NUREG/CR-1692
R1, R2, R4

Flow Regime Identification and Void Fraction Measurement Techniques in Two-Phase Flow

Manuscript Completed: May 1980
Date Published: October 1980

Prepared by
M. A. Vince, R. T. Lahey, Jr.

Department of Nuclear Engineering
Rensselaer Polytechnic Institute
Troy, NY 12181

Prepared for
Division of Reactor Safety Research
Office of Nuclear Regulatory Research
U.S. Nuclear Regulatory Commission
Washington, D.C. 20555
NRC FIN No. B7272

ABSTRACT

Flow regime identification and void fraction measurement are two important areas considered in vertical two-phase flow. A series of chordal void fraction measurements were made and formed into the probability density function (PDF) and power spectral density (PSD) function. The first four moments associated with these distributions were studied to obtain an objective flow regime indicator.

The moments of the PDF indicated the various flow regime transitions. The moments of the PSD also show some flow regime transition information, but are very sensitive to liquid phase velocity. The PDF variance, or second moment about the mean, was found to be the best indicator of flow regime. A variance of 0.04 appear to adequately discriminate between the bubbly, slug and annular flow regimes in low pressure air/water flow in tubes.

A dual beam x-ray system was designed and constructed to make the chordal void fraction measurement required. This x-ray system employs a DC excited tube filament, full wave rectification and voltage filtering to produce a stable photon source. The large photon flux made analog linearization of the signal possible.

Vertical two-phase was produced with air and water at atmospheric pressure. Calibrated rotameters were used to regulate the flow rates into the one inch I.D., plexiglass tubular test section.

Local void fraction measurements were made with a Karlsruhe impedance probe. The probe was operated at radio frequency to minimize sensitivity to liquid phase resistivity. Two types of signal thresholding were used: level and derivative. The dual beam x-ray system was used as a calibration standard for the radio frequency excited impedance probe. Calibration was performed in vertical air/water flows. Derivative thresholding was found to be preferable to level thresholding, however, in both schemes the effects of surface tension were observed below a liquid superficial velocity of 0.5 m/sec.

Table salt was added to the water to verify the probe's response to changing water resistivity. Derivative thresholding provided reasonable void fraction measurements. Level thresholding was found to be inadequate due to a shifting baseline capacitance.

Several novel void fraction measurement techniques were also investigated. A diamond tipped optical local void probe was developed and tested. A global void probe using scanning light beams was constructed and tested. Both systems appear to be promising but need further development.

Table of Contents

LIST OF FIGURES

FIGURES

Chapter 4

Chapter 5

Appendix A.4

Appendix A.6

Appendix A.9

ACKNOWLEDGEMENTS

The authors wish to thank the following individuals for their help in the development of the two-phase instrumentation reported on herein:

- Mr. G. Krycuk (RPI)
- Mr. S. Moreira (RPI)
- Mr. M. Anderson (RPI)
- Mr. W. Stronge (RPI)

In addition, the following staff helped in the setup and conduct of the experiments:

- Mr. J. Westhead (RPI)
- Mr. R. Pendt (RPI)
- Mr. J. Kelly (RPI)
- Mr. J. Schatz (RPI)
- Mr. D. Roeser (RPI)
- Mr. D. Waters (RPI)

Professor B. Malaviya (RPI) contributed to the development of the dual beam X-ray analysis and Mr. J. Pettit (RPI) helped with the development of the PDP-9 software. Without their assistance, progress would not have been as rapid.

The stimulating discussions, and help of the following graduate students was also appreciated:

- Mr. W. Conlon (RPI)
- Mr. R. Hietherington (RPI)
- Mr. N. Lombardo (RPI)
- Mr. S. Feng (RPI)

Moreover, the fine typing and clerical assistance of Ms. M. Mamone (RPI) and Ms. C. Vince was very much appreciated.

Finally, the advice, encouragement and financial assistance given this project by Dr. Y. Y. Hsu (USNRC) is greatly appreciated.

It can be seen that, to be successful, a project of this magnitude and scope involves the work of many dedicated people. The purpose of this acknowledgement section is to let them know that their efforts were appreciated.

1. INTRODUCTION

1.1 Background

Multiphase flow phenomena are observed in many industrial applications. Petroleum, chemical and nuclear industries commonly utilize multiphase flows. Efficient plant operation and optimum equipment design require accurate knowledge of the various parameters associated with this phenomena.

The recent accident at Three Mile Island has raised additional interest in light water nuclear reactor (LWR) safety. Accurate techniques for the measurement of two-phase parameters are required to conduct the necessary safety experiments.

Void fractions are central parameters associated with two-phase phenomena. The volumetric (or global) void fraction is defined as the ratio of the vapor volume to the total volume of the control volume under consideration. An area-average void fraction is the ratio of the vapor area to the total cross sectional area. In a similiar fashion, the chordal-average void fraction is the ratio of pathlength through vapor to the total chordal pathlength. The local void fraction is defined as the ratio of the time that a given point is in the vapor phase to the total observation time. All void fraction definitions indicate that this parameter ranges numerically from zero (all liquid phase) to one (all vapor phase).

The measurement of void fraction in many systems of practical concern is difficult. High temperature and mass flows place considerable demands on any void measuring device. Moreover, massive pressure vessels and thick walled piping may require penetrations to insert the appropriate instrumentation.

All void fraction measuring devices can be classified into two groups; intrusive or non-intrusive. An intrusive device would be placed in direct contact with the two-phase flow. Typical examples include a local impedance probe or drag disk turbine transducer(DTT). Non-intrusive devices do not require intimate contact with the media being measured. They include radiation attenuation or ultrasound techniques.

Two phases, flowing simultaneously, will configure themselves in different fashions depending upon the void fraction. Vertical two-phase flow can be classified into four basic categories or flow regimes [1]:

1) Bubbly
2) Slug
3) Churn-turbulent
4) Annular

These various regimes are shown schematically in Figure 1.1.

Bubbly flow is characterized by small, discrete bubbles surrounded by liquid. A spherical-capped "Taylor" bubble may occasionally appear, but this flow regime usually consists of low void fraction.

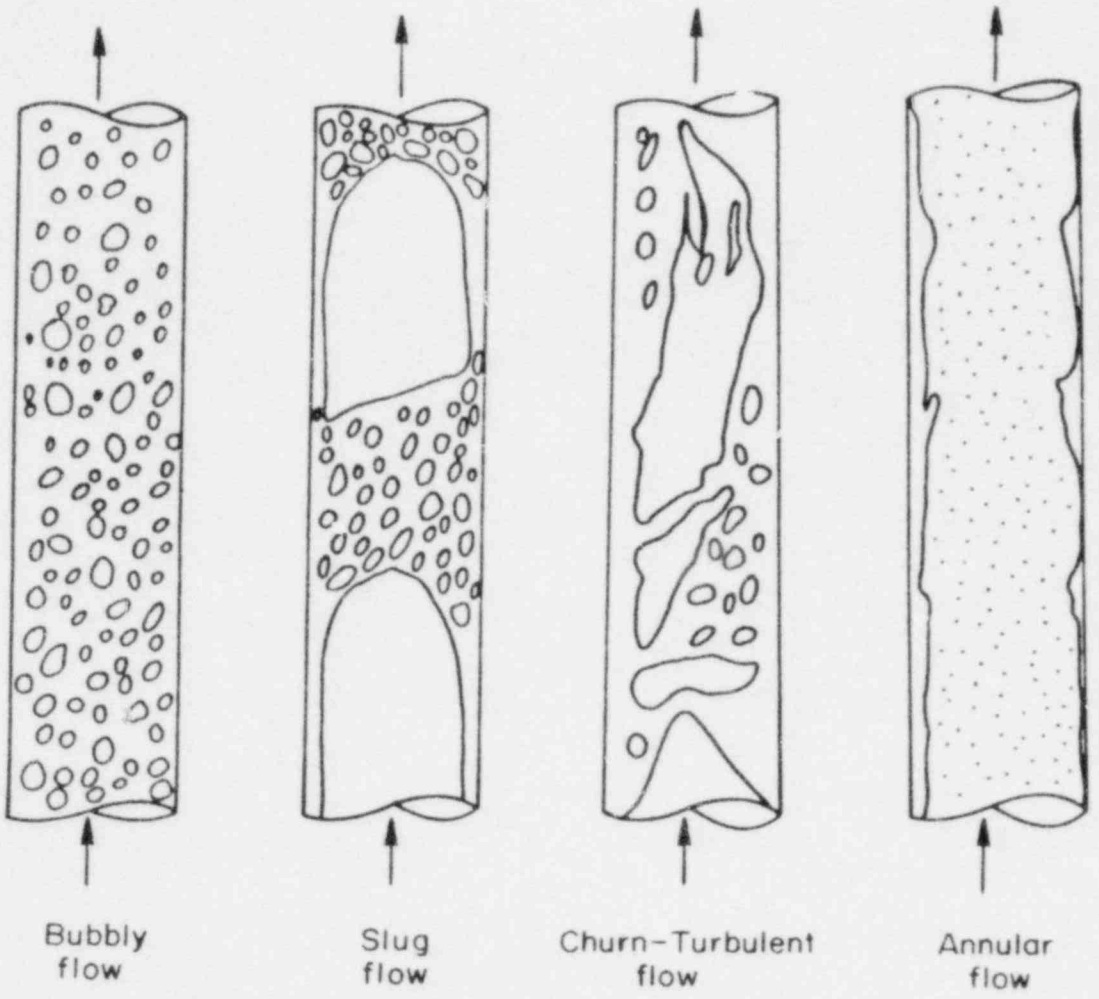

Figure 1.1
The four flow regimes observed in vertical two-phase flow

Slug flow consists of slugs of liquid separated by regions of high vapor content. The vapor phase apppears as large, spherical-capped bubbles, followed by a collection of much smaller voids, in bubbly form. At the lower flow rates, this flow regime represents a transition between bubbly and annular flow.

Churn-turbulent is a special case which occurs at high flow rates, and is characterized by chaotic motion between the phases. This flow regime can be considered to be a transition between the bubbly and annular flow regimes at high flow rates. Liquid bridging, a characteristic of slug flows, is still observed, however it is quite intermittent.

Annular flow occurs at high void fractions and is characterized by a central vapor core surrounded by an annulus of liquid. Liquid phase entrainment, i.e. droplets moving in the vapor core, are also frequently observed. Roll waves may move along the interface, however the liquid bridging, observed in slug flow, does not exist.

Heat transfer rate and the pressure drop depend on the existing flow regime. Correlations for these parameters must be related to flow regime. The various flow regimes must then be objectively identified if accurate predictions are to be made.

The flow regime is a global phenomena. Thus any objective indicator must be based on a measurement which characterizes the entire conduit. Several of the void

fractions previously discussed are such a parameter. Hence, any correlation for flow regime should include this fundamental quantity.

Flow regime identification is normally performed by visual observation [2,3]. This technique is usually based on a review of photographs or on an actual real-time observation. Flow regime identification by visual means is quite subjective. The results of various investigations rarely agree, particularly near the flow regime boundaries.

Several other schemes have previously been employed to predict flow regimes. Channel pressure drop changes have been used [4] to indicate flow regime transitions. More objective techniques, such as the power spectral density (PSD) function, determined from pressure transducer measurements [5], or the probability density function (PDF) and PSD computed from chordal x-ray measurements [6] have been proposed. Interpretation of the results of these methods is still subjective and cumbersome, consequently these techniques have not been widely used. Two fundamental problems clearly exist:

1) How to measure void fraction.
2) How to objectively identify the flow regime.

1.2 Purpose of The Study

The basic purpose of this study was to develop accurate and reliable instrumentation for the measurement of void fraction in two-phase flows. In addition, these instruments were utilized to develop an objective flow

regime indicator. This study investigated techniques for area-average, chordal-average and local void fraction measurements. Several previously employed schemes involving x-ray attenuation and impedance probes were improved and used. Novel techniques, such as an optical digital interferometer, and a diamond tipped optical local probe, were developed and tested.

An objective flow regime indicator was formulated from the PDF and PSD associated with the measured instantaneous void fractions. In principle, the moments computed from the void fraction PDF and PSD should provide an objective measure of the flow regime because of a well known theorem of statistics [7,8], which states that any distribution can be completely characterized by its moments.

Calculation of the PSD requires a Fast Fourier Transform(FFT) algorithm [9,10] to convert the time domain data into the frequency domain. If the frequencies associated with void passage are to be resolved, the void measuring device must have a sufficiently fast time response and high accuracy. Such a device will also allow for many void fraction measurements in a relatively short period of time, thus making ensemble averaging possible.

In summary, the three major objectives of this study were:

1) To develop a local void probe.
2) To develop a global void probe.
3) To develop an objective flow regime indicator.

1.3 Techniques

Many techniques are available for void fraction measurement [11,12]. X-ray attenuation was selected as the standard for calibration of local probe measurements and to provide the statistical data required for the calculation of the PDF and PSD. The technique developed provided the fast response and accuracy necessary.

1.3.1 RPI X-Ray System

Several design criteria were incorporated into the x-ray system developed at RPI for chordal-average void measurement:

1) Relative chordal-average void fraction error, $(\Delta\alpha/\alpha)$ of less than five percent in one millisecond, along the test section diameter, for the lowest void fraction of interest.
2) Test and reference beams from the same source (which allows for the application of a D.C. bias to the reference beam to reduce common mode noise).
3) Analog linearization of the void signal before digitization (to eliminate dynamic bias).
4) DC excitation of the x-ray tube's filament for photon output stability.
5) Mobility so that a conduit could be scanned laterally and vertically.

A system based on the above criteria will be able to

accurately measure the instantaneous chordal-average void fraction and provide data for the formation of the PDF and PSD.

1.3.2 X-Ray Data Analysis

Five moments are commonly associated with any distribution:

1) The mean, or first moment about the origin.
2) The second raw moment, or second moment about the origin.
3) The variance, or second moment about the mean.
4) The skewness, or third moment about the mean.
5) The kurtosis, or fourth moment about the mean.

The mean is the average value of a distribution. The second raw moment is a measure of the spread of the distribution from the origin. Variance is a measure of the distribution about the mean.

The third moment, skewness, is a measure of the asymmetry of a distribution. A symmetric distribution such as a normal distribution, has zero skewness since the mean and the median coincide. A unimodal distribution which has a median to the left of the mean, (i.e., it is skewed to the left) has a negative skewness. If the distribution is skewed to the right it will have a positive skewness. This moment is usually normalized by the variance to the 1.5 power. The resulting value is called the coefficient of skewness and relates the skewness to the spread of the

distribution.

Kurtosis is the fourth moment and is a measure of the distribution's peakedness. Similar to the skewness, this moment is often normalized by the square of the variance and the resultant parameter is called the coefficient of kurtosis. The normal distribution is mesokurtic, i.e., it has a coefficient of kurtosis equal to three. A distribution with a coefficient of kurtosis less than three is called platykurtic. These distributions are flatter than a normal distribution. Distributions with more peakedness than a normal distribution are called leptokurtic, i.e., the coefficient of kurtosis is greater than three.

These moments have physical significance and can be related to the various two-phase flow regimes. The variance of the void distribution should be small in bubbly and annular flows. These flows should also be leptokurtic and possess large positive or negative skewness. Slug flow void distributions, on the contrary, should have a large variance and near zero skewness. The slug flow void distribution is normally platykurtic. Flow regime identification should thus be possible with these moments.

Calculation of the moments of a discrete distribution is straight forward. The mean is the sum of the products of the possible void fractions and their associated probabilities, as shown in Equation (1.1),

$$\alpha = \sum_{i=1}^{N} \alpha_i p_i \qquad (1.1)$$

where,

α = mean chordal-average void fraction

p_i = probability of i^{th} void fraction

α_i = the i^{th} void fraction

The second raw moment about the origin is calculated by squaring the instantaneous void measurement before summation, Equation (1.2),

$$M_{sr} = \sum_{i=1}^{N} \alpha_i^2 p_i \qquad (1.2)$$

where,

M_{sr} = second raw moment about the mean

Moments about the mean are calculated in similar fashion, as shown in Equation (1.3),

$$M_n = \sum_{i=1}^{N} (\alpha_i - \alpha)^n p_i \qquad (1.3)$$

where,

M_n = n^{th} moment

n = 2 for variance

n = 3 for skewness

n = 4 for kurtosis

The coefficients of skewness and kurtosis are formed by dividing the skewness and kurtosis by the variance raised to the appropriate power. That is,

$$C_{M_3} = M_3/M_2^{1.5} \tag{1.4}$$

$$C_{M_4} = M_4/M_2^{2} \tag{1.5}$$

where,

C_{M_3} = the coefficient of skewness
C_{M_4} = the coefficient of kurtosis
M_2 = the variance
M_3 = the skewness
M_4 = the kurtosis

Later reference to skewness and kurtosis should be taken to mean the coefficient of skewness or the coefficient of kurtosis.

1.3.3 Local Void Probes

Let us now turn our attention from flow regime identification to the measurement of local void fraction. An ideal local void fraction probe should have several properties. This device should be very small so as to permit rapid two-phase interface penetration. The small size will also minimize void or droplet deflection caused by the probe's presence. Mechanical considerations will limit

the amount of miniaturization possible since the probe must be able to endure the harsh two-phase environment. The probe's sensitive region should be a non-wetting surface so that any liquid will not cover the probe tip during the presence of the vapor phase. In addition, an ideal local void measuring device would be independent of local temperature, local pressure and local phase velocities since these parameters are rarely controllable.

While no probes possess all these characteristics, two techniques were identified for local void fraction measurement: impedance and optical techniques.

1.3.3.1 Impedance Probes

An impedance type local void probe measures the impedance associated with each phase. Most of these techniques measure only the resistive component of the impedance. During transients, however, the liquid phase resistivity will change radically with temperature. Moreover, it is not unusual to have water purity vary with time. Thus data obtained with a resistive probe can be very unreliable.

The characteristic impedance of a measurement is made up of resistance, capacitance, and inductance. Resistance effects can be minimized by emphasizing the capacitive or inductive components. A novel capacitive excitation scheme for commerically available impedance probes, such as the Karlsruhe (KfK) type [13], was developed

at RPI. The (KfK) probe was used a capacitive element in a variable frequency oscillator (VFC). Polarization effects were eliminated as the probe operates at ground potential. The different dielectric constant associated with each phase produces the needed discrimination.

1.3.3.2 Optical Probes

An optical void probe measures the refractive index associated with each phase. The refractive index of each phase is different and they are relatively independent of the phasic temperatures and water purity, giving the optical probe an inherent advantage over an impedance probe.

Critical angle reflection is used to make the void fraction measurement. Light, incident on the probe/media interface, undergoes total internal reflection when the vapor phase surrounds the probe tip. Existence of the liquid phase at the probe tip results in light transmission into the liquid. Measurement of the reflected signal will yield the local void fraction.

Unfortunately, the two-phase environment imposes harsh operating conditions on an optical probe. Destruction of a glass probe tip can result from the high temperature fluid encountered. Fortunately, optical quality sapphire or diamond tips may be able to withstand such an environment.

A diamond-tipped optical void probe should have good void measuring characteristics. Diamonds have a high refractive index: indeed, the largest known to exist [14].

Moreover, the mechanical properties of this material are constant up to fifteen hundred degrees Fahrenheit [15]. In addition, operation of this probe in the visible light range is possible because no absorption resonances exist at these frequencies [16,17].

Standard glass fiber optics can be used for light input and output, however, an optical interface will be required between the diamond tip and the fiber optic bundle. In addition, a seal is required between diamond tip and the outer sheath, since the two-phase mixture must not come into direct contact with the glass fibers. A typical local optical probe is shown schematically in Figure 1.2.

Several mechanical design considerations are also significant. Differential thermal expansion, associated with the probe components, must be considered if the seal is to remain intact. Finally, manufacture of a diamond tipped local void probe is difficult because of the small size required.

1.3.4 Global Void Probes

An ideal global void probe would require many of the characteristics associated with a local void probe. In addition, this device should not interfere with the two-phase flow. A short response time is also an important consideration. Moreover, the phase distribution within the sensitive region should not affect the indicated void fraction.

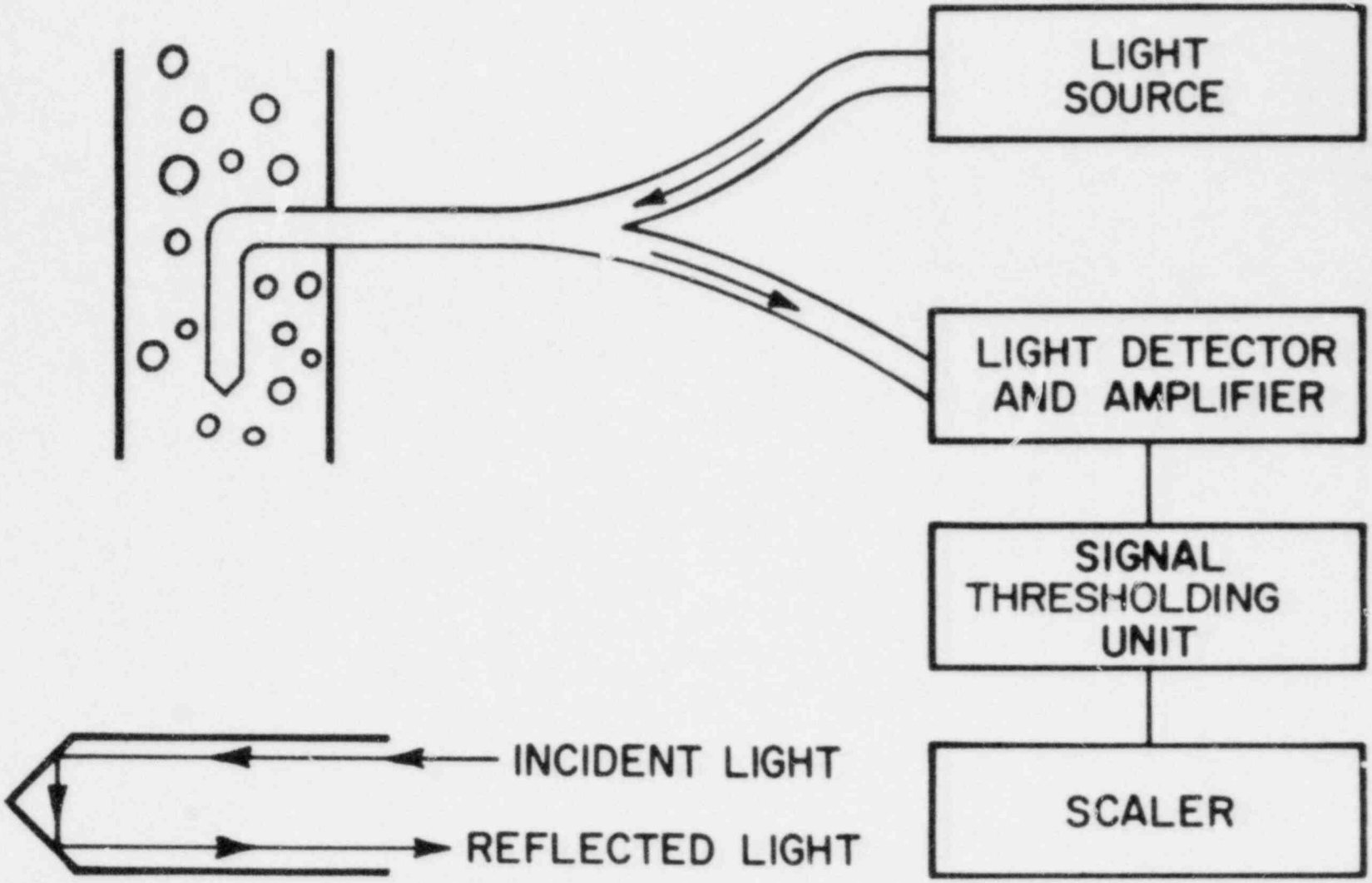

Figure 1.2
A typical optical local void probe

Global void measurements can be made using optical techniques. Light transmission techniques have been used previously [18], particularly at low void fractions. The transmitted intensity is usually measured and related to void fraction.

A void can be considered a lens system. Light incident on a bubble will initially be scattered and refracted. Due to refraction, the back interface of the void acts to further disperse the light rays as shown schematically in Figure 1.3. Clearly, the voidage will affect the transmitted intensity.

A system of well collimated light beams, as shown in Figure 1.4, can be employed to measure global void fraction. The x-y plane arrangement, through a logic interface, can detect the presence of voids at the beam intersection points.

A critical design parameter will be the ability to introduce and detect the collimated light beams, in view of the temperature and pressure considerations and the conduit size. Sapphire has exhibited good resistance to erosion under these conditons. However, transmission losses at the (light) source/sapphire wave-guide junction can substantially reduce the intensity in the two-phase mixture. Ideally, this optical junction should also act as a thermal expansion buffer between the sapphire and the light source.

Light beam detection can be achieved in a number of ways. Phototransistors, or photocells, can be used to

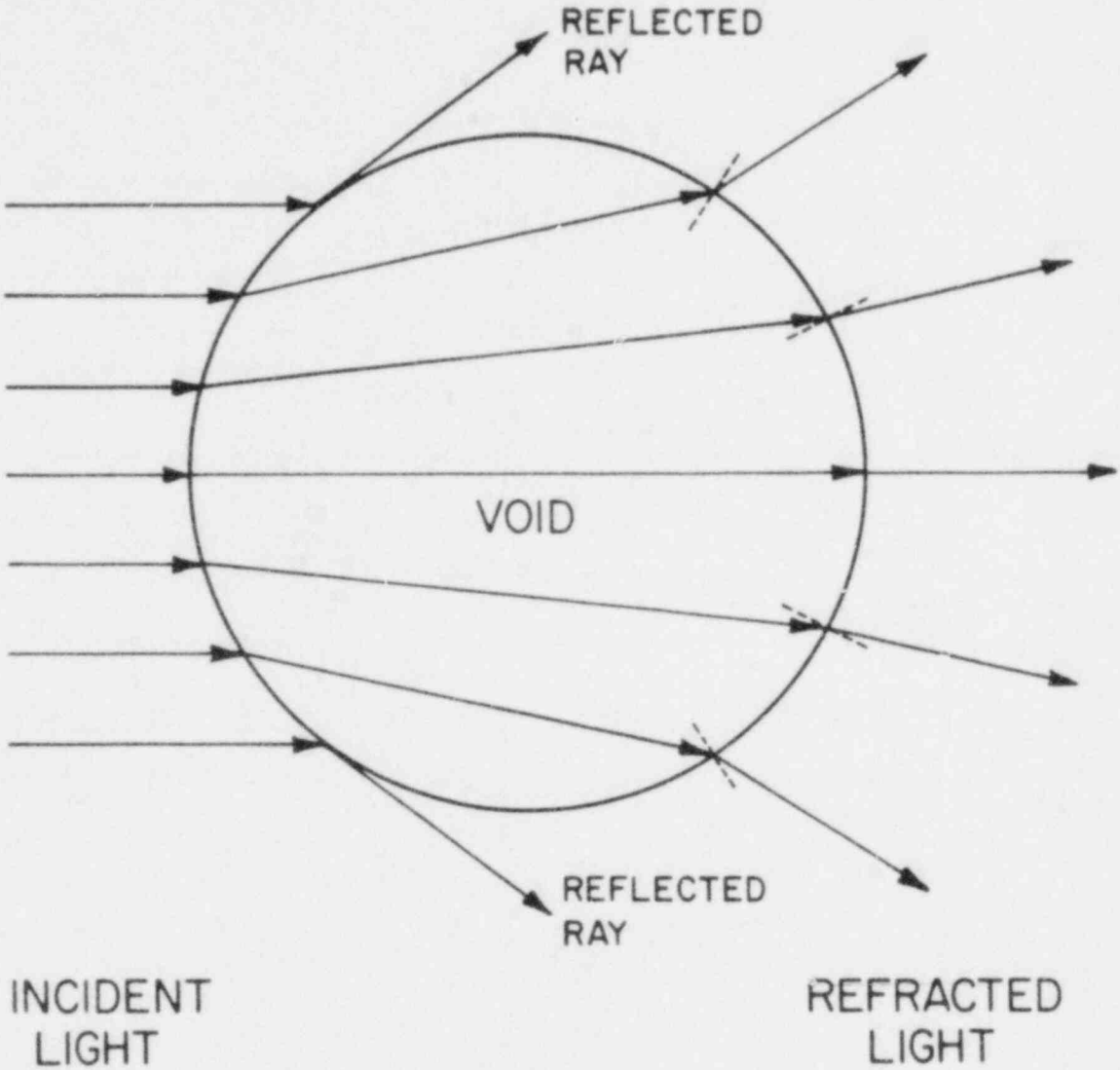

Figure 1.3
The divergence of light rays incident on a void in two-phase flow

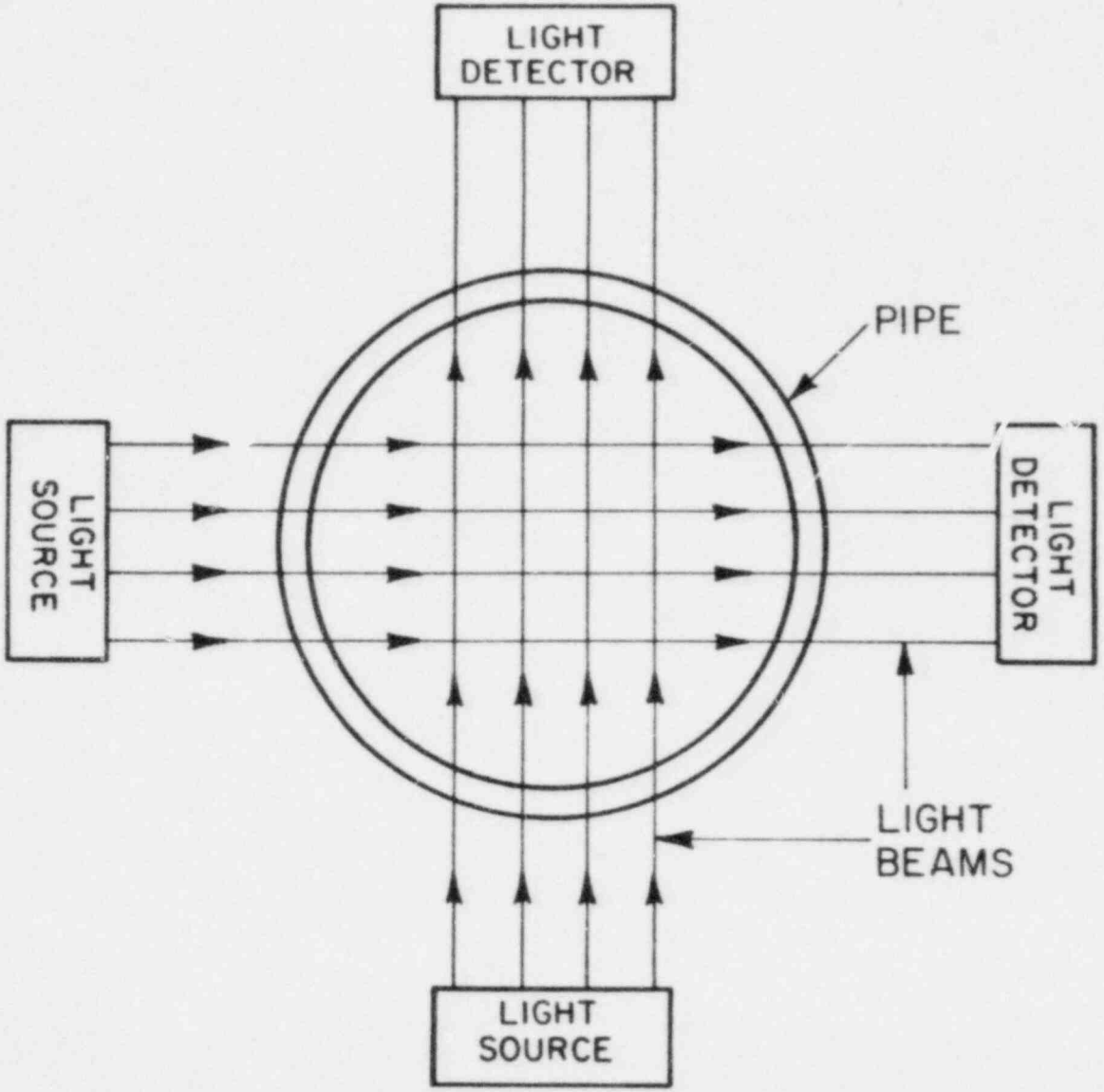

Figure 1.4
A system of well collimated light beams for global void fraction measurement

detect light. Miniature linear arrays of phototransistors are also commercially available for fine spatial resolution.

Many light sources can be considered. A laser, striking a rotating mirror, can provide a scanning light beam. Light emitting diodes (LEDs) can be interfaced directly for each beam required. These LEDs are available individually or in minature arrays. The LEDs have an excellent frequency response and thus can be pulsed at a fast rate.

Each of the void measurement techniques, discussed above, was developed at RPI. Operational prototypes were constructed for each device, and these prototypes were used to measure two-phase void fraction.

2. DISCUSSION

2.1 Flow Regime Analysis

Flow regime maps represent a convenient way to indicate the phase distribution of a two-phase mixture. Flow regime boundaries can be indicated on a plot of parameters commonly measured or calculated. The map's coordinate axis will depend on the particular application. and generalization of results is difficult.

The best known of the early flow regime maps was developed by Baker [19]. He studied the pressure drop resulting from natural gas and oil flowing simultaneously in a horizontal pipe. This pressure drop was greater than the drop associated with a single-phase flow. Baker correlated his results in terms of the mass flux of the vapor phase, G_g, and the ratio of the liquid to gas mass fluxes, G_ℓ/G_g. Figure 2.1 shows a Baker plot. A pressure correction, shown in Equation (2.1), is applied to the gas mass flux,

$$\lambda = \left[\left(\frac{\rho_g}{0.075}\right)\left(\frac{\rho_\ell}{62.3}\right)\right]^{1/2} \qquad (2.1)$$

where,

λ = density correction factor for the gas mass flux

ρ_g = gas phase density, lbm/cu ft

ρ_ℓ = liquid phase density, lbm/cu ft

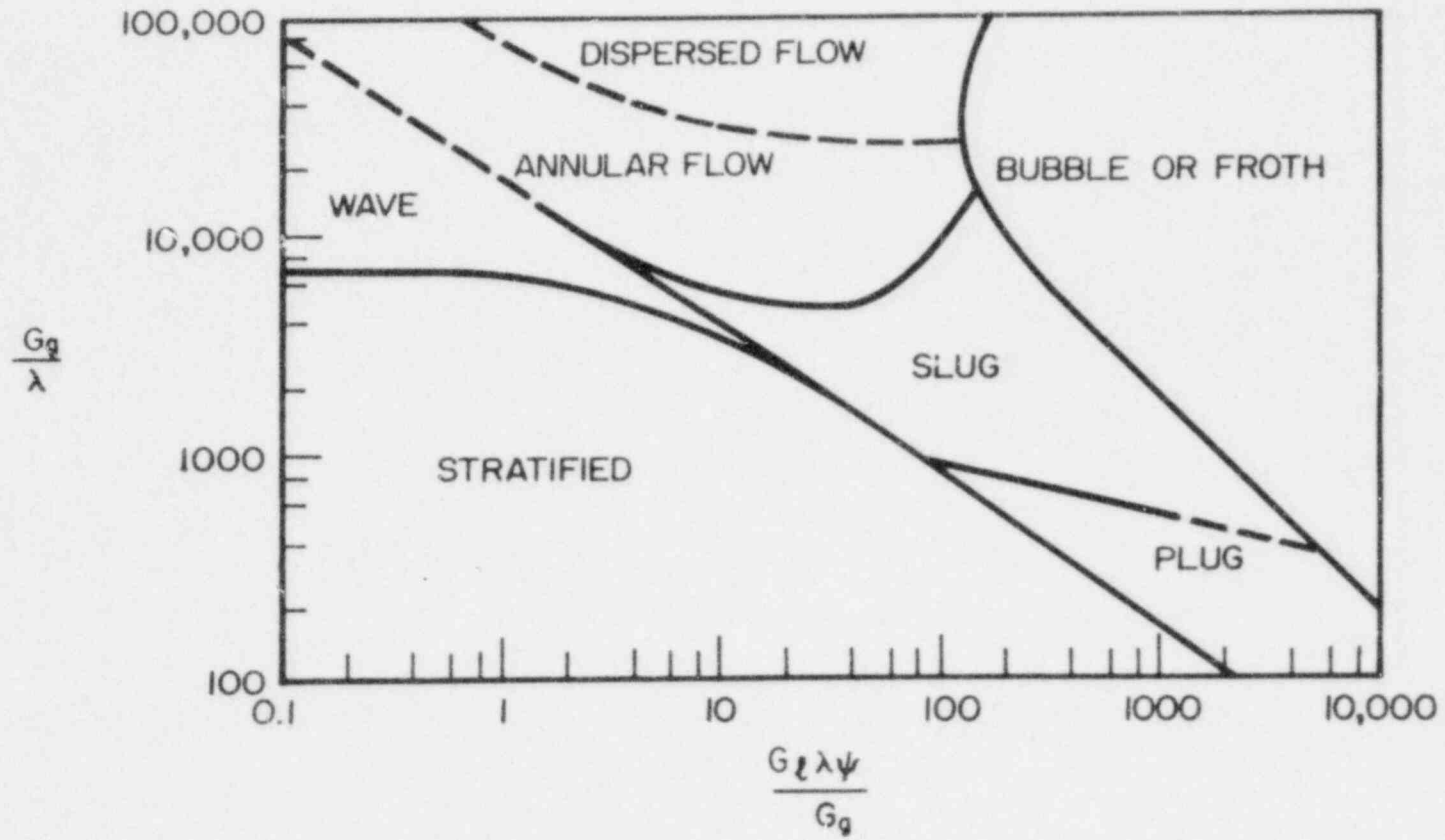

Figure 2.1
A Baker plot for flow regime identification

An aditional correction factor was used to account for viscosity effects. This expression is shown in Equation (2.2),

$$\psi = \left(\frac{73}{\sigma}\right)\left[\left(\frac{62.3}{\rho_\ell}\right)^2 \mu_\ell\right]^{1/3} \qquad (2.2)$$

where,

ψ = viscous correction factor for the liquid mass flux

μ_ℓ = liquid phase viscosity, centipoise

σ = surface tension, dynes/cm

The Baker plot shows sharp transition lines on the graph, however, the boundaries are really broad transition regions.

One of the first vertical flow regime maps was proposed by Govier, et.al. [4,20]. These experiments used air and water to simulate the two-phase flow. They investigated the effects of pipe diameter and air and water flow rates on flow pattern, "holdup" void fraction and pressure drop. Measurements of the pressure drop and void fraction were plotted against the air-to-water volumetric flux ratio. A change in pressure drop accompanies a change of flow regime. Govier, et. al. thus correlated the superficial water velocity and the air-to-water volumetric flux ratio. They indicated that the flow regime transistions occur at inflection points of the void fraction curves and at minimums in the pressure drop curves.

Griffith and Wallis [21] proposed a flow regime

map for vertical fully-developed slug flow. Their experiment consisted of an eighteen foot plexiglass air/water loop. Pressure drop measurements were made with a manometer. A plot of the relative gas flow rate verses the mixture Froude number results in a curve separating annular and bubbly flow from fully developed slug flow. This map attempts to incorporate the effect of pipe size into the correlation. Unfortunately, this correlation is only valid for fully-developed slug flow.

Hubbard and Dukler [5] measured the pressure fluctuations at the wall of a one and a half inch diameter horiziontal pipe, containing various two phase mixtures. The time response of the pressure transducer was digitized. The power spectral density (PSD) function was computed from the autocorrelation. The resulting power spectrum could be classified into three broad categories. The various flow regimes were categorized by considering the energy distribution. Apparently, this work represents the first attempt at objective classification of flow regimes.

Taitel, et.al. [22] developed models for predicting flow regime transitions in vertical flow. These models are based on the physical mechanisms associated with each transition. The effects of fluid properties and pipe size were considered. The Taitel-Dukler flow regime maps are plots based on superficial velocities; a parameter commonly measured in experiments. Several criteria are proposed. A criterion for the existence of bubble flow is

shown in Equation (2.3),

$$\left[\frac{\rho_\ell g D^2}{(\rho_\ell - \rho_g)\sigma}\right]^{1/4} \leq 4.36 \qquad (2.3)$$

where,

ρ_ℓ = liquid phase density, lbm/cu ft

ρ_g = vapor phase density, lbm/cu ft

g = acceleration due to gravity, 32.2 ft/sec^2

D = pipe diameter, ft

σ = surface tension, lbf/ft

The bubbly-to-slug transition criterion proposed is given by,

$$j_\ell = 3.0\, j_g - 1.15 \left[\frac{g(\rho_\ell - \rho_g)\sigma}{\rho_\ell^2}\right]^{1/4} \qquad (2.4)$$

where,

j_ℓ = liquid phase superficial velocity, ft/sec

j_g = vapor phase superficial velocity, ft/sec

Taitel proposed that the bubbly-to-dispersed-bubbly transition is given by,

$$j = j_\ell + j_g = 4.0 \left[\frac{D^{0.429}\left(\frac{\sigma}{\rho_\ell}\right)^{0.089}}{\nu_\ell^{0.072}} \left(\frac{g(\rho_\ell - \rho_g)}{\rho_\ell}\right)^{0.446}\right] \qquad (2.5)$$

where,

ν_ℓ = liquid kinematic viscosity

The slug-to-churn-turbulent transition was given by,

$$\frac{L_e}{D} = 40.6 \left[\frac{j}{\sqrt{gD}} + 0.22 \right] \tag{2.6}$$

where,

L_e = entrance length, ft

j = total superficial velocity, ft/sec ($j = j_\ell + j_g$)

The annular transition relationship, suggested by Taitel, is given by,

$$\frac{j_g \rho_g^{1/2}}{\left[\sigma g(\rho_\ell - \rho_g)\right]^{1/4}} = 3.1 \tag{2.7}$$

Considerable disagreement between authors exists regarding the actual location of flow pattern transition. Nevertheless, Taitel claims that his correlations, based on "theory", appeared to agree with most of the earlier experiments.

The first x-ray technique used for flow regime identification was developed by Jones [6]. This system utilized dual beams and a rectangular test section. Air and water, flowing vertically, were used to simulate the two-phase conditions. The probability density function (PDF) was formed for the data set collected. Jones observed that bubbly flow could be characterized by a single, low void, peak in the PDF. Slug flow had a bimodal PDF; the low void mode corresponding to the vapor in the liquid slug and the high void peak corresponding to the spherical-capped

bubbles. Annular flow displayed a single peak, similar to bubbly flow, but at high void fraction. Unfortunately, Jones did not attempt to deduce an objective criterion from his data.

2.2 Local Void Measurement

Electrical impedance (Z) void probe excitation schemes can be classified into two basic types; resistance, and capacitance [23]. The resistance method is the most common mode of operation. Basically the liquid short-circuits the probe, while the presence of vapor phase results in an open circuit.

The size, shape and wetability of a probe are critical parameters. Interfacial surface tension will interact with the probe tip resulting in hydrodynamic effects [24]. An ideal probe would instantly penetrate any interface. Moreover, the probe would be so small that voids are not deflected by its presence. However, any practical probe must be capable of withstanding the two-phase environment.

A high temperature probe is currently being marketed in Karlsruhe, Germany. The device has a stainless steel jacket. An inner stainless steel electrode is insulated from the jacket by aluminum oxide, as shown in Figure 2.2. A typical probe is only seven tenths (0.7mm) of a millimeter in diameter to minimize flow effects.

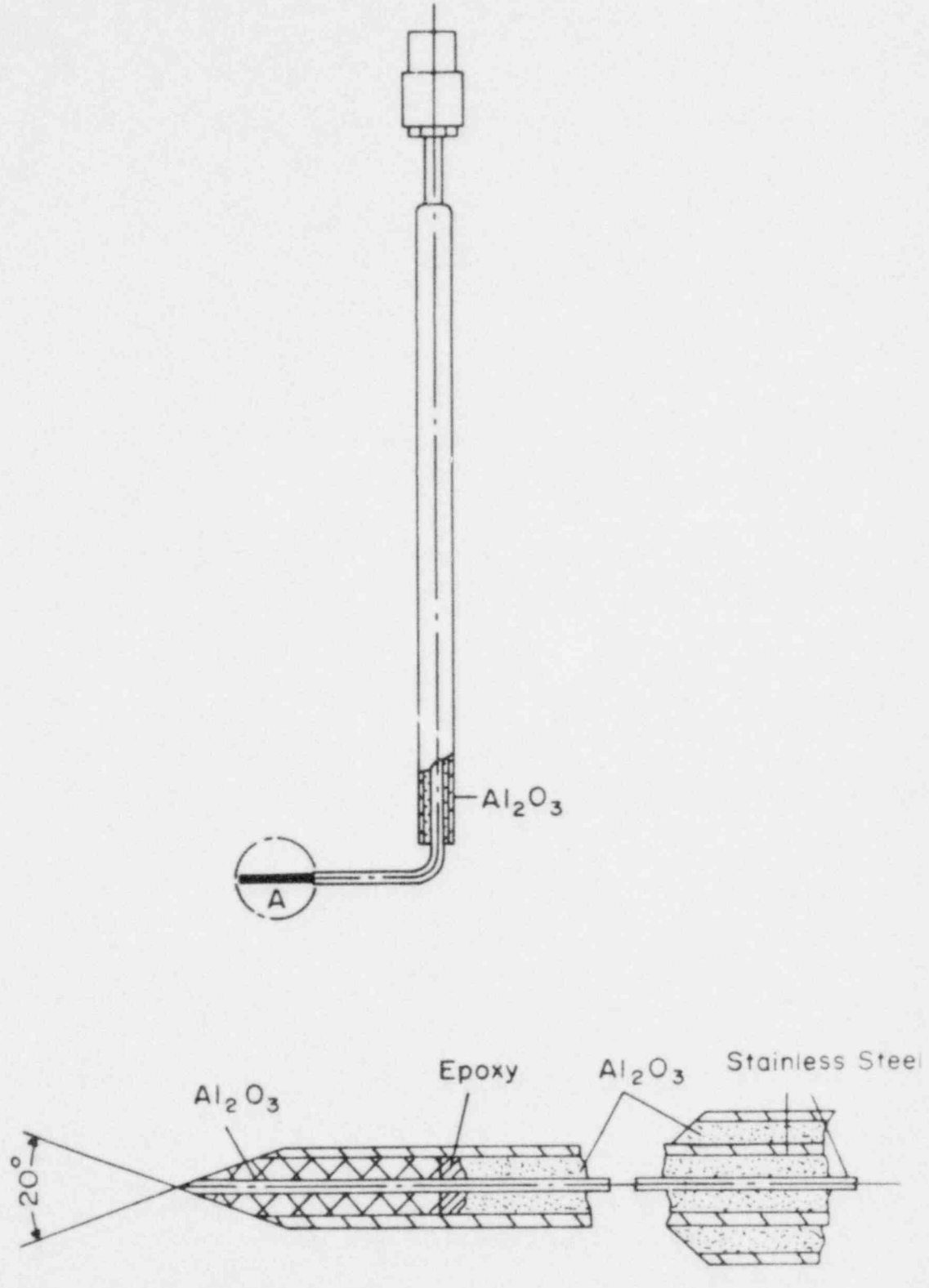

Figure 2.2
The design of a typical
Karlsruhe impedance probe

Kobori [25] has studied two methods of void probe excitation and signal processing. The two major methods of thresholding are; level and derivative thresholding. Kobori states that derivative thresholding should be more accurate because the probe output is triggering on the slope of the analog signal as opposed to the level, and thus the delays are less.

Kobori [25] also investigated the response of 'I' shaped, or straight probe, vs. 'L' shaped probes. Flow effects hamper the 'I' shaped design. He recommended the use of the 'L' shaped probe for transient blowdown tests.

The first optical probe was designed and tested by Miller and Mitchie [26]. Their device consisted of glass rod drawn to a diameter of twelve mils. The rod was either bent into an 'L' shape, parallel to the flow, or into an 'I' shape, perpendicular to the flow. The probe tip was polished into a conical shape.

The back-end components consisted of a light source, a photodetector and a thresholding unit. Light was produced by a ten watt quartz-iodine lamp and focused onto the probe's fiber optic input by a large aperature lens. Reflected light was received by a phototransistor and amplified. The signal thresholding was of the level type.

Testing of the probe was performed in air/water and Freon-12 flows. High speed photography was employed to verify the probe's operation. A correlation of the voidage measured by the probe, and that measured by quick-closing

valves, indicates that the device responds appropriately. This testing occurred in two sizes of small bore pipe.

Danel and Delhaye [27] developed a local void probe using a smaller diameter tip and weaker light source than Miller and Mitchie. This probe has a U-shaped, one hundred micrometer diameter, tip. A fiber optic, bent one hundred and eighty degrees, made the sensitive region. This small size made the device very fragile.

Reflected light was detected by a phototransistor having a fast response. Like the Miller and Mitchie design, this scheme used level thresholding to process the signal. Two thresholds, one corresponding to the rising signal and the other corresponding to the decaying signal, are employed for formation of the digital void fraction signal.

Danel and Delhaye tested their design in an air/water flow, with free rising bubbles, and in Freon flows. The tests were conducted in a small bore pipe and the probe responded accurately.

Ga[illegible] [28] has compared the two optical devices discussed above and concludes that these probes need additional improvements to increase the response time. Nevertheless, he felt the simple principle and operation of these type of probes made them very promising for industrial applications.

DISA [29] has now made the Danel and Delhaye type optical probe a commerical product. This company also markets optical liquid level probes and void passage time

devices.

2.2.1 Optical Considerations

Let us now turn our attention to the principles underlying the development of an optical global void probe. The optics of a two-phase interface have been studied for years. Davis [30] computed the angular intensity distribution of light incident on an air bubble in water. He found that external reflections from the void interface can occur. The light may also undergo total internal reflection once inside the bubble. Most intensity was scattered in the forward direction. Indeed, light was not observed to scatter beyond eighty-two and eight tenths degreees from the forward direction because of critical angle considerations.

Calderbank [18] has employed light transmission techniques to measure interfacial area. His system was arranged so that the transmitted light received by the photocell depended only on the projected area of the dispersed phase, i.e. the photocell subtended a small solid angle. Even for small particles, forward scattering predominated. The light transmitted could then be related to the source intensity as,

$$\log_{10} \frac{I_o}{I} = \frac{a\ell}{9.210} \tag{2.8}$$

where,

I_o = initial light intensity, photons/cm^2-sec

I = transmitted light intensity, photons/cm^2-sec

a = interfacial area density, cm^{-1}

ℓ = beam path length, cm

The work of Calderbank [18] was modified by Lockett [31]. Equation (2.8) was found to be valid up to thirty one percent void fraction. Higher voidage blocked out the transmitted beam. Only scattered light could then be detected. Lockett used a glass tube and introduced bubbles at the base. The liquid phase flowed downward at a velocity large enough to hold the bubbles stationary.

It is important to note that the approach taken in the development of the optical digital interferometer (for global void measurement) is more restrictive than that used in previous investigations. Advantage has been taken of the fact that a collimated light beam can be refracted and reflected at a liquid/vapor interface, but the scattering characteristics of the the two-phase medium have not been considered. As will be discussed in more detail in Section 3.4, the approach resulted in a prototype capable of the accurate measurement of both low and high global void fraction and distribution.

3. DESIGN OF EXPERIMENT AND INSTRUMENTATION

3.1 Air/Water Loop

A crucial component in any two-phase experiment is the flow loop. This device must be able to produce a variety of two-phase conditions. Visibility of the flow is also desirable, particularly in the region where measurements are made. Adequate flow regulation and metering is required to assure steady-state conditions.

A small air and water loop was built incorporating these considerations. Operation at atmospheric pressure avoided the use of pressure vessels and specially designed piping. The vertical test section consisted of one inch diameter plexiglass pipe. The mixing section was constructed of copper tubing as illustrated in Figure 3.1. Water was introduced from the city water supply, while the air was supplied by a Quincy positive displacement air compressor. Air was injected into the test section through an aquarium type airstone or input through a vertical mixing tee. The coupling between the one inch copper tube and the test section was made with a Dresser coupling to assure a smooth transformation. After flowing through eight feet of plexiglass pipe the two-phase mixture entered a one inch copper pipe. This copper pipe was connected to the air/water phase separator by a one inch flexible hose. Air was then vented directly into the atmosphere while the water was dumped into the normal city drainage system.

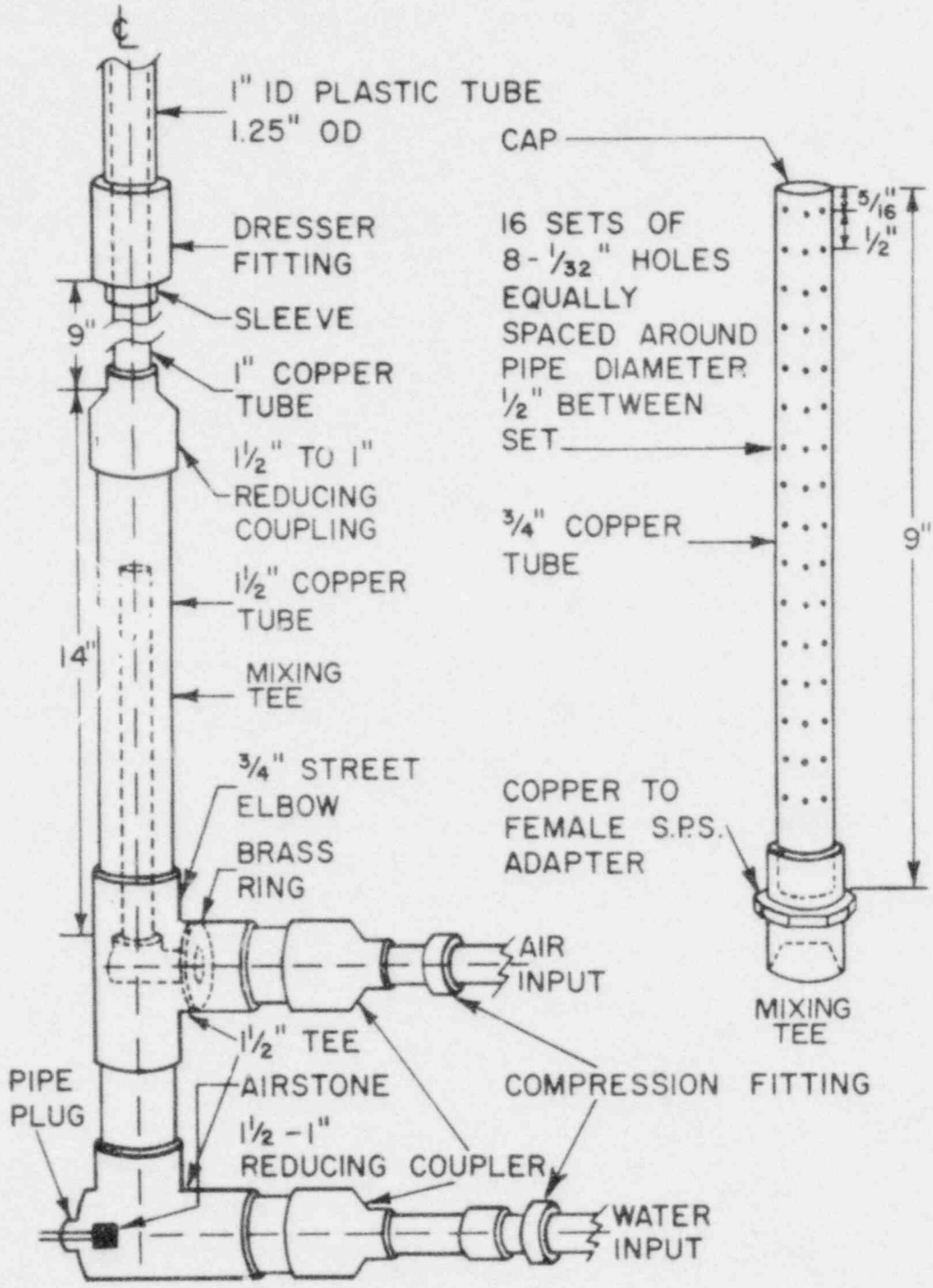

Figure 3.1
A schematic of the air/water loop mixing section

The entire loop set up is shown in Figures 3.2 and 3.3. Equipto framing was used to support the upper and lower sections of the loop. This framing was rigidly fastened to the floor and walls with studs. The test section was observed to move less than one thousandth inch [1] under all two-phase operating conditions studied.

Flow instrumentation for this loop is shown in Figure 3.4. Regulation of the air and water flow rates was performed with calibrated Dwyer rotameters. A single water rotameter with a range of one to eight gallons per minute (gpm) was used. Three air rotameters, connected in a manifold fashion, permit control between one and one thousand standard cubic feet per hour (scfh). The pressure at the inlet and outlet of the rotameter manifold was measured to determine the appropriate density correction. The air could be routed through the airstone or mixing tee via the appropriate valve.

A manometer was used to measure the pressure drop along the test section. Two pressure taps were located twelve and three sixteenths inches apart, straddling the point of x-ray measurement. The pressure lines are filled with water and sloped downward to avoid entrapment of air bubbles. These lines were initially plastic tubing and then connected to copper tubing. The plastic tubing permits a visual check for entrapped bubbles. A manometer fluid with a specific gravity of one and three quarters (1.75) was used

---

[1] A dial guage micrometer was placed on the pipe while the two-phase mixture was flowing to measure the movement.

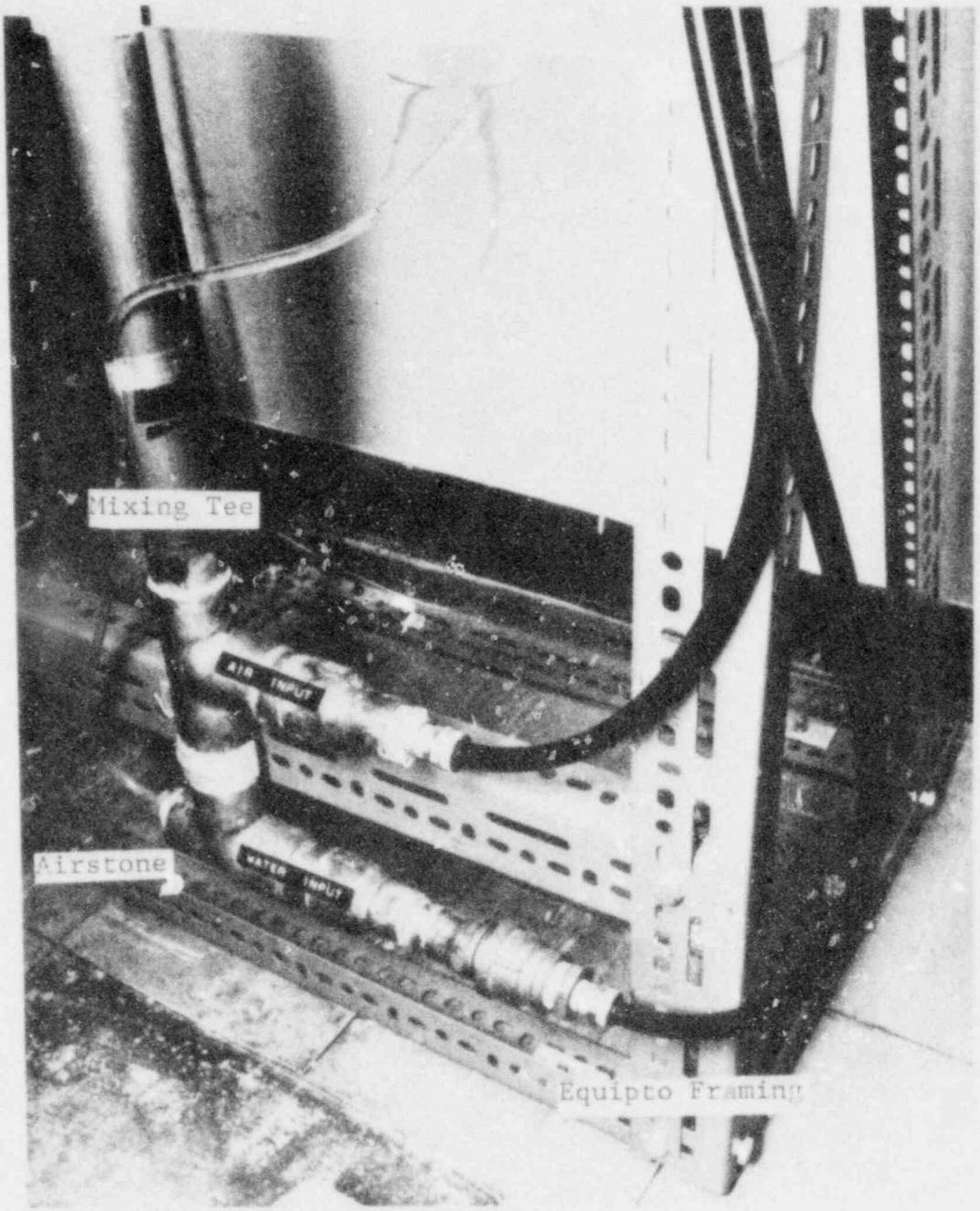

Figure 3.2
The actual air/water mixing section mounted in the x-ray test area

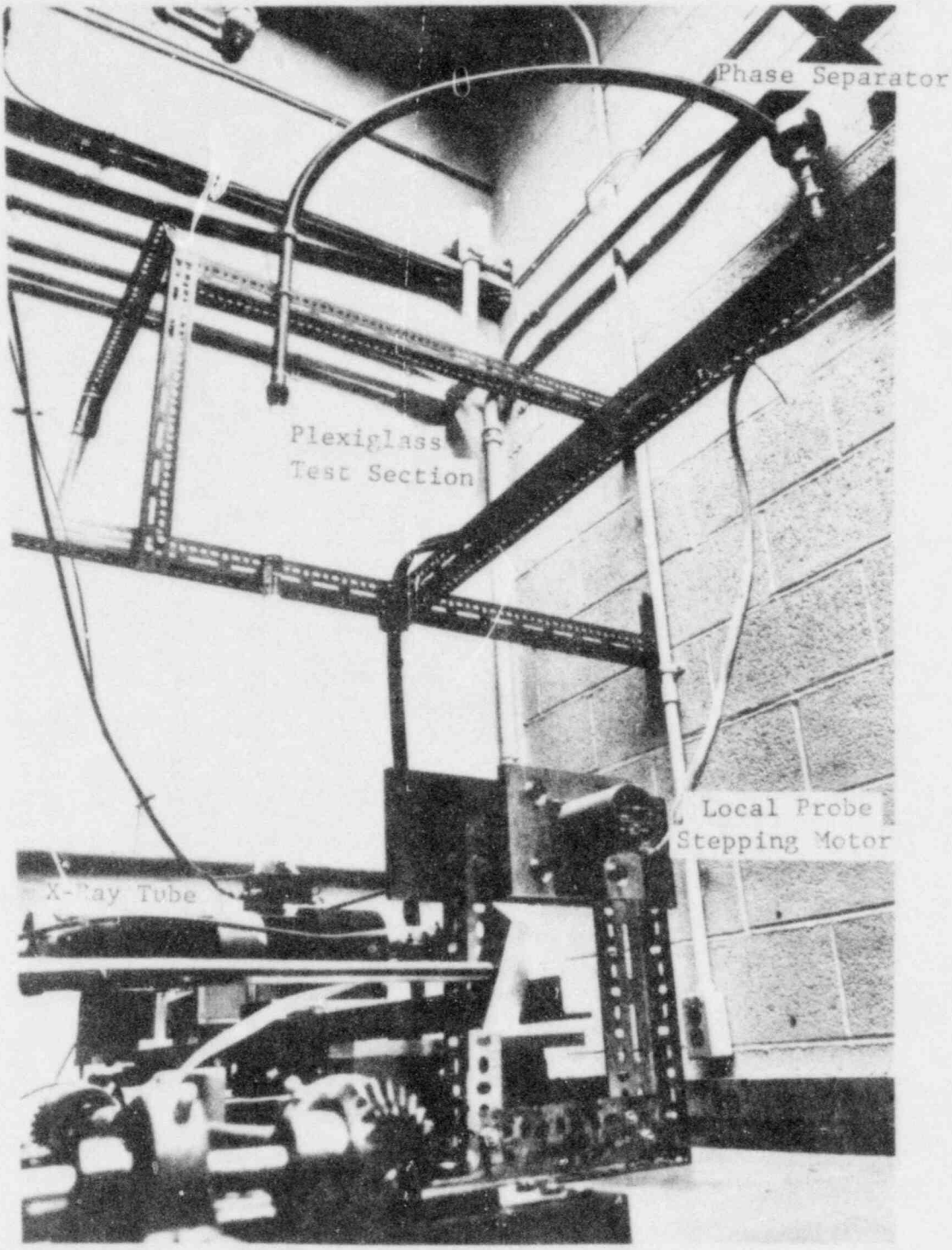

Figure 3.3
The x-ray tube, plexiglass test section and phase separator for the air/w ter loop

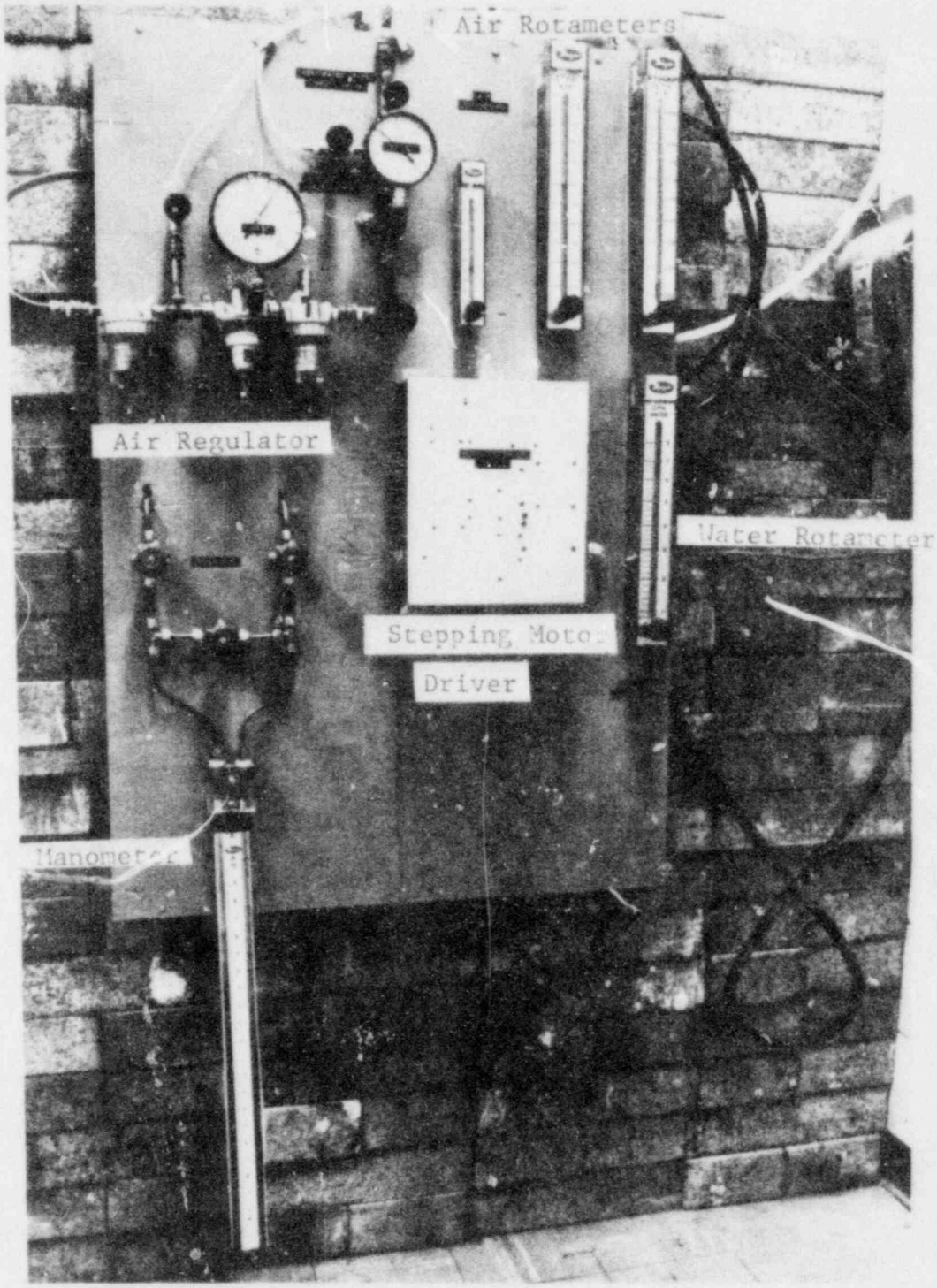

Figure 3.4
Air and water flow instrumentation for the air/water loop

for the pressure measurement. The associated valving was provided to isolate the manometer from the loop and zero the device.

Due to the low flow rates involved the global void fraction could be calculated from the manometer pressure drop. A typical two-phase condition is shown schematically in Figure 3.5. The hydrostatic pressure drop on both sides of the manometer legs must be equal. This pressure drop can be calculated as shown in Equation (3.1),

$$P_1 + \frac{\rho_\ell g h_2}{g_c} = P_2 + \frac{\rho_\ell g (h_3 - h_1)}{g_c} + \frac{\rho_{oil} g\, h_1}{g_c} \qquad (3.1)$$

where,

P_1 = pressure at point-1, psia

P_2 = pressure at point-2, psia

g = acceleration of gravity, 32 ft/sec^2

g_c = gravitation conversion factor, 32.2 lbm ft/lbf sec^2

ρ_ℓ = density of water, lbm/cu ft

ρ_{oil} = density of manometer oil, lbm/cu ft

h_1 = height of oil above datum level, in.

h_2 = total height between upper pressure tap and datum level, in.

h_3 = total height between lower pressure tap and datum level, in.

h_4 = distance between pressure taps, in.

Noting that $h_2 = h_3 + h_4$ and that $\rho_{oil} = 1.75$, Equation (3.1)

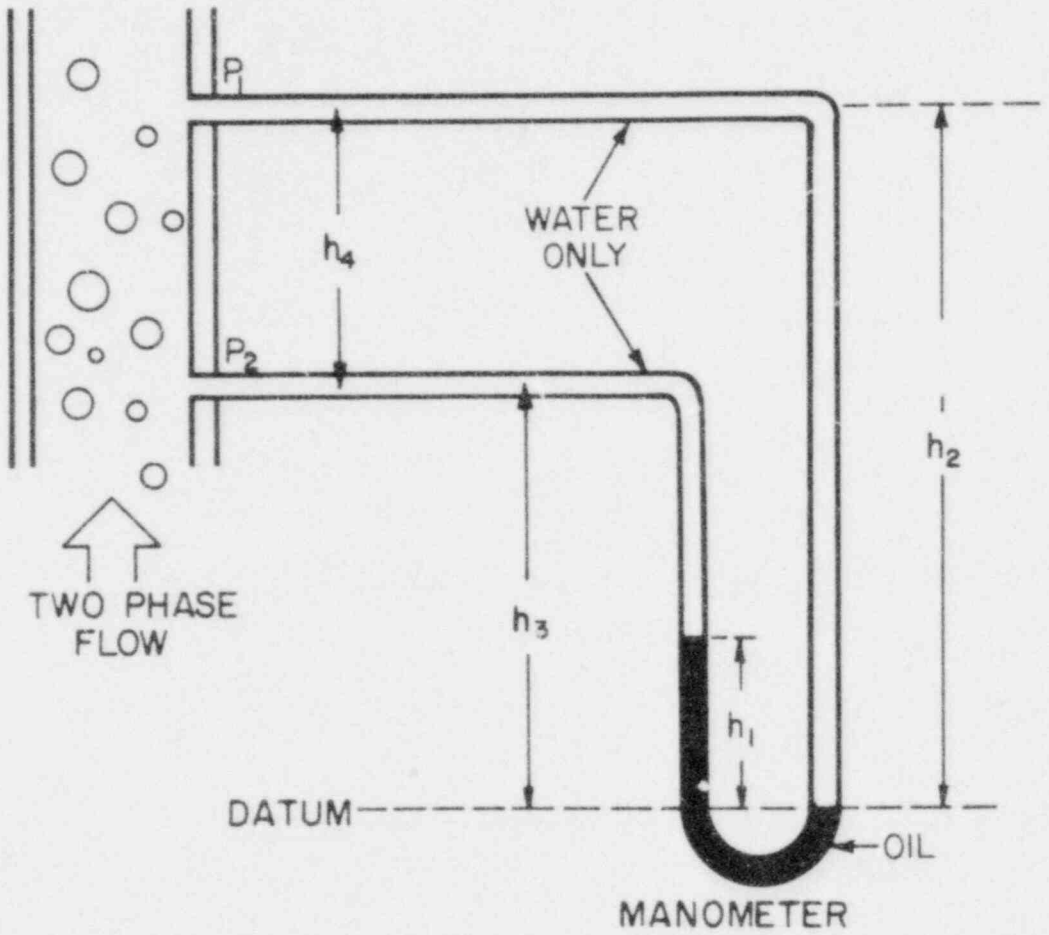

Figure 3.5
Manometer deflection in
vertical two-phase flow

can be solved for the pressure differential $P_2 - P_1$.

$$P_2 - P_1 = \frac{\rho_\ell g\, h_4}{g_c} - \frac{0.75\, \rho_\ell g\, h_1}{g_c} \qquad (3.2)$$

The hydrostatic two-phase pressure drop is:

$$P_2 - P_1 = \frac{g}{g_c}\left[\rho_\ell(1-\langle\alpha\rangle) + \rho_g \langle\alpha\rangle\right] h_4 \qquad (3.3)$$

where,

$\langle\alpha\rangle$ = global void fraction

ρ_g = density of air, lbm/cu ft

These pressure drops can now be equated. Dividing both sides by g/g_c gives an expression for the voidage in terms of measurable parameters,

$$\frac{g}{g_c}\left[\rho_\ell(1-\langle\alpha\rangle) + \rho_g\langle\alpha\rangle\right] h_4 = \frac{g}{g_c}\left[\rho_\ell h_4 - 0.75\, \rho_\ell h_1\right] \qquad (3.4)$$

Equation (3.4) can now be solved for void fraction,

$$\langle\alpha\rangle = \frac{\rho_\ell}{\rho_\ell - \rho_g}\left[\frac{0.75\, h_1}{h_4}\right] \qquad (3.5)$$

For the test under consideration: ρ_ℓ = 62.4 lbm/cu ft , ρ_g = 0.0808 lbm/cu ft and h_4= 12.1875 inches. Substituting these values into Equation (3.5), an expression to calculate the void fraction in terms of manometer height difference is obtained,

$$\langle\alpha\rangle = 0.0616\ h_1 \tag{3.6}$$

where,

h_1 = manometer fluid deflection, inches

3.2 Dual Beam X-Ray System

Monoenergetic radiation attenuation follows the well known relationship known as Beer's Law,

$$I = I_o\ e^{-\bar{\mu}x} \tag{3.7}$$

where,

I = unattenuated intensity at distance x into the media, photons/cm^2-sec

I_o = source intensity, photons/cm^2-sec

$\bar{\mu}$ = energy dependent attenuation coefficient of media, cm^{-1}

x = thickness of attenuating media, cm

Measurements of two-phase attenuation coefficient (μ) can be made using this radiation attenuation law. The two-phase attenuation coefficient can be expressed as,

$$\bar{\mu}x = \mu_g x_g + \mu_\ell x_\ell \tag{3.8}$$

where,

$\bar{\mu}$ = attenuation coefficient of two-phase mixture, cm^{-1}

x = total path length through two-phase mixture, cm

μ_g = vapor attenuation coefficient, cm^{-1}

μ_ℓ = liquid attenuation coefficient, cm^{-1}

x_g = vapor path length, cm

x_ℓ = liquid path length, cm

This expression can be substituted into Equation (3.7) to yield,

$$I = I_o e^{-(\mu_g x_g + \mu_\ell x_\ell)} \tag{3.9}$$

The attenuation coefficient of the vapor, μ_g, is usually much less than the attenuation coefficient for the liquid phase. For the (atmospheric) conditions of our test, Equation (3.9) reduces to,

$$I = I_o e^{-\mu_\ell x_\ell} \tag{3.10}$$

Several radiation sources are available for two-phase measurements [32,33]. Sources such as Cs-137 or Co-60 have photon emission rates which vary slowly with time in a well known fashion. X-ray radiation sources have strengths which depend upon their operating conditions. That is, variation in the x-ray tube's voltage or filament current will cause a change in the photon output.

Dual beam systems [6,34] use a reference beam to compensate for variations in x-ray tube photon output. This type of set-up uses two beams from the same source: one passing through the two-phase mixture and one passing through a reference attenuator. A typical arrangement [32] is shown in Figure 3.[illegible]. The instantaneous chordal void

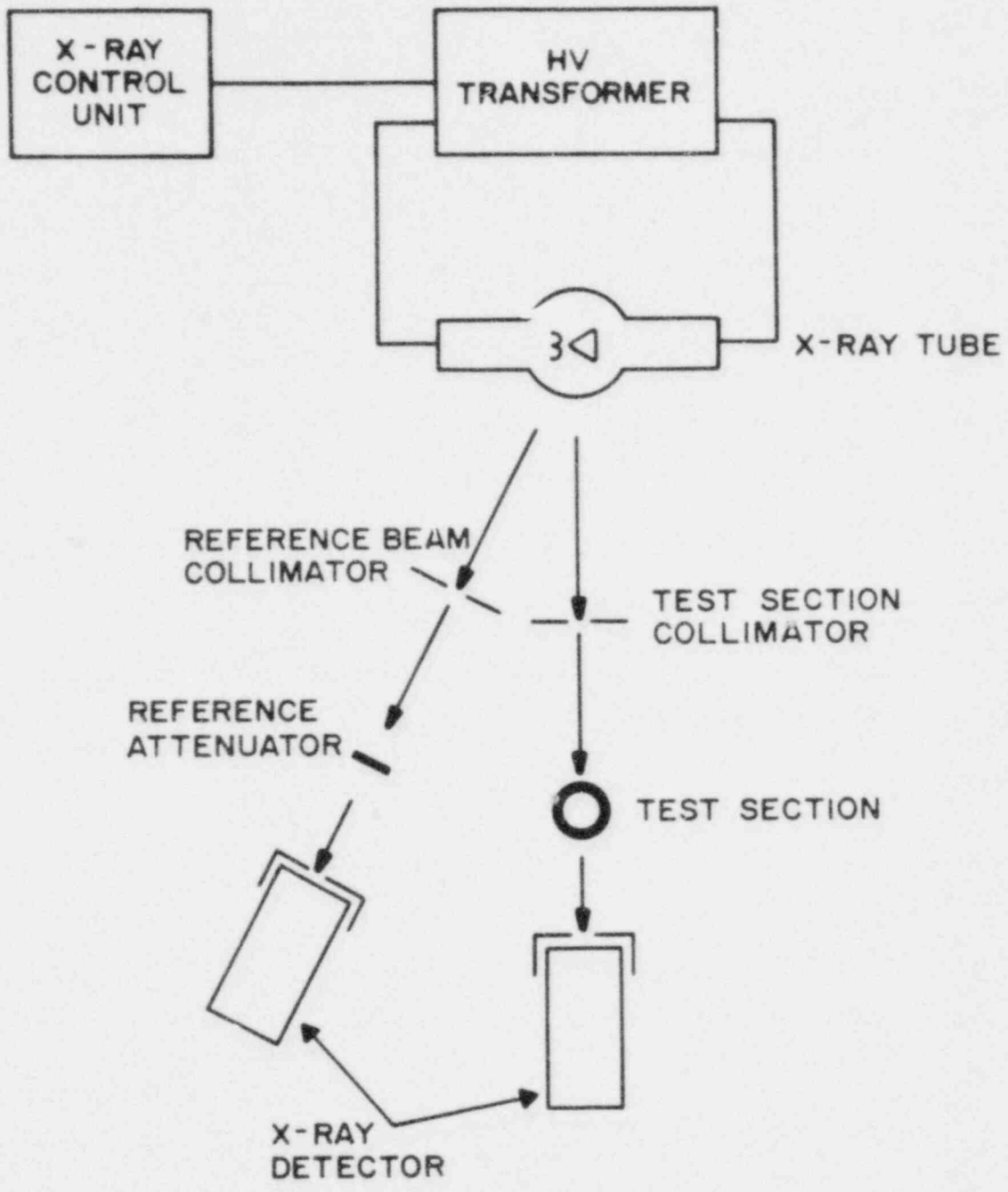

Figure 3.6
A typical dual beam x-ray system for measuring chordal void fraction

fraction will fluctuate with time, since the water pathlength, x_ℓ, will vary as a function of time. This time dependence can be introduced into Equation (3.10) yielding,

$$I(t) = I_o \, e^{-\mu_\ell x(t)} \tag{3.11}$$

where,

x(t)= time varying water path length, cm

An x-ray detector will produce an output voltage related to the incident intensity.

$$V_s(t) = V_{os} \, e^{-\mu_\ell x(t)} \tag{3.12}$$

where,

$V_s(t)$ = x-ray detector output voltage corresponding to intensity, I(t)

V_{os} = x-ray detector output voltage corresponding to initial intensity, I_o

The inherent modulation of the x-ray beam at the source causes a corresponding modulation of the detector output. Most of this fluctuation is due to noise (typically at sixty hertz; the line frequency). An expression for the fluctuating detector voltage is calculated by Equation (3.13),

$$V_s^*(t) = V_s(t) \left[1.0 + a \, f(t) \right] \tag{3.13}$$

where,

V_s^* = modulated signal voltage

a = amplitude of fluctuation resulting from

noise

$f(t)$= time dependent noise

The reference beam of a dual beam system has a response similar to the signal beam, however the reference x-ray detector should be steady since the attenuating media is constant. If we follow the suggestion of Smith [34] and include a DC bias, the modulated reference signal response is given by,

$$V_r^*(t) = V_r \left[1.0 + b\, f(t)\right] + V_{DC} \tag{3.14}$$

where,

$V_r^*(t)$ = modulated reference voltage

V_r = steady-state reference voltage

b = amplitude of reference voltage noise

V_{DC} = DC bias voltage

Equation (3.14) can be rearranged as,

$$V_r^*(t) = (V_r + V_{DC}) \left[1.0 + \frac{b\, V_r}{(V_r + V_{DC})}\, f(t)\right] \tag{3.15}$$

The measurement, Equation (3.13), and the reference, Equation (3.15), signals are separately passed through logarithmic amplifiers. The resulting signals are subtracted as shown in Equation (3.16),

$$\ln V_s^*(t) - \ln V_r^*(t) = \ln \frac{V_s(t)}{(V_r + V_{DC})} + \ln \frac{\left[1.0 + a\, f(t)\right]}{\left[1.0 + \frac{b\, V_r f(t)}{(V_r + V_{DC})}\right]} \tag{3.16}$$

This equation establishes the value of the necessary DC

bias. The last term on the right hand side of Equation (3.16) will vanish if,

$$a = \frac{b\ V_r}{V_r + V_{DC}} \tag{3.17}$$

In theory the DC bias necessary for the elimination of the common-mode noise is obtained from Equation (3.17) as,

$$V_{DC} = V_r\left[\frac{b-a}{a}\right] = V_r\left[\frac{b}{a} - 1\right] \tag{3.18}$$

Unfortunately, no two detectors will have exactly the same response, therefore, 'b' will not equal 'a'. Nevertheless, application of Equation (3.18) will simplify Equation (3.16) to,

$$\ln \frac{V_s^*(t)}{V_r^*(t)} = \ln \frac{V_s(t)}{V_r + V_{DC}} \tag{3.19}$$

The expression for $V_s(t)$, Equation (3.12), can be combined with Equation (3.19) to yield,

$$\ln \frac{V_s^*(t)}{V_r^*(t)} = \ln \frac{V_{os}}{V_r + V_{DC}} - \mu_\ell x(t) \tag{3.20}$$

Rearrangement of Equation (3.20) yields a linear expression of the instantaneous water path length in terms of measured voltages,

$$x(t) = -\frac{1}{\mu_\ell} \ln \frac{V_s^*(t)}{V_r^*(t)} - \ln \frac{V_{os}}{V_r + V_{DC}} \tag{3.21}$$

This expression does not contain any noise terms. As discussed previously, in actual practice it has been found that all noise can not be eliminated. Nevertheless, the DC bias can be used to effectively reduce most of the undesirable noise.

The instantaneous water path length is easily related to the chordal-average void fraction by,

$$\alpha(t) = 1 - \frac{x(t)}{C} \tag{3.22}$$

where,

$\alpha(t)$ = instantaneous chordal-average void fraction

C = chord length

The instantaneous chordal-average void fraction is defined by Equation (3.22). This expression can be solved for x(t) and substituted in Equation (3.21), yielding,

$$\alpha(t) = 1.0 + \frac{1.0}{\mu_\ell C}\left[\ell n\left(\frac{V_s^*(t)}{V_r^*(t)}\right) - \ell n\left(\frac{V_{os}}{V_r + V_{DC}}\right)\right] \tag{3.23}$$

Two bounds limit Equation (3.23), an empty pipe where $\langle\alpha\rangle = 1.0$ and a full pipe where $\langle\alpha\rangle = 0.0$. The expression for an empty pipe is given by,

$$1.0 = 1.0 + \frac{1.0}{\mu_\ell C}\left[\ell n\left(\frac{V_s^*}{V_r^*}\right)_G - \ell n\left(\frac{V_{os}}{V_r + V_{DC}}\right)\right] \tag{3.24}$$

while the expression for a pipe full of liquid is given by,

$$0.0 = 1.0 + \frac{1.0}{\mu_\ell C}\left[\ell n\left(\frac{V_s^*}{V_r^*}\right)_L - \ell n\left(\frac{V_{os}}{V_r + V_{DC}}\right)\right] \tag{3.25}$$

where,

L = subscript denoting all liquid

G = subscript denoting all vapor

The time dependence is removed since these equations can be considered to be time-averaged. Equations (3.24) and (3.25) can be solved for the last term on the right as shown in Equations (3.26) and (3.27),

$$\ell n\left(\frac{V_{os}}{V_r + V_{DC}}\right) = \ell n\left(\frac{V_s^*}{V_r^*}\right)_G \tag{3.26}$$

and,

$$\ell n\left(\frac{V_{os}}{V_r + V_{DC}}\right) = \ell n\left(\frac{V_s^*}{V_r^*}\right)_L + \mu_\ell C \tag{3.27}$$

These expressions can be combined with Equation (3.23) to yield two expressions for $\alpha(t)$,

$$\alpha(t) = 1.0 + \frac{1.0}{\mu_\ell C}\left[\ell n\left(\frac{V_s^*(t)}{V_r^*(t)}\right) - \ell n\left(\frac{V_s^*}{V_r^*}\right)_G\right] \tag{3.28}$$

and,

$$\alpha(t) = 1.0 + \frac{1.0}{\mu_\ell C}\left[\ell n\left(\frac{V_s^*(t)}{V_r^*(t)}\right) - \ell n\left(\frac{V_s^*}{V_r^*}\right)_L - \mu_\ell C\right] \tag{3.29}$$

It is convenient to redefine several of these ratios,

$$P_L \triangleq \ell n\left(\frac{V_s^*}{V_r^*}\right)_L \tag{3.30}$$

$$R_G \triangleq \ln\left(\frac{V_s^*}{V_r^*}\right)_G \tag{3.31}$$

$$R(t) \triangleq \ln\left(\frac{V_s^*(t)}{V_r^*(t)}\right) \tag{3.32}$$

Using these definitions, and subtracting Equation (3.26) from (3.29) yields,

$$\mu_\ell C = R_G - R_L \tag{3.33}$$

Equations (3.28) and (3.29) are equivalent, thus substitution of Equations (3.30), (3.31), (3.32), and (3.33) into either void fraction expression yields,

$$\alpha(t) = 1.0 + \frac{R(t)-R_G}{R_G - R_L} = \frac{R(t)-R_L}{R_G - R_L} \tag{3.34}$$

This expression for the time varying void fraction obviously has the correct endpoints. For all liquid, $R(t) = R_L$, and thus $\alpha(t) = 0.0$; for all vapor, $R(t) = R_G$, and thus $\alpha(t) = 1.0$. Measurements made with a dual beam system can easily be converted into instantaneous chordal void fraction readings using the linear expression given in Equation (3.34).

The design parameters for an actual dual beam x-ray system can be calculated from the radiation attenuation law, Equation (3.10), and geometrical

considerations. Predesign specifications, such as the desired relative void fraction error and response time, enter the analysis. Two major parameters must be computed; source strength and geometric positioning of components.

The source intensity and the detector intensity, shown in Figure 3.7 are related as indicated in Equation (3.35),

$$\frac{I_d}{R_{ST}^2} = \frac{I_o}{R_{SD}^2} e^{-(2\mu_W T)} e^{-(\bar{\mu} C)} \tag{3.35}$$

where,

I_d = intensity incident on detector, photons/cm^2-sec

I_o = source intensity on the test section, photons/cm^2-sec

R_{ST} = source to test section distance, cm

R_{SD} = source to detector distance, cm

μ_W = attenuation coefficient of walls of test section, cm^{-1}

$\bar{\mu}$ = average attenuation coefficient for two-phase mixture, cm^{-1}

T = wall thickness of conduit, cm

C = chord length through two-phase mixture, cm

The attenuation coefficient of the two-phase media can be expressed as,

$$\bar{\mu} = \alpha\mu_g + (1-\alpha)\mu_\ell = \mu_\ell + \alpha\,(\mu_g - \mu_\ell) \tag{3.36}$$

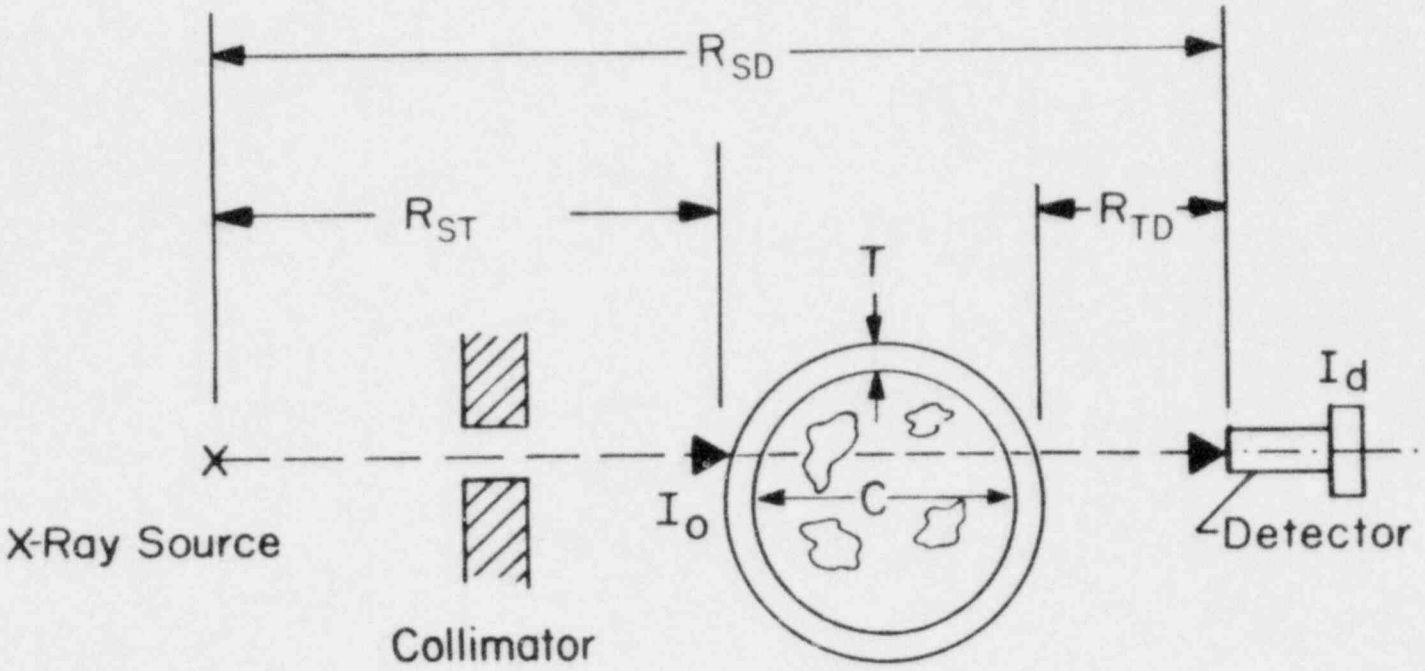

Figure 3.7
The geometric considerations
of an x-ray beam measuring
void fraction

Equations (3.35) and (3.36) can be combined, and rearranged, to yield the intensity ratio in terms of the chordal-average void fraction

$$\frac{I_d}{I_o} = \left(\frac{R_{ST}}{R_{SD}}\right)^2 e^{-(2\mu_W T + C\left[\mu_\ell + \alpha(\mu_g - \mu_\ell)\right])} \tag{3.37}$$

The photons emitted by an x-ray tube are statistical in nature and occur with the associated statistical fluctuations. "Propagation of errors" [35] can be applied to Equation (3.34), the expression for the instantaneous void fraction for a dual beam system, resulting in an expression for the absolute void fraction error,

$$(\Delta\alpha)^2 = \left(\frac{\partial\alpha}{\partial R_L}\right)^2 (\Delta R_L)^2 + \left(\frac{\partial\alpha}{\partial R_G}\right)^2 (\Delta R_G)^2 + \left(\frac{\partial\alpha}{\partial R}\right)^2 (\Delta R)^2 \tag{3.38}$$

The partial derivatives for this expression are from Equation (3.34),

$$\frac{\partial\alpha}{\partial R_L} = \frac{1-\alpha}{R_G - R_L} \tag{3.39}$$

$$\frac{\partial\alpha}{\partial R_G} = \frac{-\alpha}{R_G - R_L} \tag{3.40}$$

$$\frac{\partial\alpha}{\partial R} = \frac{1}{R_G - R_L} \tag{3.41}$$

Three unknowns still exist in Equation (3.38): ΔR_L, ΔR_G, and ΔR. These parameters can be calculated if we assume that the x-ray detection counts follow Poission statistics. The expression for R_L, indicated in Equation (3.30), can be rewritten as,

$$R_L = \ell n\ (V_s^*)_L - \ell n\ (V_r^*)_L \tag{3.42}$$

This expression can be formed into an error expression in a straignt forward fashion. Assuming that the variation of each signal with respect to the mean value of the signal, is the same, "propagation of errors" yields,

$$(\Delta R_L)^2 = \left(\frac{\partial R_L}{\partial V_s^*}\right)^2 (\Delta V_s^*)^2 + \left(\frac{\partial R_L}{\partial V_r^*}\right)^2 (\Delta V_r^*)^2$$

or,

$$(\Delta R_L)^2 = \left(\frac{\Delta V_s^*}{V_s^*}\right)^2 + \left(\frac{\Delta V_r^*}{V_r^*}\right)^2 \tag{3.43}$$

If we can employ a well known Poission statistical relationship,

$$\frac{\Delta V_s^*}{V_s} \approx \frac{\Delta V_r^*}{V_r} \approx \frac{\Delta N}{N} = \frac{1}{\sqrt{N}} \tag{3.44}$$

where,

N = number of counts registered on the photon detectors

The expression, shown in Equation (3.44) can be substituted into Equation (3.43) to yield,

$$(\Delta R_L)^2 = \left(\frac{1}{\sqrt{N}}\right)^2 + \left(\frac{1}{\sqrt{N}}\right)^2 = \frac{2}{N} \tag{3.45}$$

Similar expressions can be calculated for ΔR_G and ΔR because Equations (3.31) and (3.32) have the same form as Equation (3.30). Thus assuming that the statistical error is independent of the fluid in the test section,

$$(\Delta R_L)^2 = (\Delta R_G)^2 = (\Delta R)^2 = \frac{2}{N} \tag{3.46}$$

Thus, combination of Equations (3.38) through (3.46) results in,

$$(\Delta\alpha)^2 = \frac{4}{(R_G - R_L)^2 N} \left[1 - \alpha + \alpha^2\right] \tag{3.47}$$

The relative error can be calculated by taking the square root of both sides of Equation (3.47), and dividing by the chordal-average void fraction. The resulting expression is,

$$\frac{\Delta\alpha}{\alpha} = \frac{2}{\alpha(R_G - R_L)\sqrt{N}} \sqrt{1-\alpha+\alpha^2} \tag{3.48}$$

An equation relating the relative void fraction error, as a

function of chordal average void fraction, the given chordal position, material parameters and the accumulated counts, is formed by combining Equations (3.48) and (3.33),

$$\frac{\Delta\alpha}{\alpha} = \frac{1}{\sqrt{N}} \left[\frac{2}{\mu_\ell C}\right] \frac{\sqrt{1-\alpha+\alpha^2}}{\alpha} \tag{3.49}$$

Noting that the counts (N) can be related to the intensity by,

$$N = \theta I_d A_d \varepsilon \tag{3.50}$$

where,

θ = counting time, sec

ε = detector efficiency

A_d = detector area, cm^2

I_d = photon intensity on detector, photons/cm^2 sec

A combination of Equations (3.49), (3.50) and (3.37) yields,

$$I_o = \frac{4\left(\frac{R_{SD}}{R_{ST}}\right)^2 (1-\alpha+\alpha^2)\, e^{(2\mu_w T + \mu_\ell C + \alpha(\mu_g-\mu_\ell)C)}}{A_d \theta \varepsilon \left(\frac{\Delta\alpha}{\alpha}\right)^2 \mu_\ell C^2 \alpha^2} \tag{3.51}$$

The inverse square law terms, R_{SD} and R_{ST}, are calculated from geometric considerations. Ideally, the collimators, test section and detectors should be close to the x-ray source to minimize inverse square law attenuation. Physical constraints, i.e., the size of the radiation

detector and their associated magnetic and radiation shielding, and the size of the collimators, help determine the minimum distance.

The maximum angle of uniform photon illumination is specified by the x-ray tube manufacturer. Both reference and test beams should receive the same intensity so the two detectors must be separated by an angle less than the maximum. Thus the physical constraints associated with the size of radiation detector or collimator and the angle of uniform x-ray emission basically fix the minimum source-to-detector distance. It is important to note that both reference and test detectors should be the same distance from the source, thus each detector will see the same inverse square law attenuation.

Collimator design and position is calculated from intensity, detector size and distance considerations. Consider the isotropic point source shown in Figure 3.8. The collimator dimensions can be related to the area of the detector by the law of similar triangles,

$$C_X = \frac{R_{SC}}{R_{SD}} D_X \tag{3.52}$$

$$C_Y = \frac{R_{SC}}{R_{SD}} D_Y \tag{3.53}$$

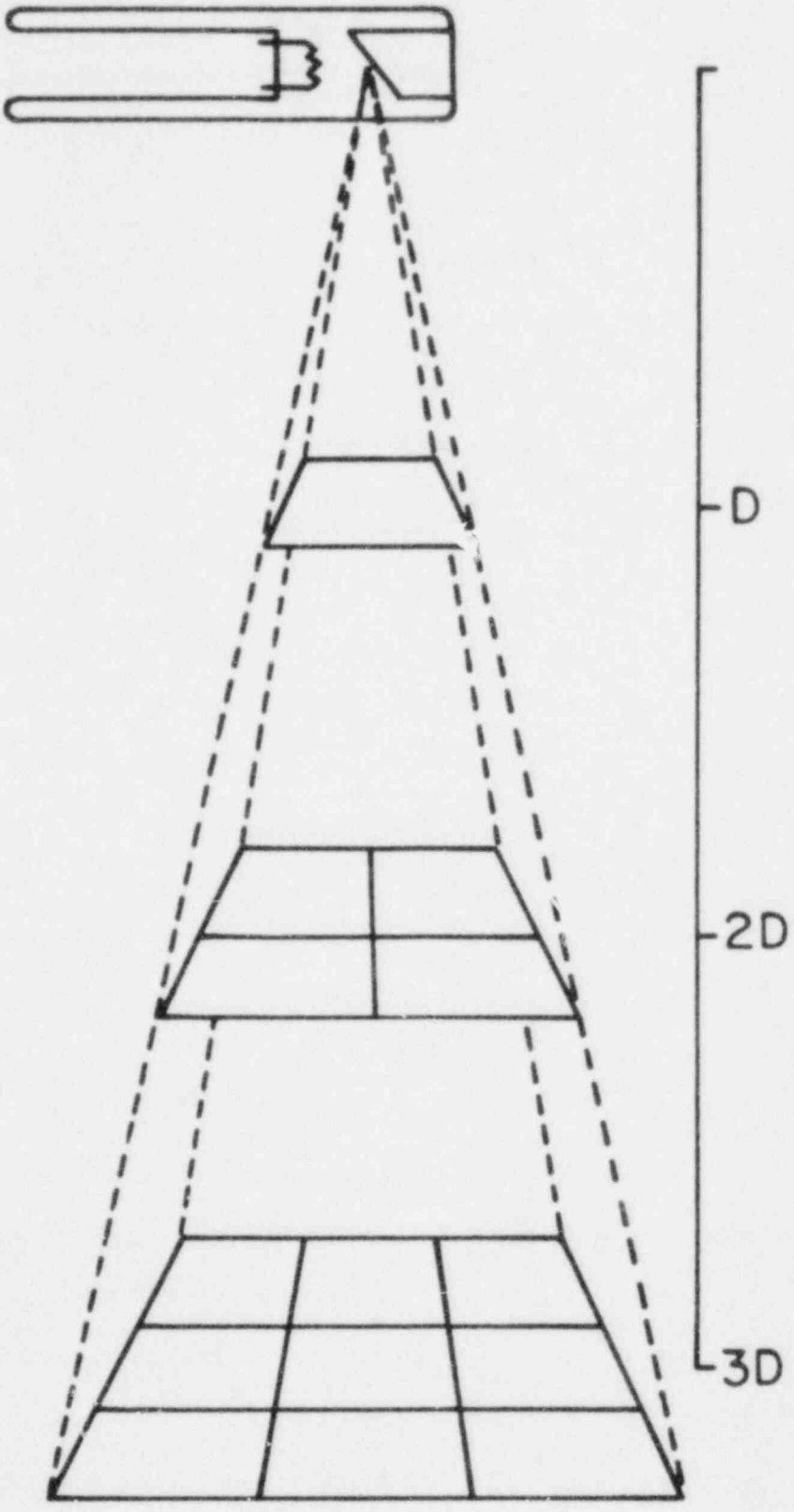

Figure 3.3
A schematic of the inverse square law for radiation attenuation

where,

C_x = x-dimension of collimator, cm

C_y = y-dimension of collimator, cm

D_x = x-dimension of area of detector, cm

D_y = y-dimension of area of detector, cm

R_{SC} = source to collimator distance, cm

R_{SD} = source to detector distance, cm

Inverse square law attenuation considerations indicate that R_{SC} should be equal to R_{SD} for maximum photon intensity. However, physical constraints, such as the test section size, collimator supports and detector shielding, require that R_{SC} is less than R_{SD}. Equation (3.51) shows that the intensity is inversely proportional to the detector area (A_d). Thus, a small detector area will increase substantially the source intensity required.

It is desirable to make the collimator area as small as possible to minimize photon streaming errors [36]. On the other hand, intensity considerations favor a large collimator, however, the size of the collimator, combined with the position, must not result in an incident beam larger than the sensitive area of the detectors. The exact size of the collimator depends on the size of the desired region to be measured. Normally the design of a collimation

system is iterative, in which the first guess is based on the considerations just discussed.

The photon output spectrum of an x-ray tube depend on the operating voltage and current. Thus the intensity calculated with Equation (3.51) must be related to a set of operating conditions Collimated x-ray photons can be considered uniaxial if scattering is neglected. The total energy-integrated intensity which strikes the radiation detector is,

$$I_o = \int_{E_{min}}^{E_{max}} I(E)\,dE \tag{3.54}$$

where,

E = photon energy, ev

$I(E)$ = photon intensity as a function of energy

E_{max} = maximum energy in spectrum, ev

E_{min} = minimum energy in spectrum, ev

The maximum energy associated with an x-ray spectrum is fixed by the tube's high voltage. The minimum energy, theoretically, can be very close to zero. In practice, filtering of the spectrum, due to the increasing attenuation coefficient at lower energy, causes the existence of a non-zero minimum. Krammer [37] suggests,[2]

$$I(E) \propto \frac{iZ}{(hc)^3} E^2(E_{max} - E) \tag{3.55}$$

---

[2] Recall $E=hc/\lambda$ where 'h' is Planck's constant, 'λ' is the wavelength and 'c' is the speed of light.

where,

$I(E)$ = intensity at a given energy, kev

Z = atomic number of target

i = x-ray tube filament current, amps

E_{max} = maximum energy of photons

To calculate the spectrum's relative intensity, Equation (3.54) can be divided into small energy subintervals and combined with the relative intensities calculated by Equation (3.55) to yield an expression for photon intensity as a function of energy, I(E).

$$\int_{E_{min}}^{E_{max}} I(E)dE = \int_{E_{min}}^{E_1} I(\bar{E})dE + \int_{E_1}^{E_2} I(\bar{E})dE + \ldots$$

$$+ \int_{E_n}^{E_{max}} I(\bar{E})dE = I_o \qquad (3.56)$$

where,

$\bar{E}$ = average photon energy within each energy interval

The operational curves for each x-ray tube can be used to provide the relationship between tube current and voltage. A typical curve is illustrated in Figure 3.9. Trial and error substitution of points on the FA-60 tube's operating curve into Equation (3.56) will result in the selection of appropriate operating conditions.

These design considerations were incorporated into

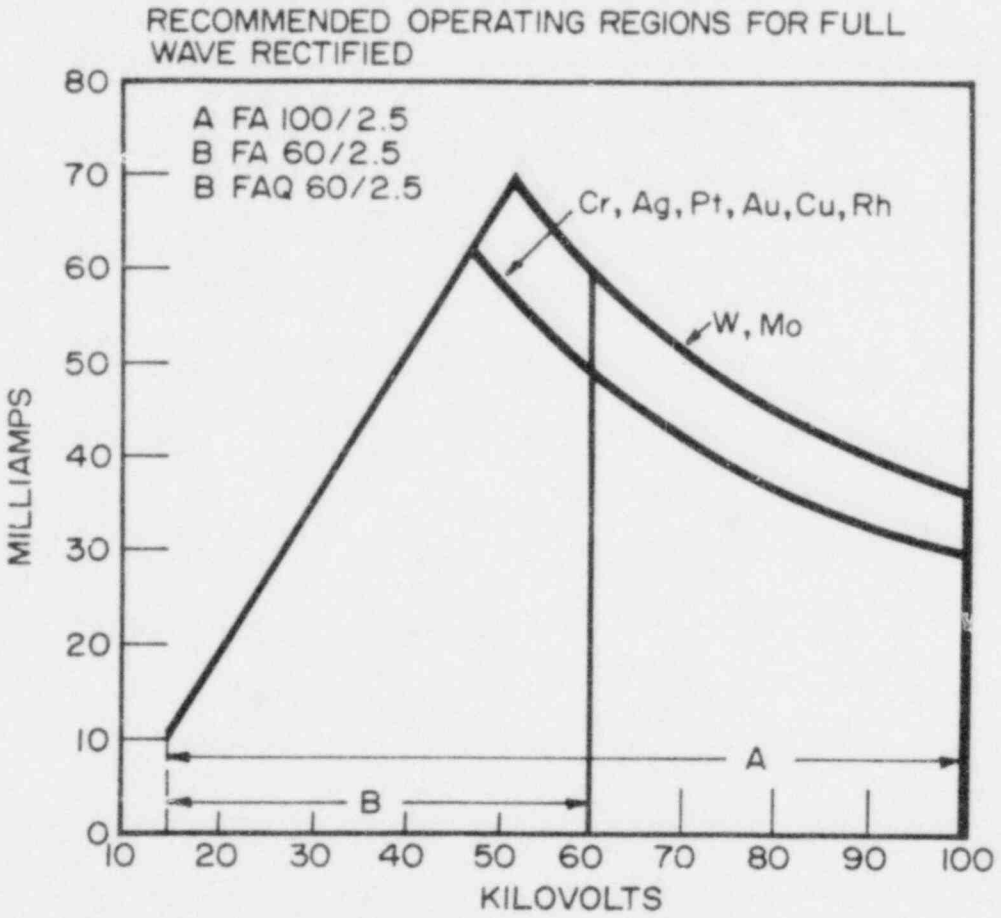

Figure 3.9
A typical operational curve
for a Philips FA series
x-ray tube

the RPI dual beam x-ray system. The system employed in this experiment is shown schematically in Figure 3.10. It features full-wave rectification and high voltage filtering to insure a stable high voltage source. The x-ray tube filament is excited by a battery current source. This provides additional stability to the photon spectrum. Figure 3.11 shows the batteries and the resistors and capacitors which comprise the high voltage filter.

A Philips FA-60 x-ray tube, rated for two and a half kilowatts, provides the x-ray source. Water cooling was necessary for stability because of the high power of the tube. Radiation detection was accomplished using thick plastic scintillators coupled to RCA 8575 photomultipliers. These detectors were operated in the dynode current mode and were covered with a lead shielding shroud to stop scattered radiation. Mu metal also covers the detector to insure magnetic shielding. Background light was removed by a thin aluminum sheet taped over the apperature to the plastic scintillator. Two identical systems were assembled for the test and reference x-ray beams. Both systems were driven by the same, stable, high voltage supply.

Rectangular, lead collimators were used. These collimators were one quarter inch thick and have rectangular openings of fifty mils wide by one hundred mils high. The rectangular design was chosen because more photons can be passed to the detector without sacrificing, lateral resolution. These collimators were mounted in vertically

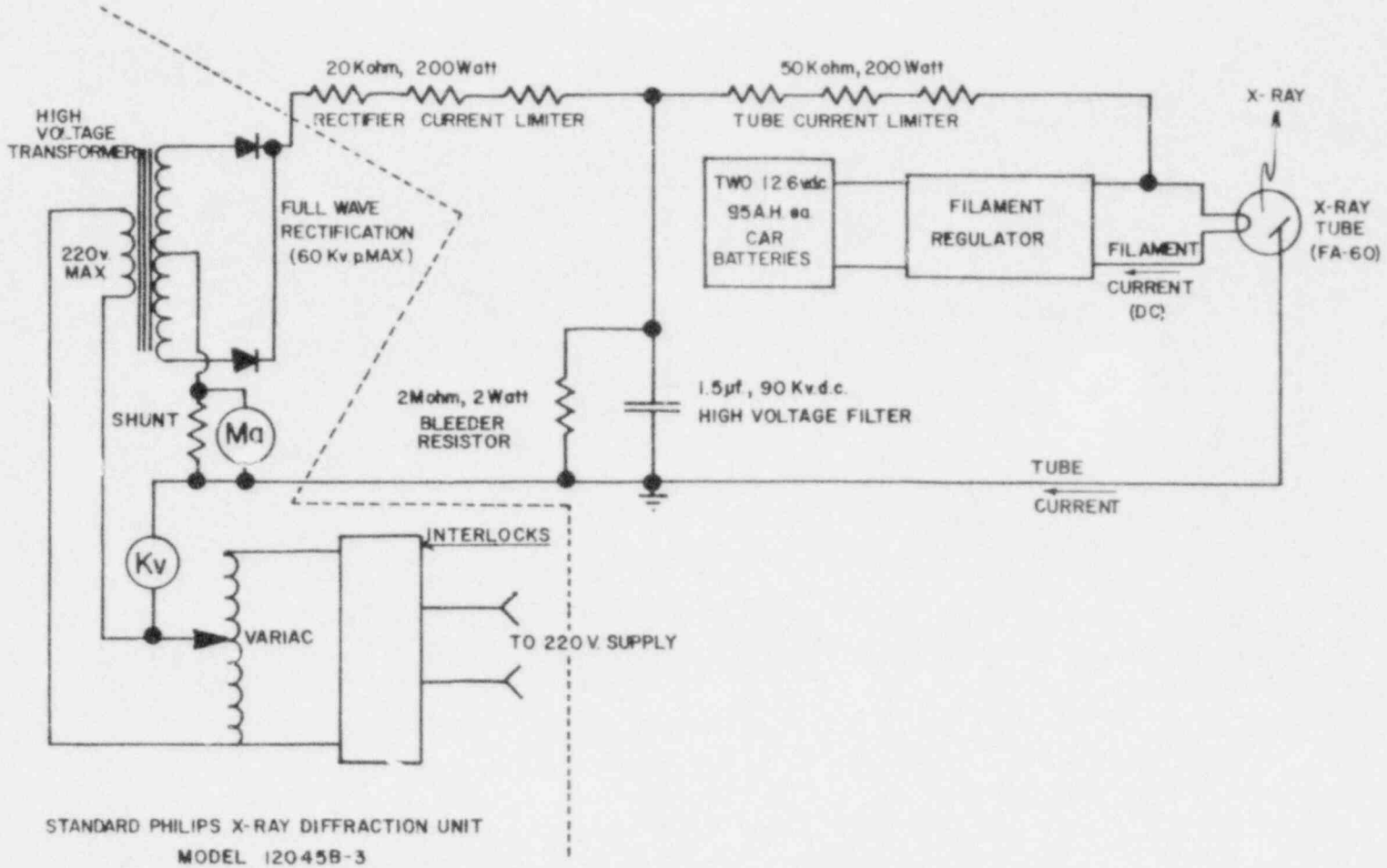

Figure 3.10
A schematic of the Philips x-ray diffraction unit as modified for chordal void fraction measurements

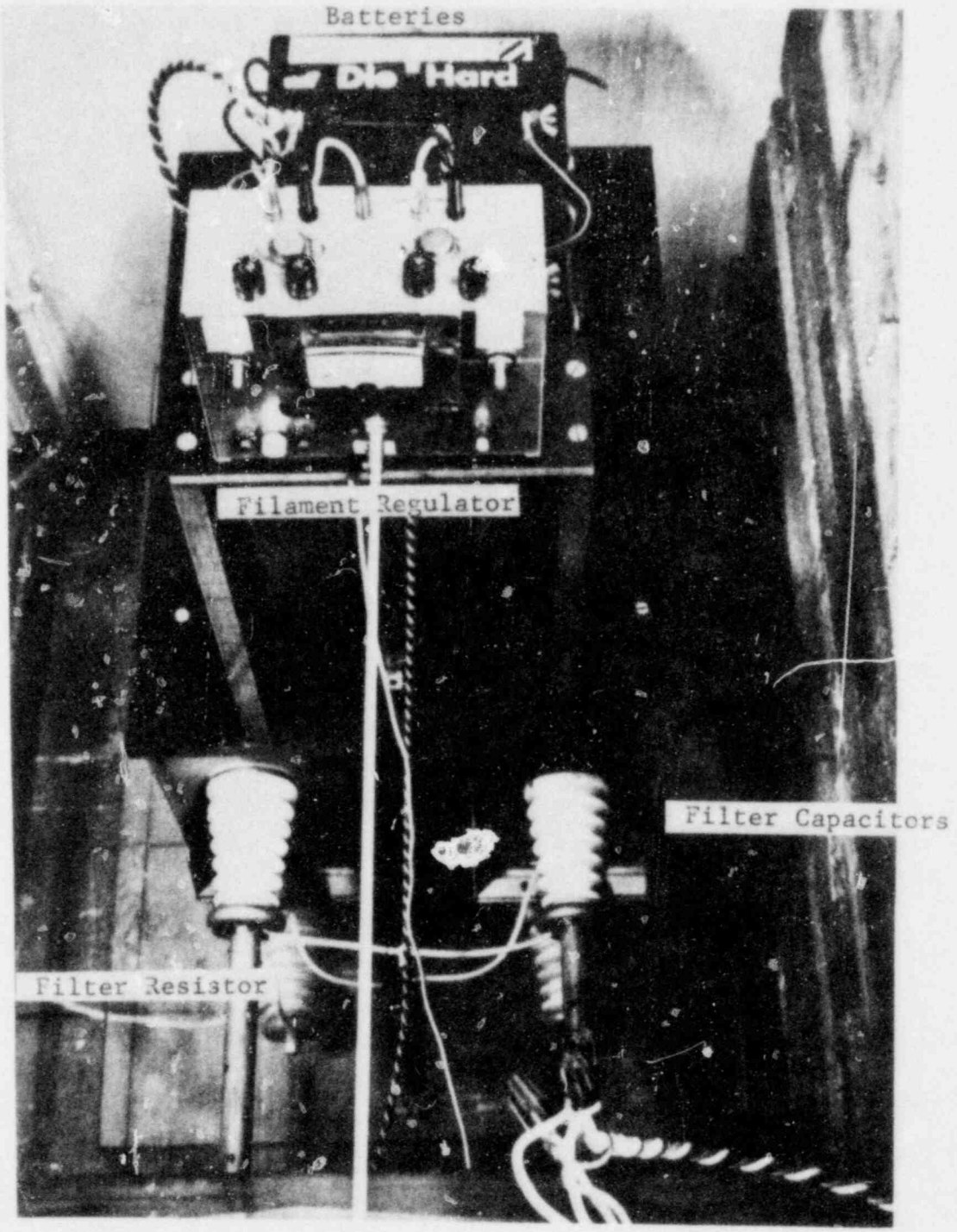

Figure 3.11
The high voltage filter and
DC filament current supply
for the x-ray system

and horizontally adjustable stainless steel cradles. The collimators are bolted firmly in place after positioning. A closeup of the detectors and collimators is shown in Figure 3.12.

The x-ray tube, radiation detectors and collimators are mounted on a machinist's table. This table permits accurate lateral movement of the x-ray system about the test section. A system of gears and shafts permit remote positioning of the table. A dial gauge micrometer is used to measure the exact table position. The actual set-up is shown in Figure 3.13.

A reference attenuator is also affixed to the machinist table. This device is a plastic cone on a micrometer drive. The plastic is remotely driven into the reference x-ray beam to compensate for the attenuation of the walls of the test section along the diameter. This attenuator is also shown in Figure 3.12.

The reference attenuator is not readjusted when off-diameter chordal void fraction measurements are made. Prior to running the actual two-phase flow conditions, measurements of the diameter and off-diameter chords with only single phase air and single phase water present were made. The all water and all air measurements are substituted directly into Equation (3.37) for R_L and R_G, respectively, to calculate the chordal void fraction along each chordal position.

Two major hazards associated with these types of

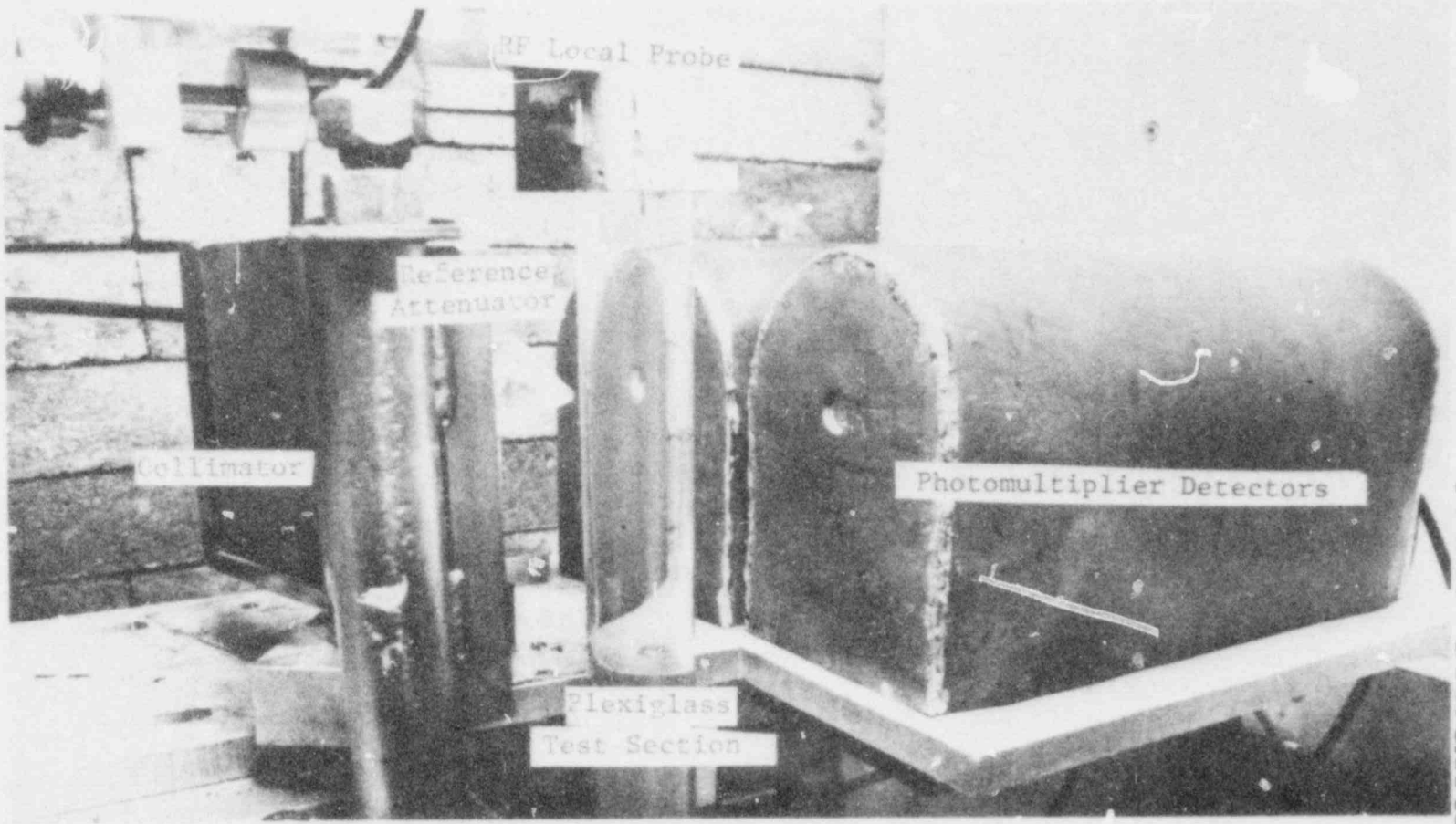

Figure 3.12
A close-up of the plexiglass test section, collimators and photomultiplier detectors

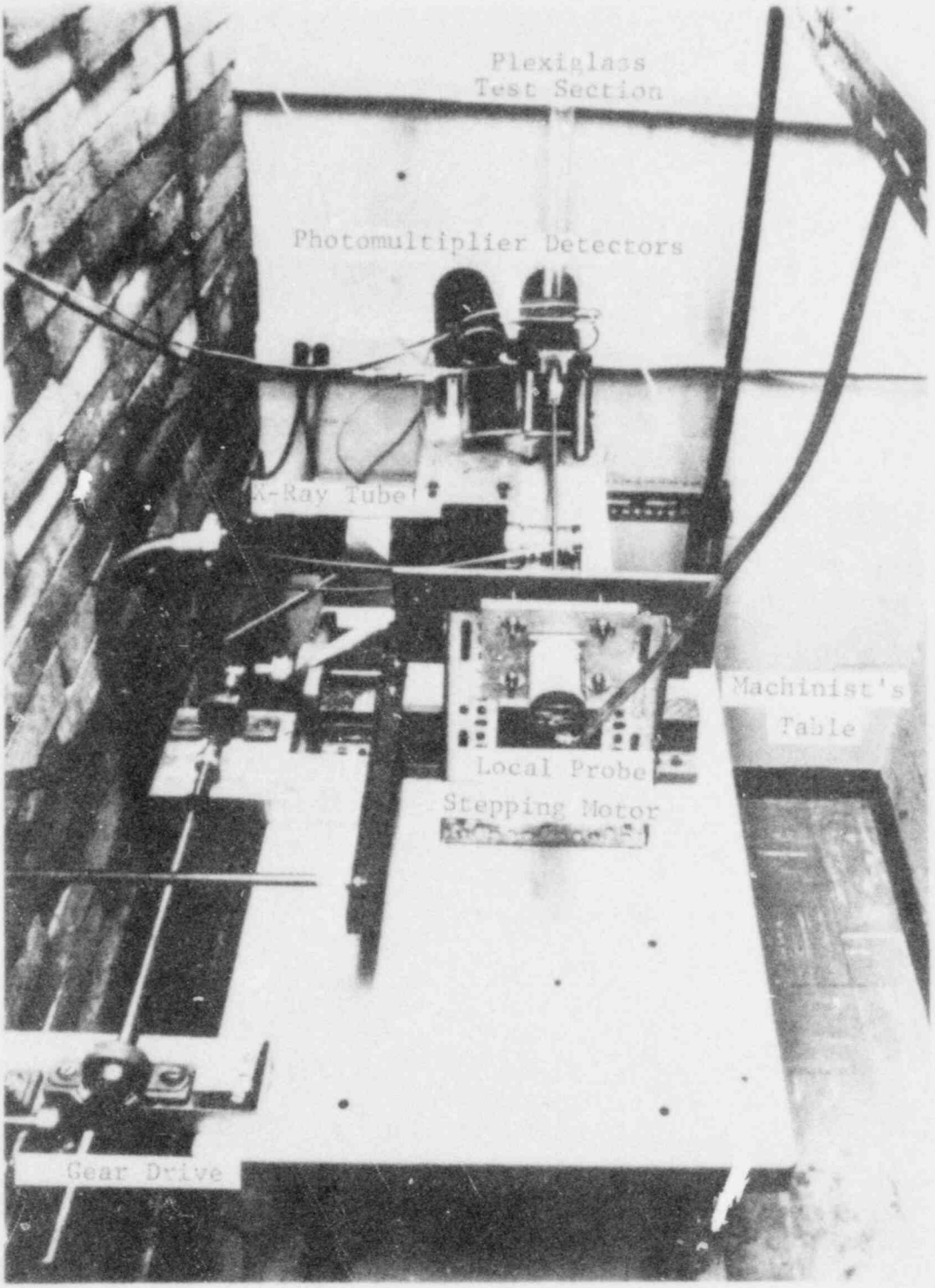

Figure 3.13
An overall view of the dual beam x-ray system

measurement are; high voltage and high radiation. Personnel must not have access to the dangerous areas during operation. High voltage protection was achieved by fencing off the appropriate area. The fence is tied to ground. Access to the high voltage region is possible only if the capacitors are grounded by a grounding rod. This rod has an alarmed holder, i.e., removal of the rod from the device trips the x-ray system. The primary x-ray beam is direct at a six foot thick concrete wall. Protection from scattered radiation is achieved by an sixteen inch thick high density concrete brick wall. Access to the measurement area is permitted via a lead covered door. This is interlocked to the x-ray system; opening the door automatically trips the x-ray unit. Radiation surveys were conducted with the x-ray unit in operation to insure that adequate shielding had been installed. Figure 3.14 shows the main x-ray system control panel, the high voltage fencing, radiation indicators and the door interlock.

Analog signal processing for this system, which follows the analysis discussed previously, is shown schematically in Figure 3.15. The current output from the test and reference photomultipliers were fed, via shielded cables, to logarithmic amplifiers and differenced electronically. Figure 3.16 shows a schematic of the electronics employed. As discussed previously a DC bias voltage was applied to the reference signal to reduce noise. The photomultipliers produce a current output, which was

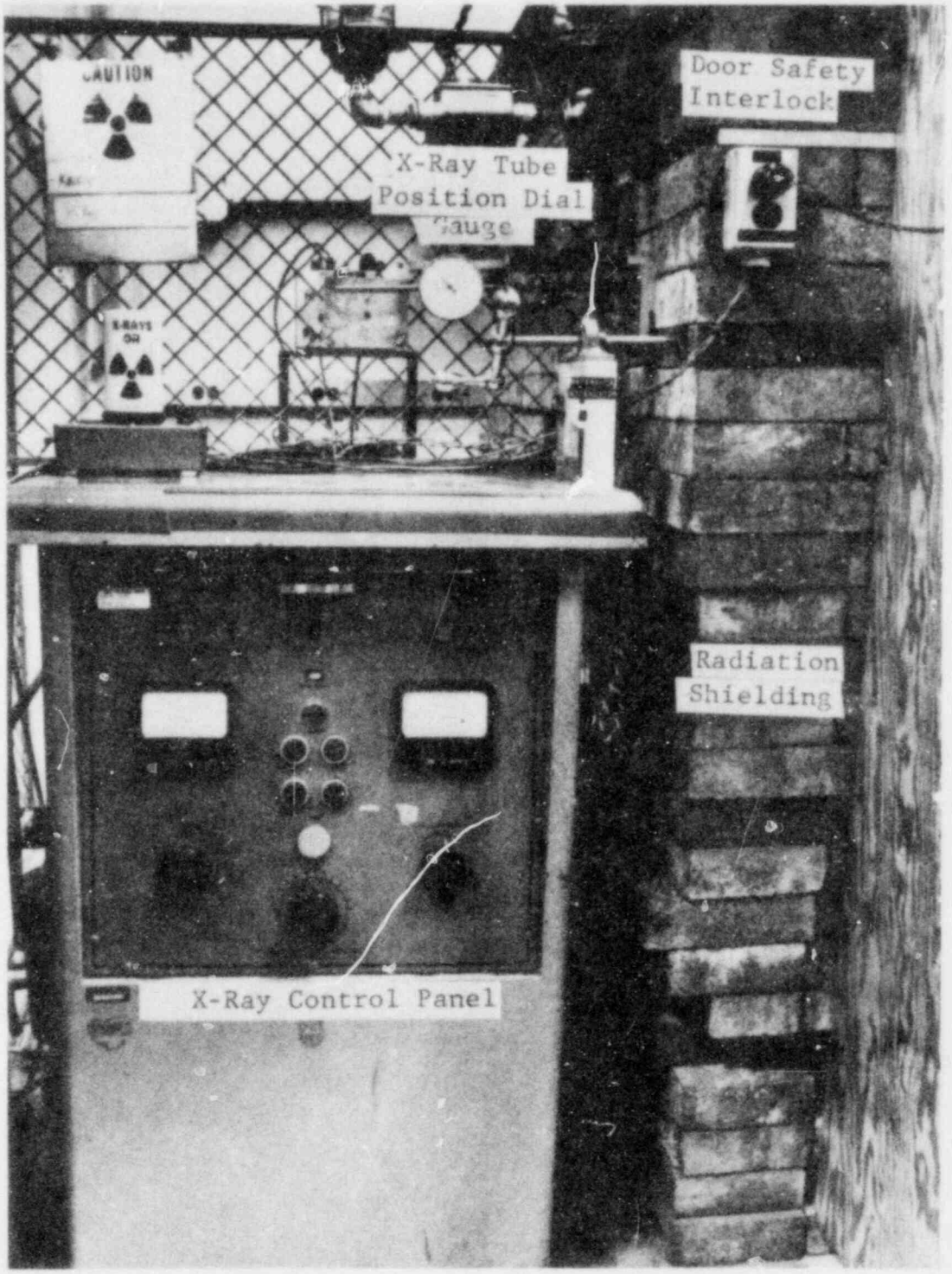

Figure 3.14
The main x-ray system control panel

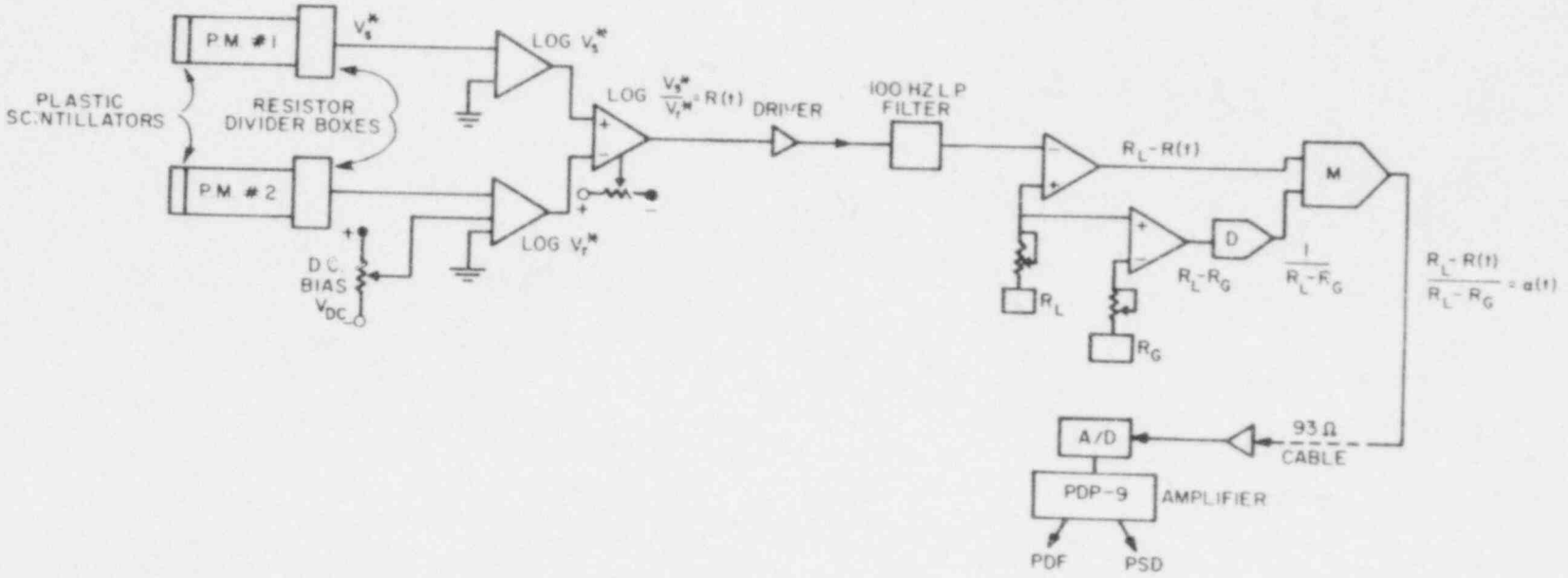

Figure 3.15
A schematic of the analog signal processing associated with the dual beam x-ray system

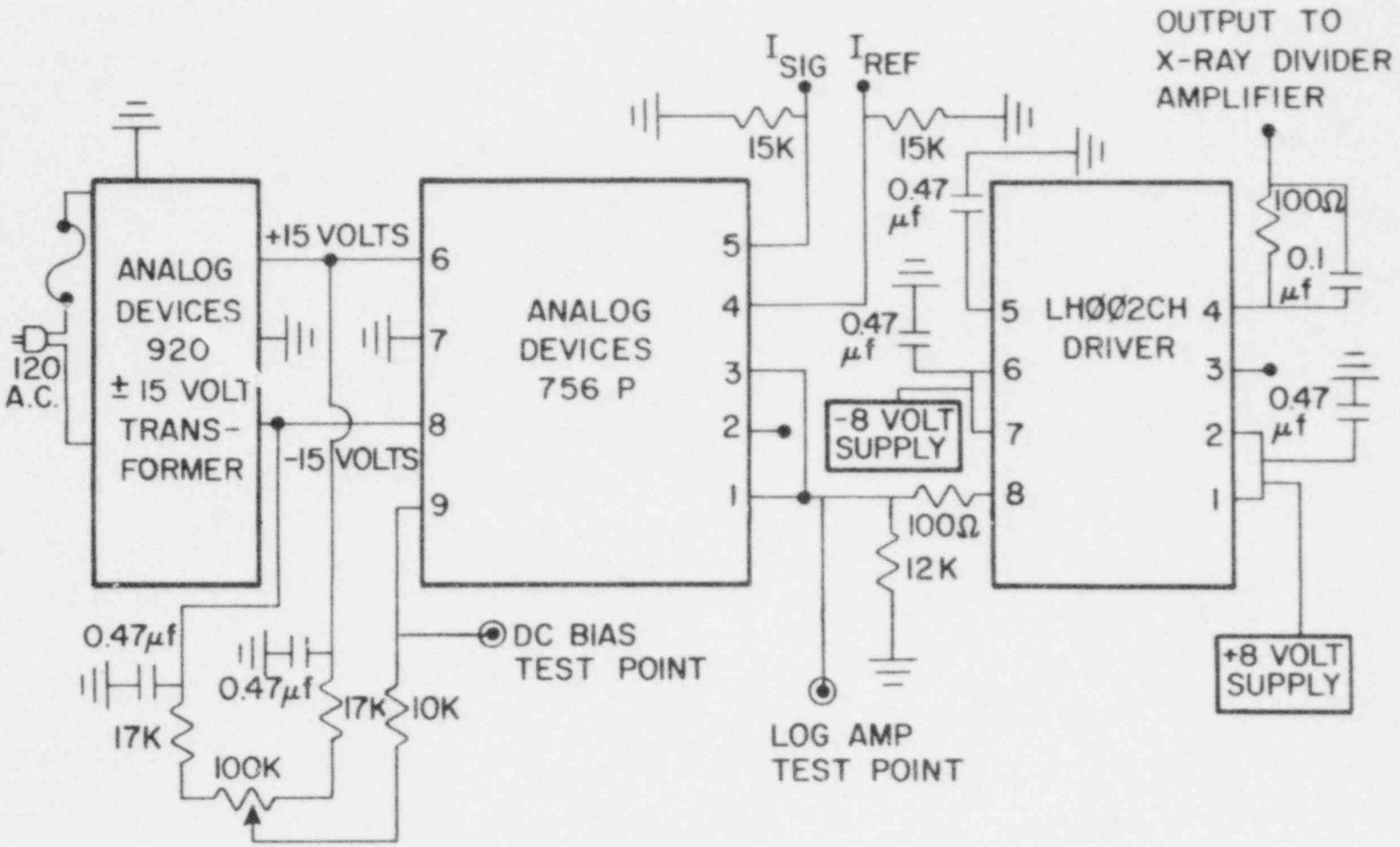

Figure 3.16
A schematic of the logarithmic difference amplifier for the dual beam x-ray system

converted to a voltage just prior to entering the logarithmic amplifier. The DC bias was applied to the trim pin of the AD 756-P integrated circuit. A driver was provided to isolate the internal circuitry. The logarithmic difference electronics were well shielded and located very close to the photomultipliers to reduce noise. A shielded cable transfers this analog signal out of the high radiation region.

Further amplification was performed before sending the void signal from the experiment to the data acquistion computer. The signal was initially passed through a four pole active filter, having a break frequency at 100 hz. The amplifier schematic is shown in Figure 3.17. This device takes a 0 to -1.3 volt signal and amplifies it to -7.70 to 0.2 volts, respectively. The amplified analog signal was now passed via shielded cable to the Gaerttner Laboratory computer room.

Further signal amplification and digitization occurs prior to entry into the PDP-9 computer shown in Figure 3.18. An operational amplifier inverts the signal. The signal is now passed to a Tennelec TC301 Linear Gate. This gate is normally closed. An external pulser is used to open this gate [illegible] that the analog x-ray signal can be sampled. The [illegible] output from the linear gate now enters a Northern NS-623 analog-to-digital (A/D) converter as shown in Figure 3.19. This digital output is passed into the PDP-9 system via a CAMAC Module.

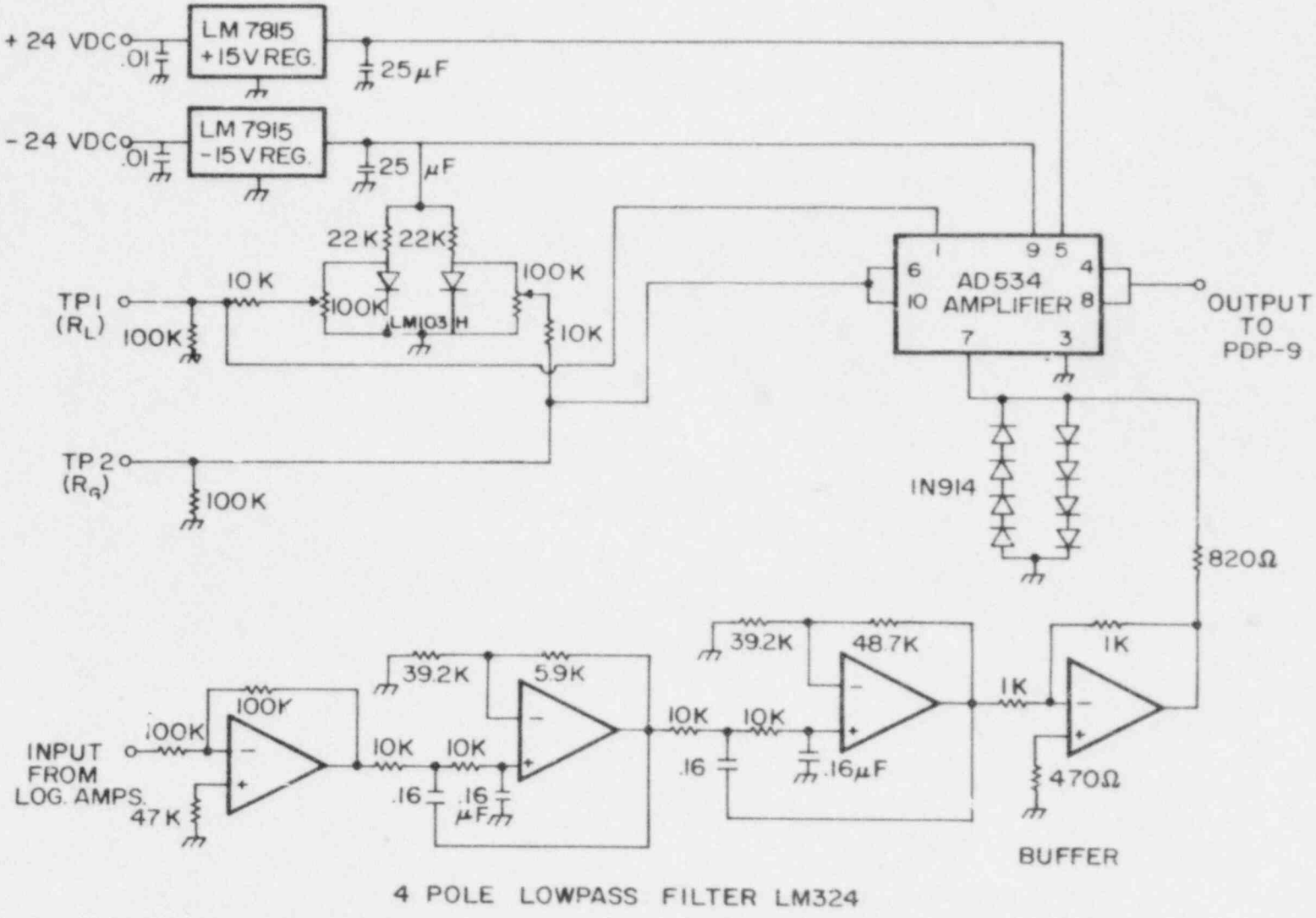

Figure 3.17
The four pole low pass
filter and signal amplifier

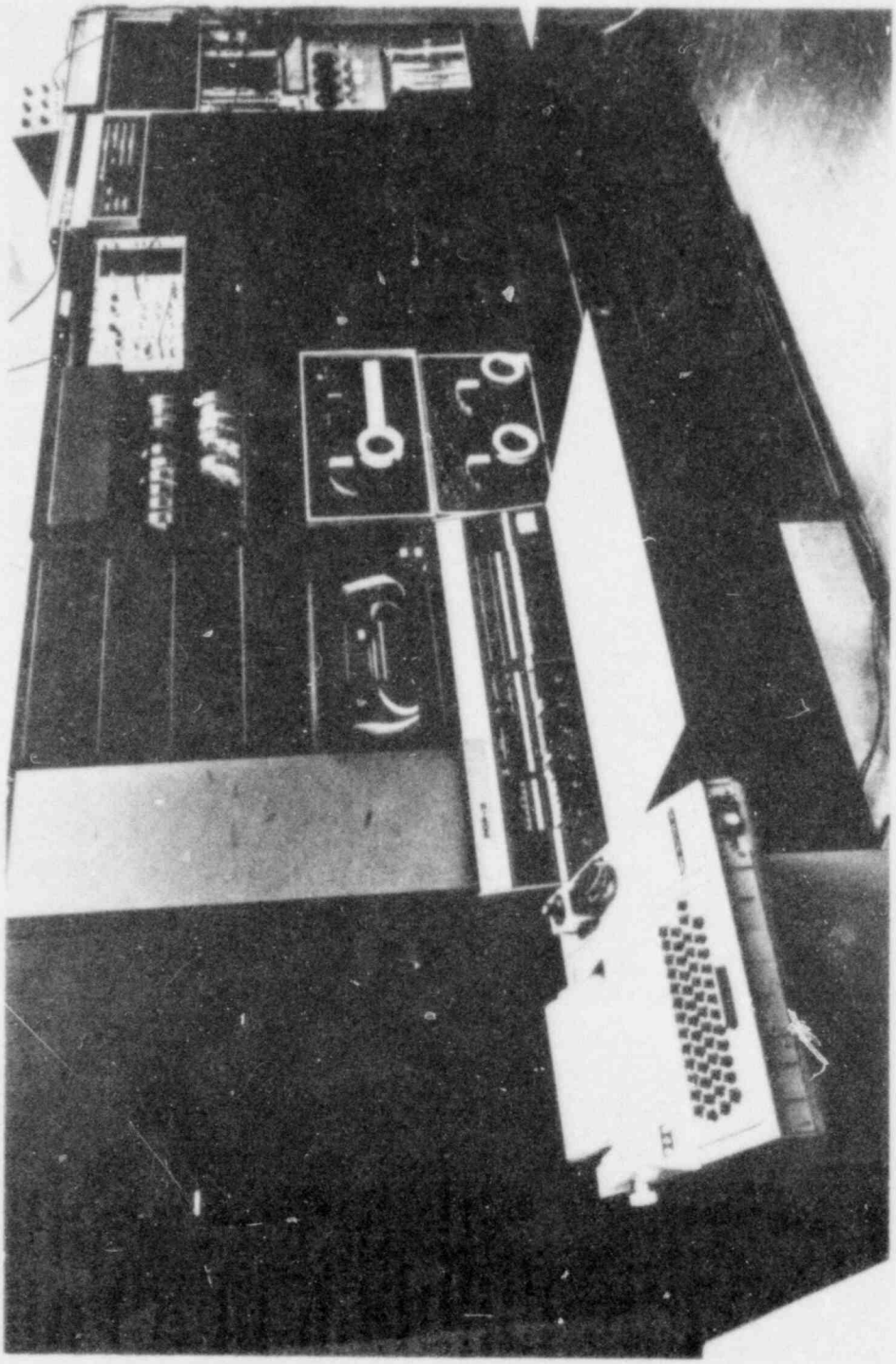

Figure 3.15
The PDP-9 Computer

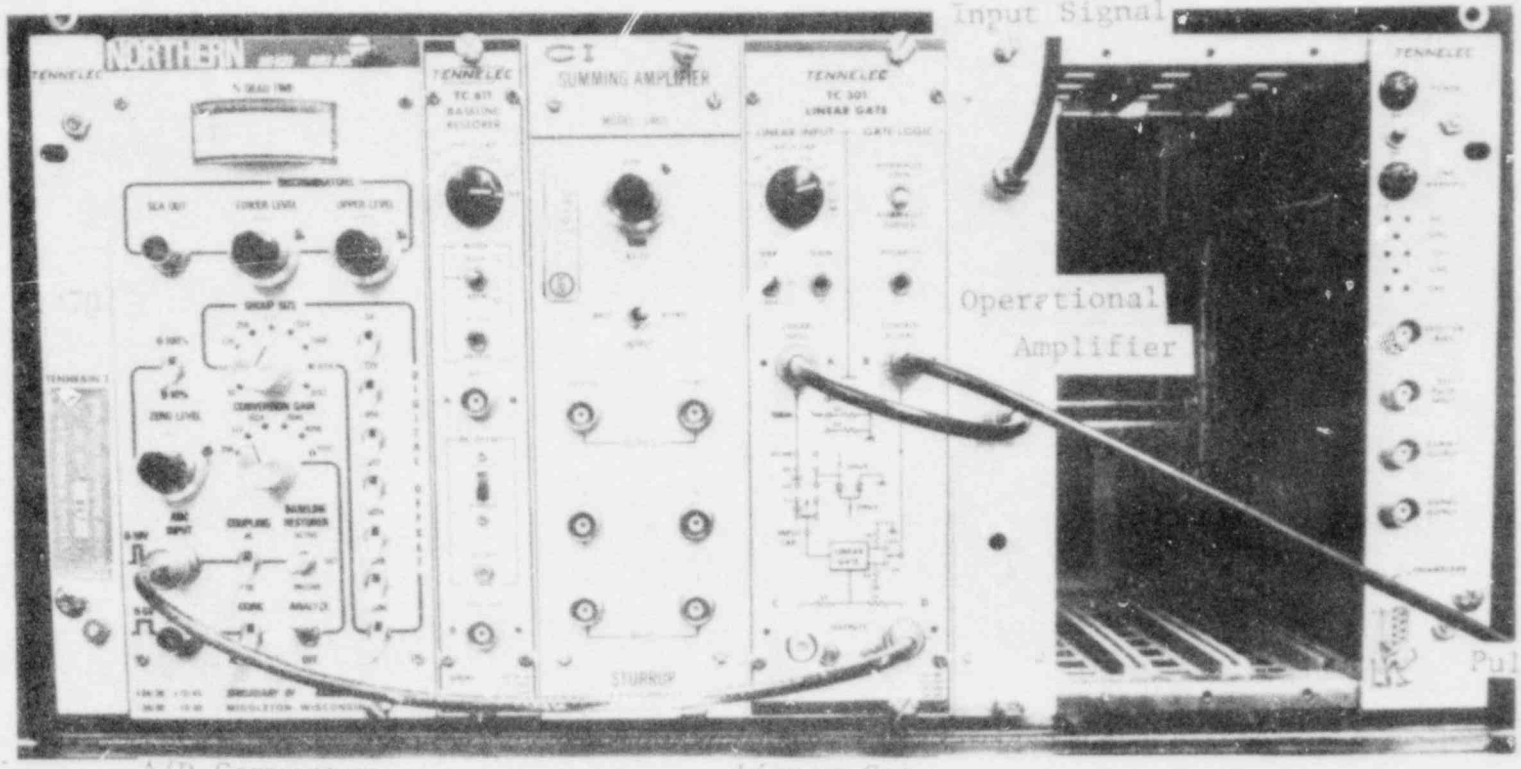

Figure 3.19
The operational amplifier, linear gate and Northern NS-623 analog-to-digital converter for the dual beam x-ray system

Special precaution must be taken to permit only a pre-specified number of pulses to pass from the external pulser to the linear gate. Should an extraneous external pulse be present after the computer has completed its sampling, the gate will open and pass another x-ray signal pulse. This unexpected data will disable the A/D converter.

Substantial software is used to acquire and process the x-ray data. Three basic steps are required:

1) Collect and store the data on the PDP-9 disk.
2) Convert data to Fortran-IV format and write it on DEC tape.
3) Analyze, print and permanently store data on a RK05 Disk.

Three programs were written to perform these functions. The data acquistion and conversion programs can be found in Appendix A.1. The data processing program is described and listed in Appendix A.2. Flow charts, which are shown in Figures 3.20, 3.21, and 3.22, describe the three basic operations.

Linearity between the void fraction reading at the PDP-9 and the actual water path length along a chord must be proven. A simple device, shown in Figure 3.23, was designed to show this relationship. This equipment consists of a plastic block with a series of steps machined into it. A frame was designed to allow the machined block to slide horizontially. This frame attached to the test beam's collimator to insure that the plastic block passed

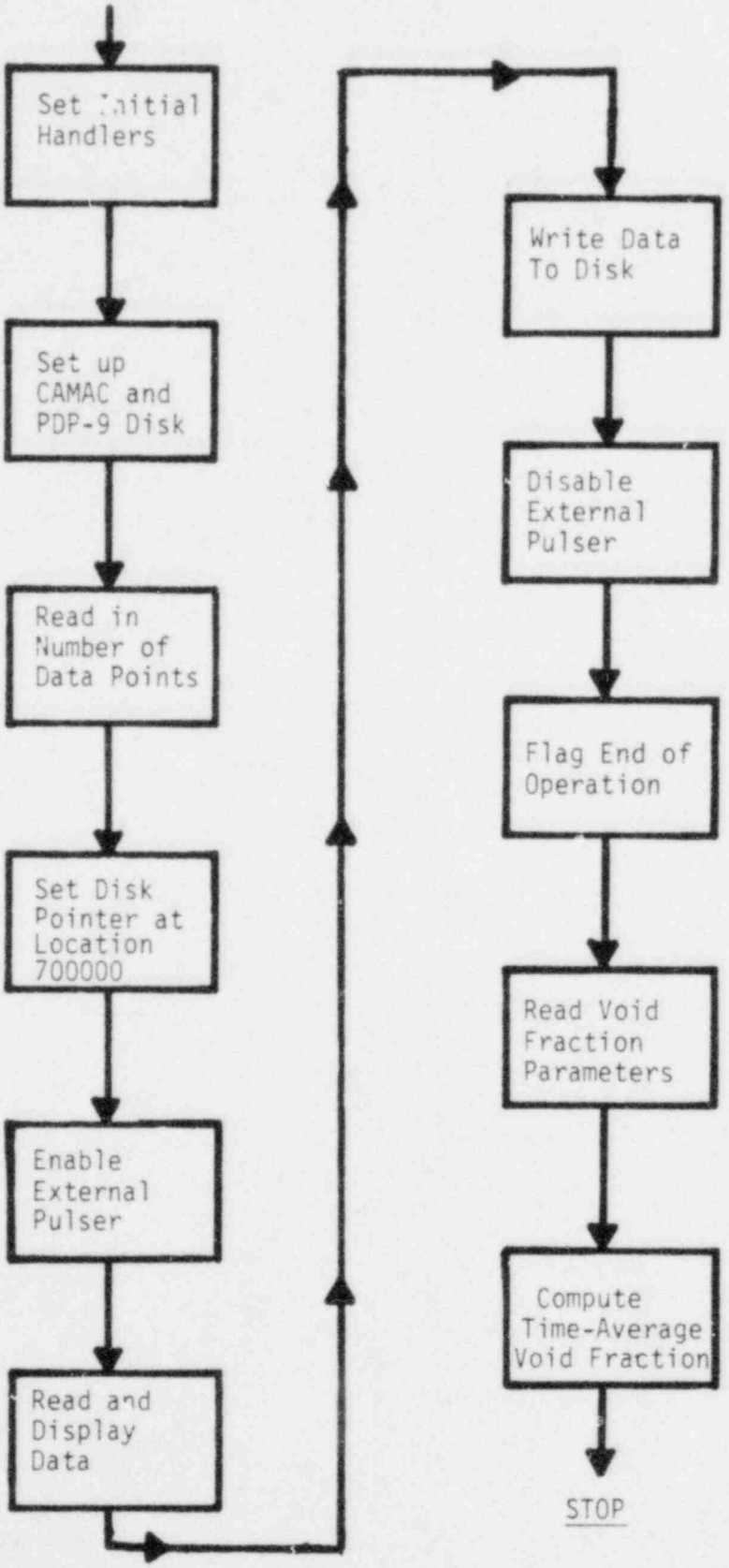

Figure 3.20 A flowchart of the data acquistion software for the x-ray void fraction measuring system

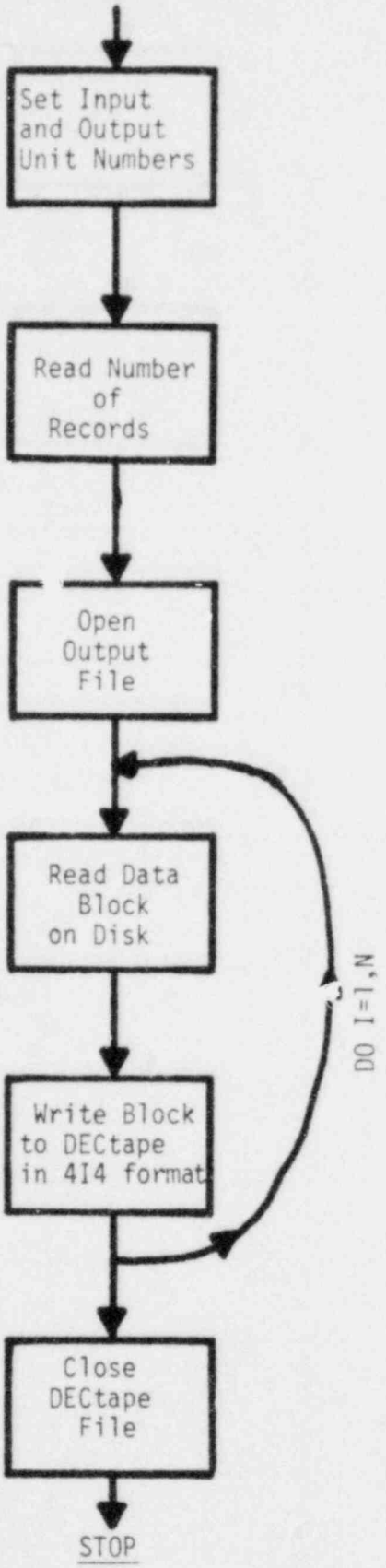

Figure 3.21 A flowchart of the conversion code to convert x-ray data from binary code to Fortran 4I4 format

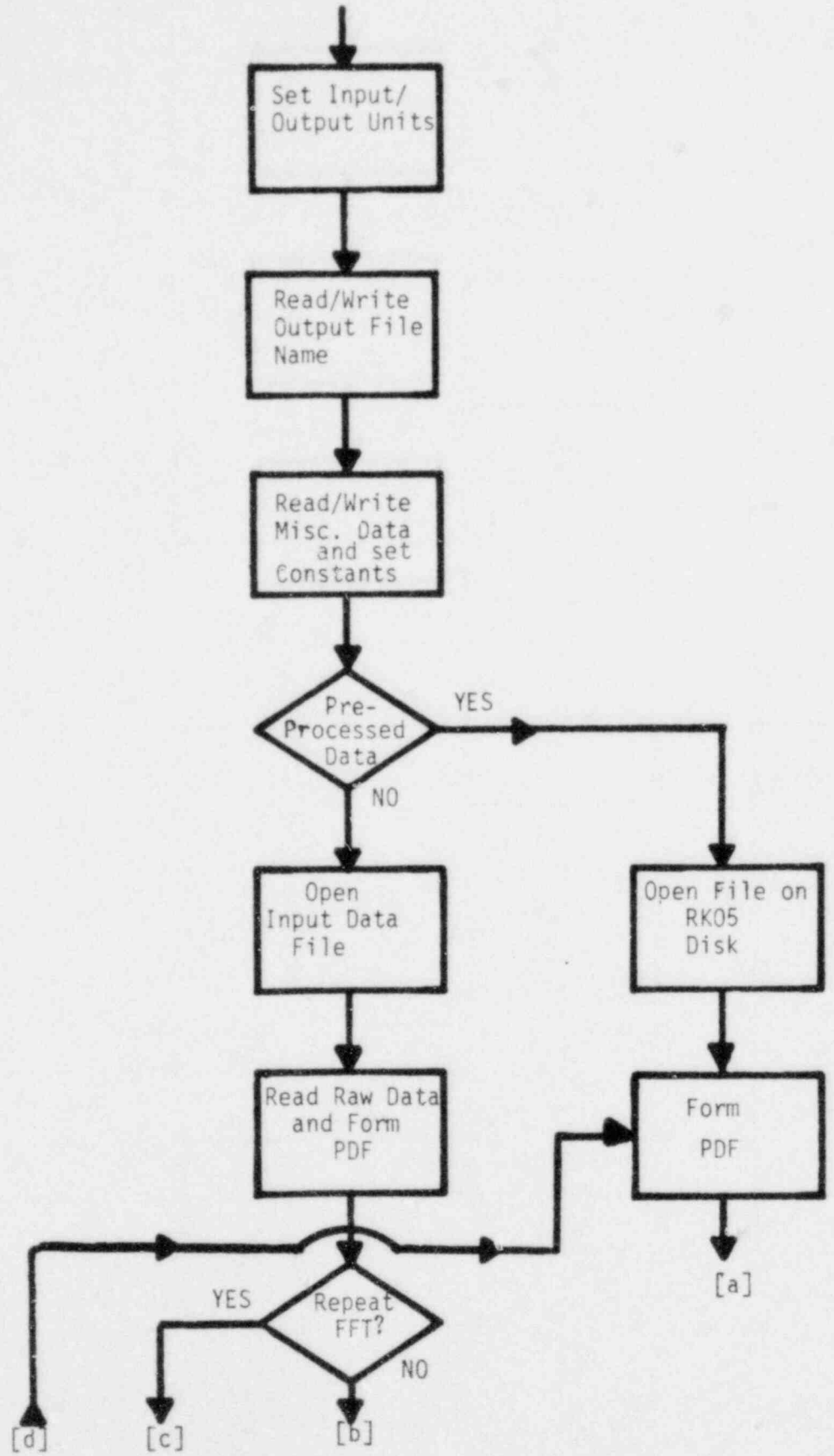

Figure 3.22a A flowchart of the computer code for the PDF, PSD and moments calculation

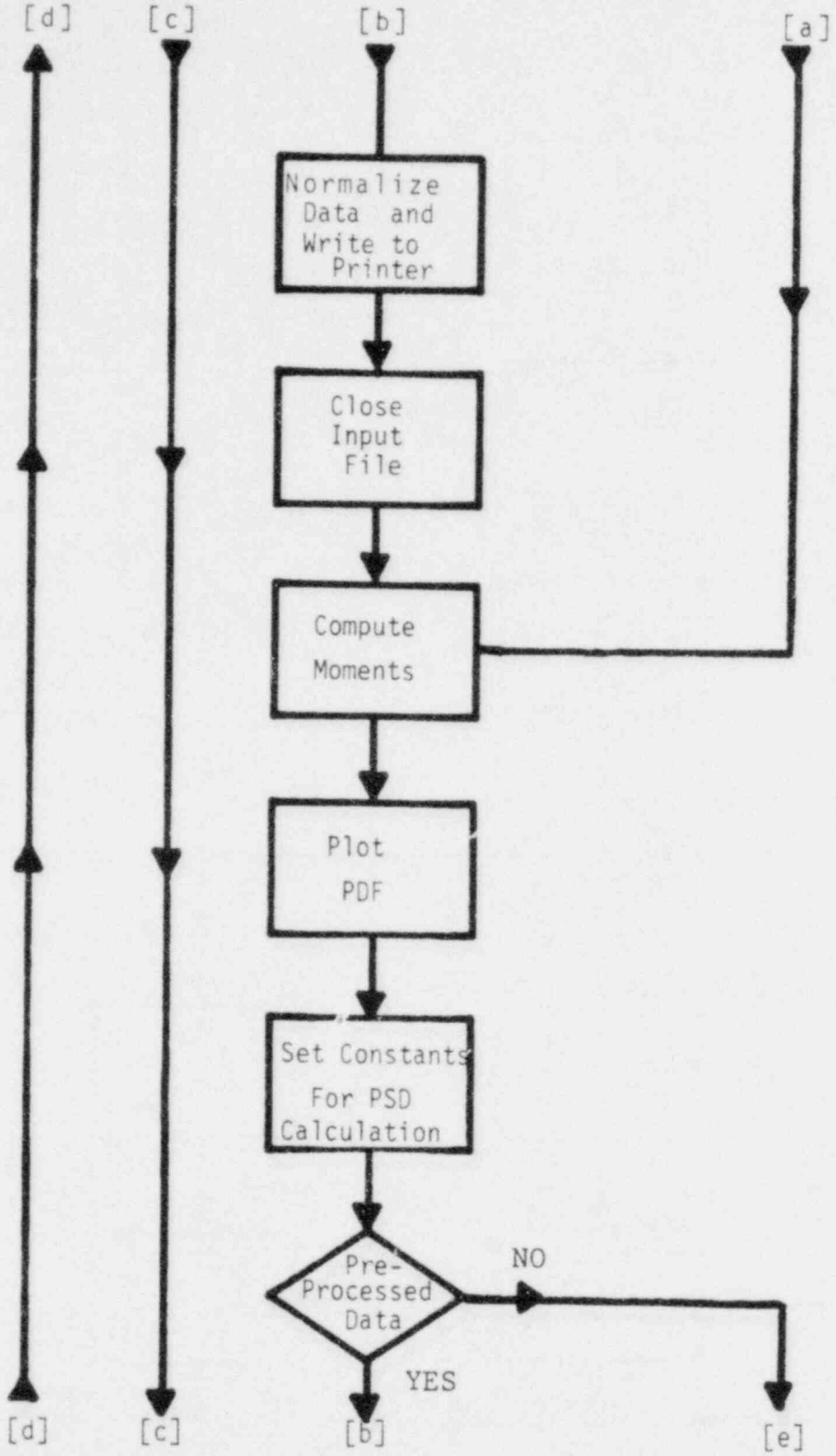

Figure 3.22b Continued

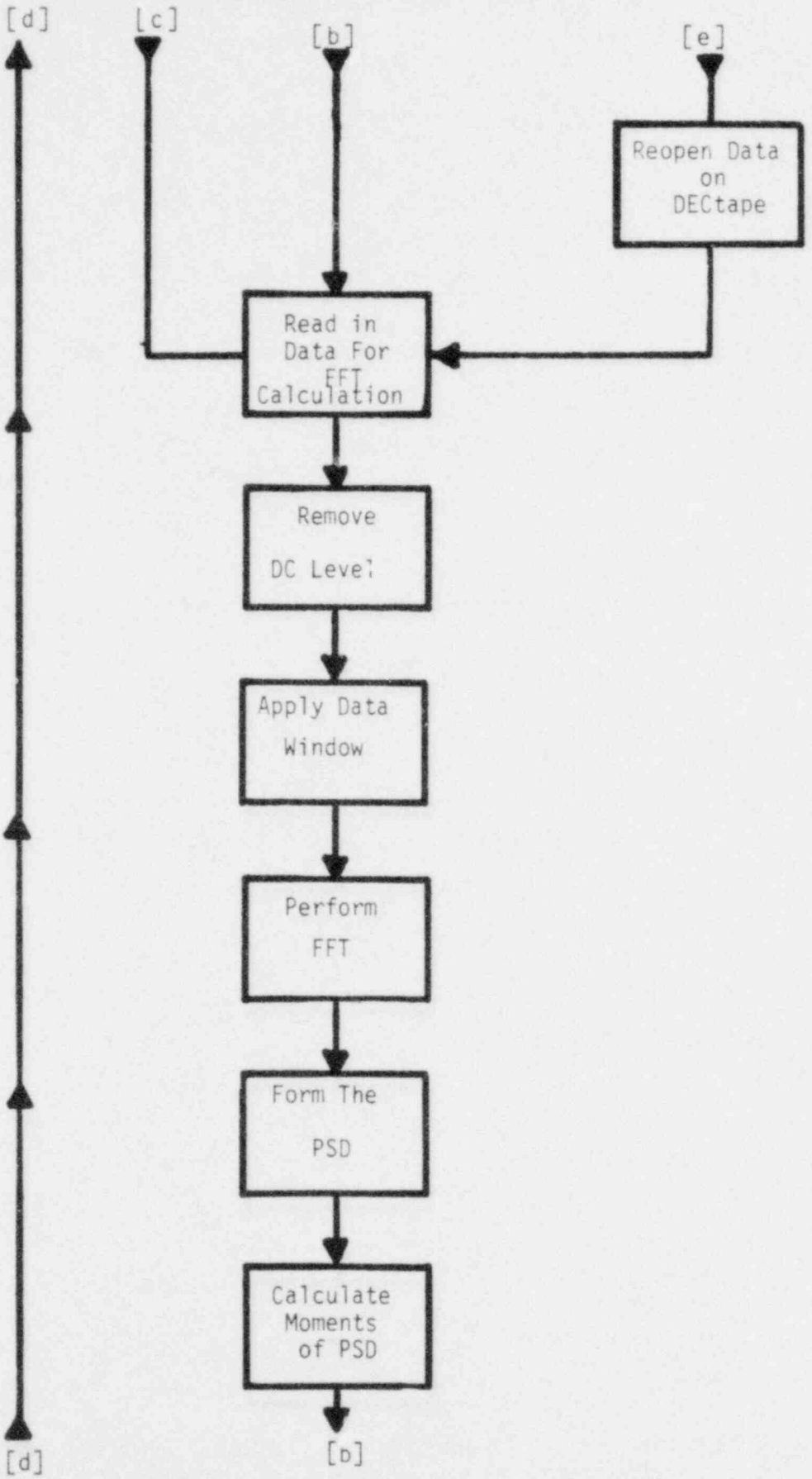

Figure 3.22c Continued

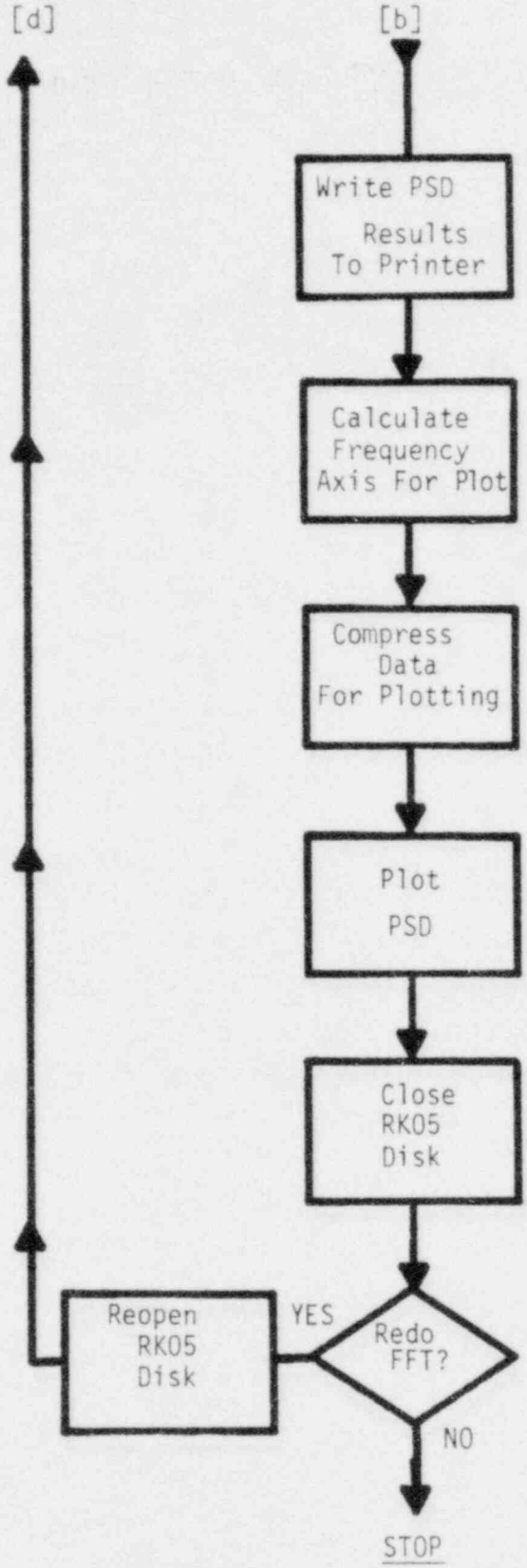

Figure 3.22d Continued

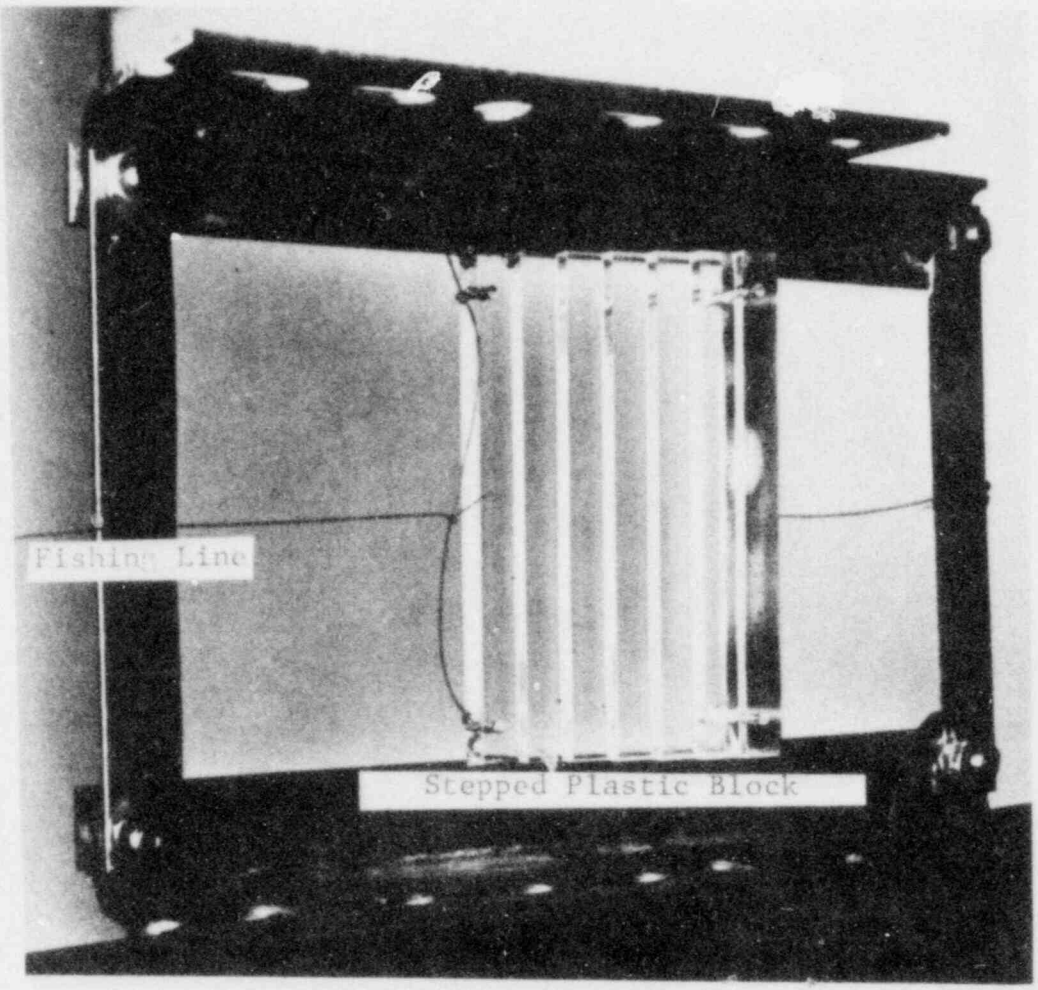

Figure 3.23
A stepped plastic block for verification of the linearity of the signal processing circuitry

perpendicular to the beam. Ten pound test fishing tackle was used to move the block remotely. The design of such a stepped block insured that the maximum attenuation in the plastic is greater than the largest expected in the test section.

The plastic thickness at each step was accurately measured. This device was then placed in the test x-ray beam. The PDP-9 equivalent void fraction reading for each step will be a linear function of plastic thickness if the signal processing is operating properly. Moreover, the slope of the line representing this relationship is the linear attenuation coefficient of the plastic block. A test curve for the previously described system is illustrated in Figure 3.24. It can be seen to be a linear relationship; the measured value of $\mu = 0.394\ cm^{-1}$, agrees with tabulated values for plastic. The graph does not extrapolate to zero because the plastic steps were not exactly perpendicular to the x-ray beam, nevertheless, this calibration is adequate because each x-ray pathlength is multiplied by the same constant.

Most previous systems of this type have used rear collimation of the transmitted beam prior to detection. The close proximity of the front collimator and detector reduce substantially the angle required for scattered radiation to enter the detector. This geometry effectively eliminated the need for a rear collimator. Test runs, using the stepped plastic device described above, and a rear

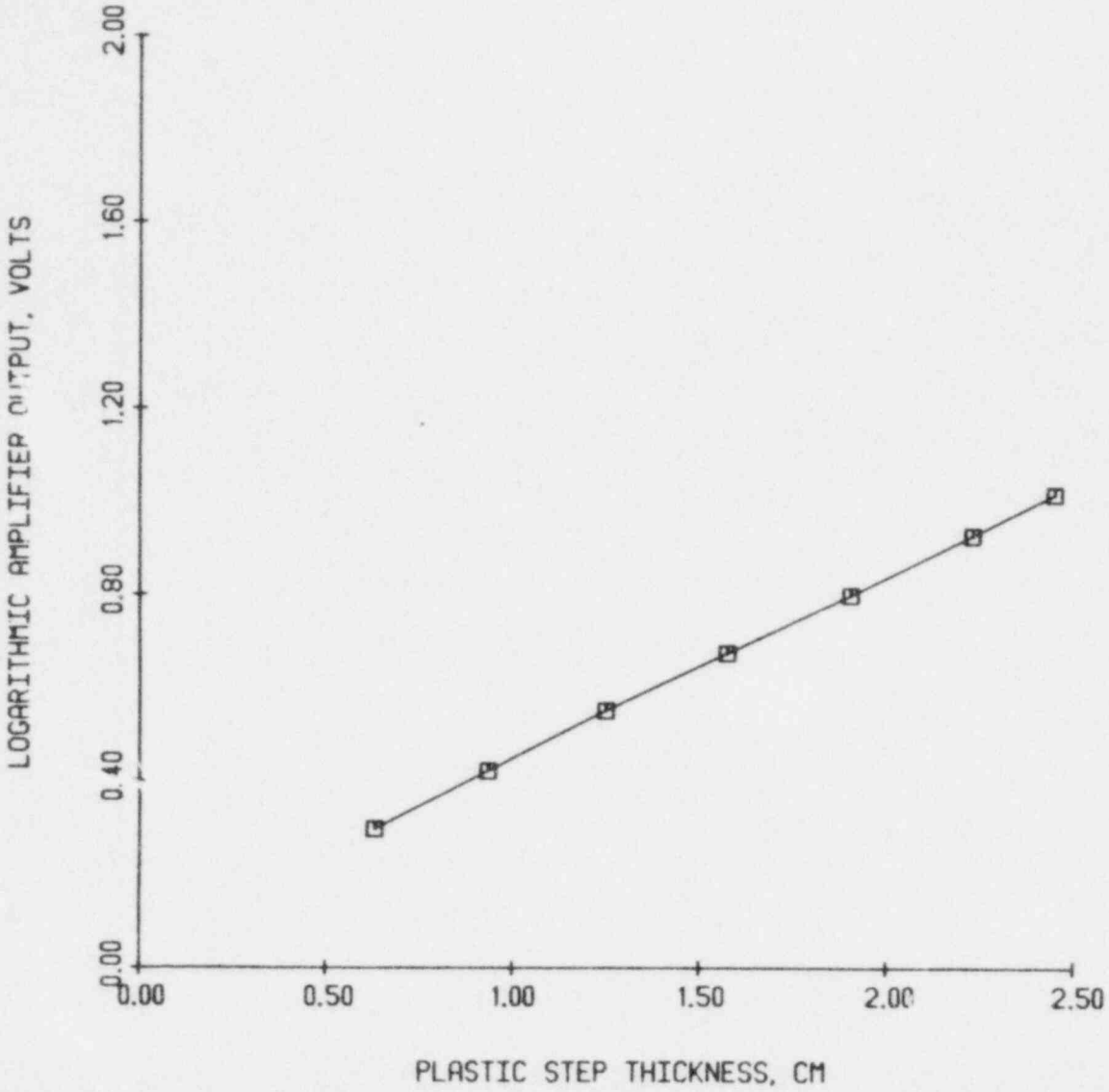

Figure 3.24 Logarithmic amplifier output voltage vs. plastic step thickness

collimator, confirmed this assertion.

3.3 Local Void Fraction Probes

Two techniques were explored for local void fraction measurements; electrical (radio frequency) and optical. The radio frequency excited device employed a local impedance probe as a capacitive element of the circuitry and thus responded to the different dielectric constant associated with each phase. The optical void probe used the different refractive index associated with each phase to determine void fraction.

3.3.1 Electrical Probes

Three criteria were addressed in the design of the local electrical probe:

1) Minimize sensitivity to liquid phase resistivity changes.
2) Avoid polarization of the fluid in contact with the probe tip.
3) Build electronics compatable with commercially available probes.

Satisfaction of the first criterion posed the largest problem, however, a quick review of basic electrical theory indicated a possible solution. Electrical circuits are composed of three components; resistive, capacitive, and inductive. The reactance of the later two components are defined as,

$$X_c = \frac{1}{\omega C} \tag{3.57}$$

$$X_L = \omega L \tag{3.58}$$

where,

X_c = capacitive reactance, ohms

ω = angular frequency, radians/sec.

C = capacitance, farads

X_L = inductive reactance, ohms

L = inductance, henries

These definitions can be used to extend Ohm's Law,

$$V = IR \tag{3.59}$$

where,

V = voltage, volts

I = current, amps

R = resistance, ohms

Notice that the units of reactance are ohms. The voltage/current relationship indicated by Ohm's Law can be applied to non-resistive type components as indicated in Equations (3.60) and (3.61),

$$V_c = IX_c \tag{3.60}$$

$$V_L = IX_L \tag{3.61}$$

where,

V_c = voltage change associated with a capacitance

V_L = voltage change associated with an inductance

The measurement of local or global void fraction with an impedance probe can be modelled as a parallel arrangement of these components in an AC circuit, as shown in Figure 3.25. An expression for the impedance of this circuit is developed by Kirchoff's current relationship. A resistive element has current and voltage in phase while the current of a capacitive element leads the voltage by ninety degrees. Inductive elements have a current that lags the voltage by ninety degrees. The currents associated with an inductor and capacitor act opposite each other. Thus the total current in a general circuit is,

$$I = \sqrt{I_R^2 + (I_c - I_L)^2} \tag{3.62}$$

where,

I_R = current associated with a resistive element

I_c = current associated with a capacitive element

I_L = current associated with an inductive element

Substitution of Equations (3.59), (3.60) and (3.61) into this expression introduces the associated impedances. The voltage is constant across each leg of a parallel circuit and can be factored out as indicated in Equation (3.63),

$$I = V \sqrt{\frac{1}{R^2} + \left(\frac{1}{X_c} - \frac{1}{X_L}\right)^2} \tag{3.63}$$

This expression can be recast to obtain a relationship for the impedance, (Z),

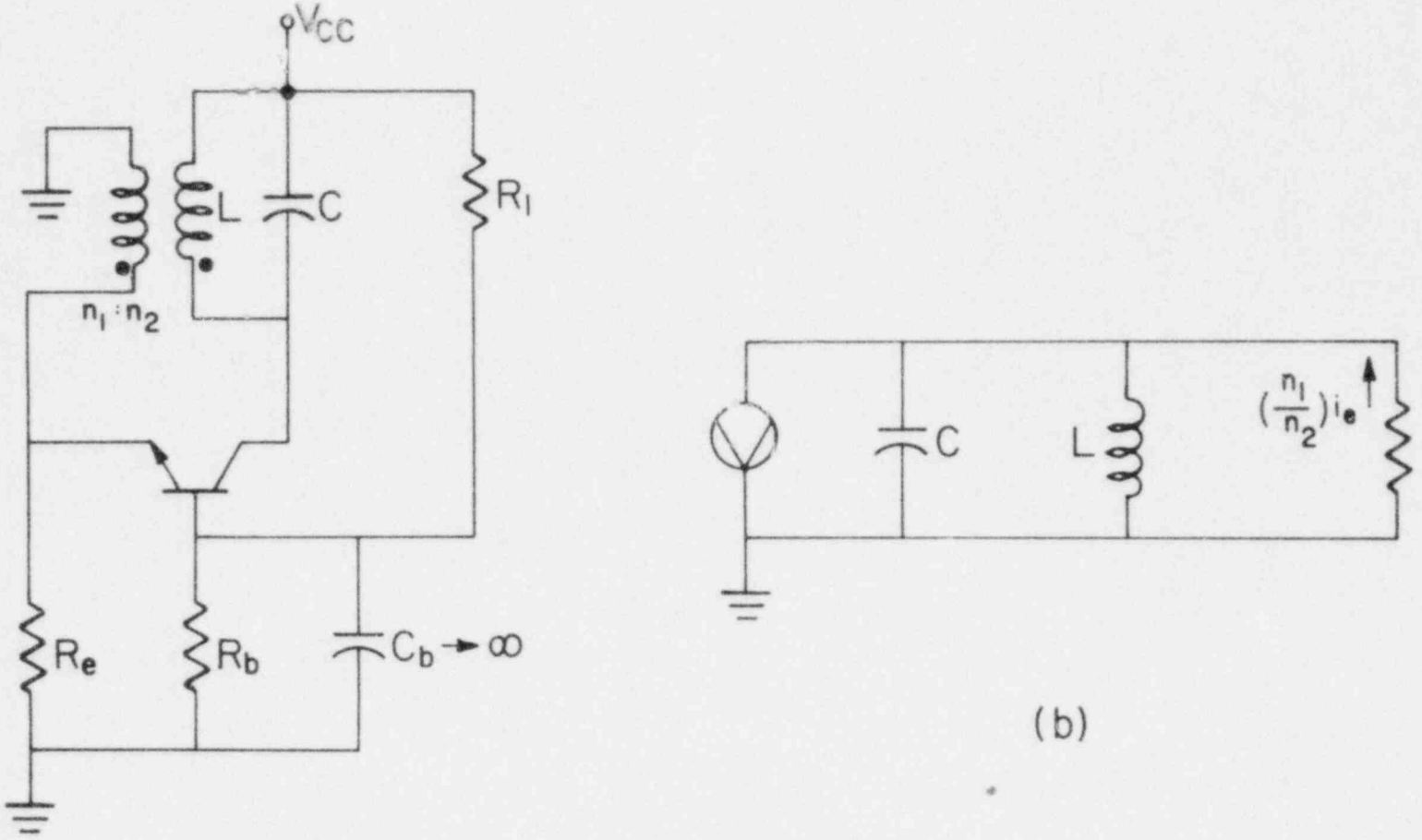

Figure 3.25
A schematic and equivalent circuit for a Hartley oscillator

$$\frac{V}{I} = \frac{1}{\sqrt{\frac{1}{R^2} + \left(\frac{1}{X_c} - \frac{1}{X_L}\right)^2}} \triangleq Z \qquad (3.64)$$

where,

Z = characteristic impedance, ohms

The denominator of Equation (3.64) can now be expanded as,

$$Z = \frac{1}{\sqrt{\frac{X_c^2 X_L^2 + R^2 X_L^2 - 2R^2 X_c X_L + R^2 X_c^2}{R^2 X_c^2 X_L^2}}} \qquad (3.65)$$

After a minor rearrangement of Equation (3.65), and substitution of Equations (3.57) and (3.58) into this expression we obtain,

$$Z = \frac{RL}{C} \sqrt{\frac{1}{\frac{L^2}{C^2} + R^2\omega^2L^2 - \frac{2R^2L}{C} + \frac{R^2}{\omega^2C^2}}} \qquad (3.66)$$

By multiplying the numerator and denominator of the radical by $(\omega c)^2$, this expression can be cast into the form,

$$Z = \omega RL \sqrt{\frac{1}{\omega^2L^2 + \omega^4C^2R^2L^2 - 2\omega^2R^2LC + R^2}} \qquad (3.67)$$

Operation at high frequency will cause the second term of the denominator to become large. Thus for high frequency the impedance can be approximated as,

$$Z \approx \omega RL \sqrt{\frac{1}{\omega^4 C^2 R^2 L^2}} = \frac{1}{\omega C} \qquad (3.68)$$

which is the characteristic impedance of a capacitor, i.e.,

$$Z \approx \frac{1}{\omega C} = X_C \qquad (3.69)$$

Thus an impedance probe which is insensitive to resistivity must operate at a high frequency.

The second previously mentioned criterion was the easiest to solve. That is, operating the probe at ground potential. The third criterion specified the circuit components to be used in conjunction with a Karlsruhe type Z-Probe.

The most basic component of the RPI radio frequency (RF) excitation system is the variable frequency oscillator (VFO). This device must be very stable, particularly with regard to temperature changes. A standard Hartley high frequency oscillator design, was selected as the RF probe driver. The probe was placed in parallel with the oscillating circuit. This arrangement solved polarization problems by keeping the probe tip at ground potential. A parallel arrangement of capacitors has total capacitance equal to the sum of all components. In this arrangement the effect of the probe's capacitance change with fluid phase will be maximized.

A Hartley oscillator will run at a frequency given by,

$$f_o = \frac{1}{2\pi\sqrt{LC}} \tag{3.70}$$

where,

f_o = frequency of oscillation, hz

L = oscillator coil inductance, henries

C = oscillator capacitance, farads

The total capacitance is the sum of the tuning, oscillator-to-probe cable, stray and probe capacitance. Under operating conditions, the oscillator will run at one frequency when the probe is immersed in the vapor phase and at a slightly lower frequency when in the liquid phase. This frequency shift is easily understood by considering the dielectric constants asociated with the two phases. Vapor has a dielectric constant of about 1.0; while for water it is 75.0.

It is desirable to make the associated frequency shift as large as possible. Stray, tuning and cable capacitances were thus minimized. The probe capacitance would add directly to these capacitances, so the smaller these constant capacitances are, the greater portion of the total capacitance associated with the probe. The Hartley oscillator output is mixed with a crystal oscillator. The resultant frequencies are filtered so that only the difference between the VFO and the crystal oscillator frequencies are passed. This technique produces a

relatively large change in signal for a given capacitance change.

The probe was designed to detect a one hundredth of a foot diameter bubble moving at fifty feet per second. A maximum information rate is thus directly calculated,

$$\left[\frac{1}{\frac{0.01 \text{ ft}}{50 \frac{\text{ft}}{\text{sec}}}}\right] = 5 \text{ khz} \tag{3.71}$$

Lower frequency systems are less expensive to build thus a very high frequency device was not considered desirable. Basic radio electronics dictates that the lowest carrier frequency should be at least ten times the information rate for effective modulation. The frequency difference required can be expressed as,

$$f_\ell - f_m = f_{c\ell} = 50 \text{ khz} \tag{3.72}$$

where,

f_ℓ = probe oscillator frequency when tip is in the liquid phase, khz

f_m = crystal mixing frequency, khz

$f_{c\ell}$ = lowest carrier frequency, khz

A carrier frequency in the vapor phase that is twice the liquid phase carrier would permit easy phasic discrimination. This one octave frequency difference could be translated into a twenty-four decibel (more than a factor of ten) amplitude change, using a simple four pole active

filter. The twenty-four decibel change will provide adequate range for phase discrimination. The required frequency when the probe is immersed in vapor is expressed by,

$$f_g - f_m = f_{cg} = 2(50khz) = 100\ khz \tag{3.73}$$

where,

f_g = probe oscillator frequency when tip is in the vapor phase, khz

f_{cg} = vapor phase carrier frequency, khz

The required change in frequency is obtained by subtracting Equation (3.72) from (3.73),

$$f_g - f_\ell = \Delta f = f_{cg} - f_{c\ell} = 50\ khz \tag{3.74}$$

The appropriate oscillator frequency can now be calculated. Equation (3.74) can be combined with Equation (3.70) to obtain,

$$\Delta f = f_g - f_\ell = \frac{1}{2\pi\sqrt{LC_\ell}} - \frac{1}{2\pi\sqrt{LC_g}} \tag{3.75}$$

where,

C_ℓ = total system capacitance with the probe's tip in liquid phase, farads

C_g = total system capacitance with the probe's tip in vapor phase, farads

This expression can be rewritten as,

$$\Delta f = \frac{\sqrt{C_\ell} - \sqrt{C_g}}{2\pi \sqrt{LC_\ell C_g}} \tag{3.76}$$

Simplification can be made by noting from Equation (3.70) that the frequency of oscillation in the liquid phase can be factored out, resulting in,

$$\Delta f = f_\ell \left[\frac{\sqrt{C_\ell} - \sqrt{C_g}}{\sqrt{C_g}} \right] \tag{3.77}$$

The probe and cable capacitance was measured using a capacitance meter. The all vapor capacitance was found to be 35.85 picofarads (pf), and the all liquid capacitance was 36pf. Substitution of these values into Equation (3.77) and noting the Δf is fifty kilohertz, f_ℓ is found to be 24 megahertz (Mhz). This value constitutes the minimum frequency.

A 27.001 Mhz crystal was used because of availability. The probe's Hartley oscillator was tuned to 27.051 Mhz in water. This is 50 khz greater than the crystal frequency. The carrier frequency in air was now measured at 117 khz, resulting in a difference of 67 khz.

Filtering was necessary since the carrier amplitude is relatively constant. Two two-pole Butterworth filters with a break frequency of 50 khz amplify the phasic difference.

A useful signal is not yet available since the

carrier is still AC. It must be rectified and filtered further before it can be sent to a comparator for thresholding. Filtering requirements can be relaxed if full wave rectification is performed at this stage. Diodes are too slow and have too large a turn-on voltage for this application. As a result, standard full wave rectifying circuits could not be used.

A new circuit was designed to full wave rectify this type of signal. In this circuit, a comparator goes high when subjected to a positive input voltage. This gate turns on an analog switch and the circuit becomes a unity gain inverting amplifier. A negative input voltage to the comparator causes it to go low. This gate also opens the analog switch but the circuit is now a unity gain noninverting amplifier. The output from this system is full wave rectified signal since the positive half cycles are inverted and negative half cycles are untouched. This signal is then applied to a resistor/capacitor single pole filter. A fifteen microsecond time constant at this stage is crucial, since the speed of the last filter usually determines the device's overall response time.

Due to extensive filtering, the signal quality is very good. One hundred millivolts of ripple on a six and one half volt signal exist when the probe is in the vapor phase. The liquid phase shows a one half volt signal with fifty millivolts of ripple.

The final stages of this RF impedance probe

contains either a comparator or derivative box for signal thresholding. This comparator produces output voltages compatable with a zero to ten volt A/D converter. The output of this comparator is used to gate a one hundred khz oscillator. The pulses passing through the gate are counted. Local, time-averaged void fraction can be calculated as,

$$\alpha_p = \frac{N_s}{10^5 T_c} \tag{3.78}$$

where,

α_p = local void fraction

N_s = pulses counted on scalar

T_c = counting interval, seconds

A block diagram of the radio frequency probe electronics is shown in Figure 3.26, and a circuit diagram is shown in Figure 3.27. The actual probe, VFO and micrometer driver mounted in the air/water loop are shown in Figure 3.28.

3.3.2 High Temperature Optical Probe

As discussed previously, local void measurements can also be made by optical techniques. A diamond tipped, optical probe was developed for this purpose. Fiber optics delivered visible light to the specially cut tip. Reflected light from the tip was transmitted through fiber optics to a phototransistor. The phototransistor converted the returning light to a voltage, which was processed to yield

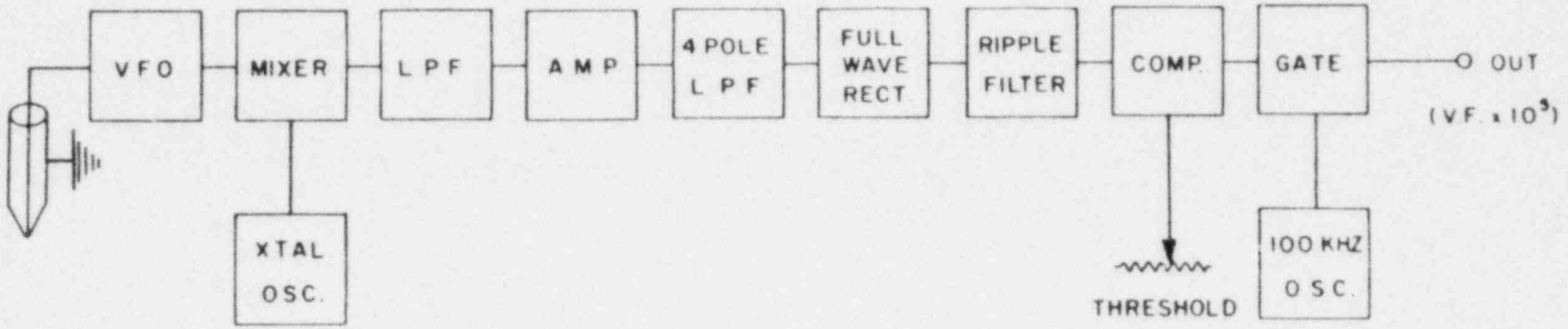

Figure 3.26
A block diagram of radio frequency local void fraction probe electronics

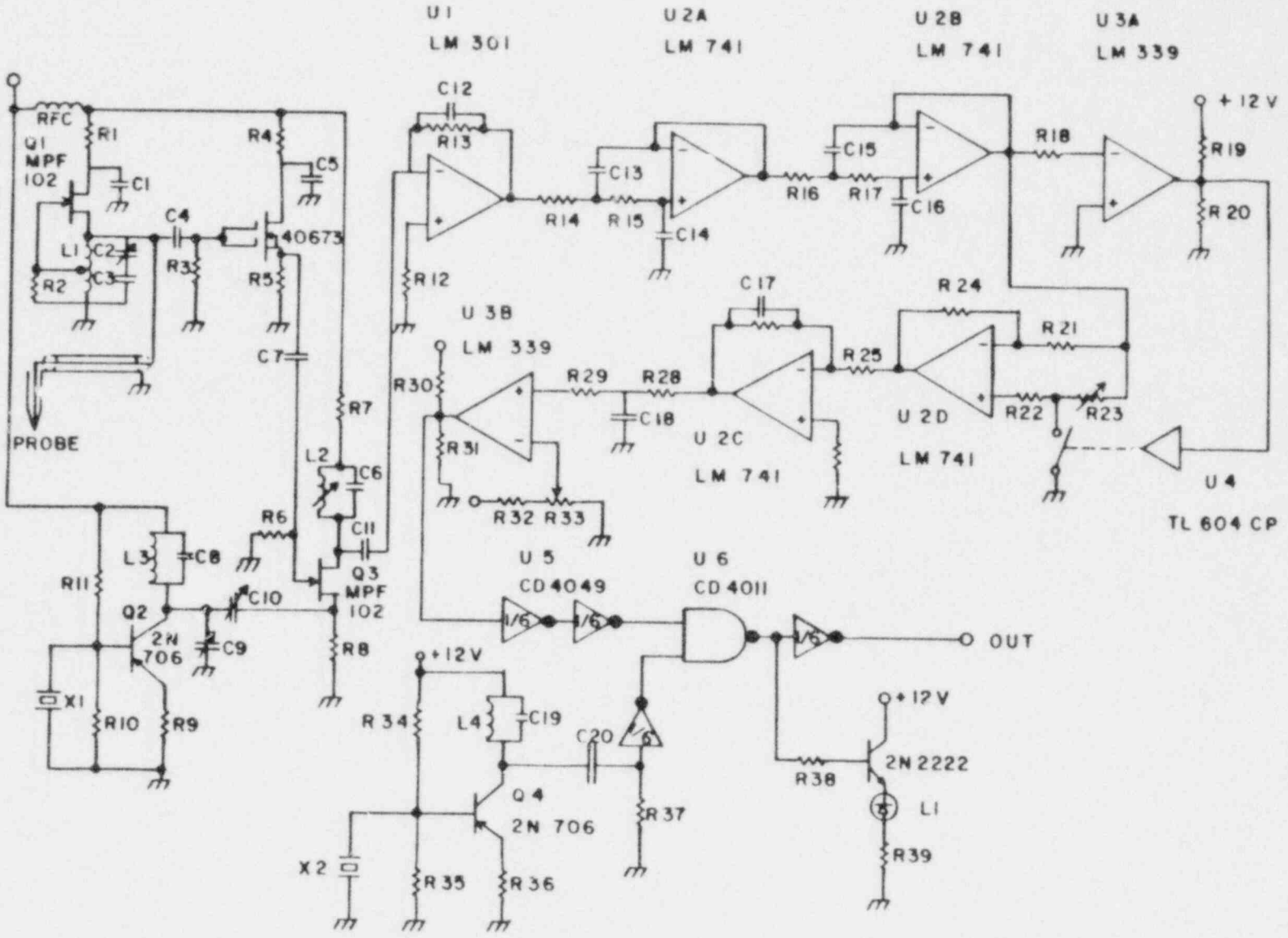

Figure 3.27
The circuit diagram for the radio frequency local void probe electronics

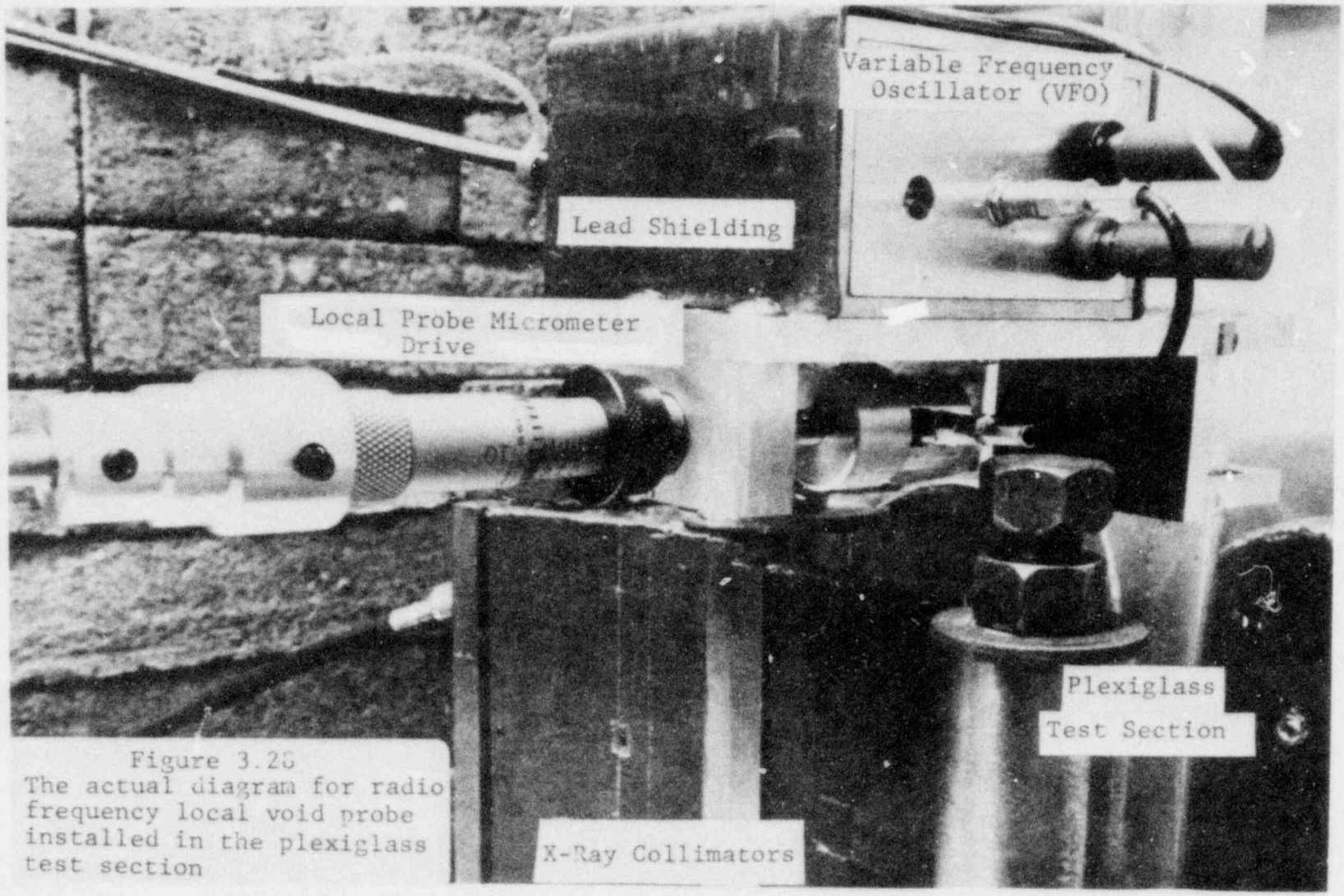

Figure 3.28
The actual diagram for radio frequency local void probe installed in the plexiglass test section

the local void fraction.

Snell's Law forms the principle of all optical void probe's operation,

$$n_1 \sin \phi_1 = n_2 \sin \phi_2 \tag{3.79}$$

where,

n_1 = refractive index of media-1

ϕ_1 = angle of incidence, with respect to the surface normal

n_2 = refractive index of media-2

ϕ_2 = angle of refraction, with respect to the surface normal

Phase detection occurs at the surface of the probe tip. This surface is shaped to internally reflect incoming light if vapor surrounds it, and to refract light if liquid surrounds it. Measurement of the reflected light can yield the void fraction.

Light, in passing from a more dense to a less dense media, can be totally internally reflected. This reflection occurs when the angle of refraction becomes ninety degrees. Snell's Law, Equation (3.79), can be solved for the angle of incidence,

$$\phi_1 = \mathrm{Sin}^{-1}\left(\frac{n_2 \sin \phi_2}{n_1}\right) \tag{3.80}$$

At the critical angle, $\sin\phi_2$ equals one and Equation (3.80) reduces to

$$\phi_1 = \mathrm{Sin}^{-1}\left(\frac{n_2}{n_1}\right) \tag{3.81}$$

This relationship holds only for light going into a less dense media. Light moving into a more dense media is always refracted.

Both sapphire and diamond have desirable optical and high temperature properties. A diamond tip was selected in this study because of its availability and physical properties. The hardness of a diamond should insure endurance and diamonds are known for their outstanding clarity, having no absorption resonances in the visible light band. This material also has a very high refractive index, about 2.4.

Proper operation of an optical probe crucially depends on the sensing tip's construction. Several parameters must be considered in the tip's design:

1) The ability to cut the stone accurately.
2) The proper tip angle to insure maximum phasic discrimination.
3) Streamlined shape to insure easy interface penetration.
4) Correct diamond shaft length.
5) Small tip diameter to minimize hydrodynamic effects.

6) The proper ratio, and position, of input and output fibers.

7) Tip and fiber availability.

8) Tip-to-optical fiber optical coupling

9) Leaktight seal of tip-to-sheath seal.

Some of these parameters are shown schematically in Figure 3.29.

Several tip designs were considered. Curved tip shapes such as spherical or elliptical are desirable for optical reasons. Hydrodynamically, however, these shapes have poor interface penetration chacteristics, and small voids may be deflected by the tip surface. Impedance probes normally use a conical tip and generally have acceptable hydrodynamic characteristics. It was reasoned that a conical diamond tipped probe should possess similar flow hydrodynamic characteristics.

The geometric parameters of the tip were investigated by computerized ray tracing. The code, DOPE-1 (Diamond Optical Probe Evaluation), simulated the two-dimensional ray paths inside the tip. Ten rays were initialized along the back face. The rays were equally spaced in the areas designated as input fibers. The light was assumed to move in a straight line. Its path was traced through the tip and back to the rear face unless it was transmitted out of the diamond.

Several runs of the code were made to optimize the various parameters. Figure 3.30 illustrates the effect of

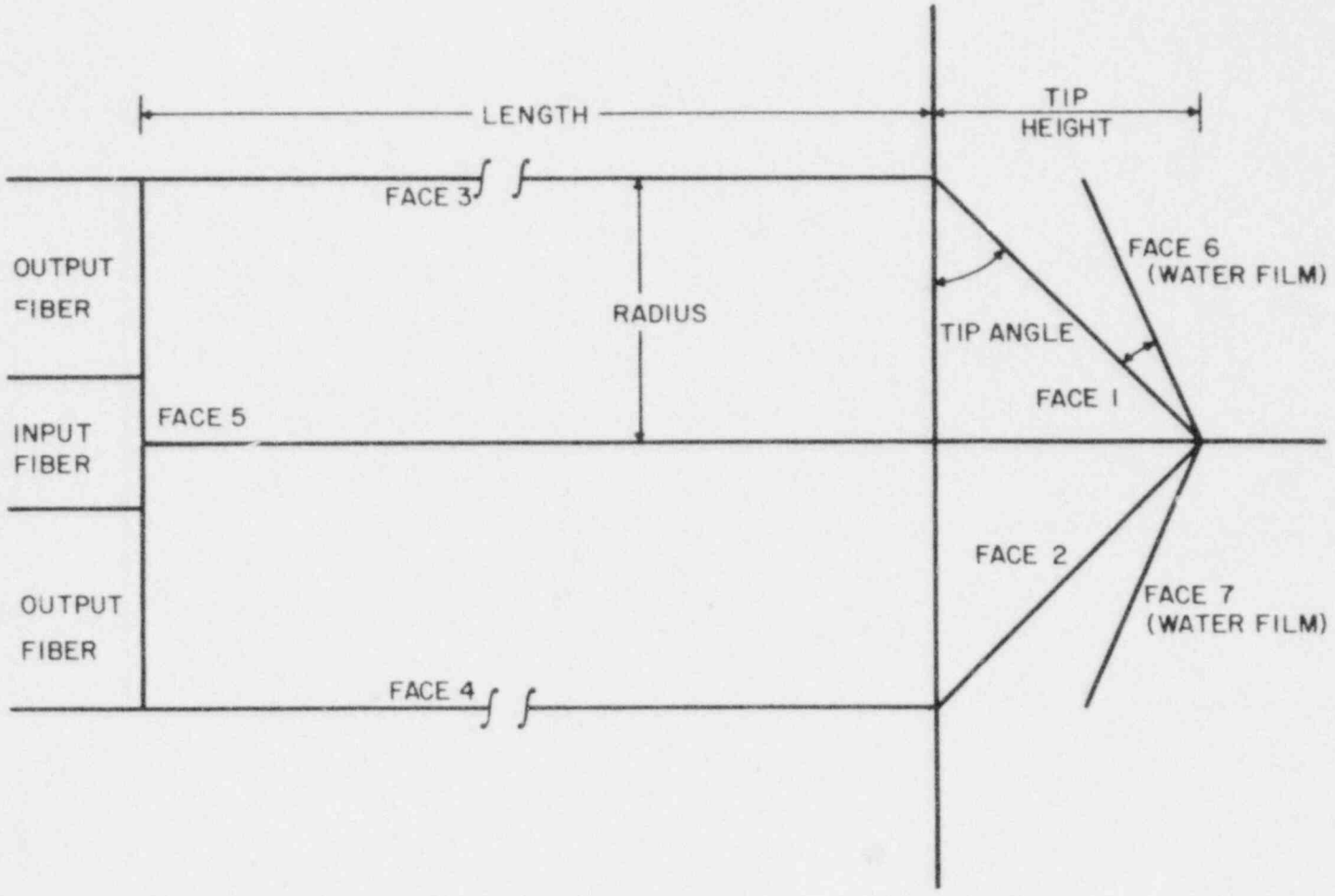

Figure 3.29
Typical parameters considered in the analysis of the sensing tip of an optical probe

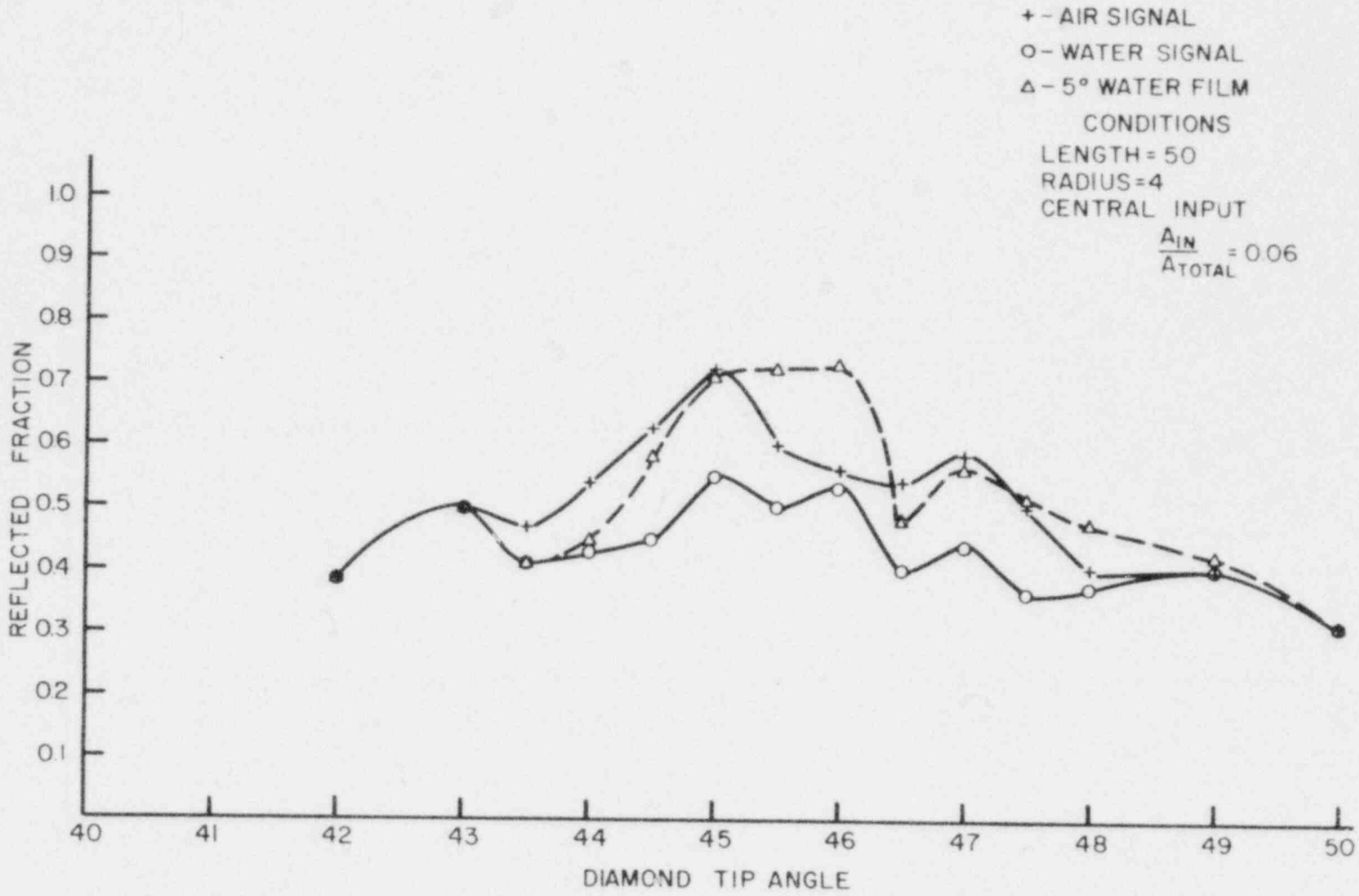

Figure 3.30 REFLECTED LIGHT FRACTION AS A FUNCTION OF DIAMOND TIP ANGLE

changing the tip angle. For small tip angles, no phase discrimination is possible since the light is refracted out of the tip. Large tip angles, while adequately returning light to the output fibers, produce rays which exceed the optical fiber's acceptance angle. Indeed, phasic discrimination is only possible over a relatively small range of angles.

Figure 3.31 shows the effects of a changing shaft length for a tip angle of 45 degrees and a constant tip diameter. The shaft length was not considered a critical parameter as long as some minimum length was exceeded, since diamond availability and cost will limit the length.

The phasic discrimination made possible by varying the input to output optical fiber area is illustrated in Figure 3.32 and 3.33. The light input occurs in the center for Figure 3.32 while light enters around the periphery for Figure 3.33. Output fibers are available in all other regions along the back face for these cases. It is obvious that an optimal fiber optic bundle would input light along the periphery and detect the reflected light in the central region.

A code description and explanation of the DOPE-1 model is provided in Appendix A.4. A sample case is included, as well as the code listing, in Appendix A.5.

Several compromises were made in the final design. Initial considerations indicated that a twelve mil diameter was desired. This size turned out to be too expensive to

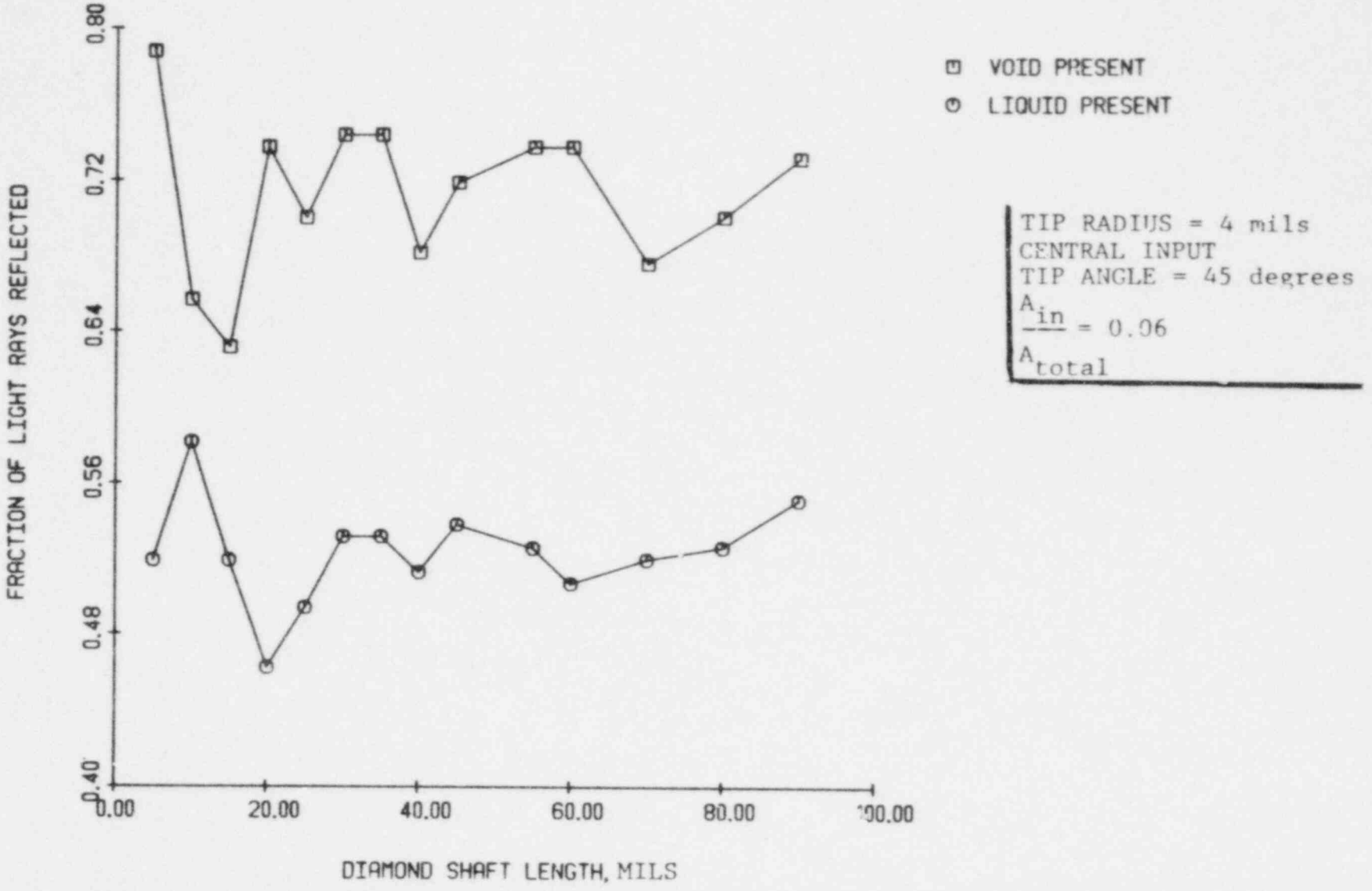

Figure 3.31 The fraction light rays reflected vs. diamond shaft length

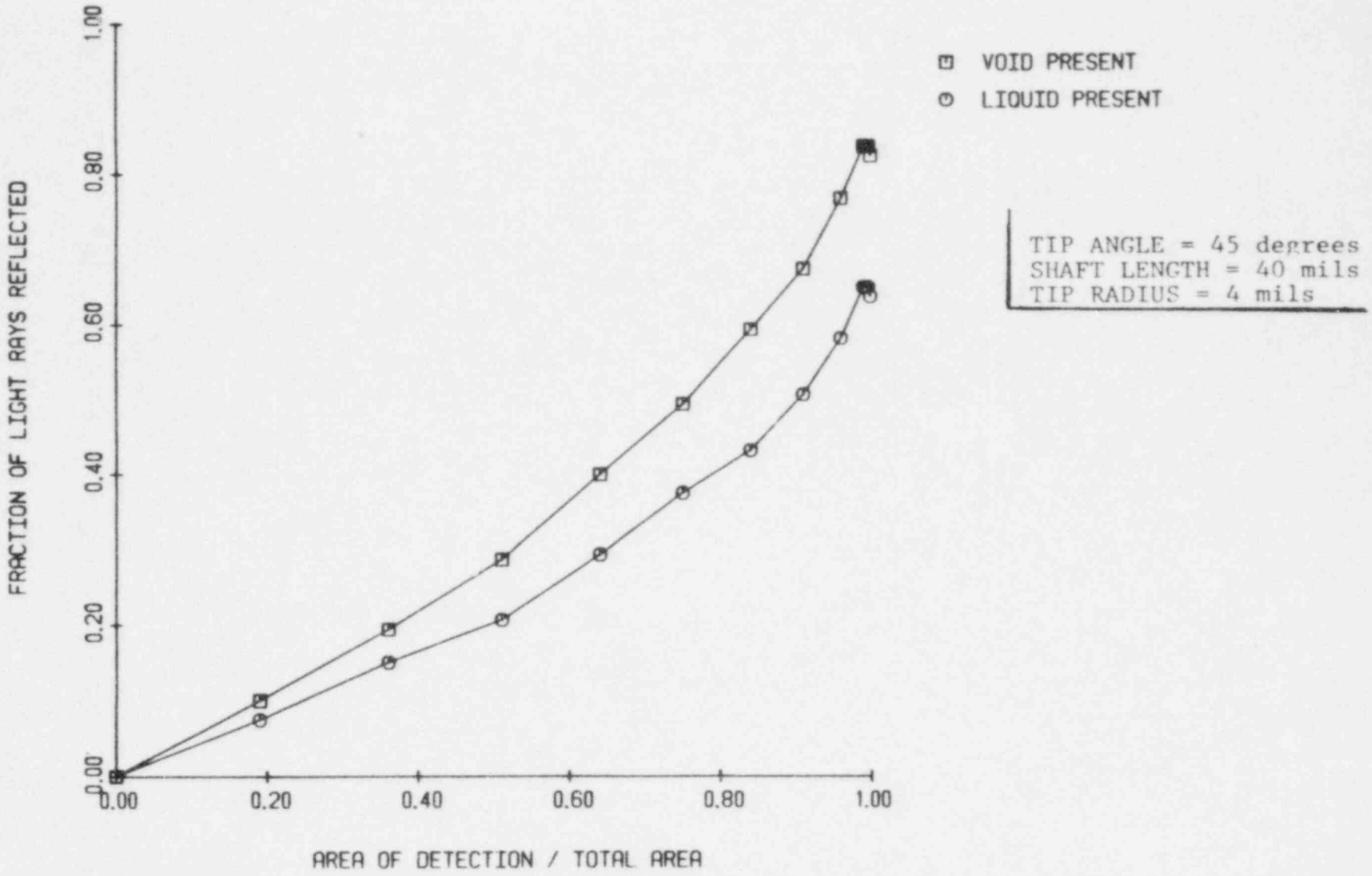

Figure 3.32 The fraction of light rays reflected vs. area of light detection ratio for a central light input / peripheral output

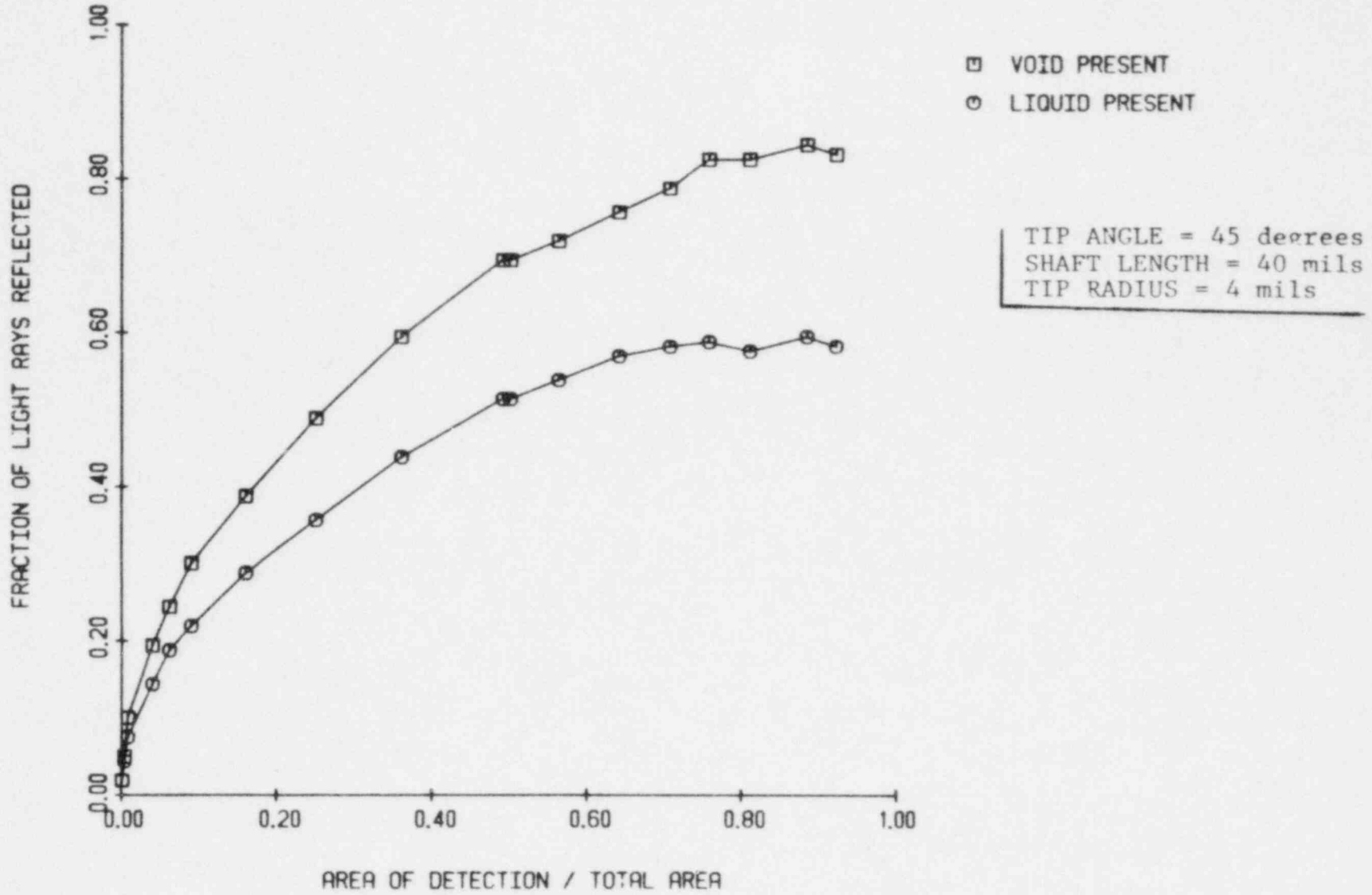

Figure 3.33 The fraction of light rays reflected vs. area of light detection ratio for a peripheral light input / central output

manufacture, thus a twenty-nine mil diameter was used to determine proof of principle. High costs forced the use of a commercial fiber optic bundle made by Skanamatics [38]. Optical contact between the fibers and diamond was made in a various fashions. Several oils and RTVs were tried, but these did not work as well as direct mechanical contact.

The diamond was mounted in a stainless steel sleeve. Neuber Industrial Diamonds cut and mounted the tip in the sleeve. This sleeve slipped onto a Skanamatic probe body, as illustrated in Figure 3.34.

Back end electronics were attached to process the phototransistor output. They consisted of an amplifier and several comparators. A light emitting diode indicated the presence of the vapor phase. The output signal was digital and could be used to trigger a gate on a high frequency clock. This clock provided counts to a scalar, similar to the RF probe design. A block diagram of the electronics is shown in Figure 3.35, while a circuitry schematic is shown in Figure 3.36.

This system was bench-tested in low pressure air/water flow and appeared to operate satisfactorily. Due to the high costs involved in the manufacture of a high temperature probe of suitably small size, it was decided not to proceed with the development of this type probe. Nevertheless, such a probe appears to be feasible and has a number of attractive features.

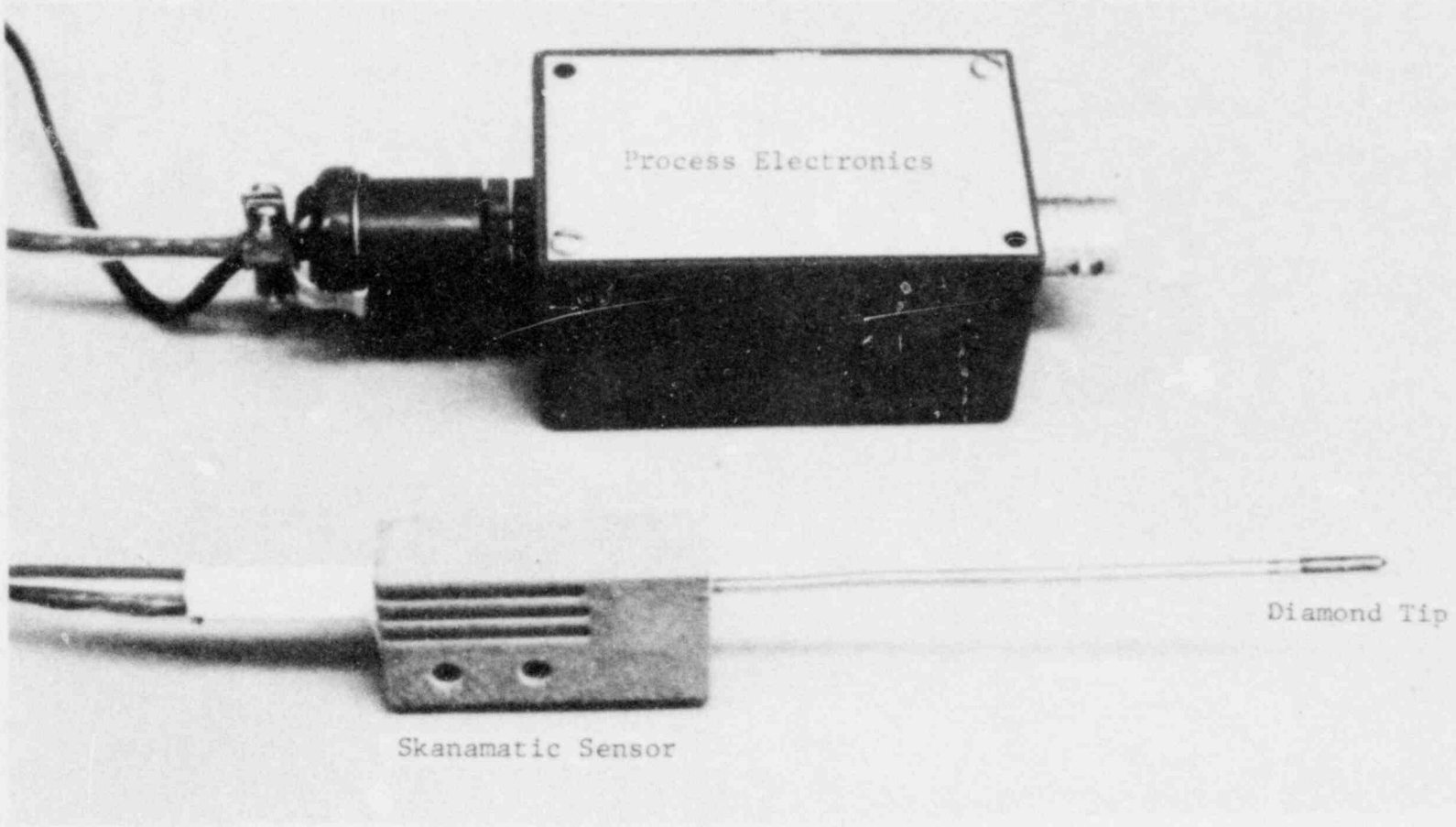

Figure 3.34
The diamond tipped optical
local void fraction probe
and process electronics

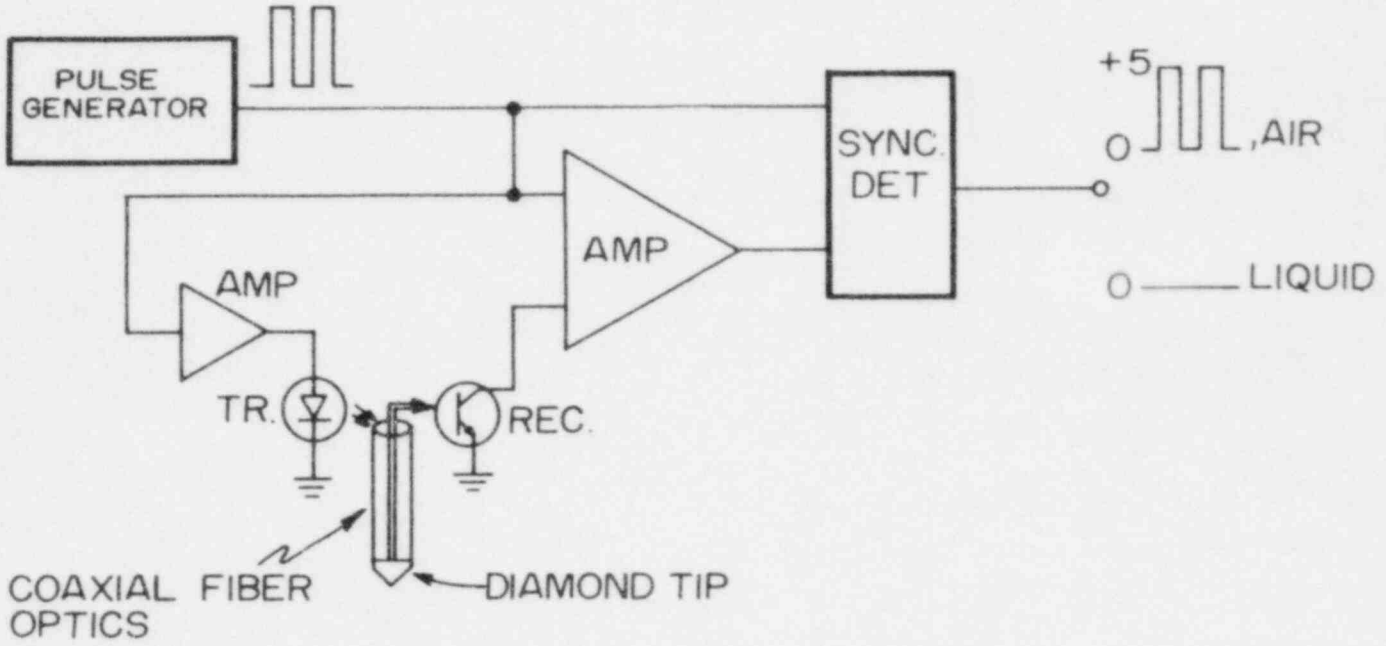

Figure 3.35
A block diagram of the diamond tipped optical void fraction probe's electronics

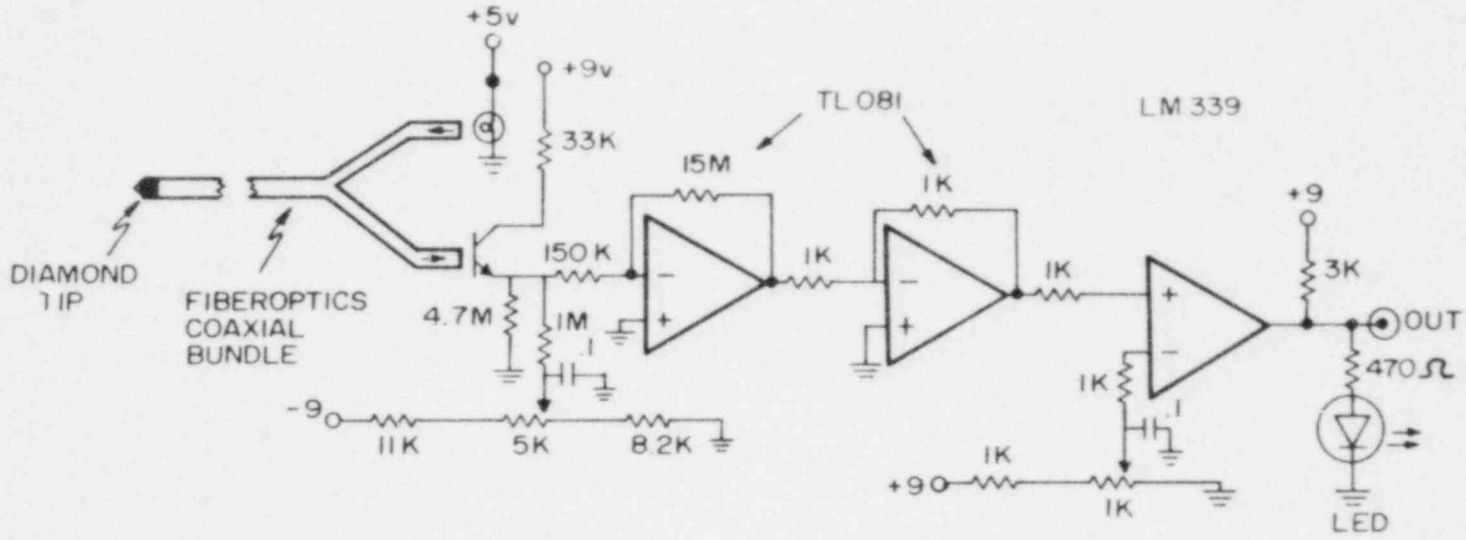

Figure 3.36
A circuit diagram of the
diamond tipped optical void
fraction probe's electronics

3..3 Signal Processing

The analog signal produced by any local probe must exceed some level above noise to result in an output. Two basic schemes exist; level thresholding and derivative thresholding.

Level thresholding has been the most widely used in the past and is the simplest to apply. This method employs an adjustable voltage level. An analog signal from the probe, which exceeds the preset threshold, opens the ouput gate. The gate remains open until the analog signal falls below the threshold level.

Derivative thresholding triggers on the slope of the analog signal. A positive sloped signal indicates probe tip entry into a void and enables the output gate. A negative sloped signal indicates probe tip exit from the void and disables the gate. A comparison of level and derivative thresholding is shown in Figure 3.37. It can be seen that level thresholding has a slower response and cannot detect small, fast moving, bubbles.

There are four chacteristic frequencies present in the analog signal:

1) A low frequency due to void passage time.
2) A higher frequency associated with probe's penetration time into the void.
3) A slightly higher frequency caused by the probe's penetration time from the void.
4) High frequency noise.

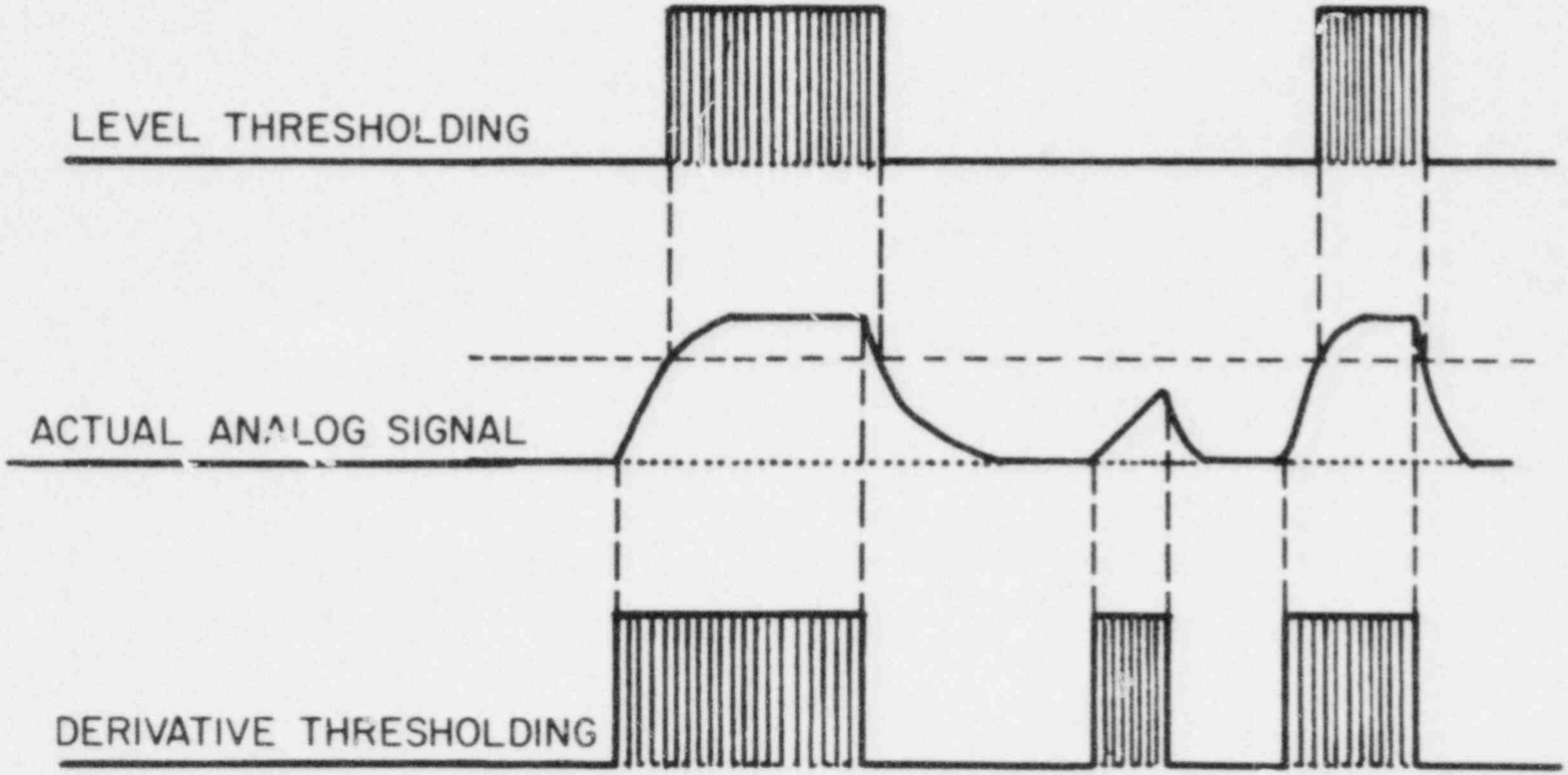

Figure 3.37
A comparison of the void fraction measured with level and derivative thresholding

Derivative thresholding may be thought of as a band-pass filter, discriminating out the low frequency due to void passage and the high frequencies associated with noise. Only the frequencies resulting from probe penetration, or departure from the void, are passed.

A block diagram of derivative thresholding is shown in Figure 3.38. The differentiator establishes the frequency associated with the analog signal change. An adjustable window determines if the frequency should be passed or filtered. The last stage consists of a flip-flop which is enabled by the positive sloped signal and disabled by a negative sloped signal. Figure 3.39 shows the derivative circuit developed for the RF probe.

Derivative thresholding has two major advantages:

1) Insensitivity to baseline capacitance drift (eg: changes in fluid temperature).
2) Ability to detect small, fast moving voids.

A level thresholding circuit is easier and cheaper to construct. However, drifts in the baseline capacitance, due to varying fluid temperature, will move the effective discriminator level.

The RF excited impedance probe was selected for further development because of cost. Impedance probes are commonly used in two-phase measurements thus further development of this scheme is valuable. Moreover, such probes are some of the only ones known to withstand the harsh environment usually associated with diabatic two-phase

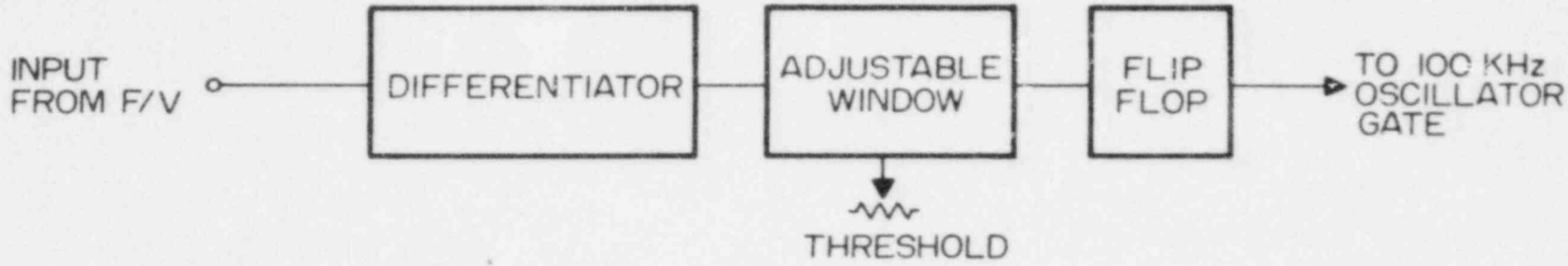

Figure 3.38
A block diagram of the derivative thresholding scheme

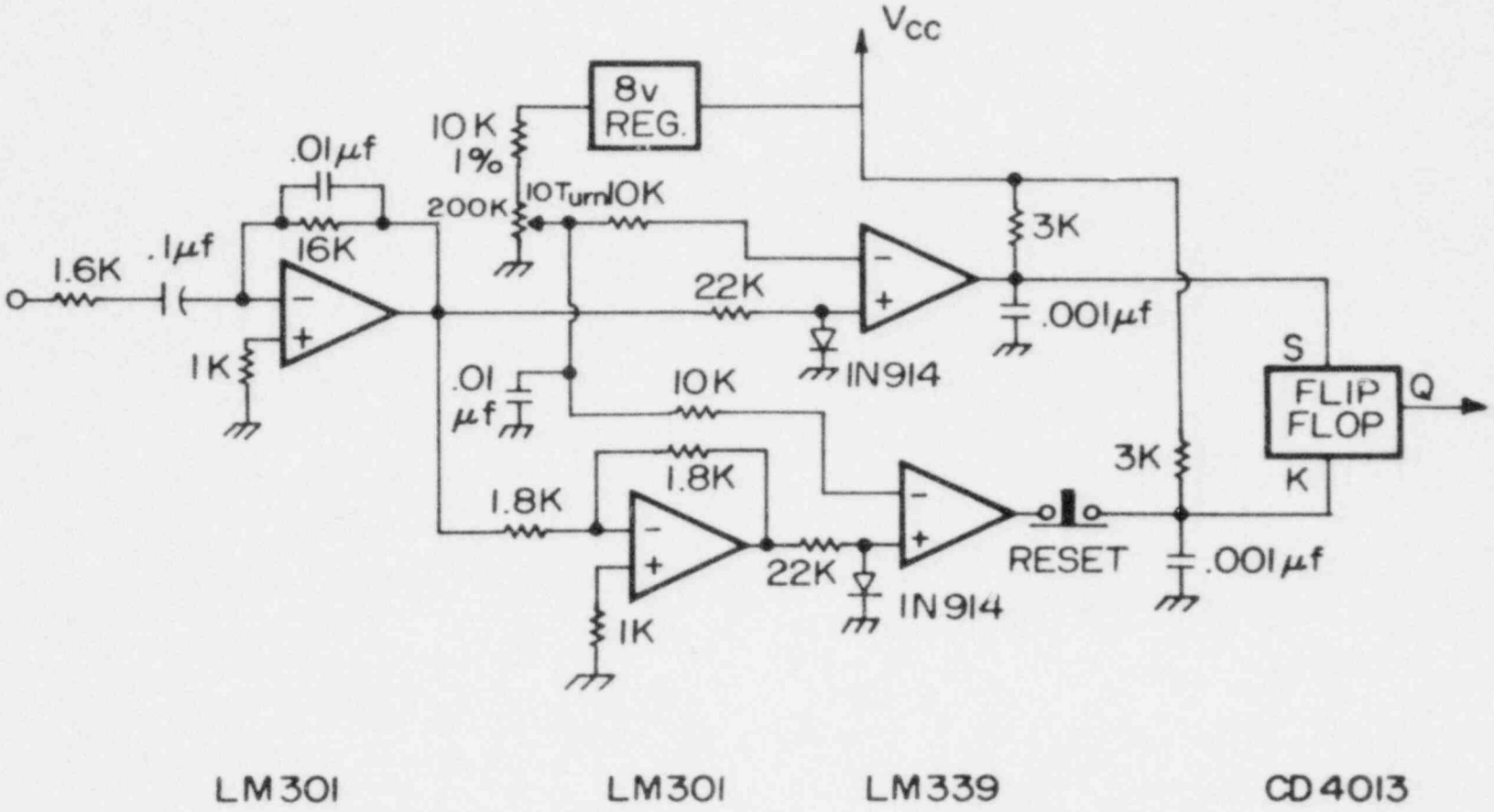

Figure 3.39
Derivative thresholding circuitry developed for the RF probe

flows.

In this study both thresholding schemes were employed in conjunction with the RF local void probe. The results are presented later in the text. A picture of the actual electronics is shown in Figure 3.40.

The previously described air/water loop was outfitted to test and calibrate the RF impedance probe. The probe mounting and micrometer drive needed for accurate probe positioning were previously shown in Figure 3.28. Remote movement of the probe is performed by a stepping motor as shown earlier in Figure 3.13. The driver for the stepping motor was mounted outside the high radiation area associated with the x-ray machine. Hence, the local RF void probe could be moved along the tube diameter while simultaneously measuring the chordal-average void fraction along the diameter with the x-ray system. Integration of the measured local void fractions and comparison with chordal x-ray measured chordal-average void fraction will yield a local probe calibration curve.

3.4 Optical Global Void Fraction Technique

Light rays striking a two-phase interface will be refracted or reflected, the amount depending on the surface curvature. The optics of refraction at this interface are described by Snell's Law, Equation (3.79).

Global two-phase void fraction measurements can be made with this principle. That is, a collimated light beam

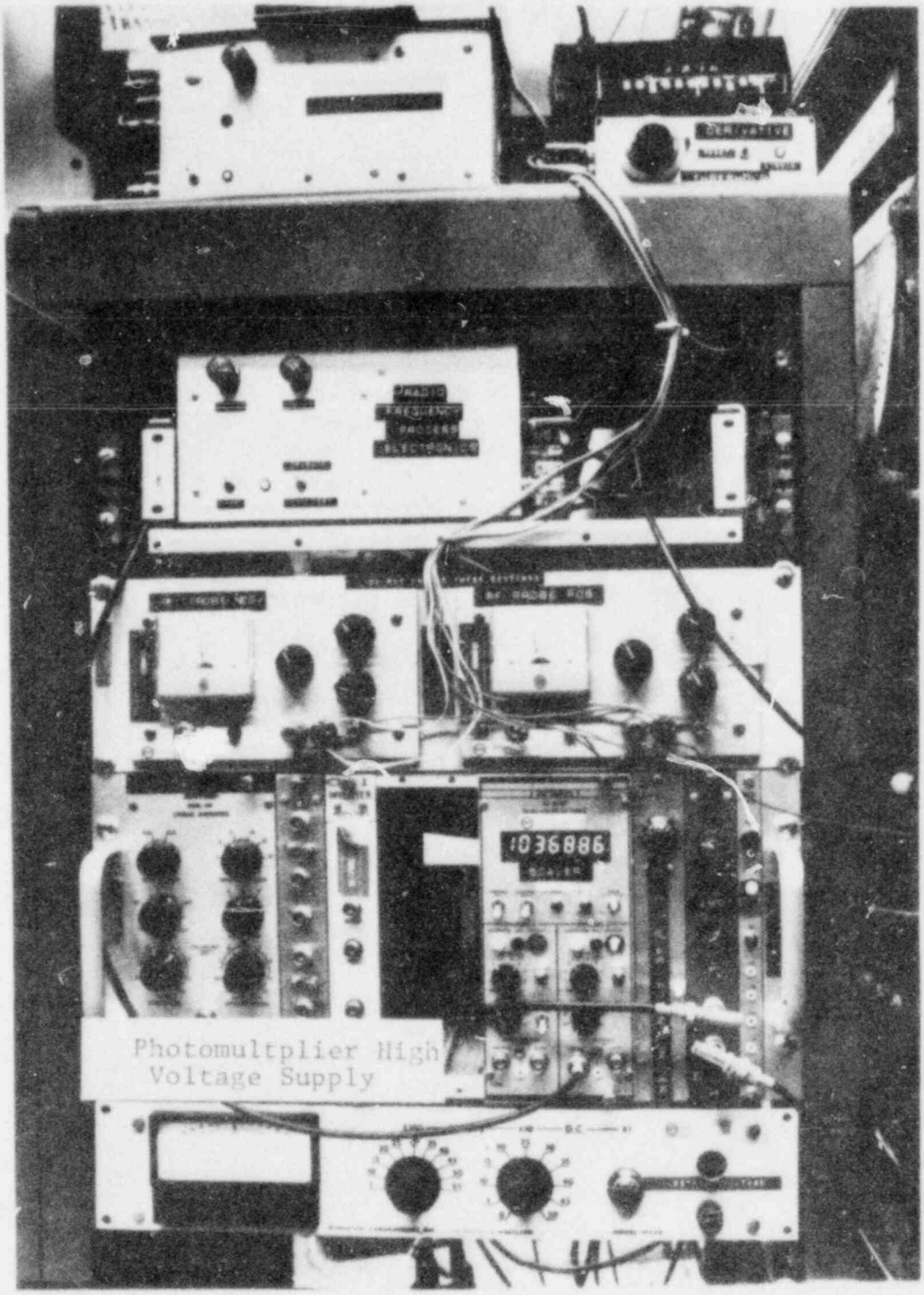

Figure 3.40
The actual level and derivative thresholding electronics in operation

can be directed through the two-phase mixture and the transmitted intensity measured. Obviously the light does not disturb the flow.

A global void fraction measuring device was constructed based on this principle. The device, called an optical digital interferometer, consists of a four by four perpendicular arrangement of light beams, These beams are directed at opposing phototransistors. This arrangement cross hatches a pipe with an optical grid. Interfaces are detected by pulsing the light beams and simultaneously scanning the phototransistor outputs. This technique eliminates cross-talk between the various beams and detectors.

A simple logic system was employed to unfold the void fraction and phase distribution. A void present at a given location will trigger the two corresponding x and y direction phototransistors. These digital signals latch a flip-flop to light the corresponding light emitting diode (LED) on the display board. A schematic of this device is shown in Figure 3.41, for an instantaneous global void fraction of 12.5 percent (2/16). It can be seen than this device should be useful for low quality (bubbly) flow and high quality (droplet) flow, but is not reliable for intermediate qualities.

Solid state electronics were used to drive the LEDs, sample the phototransistors and display the results. The interferometer's driver board is schematically shown in

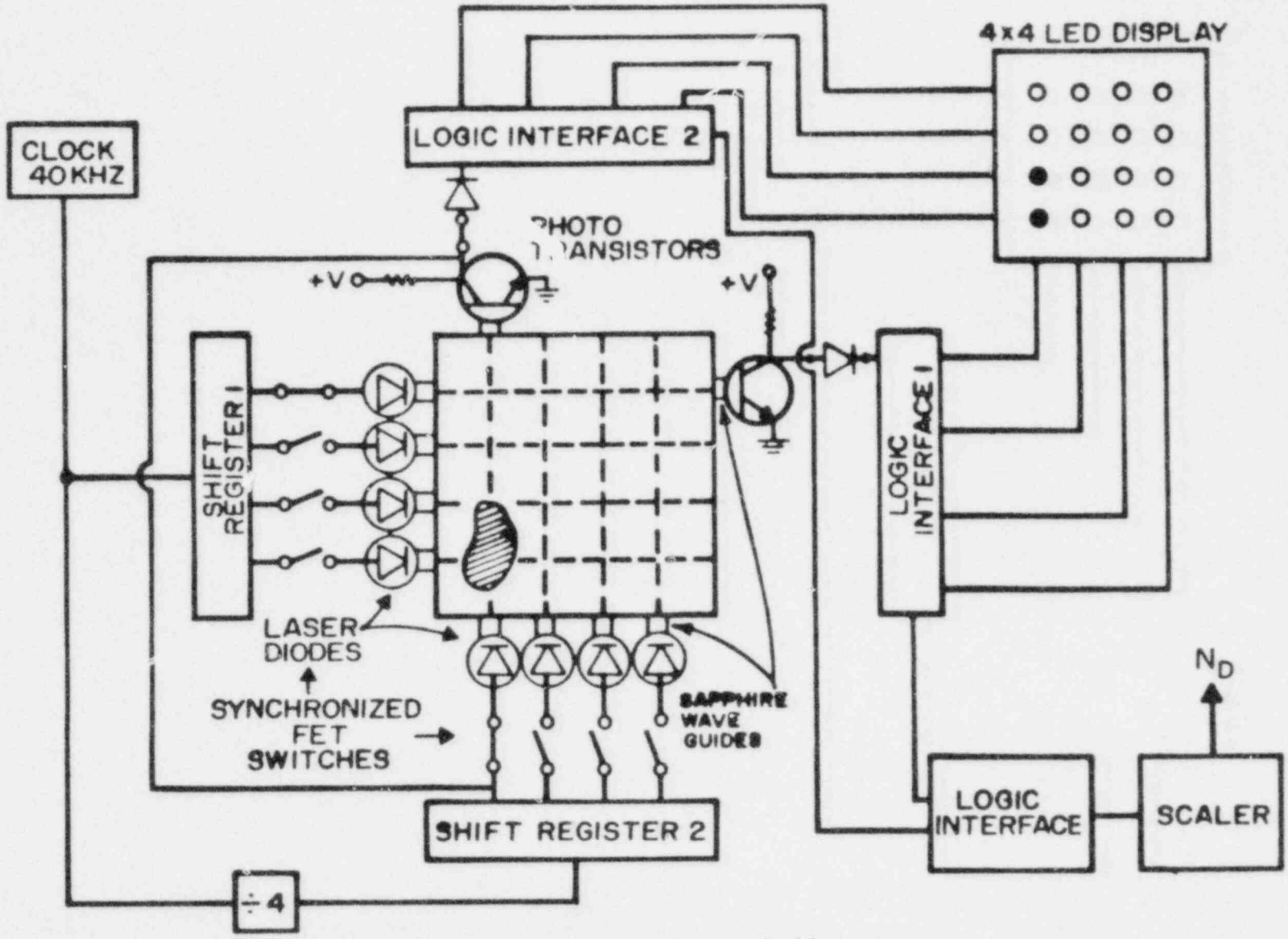

Figure 3.41
A schematic of the RPI optical digital interferometer

Figure 3.42. An adjustable NE 555 astable vibrator produces clock pulses. A SN7400 NAND gate was used to further shape these pulses. The pulse train is sent in two directions; directly to the x-axis SN7496 shift register and to a SN7493 binary counter. The binary counter produces one output pulse for four input pulses. This counter drives the y-axis SN7496 shift register at one quarter the speed of the x-axis shift register. These shift registers drive the LEDs and sample the corresponding phototransistors. As mentioned previously, use of the same trigger signal for the transmitter and receiver avoids crosstalk between the light beams. The shift registers are initialized by a pulse from a SN74121 monostable multivibrator.

The phototransistor output is processed as shown in Figure 3.43 to yield the void distribution. Output from a phototransistor is amplified by a 741 operational amplifier. The gain of this amplifier is adjustable so that all phototransistor channels can be equalized. A 2N2369 transistor is used to gate the operational amplifier output when triggered by the driver board. The x and y signals for corresponding channels enters a SN7410 three input positive NAND gate. This gate will inable a SN7474 flip-flop which triggers the appropriate LED on the display board. Figure 3.44 illustrates the clear and inhibit circuit for the display board.

Introduction and pick-up of the light beams in the two-phase media was done with one eighth inch diameter

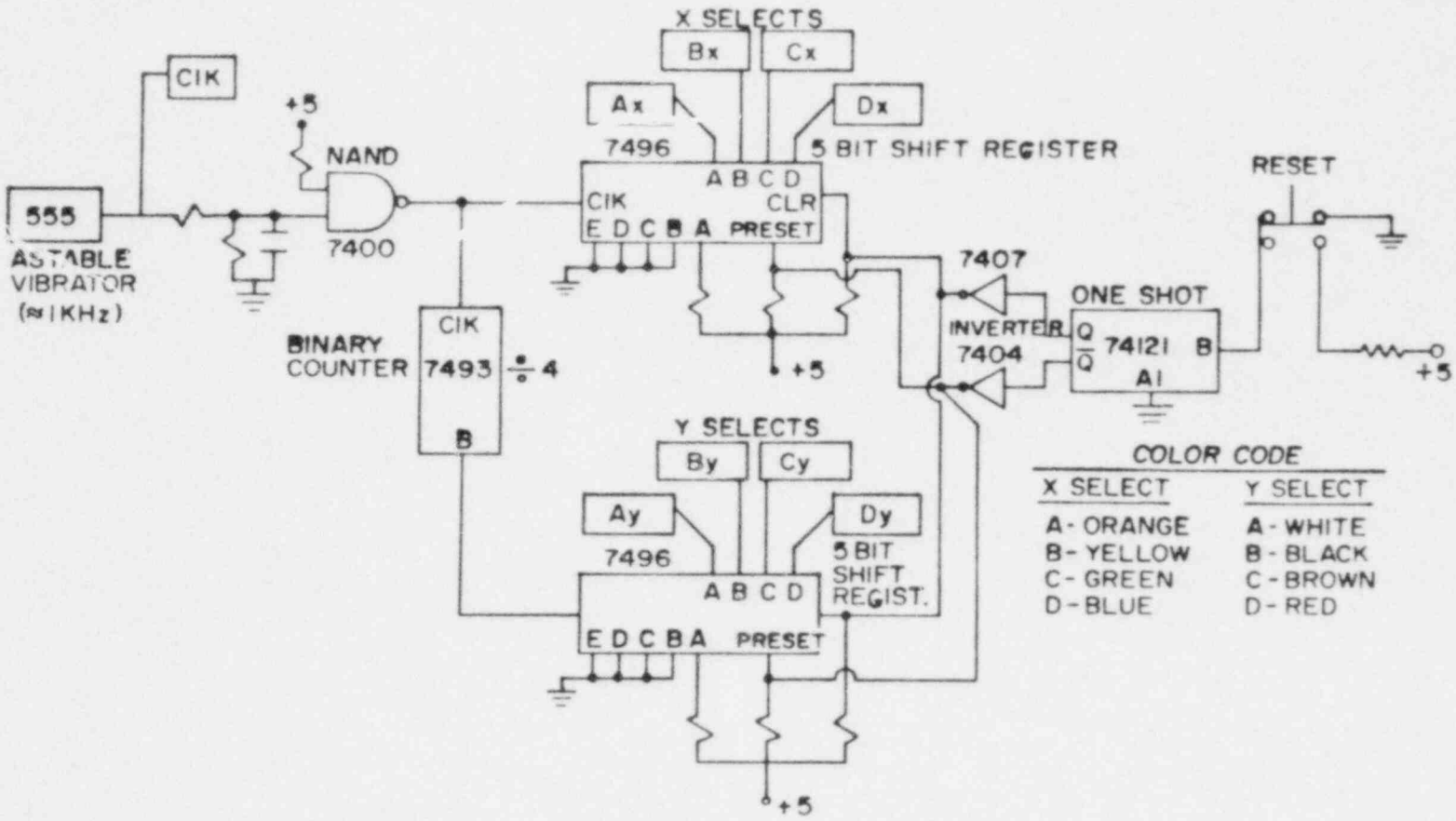

Figure 3.42
A schematic of the optical digital interferometer's driver board

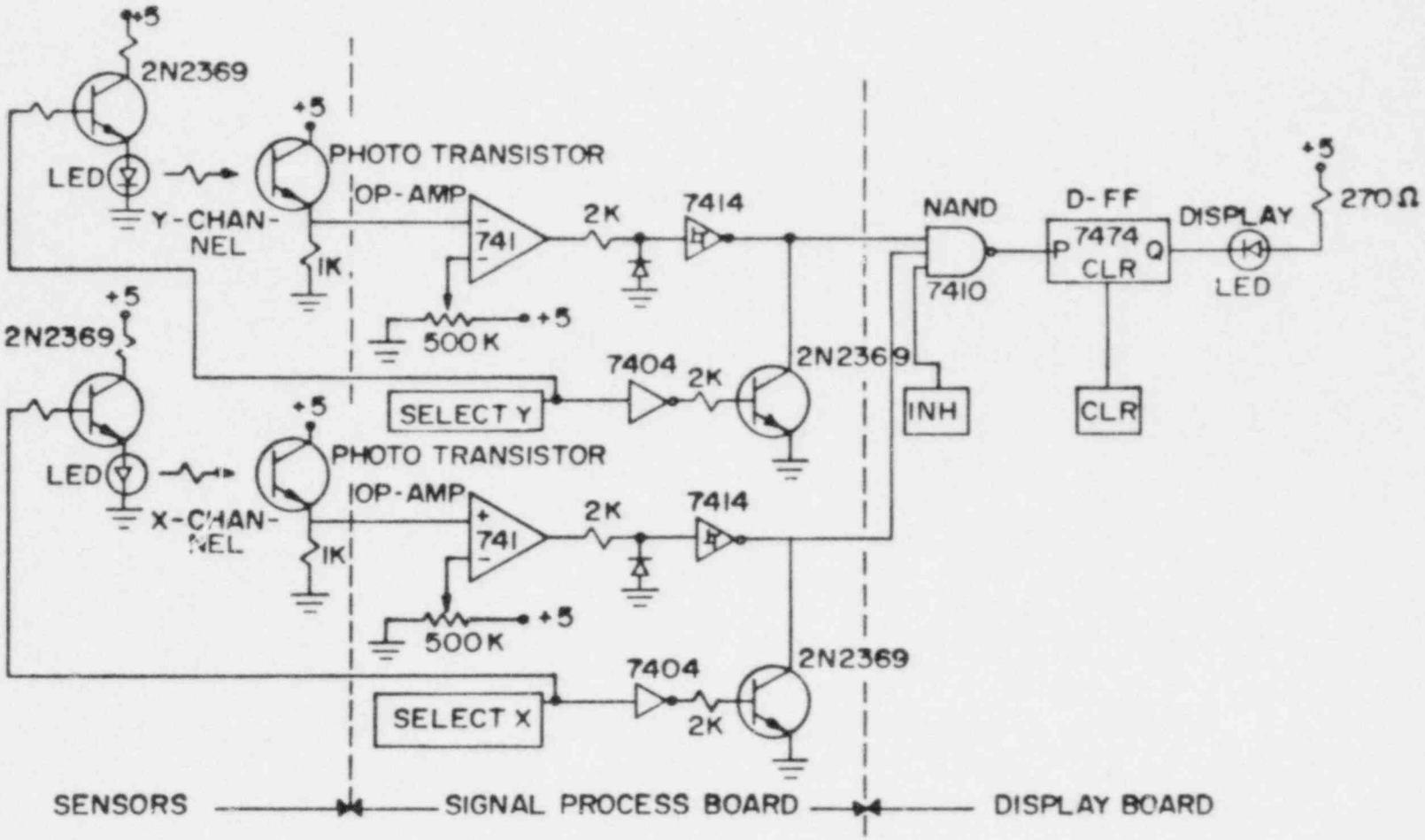

Figure 3.43
A schematic of the photo-transistor output signal processing to yield area averaged void fraction

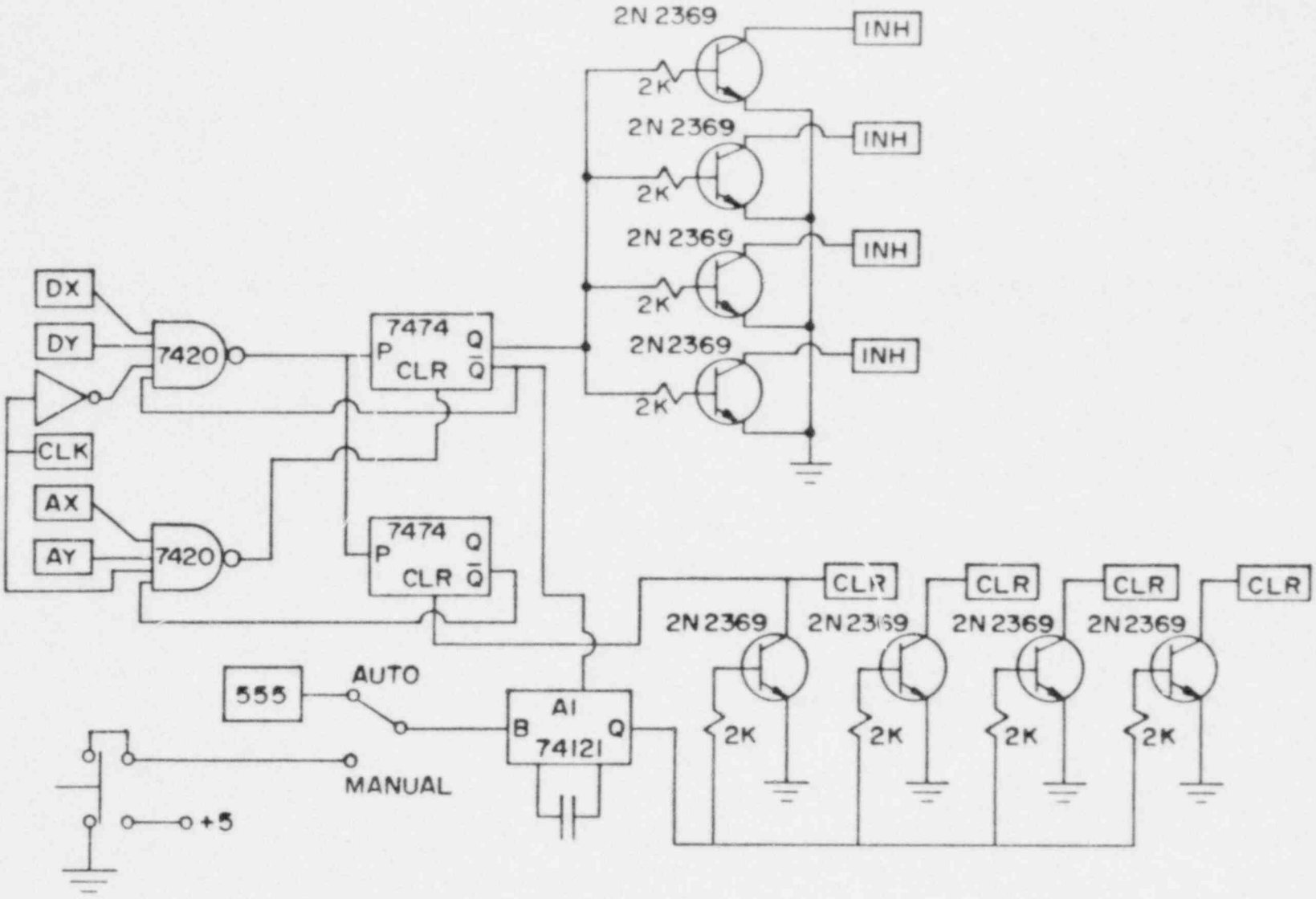

Figure 3.44
The clear and inhibit circuitry for the void fraction LED display

sapphire light pipes. These light pipes were used instead of conventional glass fiber optics because sapphire has better endurance in a high temperature environment. Thus, in principle, this device should also be useful in diabatic two-phase flows. The optical coupling between LEDs or phototransistors and the sapphire light pipes was achieved with General Electric Silicone RTV-615 and SS4120 primer.

The optical digital interferometer was installed in a special small air/water two-phase test section and packaged in a case. Figure 3.45 shows the entire system. A small air pump supplies air to an aquarium airstone located in the base of the test section. A close-up of the void fraction sensing head is shown in Figure 3.46

Light scattering by two-phase flows have been studied extensively [30,39]. A computer model, called BUBRAY, was developed to simulate the optical digital interferometer's performance. This code performs ray tracing in square or round geometries. Fifty rays are initialized at the light beam input location and allowed to reflect and refract through the two-phase media. A ray returning to the tube wall has its position calculated. The location bin associated with that region is tallied.

Output from the model includes data to form a histogram indicating the light distribution around the duct. The individual ray paths can be printed if desired. A simplified flowchart of this code is illustrated in Figure 3.47. Appendix A.6 contains a description of the models

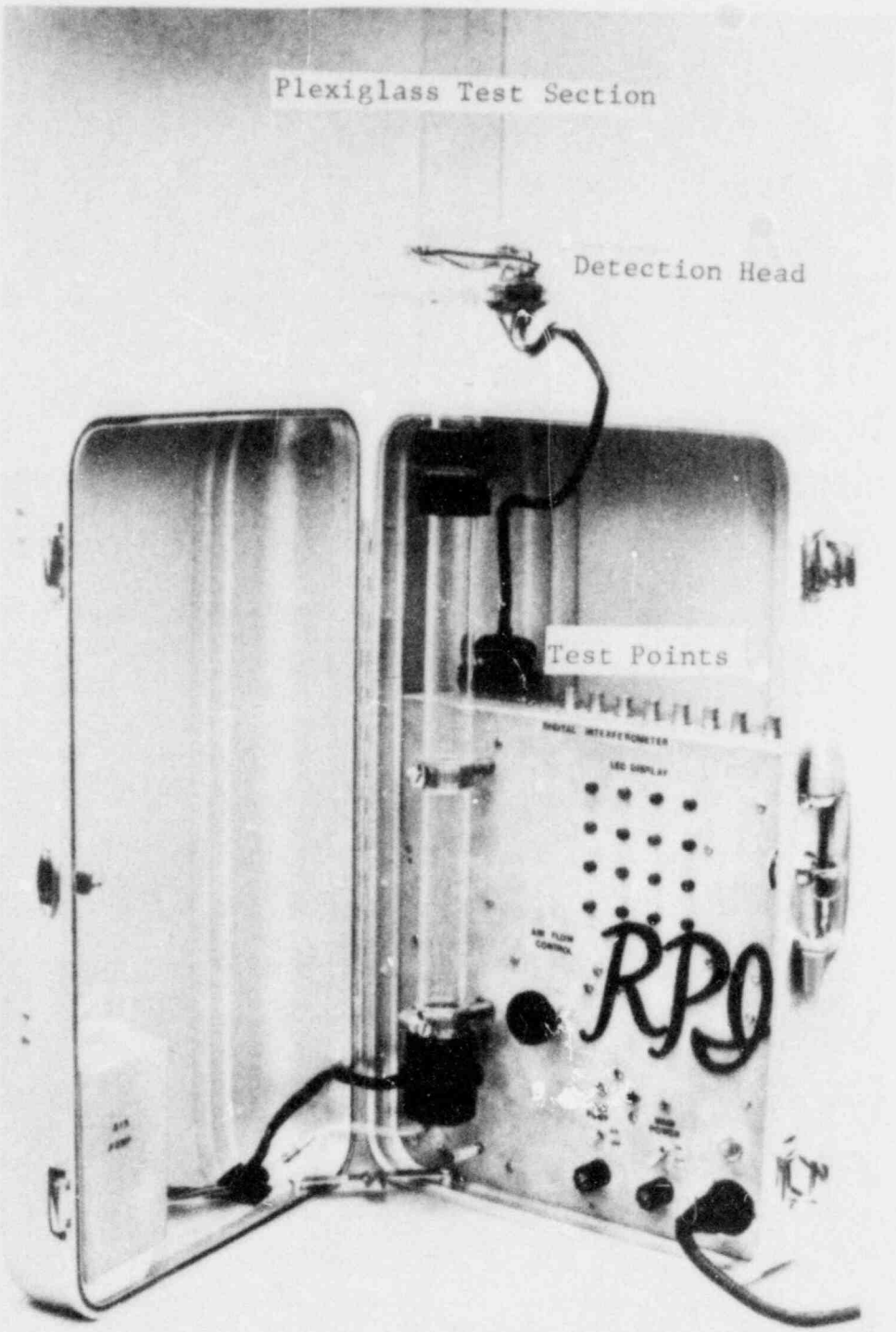

Figure 3.45
The optical digital interferometer and two phase flow loop

Figure 3.46
Close-up of the void detection head

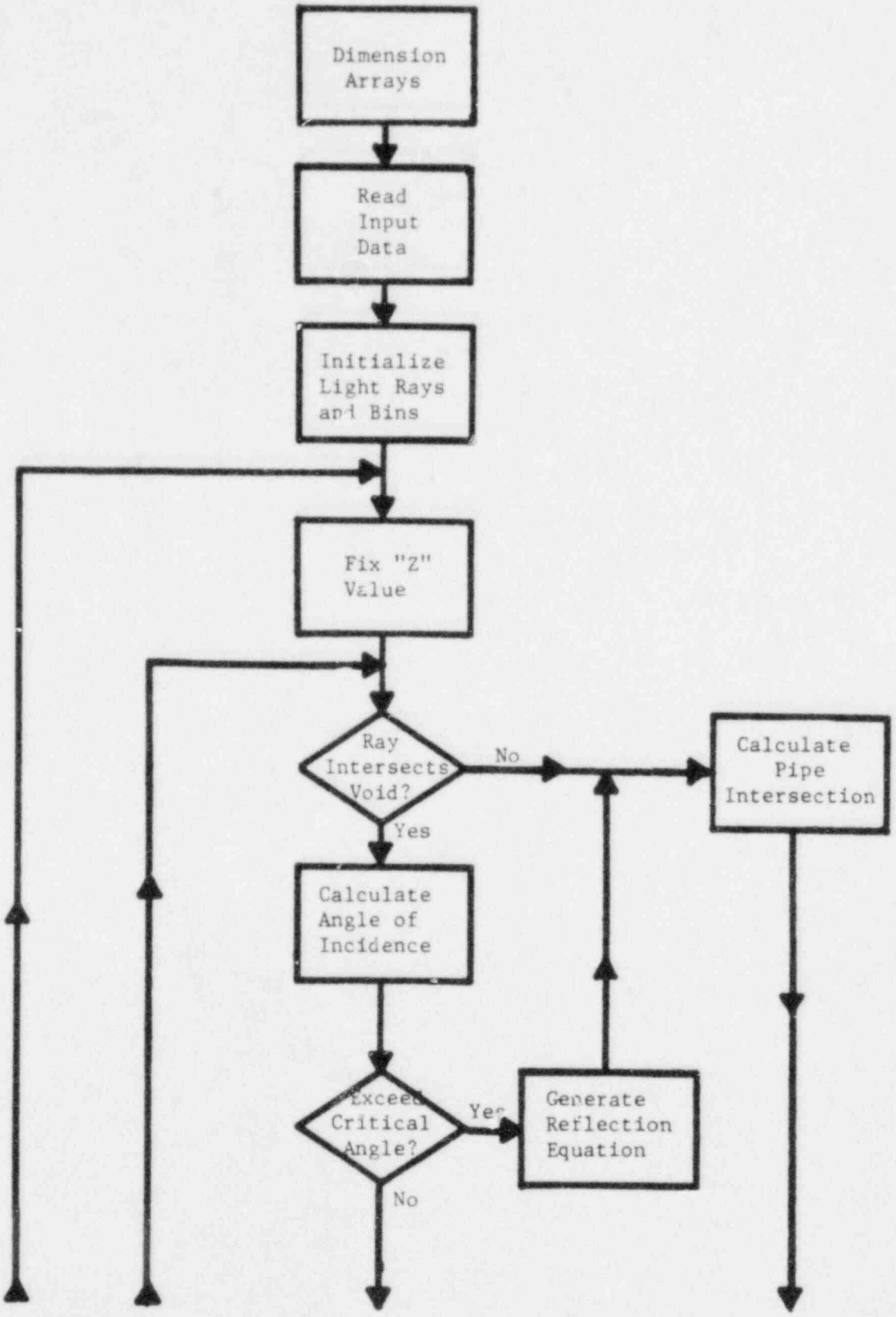

Figure 3.47a A simplified flowchart for the BUBRAY computer code

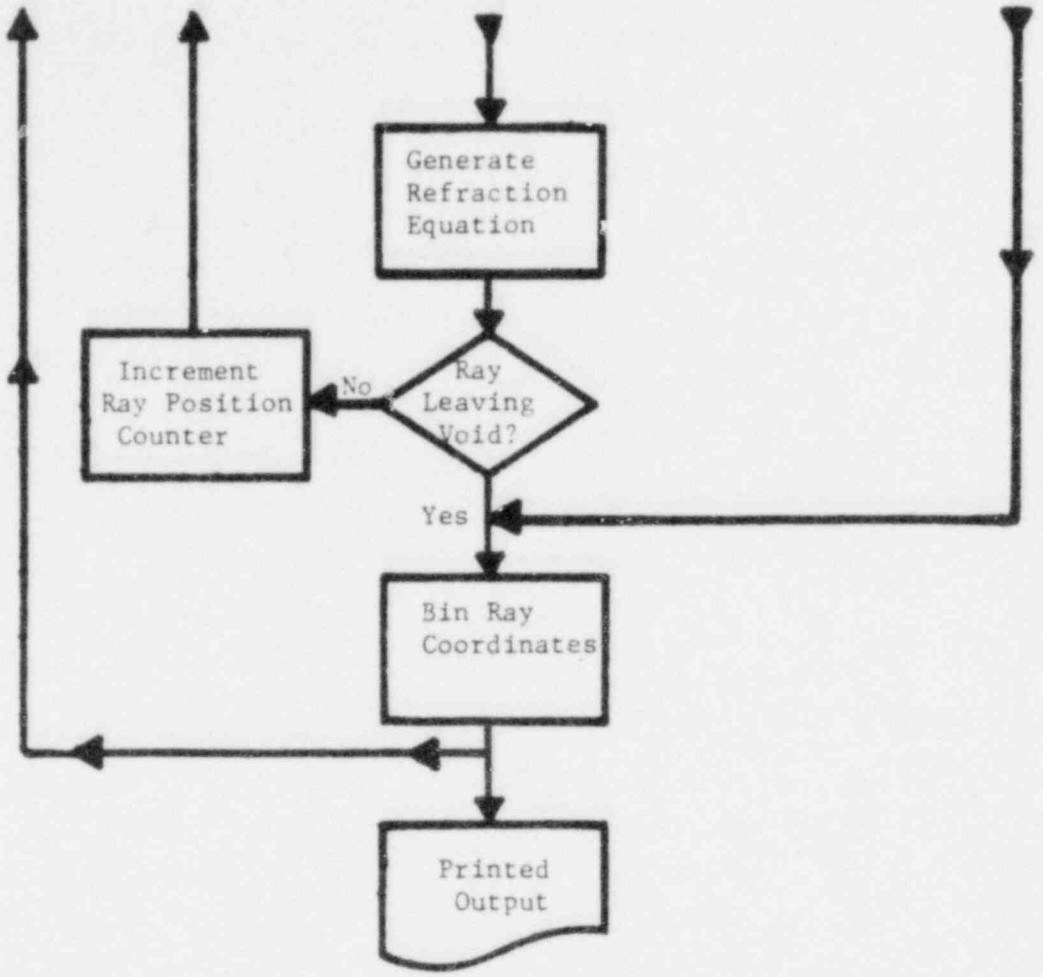

Figure 3.47b Continued

used in BUBRAY, a listing is provided in Appendix A.7.

Several parameters were studied using the BUBRAY computer code. These parameters included:

1) Water film on the duct during annular flow.
2) Bubble or droplet size.
3) Bubble position.

Small angled water films do not affect the digital interferometer's operation. However, a water film angle of thirty degrees generated the histogram as shown in Figure 3.48. This can be compared with the histogram, shown in Figure 3.49, for similiar conditions except that the water film had an angle of zero degrees. Clearly a steep film gradient (eg: in a roll wave) will refract the incident light rays considerably.

The light scattering pattern is a strong function of the bubble size. Figure 3.50 shows the scattering associated with a relatively small bubble. The large curvature of the interface causes this wide distribution. A large bubble, in contrast, barely disturbs the transmitted rays, as shown in Figure 3.51.

Bubble position was also studied. The digital interferometer should experience depth perception. Figure 3.52 displays the histogram associated with a small bubble, close to the light source. If the same conditions are maintained but the bubble is moved away from the source, the histogram, shown in Figure 3.53, exhibits considerably less scatter. This is reasonable since, a void close to the

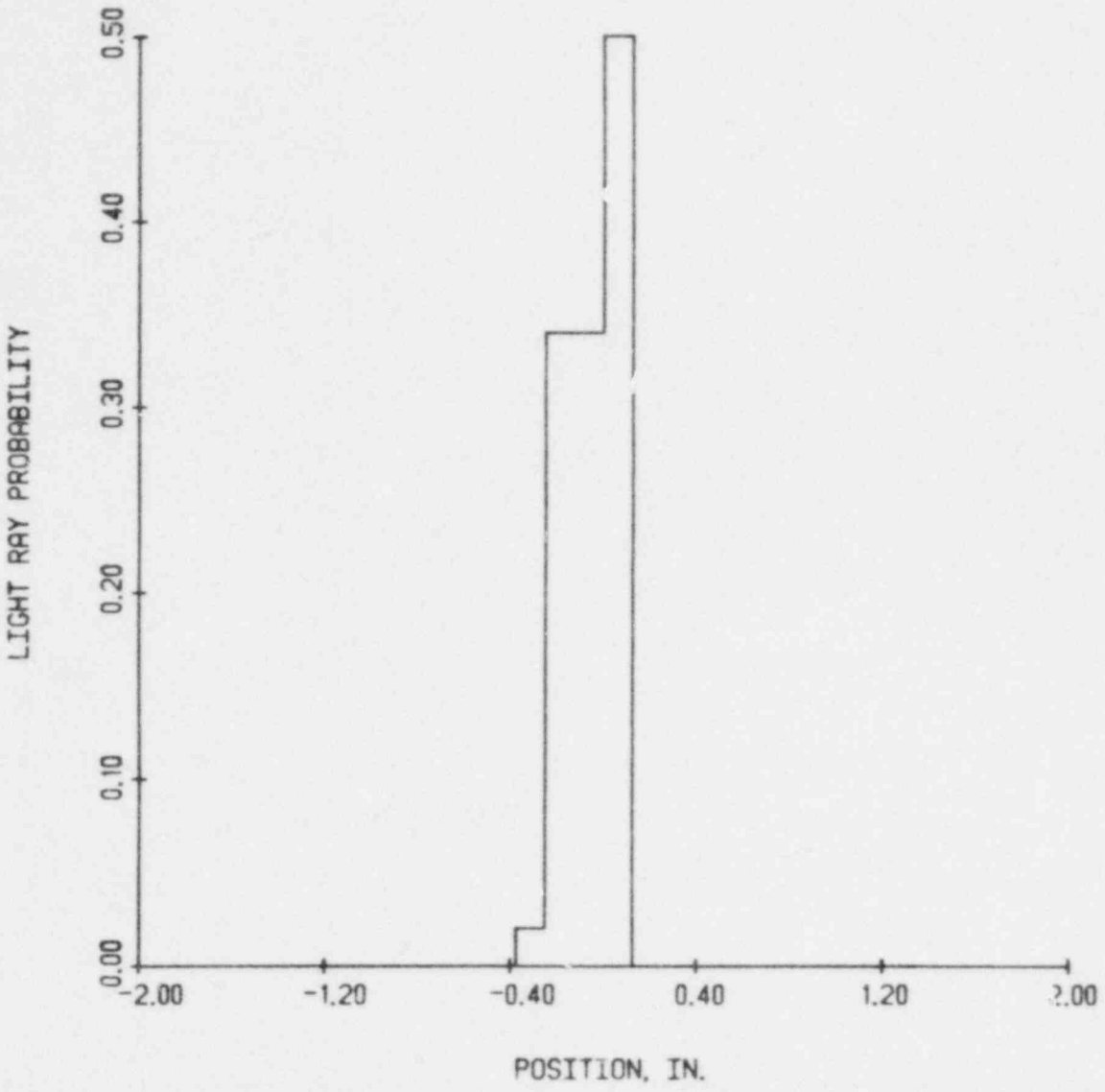

Figure 3.48 The light ray scattering in annular flow due to a water film inclined at 30 degrees

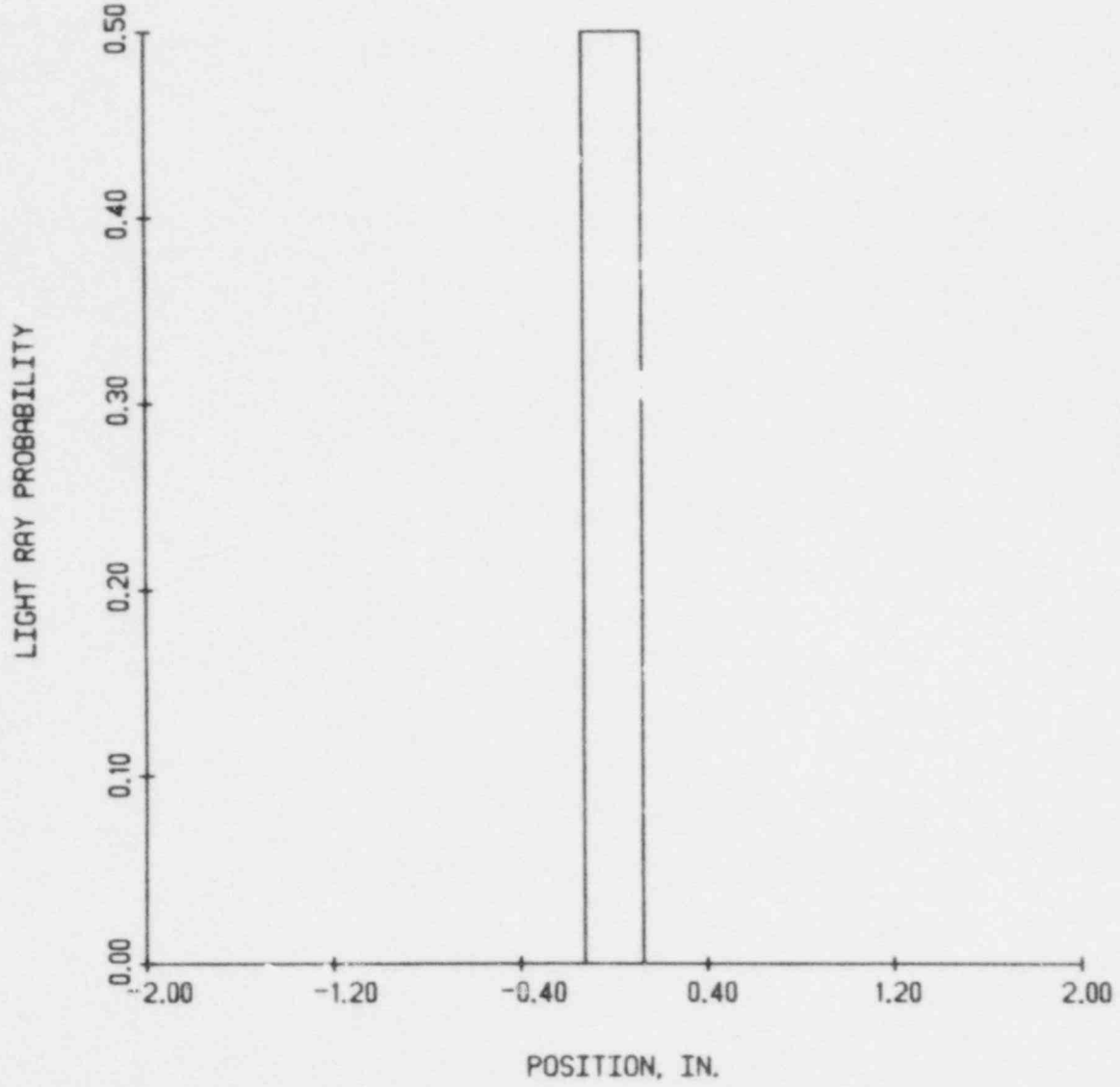

Figure 3.49 The light ray scattering in annular flow due to a water film inclined at 0 degrees

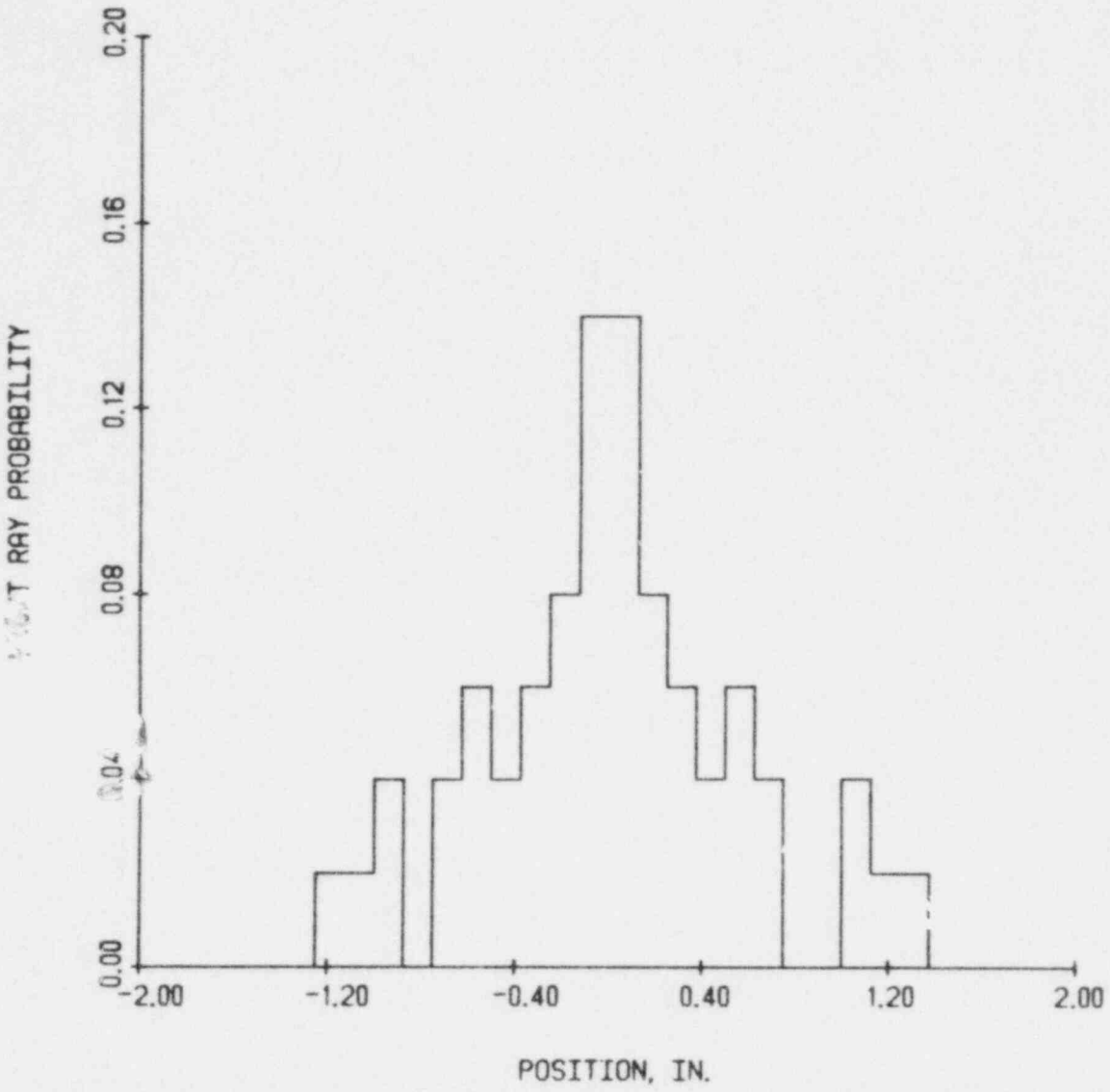

Figure 3.50 The light ray scattering due to the presence of a small void

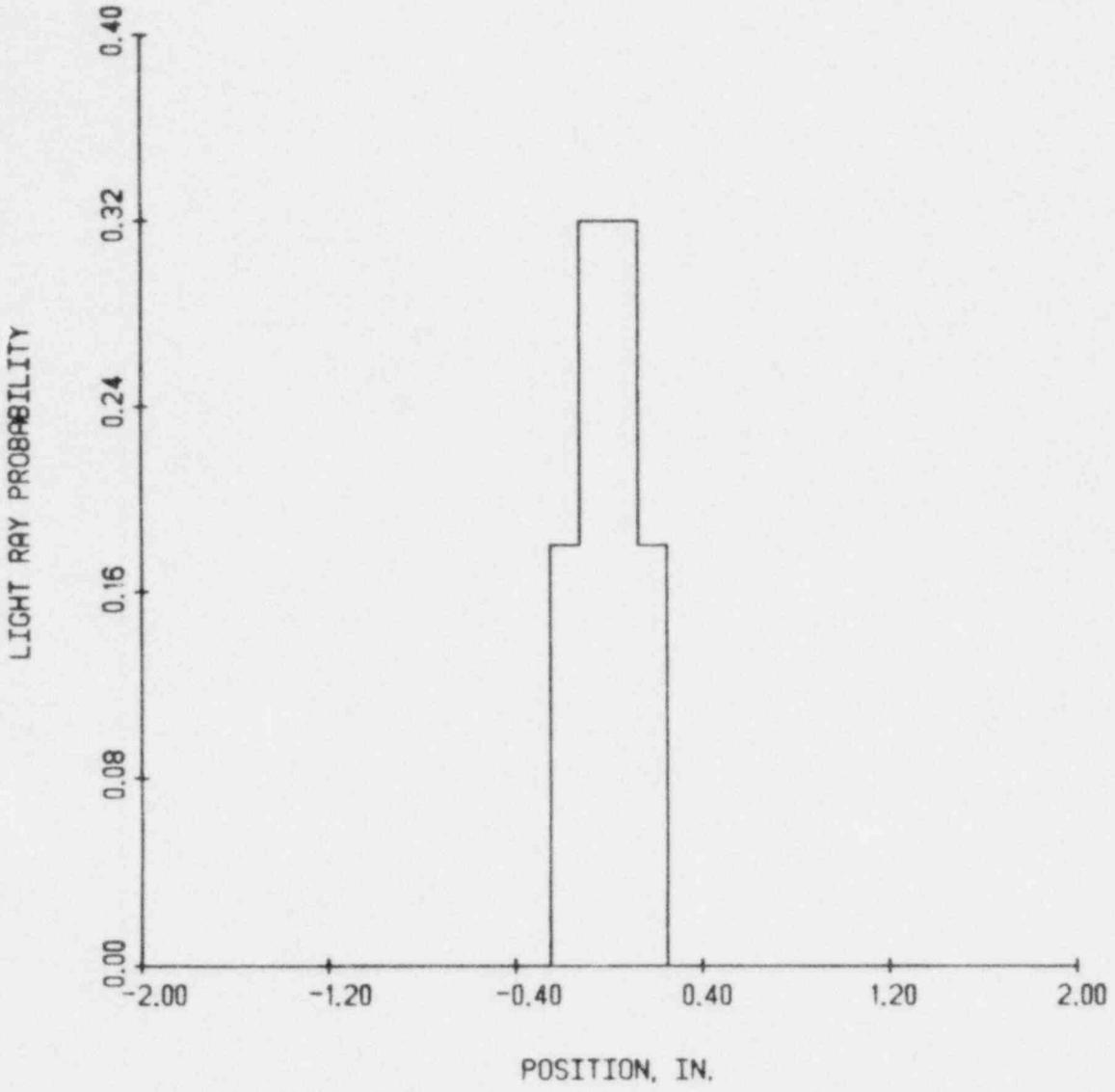

Figure 3.51 The light ray scattering due to the presence of a large void

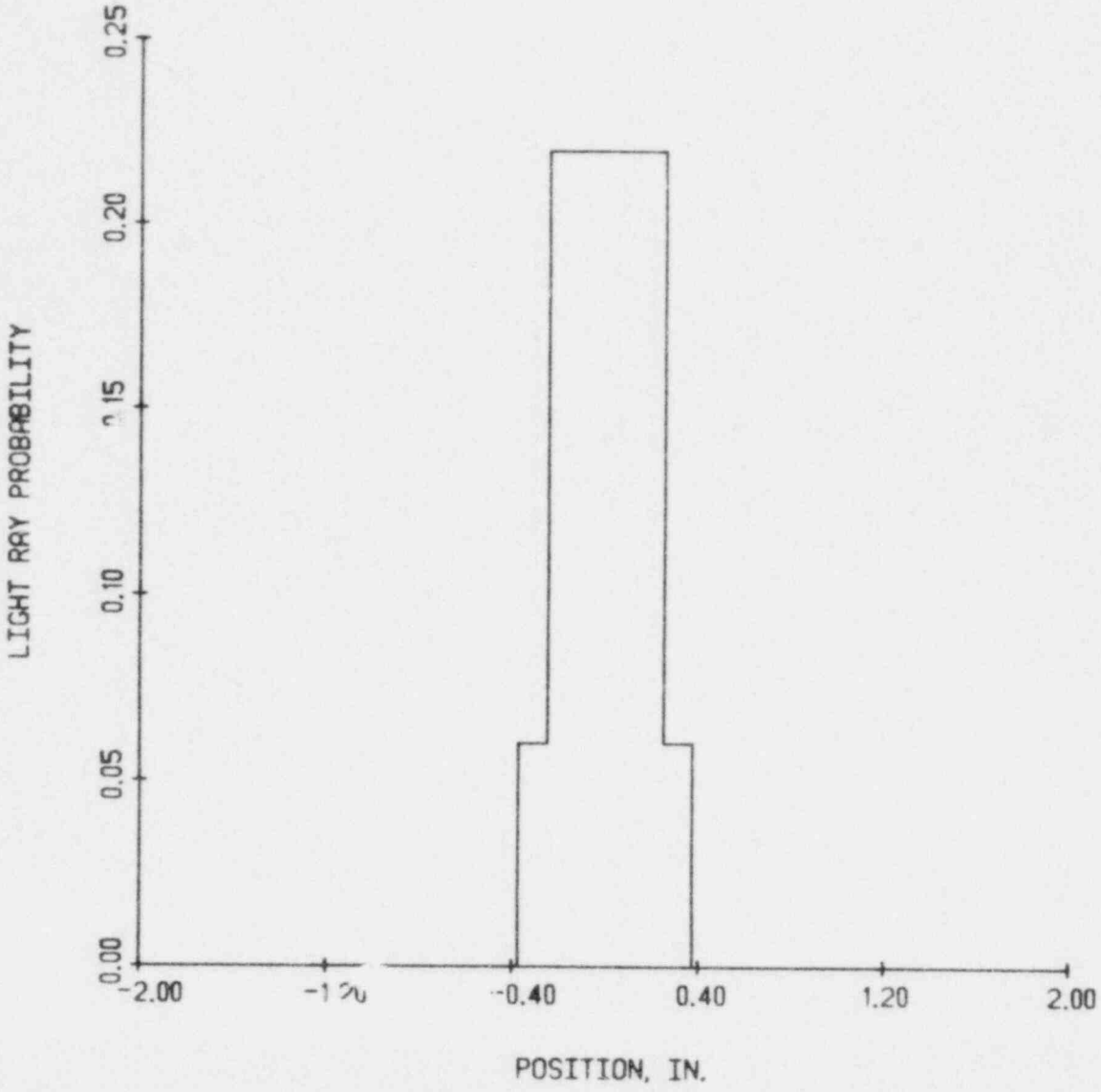

Figure 3.52 The light ray scattering caused by a void close to the light source

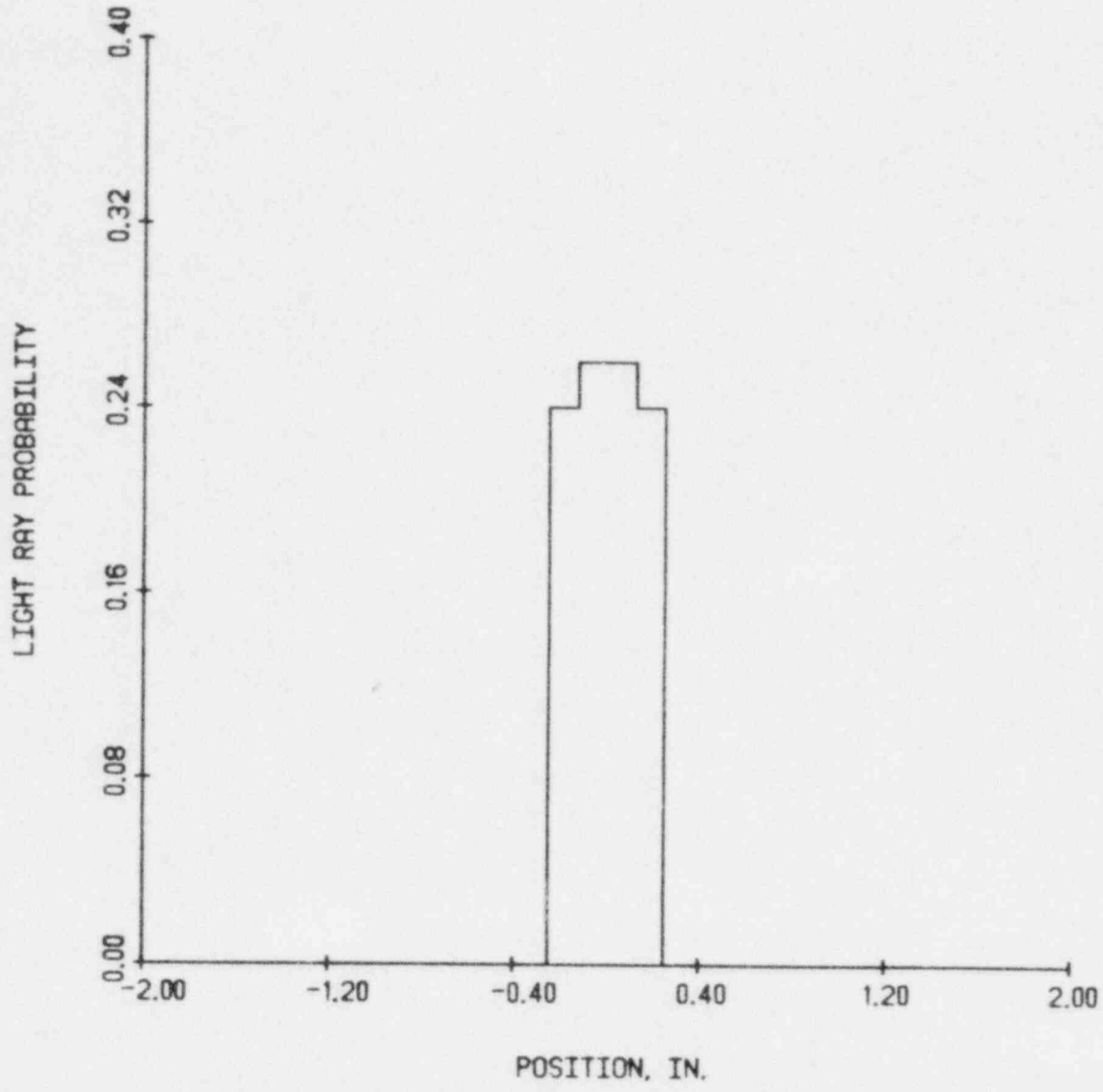

Figure 3.53 The light ray scattering caused by a void far from the light source

light source acts as a lens and causes the rays to diverge further after refracting.

Several limitations must be placed on the application of the optical digital interferometer for void fraction measurements. This device requires square light beam mesh. This arrangement is not always possible since internal components may block the light beams. However, pipes are round and a square mesh can leave regions unmapped. In addition, in a large conduit it is difficult to keep the light beams collimated.

As mentioned previously, the optical digital interferometer has application only in the low and high void ranges. It is interesting to note, however, that this device can detect droplets in annular flow. A schematic of the bench test run to verify this capability is shown in Figure 3.54.

Computer simulation and operating experience indicate that for conditions where the void fraction data obtained from the optical digital interferometer is difficult to interpret, (i.e.; intermediate void fractions), other techniques such as radiation attenuation or global capacitance gauges are reasonably reliable. This is fortunate since these devices are not reliable in the low and high void region, where the optical digital interferometer appears to be accurate.

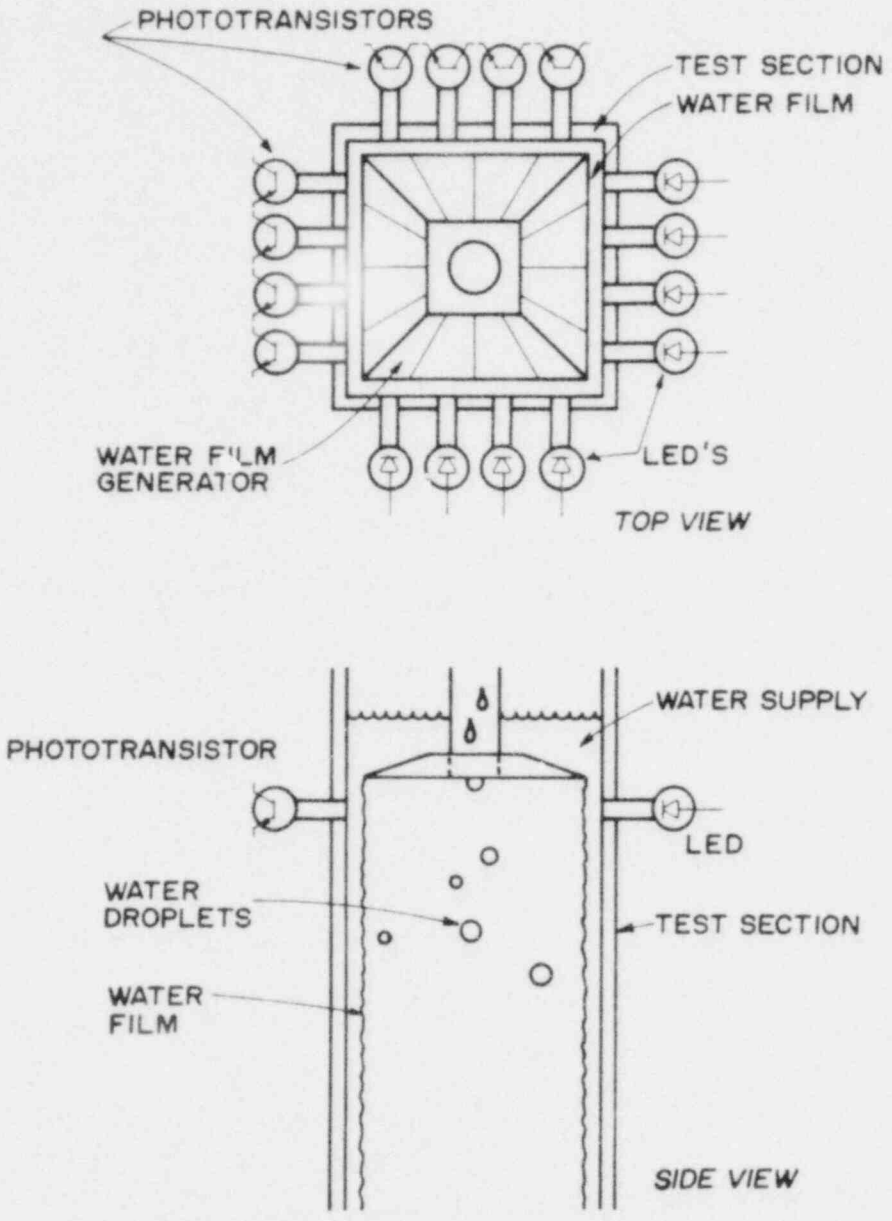

Figure 3.54
A schematic of entrained droplet detection test performed with the optical digital interferometer

4. PDF AND P. RESULTS

A large amount of air/water two phase flow chordal-average void fraction data was taken using the x-ray system. This data included zero and non-zero liquid flow cases. In all, forty-nine sets of data were acquired and processed. Each set consisted of six chordal measurements, including one along the diameter and one adjacent to the tube wall. The flow was found to be axisymetric so, as shown in Figure 4.1, data was only taken on one side of the tube. A plot of the air/water superficial velocities measured are shown in Figure 4.2 with flow regime boundaries. It can be noted that the data is concentrated in the regions in which flow regime transition was expected. For ease of display all data taken at zero liquid superficial velocity has been placed at one thousandth of a meter per second. The flow regimes indicated in Figure 4.2 were determined from direct visual information.

Each measurement consisted of twelve thousand eight hundred (12,800) instantaneous void fraction readings at each chordal location. These data were collected at a rate of two hundred samples per second. A sixty-four second sample time was determined to be large enough to insure a statistically stationary chordal-average void fraction value for all flow regimes tested.

The normalized PDF was formed from all the acquired data points in each chordal void measurement. This histogram was further analyzed by computing the various

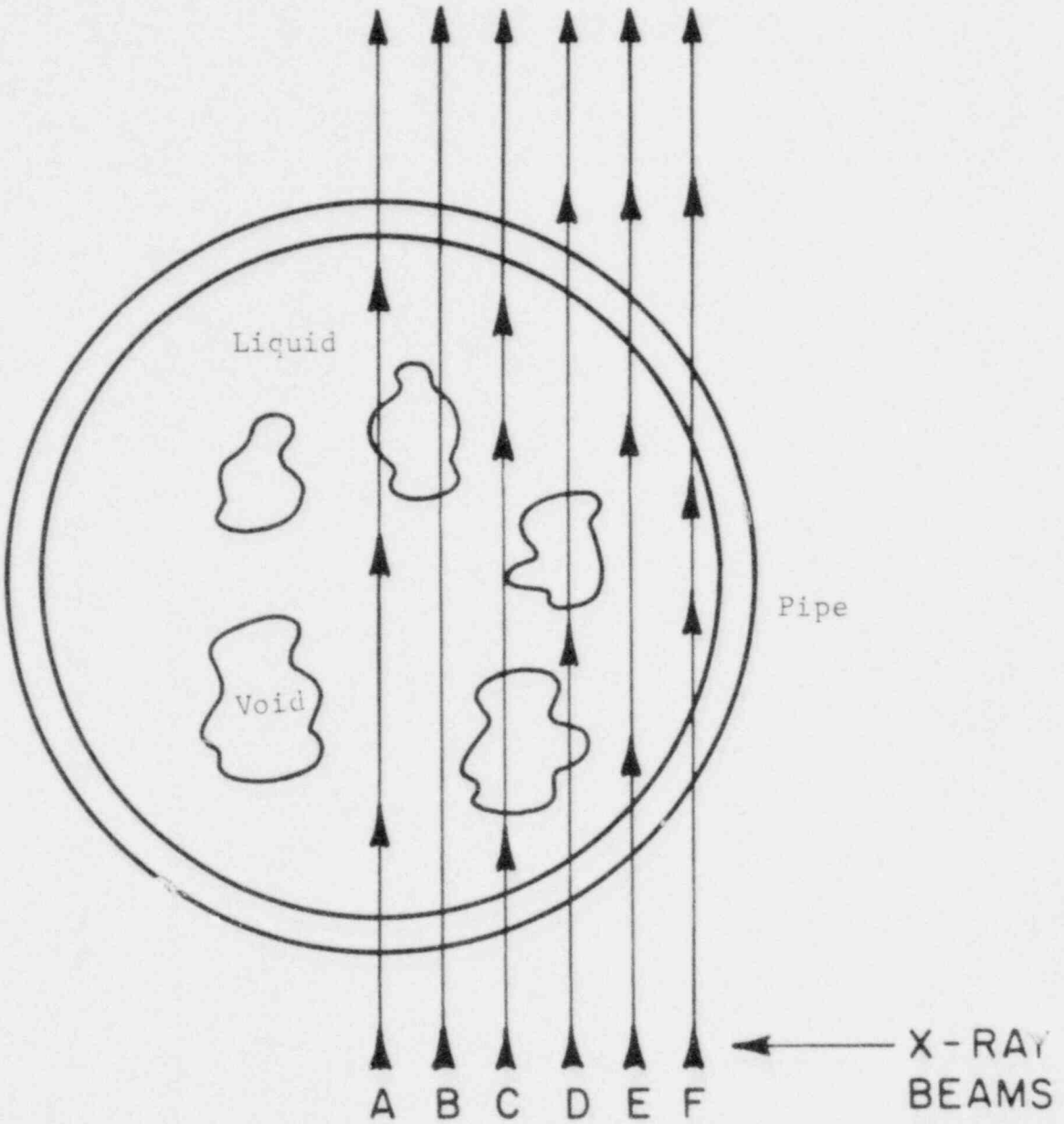

Figure 4.1
The six chords at which chordal void fraction measurements were made

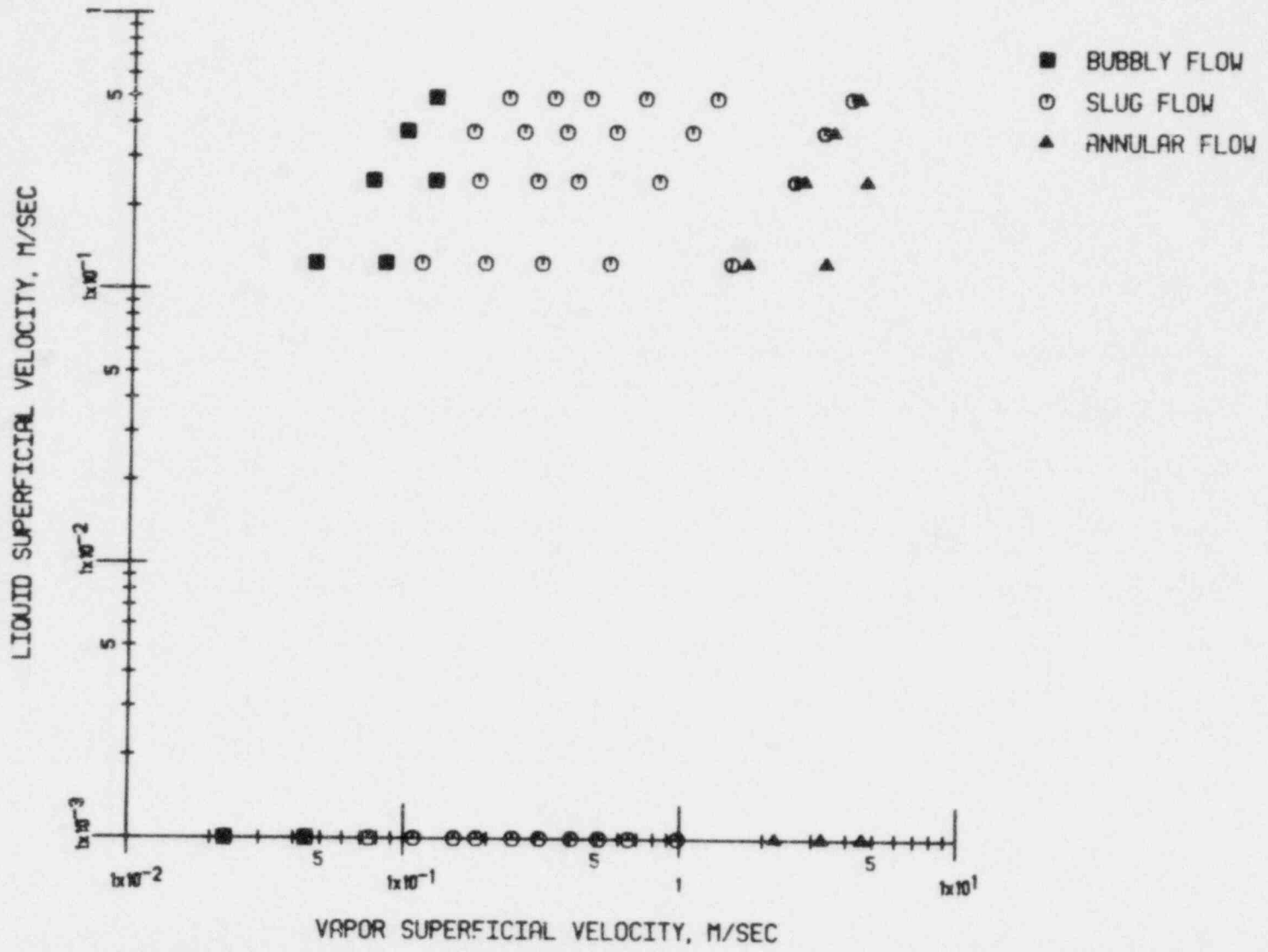

Figure 4.2 A flow regime map based on visual observation of the two-phase flow

moments associated with it.

The first one thousand twenty-four (1024) points were used in forming the PSD because of the limitations on the PDP-15 computer's central memory. A sampling frequency of two hundred per second results in a Nyquist frequency of one hundred hertz or one half the sampling rate. To minimize aliasing errors the break frequency of the active low pass filter was set at 100 hz. This data set size, and the associated Nyquist frequency, set the frequency resolution at slightly greater than one half Hertz. The moments of the PSD were calculated in a fashion identical to the PDF. Different parts of the full data set were ensemble averaged to insure that the first one thousand twenty-four point set produced a representative power spectrum.

The effects of Hamming and Hanning windows [40] were also investigated. Application of a data window changed the total amplitude of the spectrum but did not change its shape. Thus, no windowing was performed on the data presented herein.

The x-ray machine measured the PDF shown in Figure 4.3 for zero void fraction. The PDF appears to be almost a perfect spike at zero void. Actually, this distribution is a normal distribution with a very small variance. The x-ray system developed at RPI obviously had a more stable photon output than the one used previously by Jones [6].

Chordal-average void fraction profiles for zero liquid flow are shown in Figure 4.4. These profiles are

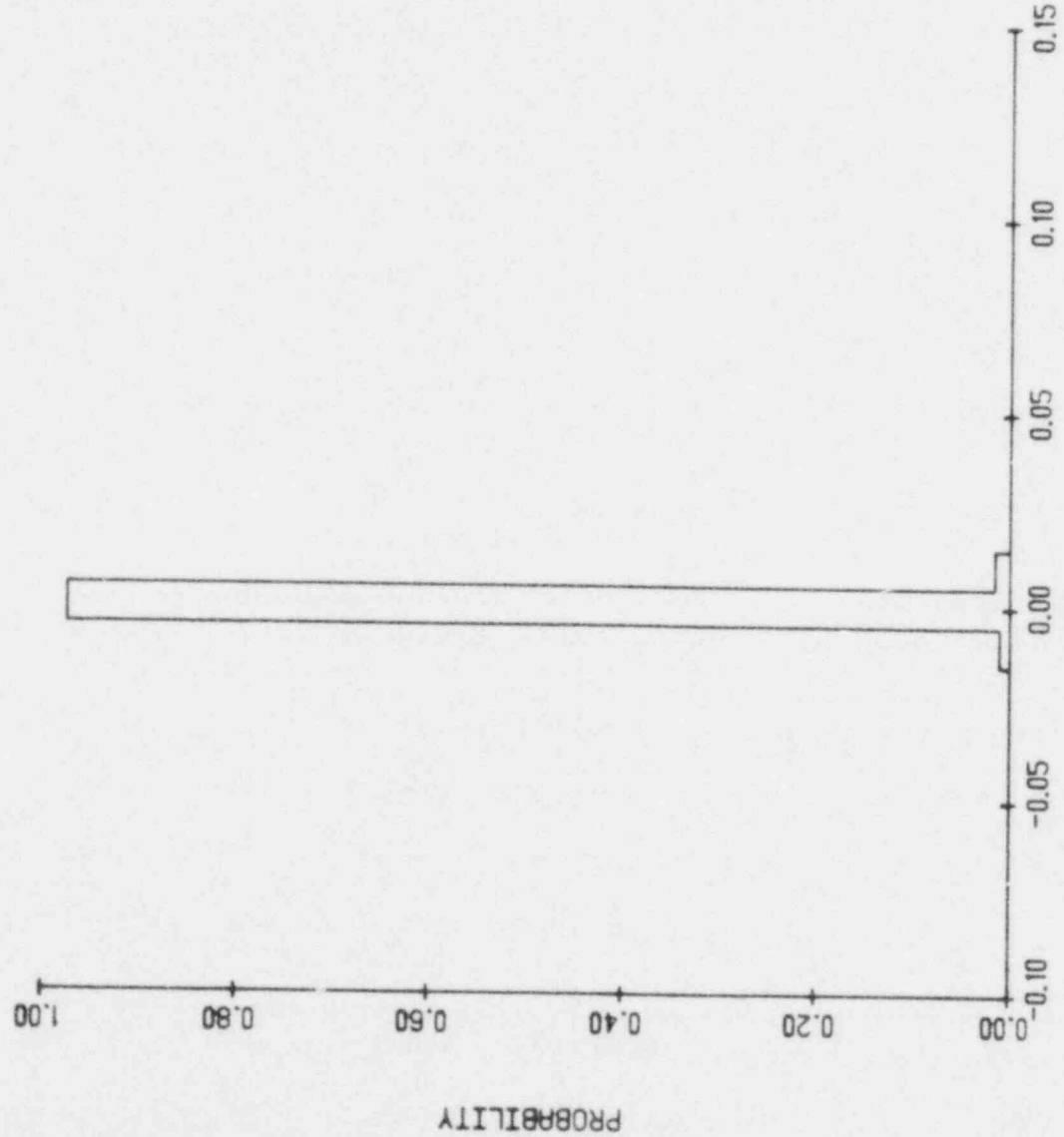

Figure 4.3 The PDF for single phase liquid flow i.e. void fraction equal zero

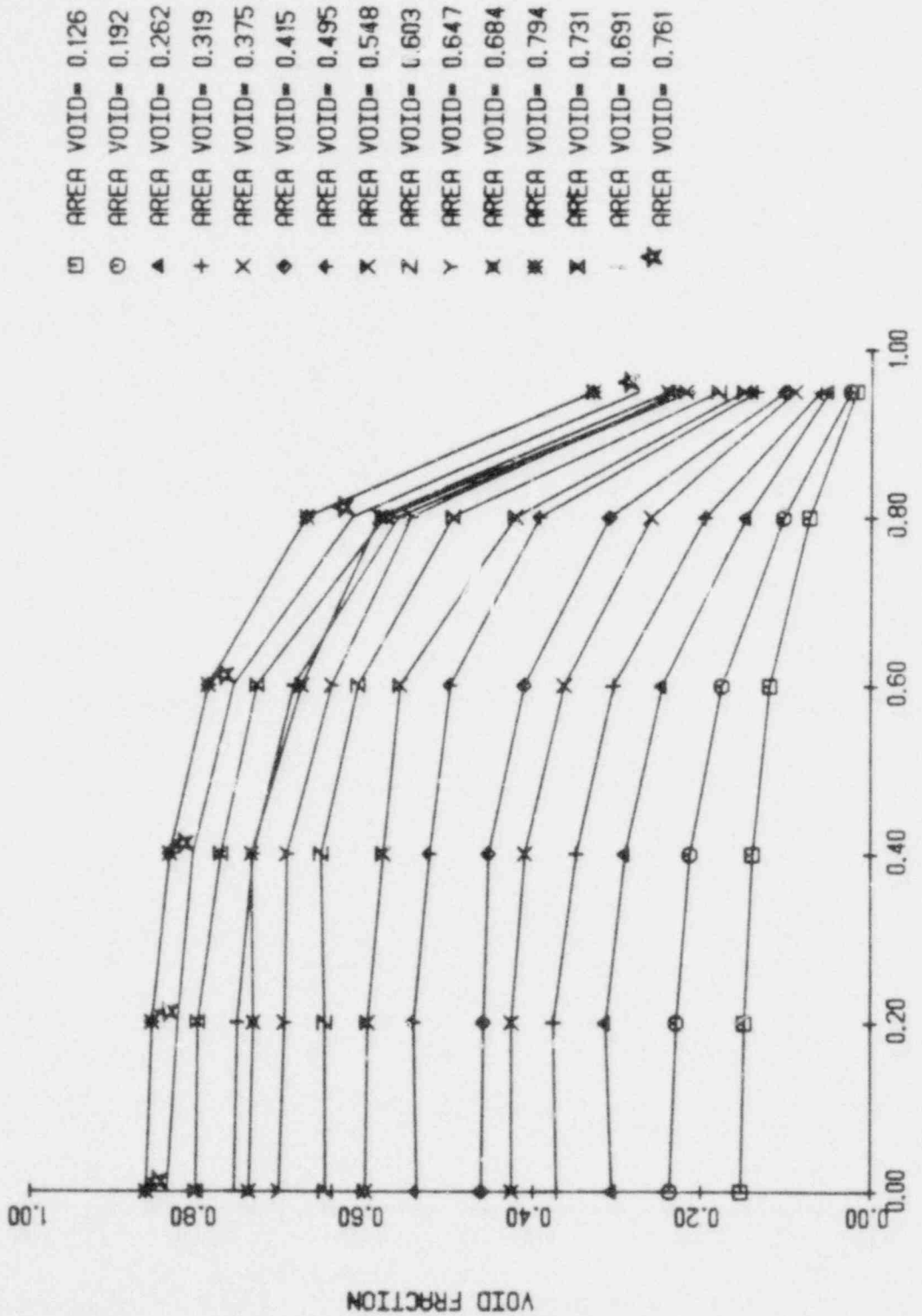

Figure 4.4 The time averaged chordal void fraction vs. radial position for J_f=0.00 m/sec

categorized by their associated area-averaged[3] void fraction, as specified in the legend of the graph. It can be seen that the void fraction profiles associated with zero liquid flow are relatively flat over most of the pipe. Non-zero liquid flow cases can have slightly lower void fractions near the wall region.

4.1 Visual Data

Photographs and visual observation were taken of each two-phase condition studied. At low liquid velocity, visual flow regime identification is easily made for bubbly or slug flow. Higher liquid velocity makes visual flow regime distinction more difficult.

Churn-turbulent flow is relatively easy to observe, however, the transistion from slug to churn-turbulent flow is very difficult to detect visually.

The conclusions drawn from visual observation can differ, depending on the observer. Photographs, while providing a fixed picture of the two-phase flow, indicate the conditions in a given region at a particular instant. Steady-state flow regimes usually span most of the test section, thus a photograph of the entire pipe is required to attempt a reasonable flow regime estimate. Visual methods are subjective and accurate conclusions regarding flow regime boundaries cannot normally be made. Photographs of

---

[3] The area-average void fractions were determined by numerically integrating the corresponding chordal-average void fractions (see Appendix A.9)

some of the two-phase conditions studied are included with the PDF and PSD measured along the tube diameter. The reader is cautioned, however, that they illustrate only the instantaneous phase configuration in one part of the test section.

4.1.1 Centerline PDF and PSD Distributions

Photographs of some of the two-phase mixtures are displayed with the diametric PDF and PSD. The diameter distributions were selected because they are representative of the conditions prevailing in the entire pipe.

The PDF, PSD and two-phase mixture associated with an area-averaged void fraction of 13 percent are illustrated in Figures 4.5 to 4.9. The liquid superficial velocity studied are 0.0, 0.12, 0.25, 0.37, and 0.50 m/sec, respectively. A unimodal PDF, typical of bubbly flow, is observed. A sharp peak is also observed at zero void fraction due to the measurement associated with the liquid phase only. Jones [6] did not observe this peak, apparently because of the resolution of his system.

The associated PSD increases in bandwidth with increasing liquid velocity. This result is expected since void transit time is decreasing. The amplitude of the PSD decreases with increasing liquid velocity as the energy is more broadly distributed.

Figures 4.10 to 4.14 illustrate the PDF, PSD and two-phase mixture associated with a 20 percent area-averaged

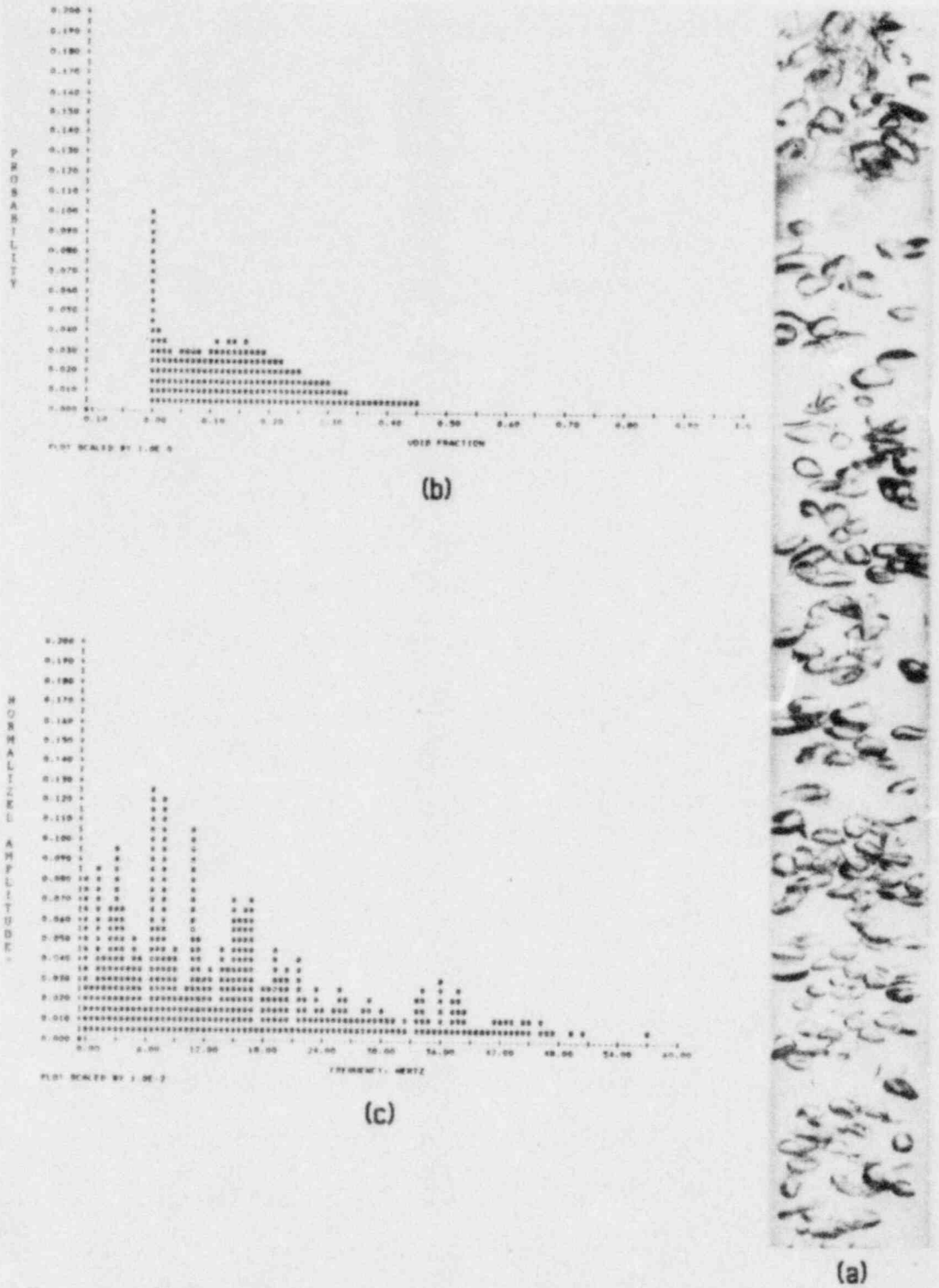

Figure 4.5

A photograph (a), diameter PDF (b), and diameter PSD (c), for 13 percent area-averaged void fraction, j_f=0.0 m/sec, j_g=0.23 m/sec

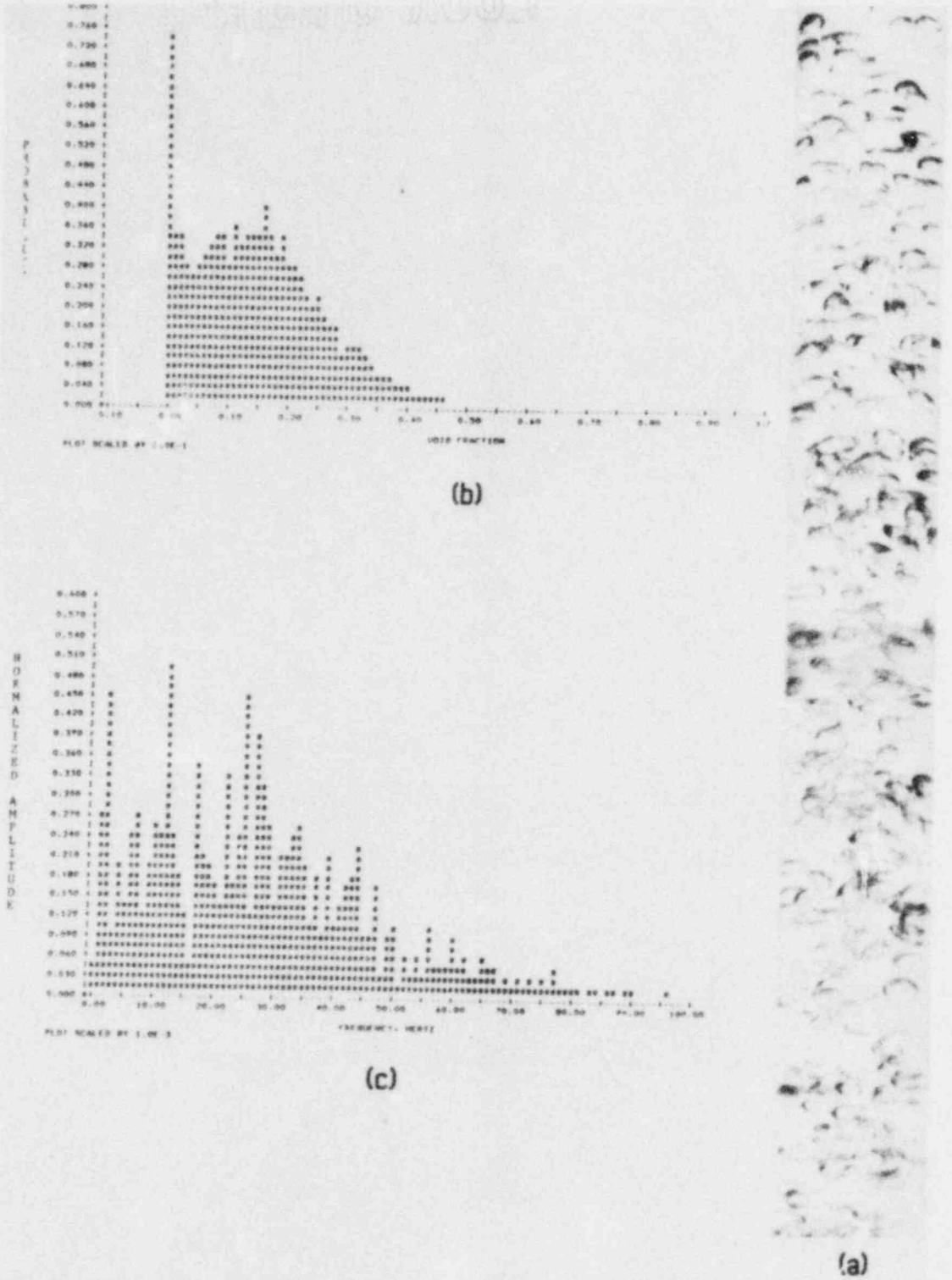

Figure 4.6

A photograph (a), diameter PDF (b), and diameter PSD (c), for 13 percent area-averaged void fraction, j_ℓ = 0.12 m/sec, j_g=0.045 m/sec

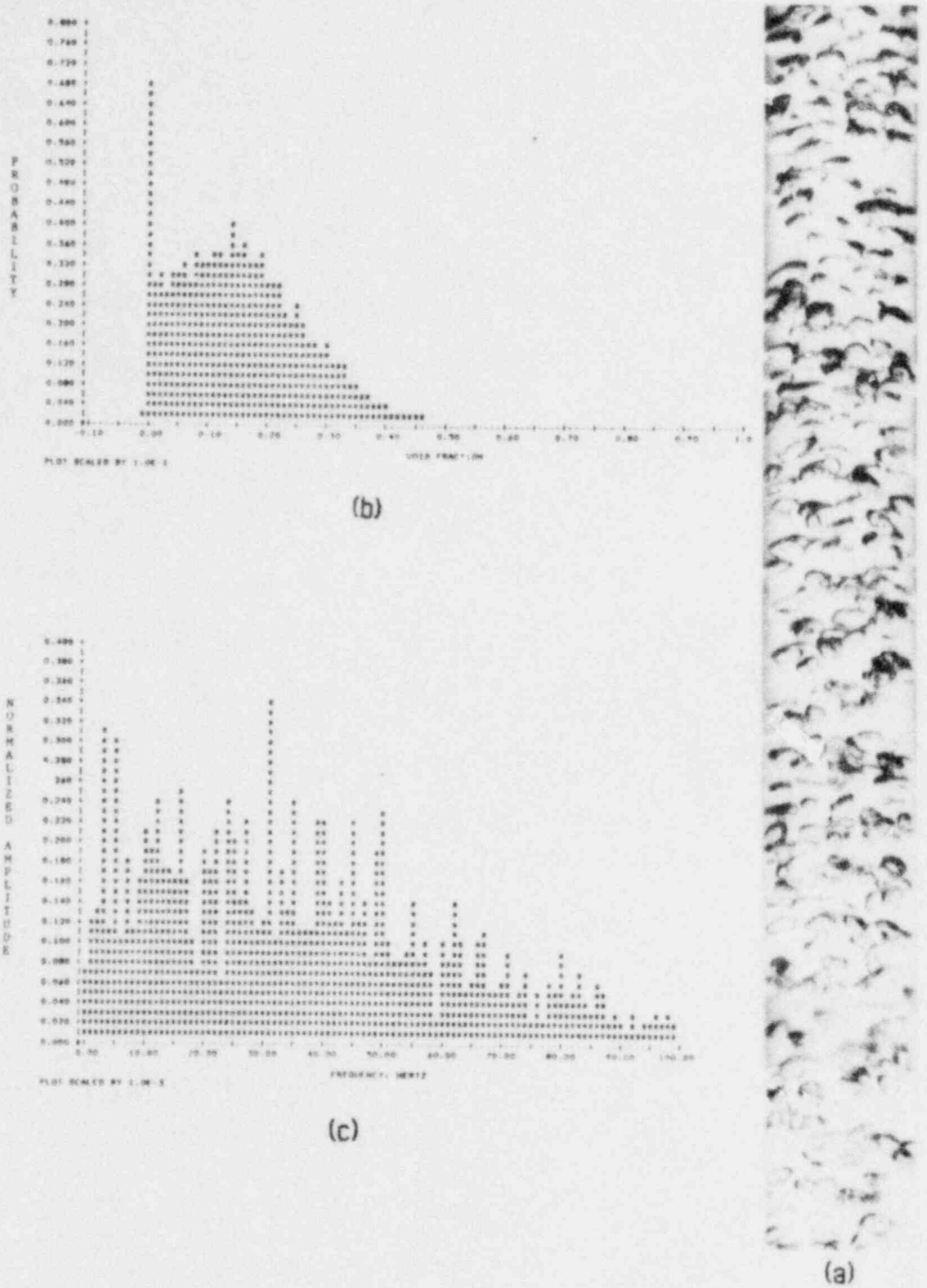

Figure 4.7
A photograph (a), diameter PDF (b), and diameter PSD (c), for 13 percent area-averaged void fraction, j_L = 0.25 m/sec, j_g=0.073 m/sec

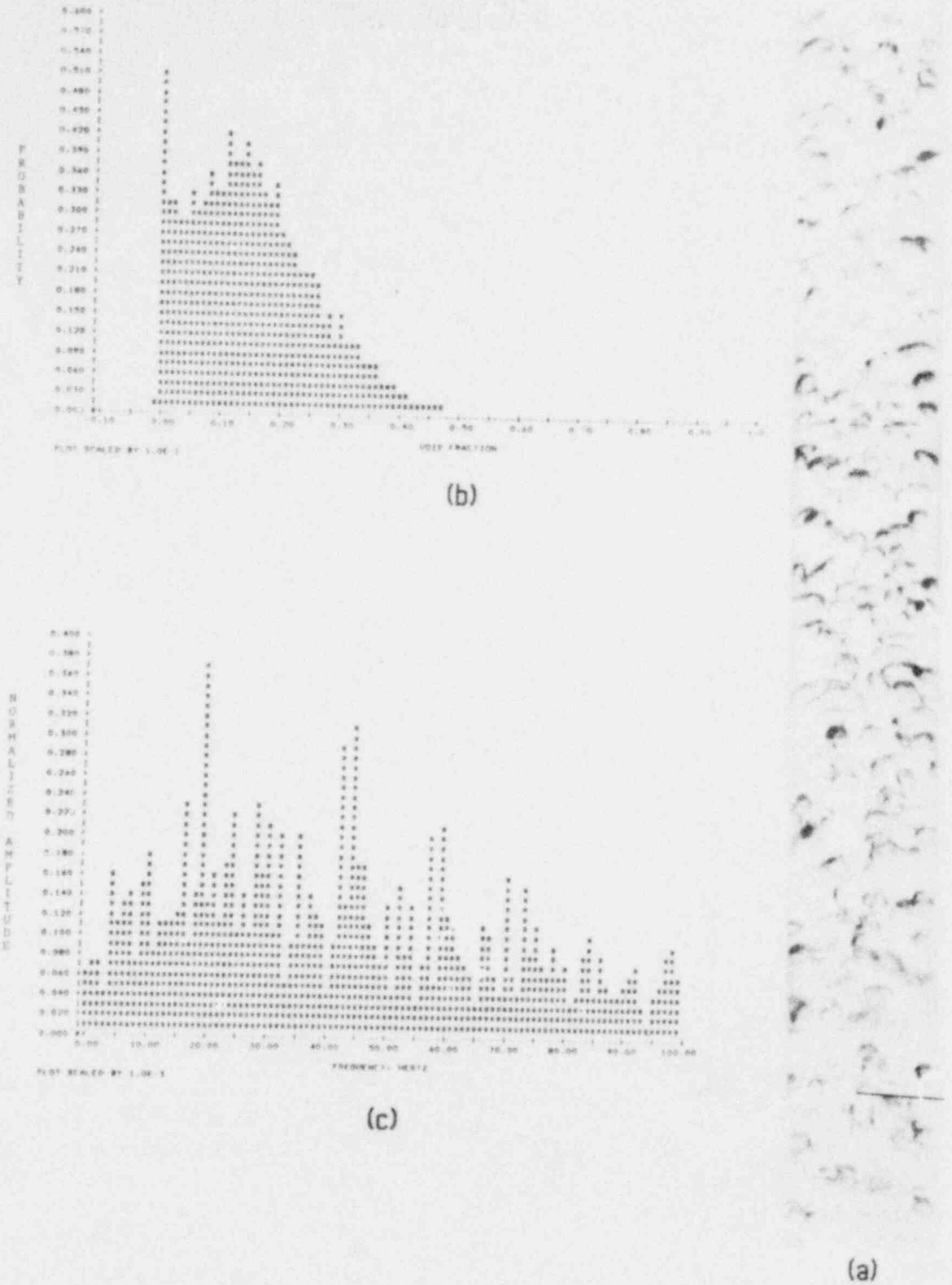

Figure 4.8
A photograph (a), diameter PDF (b), and diameter PSD (c), for 13 percent area-averaged void fraction, j_L = 0.37 m/sec, j_g=0.57 m/sec

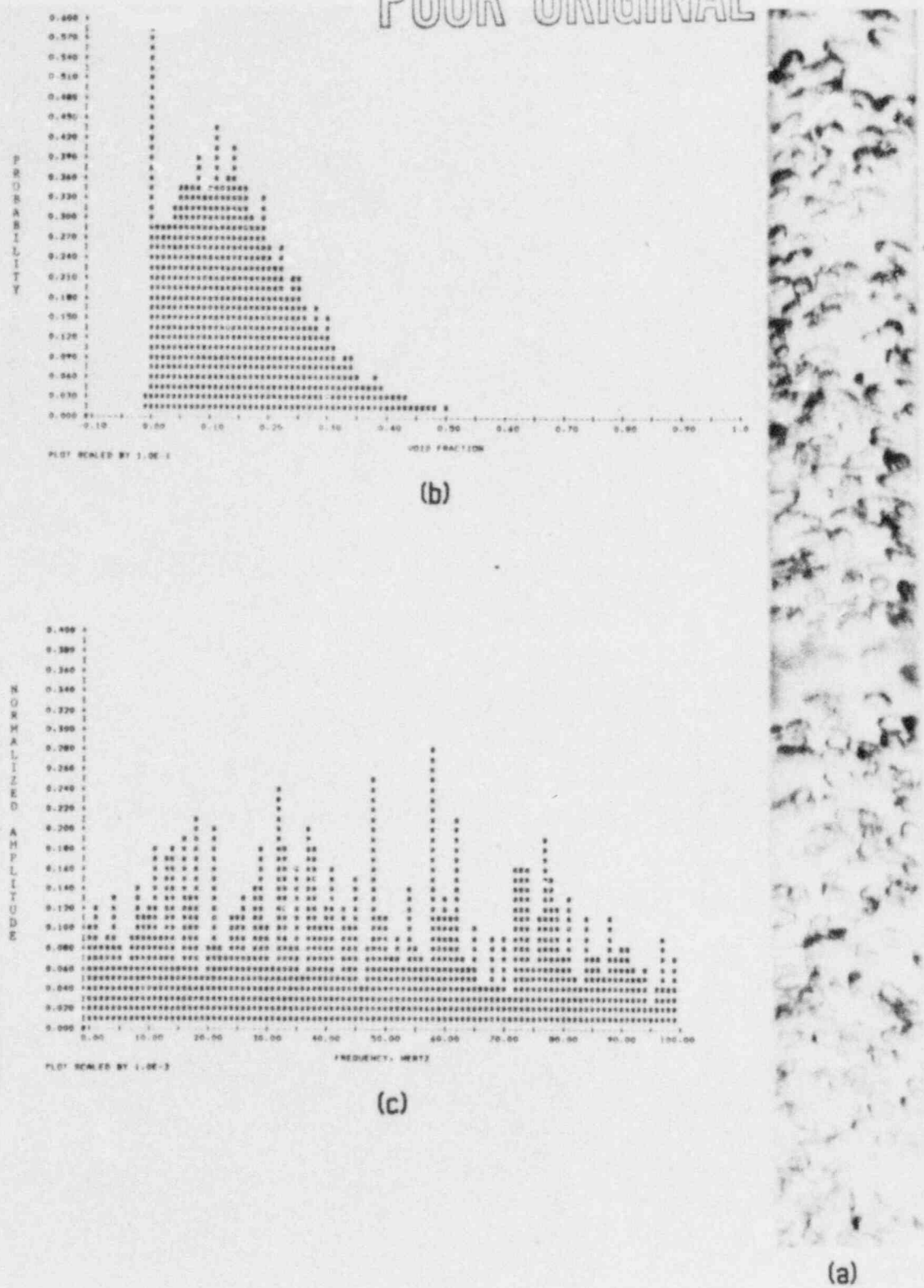

Figure 4.9

A photograph (a), diameter PDF (b), and diameter PSD (c), for 13 percent area-averaged void fraction, j_ℓ = 0.50 m/sec, j_g =0.123 m/sec

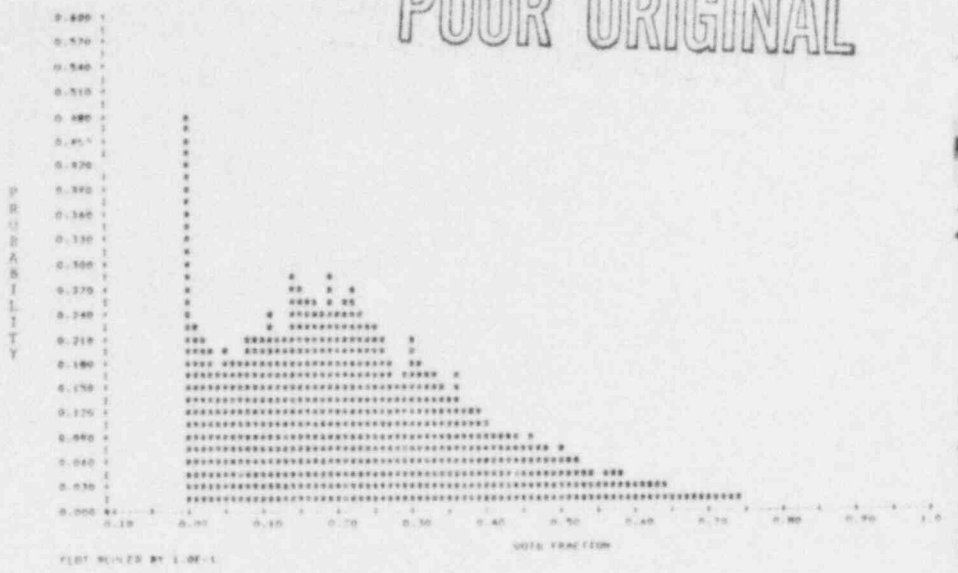

(b)

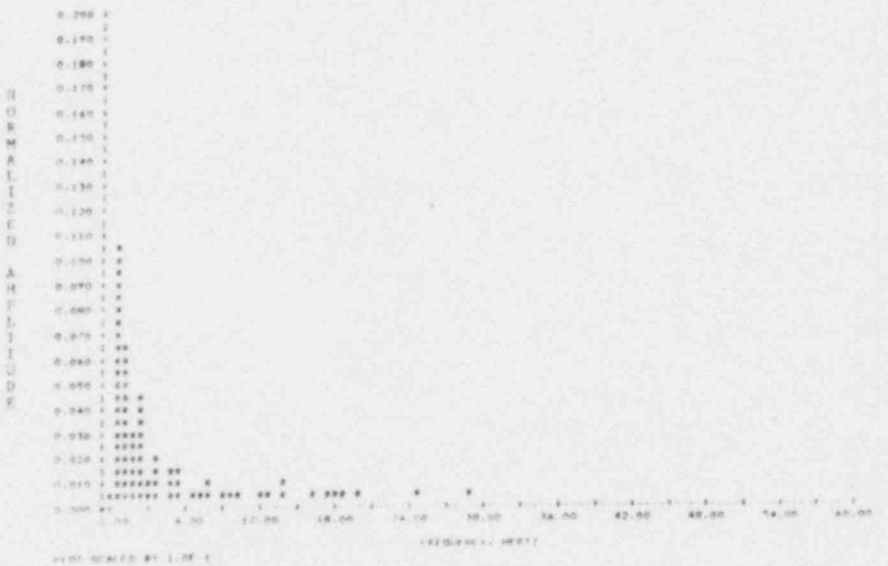

(c)

(a)

Figure 4.10
A photograph (a), diameter PDF (b), and diameter PSD (c), for 20 percent area-averaged void fraction, j_ℓ=0.0 m/sec, j_g=0.44 m/sec

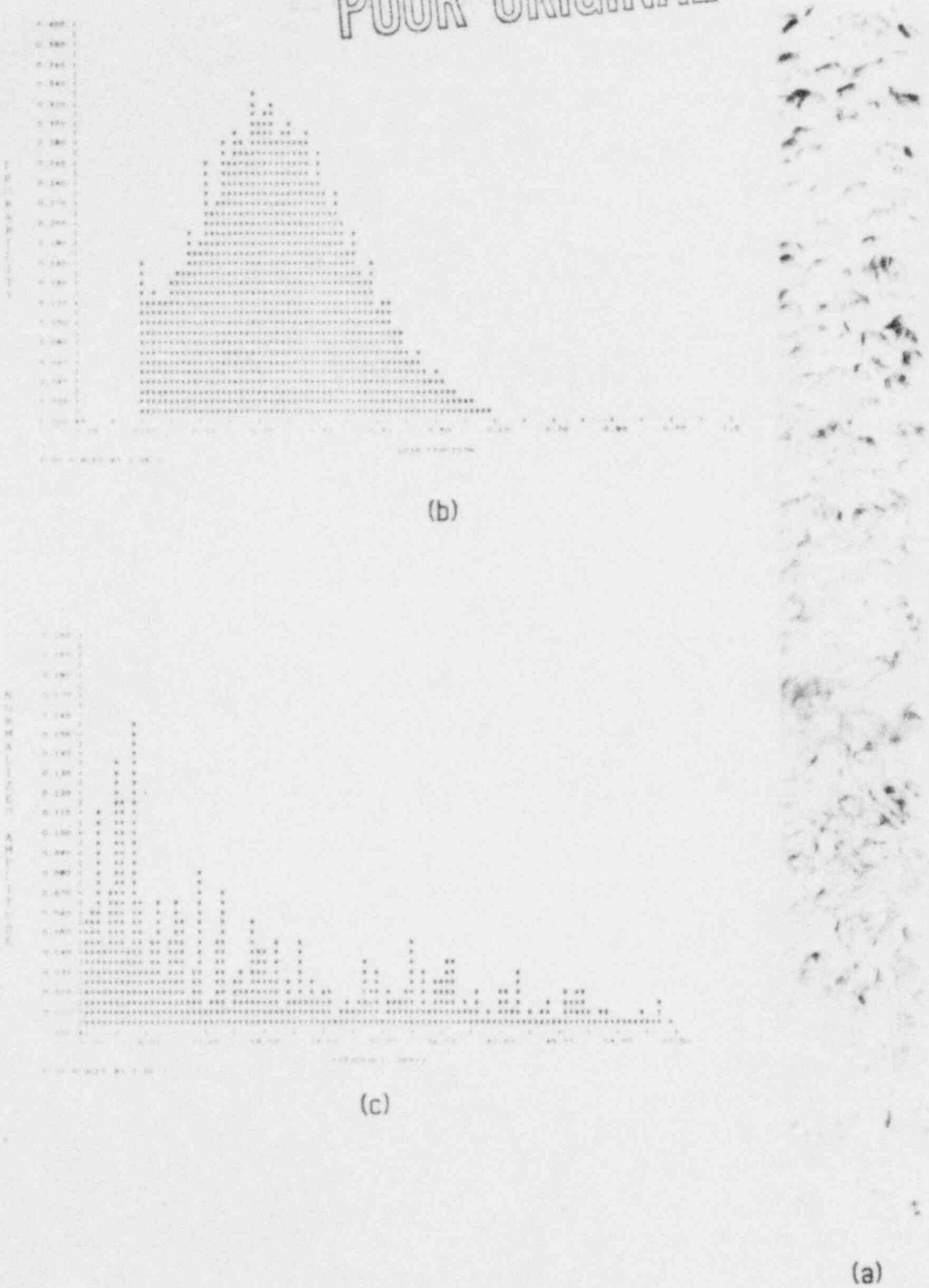

Figure 4.11
A photograph (a), diameter PDF (b), and diameter PSD (c), for 20 percent area-averaged void fraction, j_L=0.12 m/sec, j_g=0.082 m/sec

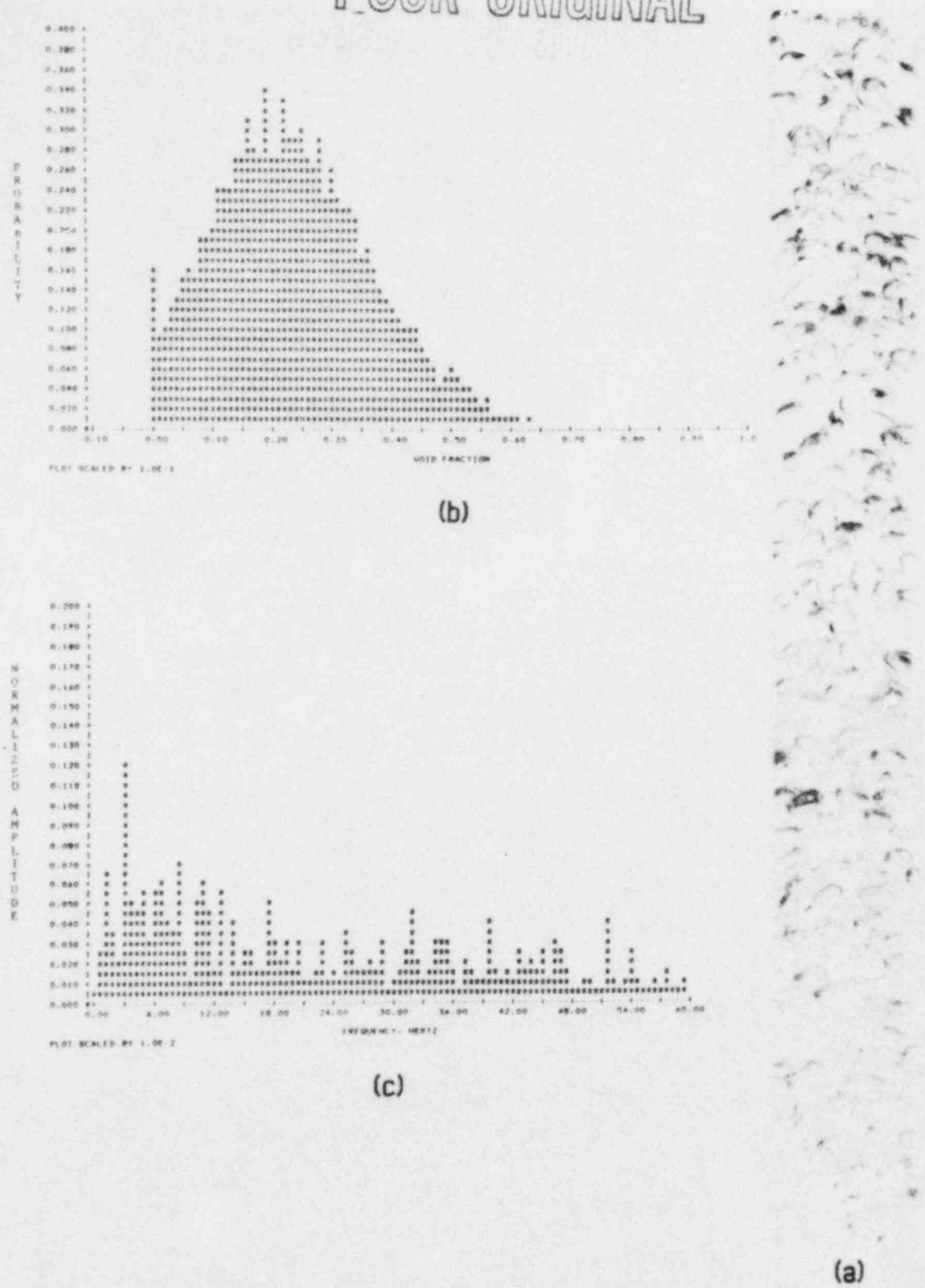

Figure 4.12
A photograph (a), diameter PDF (b), and diameter PSD (c), for 20 percent area-averaged void fraction, j_ℓ=0.25 m/sec, j_g=0.123 m/sec

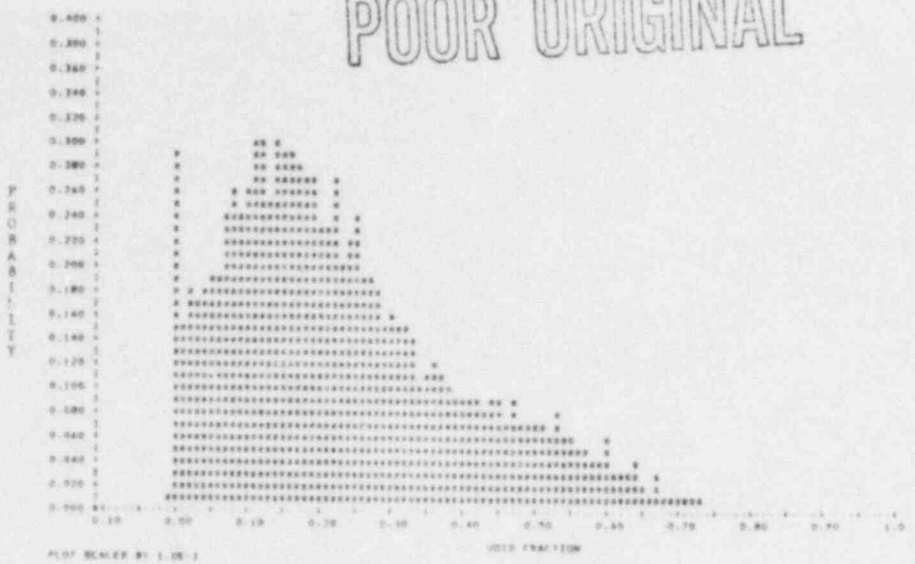

(b)

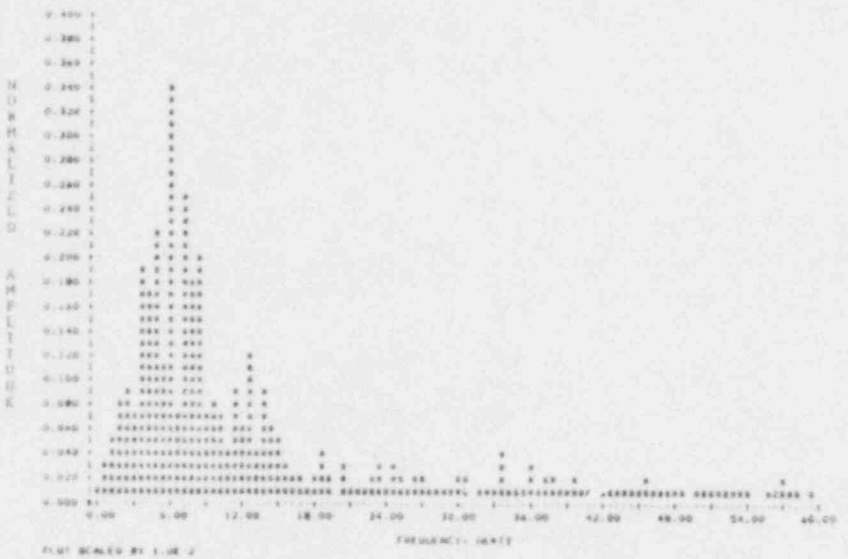

(c)

(a)

Figure 4.13

A photograph (a), diameter PDF (b), and diameter PSD (c), for 20 percent area-averaged void fraction, j_ℓ=0.37 m/sec, j_g=0.168 m/sec

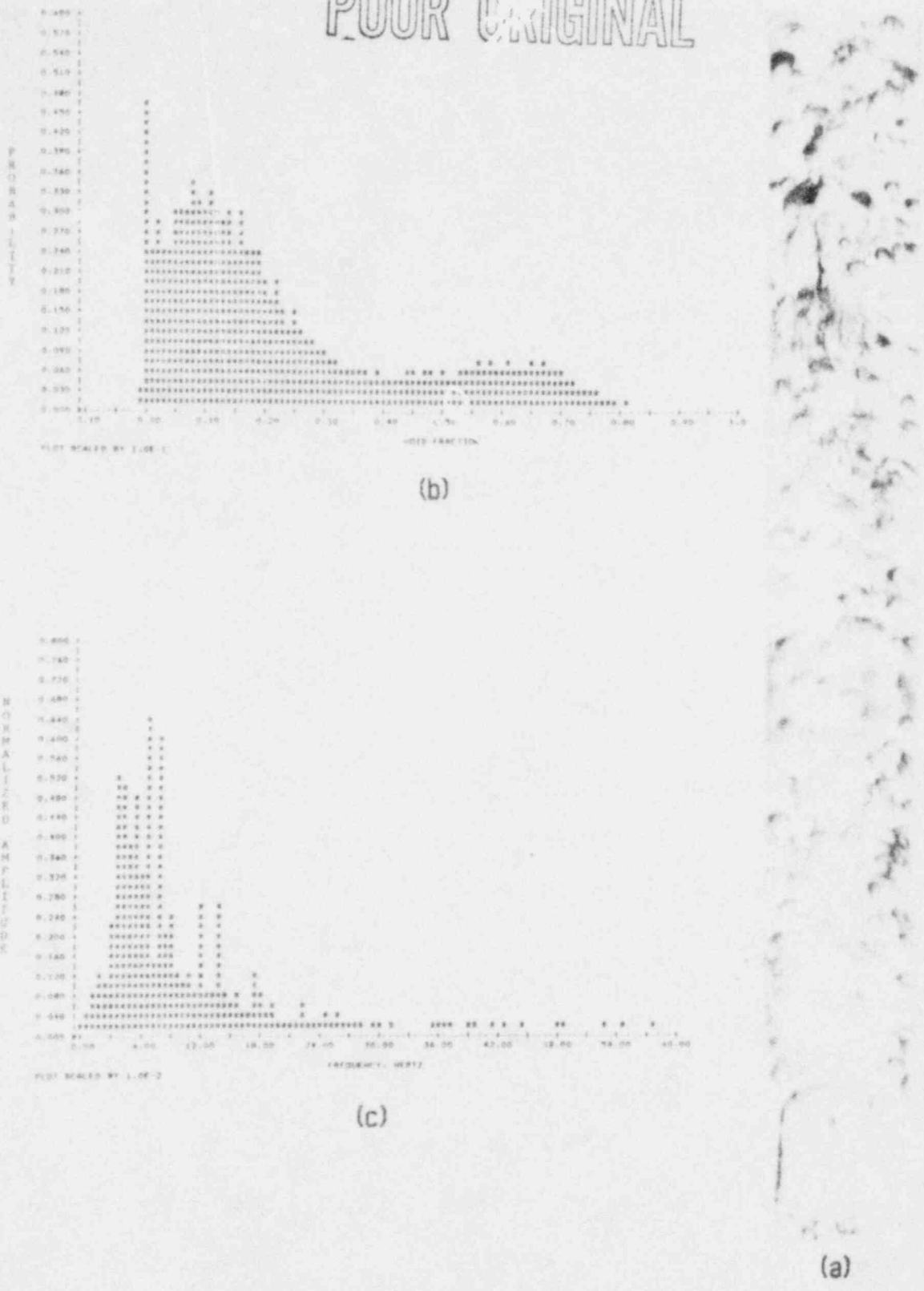

(b)

(c)

(a)

Figure 4.14

A photograph (a), diameter PDF (b), and diameter PSD (c), for 20 percent area-averaged void fraction, j_L =0.50 m/sec, j_g =0.226 m/sec

void fraction. The respective liquid superficial velocities were 0.0, 0.12, 0.25, 0.37, and 0.50 m/sec. This flow regime is also bubbly and a unimodal PDF is observed. The onset of liquid flow initially causes the PDF to become more peaked as shown in Figures 4.11 and 4.12. The PDF broadens at larger air and water flow rates because of the more frequent formation of Taylor bubbles. This broadening is shown in Figures 4.13 and 4.14.

The PSD associated with this void fraction show a fairly well defined peak in Figure 4.10. This peak is caused by the emergence of a characteristic frequency, however, the observed peak is still of an amplitude comparable to other frequencies in the PSD. PSDs shown in Figures 4.11 through 4.14 have rather broad band spectrums of relatively low amplitude. This observed trend in the PSDs is caused by the onset of liquid flow.

For 26 percent area-averaged void fraction, the PDF, PSD and two-phase picuture are shown in Figures 4.15 to 4.19 for liquid superficial velocities of 0.0, 0.12, 0.25, 0.3, and 0.5 m/sec, respectively. The PDF associated with zero liquid flow is very broad due to the presence of Taylor bubbles. As found at lower void fraction, the onset of liquid flow reduces the breadth of the PDF; this is shown in Figure 4.16. The increasing air flow associated with an increasing liquid flow, at constant area-average void fraction,promotes the transition to slug flow. A very broad PDF is observed for a superficial velocity of 0.25

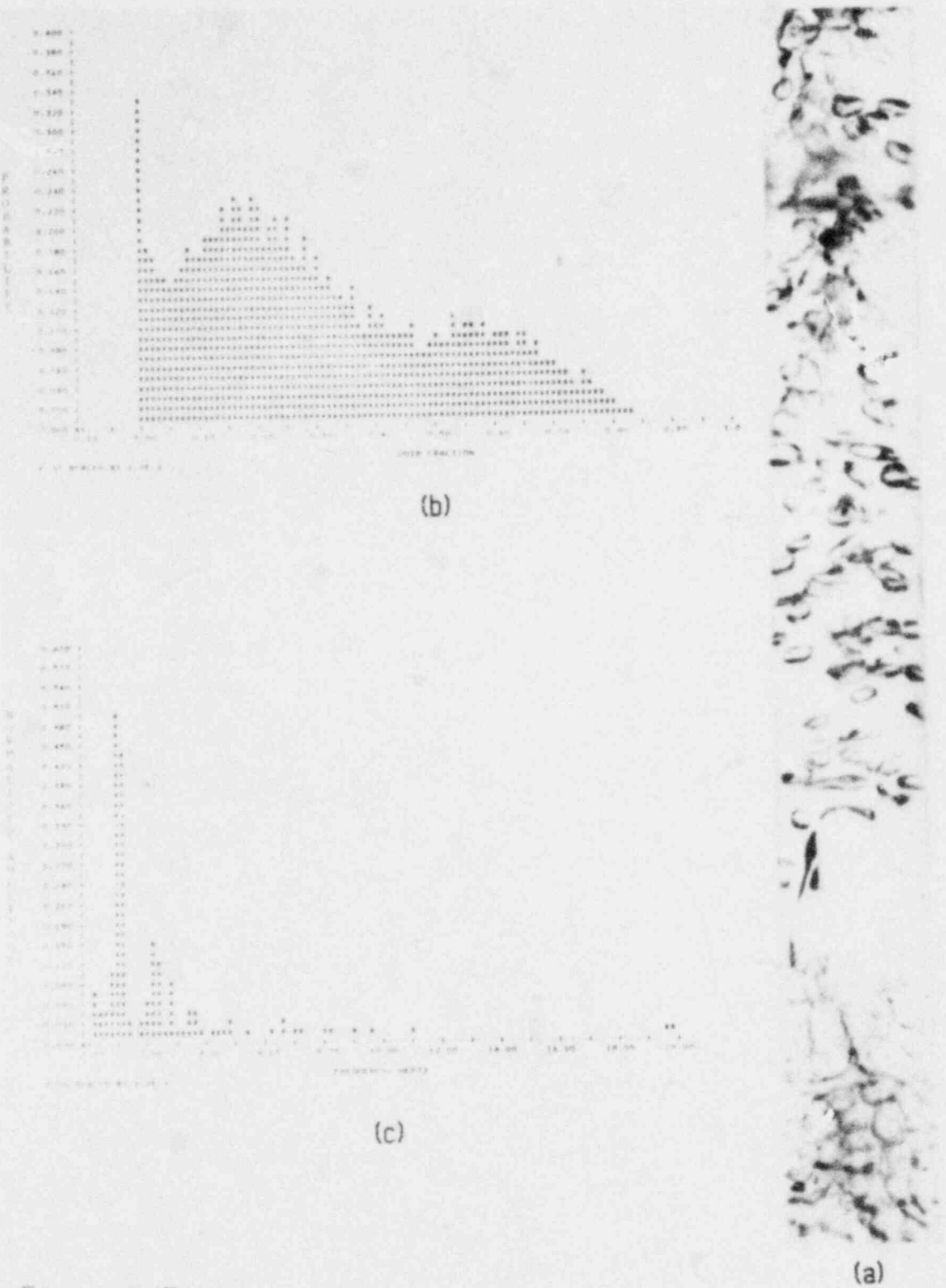

Figure 4.15
A photograph (a), diameter PDF (b), and diameter PSD (c), for 26 percent area-averaged void fraction, j_L=0.0 m/sec, j_g=0.075 m/sec

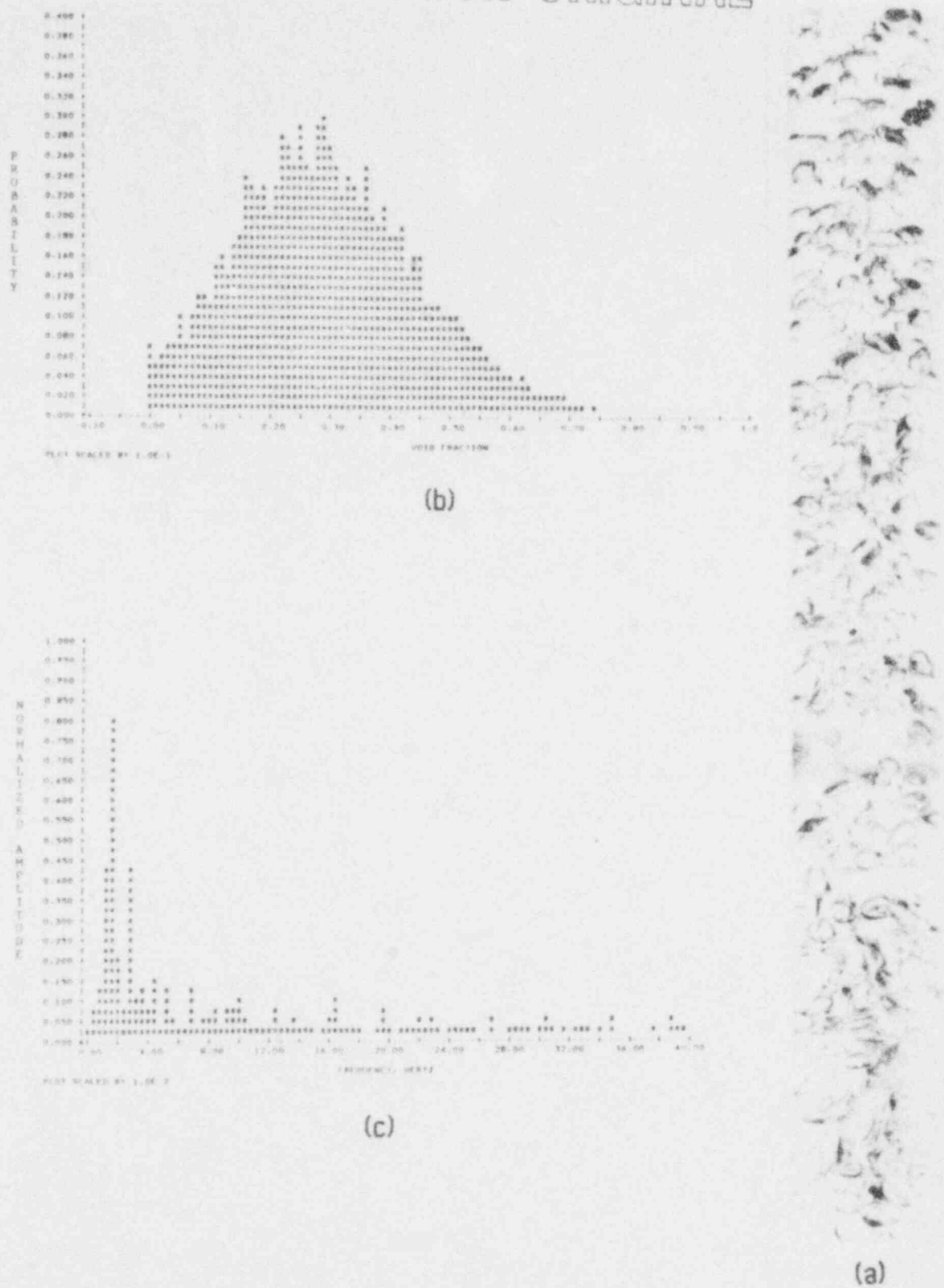

Figure 4.16
A photograph (a), diameter PDF (b), and diameter PSD (c), for 26 percent area-averaged void fraction, j_L=0.12 m/sec, j_g=0.111 m/sec

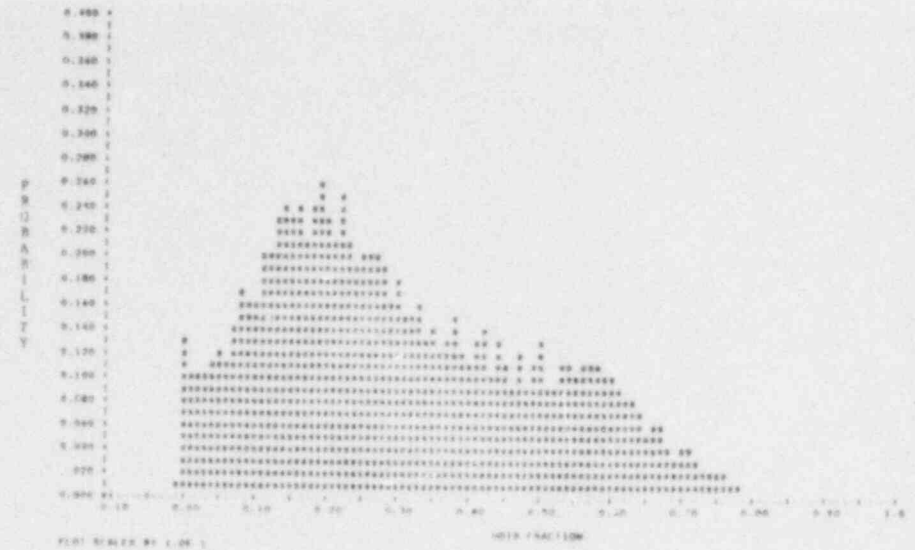

(b)

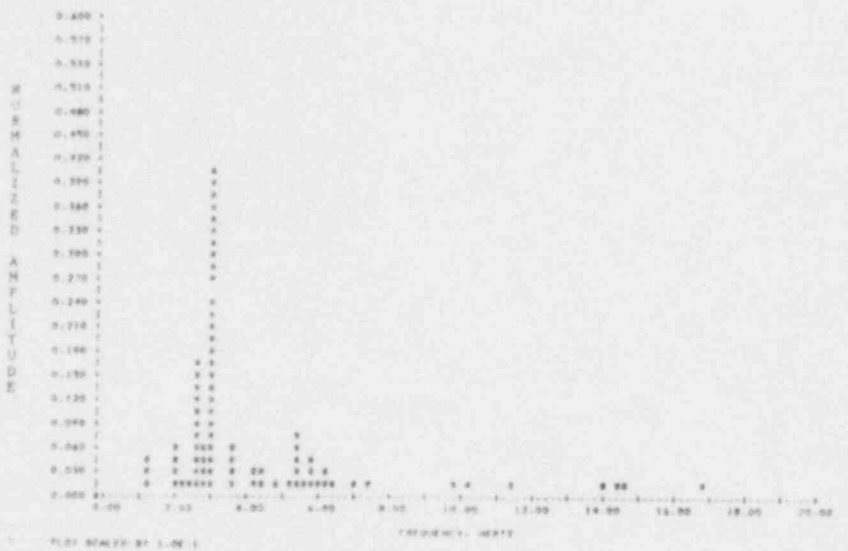

(c)

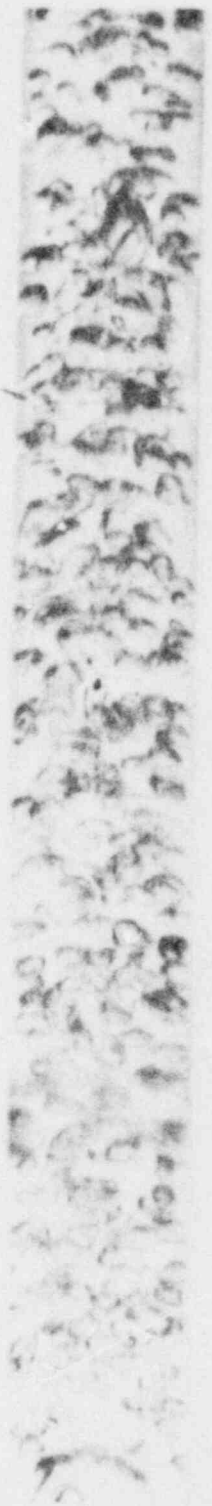

(a)

Figure 17

A photograph (a), diameter PDF (b), and diameter PSD (c), for 26 percent area-averaged void fraction, j_f =0.25 m/sec, j_g =0.177 m/sec

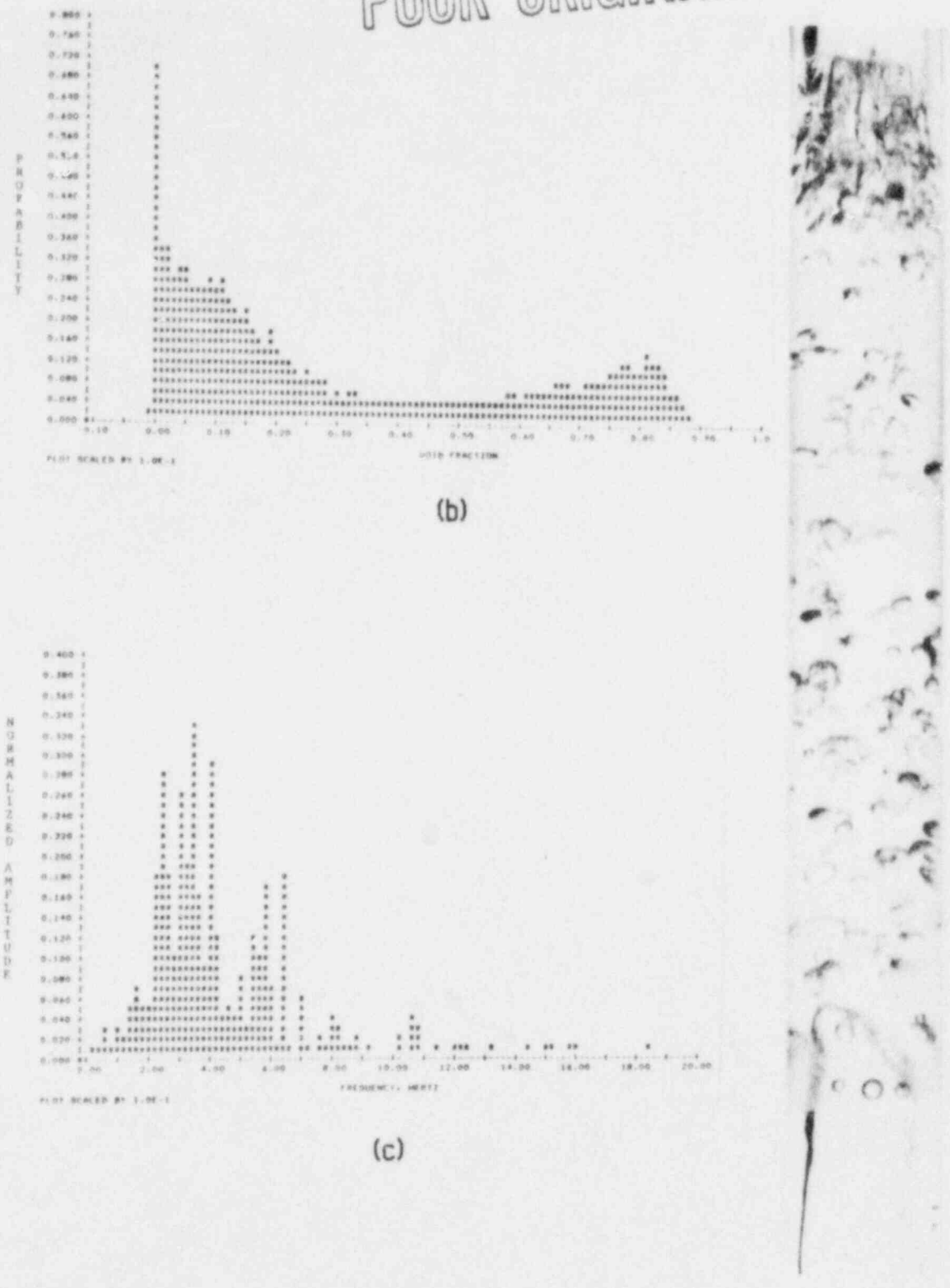

Figure 4.18

A photograph (a), diameter PDF (b), and diameter PSD (c), for 26 percent area-averaged void fraction, j_L=0.37 m/sec, j_g=0.257 m/sec

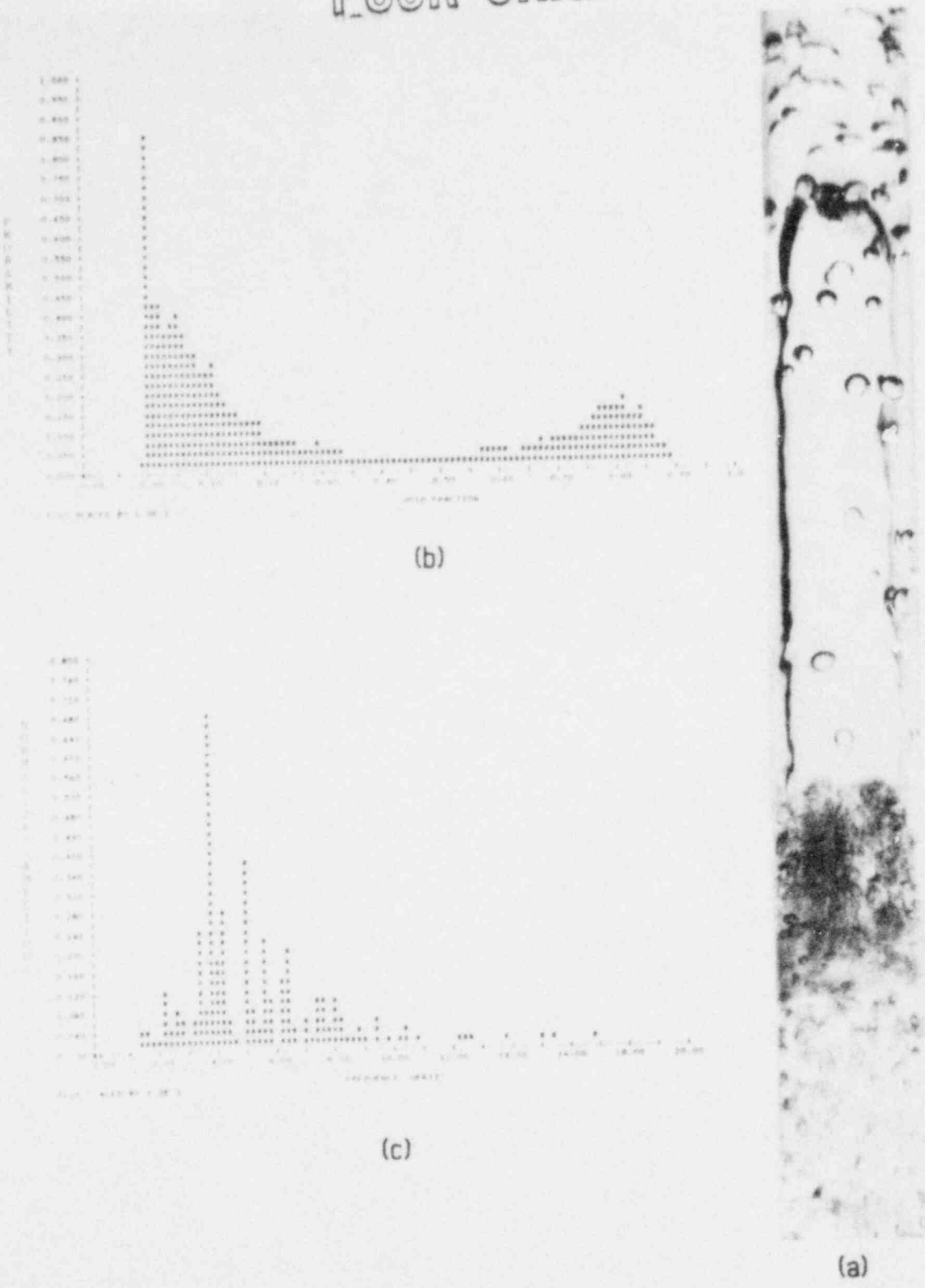

(b)

(c)

(a)

Figure 4.19

A photograph (a), diameter PDF (b), and diameter PSD (c), for 26 percent area-averaged void fraction, j_f=0.50 m/sec, j_g=0.329 m/sec

m/sec as shown in Figure 4.17. Ultimately, the liquid cannot suppress the transition to slug flow and the PDF becomes bimodal. These results are clearly shown in Figures 4.18 and 4.19. Notice that a sharp peak at zero chordal-average void fraction is still observed.

The PSDs associated with this void fraction show an interesting trend. All PSDs for this void fraction show characteristic peaks. The position of these peaks increase in frequency with increasing liquid velocity. Some of the peaks are rather broad; especially those shown in Figures 4.18 and 4.19.

A further increase in area-average void fraction to 32 percent produces the PDFs, PSDs and two-phase photographs shown in Figures 4.20 through 4.24. The superficial liquid velocities are 0.0, 0.12, 0.25, 0.37, and 0.5 m/sec. Visually, slug flow is apparent but the PDF clearly becomes totally bimodal only at the higher liquid velocities as shown in Figures 4.22 through 4.24. These PDFs clearly indicate that the transition to slug flow does not occur sharply. Moreover, the emergence of slug flow is not clear from the PDF alone.

Jones [6] has previously attempted to discriminate between flow regimes by looking at the number of modes in the PDF. The previous PDFs and photographs indicate that the transition from bubbly to slug flow can be very gradual. Discrimination based on the number of modes will not always be accurate. Jones tested a 2-dimensional conduit geometry

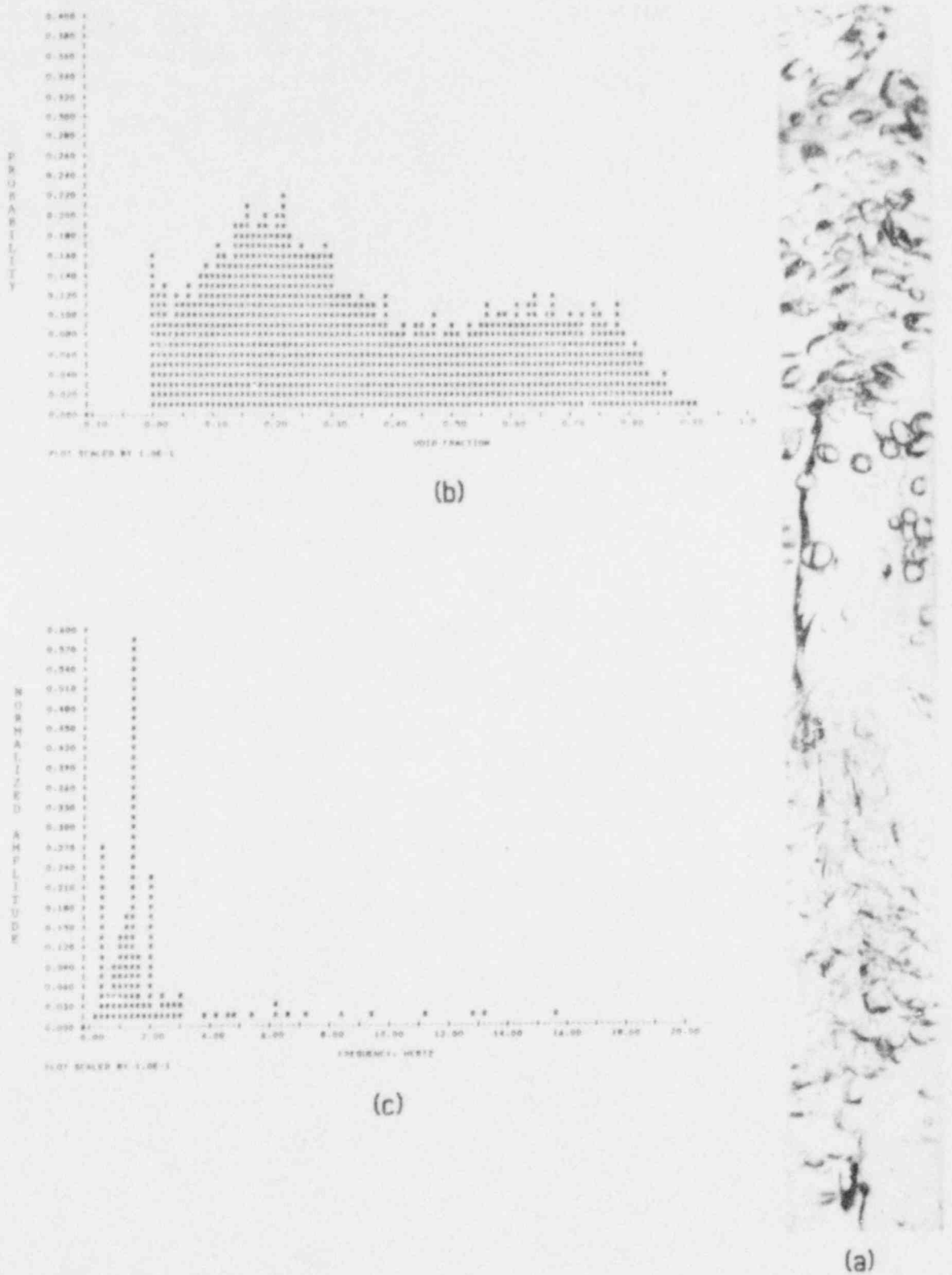

Figure 4.20

A photograph (a), diameter PDF (b), and diameter PSD (c), for 32 percent area-averaged void fraction, j_L=0.0 m/sec, j_g=0.109 m/sec

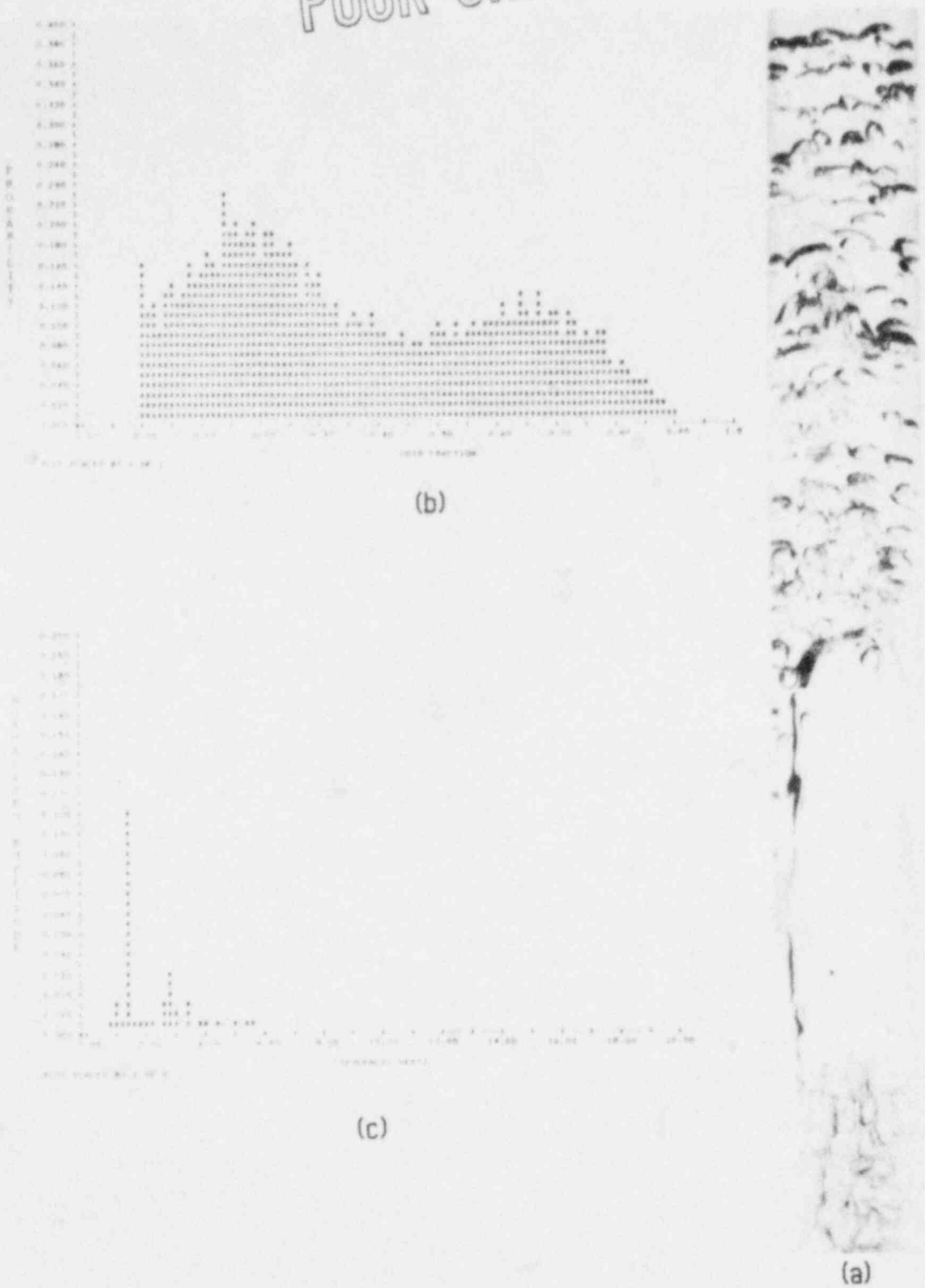

Figure 4.21
A photograph (a), diameter PDF (b), and diameter PSD (c), for 32 percent area-averaged void fraction, j_ℓ =0.12 m/sec, j_g =0.187 m/sec

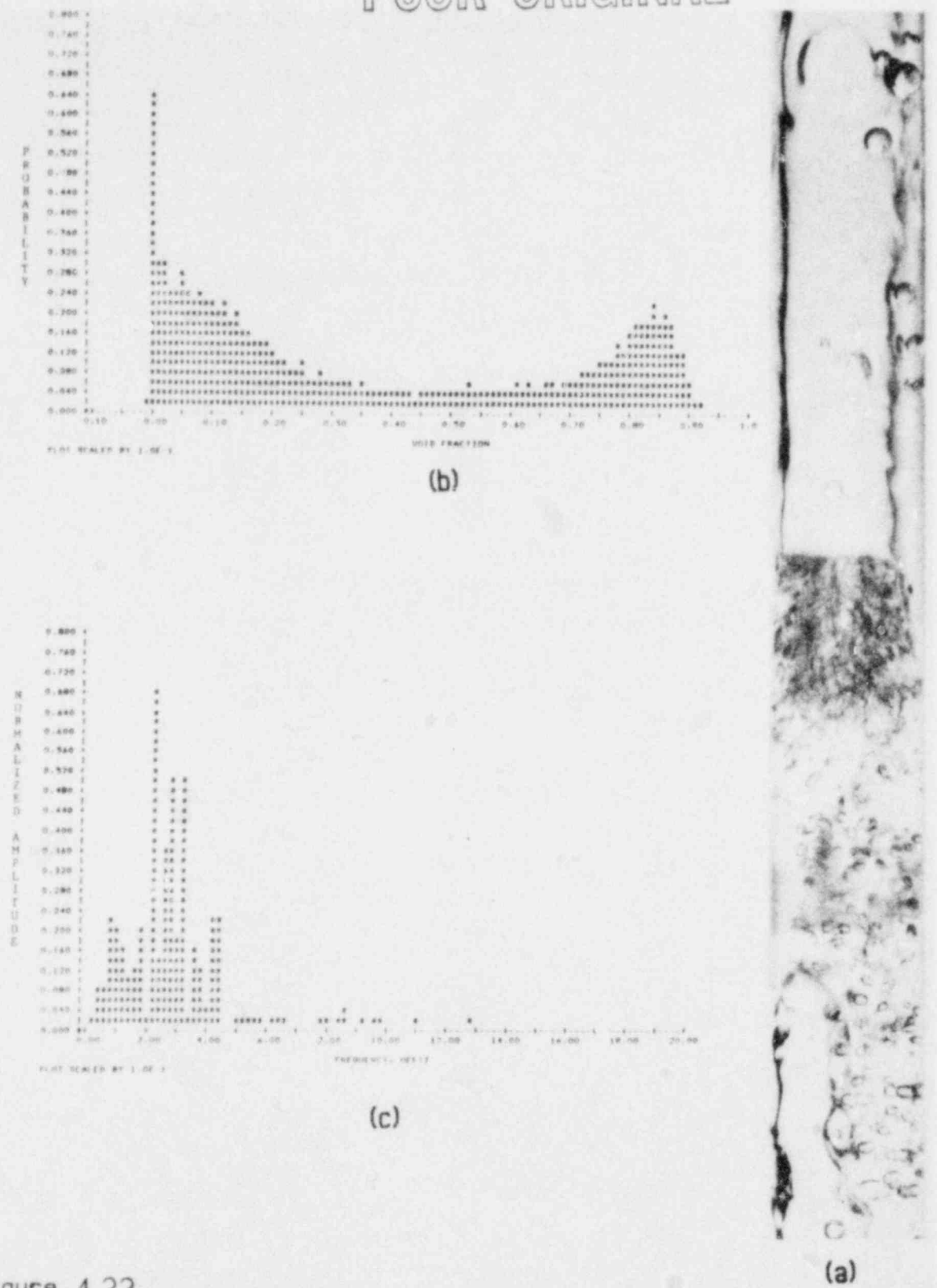

Figure 4.22

A photograph (a), diameter PDF (b), and diameter PSD (c), for 32 percent area-averaged void fraction, j_ℓ=0.25 m/sec, j_g=0.288 m/sec

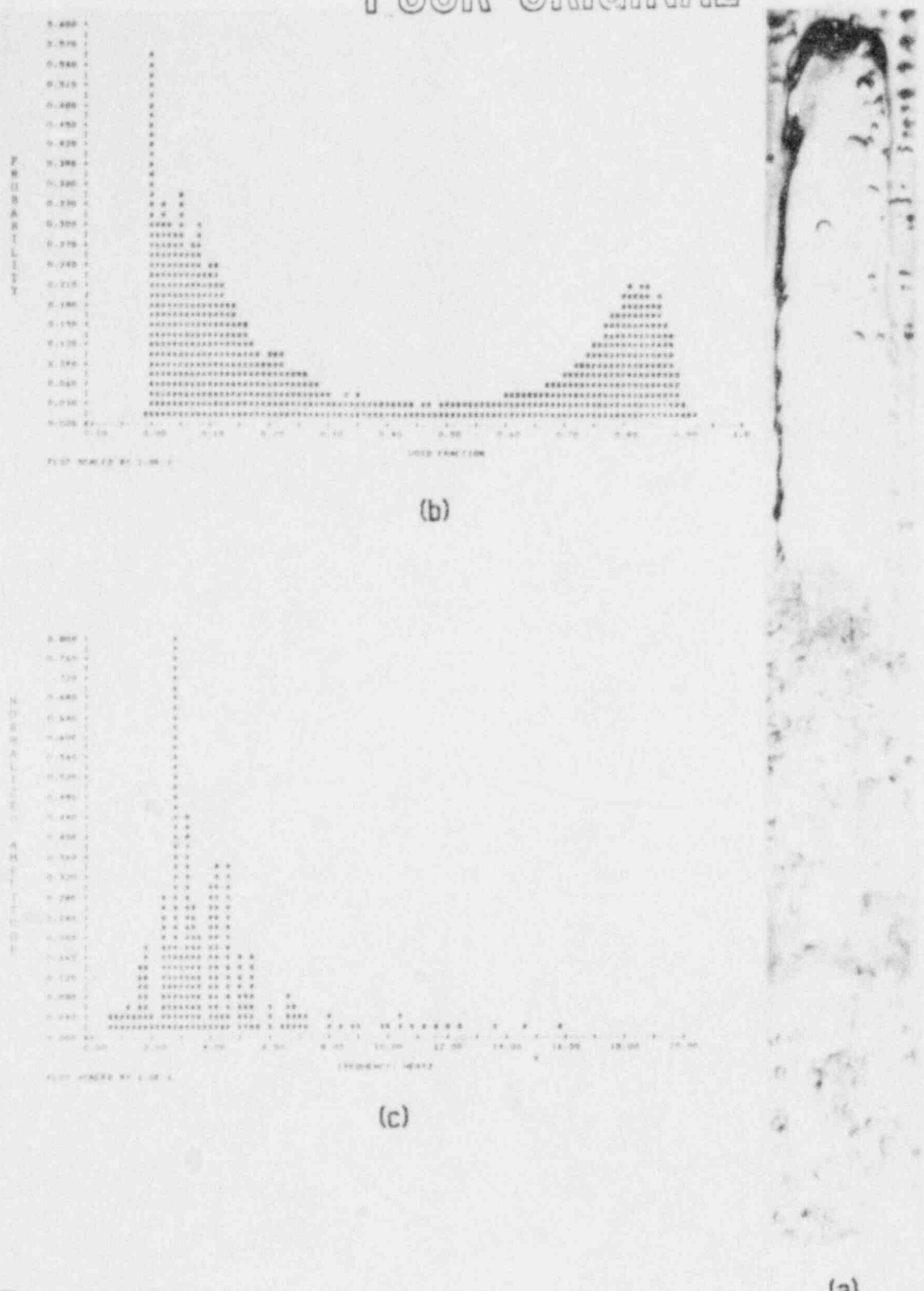

(b)

(c)

(a)

Figure 4.23

A photograph (a), diameter PDF (b), and diameter PSD (c), for 32 percent area-averaged void fraction, j_ℓ=0.37 m/sec, j_g=0.366 m/sec

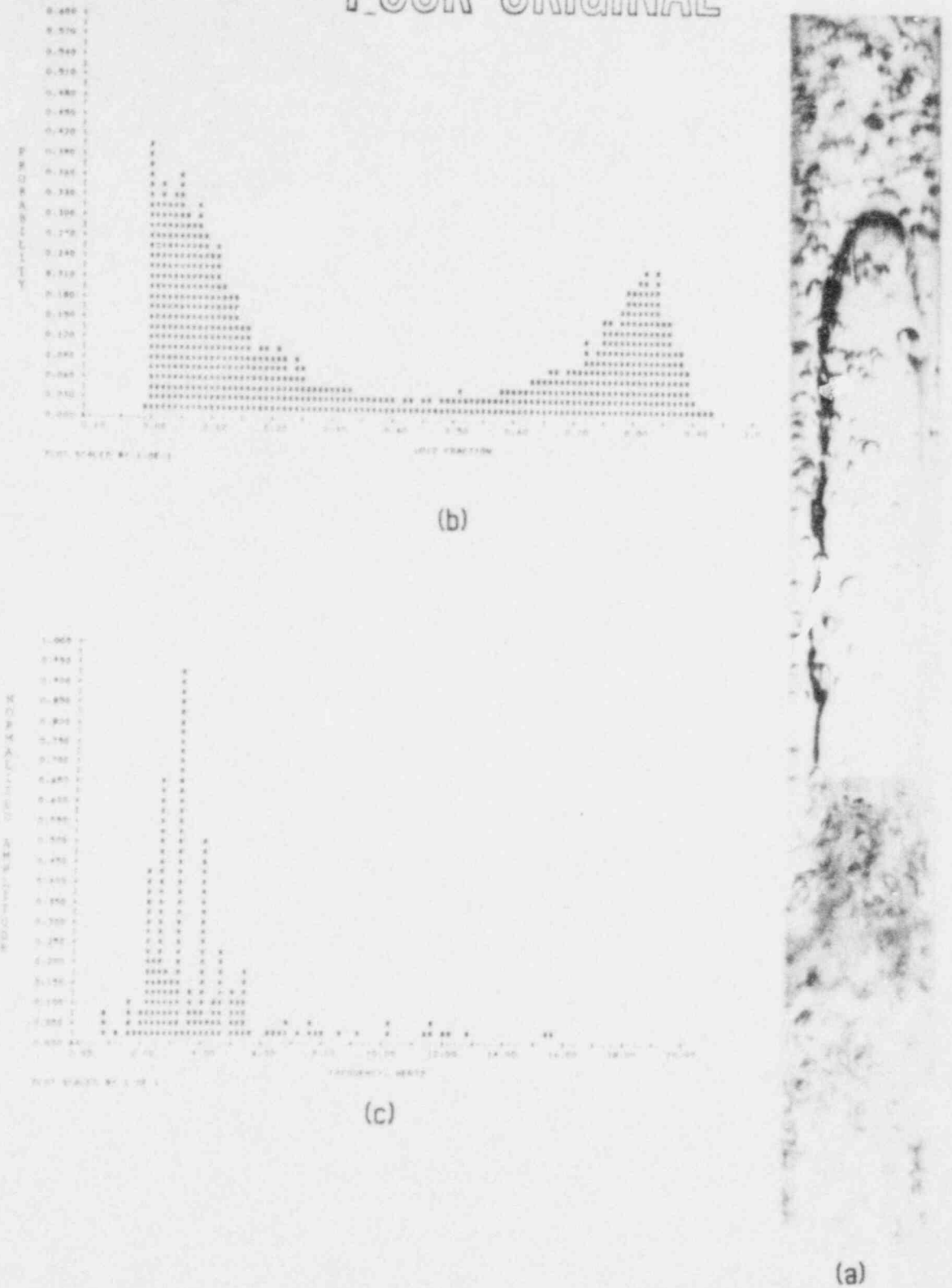

(b)

(c)

(a)

Figure 4.24

A photograph (a), diameter PDF (b), and diameter PSD (c), for 32 percent area-averaged void fraction, j_ℓ=0.50 m/sec, j_g=0.445 m/sec

which simplified data interpretation. The round conduit geometry used in this study indicates that the number of modes possessed by a PDF is not adequate for flow regime identification. However, as will be discussed in later sections, calculations of the moments provides a more objective measure.

The PSDs at 32 percent area-average void fraction are all indicative of slug flow, i.e. a large peak has emerged at low frequency. The location of the peak increases in frequency as the liquid velocity increases. This result is expected since the peak is due to the frequency associated with the liquid slug transit time.

Fully-developed slug flow is obvious in Figures 4.25 to 4.29 for 41 percent area-averaged void fraction. Like the earlier data the liquid superficial velocities studied were 0.0, 0.12, 0.25, 0.37, and 0.50 m/sec, respectively. The PDFs are all bimodal as expected.

The PSDs also show behavior characteristic of slug flow. A peak of large magnitude at low frequency is observed. This peak's location moves to higher frequency as the liquid velocity is increased.

Figures 4.30 and 4.31 give the photograph, PDF and PSD associated with 55 and 65 percent area averaged void fraction, respectively. These results were obtained at zero liquid superficial velocity. The PDFs are bimodal but show peaks at high void fraction. The PSDs indicate a large, low frequency peaks typical of slug flow.

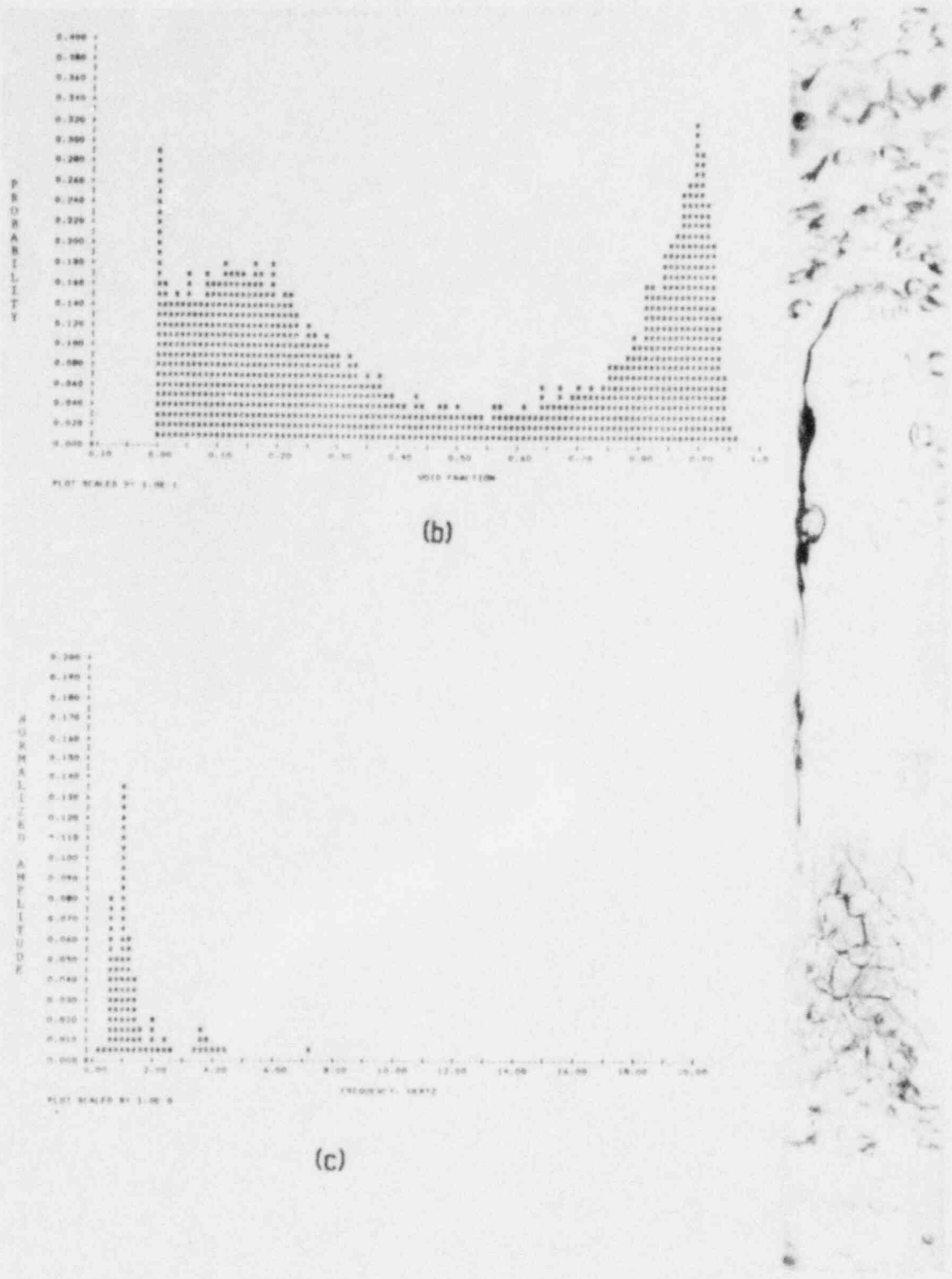

Figure 4.25

A photograph (a), diameter PDF (b), and diameter PSD (c). for 41 percent area-averaged void fraction, j_ℓ=0.0 m/sec, j_g=0 34 m/sec

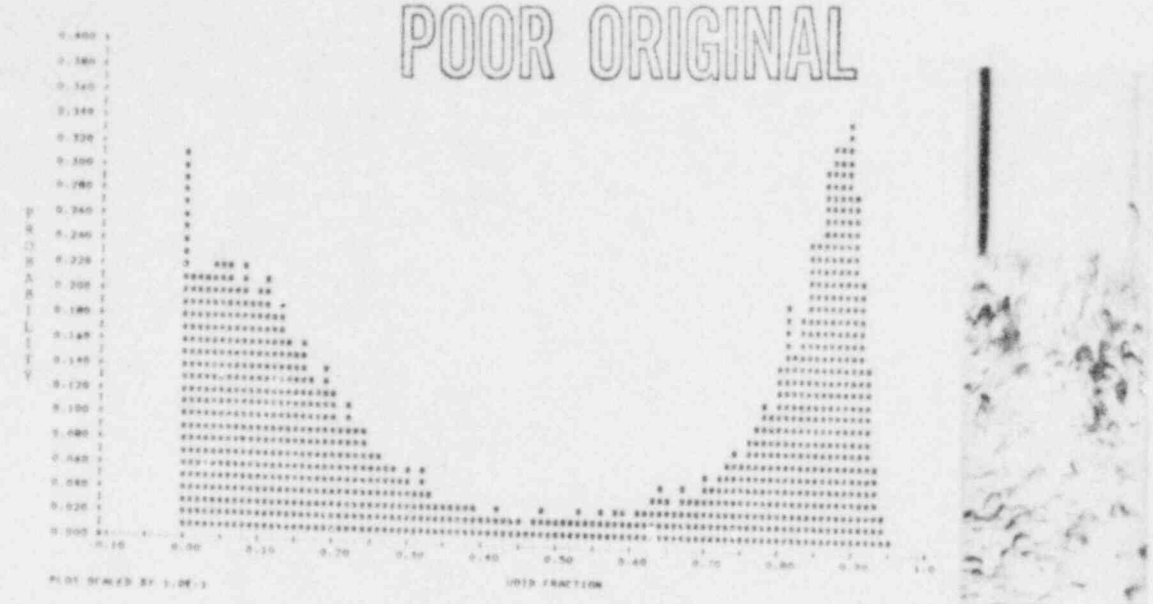

(b)

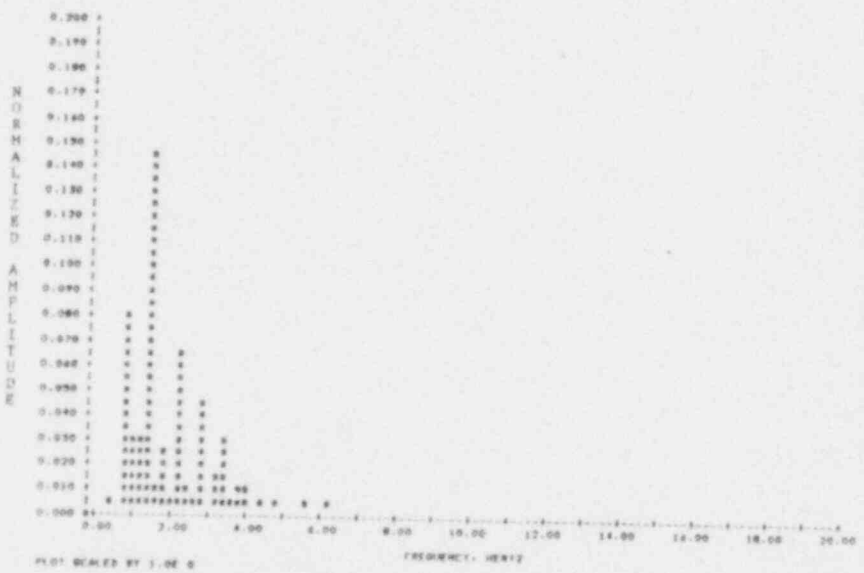

(c)

(a)

Figure 4.26

A photograph (a), diameter PDF (b), and diameter PSD (c), for 41 percent area-averaged void fraction, j_ℓ=0.12 m/sec, j_g=0.301 m/sec

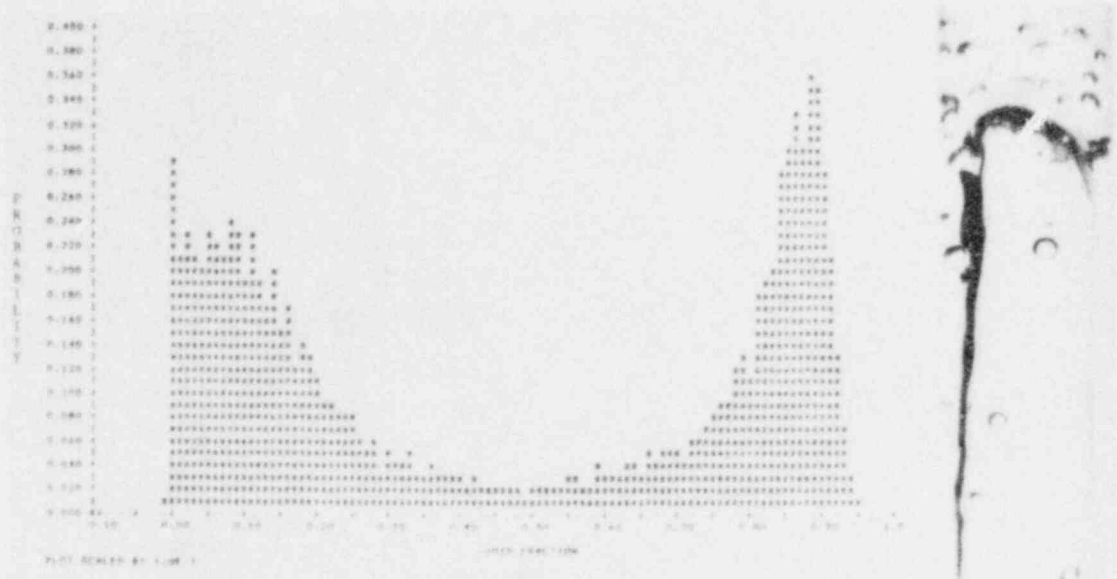

(b)

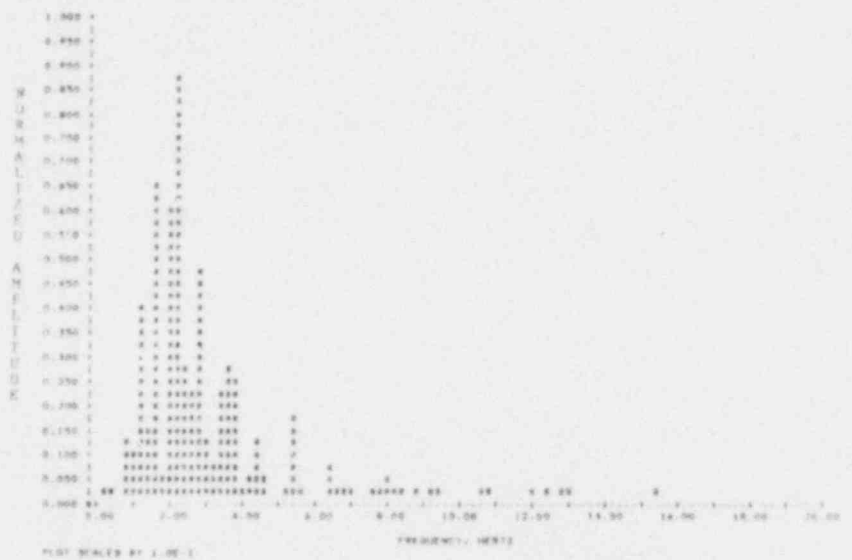

(c)

(a)

Figure 4.27

A photograph (a), diameter PDF (b), and diameter PSD (c), for 41 percent area-averaged void fraction, j_ℓ=0.25 m/sec, j_g=0.402 m/sec

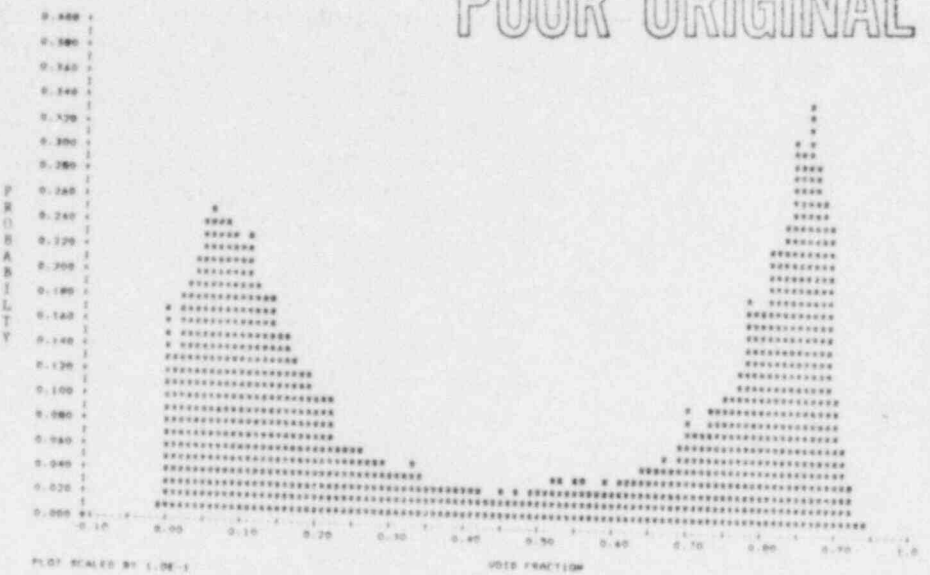

(b)

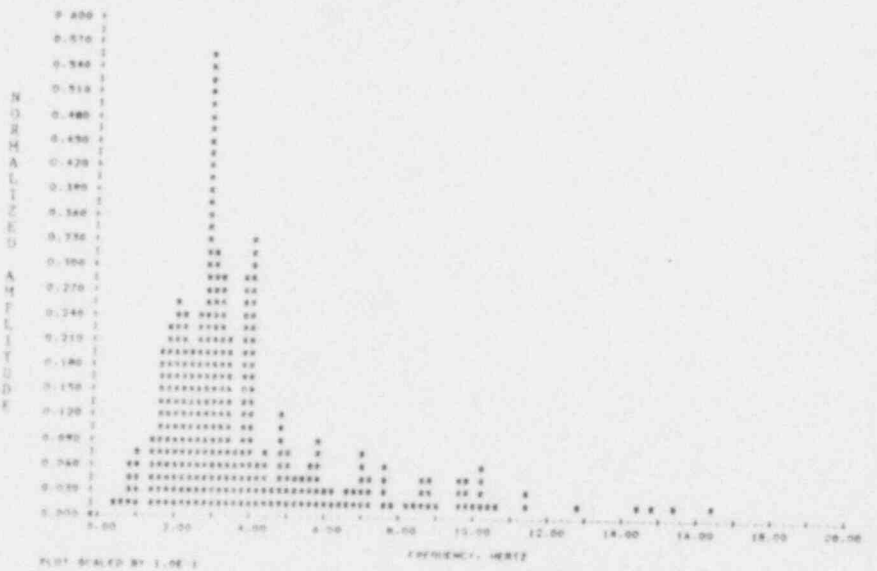

(c)

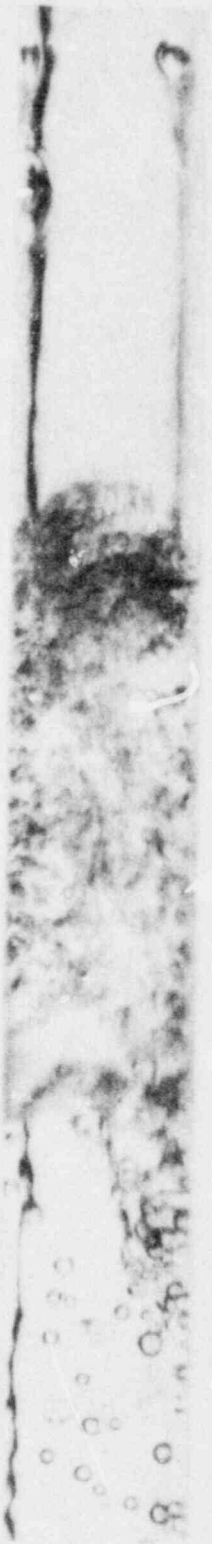

(a)

Figure 4.28

A photograph (a), diameter PDF (b), and diameter PSD (c), for 41 percent area-averaged void fraction, j_ℓ=0.37 m/sec, j_g=0.552 m/sec

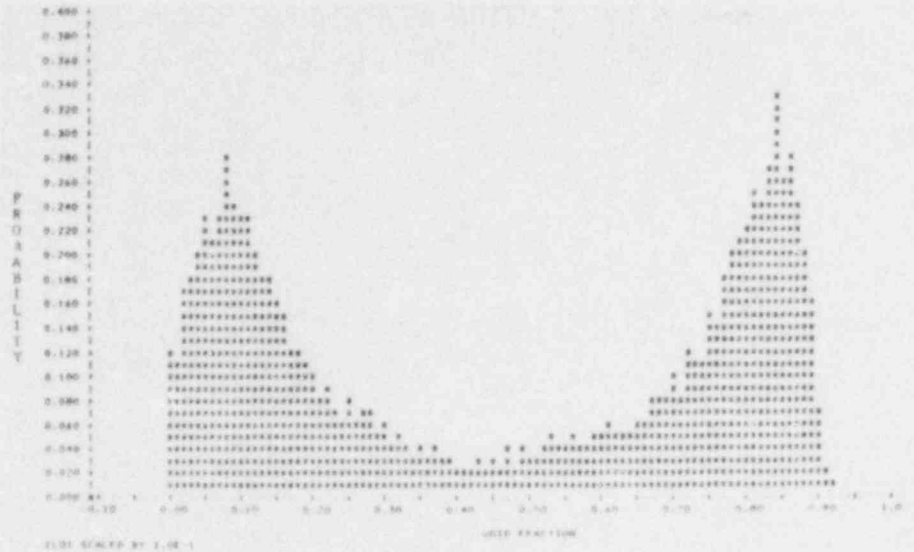

(b)

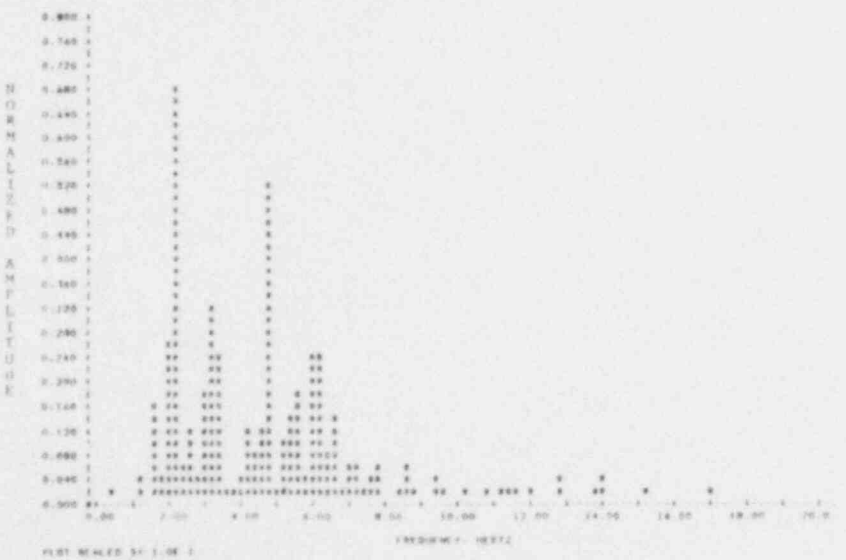

(c)

(a)

Figure 4.29

A photograph (a), diameter PDF (b), and diameter PSD (c), for 41 percent area-averaged void fraction, j_ℓ=0.50 m/sec, j_g=0.704 m/sec

(b)

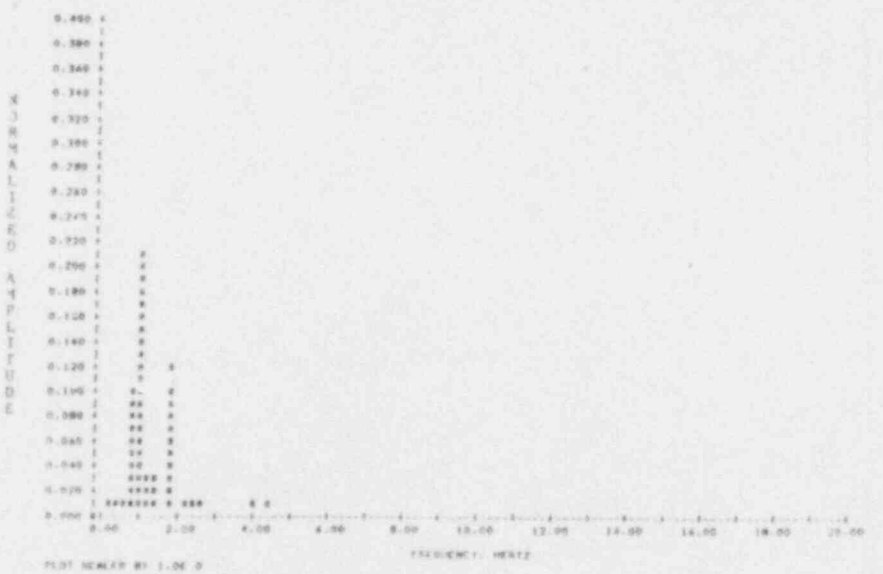

(c)

(a)

Figure 4.30

A photograph (a), diameter PDF (b), and diameter PSD (c), for 55 percent area-averaged void fraction, j_f=0.0 m/sec, j_g=0.311 m/sec

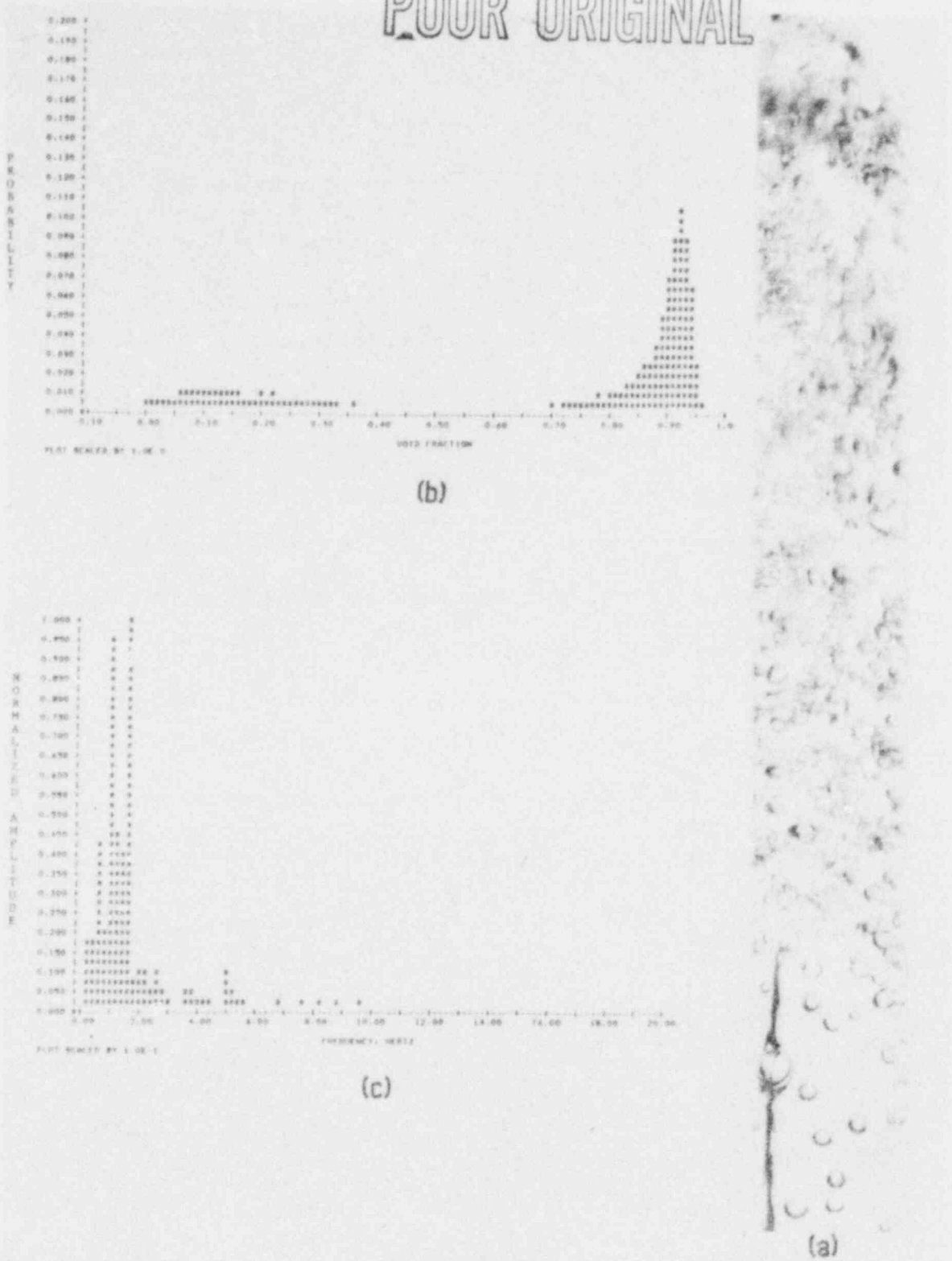

Figure 4.31
A photograph (a), diameter PDF (b), and diameter PSD (c), for 65 percent area-averaged void fraction, J_ℓ=0.0 m/sec, J_g=0.509 m/sec

Figures 4.32 through 4.36 illustrate the PDF, PSD and photograph for 68 area-averaged void fraction. The liquid superficial velocities are 0.0, 0.12, 0.25, 0.37, and 0.50 m/sec, respectively. The zero liquid flow case has a bimodal PDF and a single low frequency peak in the PSD. Liquid flow causes a unimodal PDF typical of annular flow. The PSD is broadened and reduced in amplitude as would be expected in annular flow.

An increase in area-average void fraction to 72 percent produces Figures 4.37 through 4.39 for 0.0, 0.12, and 0.25 m/sec liquid superficial velocities, respectively. The PDF clearly indicates annular flow. The PSD has a wide band of low amplitude, also characteristic of annular flow. Roll waves appeared along the vapor/liquid interface, typical of annular flow.

Data acquired at 76 and 79 percent area-average void fraction is shown in Figures 4.40 and 4.41. These data were acquired at zero liquid superficial velocity. Annular flow is clearly present. The PDF is unimodal and the PSD has a fairly broad bandwidth of low amplitude. Roll waves, characteristic of annular flow, are particularly obvious in Figure 4.40.

4.2 Statistical Data

As was discussed in a prior section, the PDF and PSD do not provide an objective flow regime indicator. Interpretation of this distribution is still subjective.

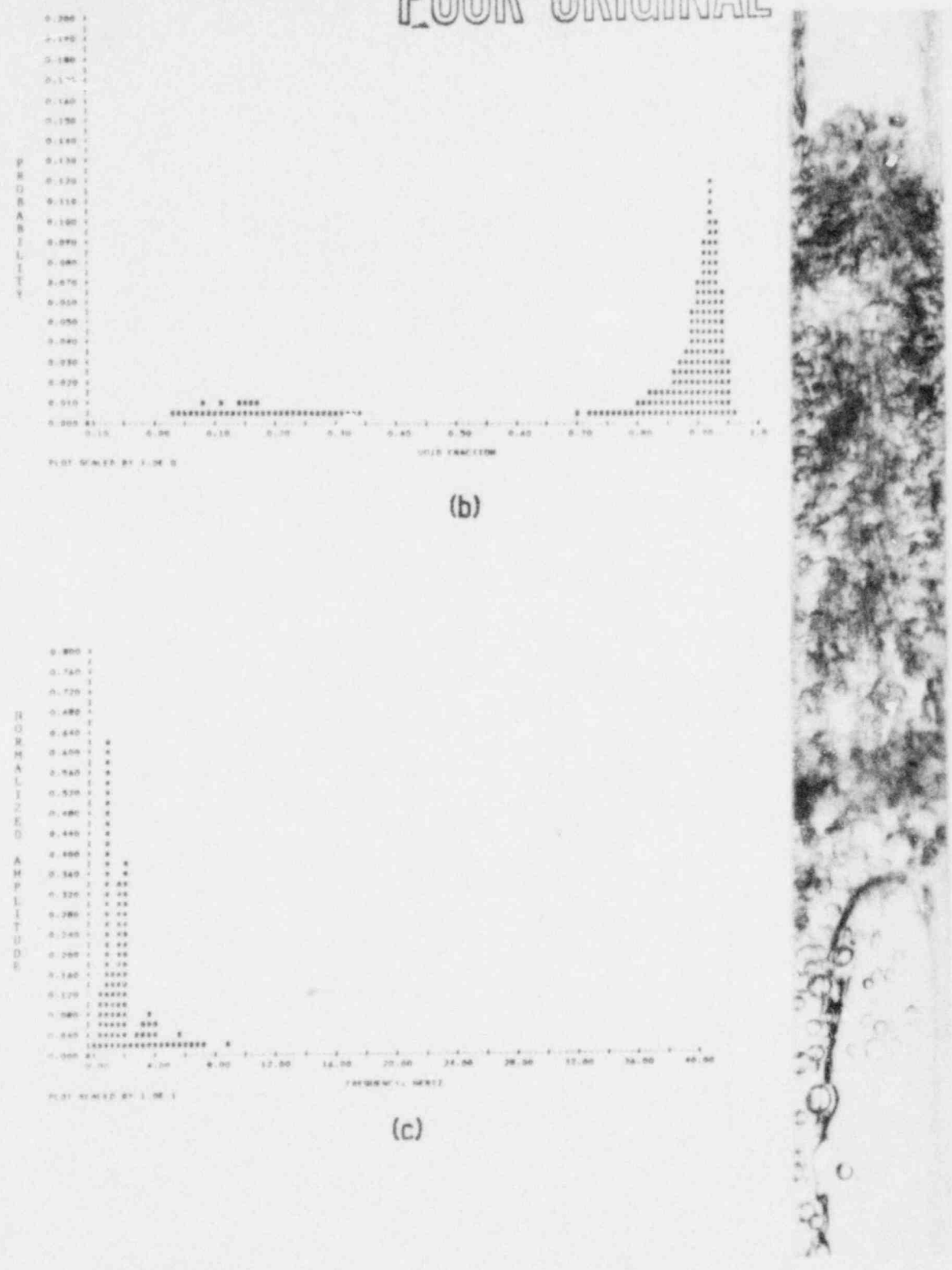

Figure 4.32

A photograph (a), diameter PDF (b), and diameter PSD (c), for 68 percent area-averaged void fraction, j_ℓ=0.0 m/sec, j_g=0.981 m/sec

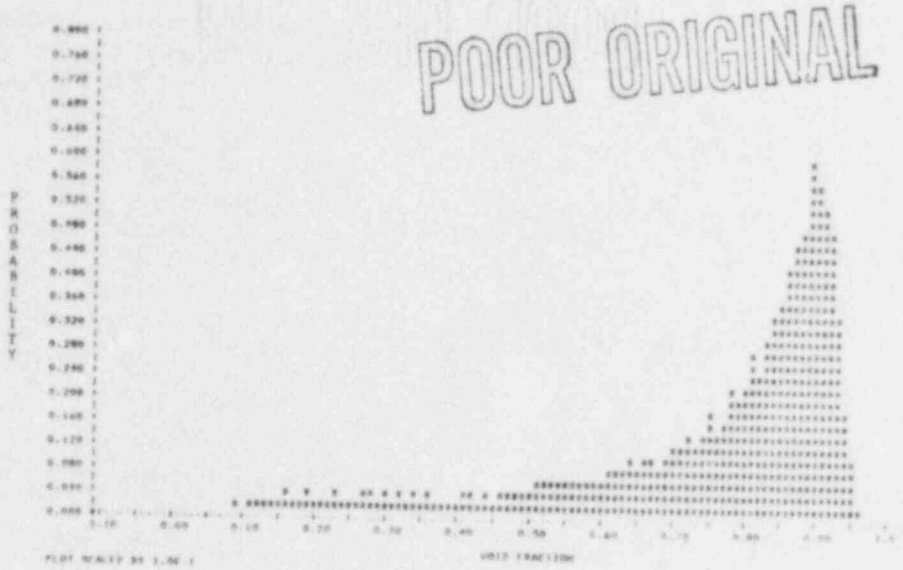

(b)

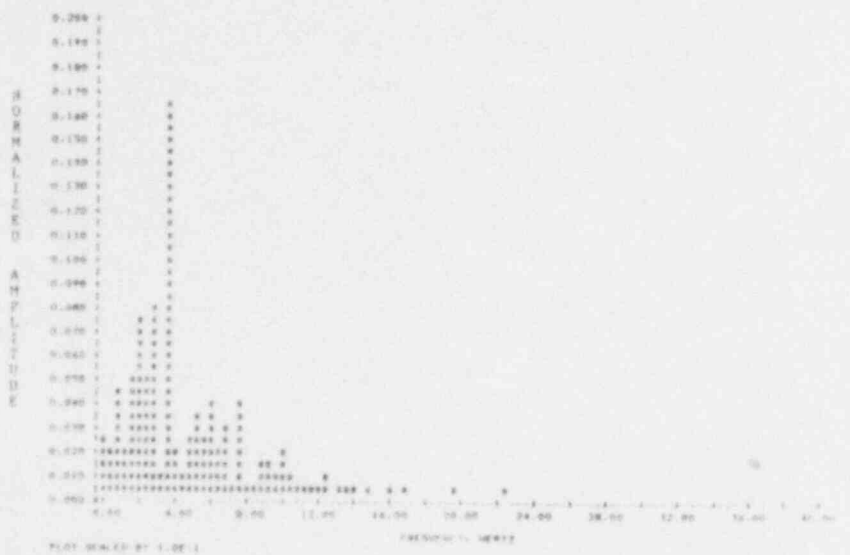

(c)

(a)

Figure 4.33

A photograph (a), diameter PDF (b), and diameter PSD (c), for [illegible] percent area-averaged void fraction, j_ℓ=0.12 m/sec, j_g=1.67 m/sec

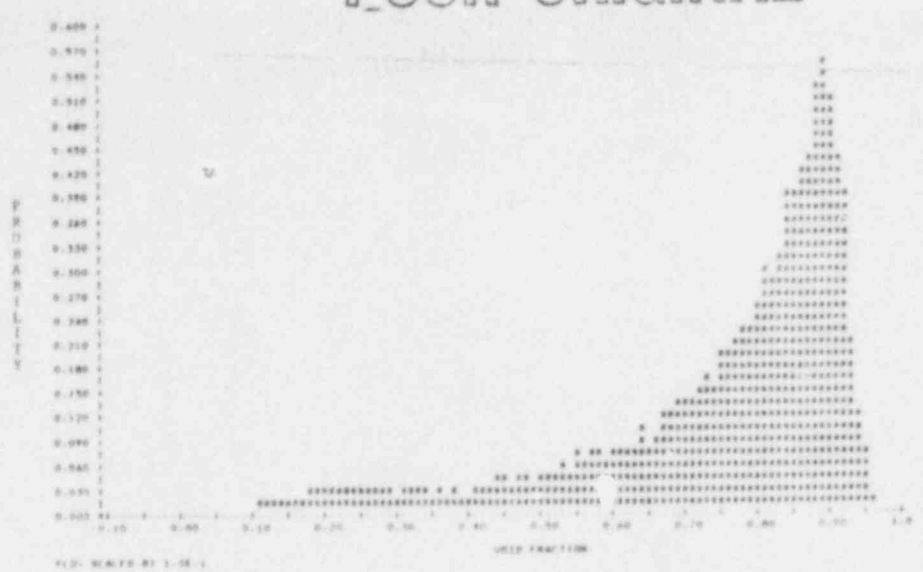

(b)

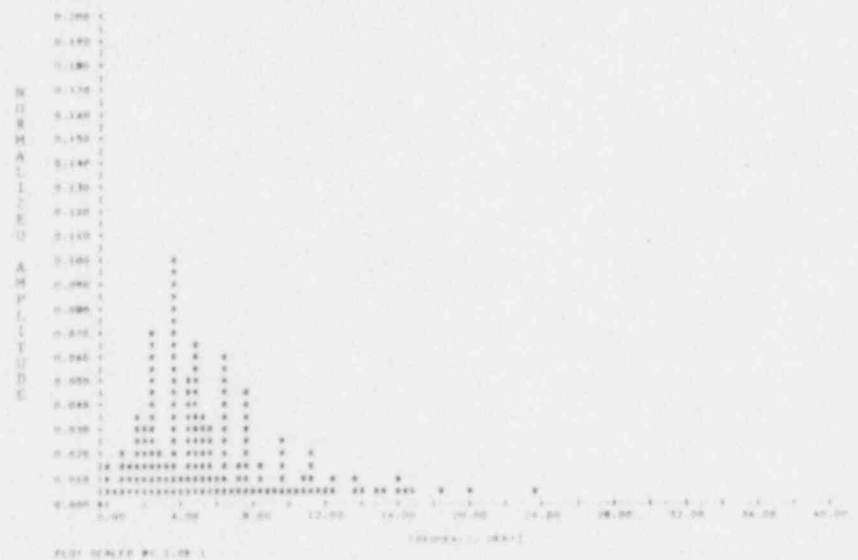

(c)

(a)

Figure 4.34

A photograph (a), diameter PDF (b), and diameter PSD (c), for 68 percent area-averaged void fraction, j_ℓ=0.25 m/sec, j_g=2.67 m/sec

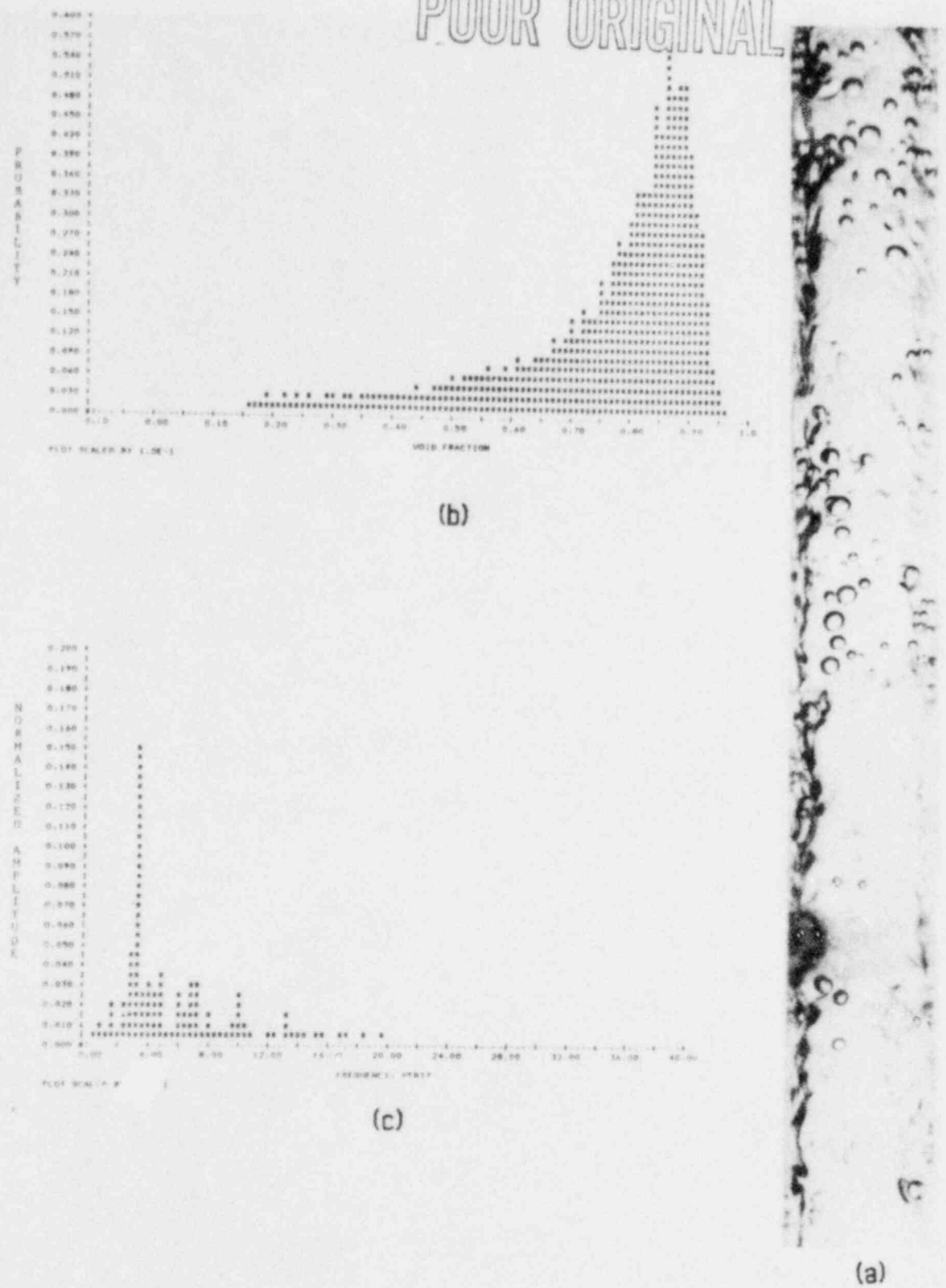

Figure 4.35

A photograph (a), diameter PDF (b), and diameter PSD (c), for 68 percent area-averaged void fraction, j_ℓ=0.37 m/sec, j_g=3.41 m/sec

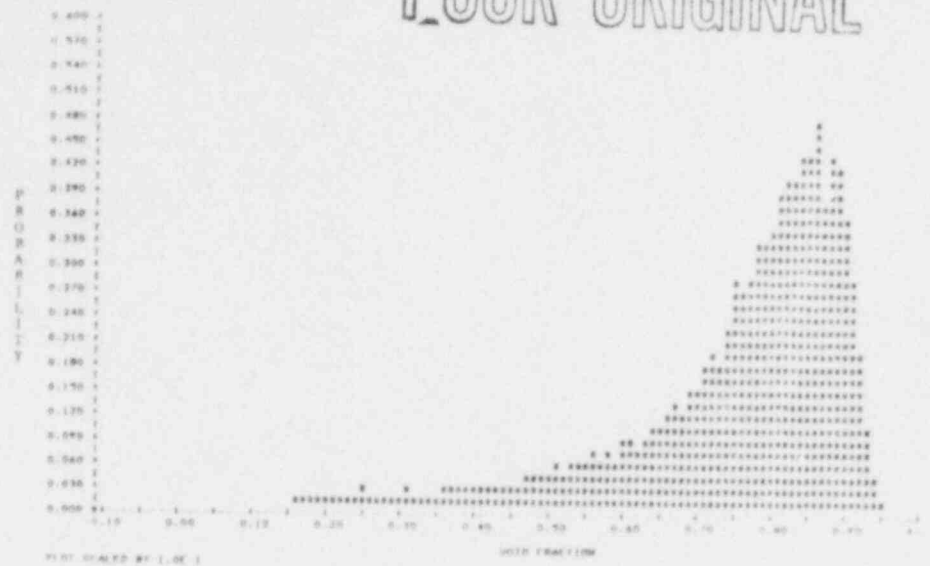

(b)

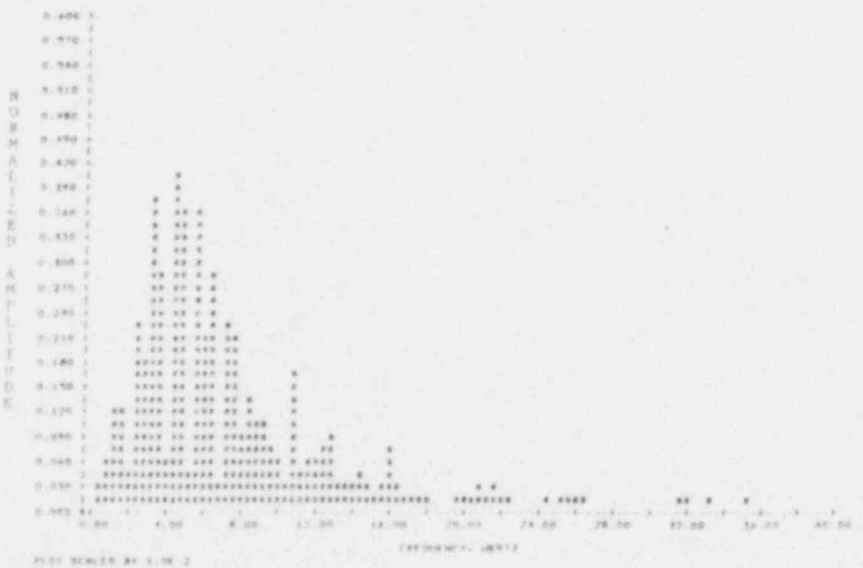

(c)

(a)

Figure 4.36

A photograph (a), diameter PDF (b), and diameter PSD (c), for 68 percent area-averaged void fraction, j_ℓ=0.50 m/sec, j_g=4.24 m/sec

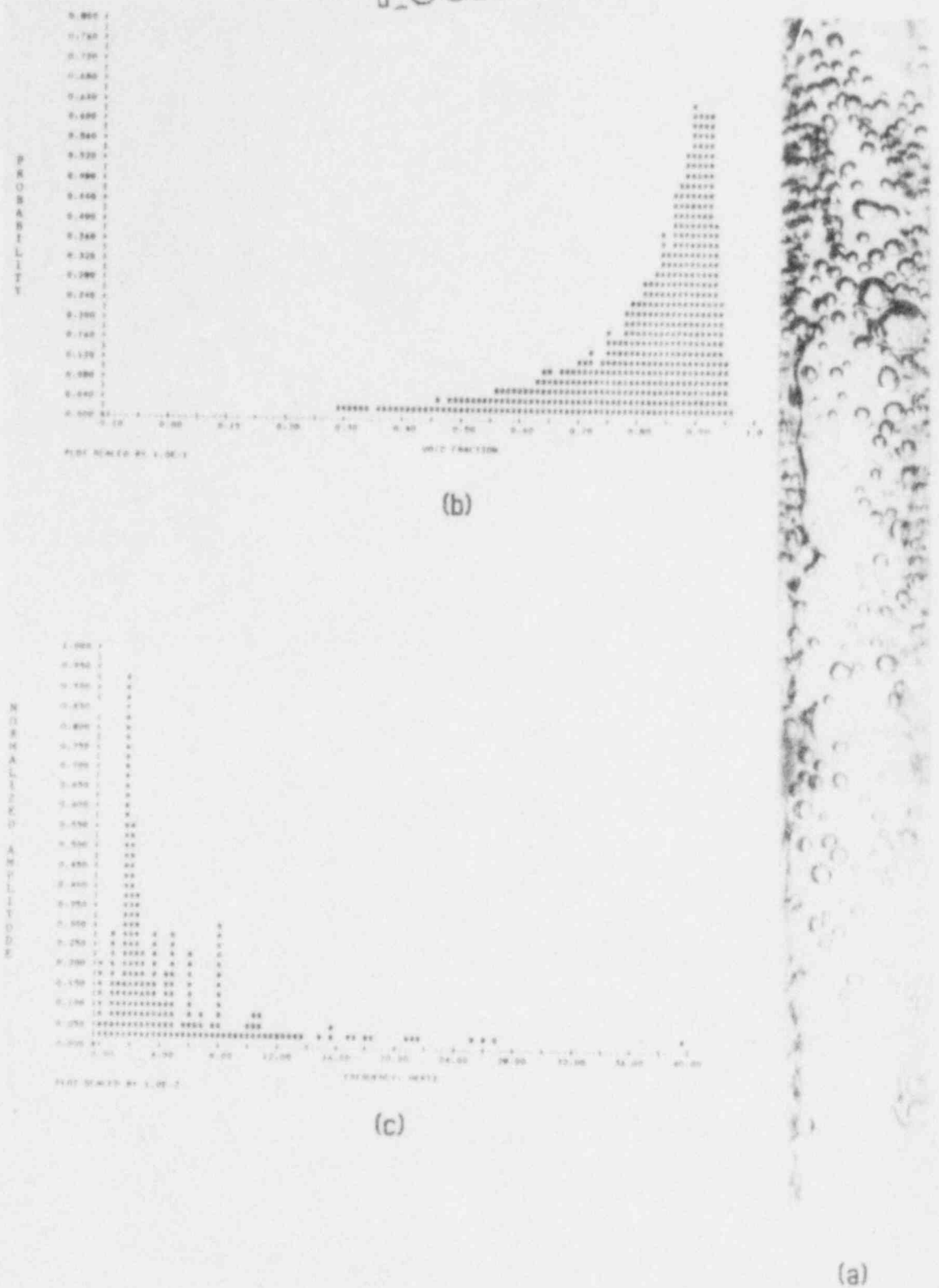

Figure 4.37

A photograph (a), diameter PDF (b), and diameter PSD (c), for 72 percent area-averaged void fraction, j_ℓ=0.0 m/sec, j_g=2.21 m/sec

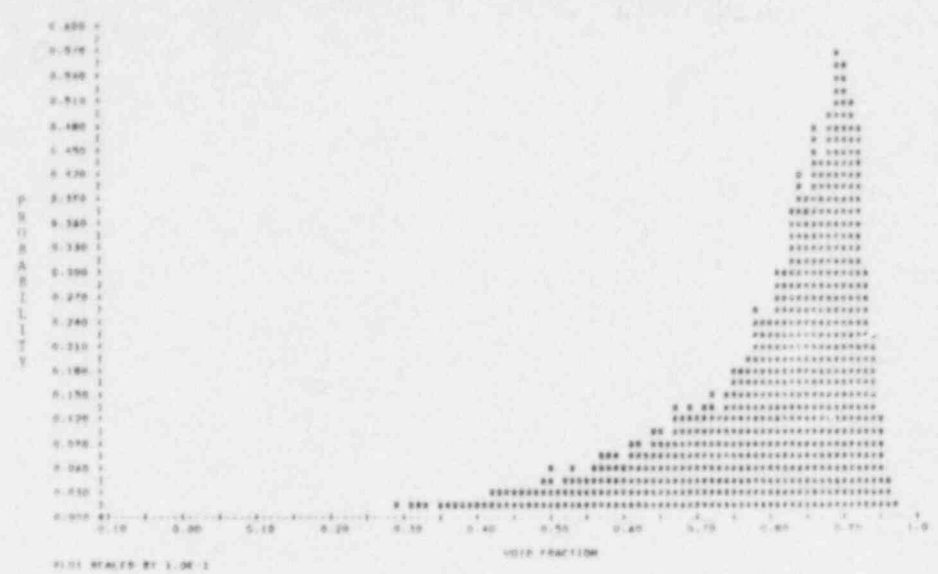

(b)

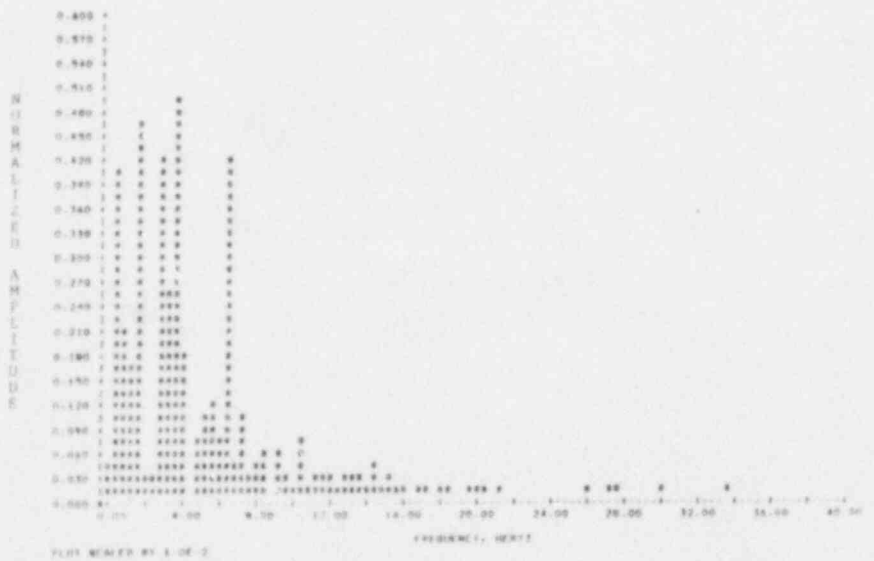

(c)

(a)

Figure 4.38
A photograph (a), diameter PDF (b), and diameter PSD (c), for 72 percent area-averaged void fraction, j_ℓ=0.12 m/sec, j_g=3.23 m/sec

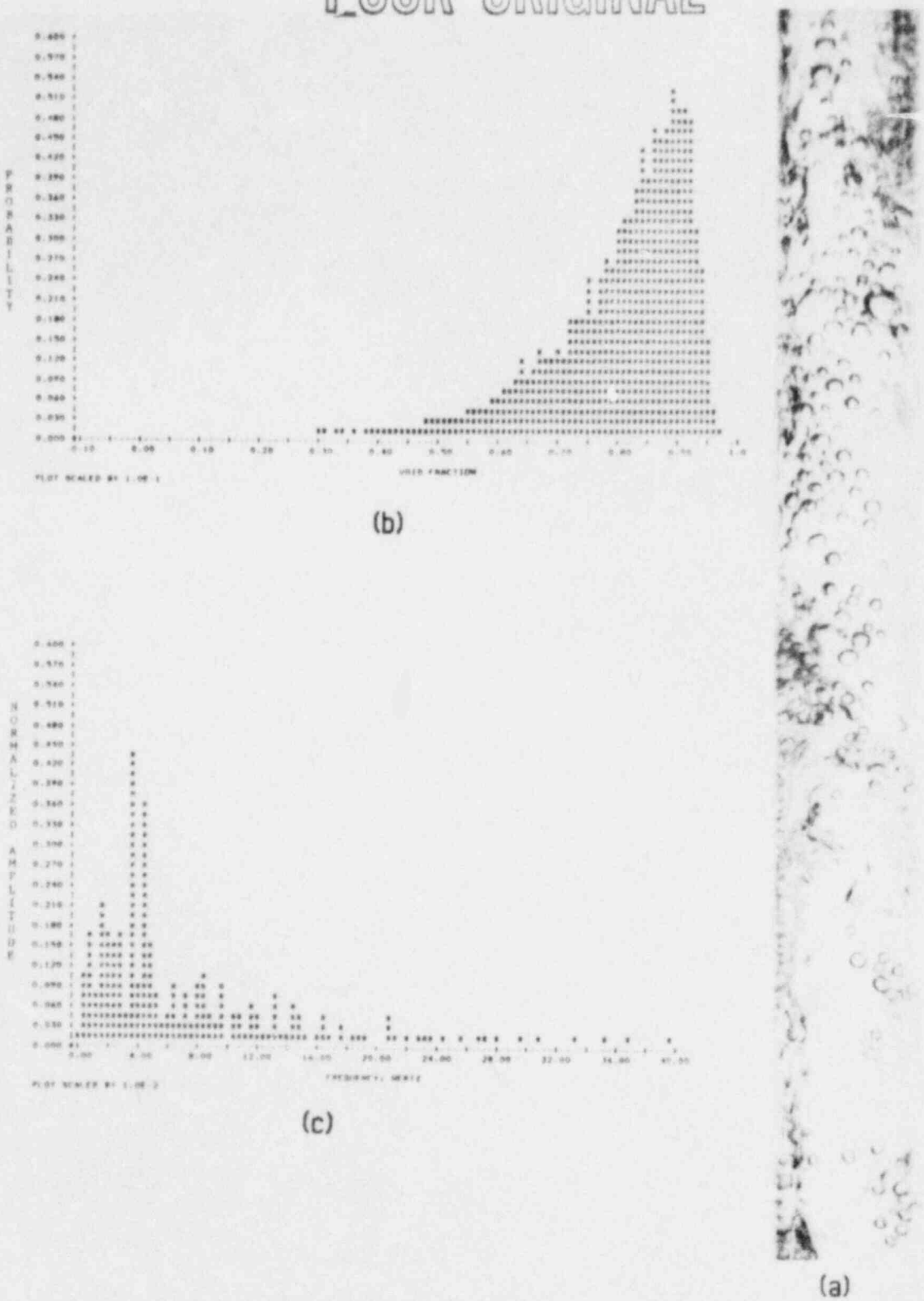

Figure 4.39
A photograph (a), diameter PDF (b), and diameter PSD (c), for 72 percent area-averaged void fraction, j_ℓ=0.25 m/sec, j_g=4.51 m/sec

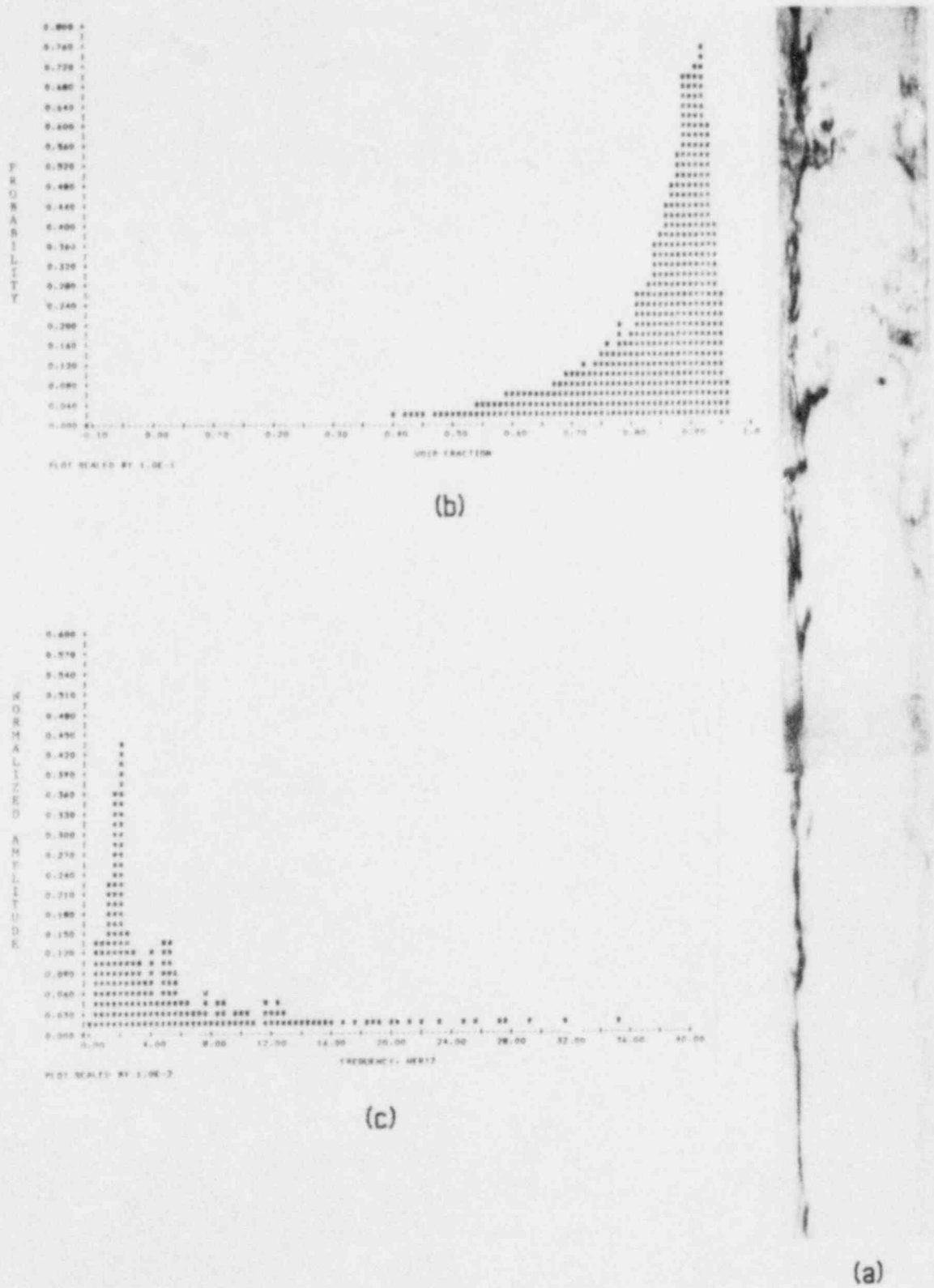

Figure 4.40

A photograph (a), diameter PDF (b), and diameter PSD (c), for 76 percent area-averaged void fraction, j_ℓ=0.0 m/sec, j_g=3.26 m/sec

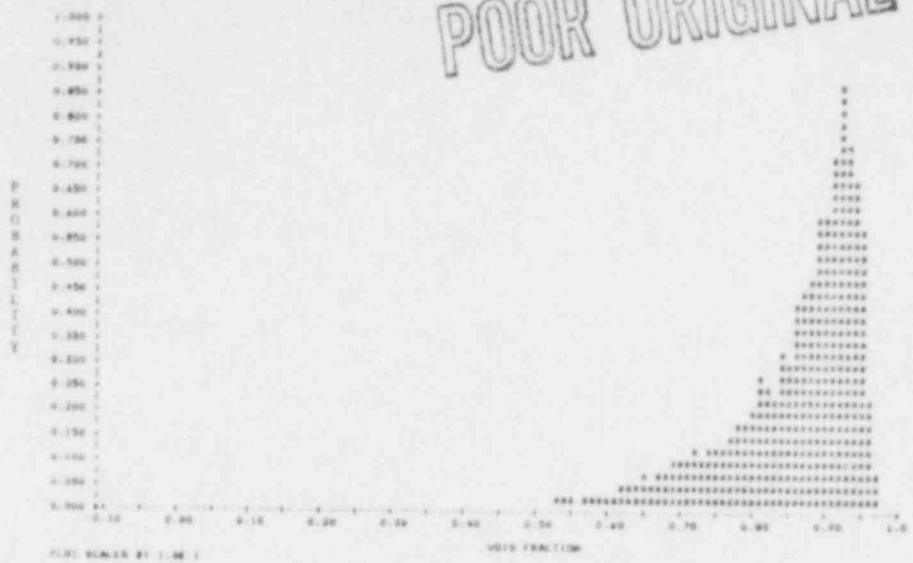

(b)

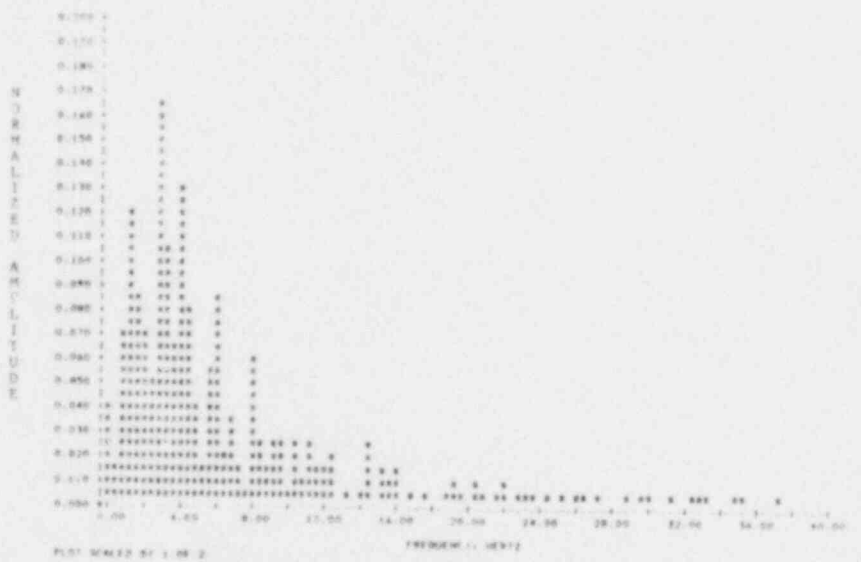

(c)

(a)

Figure 4.41
A photograph (a), diameter PDF (b), and diameter PSD (c), for 79 percent area-averaged void fraction, j_ℓ=0.0 m/sec, j_g=4.57 m/sec

The moments of a distribution, however, are a unique set of objective parameters associated with the distribution. Several moments were calculated for each void fraction data set including:

1) The mean, or first moment about the origin.
2) The second raw moment, or second moment about the origin.
3) The variance, or second moment about the mean.
4) The coefficient of skewness, or third moment about the mean divided by the variance raised to the 1.5 power.
5) The coefficient of kurtosis, or fourth moment about the mean divided by the variance squared.
6) The cummulative value, that is the integral of the distribution (i.e. the energy).

These measures of the distribution are widely used in classical signal recognition theory techniques, and were investigated in this study, as a function of void fraction.

The review of the moments to find an objective flow regime indicator was conducted in two stages. Initially, the data acquired with zero liquid flow was plotted as a function of void fraction. Secondly, the various moments were plotted as a function of liquid superficial velocity. The data acquired at constant void fraction was grouped for each plot. A good flow regime indicator will be fairly independent of measurement position, hence all data was also plotted by chordal

location.

4.2.1 Probability Density Function (PDF) Data

The PDFs resulting from void fraction measurements with the dual beam x-ray system showed three distinct regions:

1) A spike at zero void.
2) A broad peak at 15-20 percent chordal-average void.
3) A sharp pea' at 75-80 percent chordal-average void.

The zero void spike corresponds to a chordal measurement of water only. Small, discrete bubbles will produce the broad peak found at low voidage. Large voids, usually filling the entire pipe during slug or annular flow, are responsible for the high void fraction peak.

Bubbly flow exhibited the zero void spike and a single broad peak. Annular flow shows only the high void peak, as would be expected. Slug flow represents a combination of these three possiblities. Churn-turbulent flow, and higher void fraction slug flow, contains the low and high void peaks only.

4.2.1.1 Zero Liquid Flow Data

The mean void fraction, or first moment of the void distribution, will correspond exactly to the time averaged void fraction if the process is statistically

stationary. This relationship is called the Erogodic Hypothesis. Figure 4.42 compares the mean and the time averaged value. The correlation is excellent, indicating a stationary process, and that the measurements are independent of chordal position. Unfortunately, the mean does not provide information regarding the flow regime boundaries.

The second raw moment is shown in Figure 4.43 as a function of chordal void fraction. This response is relatively smooth over the void fraction range. All data, regardless of position, follows essentially the same curve. Replotting the same data as a function of the area-averaged void fraction results in Figure 4.44. The values of the moment are approximately straight lines. Chordal measurements at location 'A', 'B' and 'C' produce moments independent of position. The flow effects due to the wall appear in the data at the 'E' and 'F' chords but the linear trend is still observed.

A plot of the variance as a function of chordal-average void fraction is indicated in Figure 4.45. The curve is relatively smooth in the region expected for the bubbly-slug transition (at 20 to 30 percent void fraction). A slug-annular (at 70 to 80 percent void fraction) is also indicated since the variance changes sharply for a slight increase in void fraction. This graph does not clearly illustrate if a flow regime change has occurred. The same data replotted as a function of

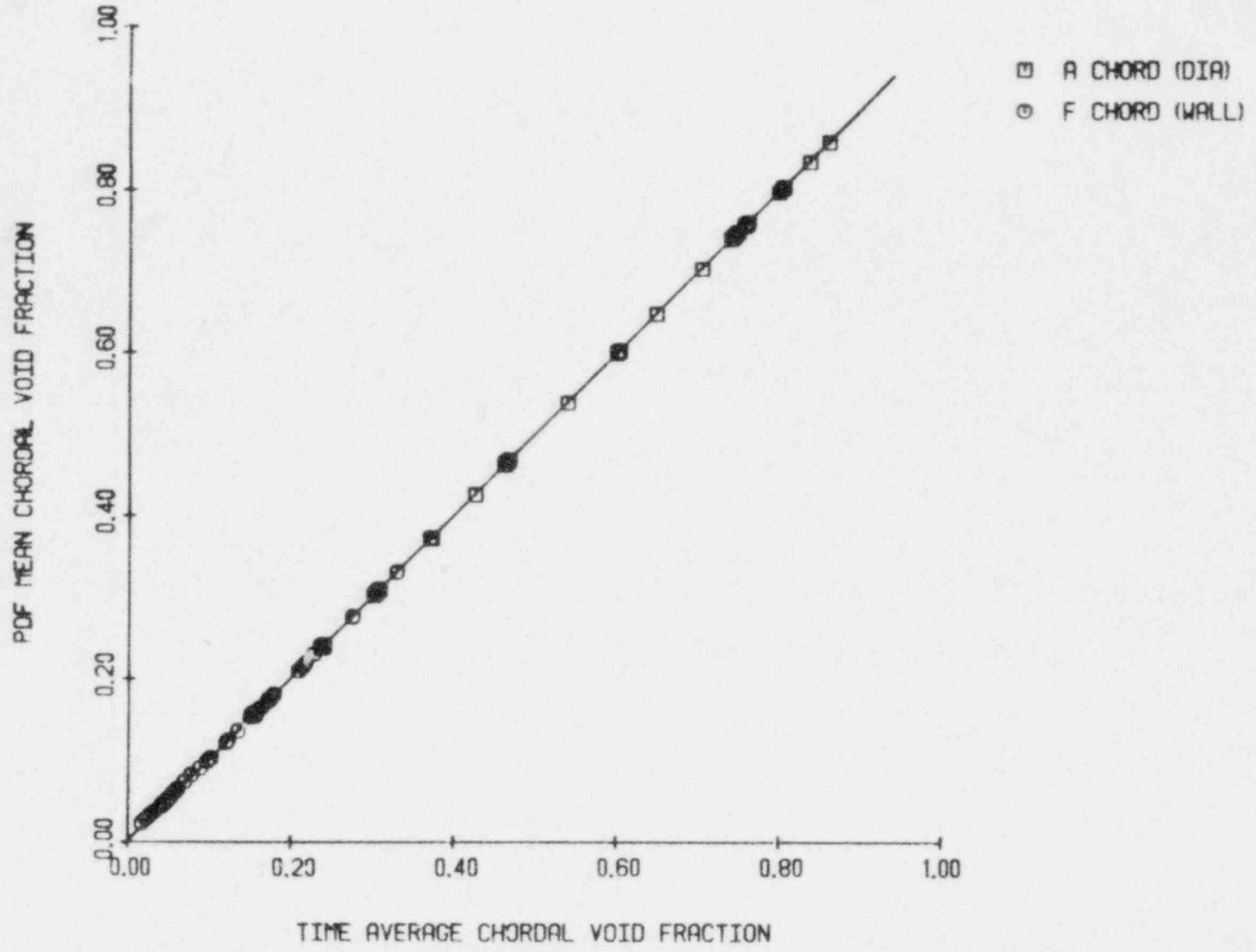

Figure 4.42 The PDF mean vs. time average chordal void fraction for all data

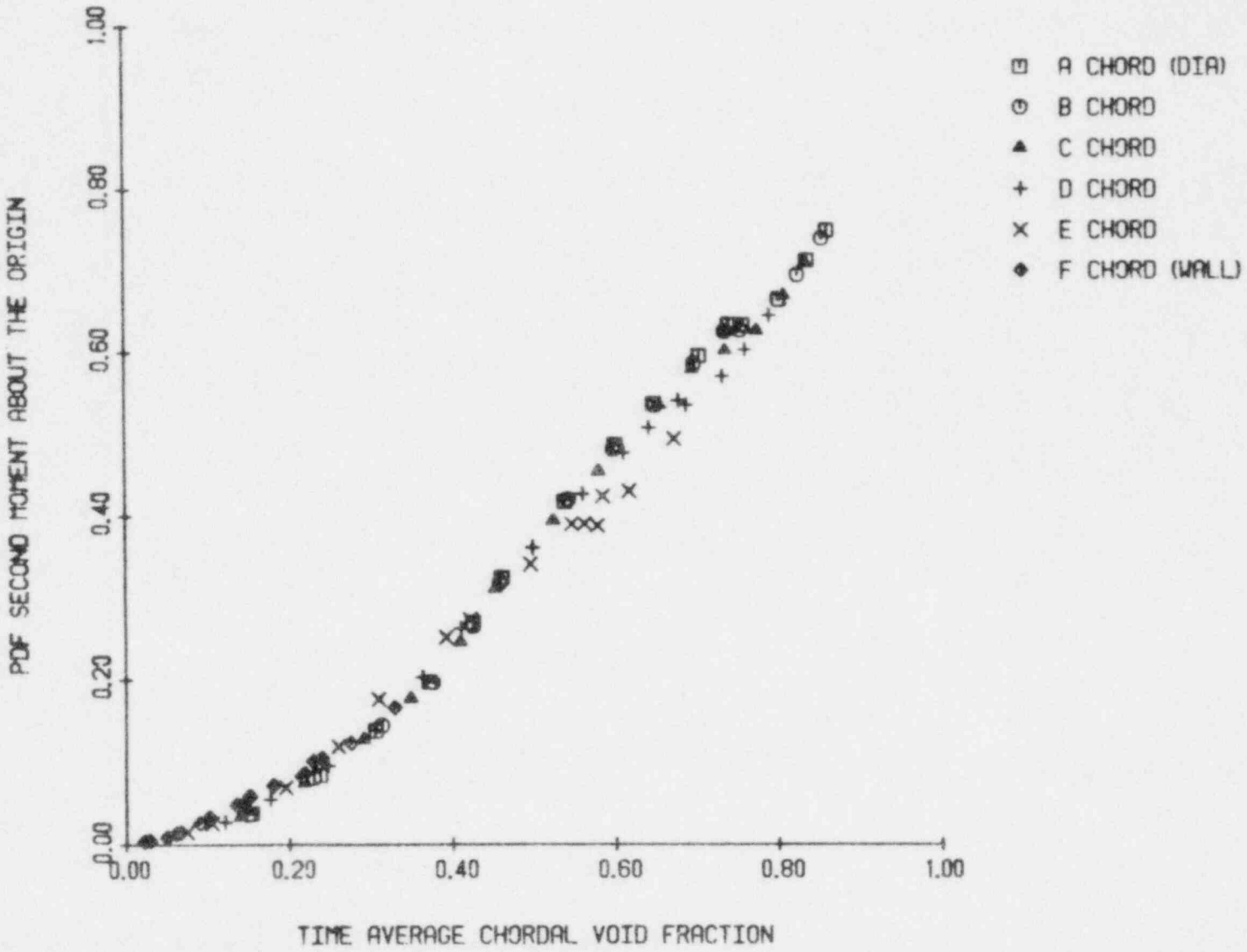

Figure 4.43 The PDF second moment about the origin vs. time average chordal void fraction for J_l=0.00 m/sec

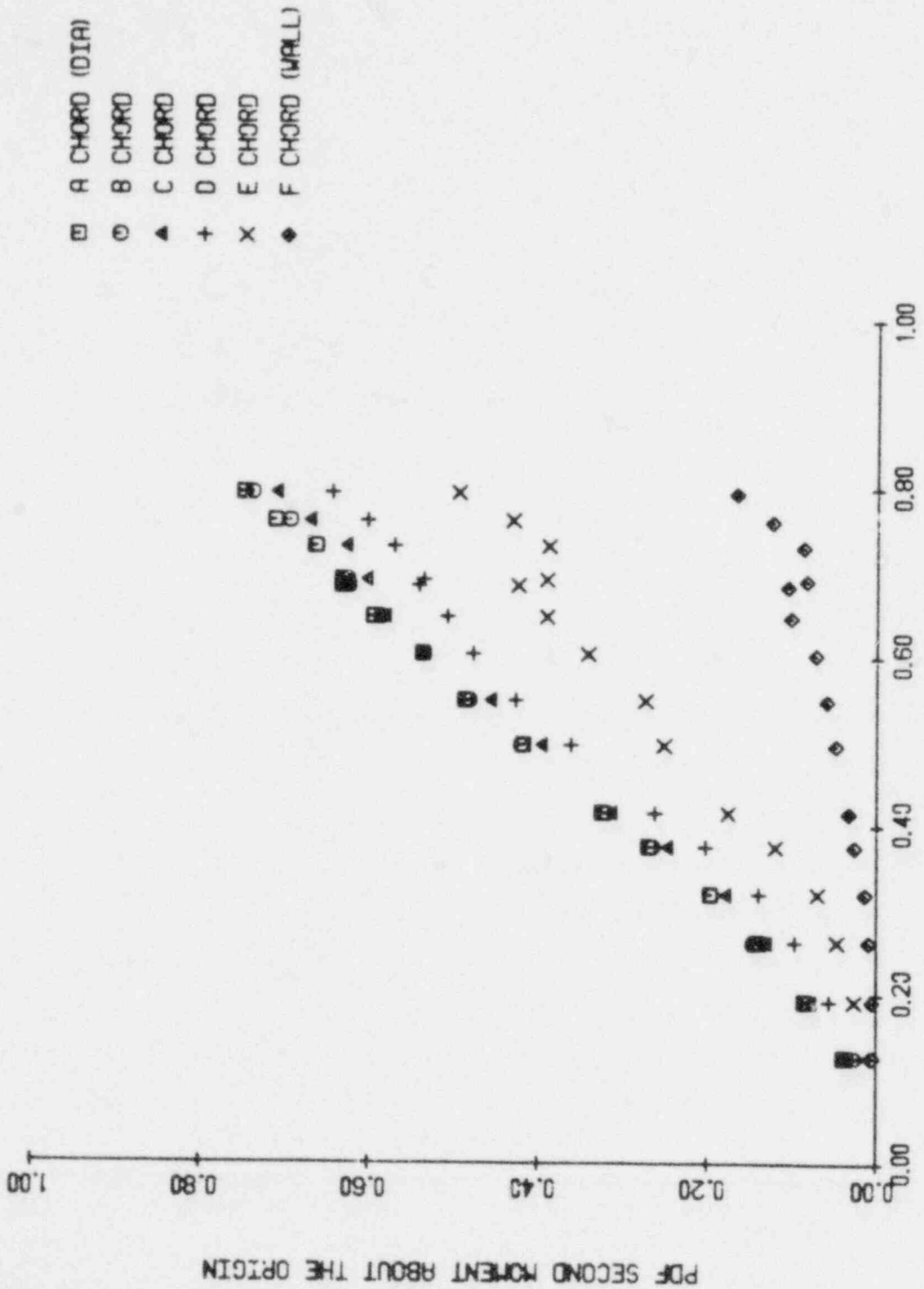

Figure 4.44 The PDF second moment about the origin vs. area-averaged void fraction for J_ℓ =0.00 m/sec

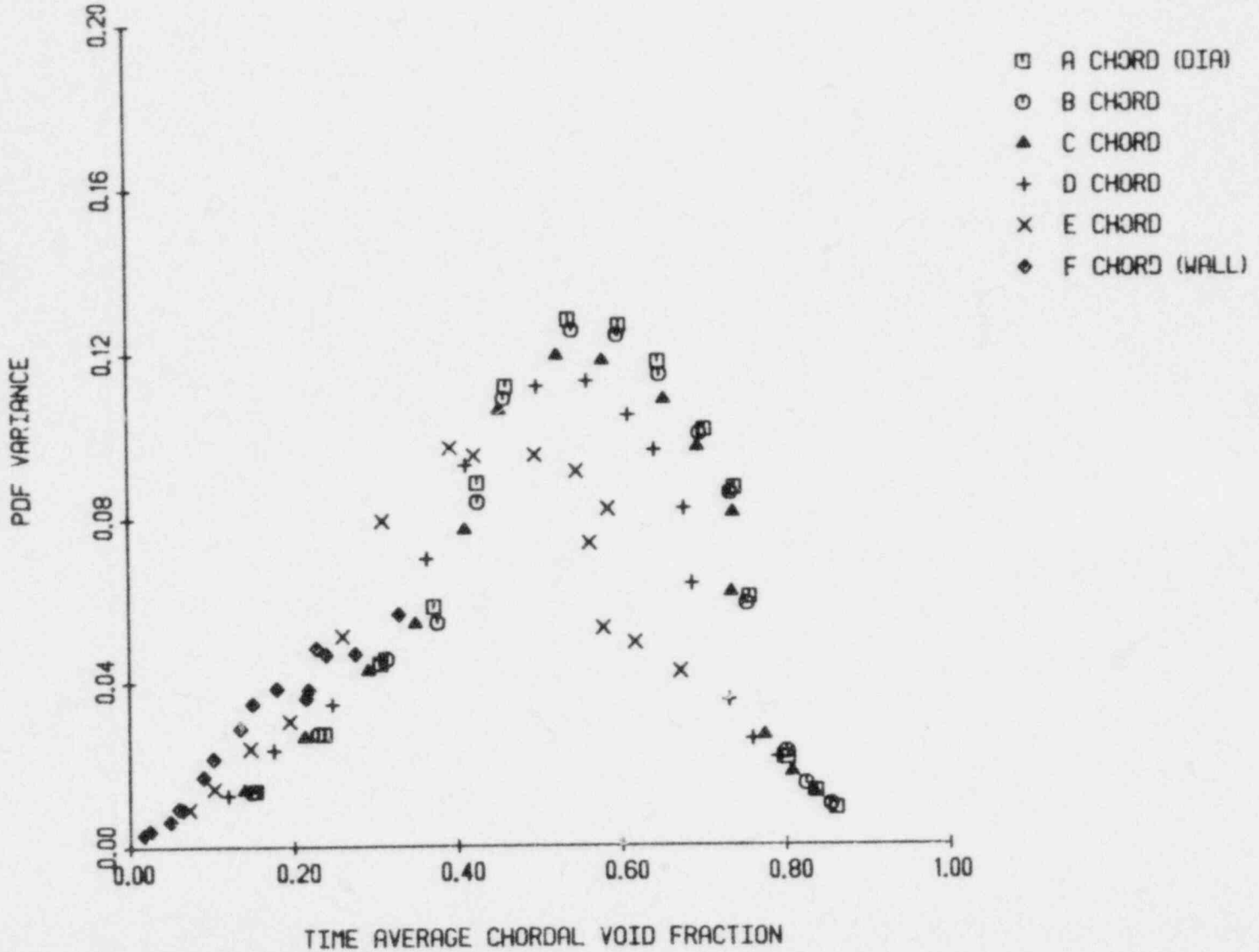

Figure 4.45 The PDF variance vs. time average chordal void fraction for j_ℓ=0.0 m/sec

area-averaged void fraction is shown in Figure 4.46. This graph reinforces the idea of using the variance as a possible slug-annular transition indicator. All data, with the exception of that along the wall chord, changes dramatically at about 70 percent area-average void fraction. The curves then tend toward zero as the void fraction approaches one. This should be expected since the mean void fraction would be centered about unity for an empty pipe. It can be noted that a variance of 0.04 predicts the slug-annular transition.

Two-phase flow structure can be easily associated with the variance. Liquid bridging across the pipe is the primary physical difference between slug and annular flow. For slug flow the presence of a low void region, associated with the liquid slug (and entrained bubbles), and a high void region associated with the large spherical cap bubbles, produces considerable variance from the mean. The disappearance of the liquid slug corresponds to a significant decrease in variance and thus indicates transition to annular flow.

The response at the wall can also easily be explained. Larger gas flow rates, associated with the higher void fractions, cause the liquid phase to flow on the walls. Thus, for annular flow, void fractions measured in the wall region will be considerably lower than in the rest of the test section. A word of caution is in order, however, since due to the effect of slight changes in

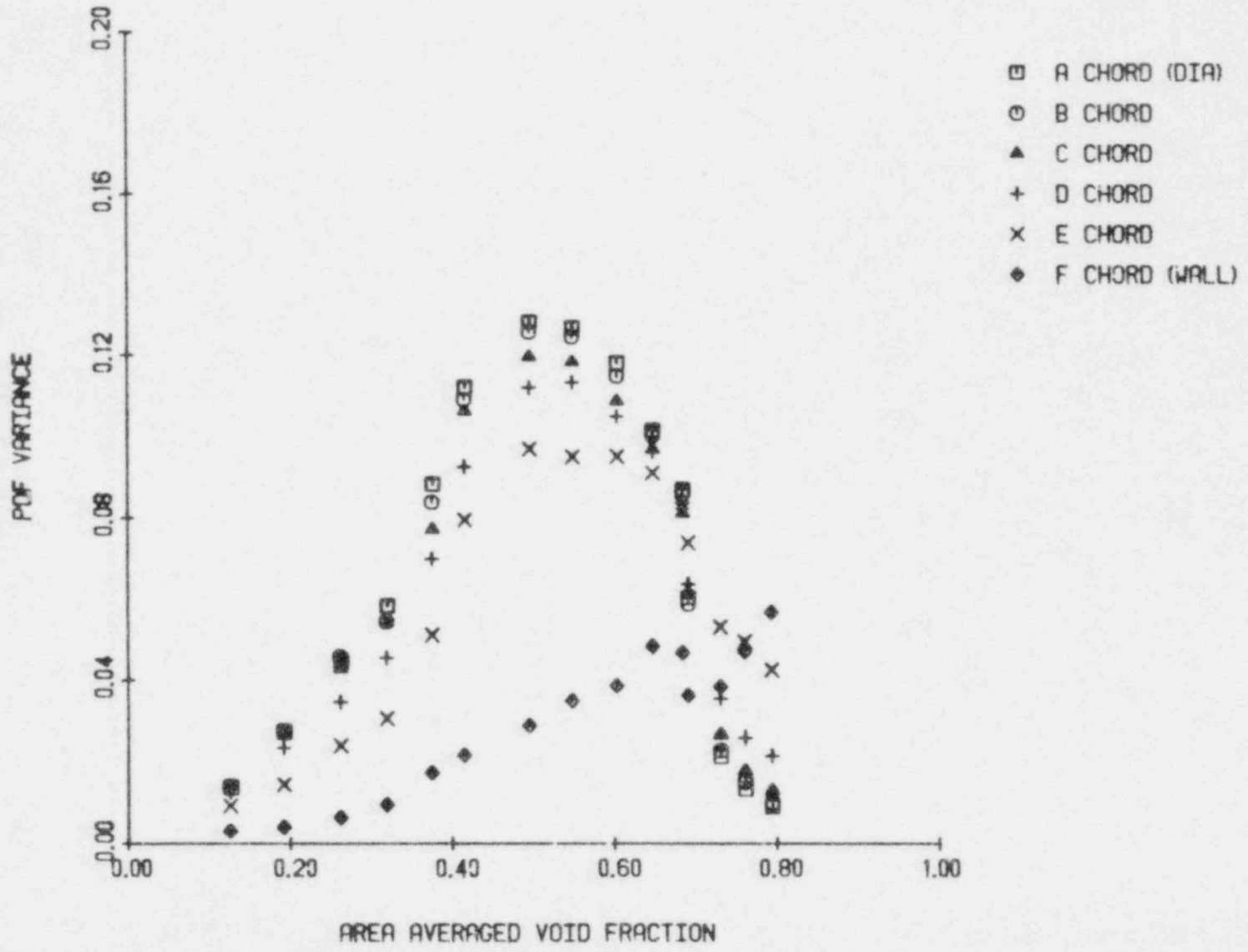

Figure 4.46 The PDF variance vs. area-averaged void fraction for J_g=0.0 m/sec

geometry, poor accuracy can be expected near the wall. In addition, radiation streaming may be occurring because of the potential for a parallel attenuation situation as shown schematically in Figure 4.47.

A plot of the third moment, the coefficient of skewness, as a function of chordal void fraction is shown in Figure 4.48. The skewness is relatively smooth in the bubbly-slug transition region, further indicating the smoothness of this occurrence. A potential slug-annular transition is indicated near 80 percent chordal void fraction. Skewness is relatively independent of position, except for the wall.

The skewness, like the variance, is a measure of the distribution with respect to the mean. The loss of liquid bridging should produce a considerable shift in the void PDF. Replotting the data in terms of area-averaged void fraction is illustrated in Figure 4.49. This graph accentuates the skewness minimum at about 70 percent area-average void. It can be seen that the 'E' and 'F' chords do not exhibit trends similar to the other chords. Note, however, that for the diametric measurements, both the skewness and variance change at the same voidage.

The fourth moment, the coefficient of kurtosis, is plotted as a function of chordal void fraction in Figure 4.50. This parameter is relatively constant in the bubbly-slug transition region. Kurtosis, or peakedness, is minimized near 50 percent chordal void fraction. This

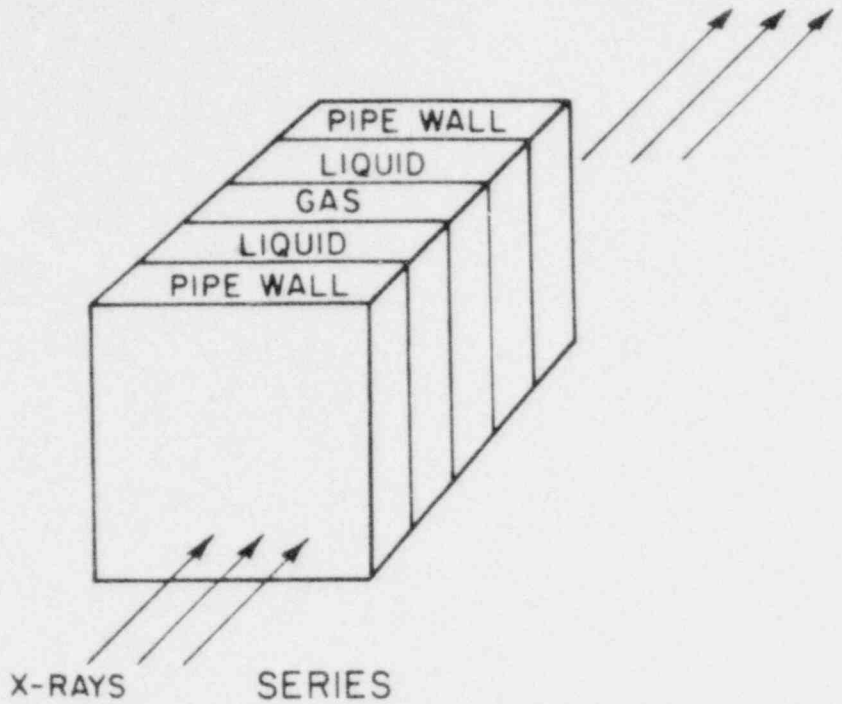

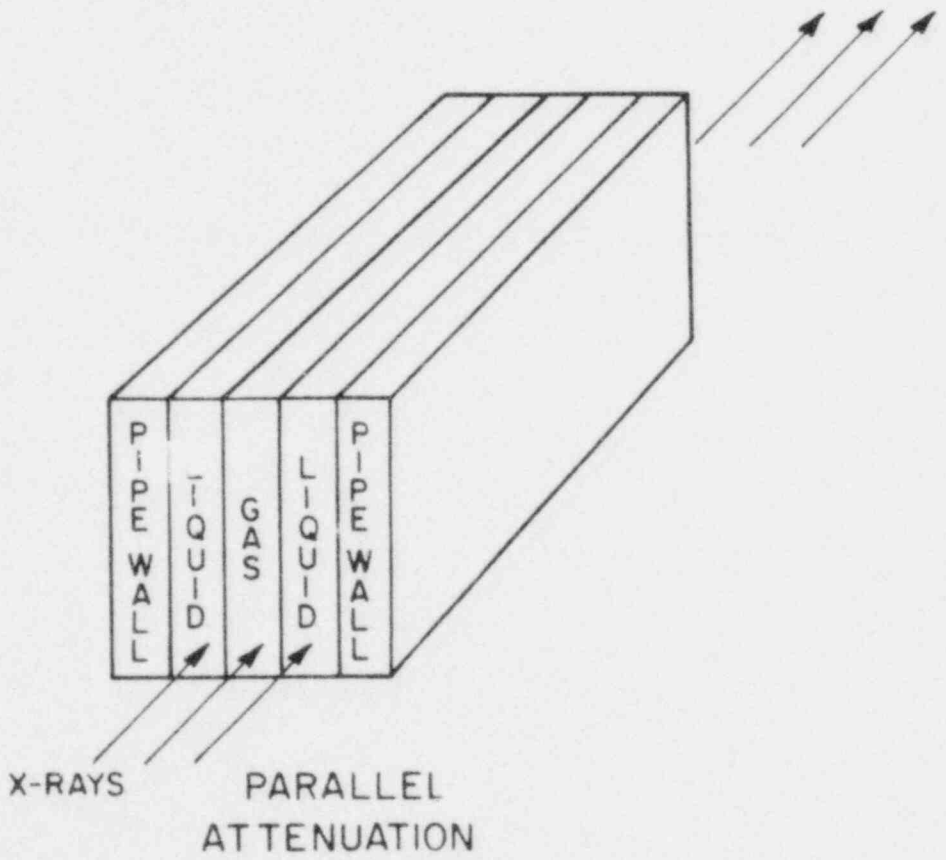

Figure 4.47
A comparison of series and parallel attenuation in two-phase flow

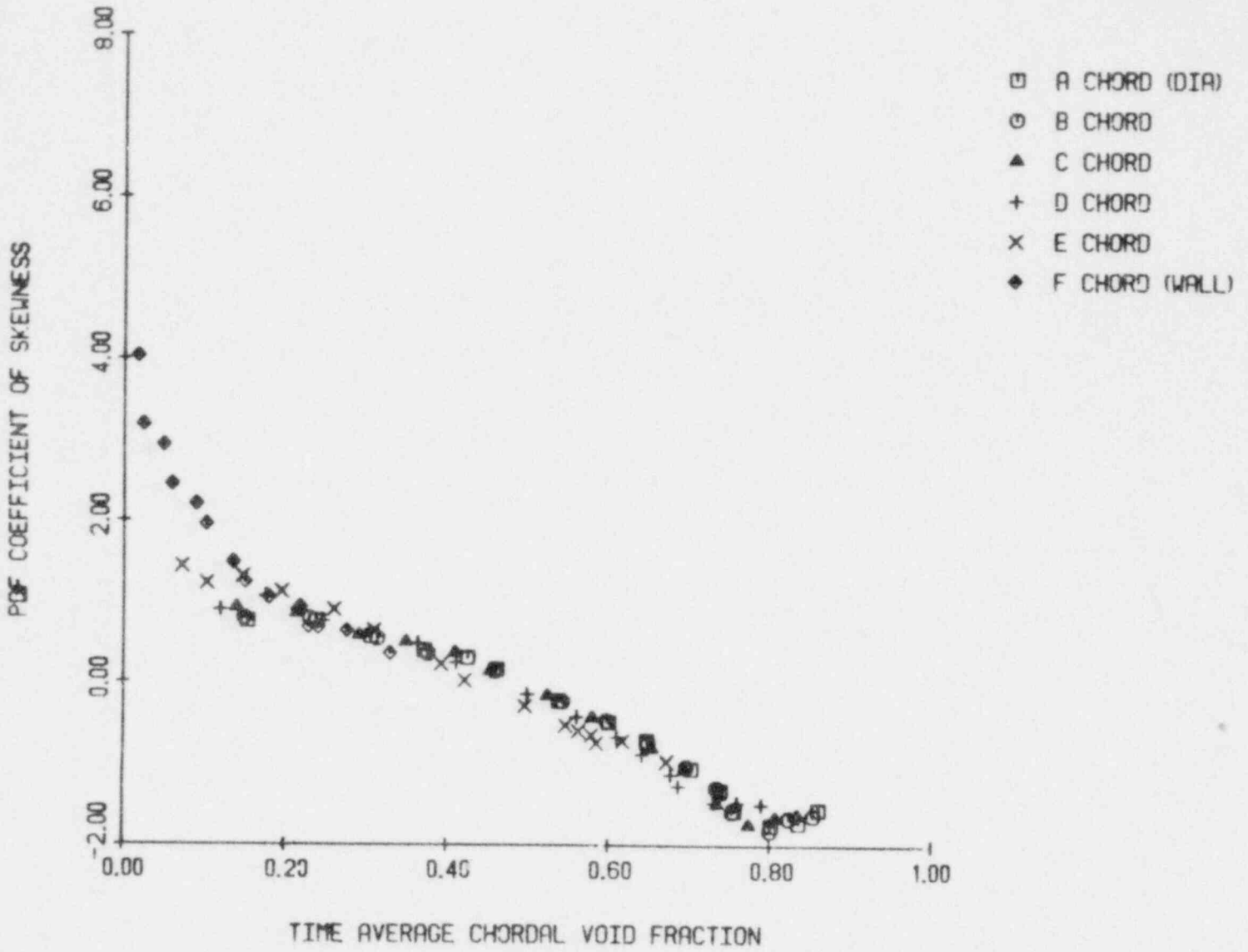

Figure 4.48 The PDF coefficient of skewness vs. time average chordal void fraction for J_L=0.00 m/sec

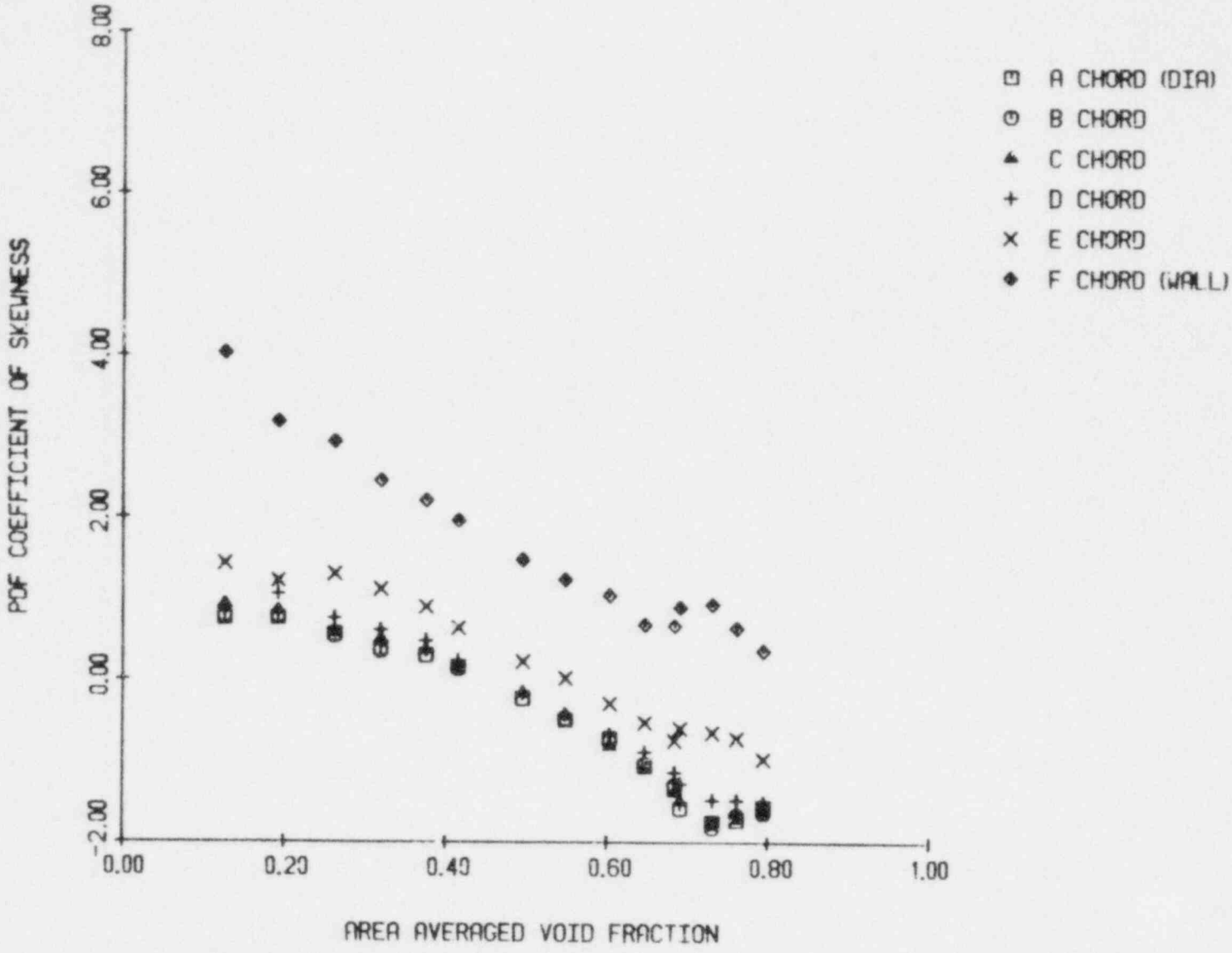

Figure 4.49 The PDF coefficient of skewness vs. area-averaged void fraction for J_L=0.00 m/sec

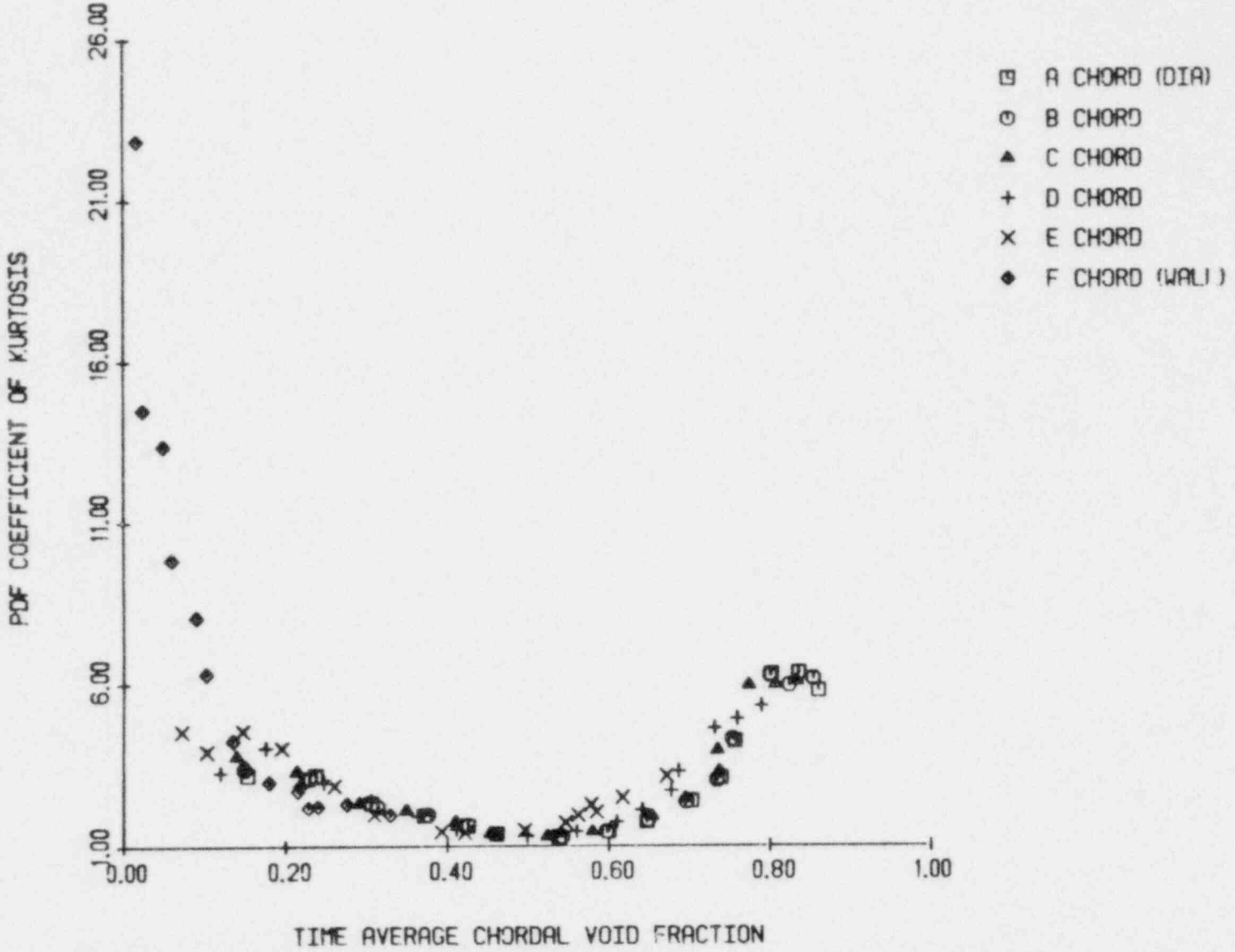

Figure 4.50 The PDF coefficient of kurtosis vs. time average chordal void fraction for J_L=0.00 m/sec

observation is explained by considering the slug flow pattern. At this voidage, an even distribution is observed between these phases, thus the high and low voidage PDF peaks offset each other and minimize the kurtosis.

The kurtosis, like the lower moments, indicates flow regime transistion near 80 percent chordal void fraction. All chordal measurements follow the same trend. As expected, the measurements made near the wall do not readily indicate a flow regime transition.

A plot of the coefficient of kurtosis as a function of area-averaged void fraction, Figure 4.51, further amplifies the slug-annular transition. The kurtosis increases rapidly at 70 percent void. This response corresponds to a substantial increase in peakedness caused by the disappearance of the liquid slugs. It should be noted that measurements made near the wall, i.e. the 'E' and 'F' chords, do not exhibit the same trends as data acquired elsewhere.

4.2.1.2 Non-Zero Liquid Flow Data

Any useful flow regime indicator should be independent of mixture velocity. Thus, the data acquired at non-zero liquid flows was compared to that acquired at zero liquid flow.

The variance was observed to be relatively constant in bubbly flow. Figure 4.52 illustrates the variance as a function of liquid superficial velocity for an

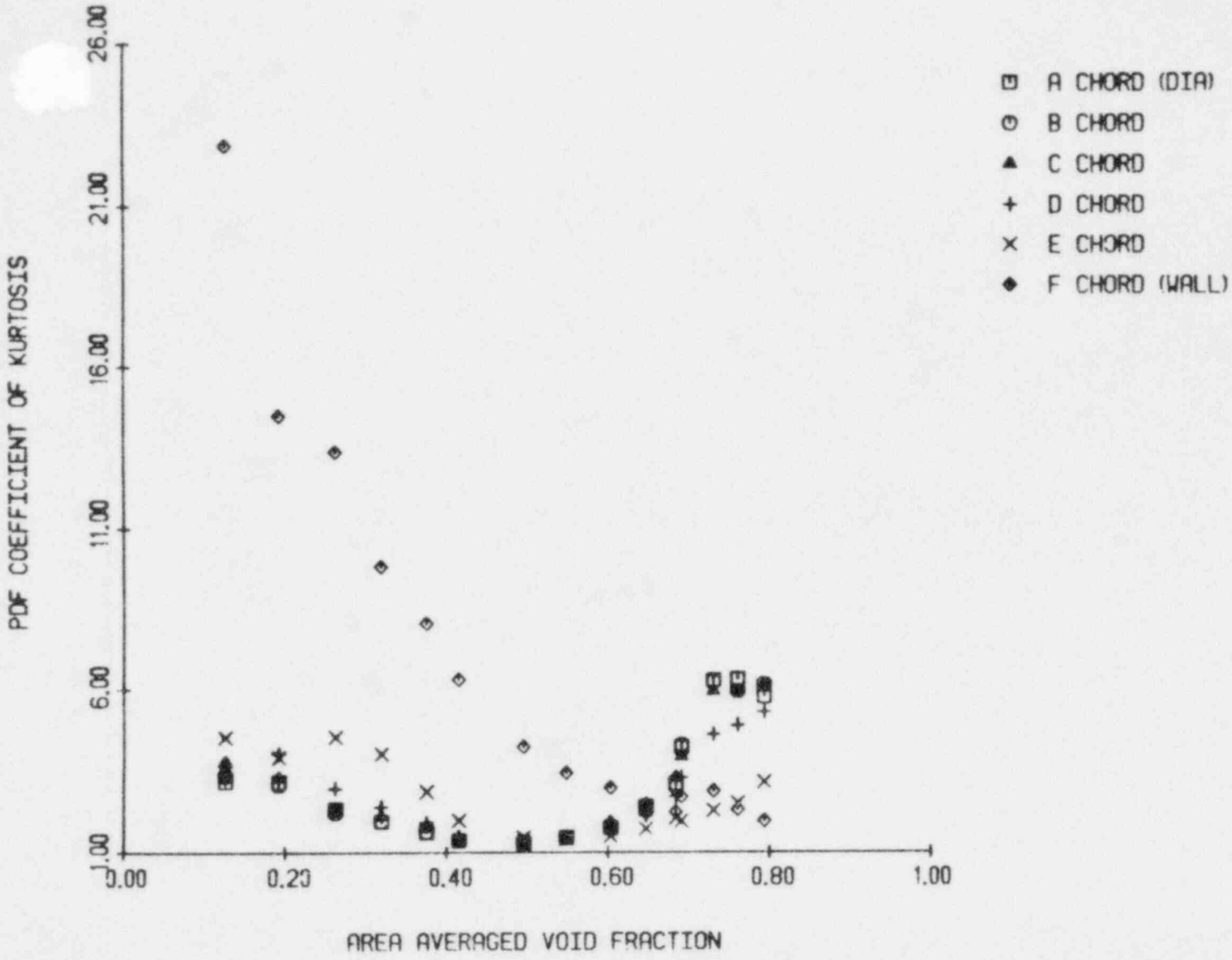

Figure 4.51 The PDF coefficient of kurtosis vs. area-averaged void fraction for J_L=0.00 m/sec

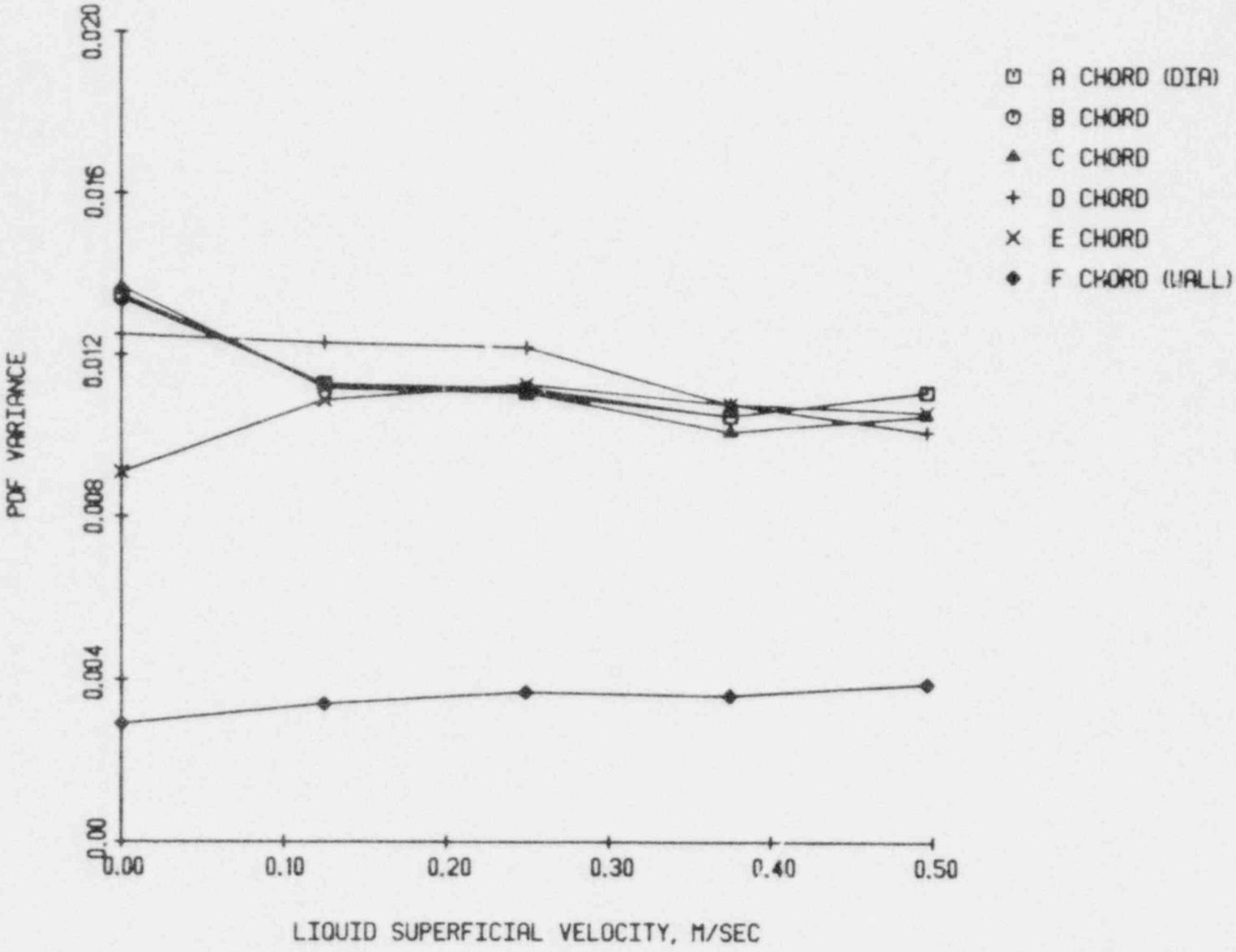

Figure 4.52 The PDF variance vs. superficial liquid velocity at 13 percent area-averaged void fraction

area-averaged void fraction of 3 percent. Increasing the area-averaged voidage to 20 percent results shown in Figure 4.53. The variance initially decreases with the onset of liquid velocity. This occurence indicates that the bubbly-slug transition is suppressed by the liquid velocity. An increase in liquid velocity ultimately cannot stop the transition to slug flow because of the corresponding increase in vapor flow rate necessary to maintain constant void fraction. This phenomena is also seen at 26 percent area-averaged void fraction, as illustrated in Figure 4.54. The onset of liquid flow initially suppresses the bubbly-slug transition. At some point, the liquid velocity can no longer stop the transition and the variance increases dramatically indicating a transition. Notice that all chords indicate similar trends. Clearly, the bubbly-slug flow regime transition does not occur at constant void fraction, however it is seen that a variance of 0.04 will predict the bubbly-slug transition.

A further increase of area-averaged void fraction to 32 percent produces the variances shown in Figure 4.55. Slug flow is obvious and the variance continues to increase with liquid flow. At 41 percent area-averaged void fraction, the variance is independent of liquid velocity as shown in Figure 4.56. All chords, except the 'F' wall chord, have a similar magnitude, and every chord exhibits the same trend.

Figure 4.57 illustrates the variance as a function

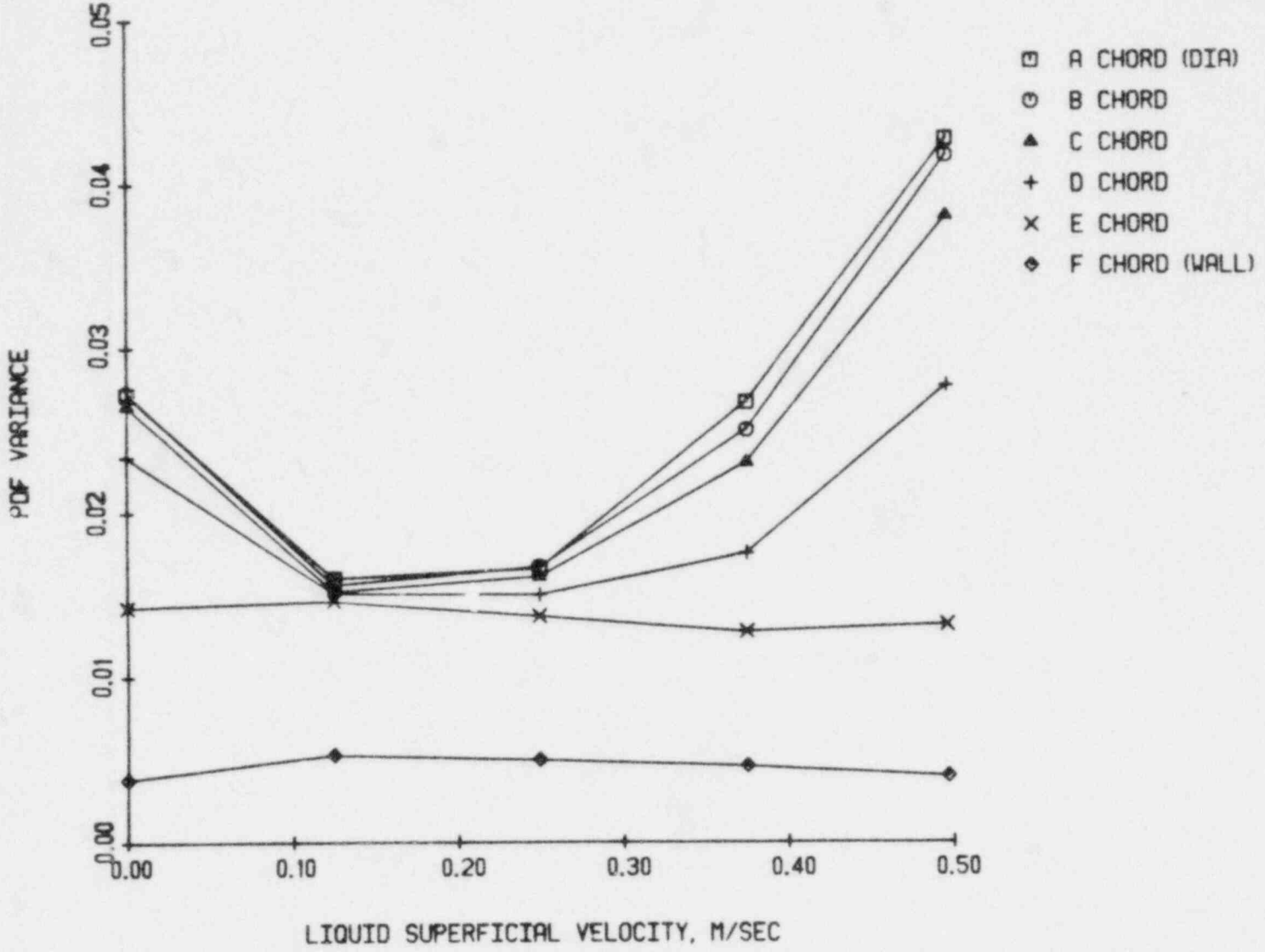

Figure 4.53 The PDF variance vs. superficial liquid velocity at 20 percent area-averaged void fraction

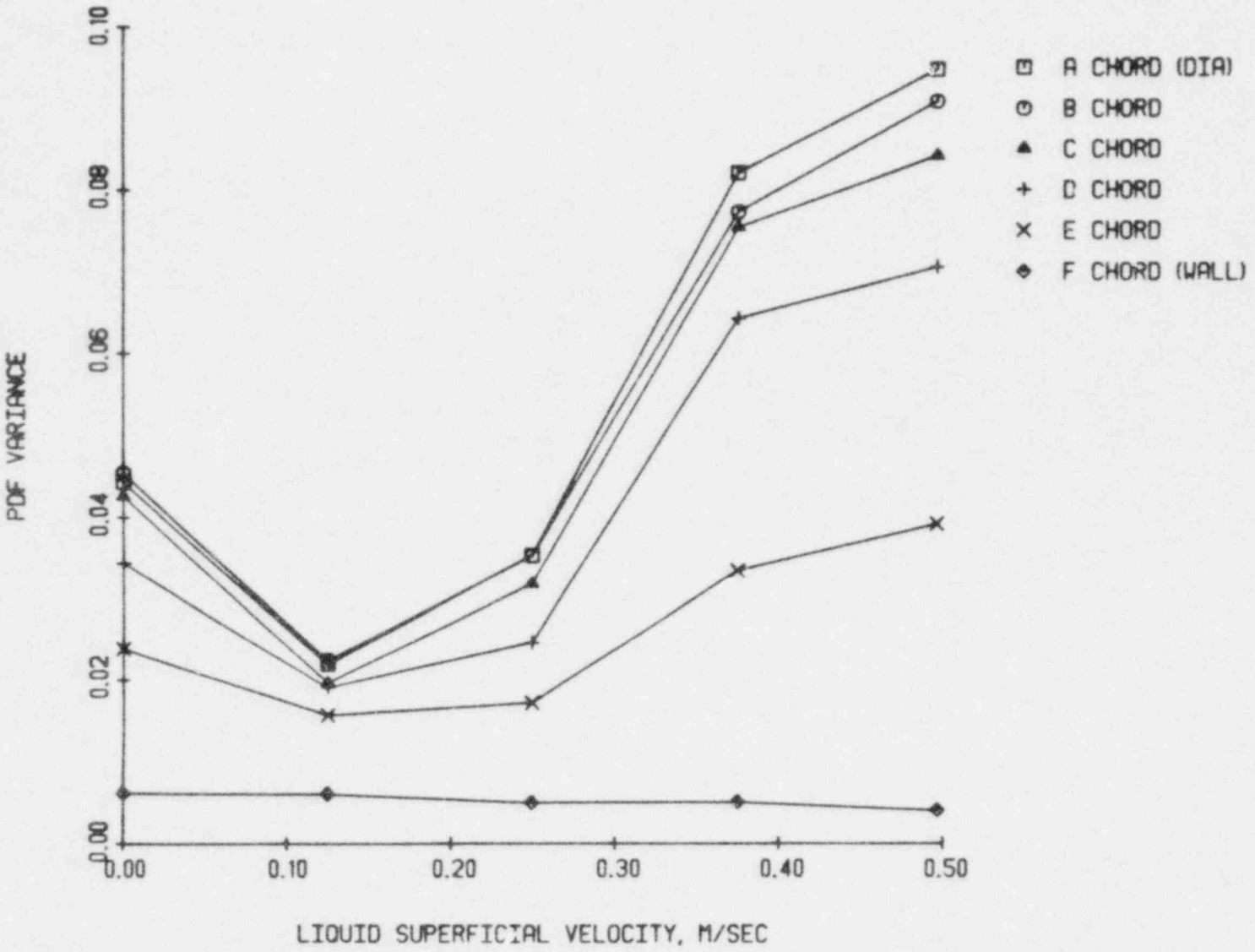

Figure 4.54 The PDF variance vs. superficial liquid velocity at 26 percent area-averaged void fraction

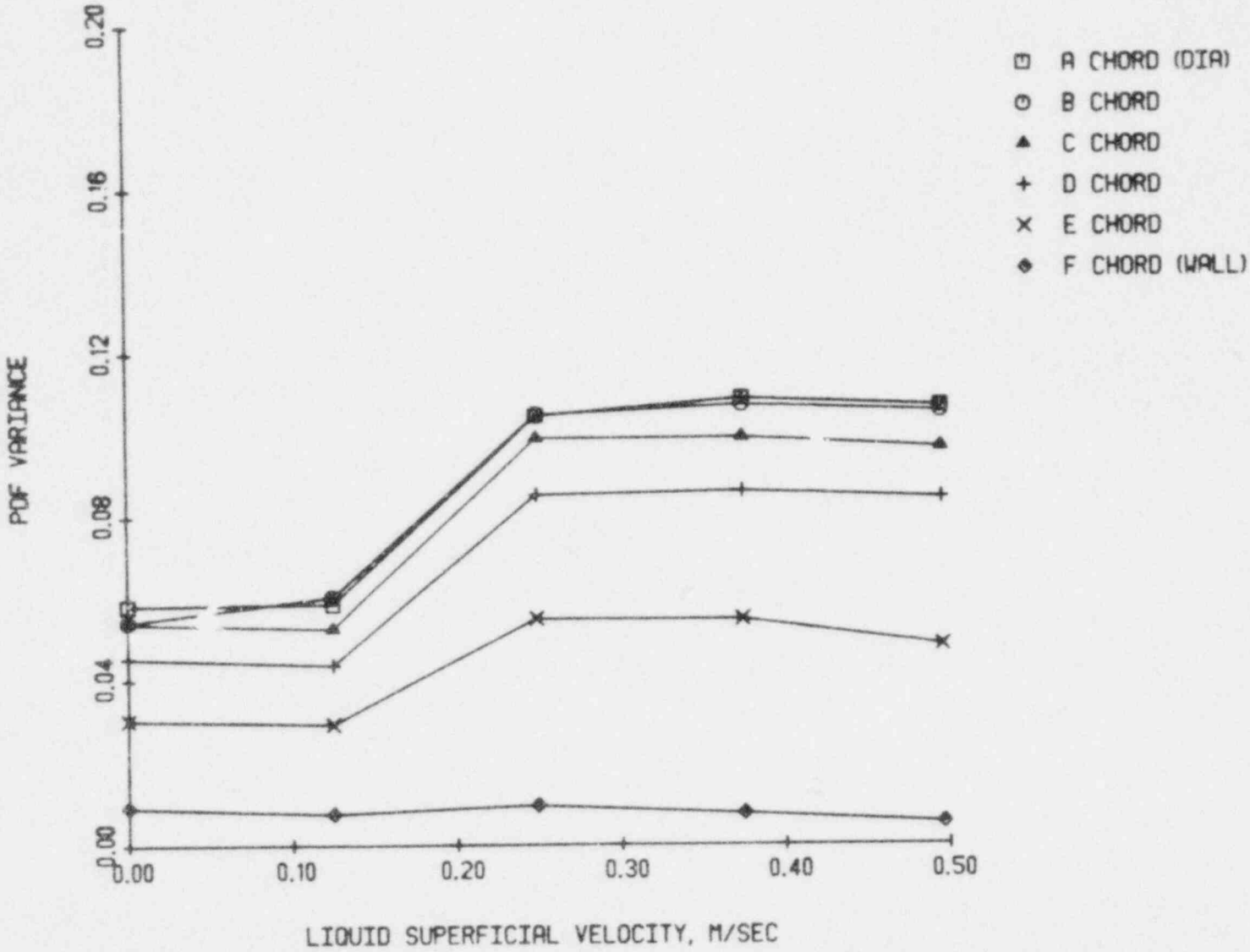

Figure 4.55 The PDF variance vs. superficial liquid velocity at 32 percent area-averaged void fraction

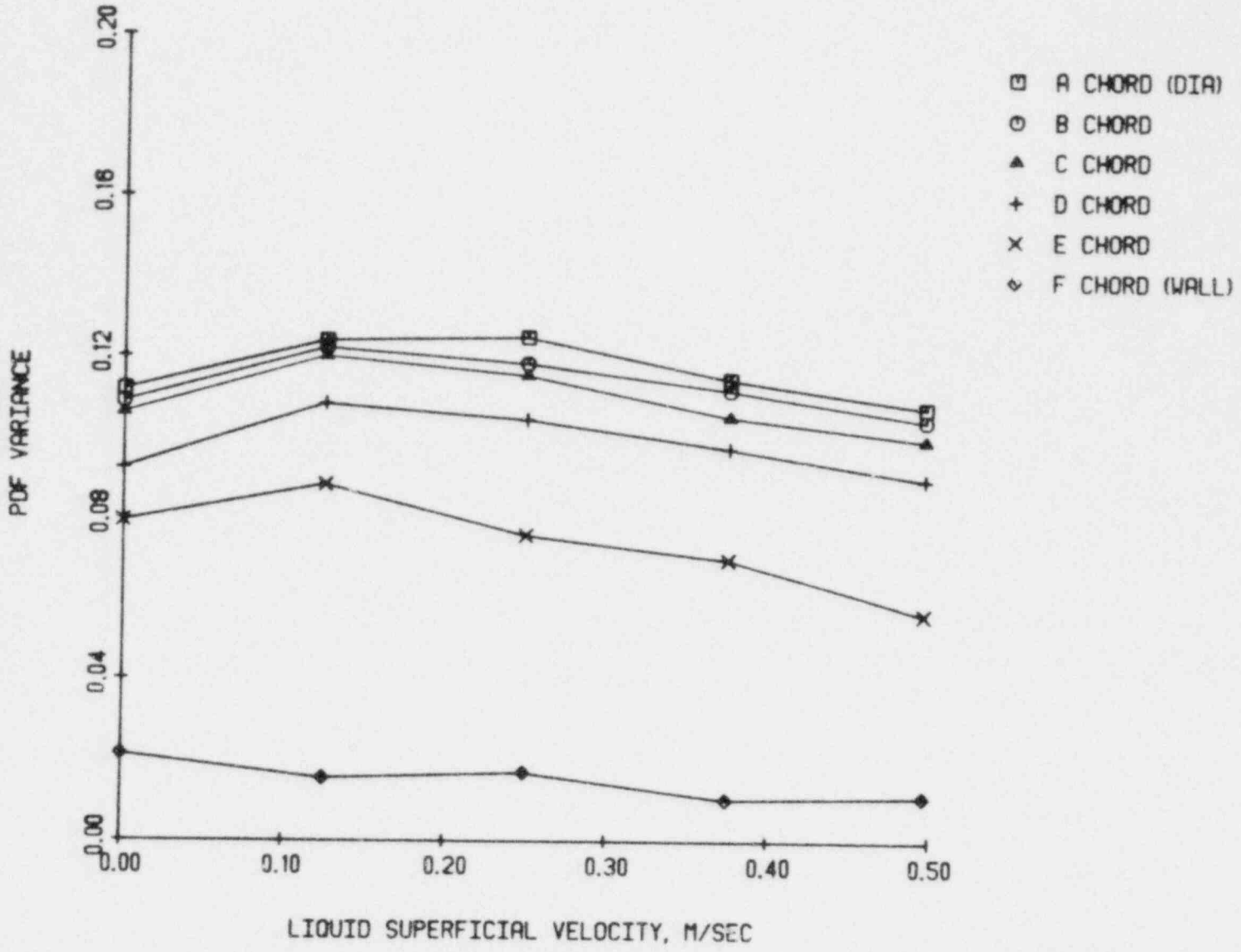

Figure 4.56 The PDF variance vs. superficial liquid velocity at 41 percent area-averaged void fraction

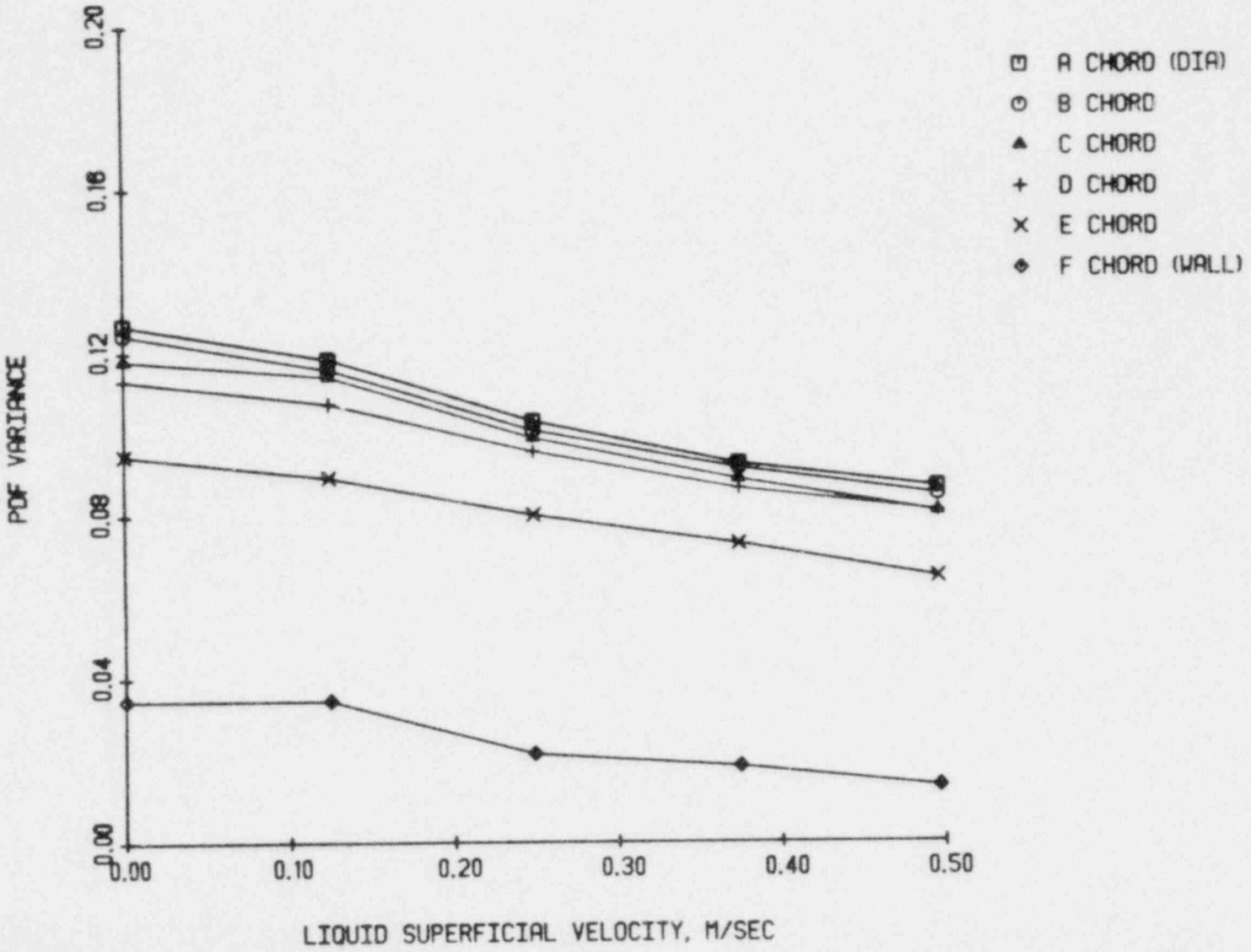

Figure 4.57 The PDF variance vs. superficial liquid velocity at 53 percent area-averaged void fraction

of liquid superficial velocity at 53 percent area-averaged void fraction. A general decrease in variance is observed. This trend continues at 66 percent void fraction. However, as shown in Figure 4.58, the rate of variance decrease is increased. The large vapor flow rates this void fraction tends to push the liquid to the wall causing a slug-annular flow regime transition.

The zero liquid flow case showed a larger variance during annular flow because it was a special situation. For this case the liquid phase drains around the updrafting vapor frequently producing a chugging phenomena. At higher vapor velocities the liquid becomes flooded, resulting in intermittent wetting of the wall. In the non-zero liquid flow cases, the liquid and vapor phases flow concurrently and continuously up the pipe. The liquid film associated with annular flow is constantly replenished thus establishing a more stable condition.

A further increase in void produce a slowly decreasing variance as shown in Figure 4.59, for 68 percent area-average void fraction, and in Figure 4.60, for 72 area-average void fraction. The variance increases as the tube wall is approached. However, the wall measurement shows a variance considerably below other measurements associated with the same data set. This result is expected since the wall chord contains primarily liquid film in annular flow. As a void fraction of 1.0 is approached, chordal measurements near the wall will exhibit an

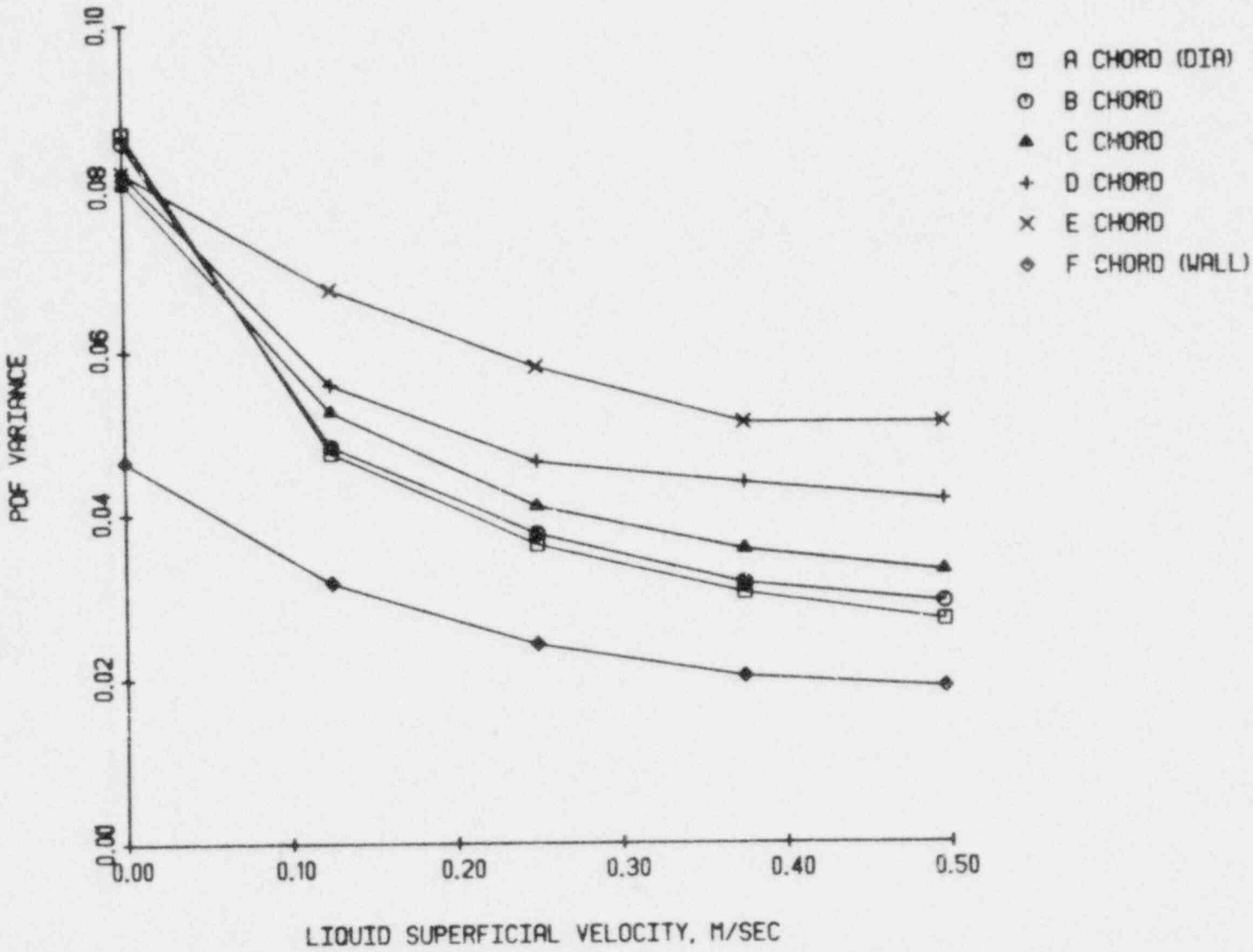

Figure 4.58 The PDF variance vs. superficial liquid velocity at 66 percent area-averaged void fraction

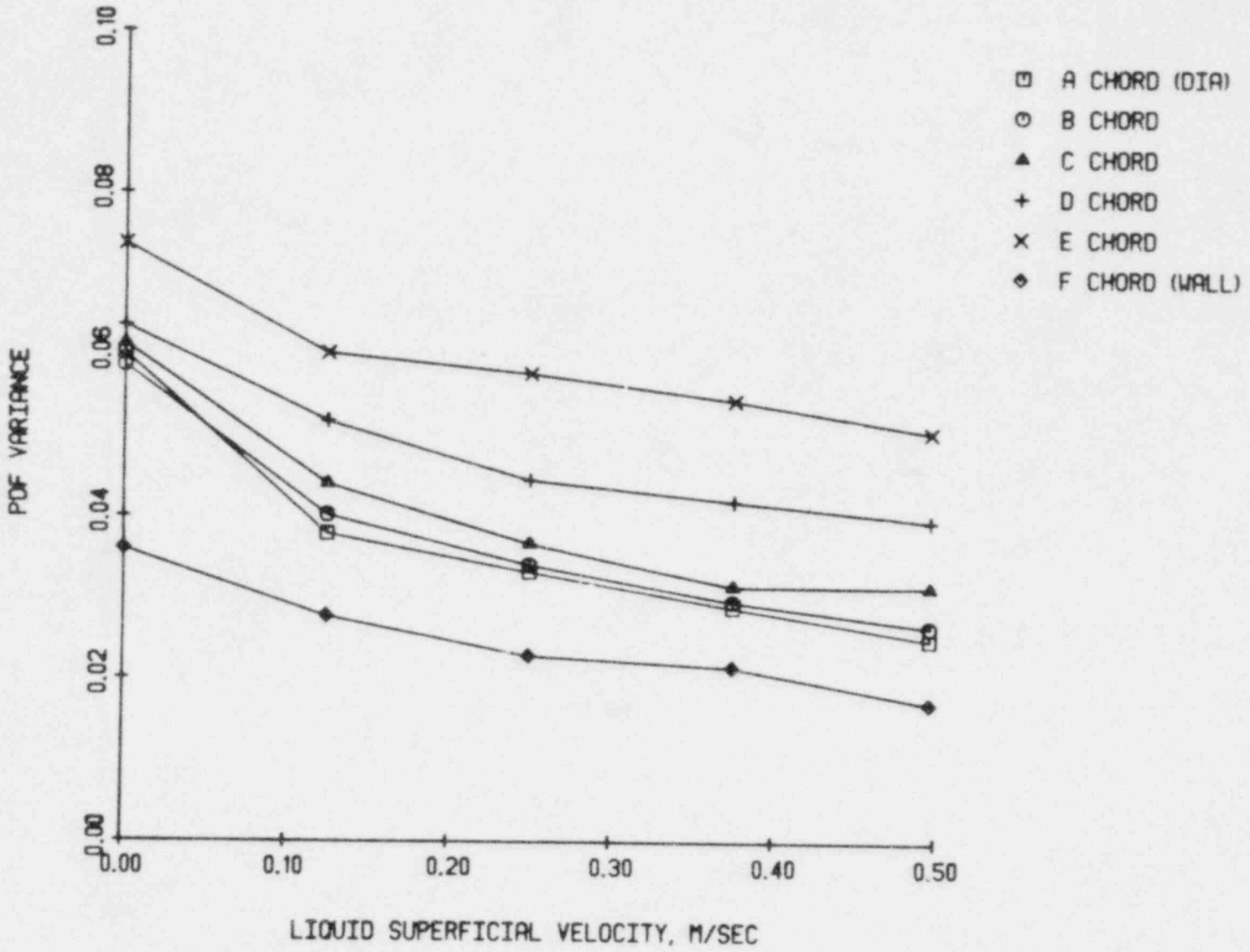

Figure 4.59 The PDF variance vs. superficial liquid velocity at 68 percent area-averaged void fraction

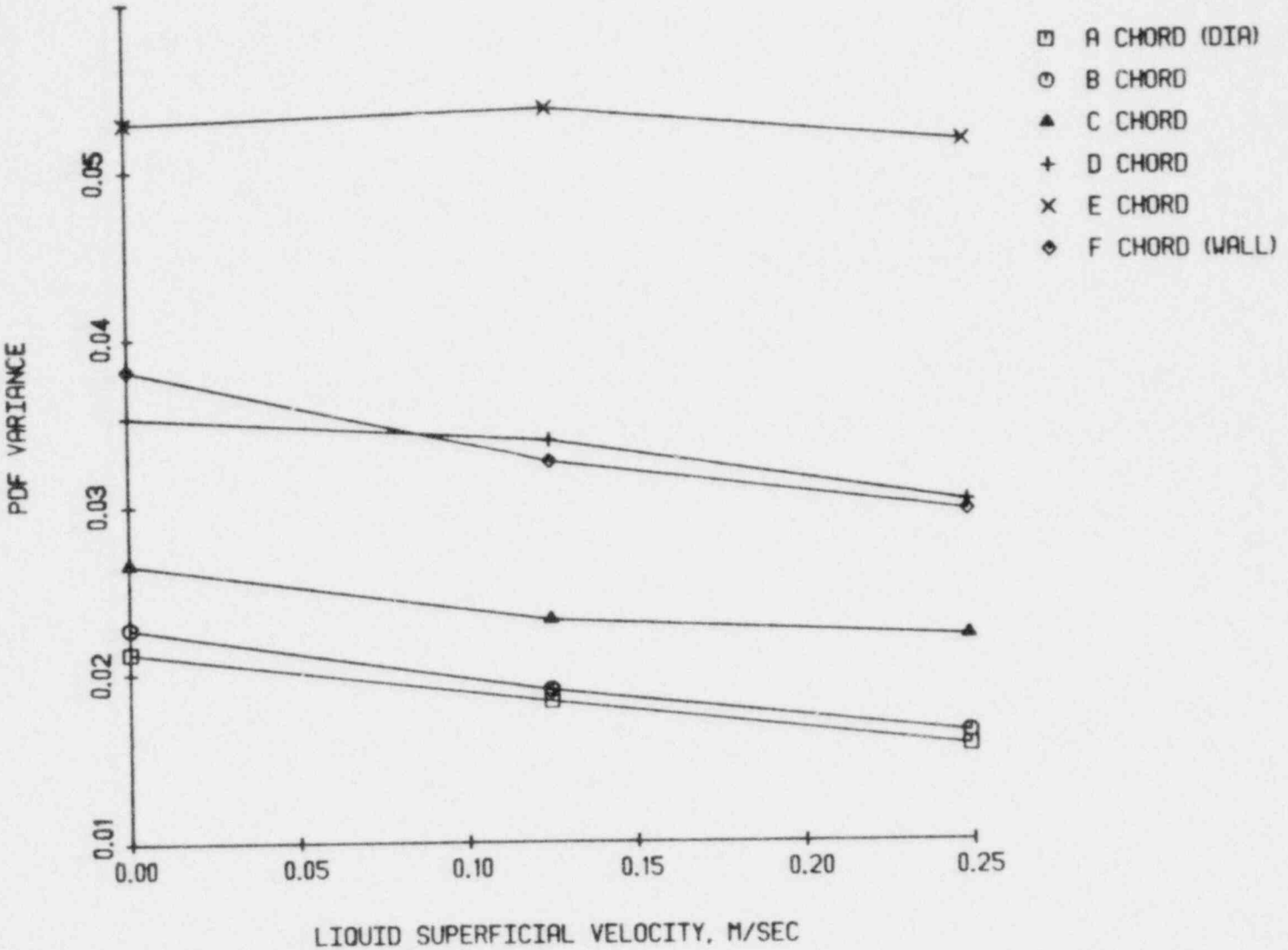

Figure 4.60 The PDF variance vs. superficial liquid velocity at 72 percent area-averaged void fraction

intermittent void fraction, and thus have larger variances than measurements nearer the tube diameter.

The skewness, or third moment about the mean exhibits some of the variance's trends. Except for the wall chord, the coefficient of skewness is relatively constant for 13 percent area-average void fraction bubbly flow as shown in Figure 4.61. Increasing the area-average void fraction to 20 percent produces the results shown in Figure 4.62. The trend with j_ℓ, observed here is very similar to the variance data shown in Figure 4.53. An area-averaged voidage of 26 percent results in Figure 4.63, while the data at 32 percent area averaged void fraction is illustrated in Figure 4.64.

The shape of the skewness verses liquid superficial velocity graph is similar to the same graph for the variance, however, the magnitude of the skewness does not change in a fashion necessary to establish a precise bubbly-slug flow regime indicator. The magnitude of the skewness generally decreases with increasing void fraction, however, a transition from bubbly to slug flow produces an increase in skewness. These two phenomena occur simultaneously and tend to offset each other.

These trends are easily explained if the meaning of skewness is considered. Skewness is a measure of the difference between the median, the 50th percentile, and the mean. Bubbly flow has positive skewness, i.e., the median is to the left of the mean. Slug flow may have either

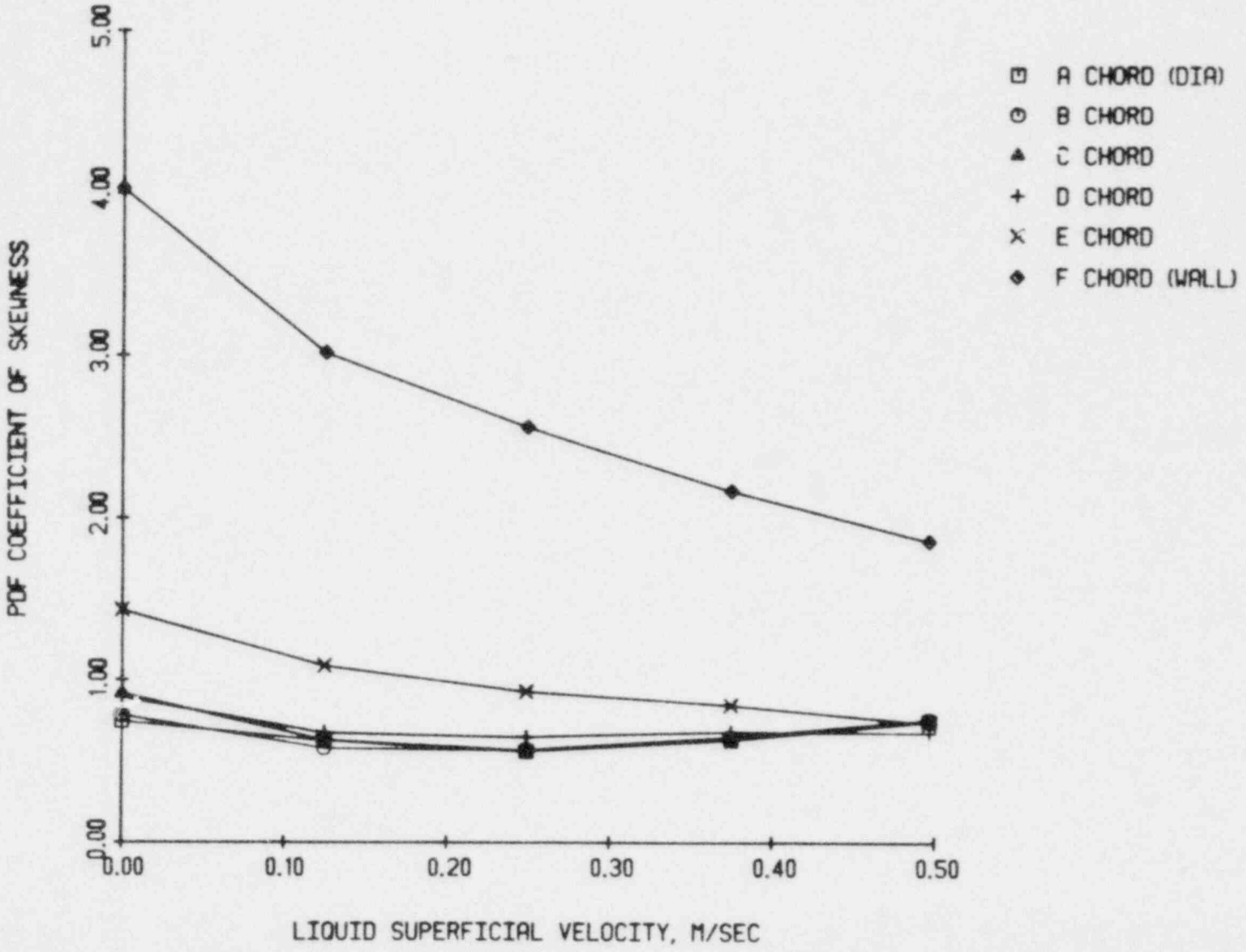

Figure 4.61 The PDF coefficient of skewness vs. superficial liquid velocity at 13 percent area-averaged void fraction

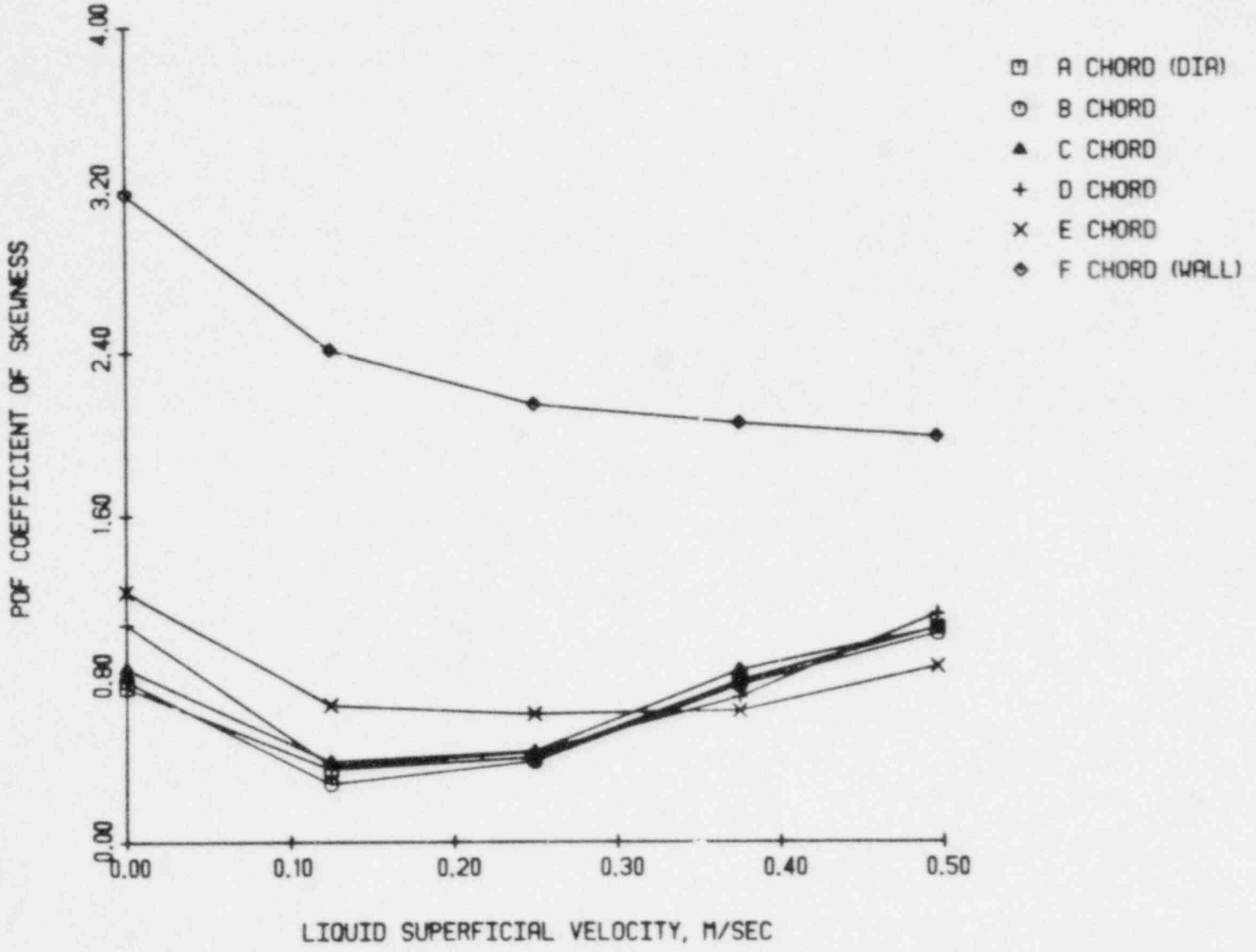

Figure 4.62 The PDF coefficient of skewness vs. superficial liquid velocity at 20 percent area-averaged void fraction

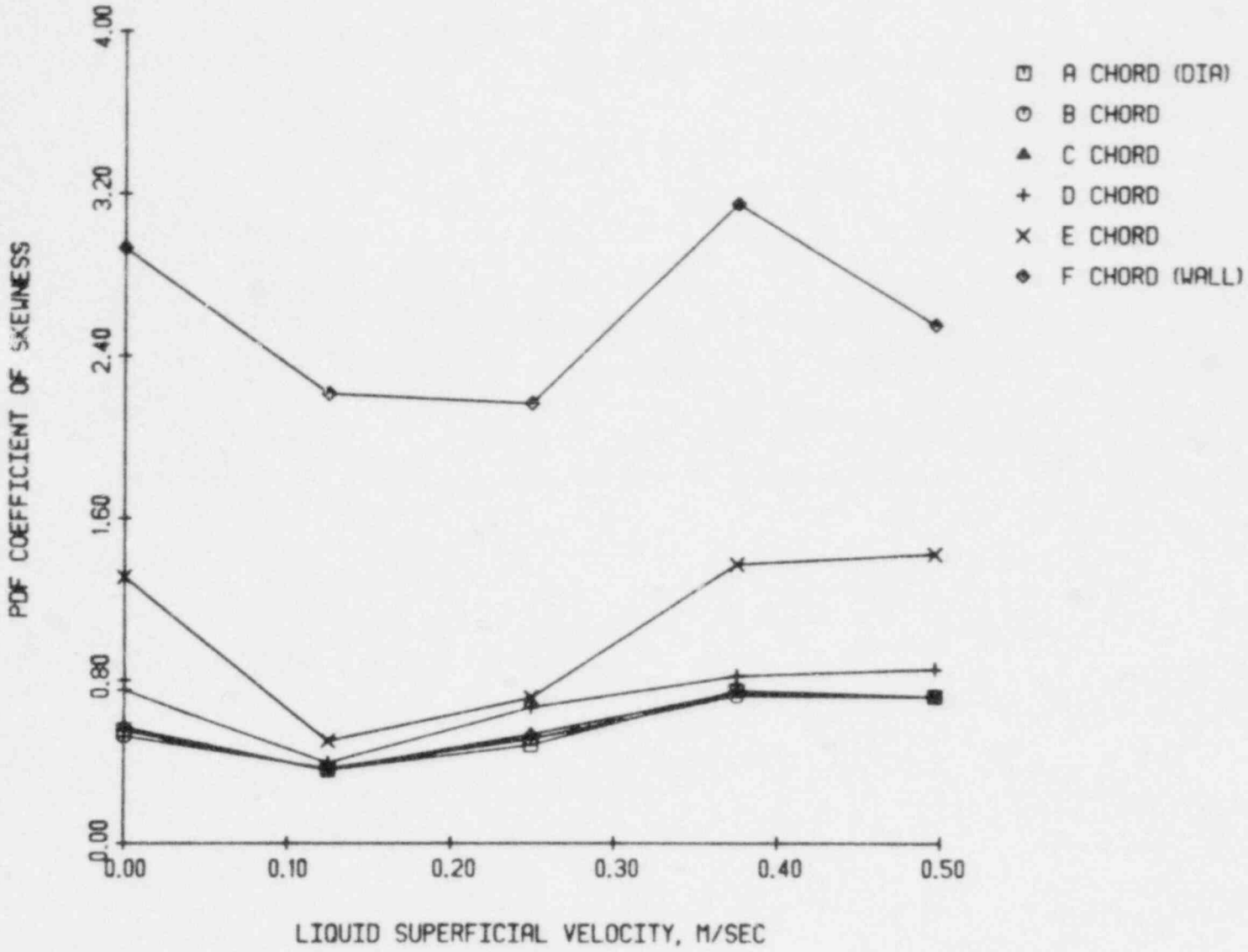

Figure 4.63 The PDF coefficient of skewness vs. superficial liquid velocity at 26 percent area-averaged void fraction

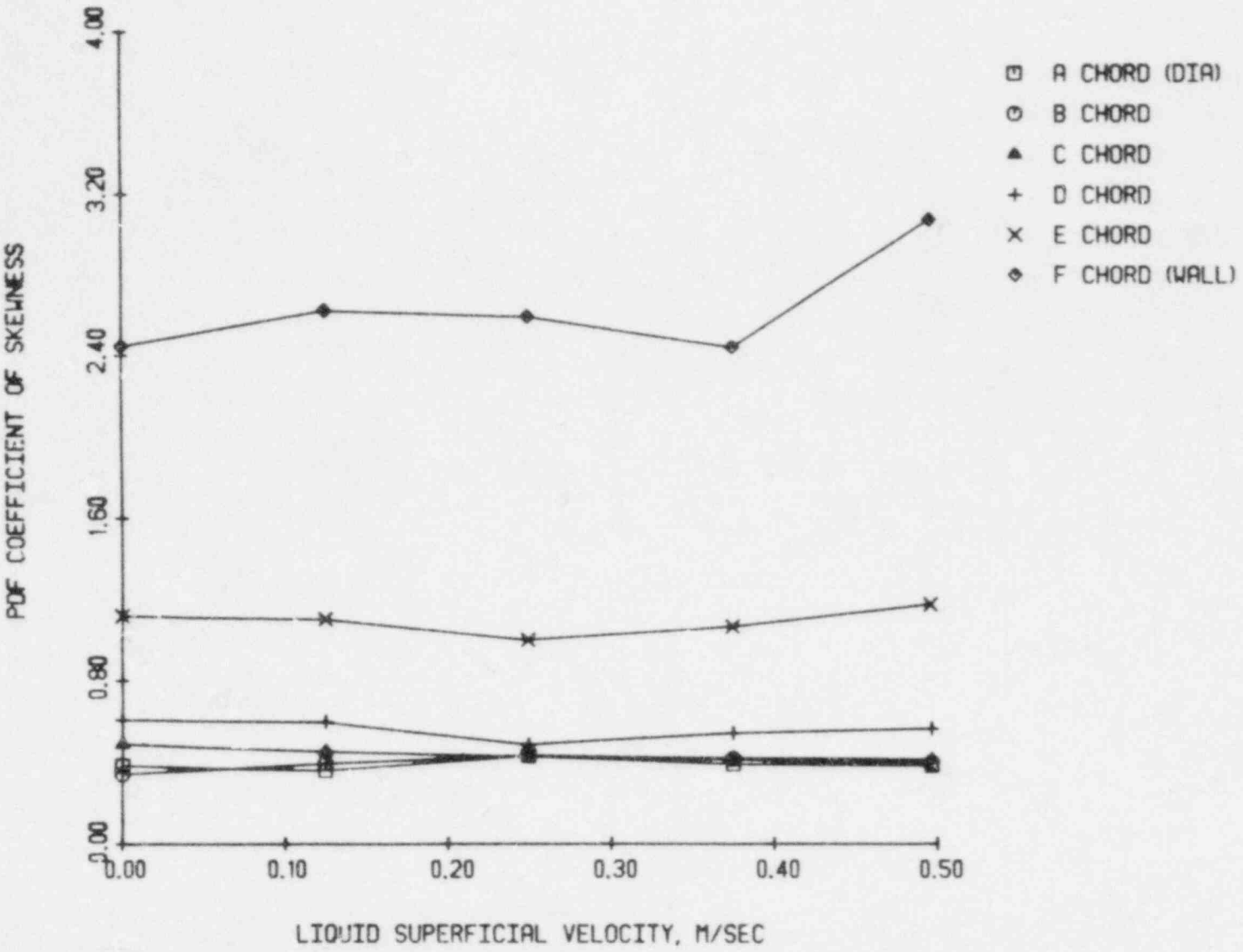

Figure 4.64 The PDF coefficient of skewness vs. superficial liquid velocity at 32 percent area-averaged void fraction

positive or negative skewness. However, most annular flows exhibit negative skewness, i.e., a median to the right of the mean. An increase in the void fraction at low void causes the median to approach the mean thus reducing the skewness. As indicated earlier, introduction of a non-zero liquid superficial velocity tends to suppress the bubbly-slug transition and not allow the median to approach the mean.

An increase in void fraction results in plots of the coefficient of skewness for various area-averaged void fractions, as shown in Figure 4.65 for 41 percent void and, in Figure 4.66 for 53 percent void fraction. As explained earlier the magnitude of skewness decreases with increasing void fraction but is independent of liquid superficial velocity.

The coefficient of skewness remains relatively independent of liquid superficial velocity for a large range of area-average void fractions. These trends are shown in Figures 4.67 and 4.68 for area-averaged void fractions of 66 and 68 percent respectively. The skewness is relatively independent of the chordal location except at the larger void fractions. As indicated earlier the data acquired close to the wall is effected by the local phenomena at the wall.

Annular flow is accompanied by an increase in skewness as shown in Figure 4.69 for 72 percent area averaged void fraction. A liquid superficial velocity greater than zero will supply fluid to the wall liquid film.

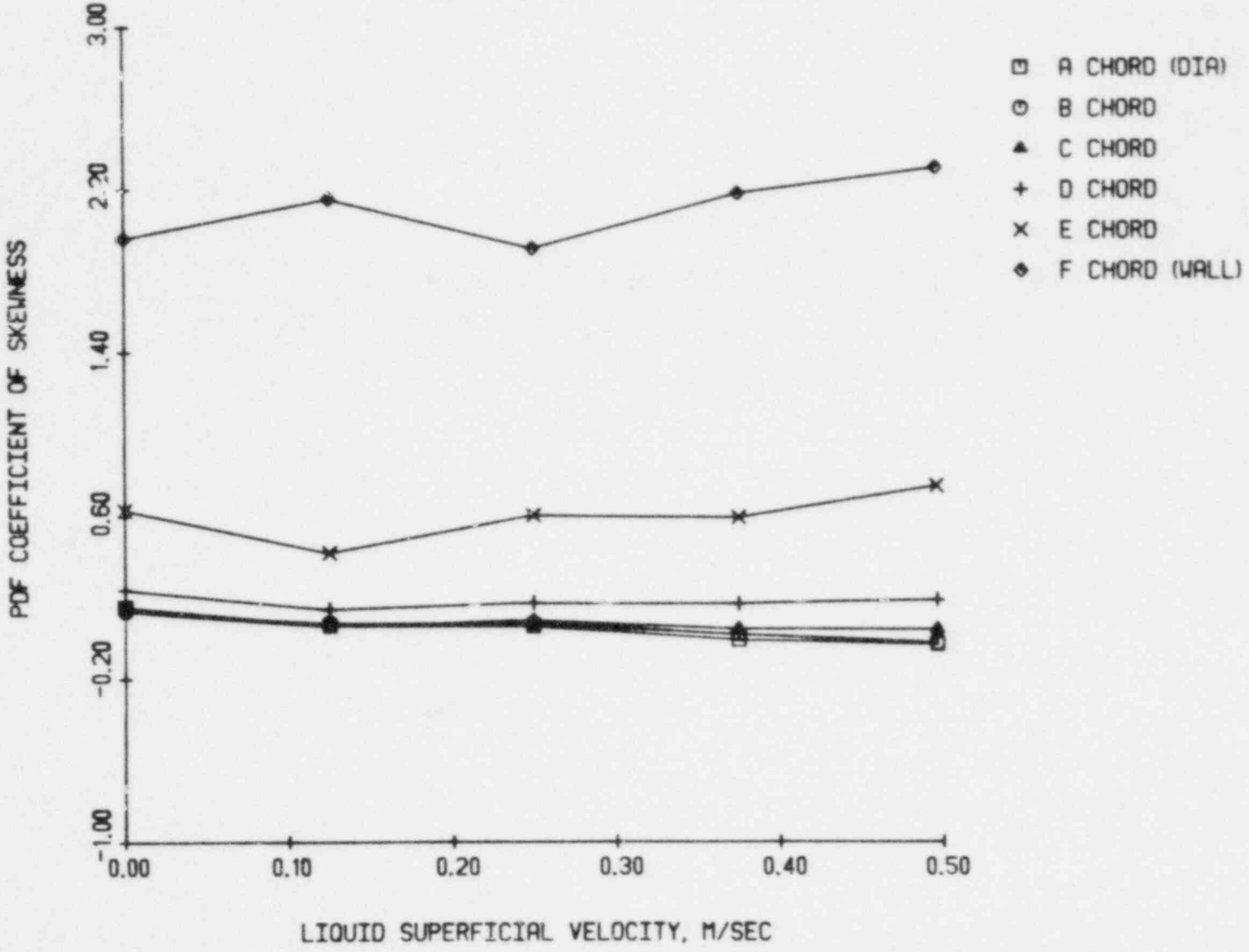

Figure 4.65 The PDF coefficient of skewness vs. superficial liquid velocity at 41 percent area-averaged void fraction

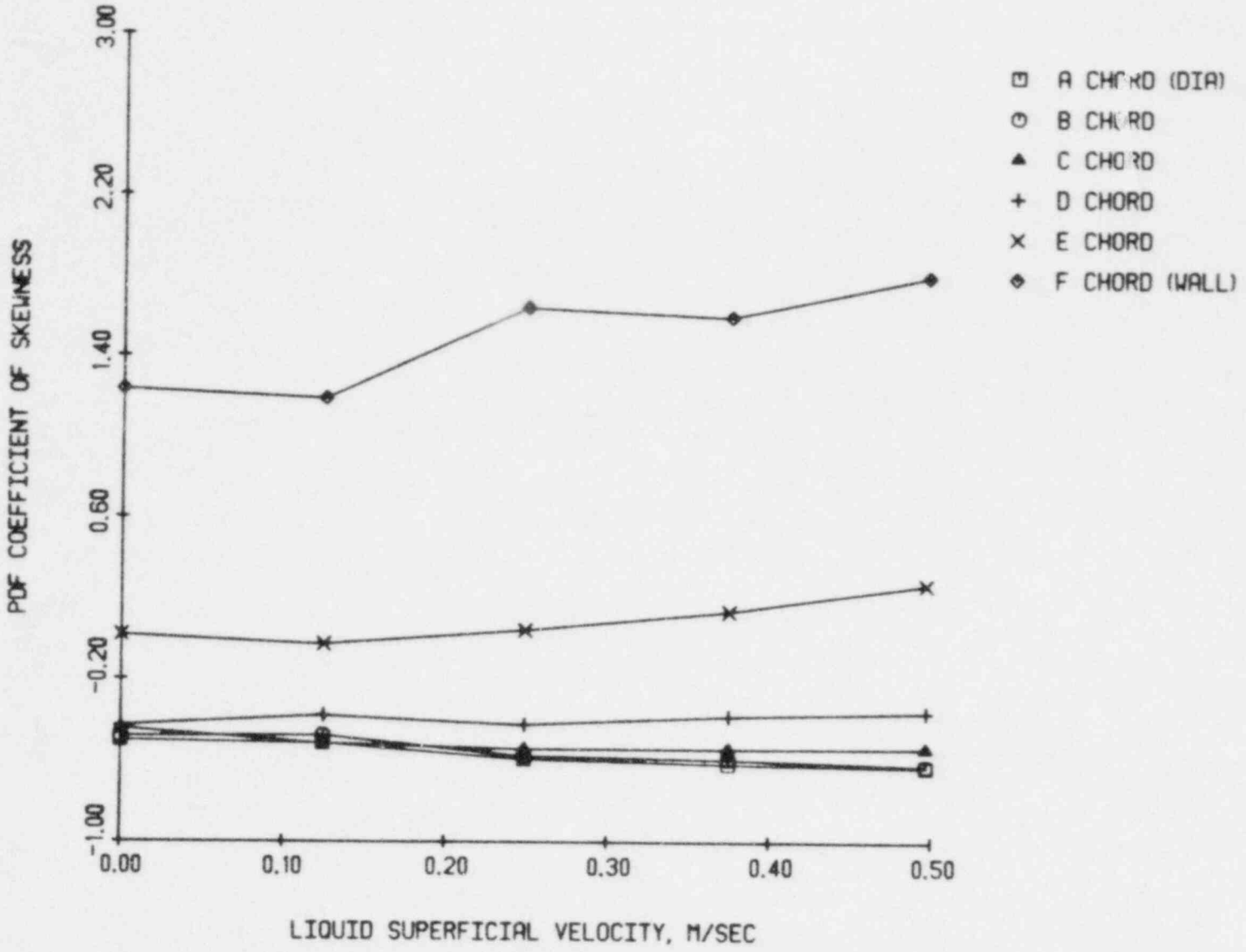

Figure 4.66 The PDF coefficient of skewness vs. superficial liquid velocity at 53 percent area-averaged void fraction

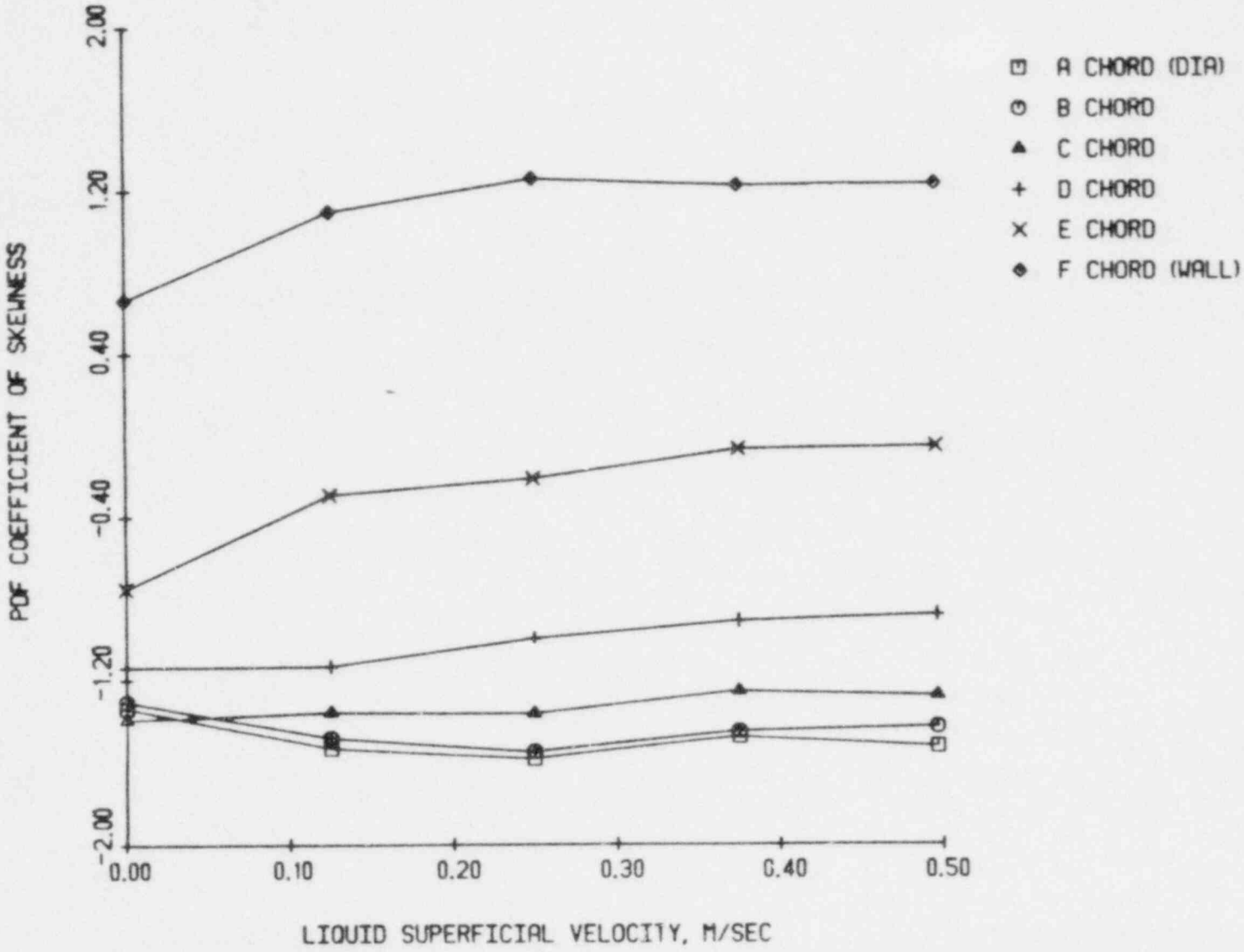

Figure 4.67 The PDF coefficient of skewness vs. superficial liquid velocity at 66 percent area-averaged void fraction

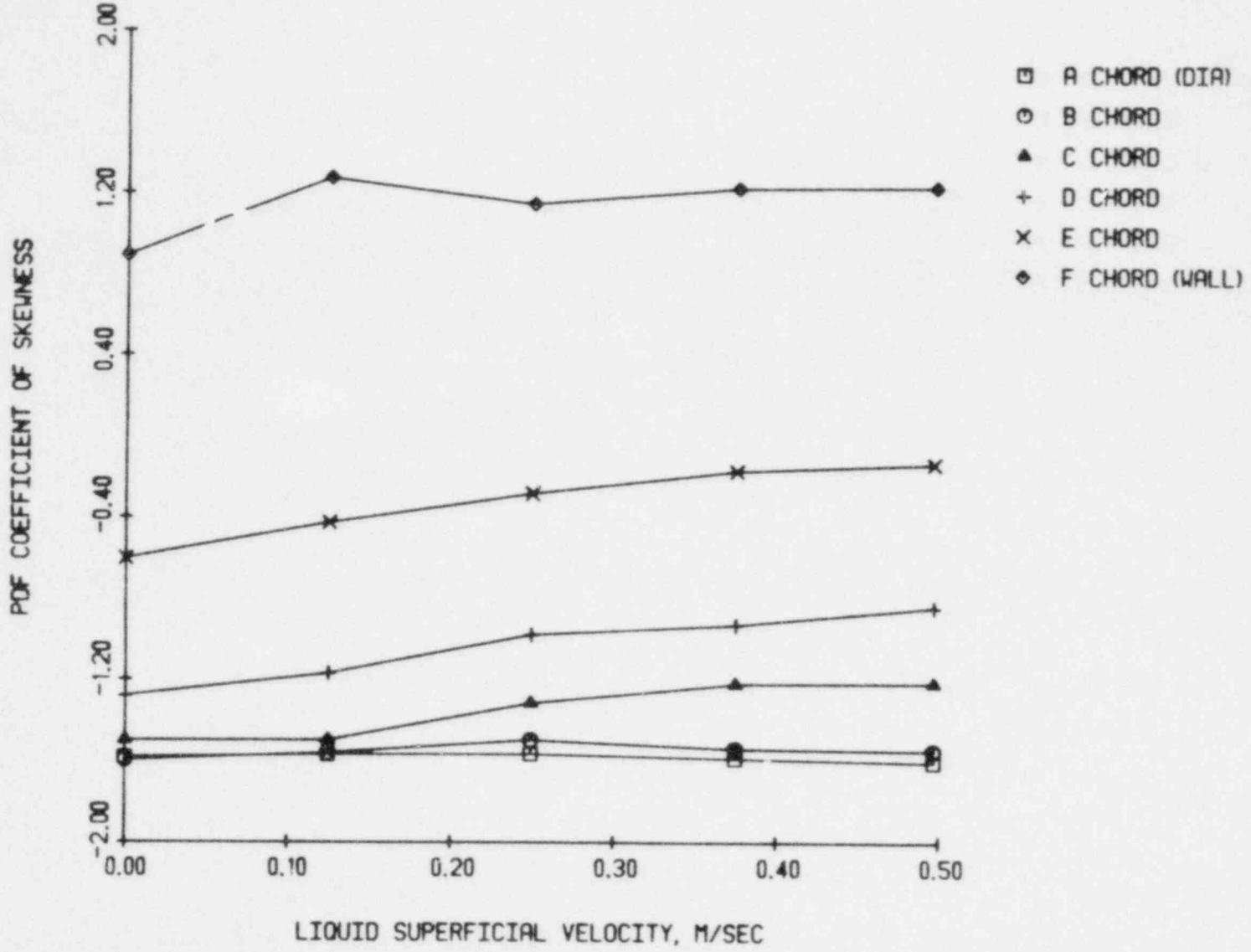

Figure 4.68 The PDF coefficient of skewness vs. superficial liquid velocity at 68 percent area-averaged void fraction

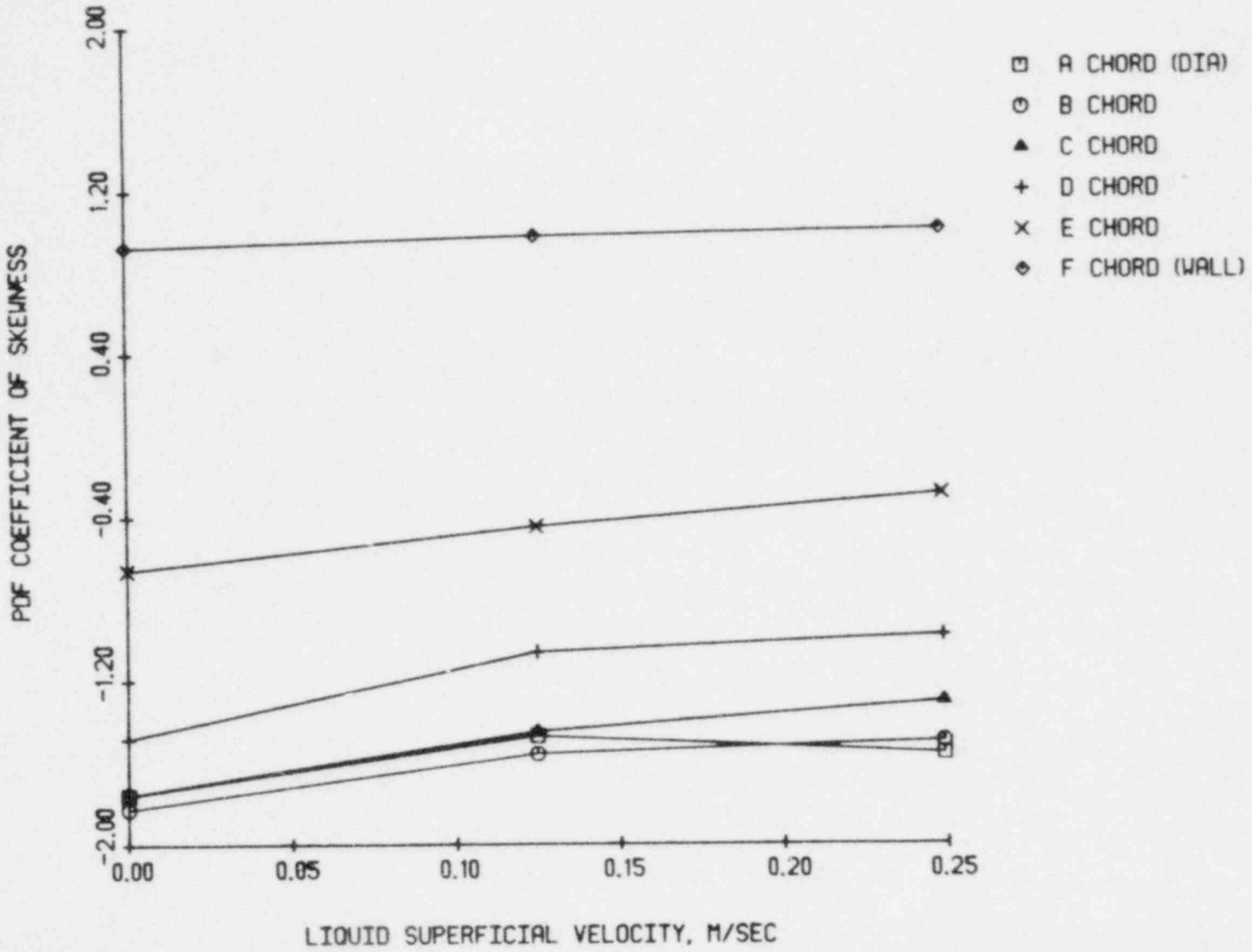

Figure 4.69 The PDF coefficient of skewness vs. superficial liquid velocity at 72 percent area-averaged void fraction

As a result, the annular flow regime can be generated more easily. The skewness will thus decrease since the liquid is not an intermittent counter-current flow.

Kurtosis, the fourth moment about the mean, is very independent of liquid velocity and correspondingly flow regime. Figures 4.70 through 4.72 indicate that, except for the wall chord, the coefficient of kurtosis is invariant with respect to liquid superficial velocity for area-averaged void fractions of 13, 20 and 26 percent. The magnitude of the coefficient of kurtosis does change as a function of voidage and is relatively independent of position. Clearly a bubbly-slug flow regime indicator is not possible using the coefficient of kurtosis.

In the slug flow regime, the coefficient of kurtosis again does not exhibit any dependence on liquid superficial velocity as shown in Figures 4.73 through 4.75 for area averaged void fractions of 32, 41, and 53 percent, respectively. Moreover, the coefficient of kurtosis is independent of chordal position.

A further increase in void fraction results in considerable variation in the coefficient of kurtosis as a function of measurement position. The coefficient of kurtosis associated with area-averaged void fractions of 66, 68, and 72 percent is shown as a function of liquid superficial velocity in Figures 4.76 through 4.78, respectively. Superficial liquid velocity effects and position effects are illustrated. These trends are expected

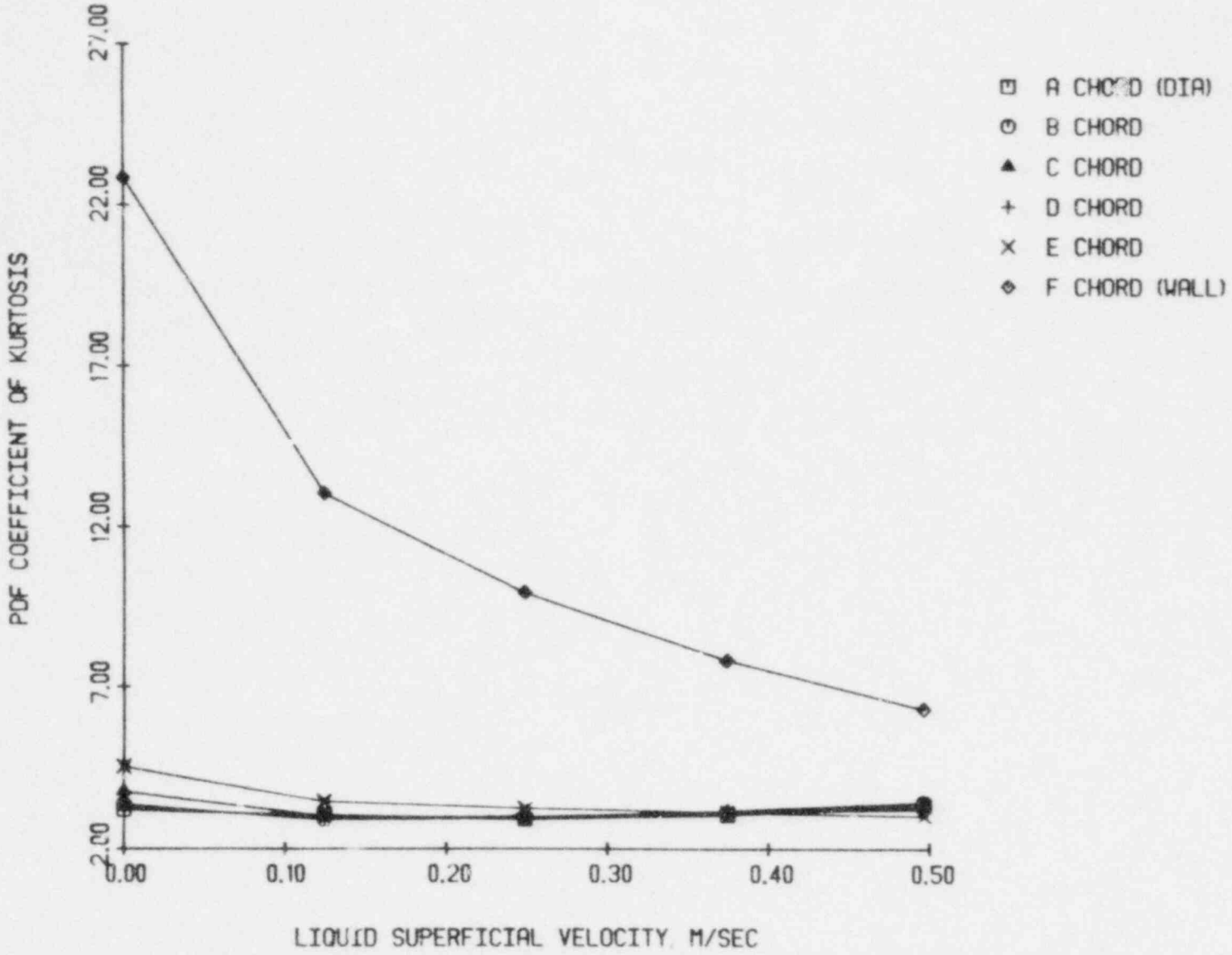

Figure 4.70 The PDF coefficient of kurtosis vs. superficial liquid velocity at 13 percent area-averaged void fraction

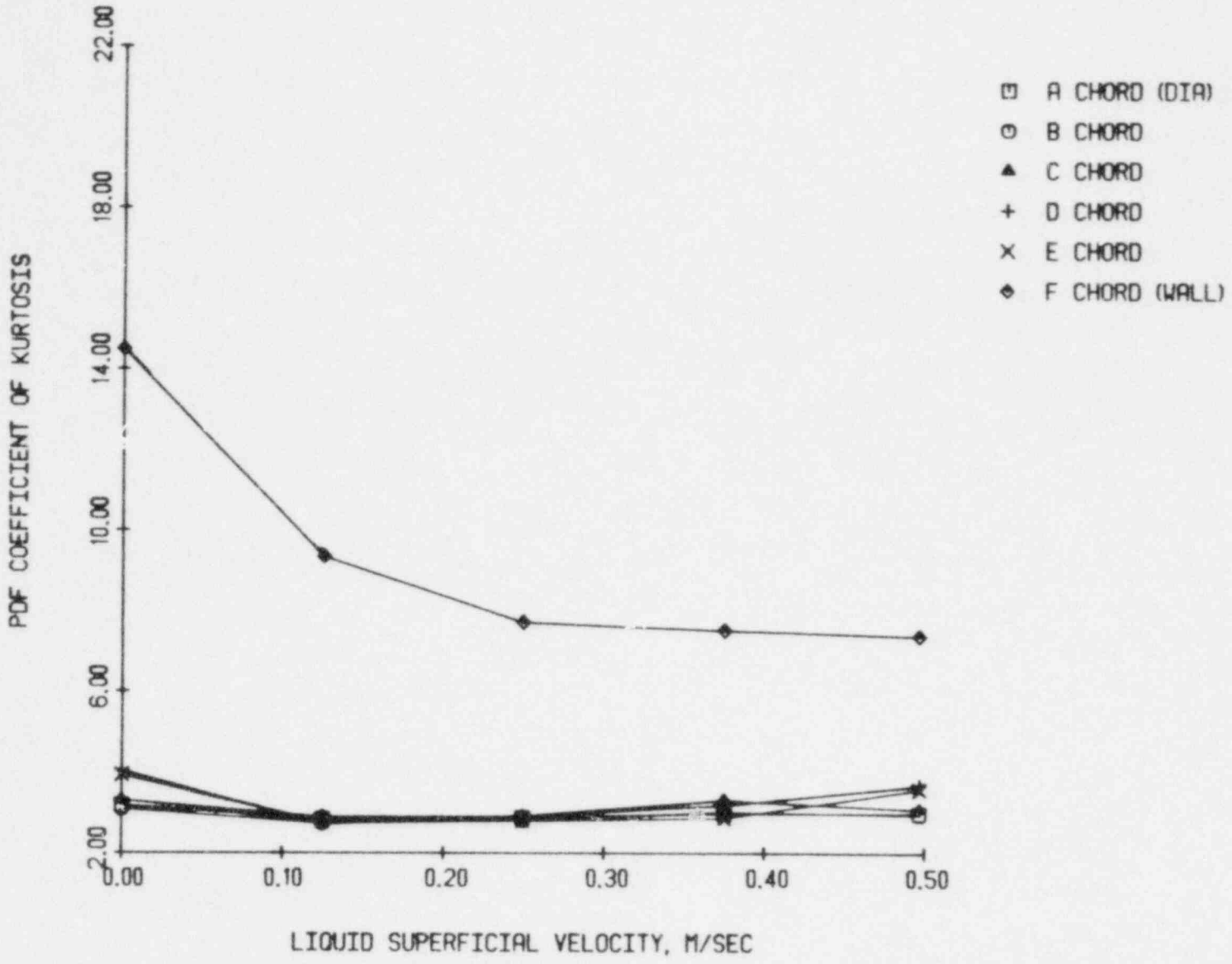

Figure 4.71 The PDF coefficient of kurtosis vs. superficial liquid velocity at 20 percent area-averaged void fraction

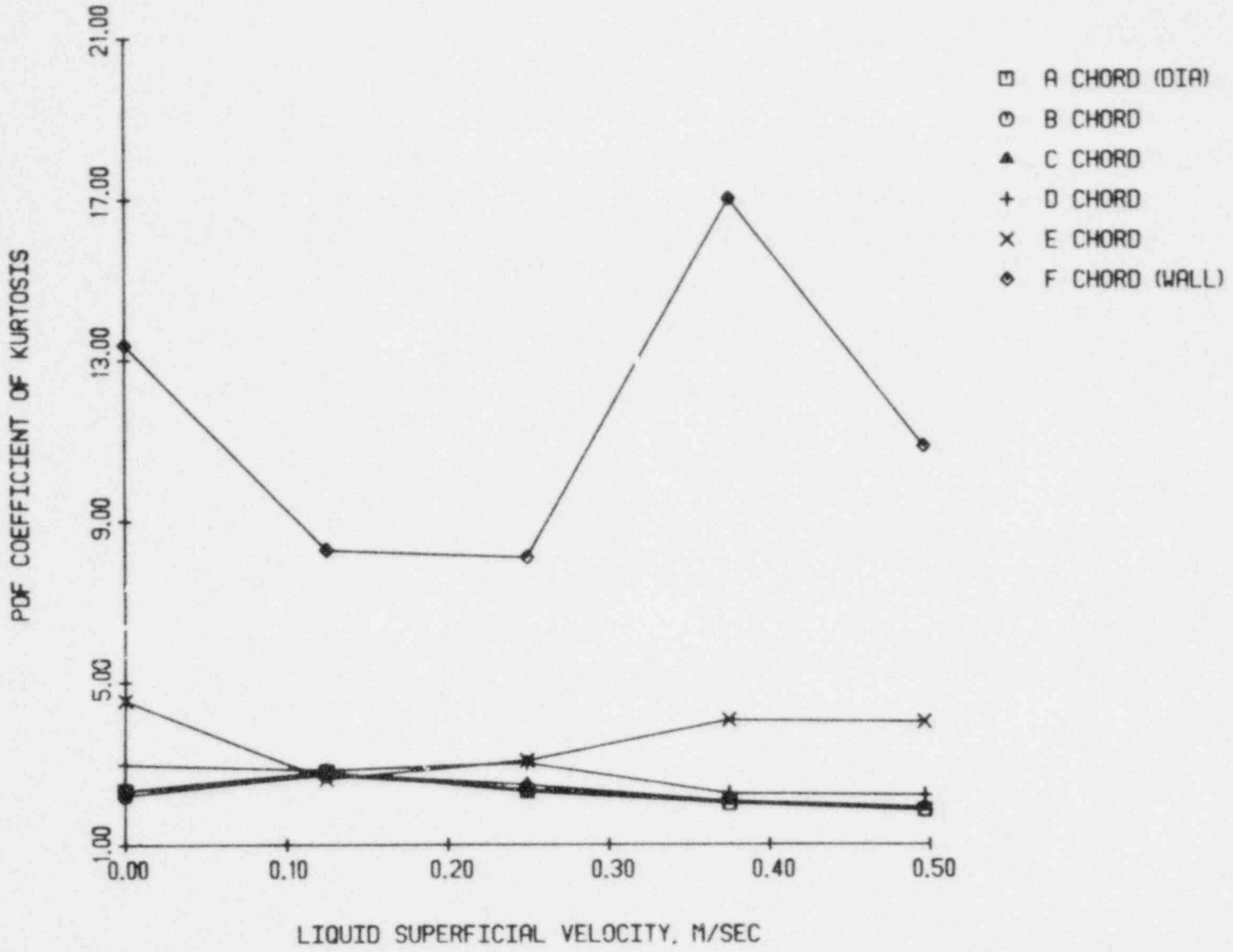

Figure 4.72 The PDF coefficient of kurtosis vs. superficial liquid velocity at 26 percent area-averaged void fraction

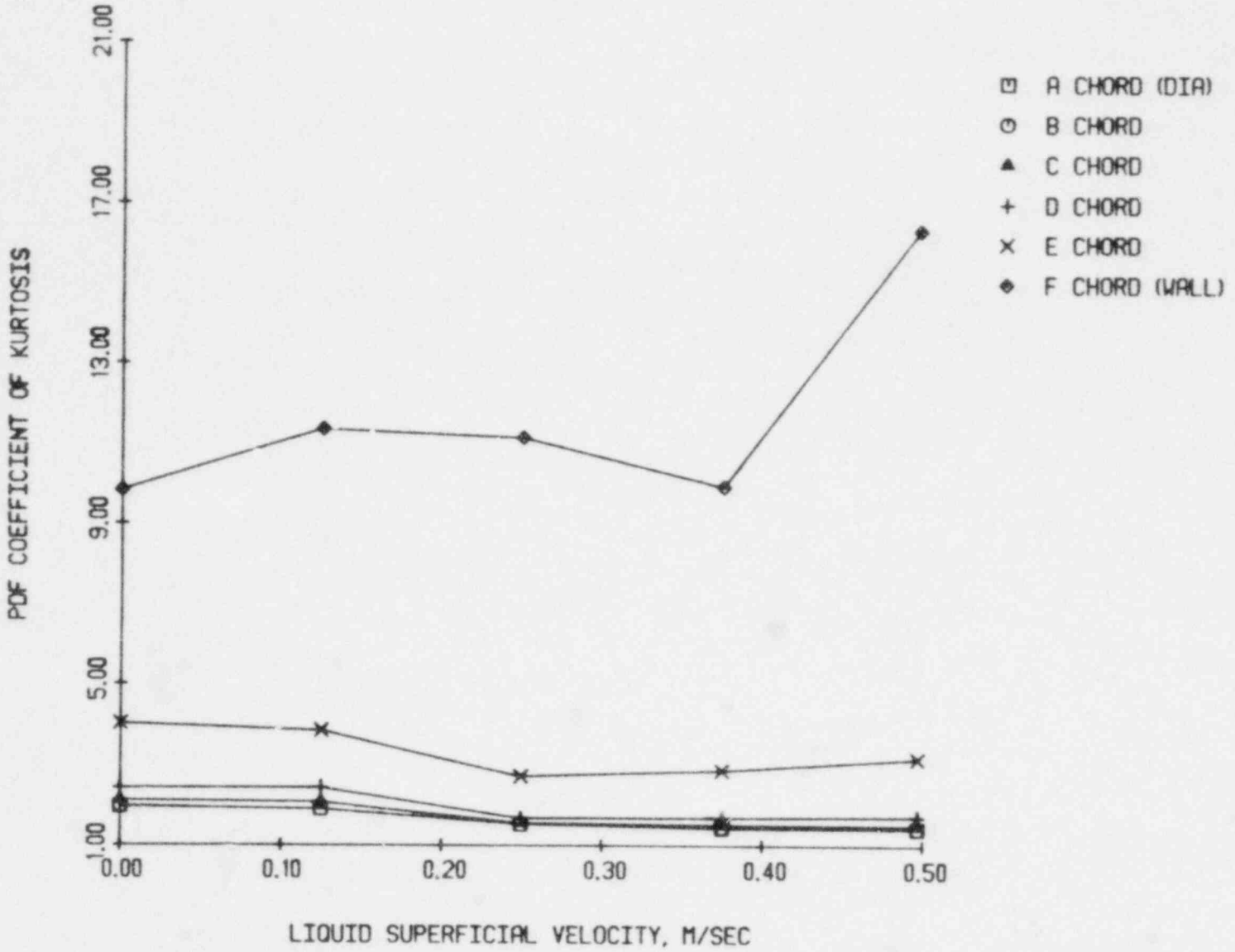

Figure 4.73 The PDF coefficient of kurtosis vs. superficial liquid velocity at 32 percent area-averaged void fraction

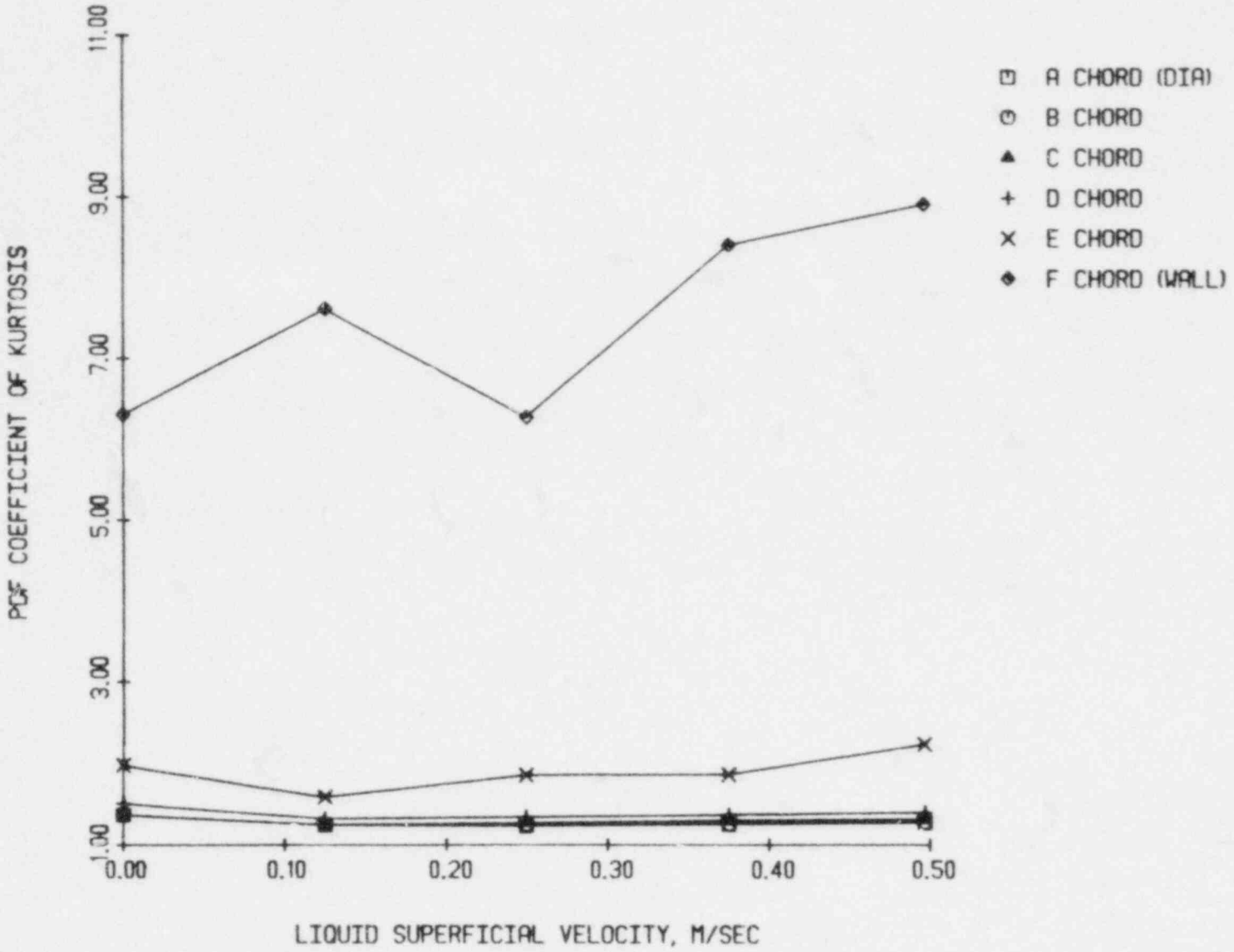

Figure 4.74 The PDF coefficient of kurtosis vs. superficial liquid velocity at 41 percent area-averaged void fraction

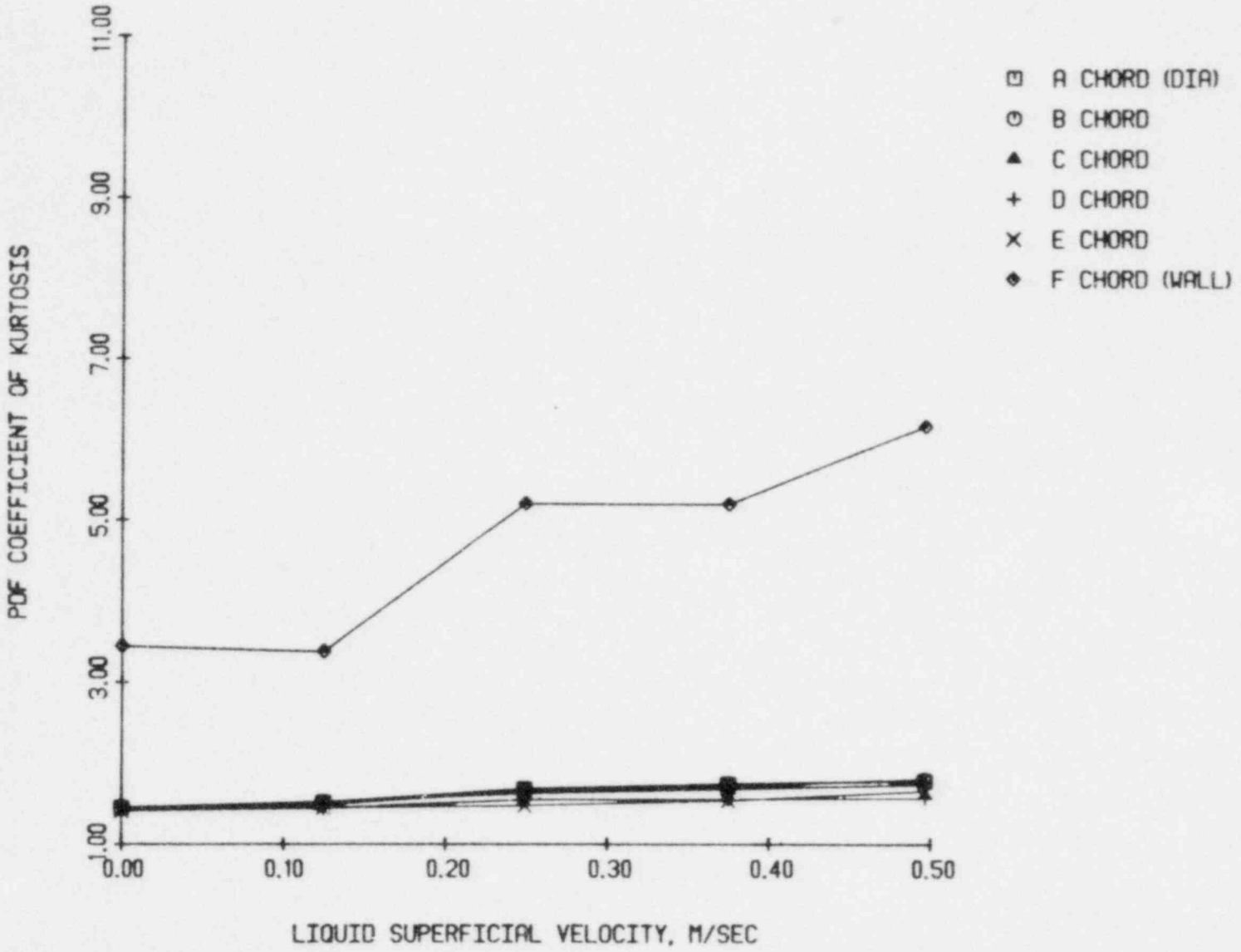

Figure 4.75 The PDF coefficient of kurtosis vs. superficial liquid velocity at 53 percent area-averaged void fraction

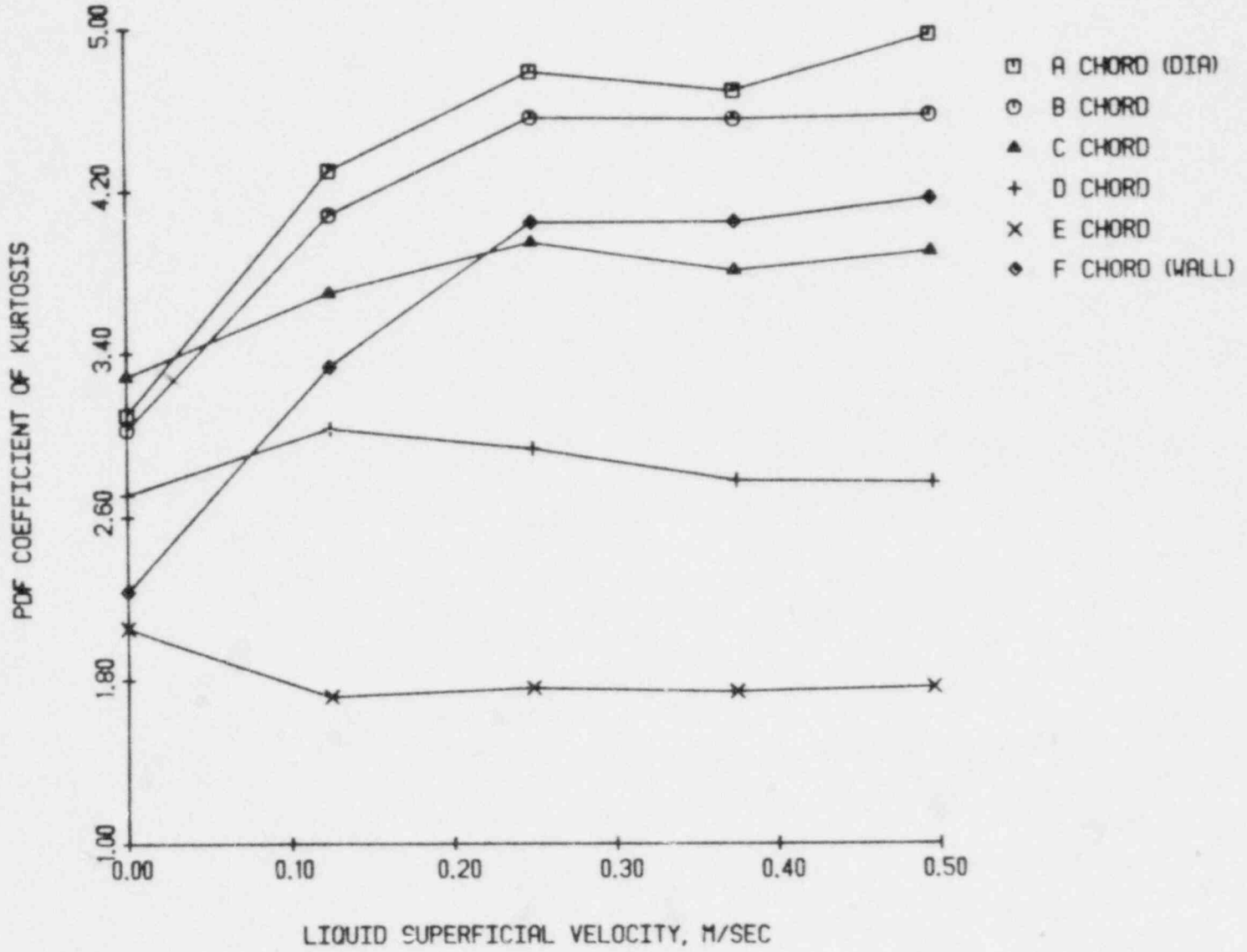

Figure 4.76 The PDF coefficient of kurtosis vs. superficial liquid velocity at 66 percent area-averaged void fraction

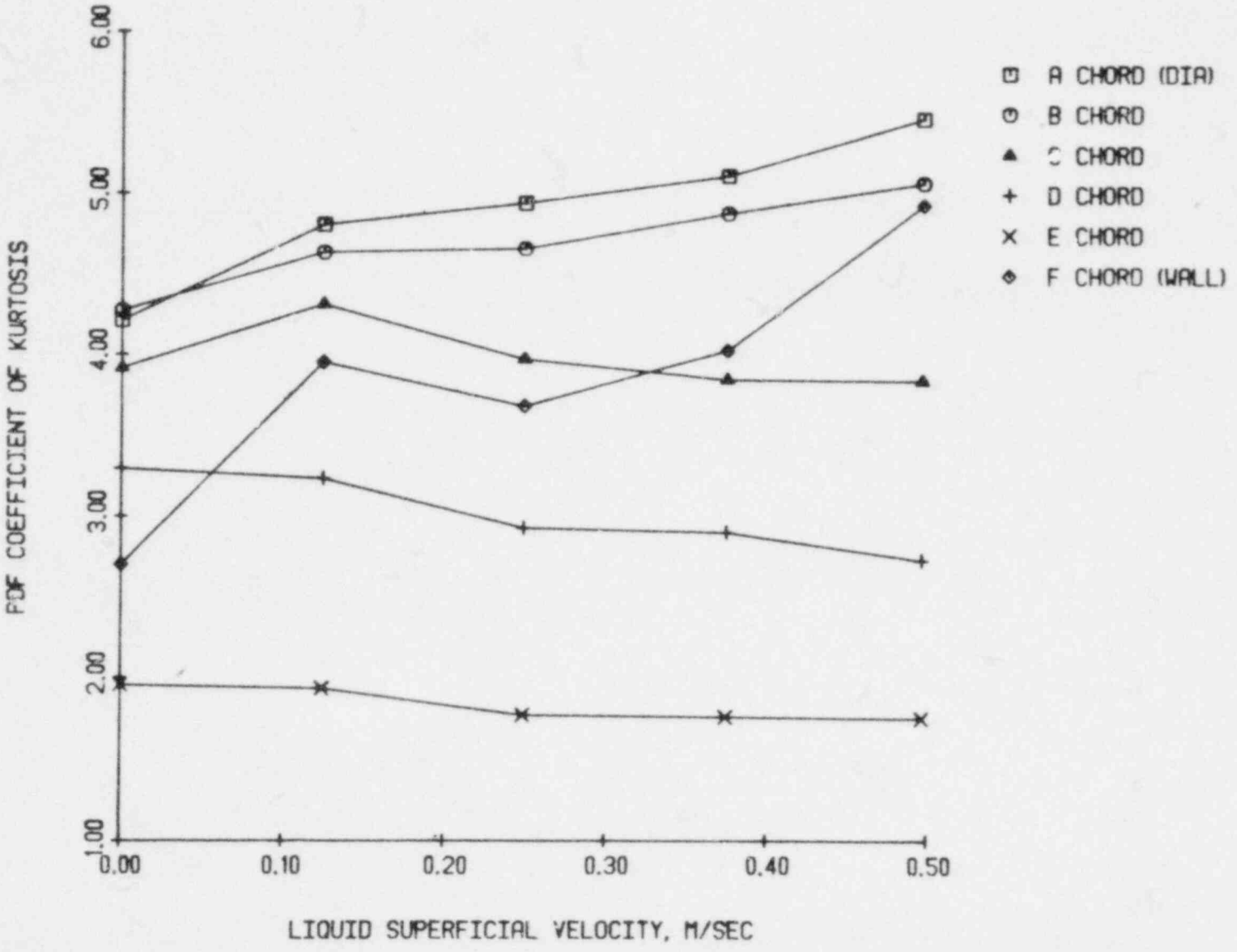

Figure 4.77 The PDF coefficient of kurtosis vs. superficial liquid velocity at 68 percent area-averaged void fraction

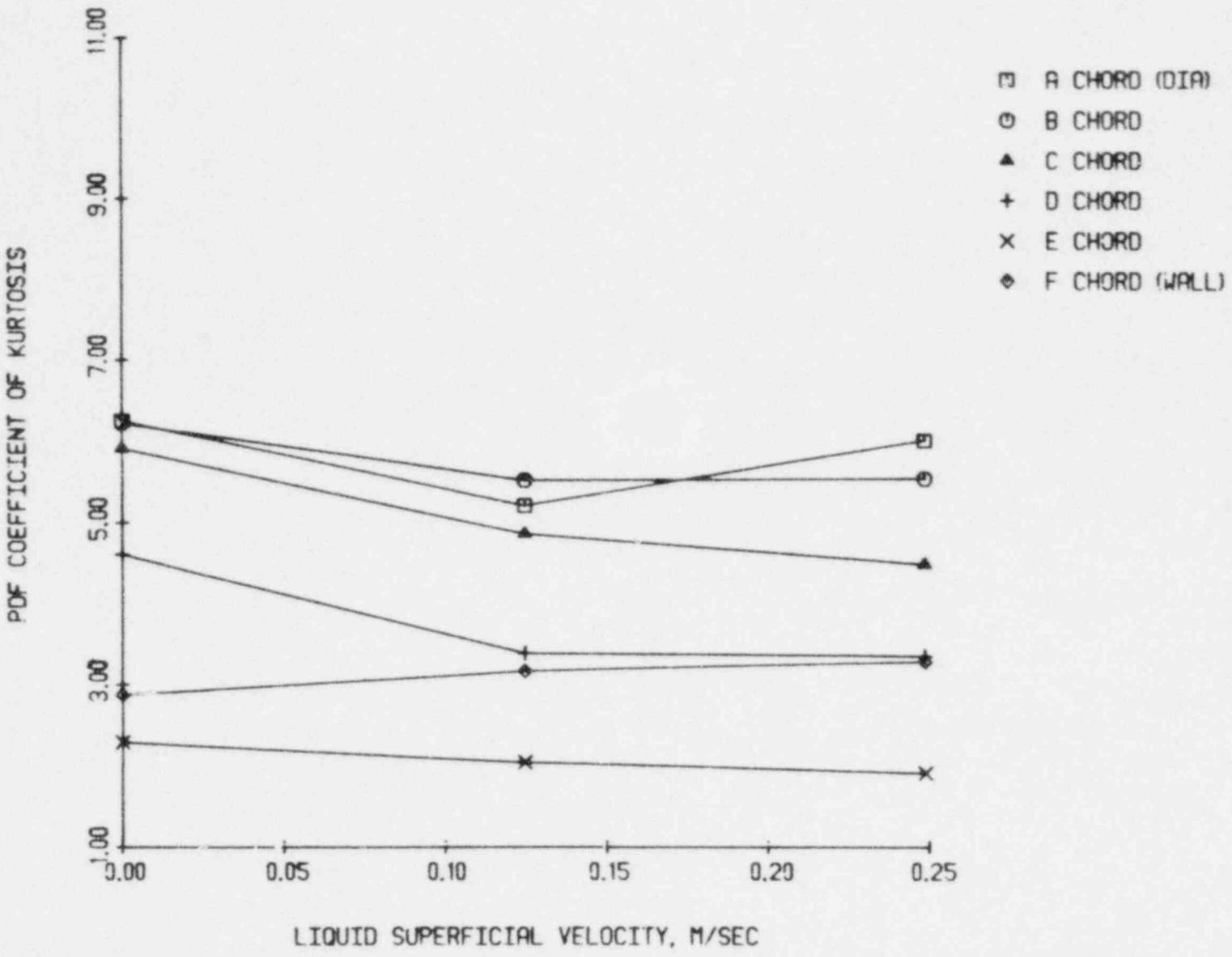

Figure 4.78 The PDF coefficient of kurtosis vs. superficial liquid velocity at 72 percent area-averaged void fraction

since the kurtosis is a measure of the distribution's peakedness. Around the slug-annular transition, the void distribution is more peaked for the chord along the diameter than the one adjacent to the wall.

Figure 4.76 also shows a very important relationship to the variance earlier illustrated in Figure 4.59. The distribution's peakedness increases with superficial liquid velocity while simultaneously the variance drops with superficial liquid velocity. This clearly indicates that a flow regime transition is occurring.

4.2.2 Power Spectral Density (PSD) Data

The first one thousand and twenty-four (1024) data points acquired from each chordal measurement were processed by a Discrete Fast Fourier Transform (DFFT). The power spectral density was formed by summing the squares of the real and imaginary components output from the DFFT, dividing by the data acquisition period and then multiplying the result by two. Multiplication by two was necessary since all the data was real, and thus the Fourier Transform is symmetric.

Three types of power spectra were observed:

1) A wide band, low amplitude spectrum usually associated with bubbly flows.
2) A low frequency peak of large amplitude usually associated with the characteristic frequency of slug flow.

3) A medium band with an amplitude spectrum corresponding to annular flow.

The band width of the bubbly flow spectrum will increase with liquid elocity since the shorter void transit time corresponds to higher frequencies. Similarily, the PSD for slug flow shifts to high frequency as the liquid superficial velocity is increased. Annular flow is composed of the frequencies of the roll waves moving along the liquid film/vapor interface and thus produces a spectrum of medium width, which increases with liquid velocity.

A comparison of the time average of the data subset used in the PSD calculation and the time average of the entire data set is shown in Figure 4.79. A reasonable correspondence is illustrated, indicating that ensemble averaging of each record of (1024) data points is unnecessary. Bubbly and annular flow regimes produce close correlation while slight discrepencies are observed in the slug flow regime. Only the 'A' and 'F' chords are shown since these measurements bound all other chords.

4.2.2.1 Zero Liquid Flow Data

The PSD was Reimann integrated to calculate the cummulative value, or total energy. These results for the zero liquid flow data are shown in Figure 4.80, as a function of chordal void fraction. As expected, the spectra have a maximum energy in the slug flow regime. Bubbly and annular flow have a wider bandwidth but small amplitudes,

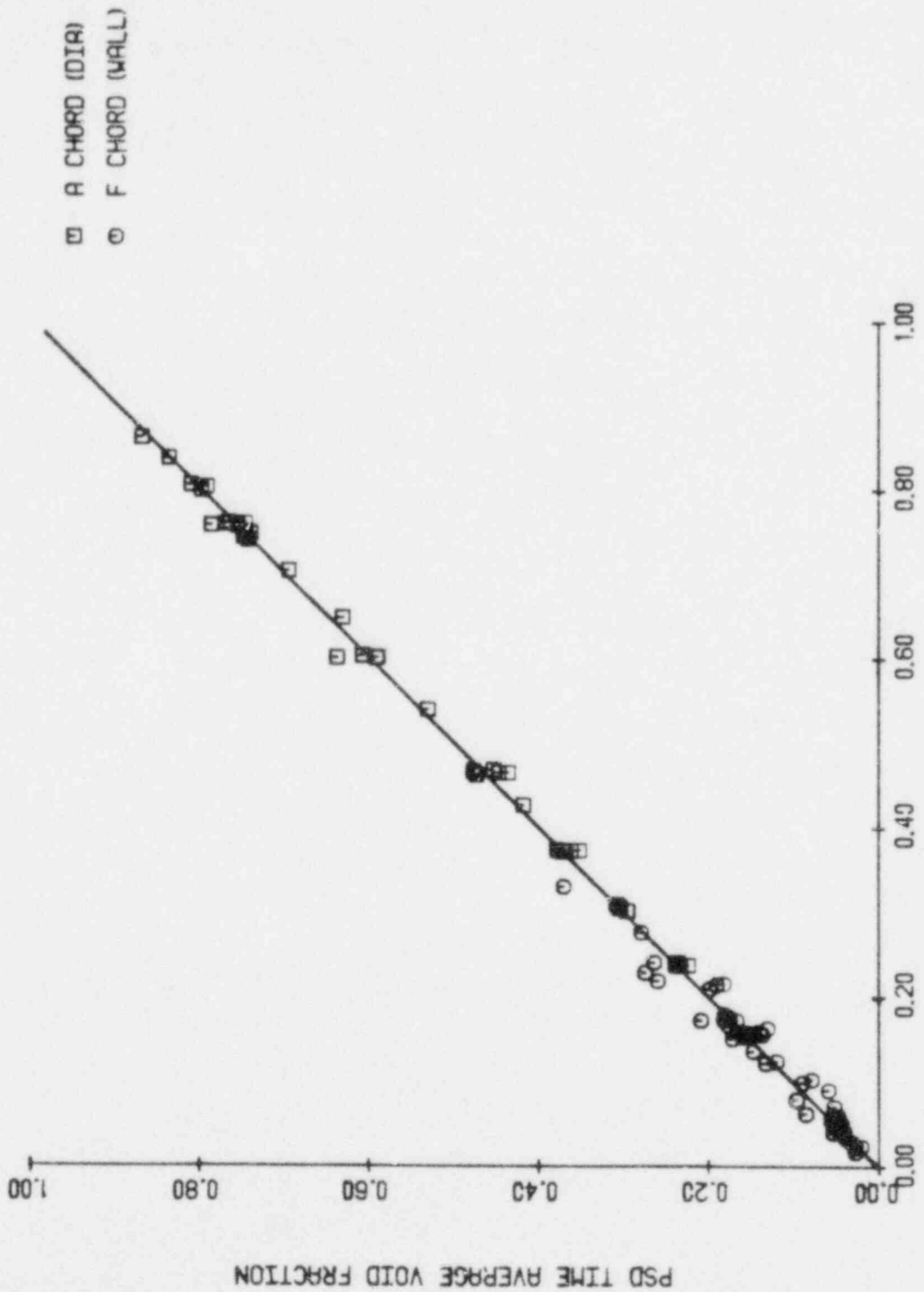

Figure 4.79 The PSD time average void fraction vs. time average chordal void fraction for A and F chords

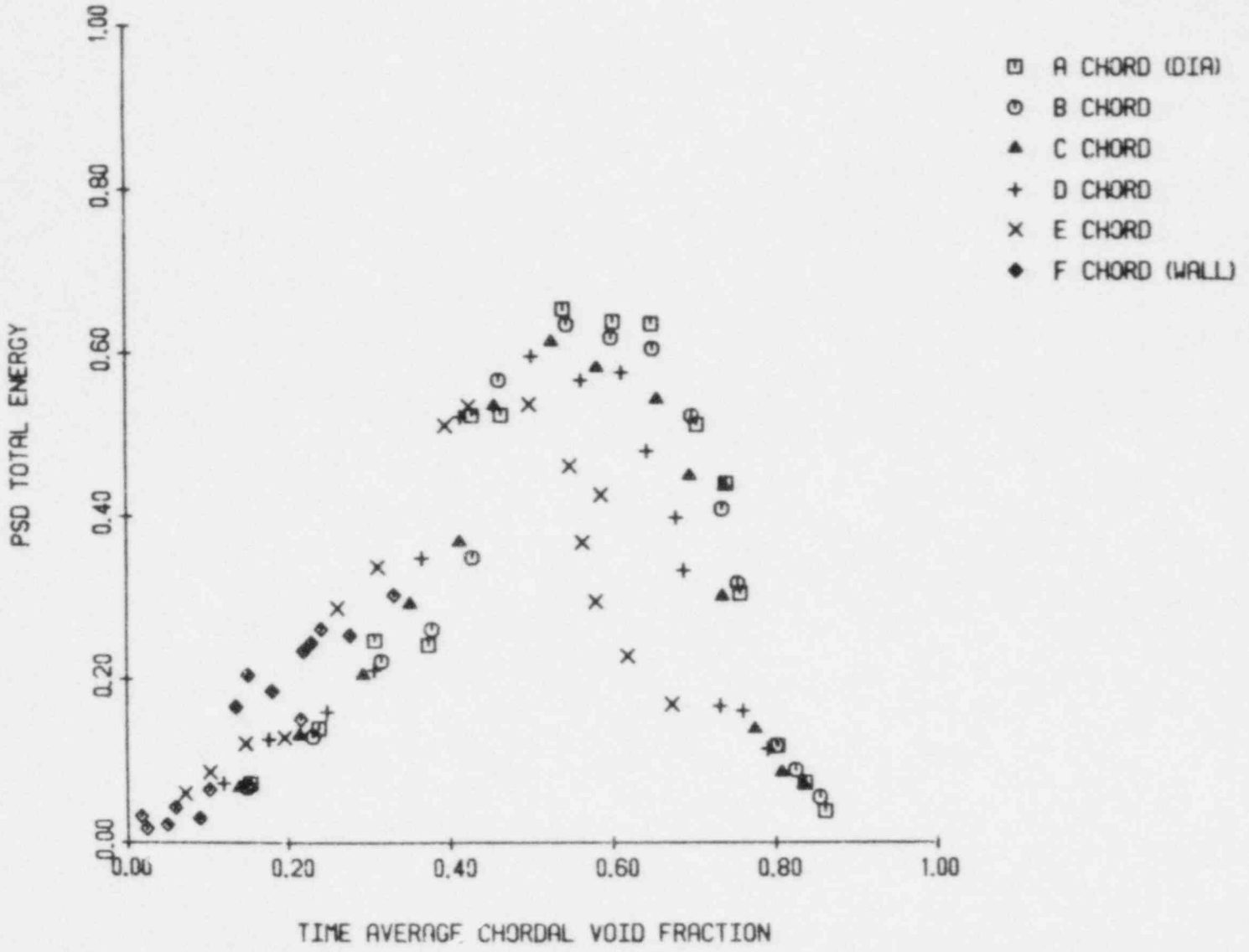

Figure 4.80 The PSD total energy vs. time average chordal void fraction for j_g=0.0 m/sec

hence less energy.

The first moment about the origin, or mean, is plotted in Figure 4.81 as a function of chordal void fraction for the zero liquid flow case. As expected, the mean increases as we go from bubbly to slug flow due to the emergence of a characteristic frequency of low amplitude. Churn-turbulent and annular flow show a decreasing average as a function of void fraction. This trend is explained since the wider bandwidth and lower amplitude associated with annular flow will result in a smaller average value.

Normalization of the PSD average by the energy results in Figure 4.82. The resulting curve is relatively smooth in the lower void fraction regions. The PSD average normalized by energy indicates a transition near 80 percent chordal void fraction. Higher moments of the PDF exhibited a similar trend at this void fraction. The smaller average value and the lower energy associated with annular flow combine to produce this flow regime transition indicator.

A plot of the PSD variance as a function of chordal void fraction is illustrated in Figure 4.83. No clear trends are apparent. Division by the total energy yields Figure 4.84. This normalization accentuates a possible slug annular transition near 80 percent chordal void fraction, however, no bubbly-slug transition is evident.

The variance normalized by the energy is mimimized between 40 and 60 percent chordal void fraction. Here a

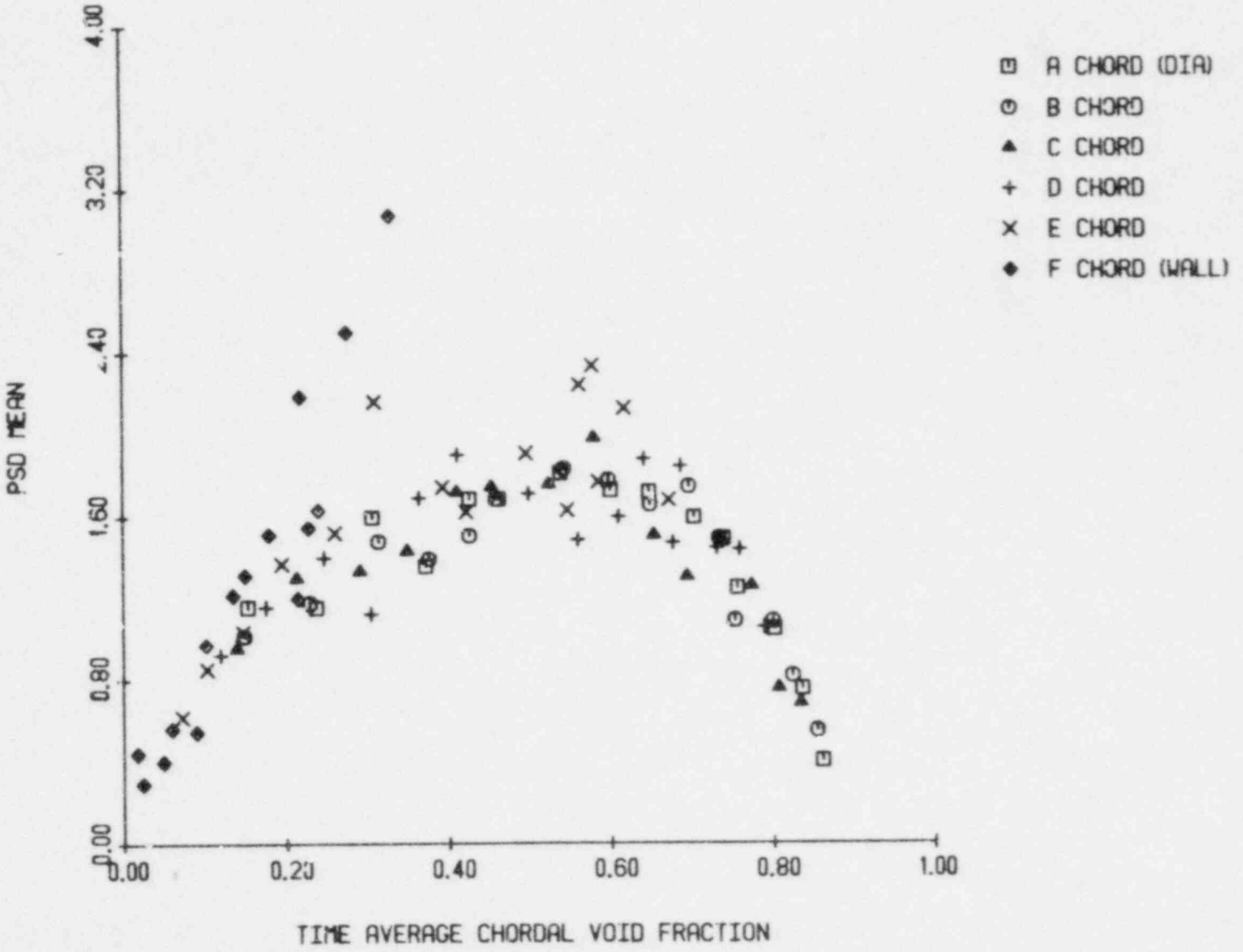

Figure 4.81 The PSD mean vs. time average chordal void fraction for j_L=0.0 m/sec

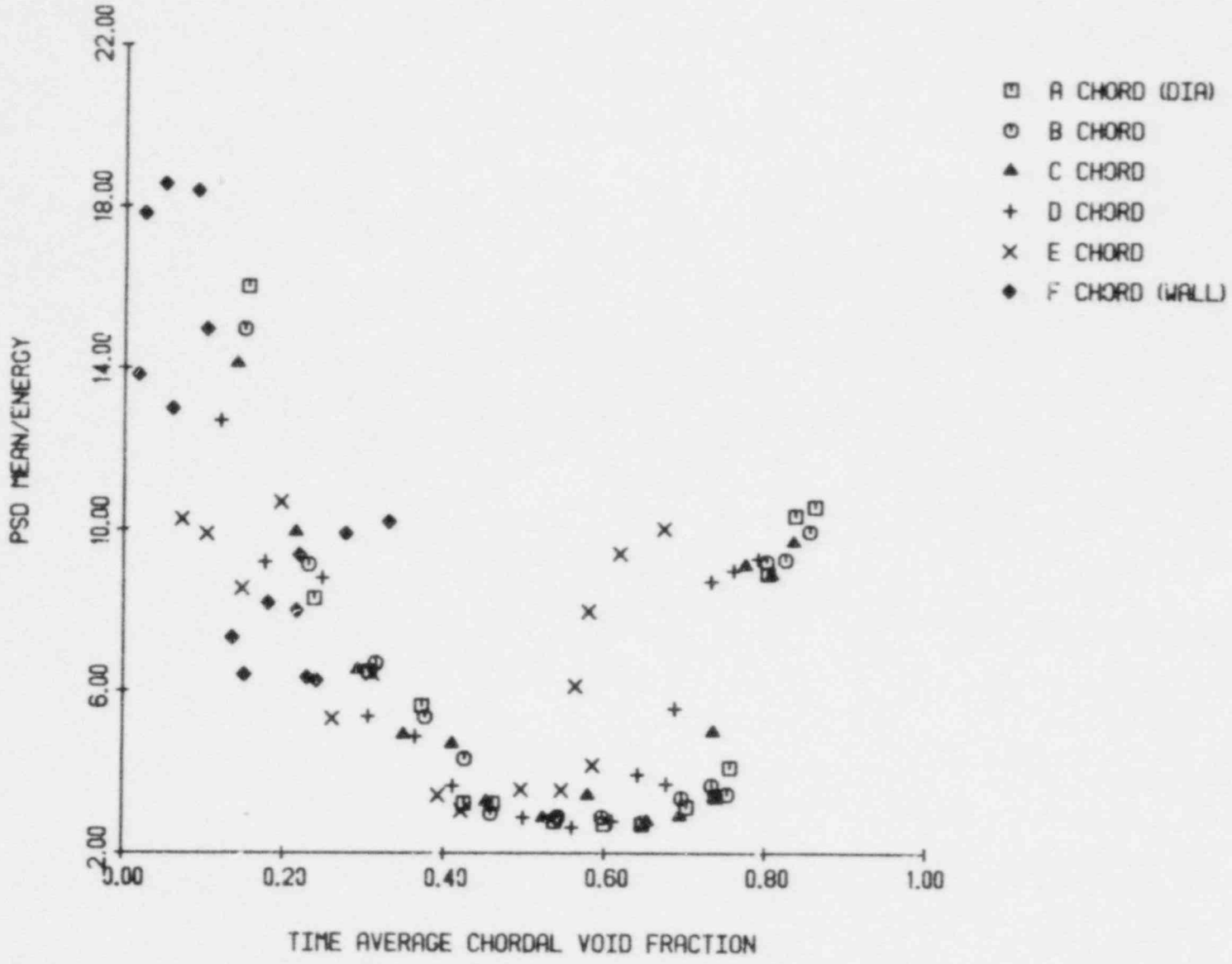

Figure 4.82 The PSD mean/energy vs. time average chordal void fraction for J_f =0.0 m/sec

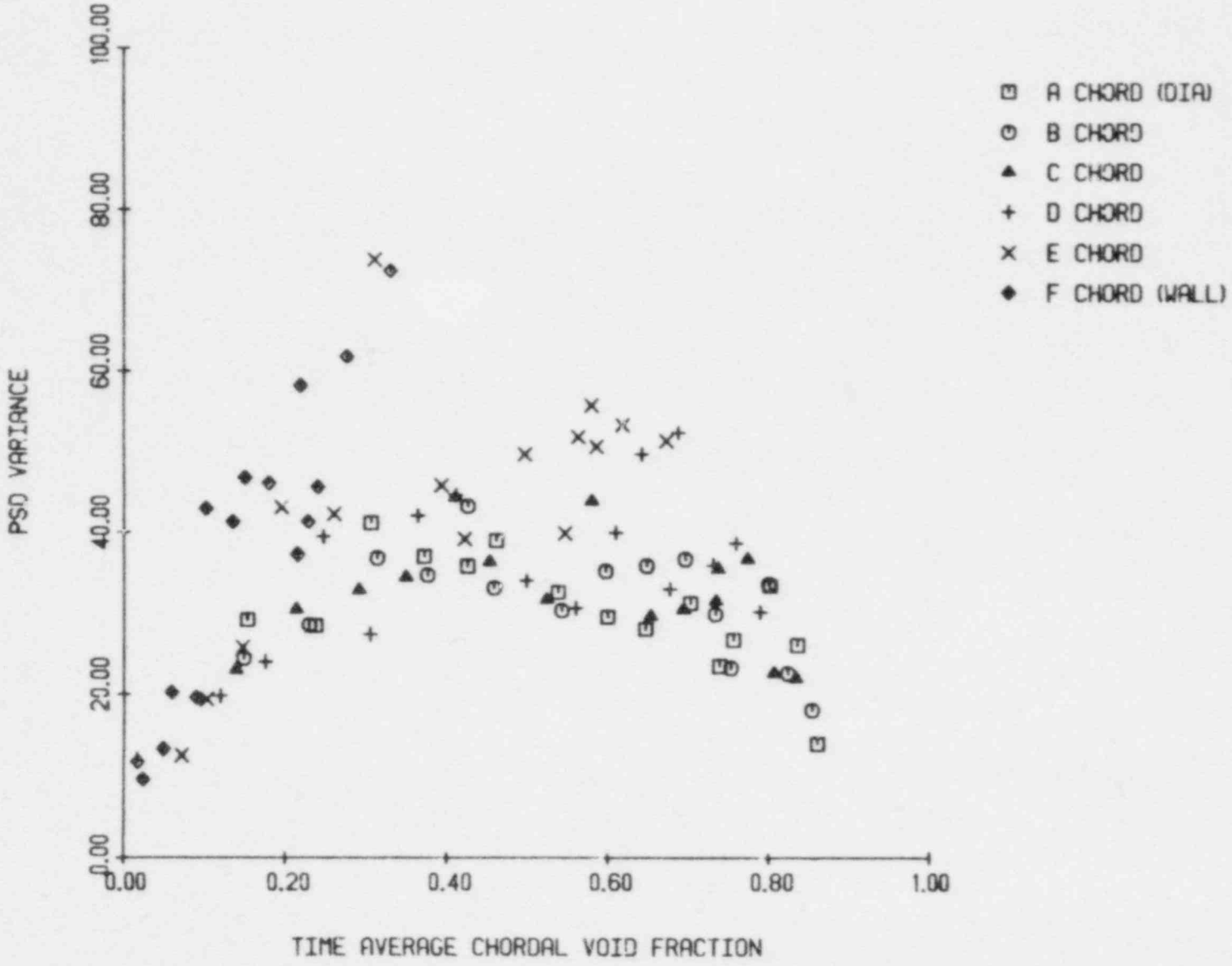

Figure 4.83 The PSD variance vs. time average chordal void fraction for J_L=0.0 m/sec

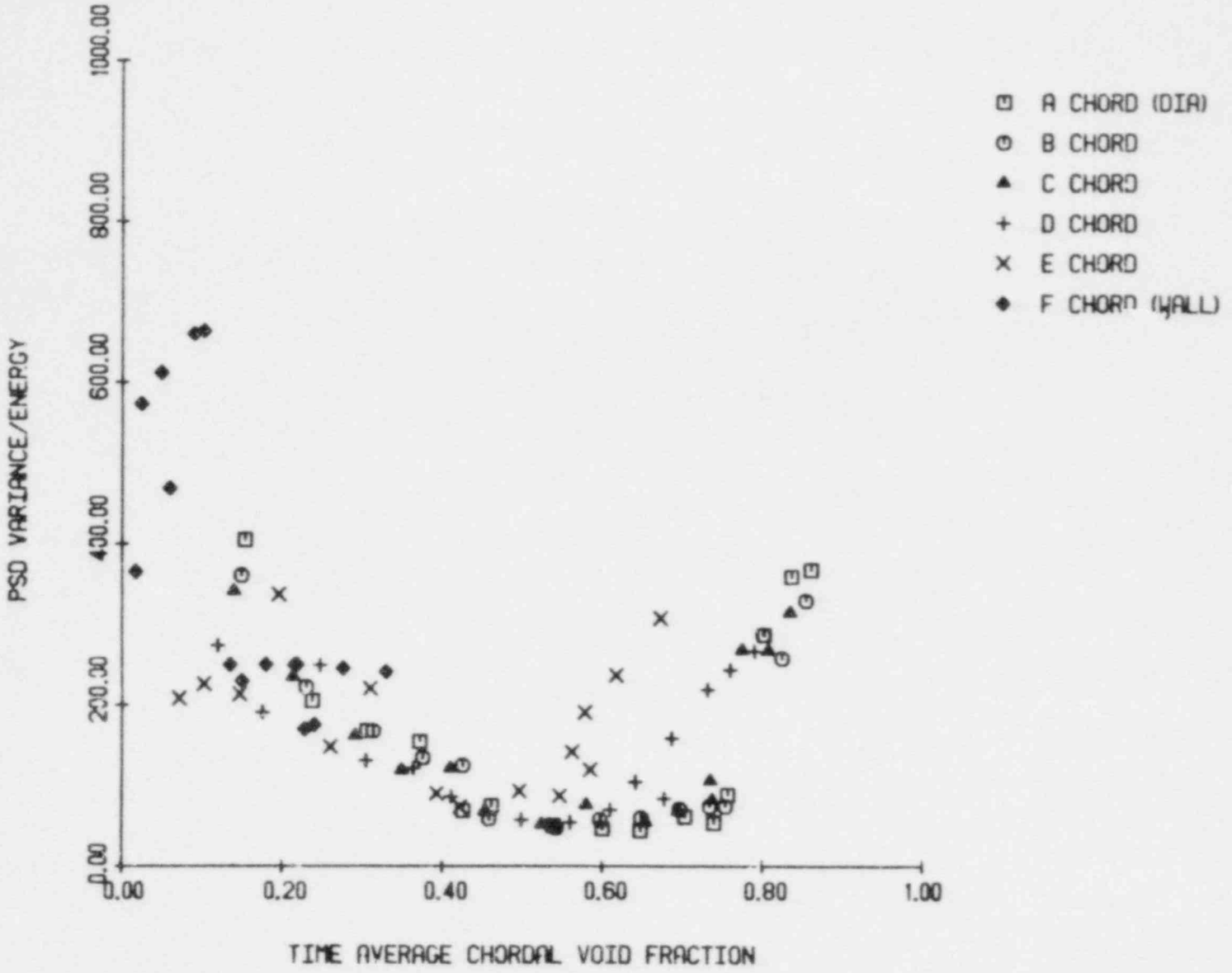

Figure 4.84 The PSD variance/energy vs. time average chordal void fraction for j_ℓ=0.0 m/sec

single, large amplitude peak has emerged from the power spectrum. The energy associated with this peak is relatively large, thus a small variance-energy quotient.

The mean PSD value is usually very close to the origin. Thus, the second raw moment, i.e., the second moment about the origin and the variance, the second moment about the mean, do not differ significantly. Any discussion regarding the variance is equally applicable to the second raw moment.

Figure 4.85 illustrates the PSD coefficient of skewness as a function of chordal void fraction. A gradually changing skewness is observed over the entire range of zero liquid flow void fraction, unfortunately, no objective regime indicator is evident.

Normalization of the skewness by the energy results in Figure 4.86. The skewness-energy quotient gradually decreases as we approach the bubbly-slug transition region. This quotient is relatively constant in the slug flow regime and independent of chordal position. Near the slug-annular transition region (suggested by other potential flow regime indicators), this quotient increases considerably. This trend would be expected since the skewness is increasing with voidage due to the widening of the PSD distribution as the annular flow regime is encountered. Simultaneously, the total energy is decreasing and thus the quotient will increase. These same trends shown in Figures 4.87 and 4.88 were observed in the PSD

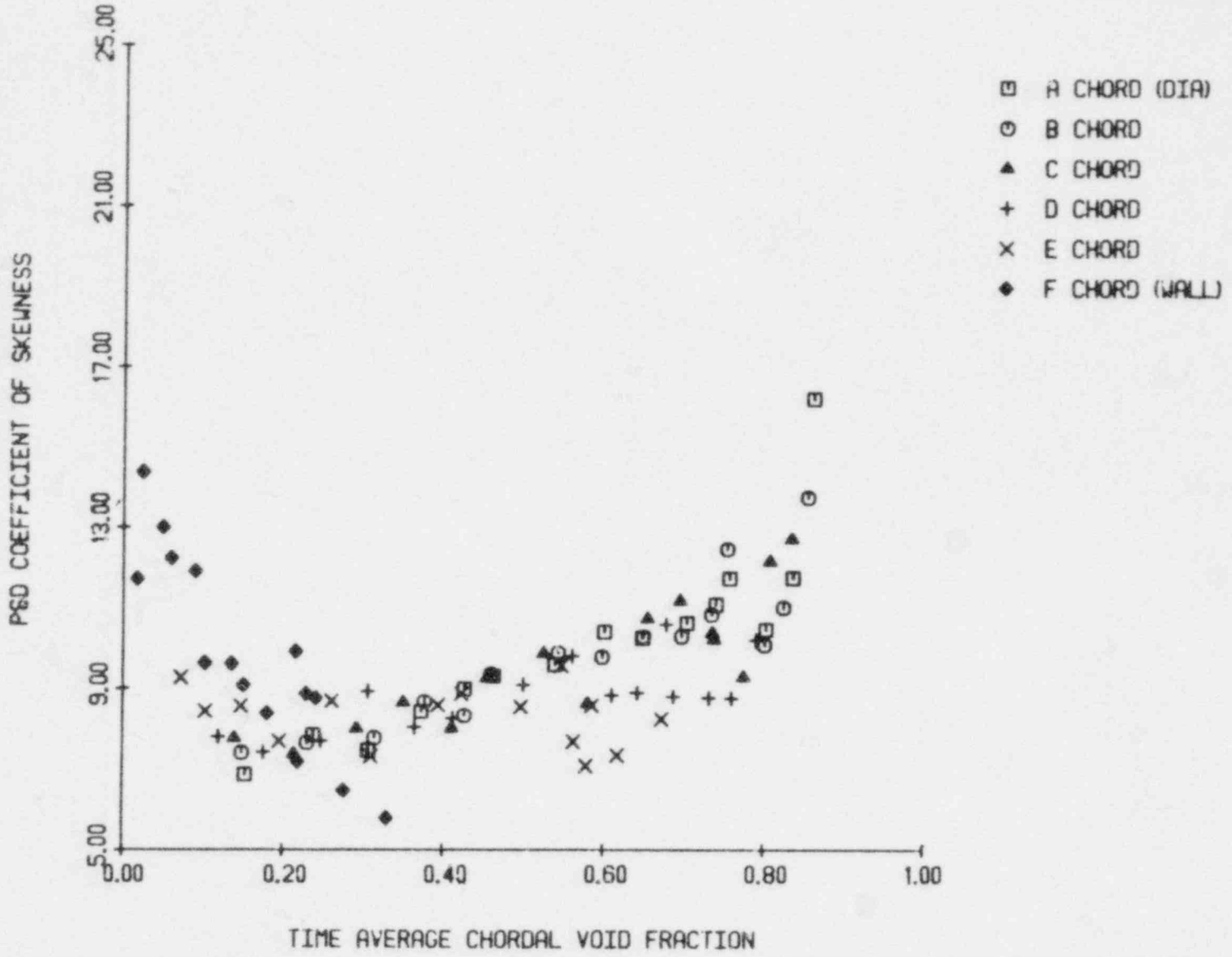

Figure 4.85 The PSD coefficient of skewness vs. time average chordal void fraction for j_ℓ = 0.00 m/sec

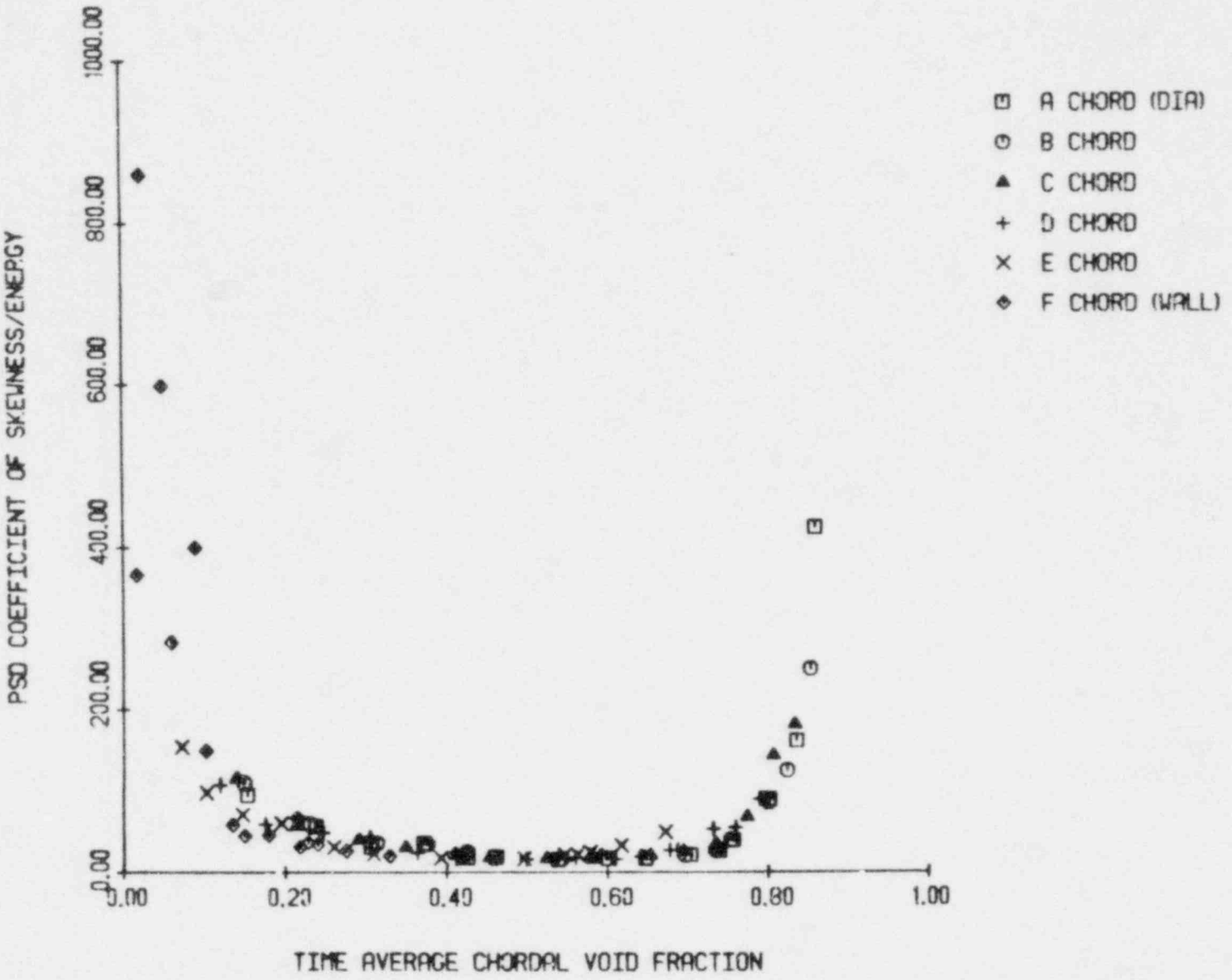

Figure 4.86 The PSD coefficient of skewness/energy vs. time average chordal void fraction for J_ℓ = 0.00 m/sec

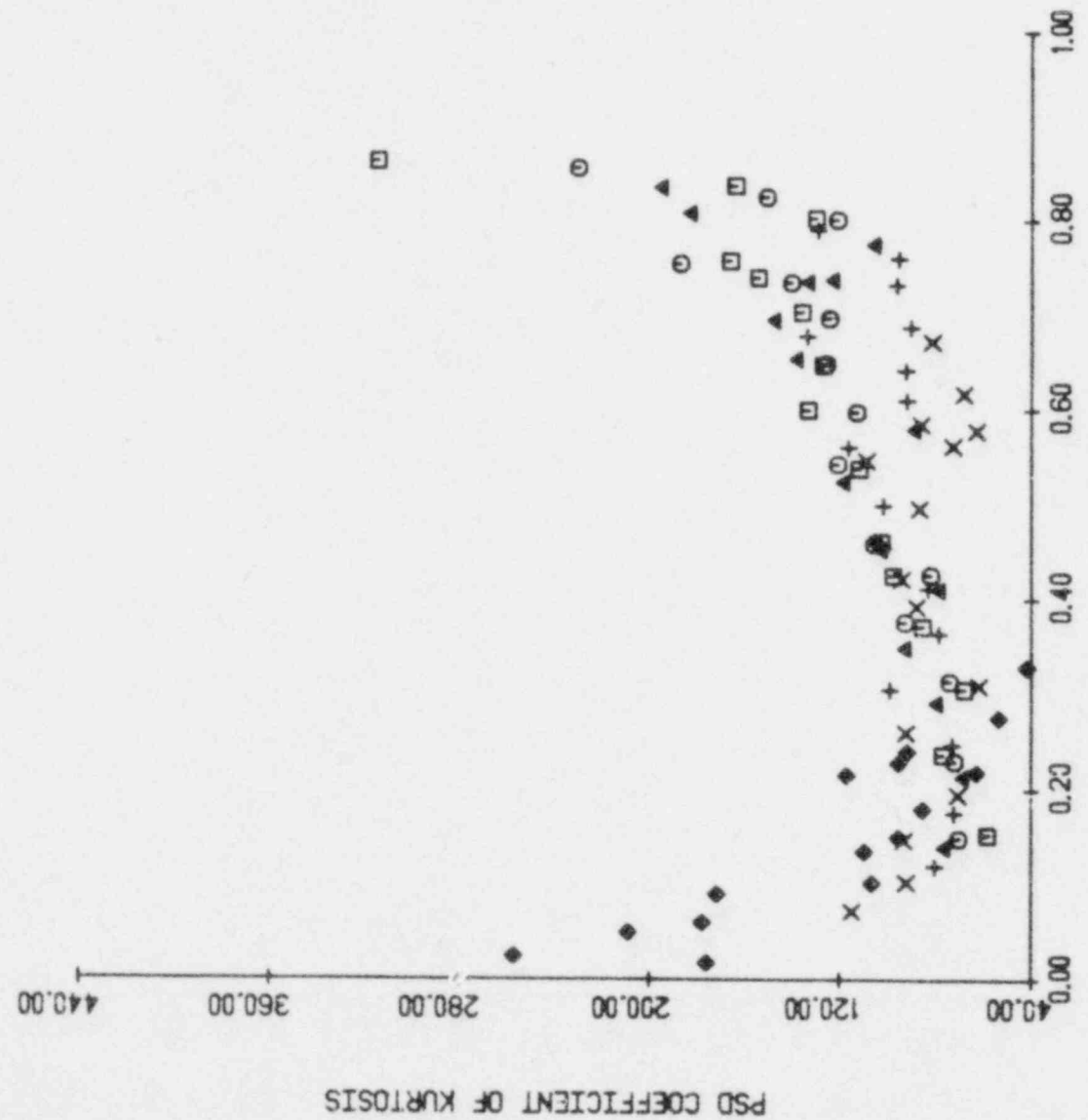

Figure 4.87 The PSD coefficient of kurtosis vs. time average chordal void fraction for j_f = 0.00 m/sec

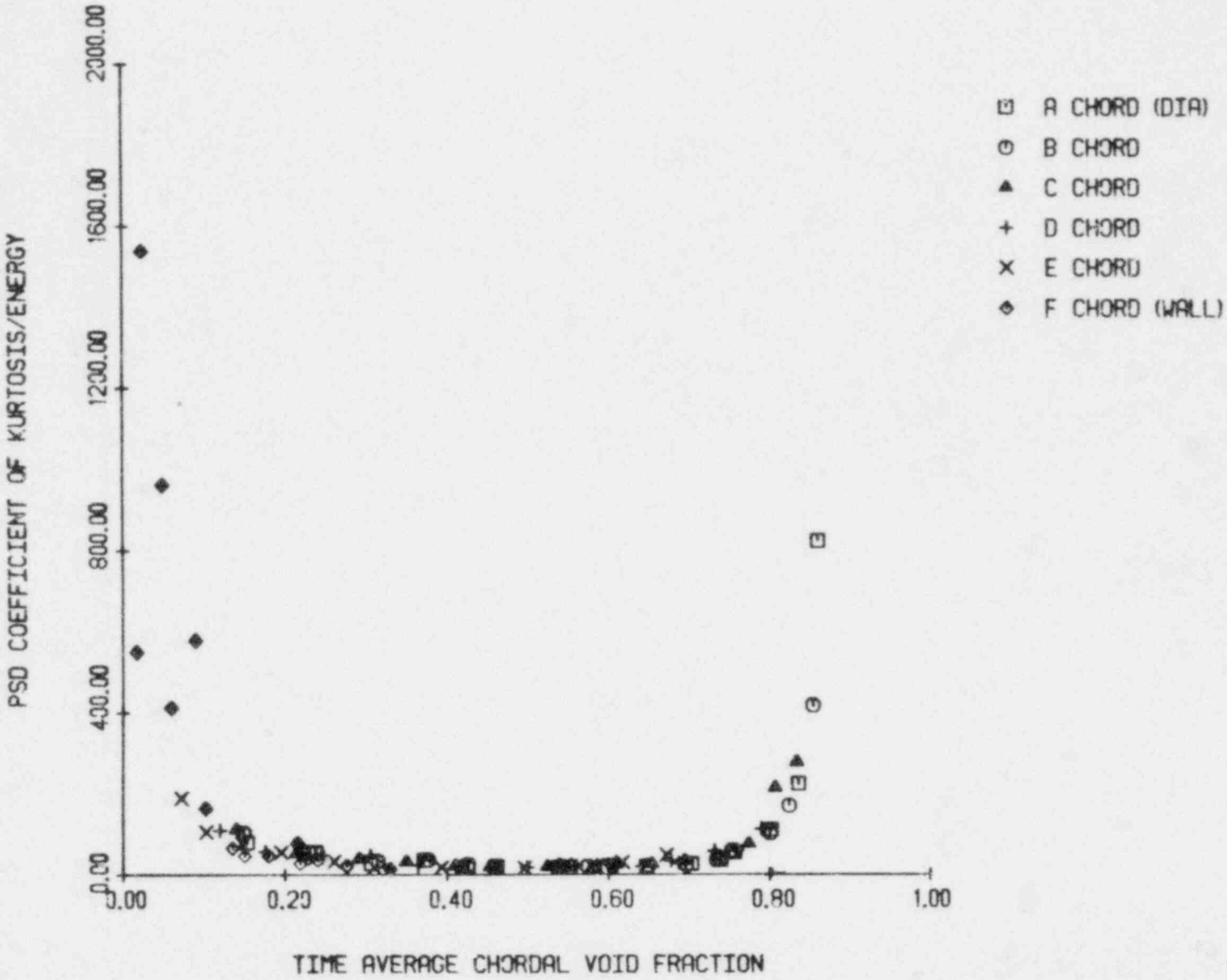

Figure 4.88 The PSD coefficient of kurtosis/energy vs. time average chordal void fraction for J_ℓ = 0.00 m/sec

coefficient of kurtosis and energy normalized coefficient of kurtosis.

4.2.2.2 Non-Zero Liquid Flow Data

Division by the total energy provided higher moment curves which were more easily interpretable. Hence, the non-zero liquid flow data was presented with all moments normalize by the total energy.

The variance divided by the total energy is plotted in Figure 4.89 for an area-averaged void fraction of 13 percent. Clearly the variance is affected by the changing liquid superficial velocity. This trend is expected since larger frequencies are available as the the liquid velocity is increased. These larger frequencies are of smaller amplitude but increase the variance. All chords yield similar results. At 20 percent area-averaged void fraction the increasing variance divided by energy trend is observed as shown in Figure 4.90. The larger liquid velocities at this voidage show a significant change. The emergence of a characteristic frequency associated with slug flow causes a substantial decrease in variance and increase in energy, thus the variance-energy quotient is substantially affected. This effect is very noticable along the centerline chords. The measurements near the wall show the increasing trend shown at lower liquid velocity.

Figure 4.91 illustrates the trend in variance divided by energy at 26 percent area-averaged void fraction.

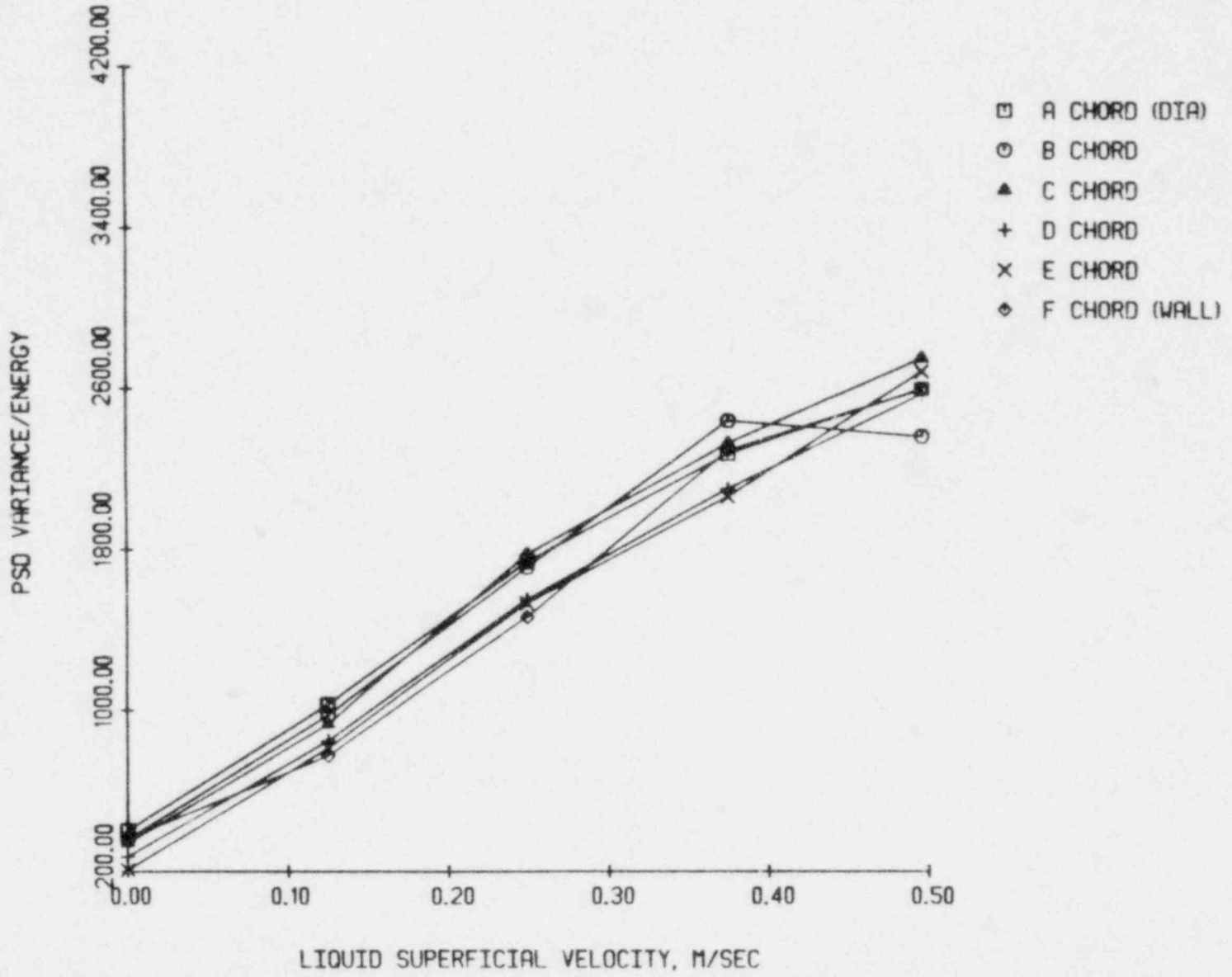

Figure 4.89 The PSD variance/energy vs. superficial liquid velocity at 13 percent area-averaged void fraction

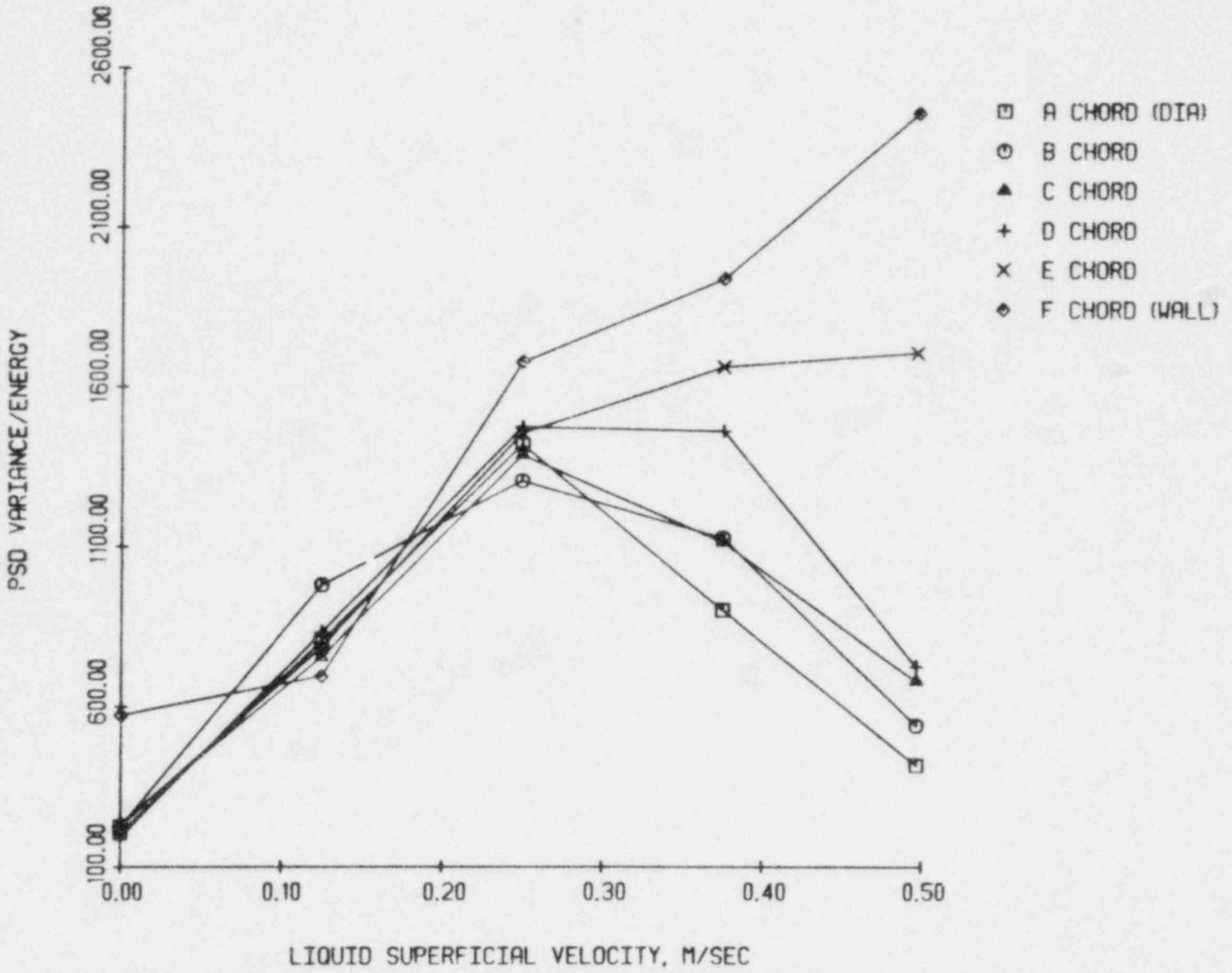

Figure 4.90 The PSD variance/energy vs. superficial liquid velocity at 20 percent area-averaged void fraction

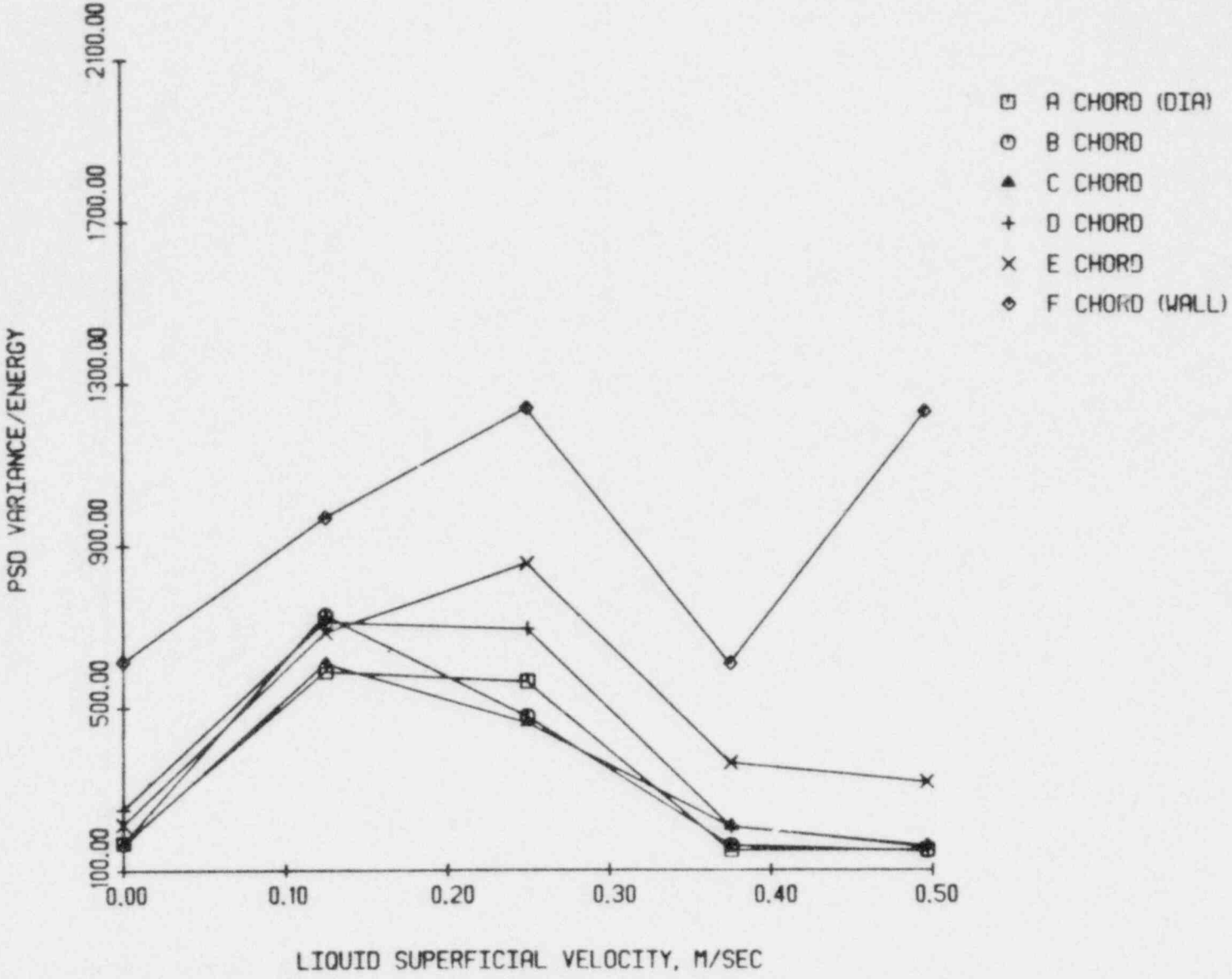

Figure 4.91 The PSD variance/energy vs. superficial liquid velocity at 26 percent area-averaged void fraction

The variance-energy quotient initially increases because the flow of liquid causes the slug flow to revert to bubbly flow. A further increase of liquid flow at constant void fraction can not suppress the bubbly-slug transition. As a result, the variance-energy quotient is reduced to a value comparable to the zero liquid flow case.

Initiation of liquid flow causes an increase in the variance-energy quotient as shown in Figure 4.92 for 32 percent area-average void fraction. Slug flow is obviously present here. A further increase in void fraction results in Figures 4.93 through 4.97 for area-average void fraction of 41, 53, 66, 68, and 72 percent, respectively. The variance-energy quotient exhibits an increase with superficial liquid velocity. This trend is expected because the higher liquid velocity will introduce more low amplitude, higher frequency components into the signal. These higher frequency components will contribute little to the total energy but significantly increase the variance. All chordal measurements, except the wall chord, followed the same trend with approximately the same magnitude.

The same trends observed in the variance were seen in the second raw moment, i.e.; the second moment about the origin. The mean is very close to the origin, hence a significant difference in the second moment magnitude was not observed. As a result, the second raw moment information is not presented.

The third and fourth moments of the PSD did not

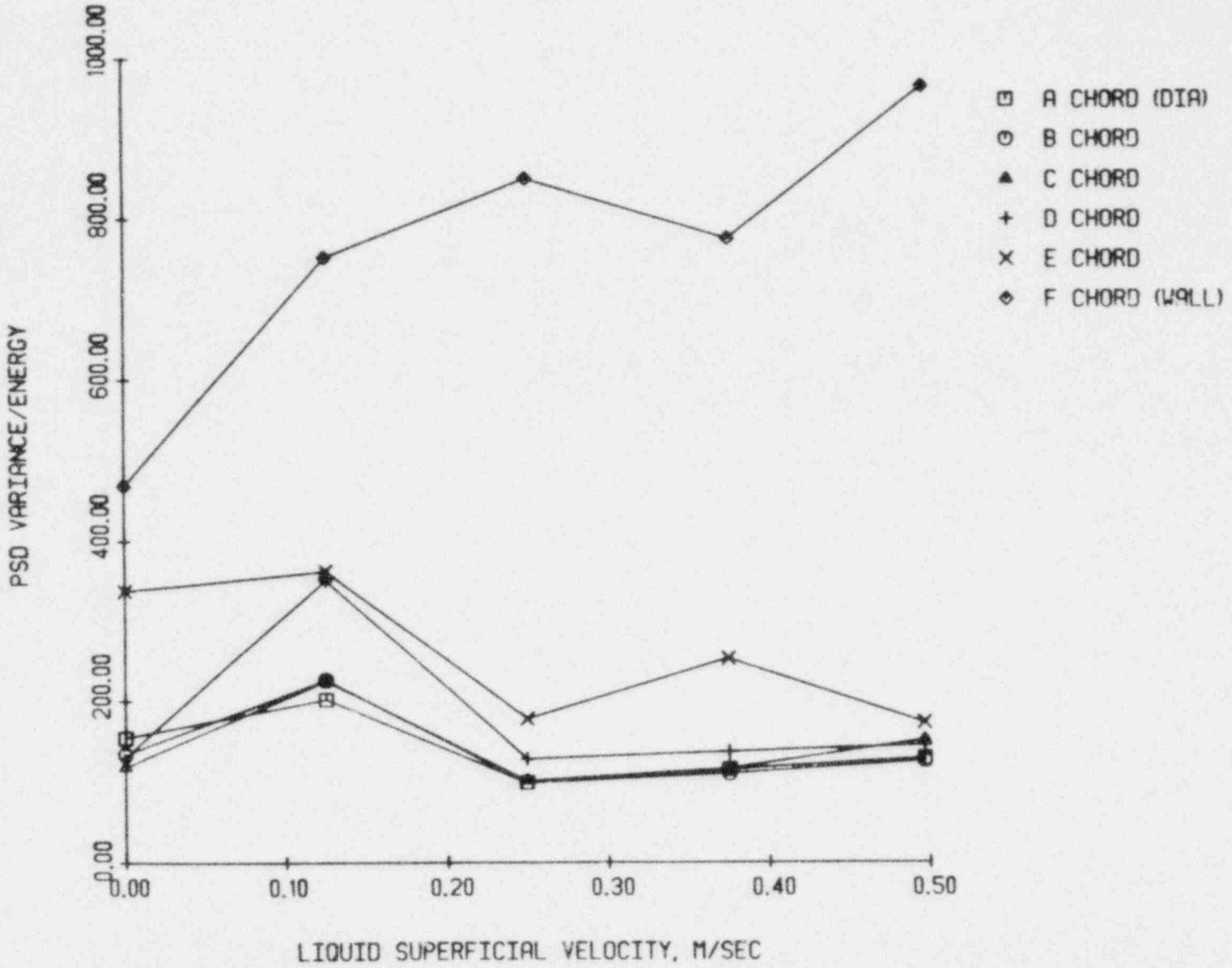

Figure 4.92 The PSD variance/energy vs. superficial liquid velocity at 32 percent area-averaged void fraction

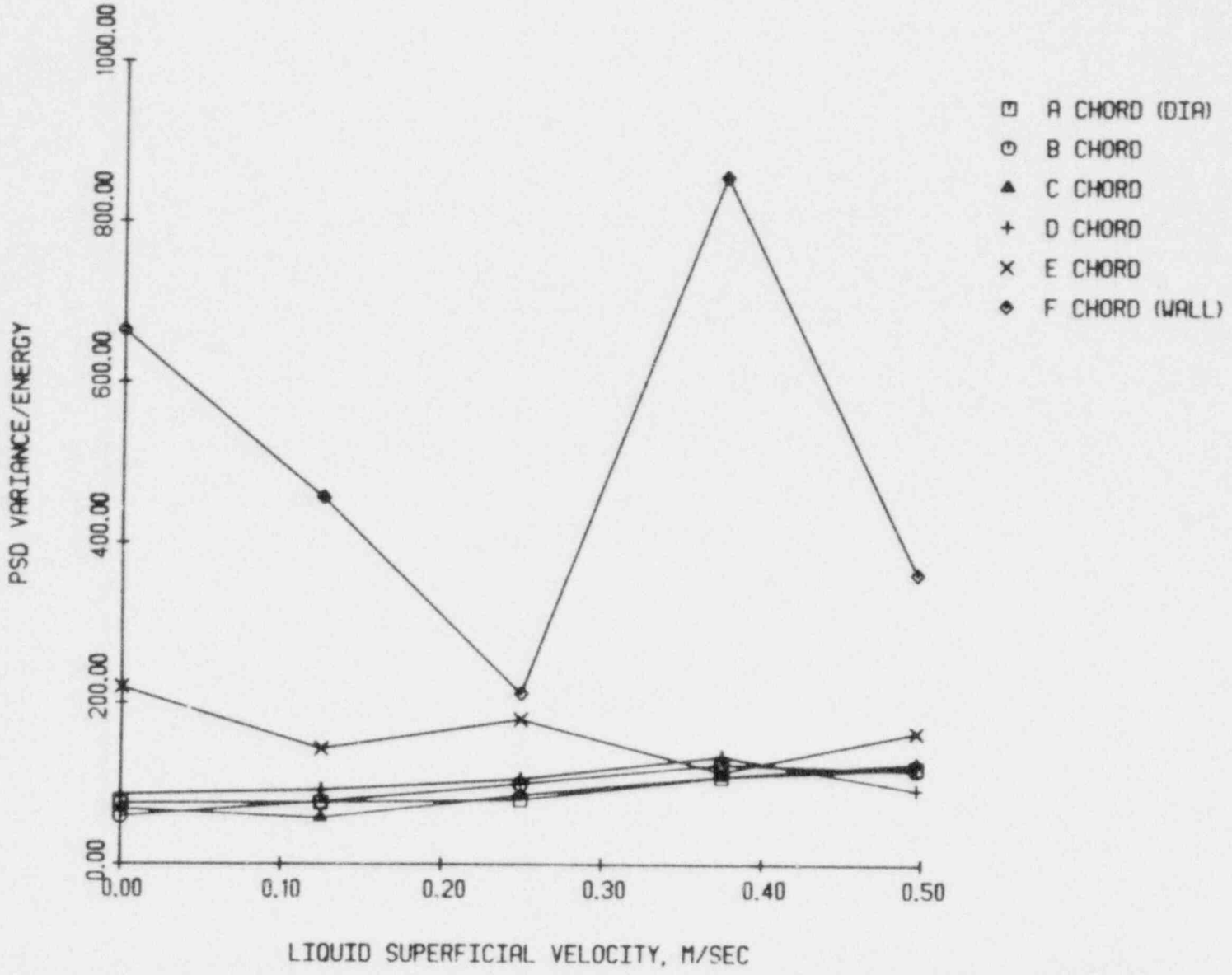

Figure 4.93 The PSD variance/energy vs. superficial liquid velocity at 41 percent area-averaged void fraction

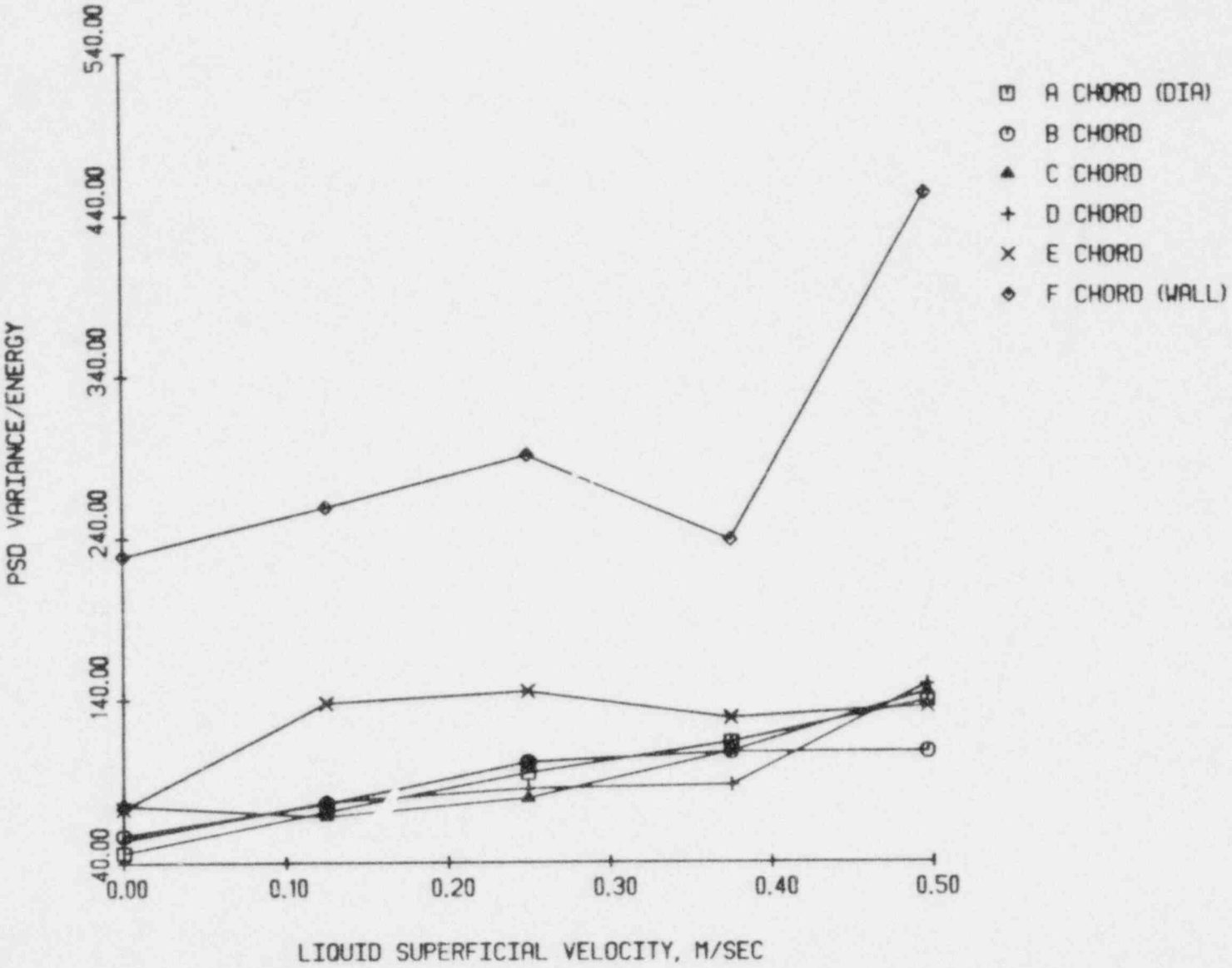

Figure 4.94 The PSD variance/energy vs. superficial liquid velocity .. 53 percent area-averaged void fraction

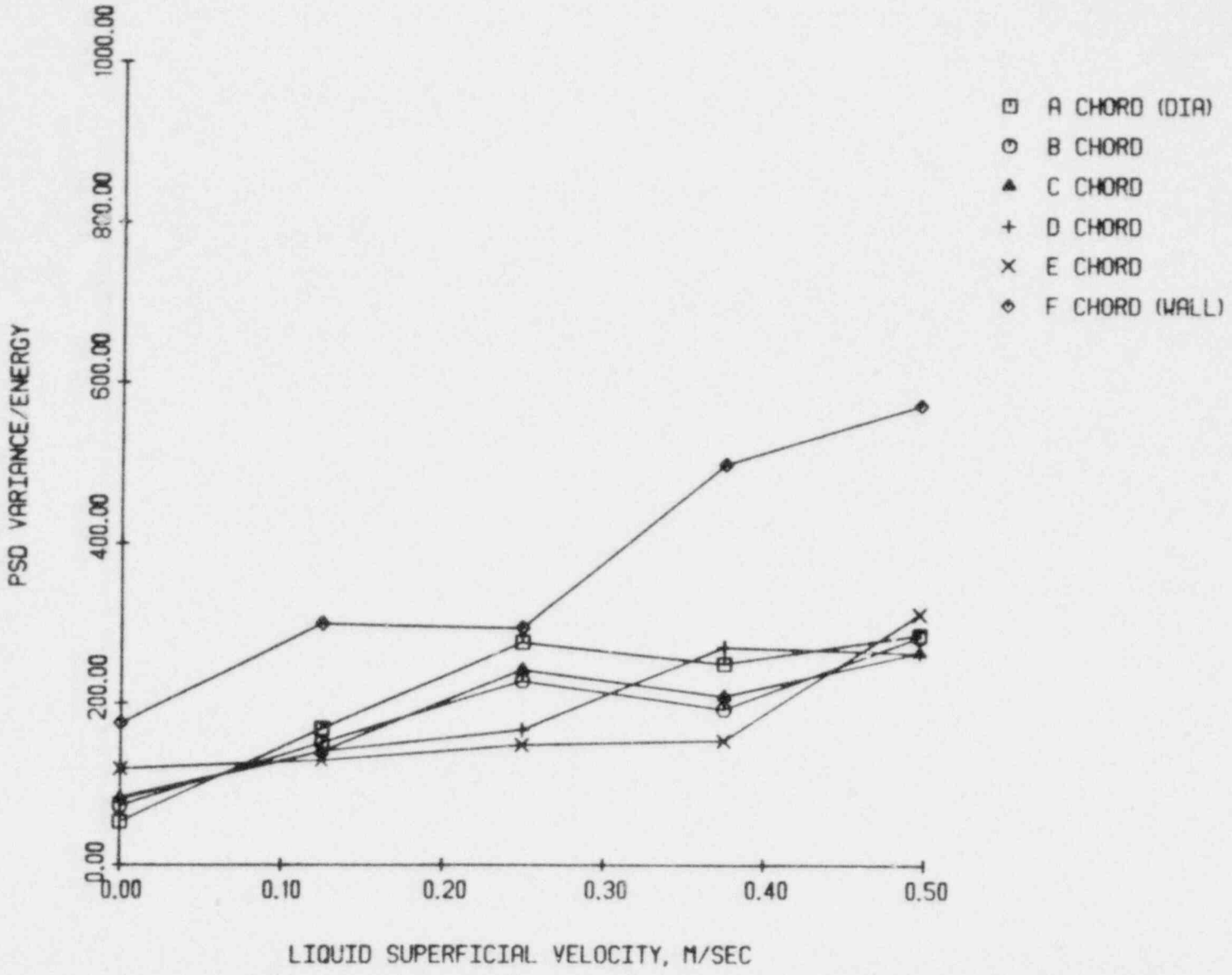

Figure 4.95 The PSD variance/energy vs. superficial liquid velocity at 66 percent area-averaged void fraction

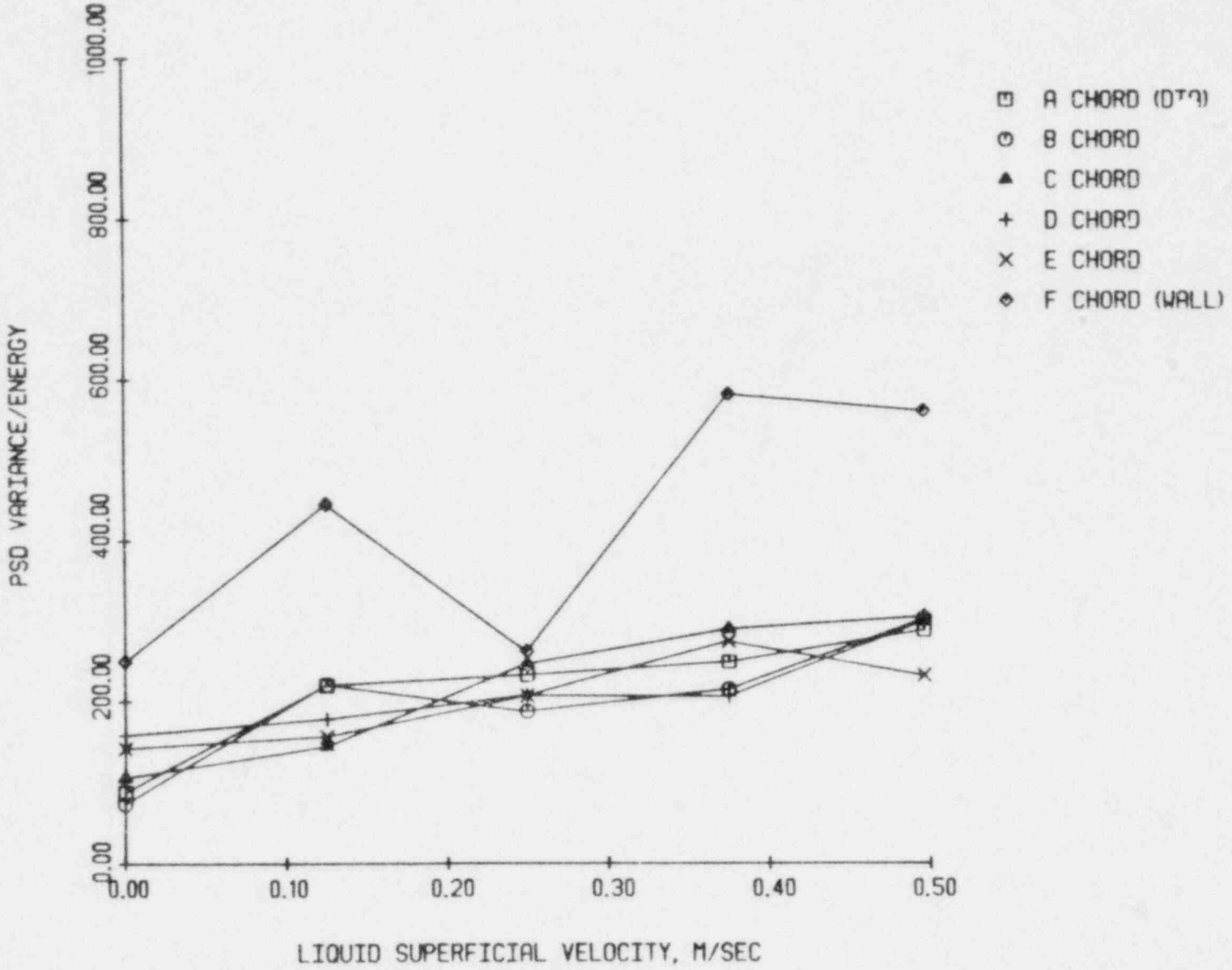

Figure 4.96 The PSD variance/energy vs. superficial liquid velocity at 68 percent area-averaged void fraction

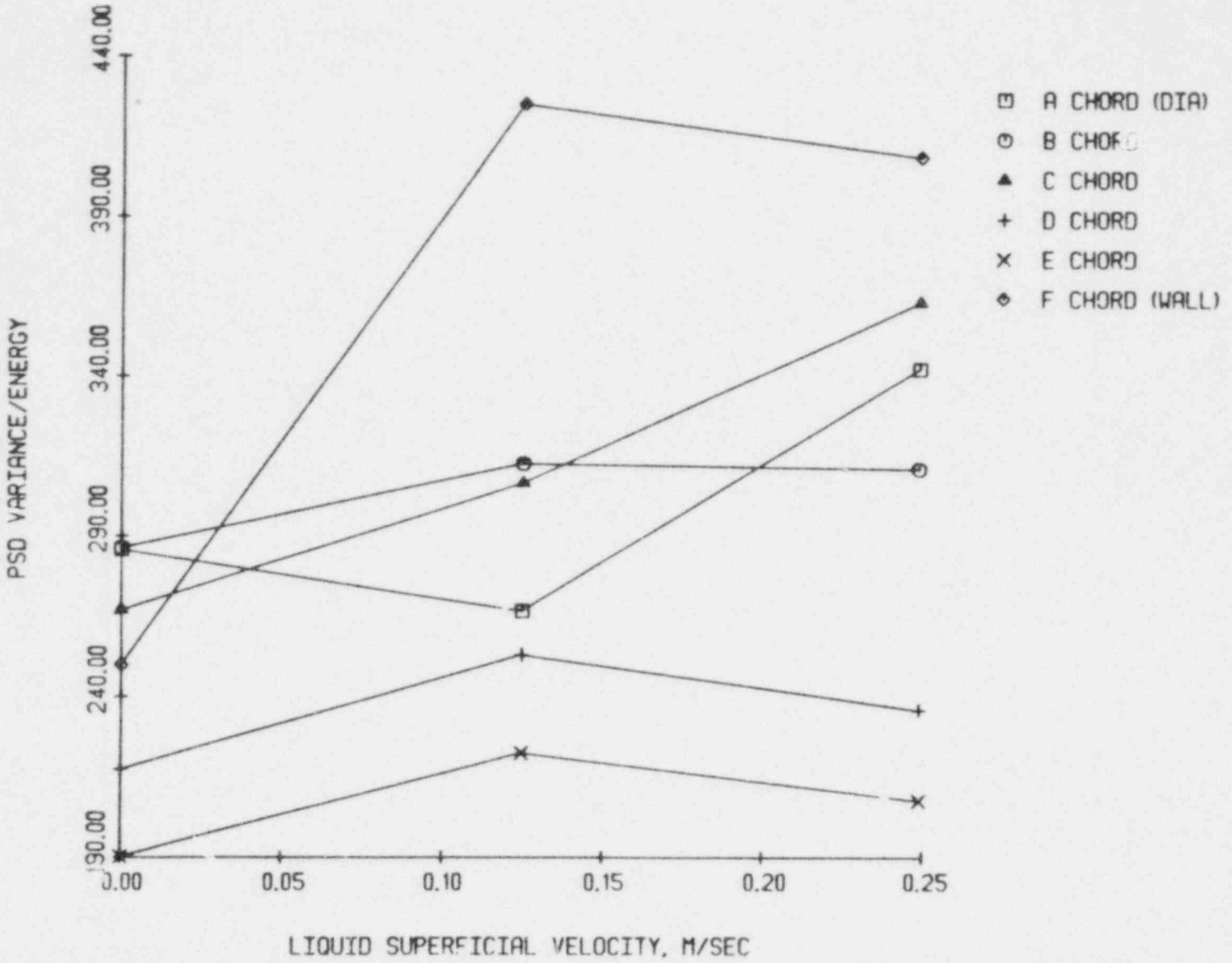

Figure 4.97 The PSD variance/energy vs. superficial liquid velocity at 72 percent area-averaged void fraction

provide any useful flow regime transition information, nevertheless, these graphs are included for completeness as Figures 4.98 through 4.115. All chordal measurements, except the wall chord, follow the same trend with about the same amplitude. For annular flow, these moments become very position dependent as shown earlier in Figures 4.114 and 4.115.

4.3 Data Consistency

Two verifications were performed to assure accuracy in the previous results. First the Ergodic Hypothesis was verified earlier, as shown in Figure 4.42. As a result the process was shown to be statistically stationary.

The second verification was obtained by comparing a global void fraction determined from pressure drop measurements with the weighted and integrated chordal x-ray measurements, i.e.; the area-average void fraction. A weighting scheme proposed by Pike [41] (see Appendix A.9) was employed. The results are shown in Figure 4.116. Considering that fluctuation in pressure drop made an accurate manometer reading difficult (particularly for the slug flow regime), the observed correlation is excellent.

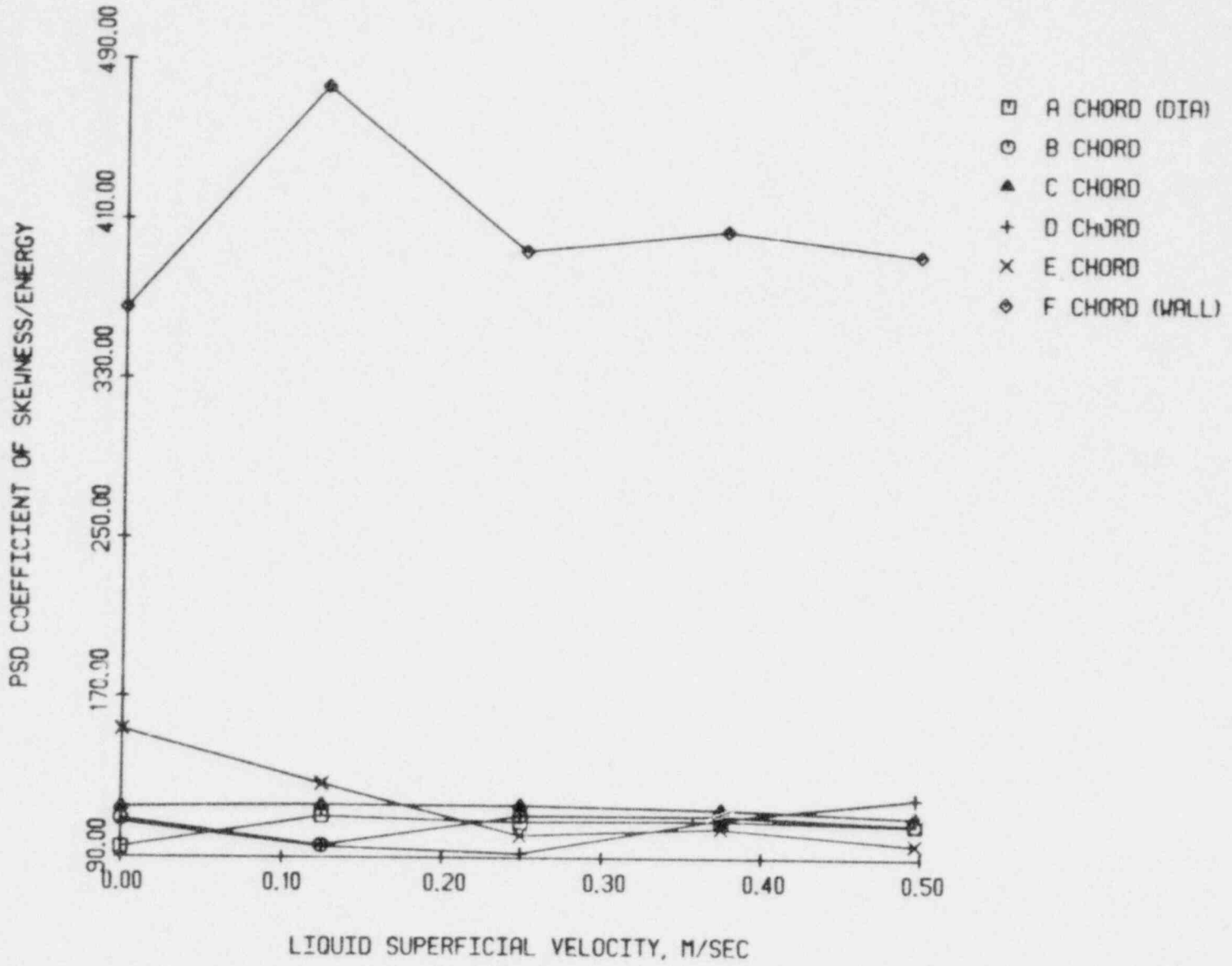

Figure 4.98 The PSD coefficient of skewness/energy vs. superficial liquid velocity at 13 percent area-averaged void fraction

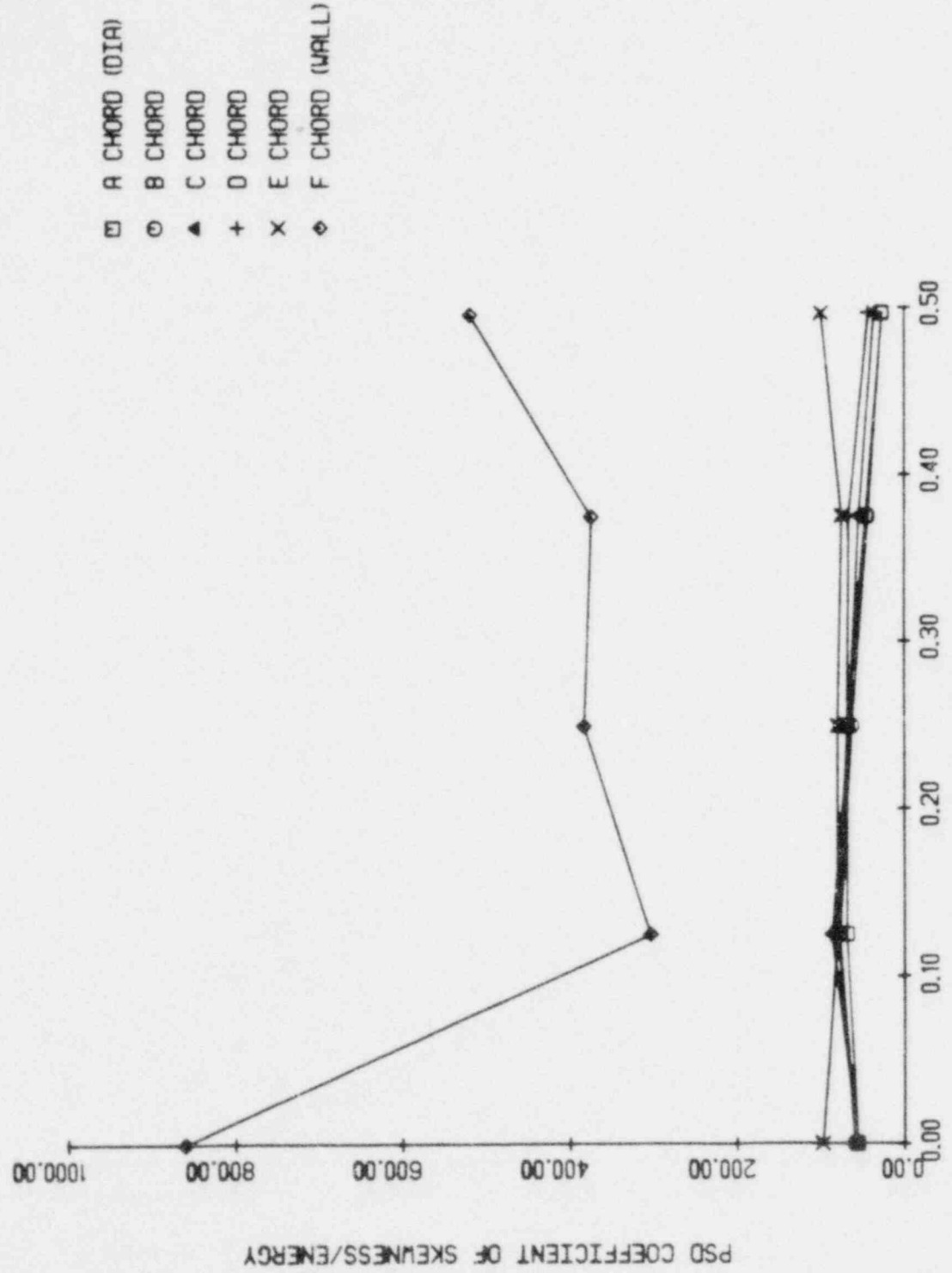

Figure 4.99 The PSD coefficient of skewness/energy vs. superficial liquid velocity at 20 percent area-averaged void fraction

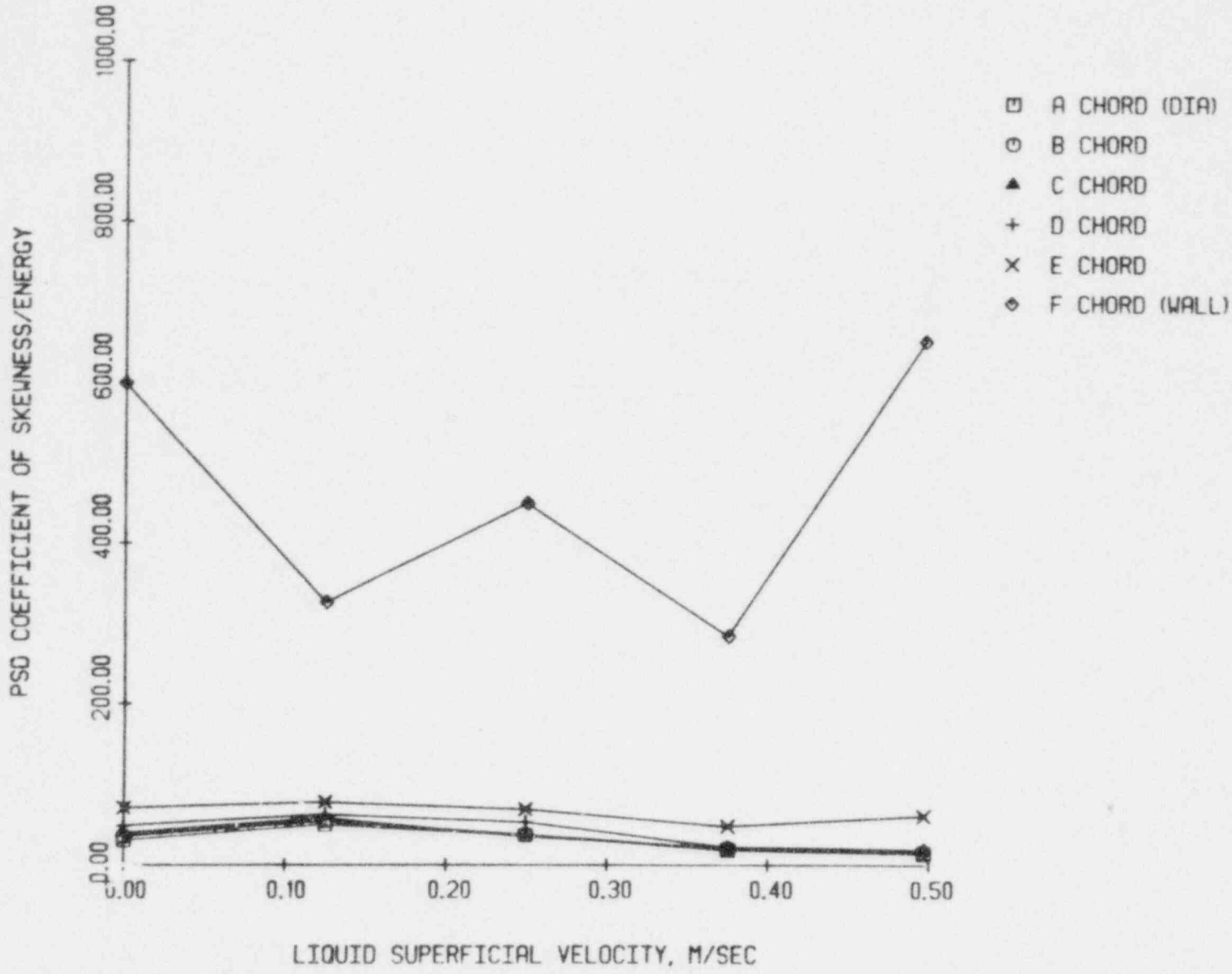

Figure 4.100 The PSD coefficient of skewness/energy vs. superficial liquid velocity at 26 percent area-averaged void fraction

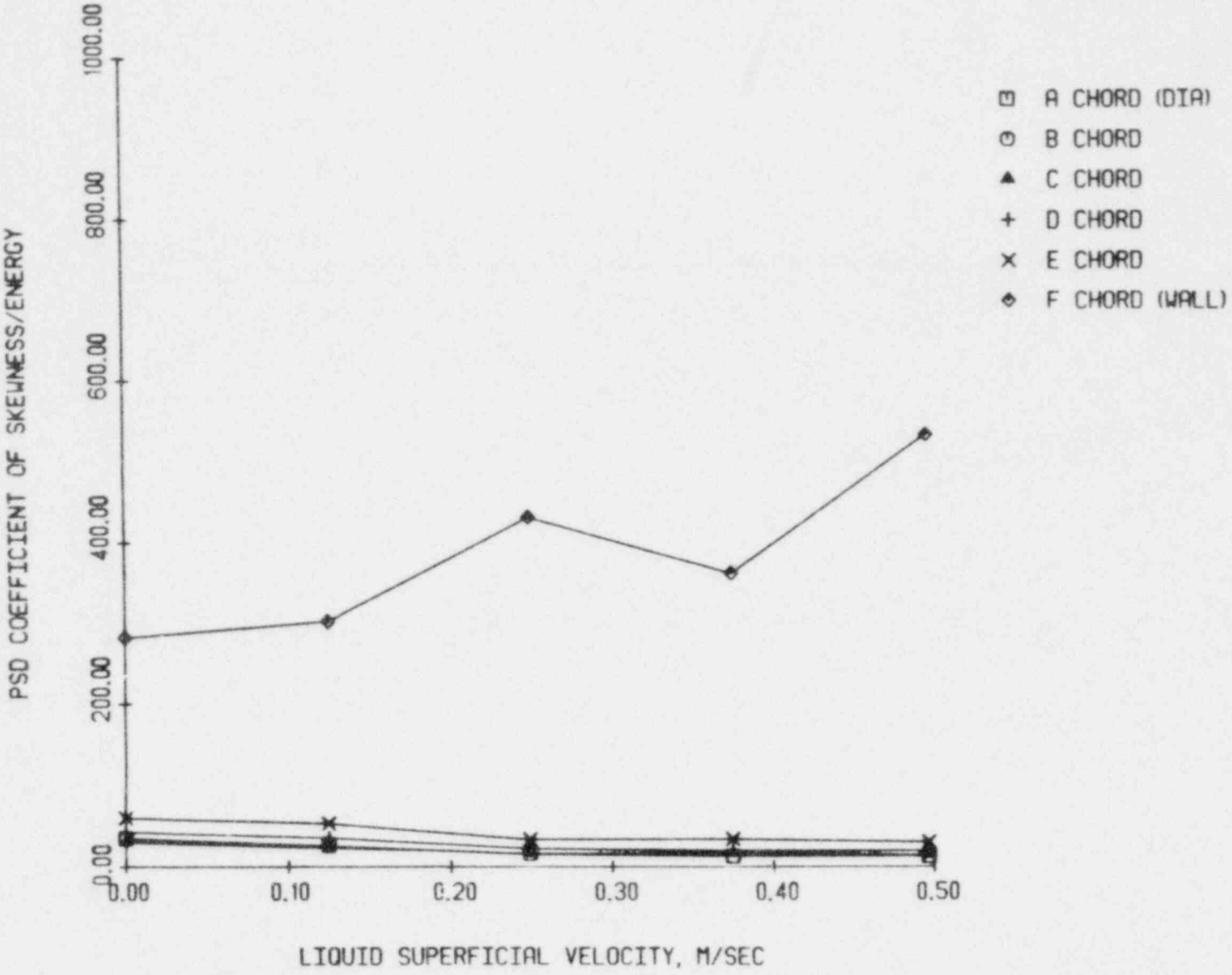

Figure 4.101 The PSD coefficient of skewness/energy vs. superficial liquid velocity at 32 percent area-averaged void fraction

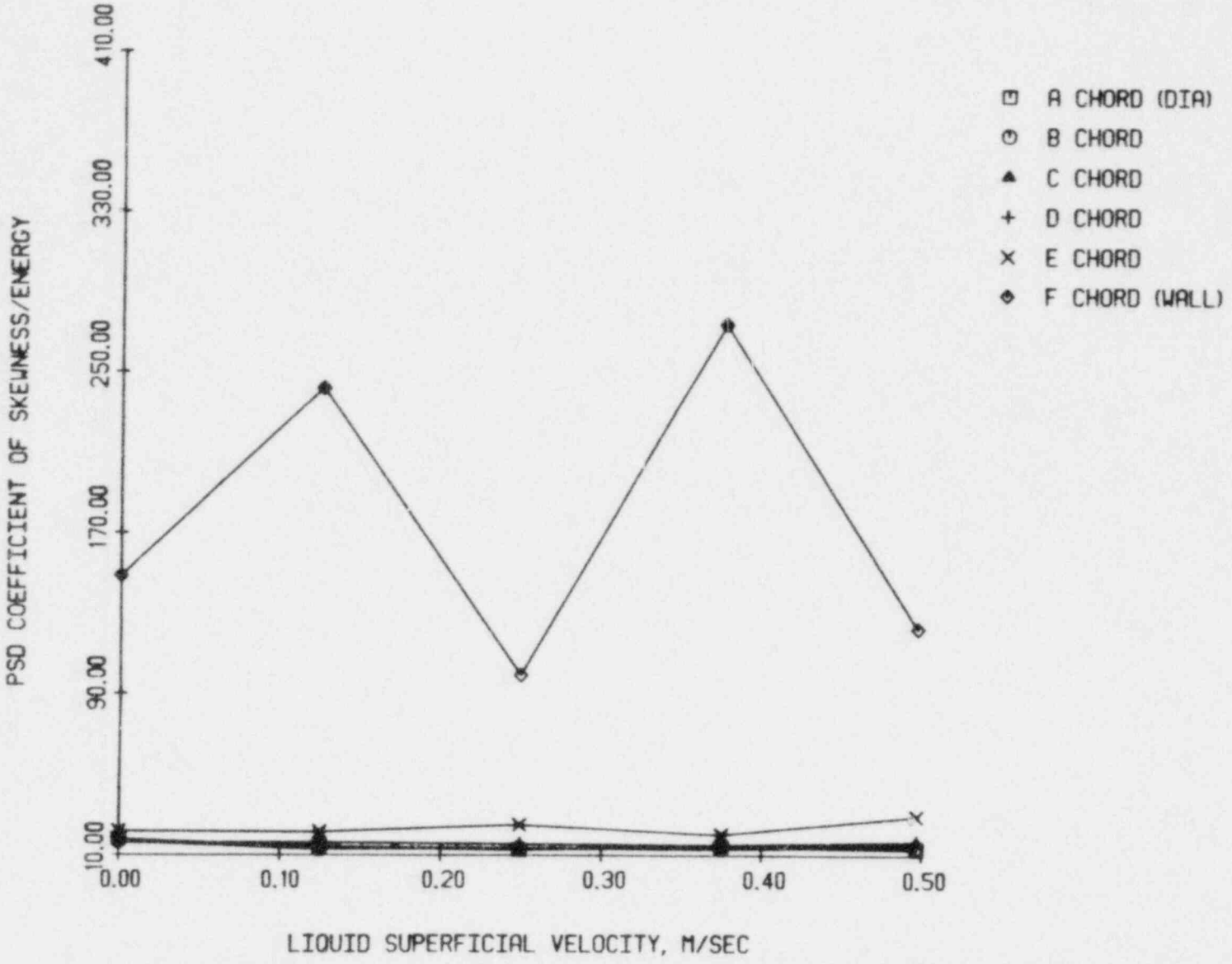

Figure 4.102 The PSD coefficient of skewness/energy vs. superficial liquid velocity at 41 percent area-averaged void fraction

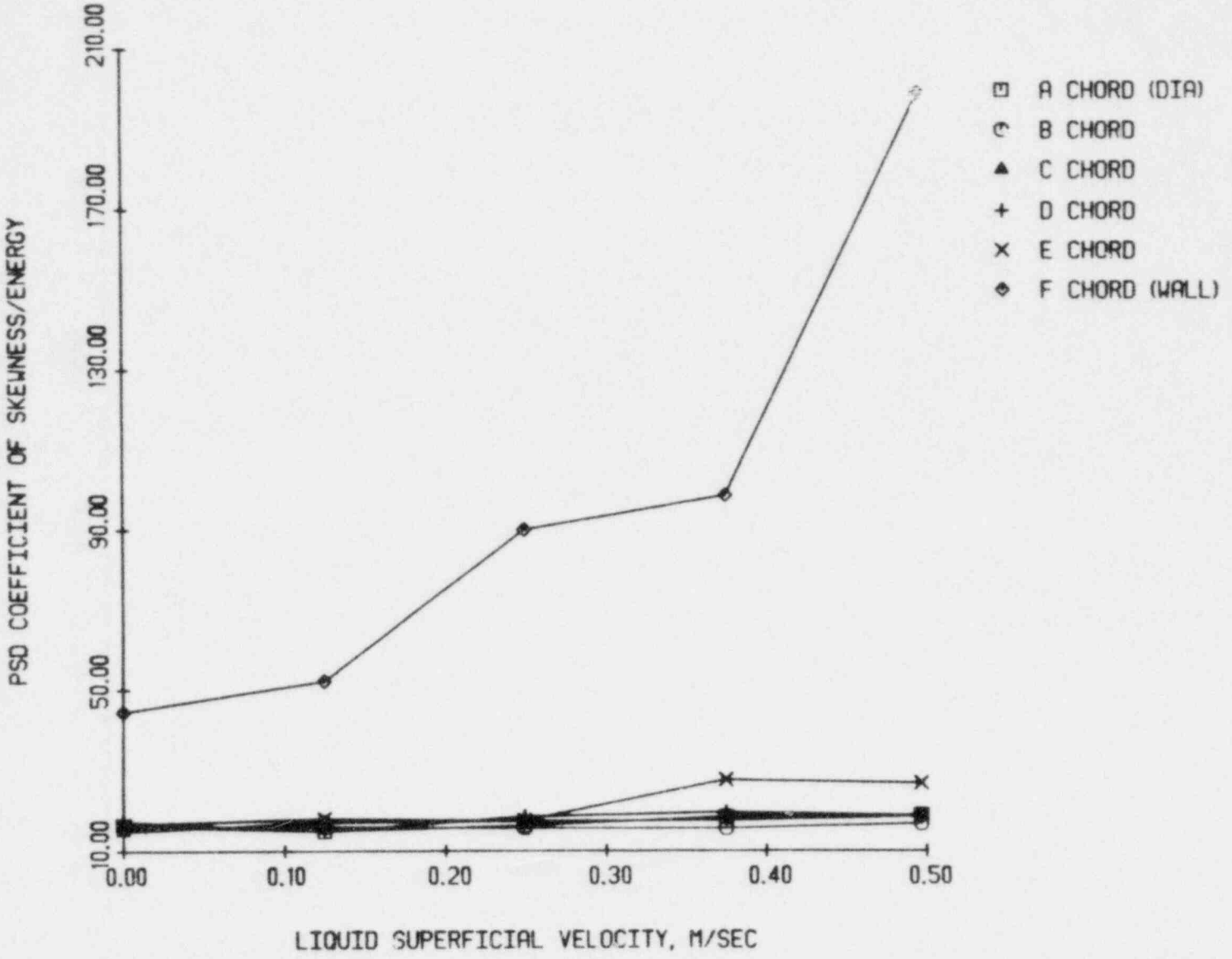

Figure 4.103 The PSD coefficient of skewness/energy vs. superficial liquid velocity at 53 percent area-averaged void fraction

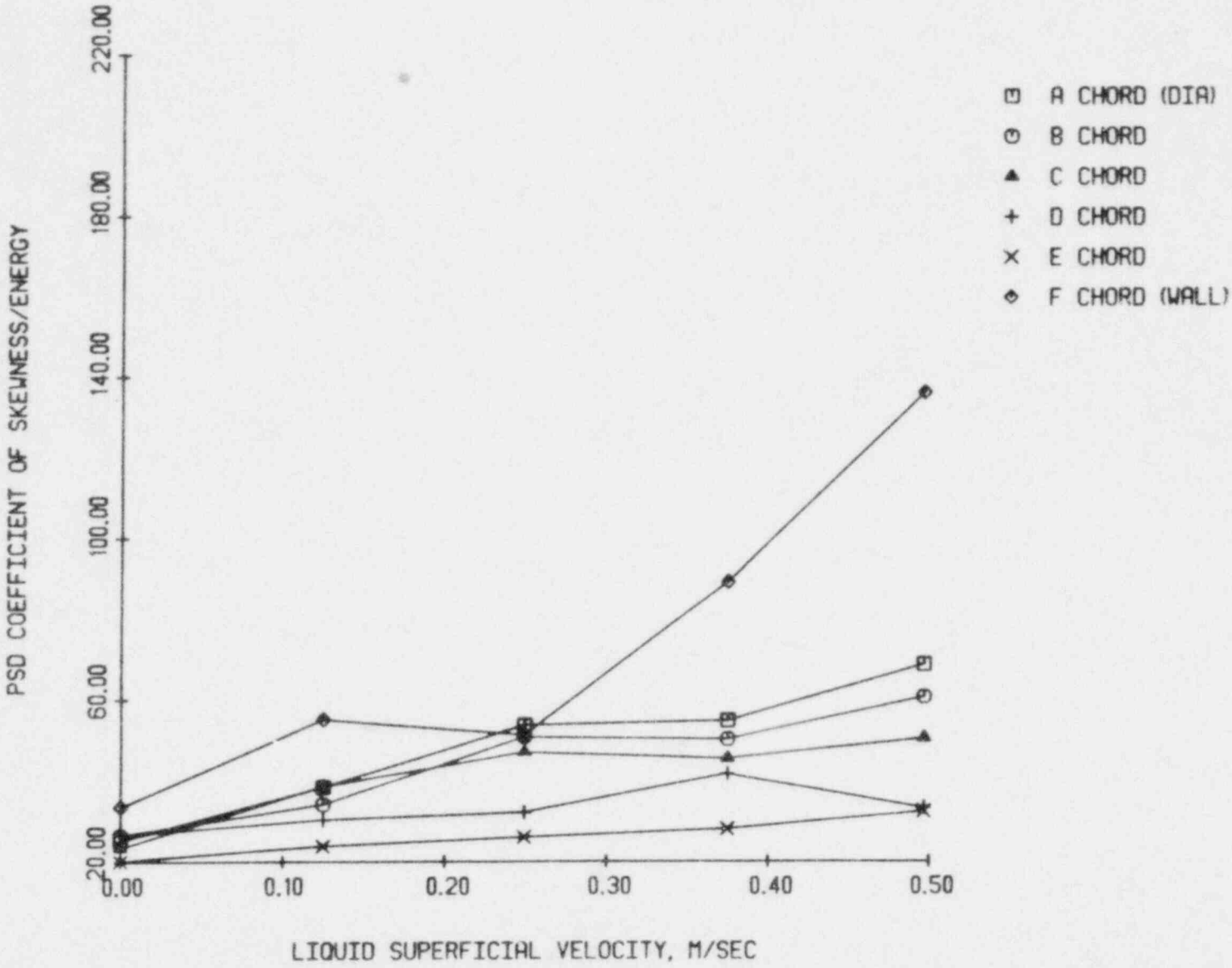

Figure 4.104 The PSD coefficient of skewness/energy vs. superficial liquid velocity at 66 percent area-averaged void fraction

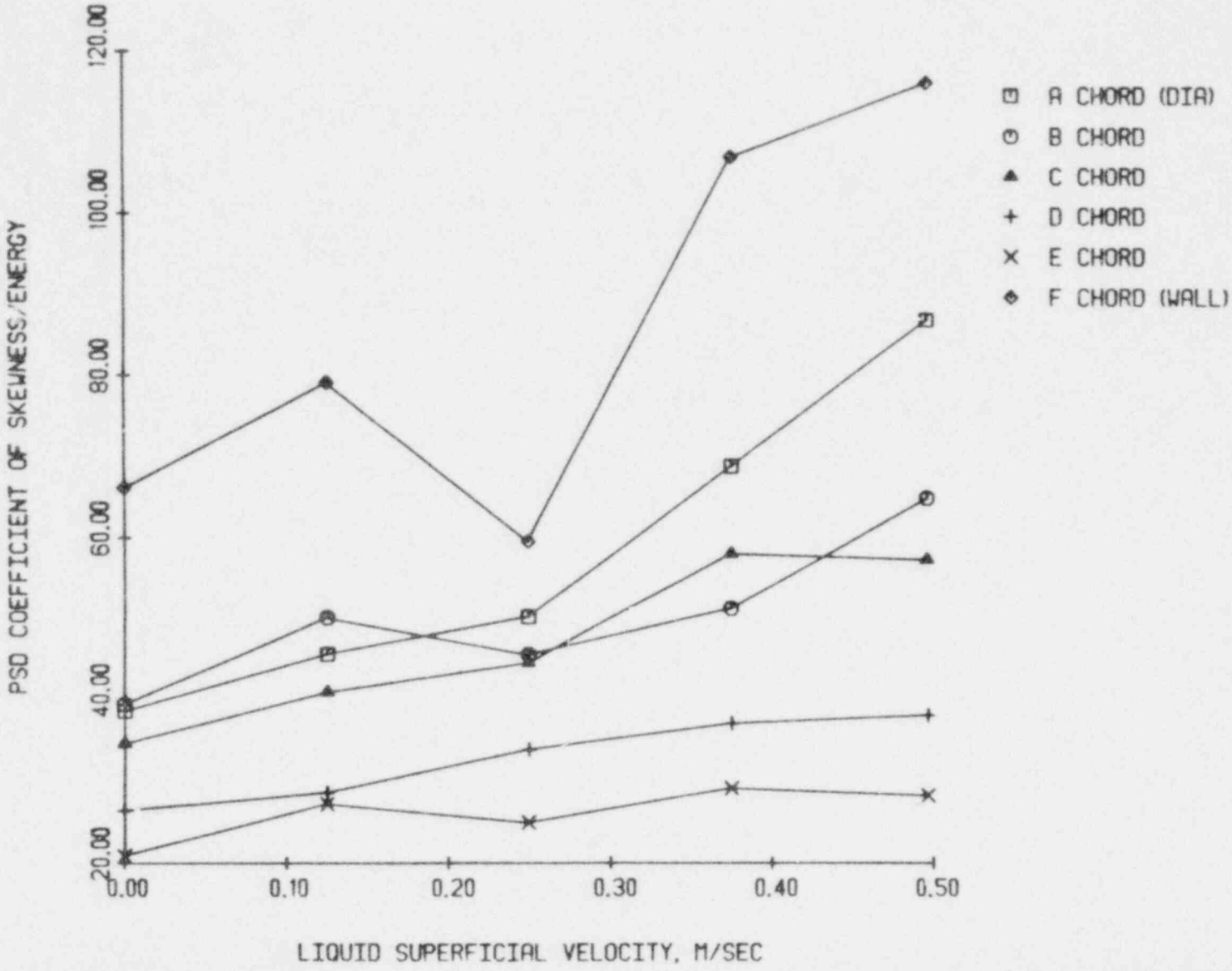

Figure 4.105 The PSD coefficient of skewness/energy vs. superficial liquid velocity at 68 percent area-averaged void fraction

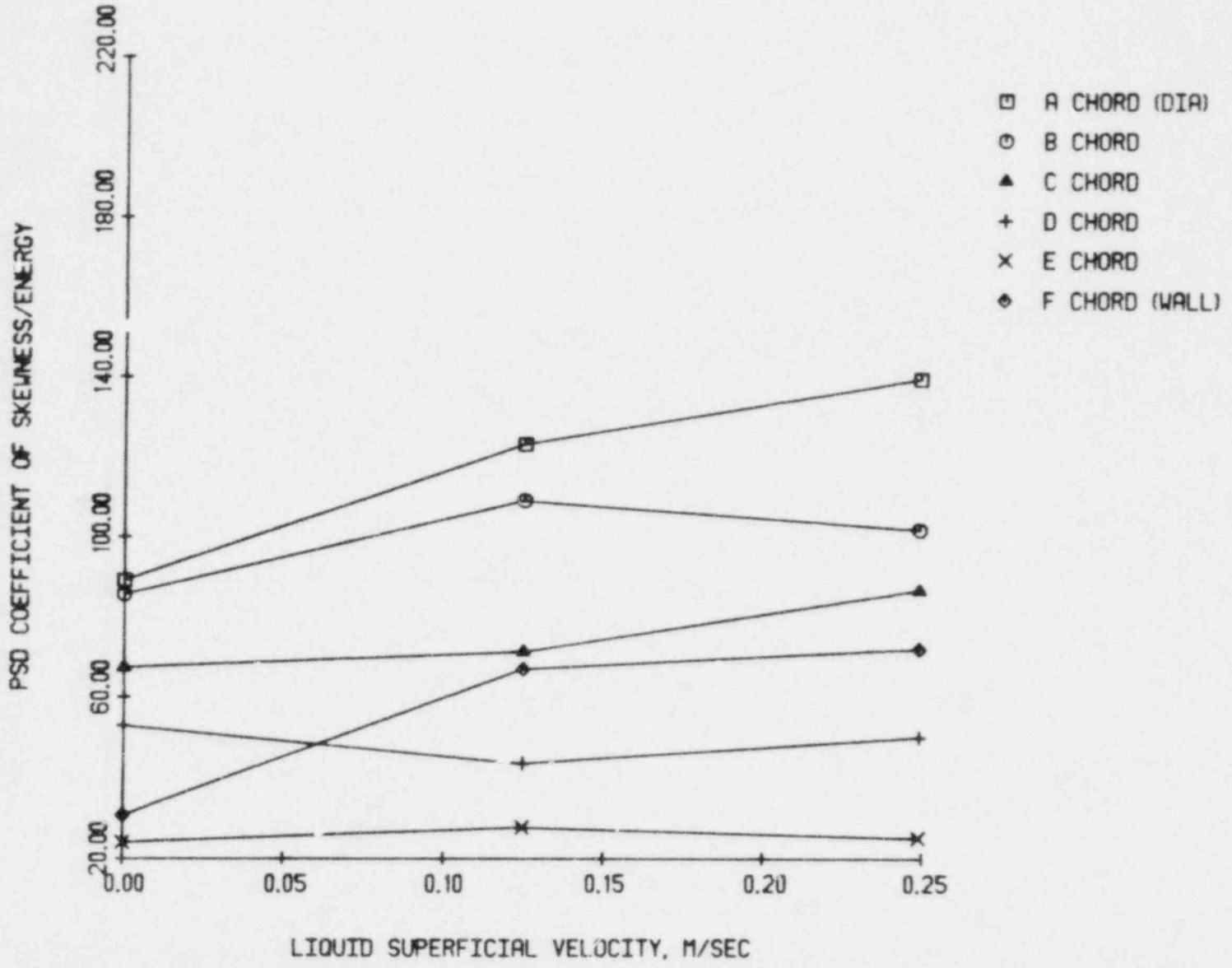

Figure 4.106 The PSD coefficient of skewness/energy vs. superficial liquid velocity at 72 percent area-averaged void fraction

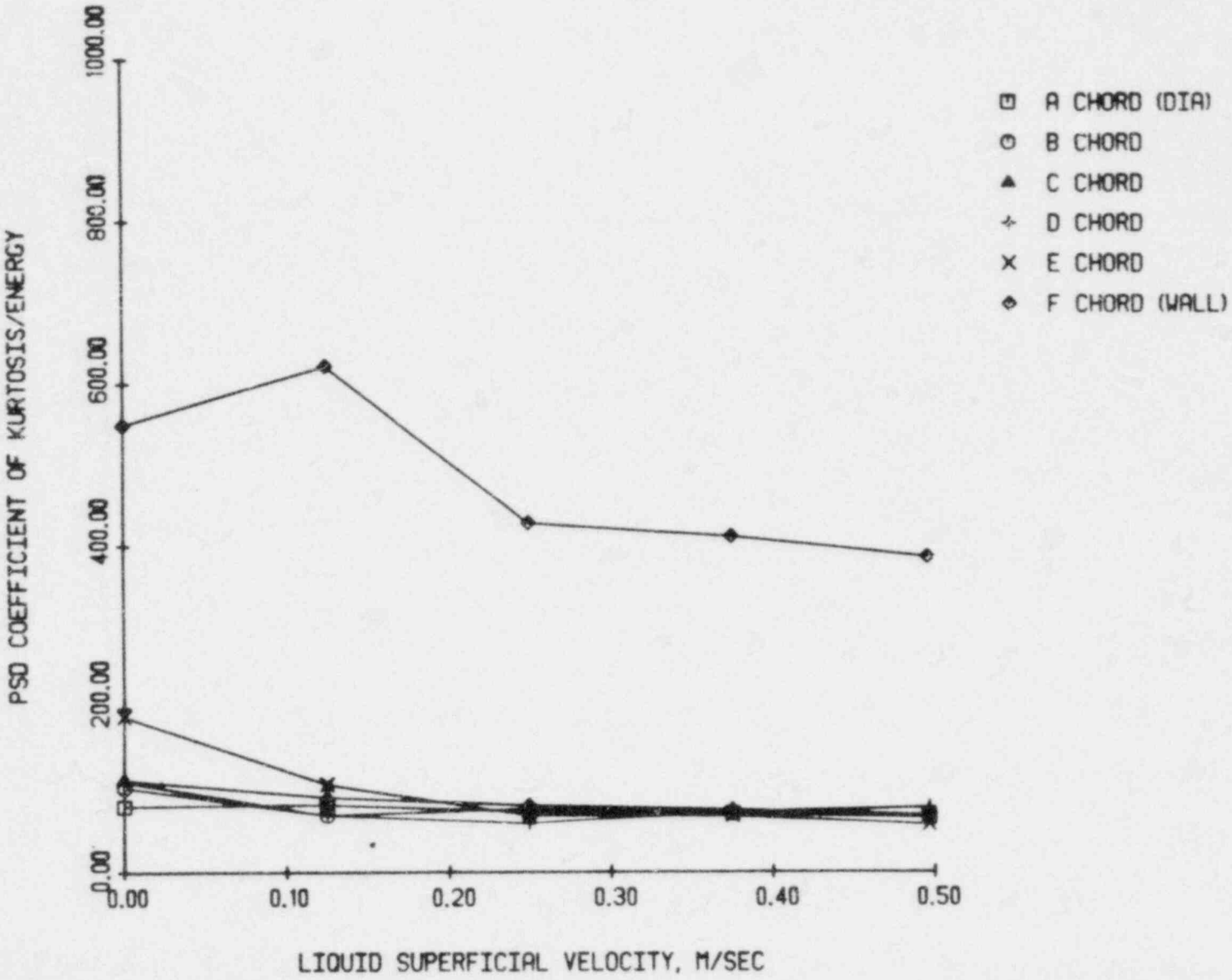

Figure 4.107 The PSD coefficient of kurtosis/energy vs. superficial liquid velocity at 13 percent area-averaged void fraction

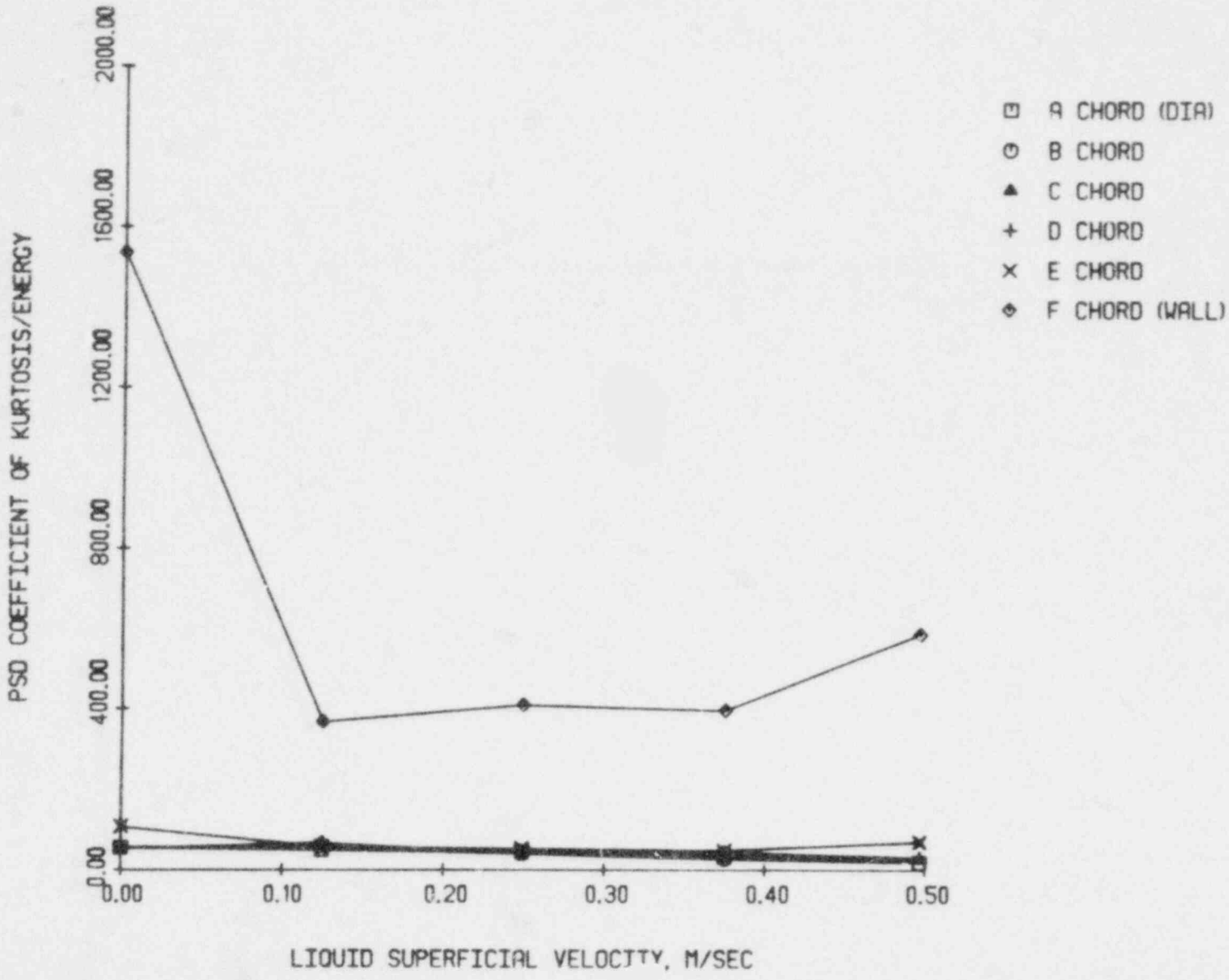

Figure 4.108 The PSD coefficient of kurtosis/energy vs. superficial liquid velocity at 20 percent area-averaged void fraction

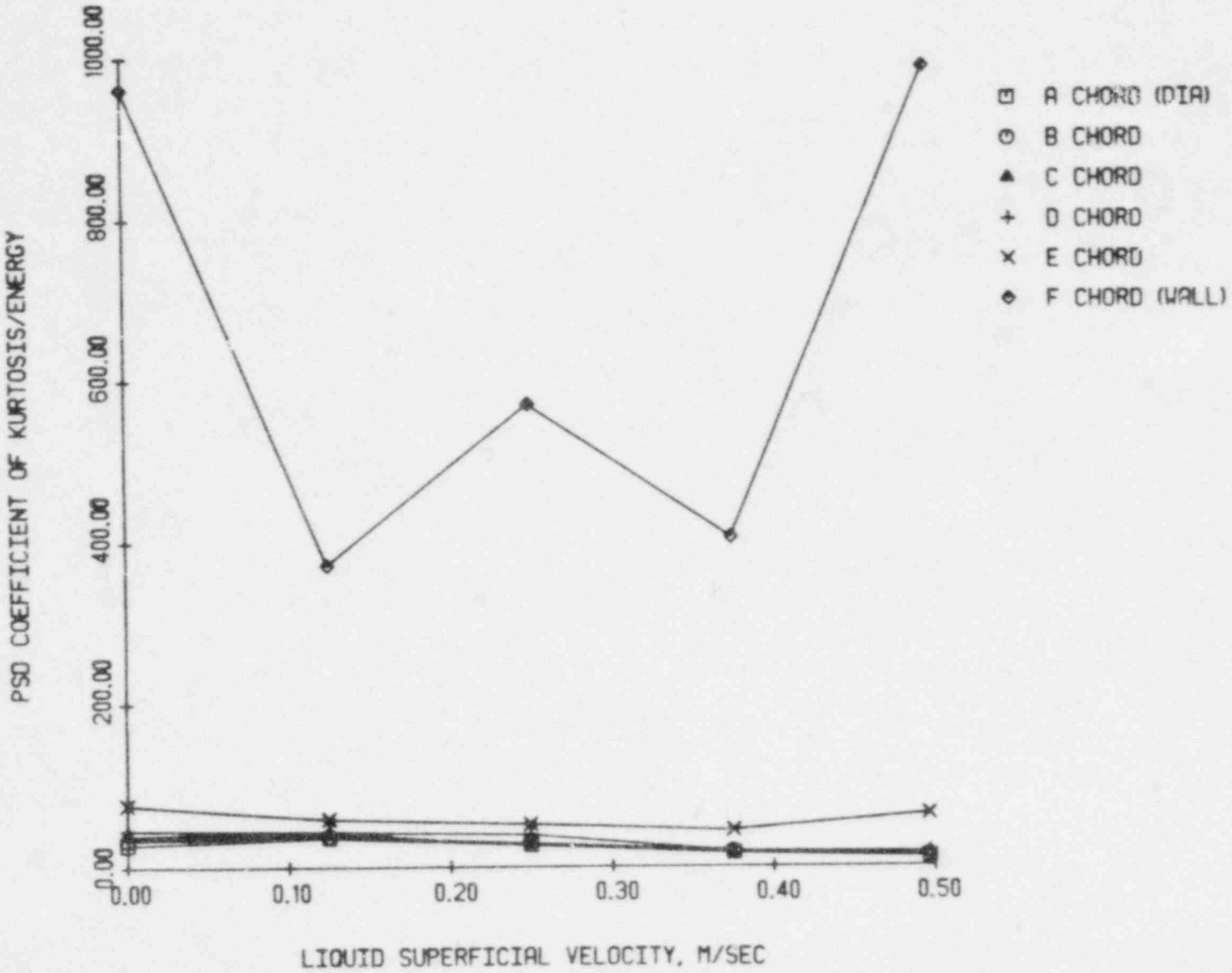

Figure 4.109 The PSD coefficient of kurtosis/energy vs. superficial liquid velocity at 26 percent area-averaged void fraction

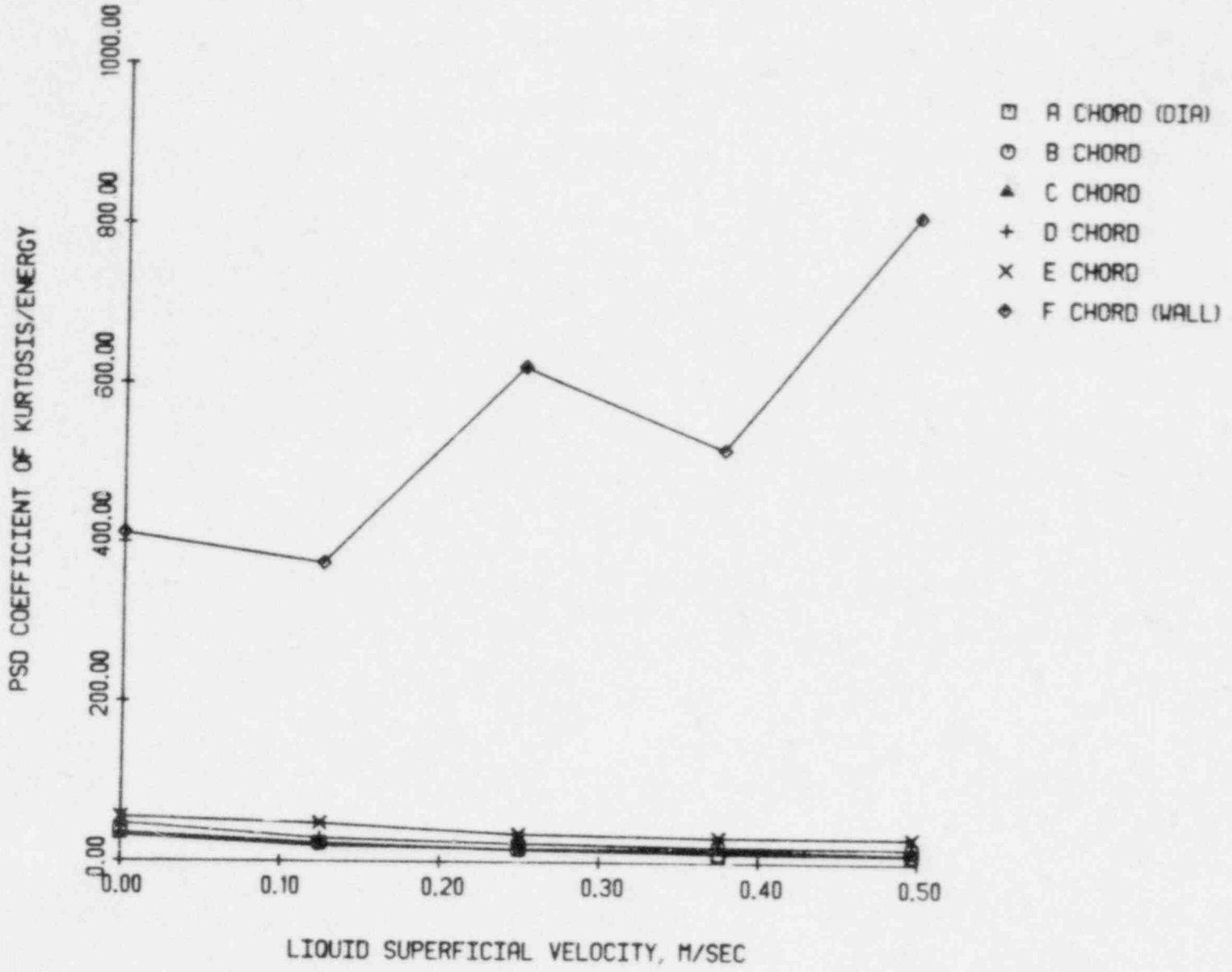

Figure 4.110 The PSD coefficient of kurtosis/energy vs. superficial liquid velocity at 32 percent area-averaged void fraction

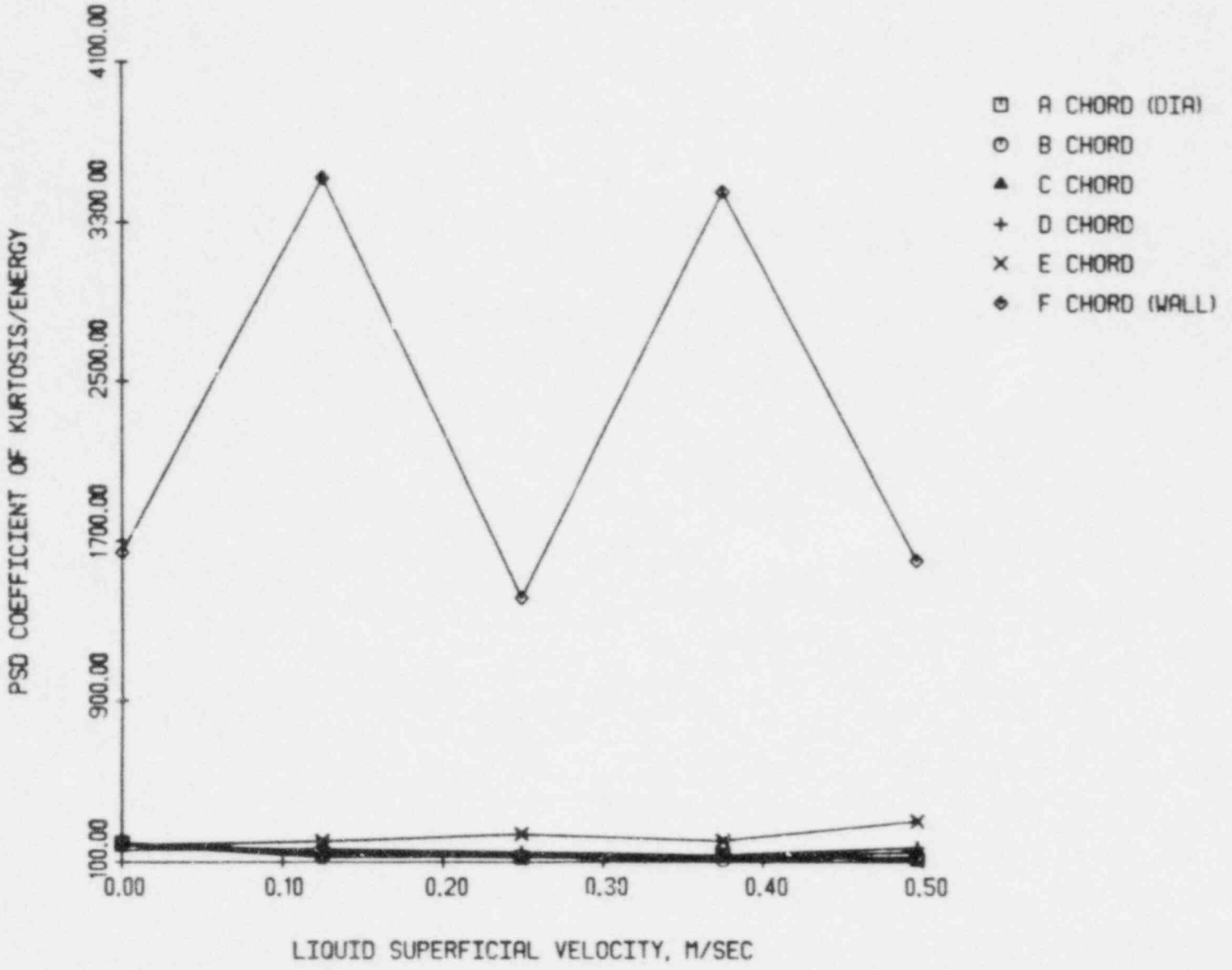

Figure 4.111 The PSD coefficient of kurtosis/energy vs. superficial liquid velocity at 41 percent area-averaged void fraction

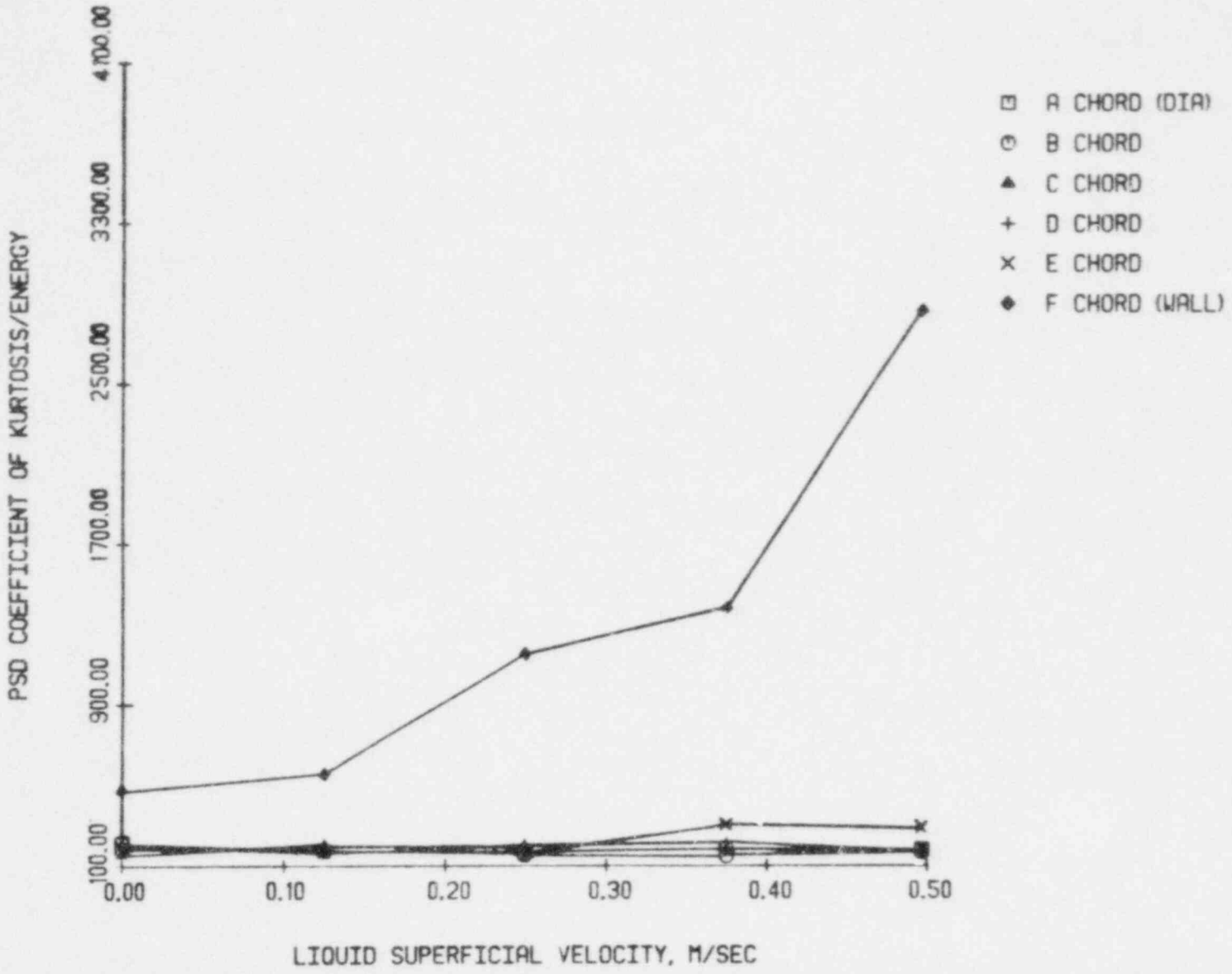

Figure 4.112 The PSD coefficient of kurtosis/energy vs. superficial liquid velocity at 53 percent area-averaged void fraction

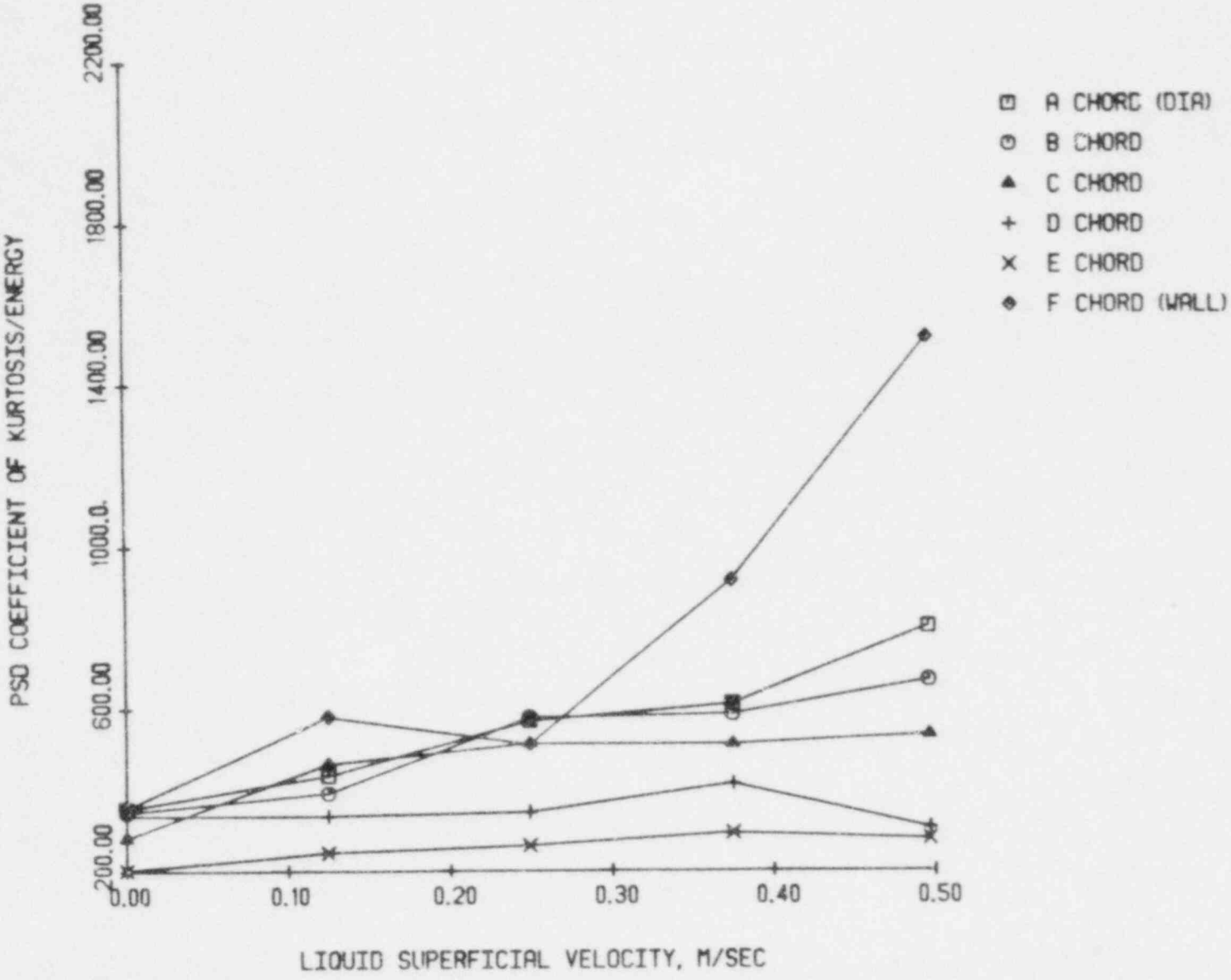

Figure 4.113 The PSD coefficient of kurtosis/energy vs. superficial liquid velocity at 66 percent area-averaged void fraction

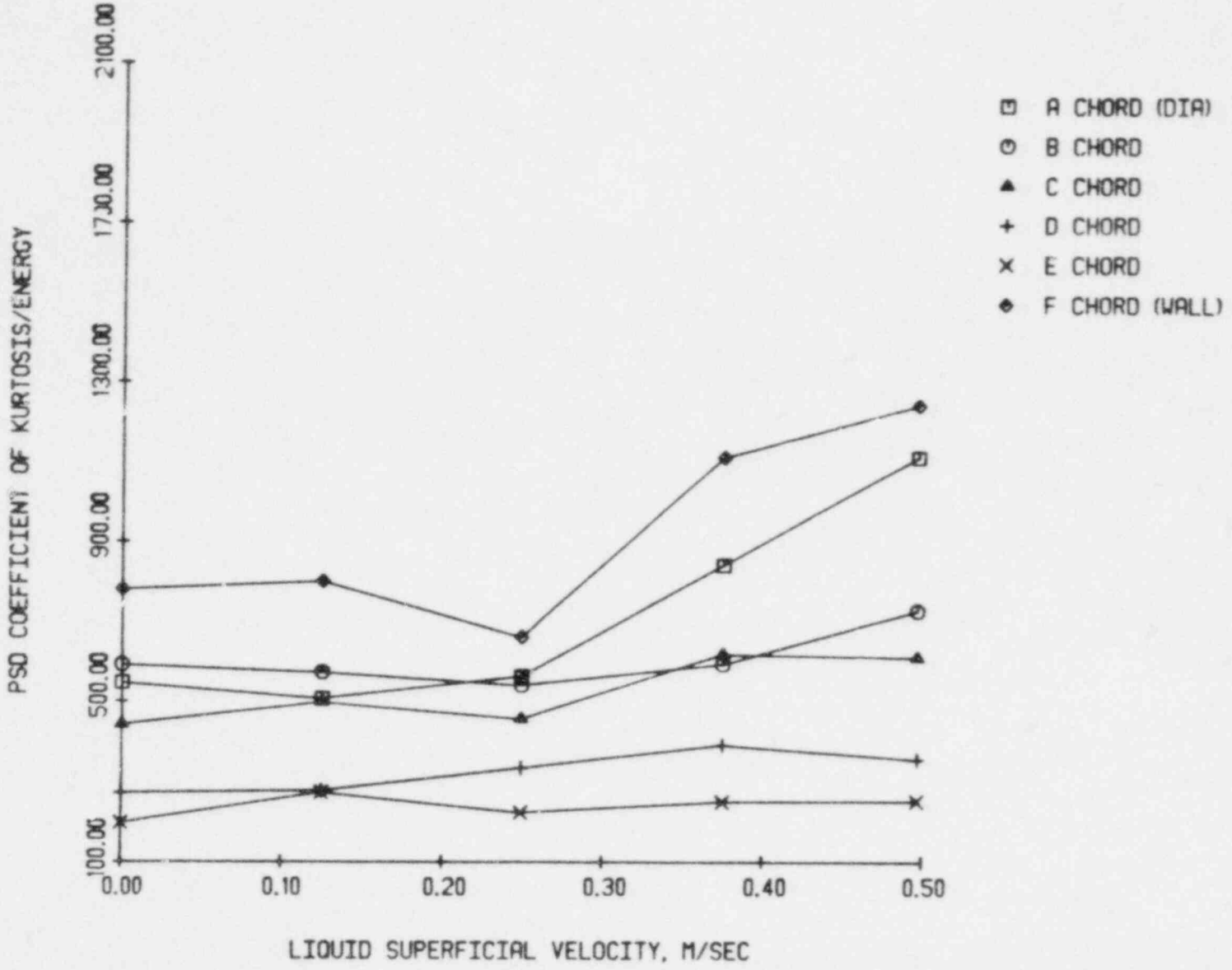

Figure 4.114 The PSD coefficient of kurtosis/energy vs. superficial liquid velocity at 68 percent area-averaged void fraction

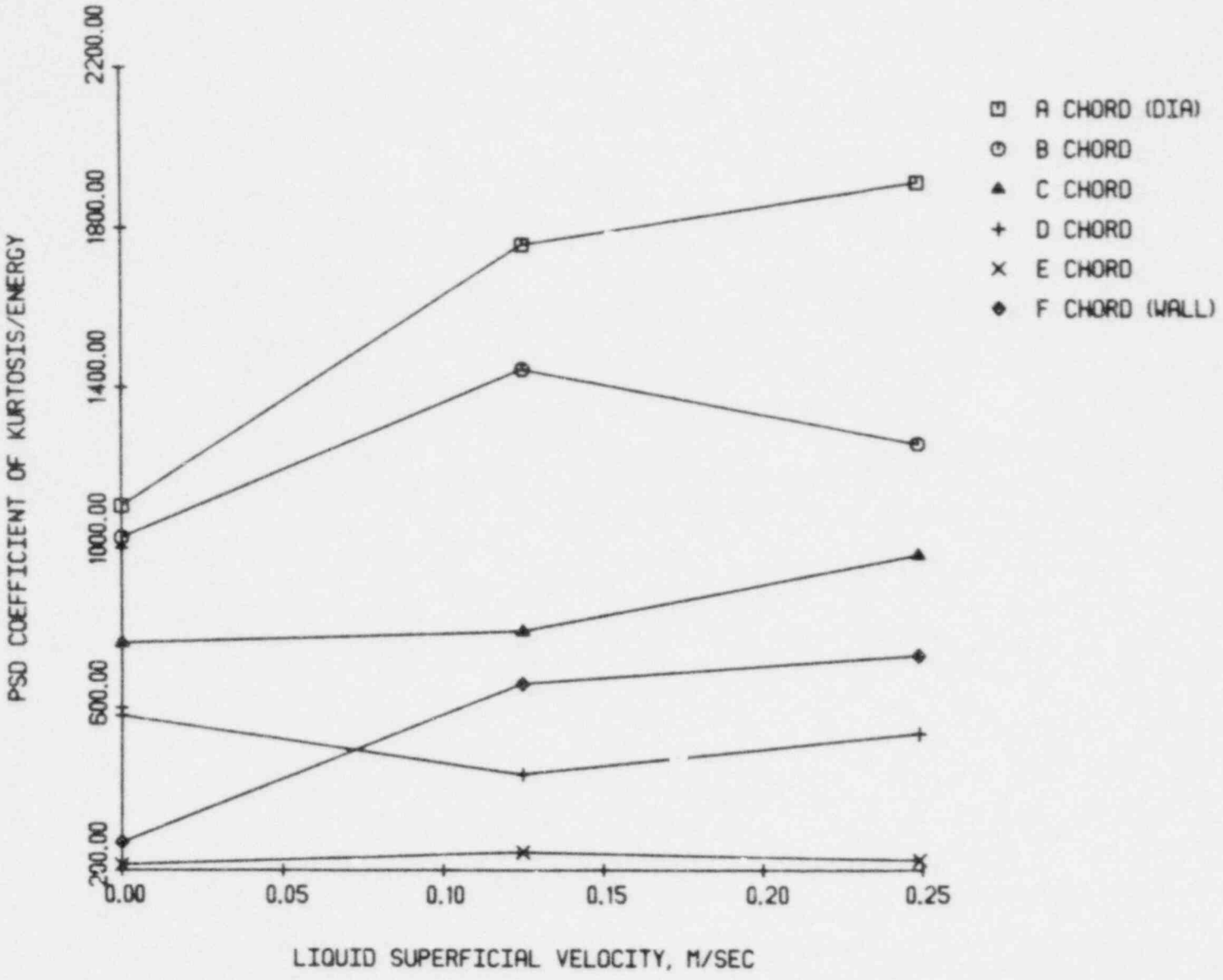

Figure 4.115 The PSD coefficient of kurtosis/energy vs. superficial liquid velocity at 72 percent area-averaged void fraction

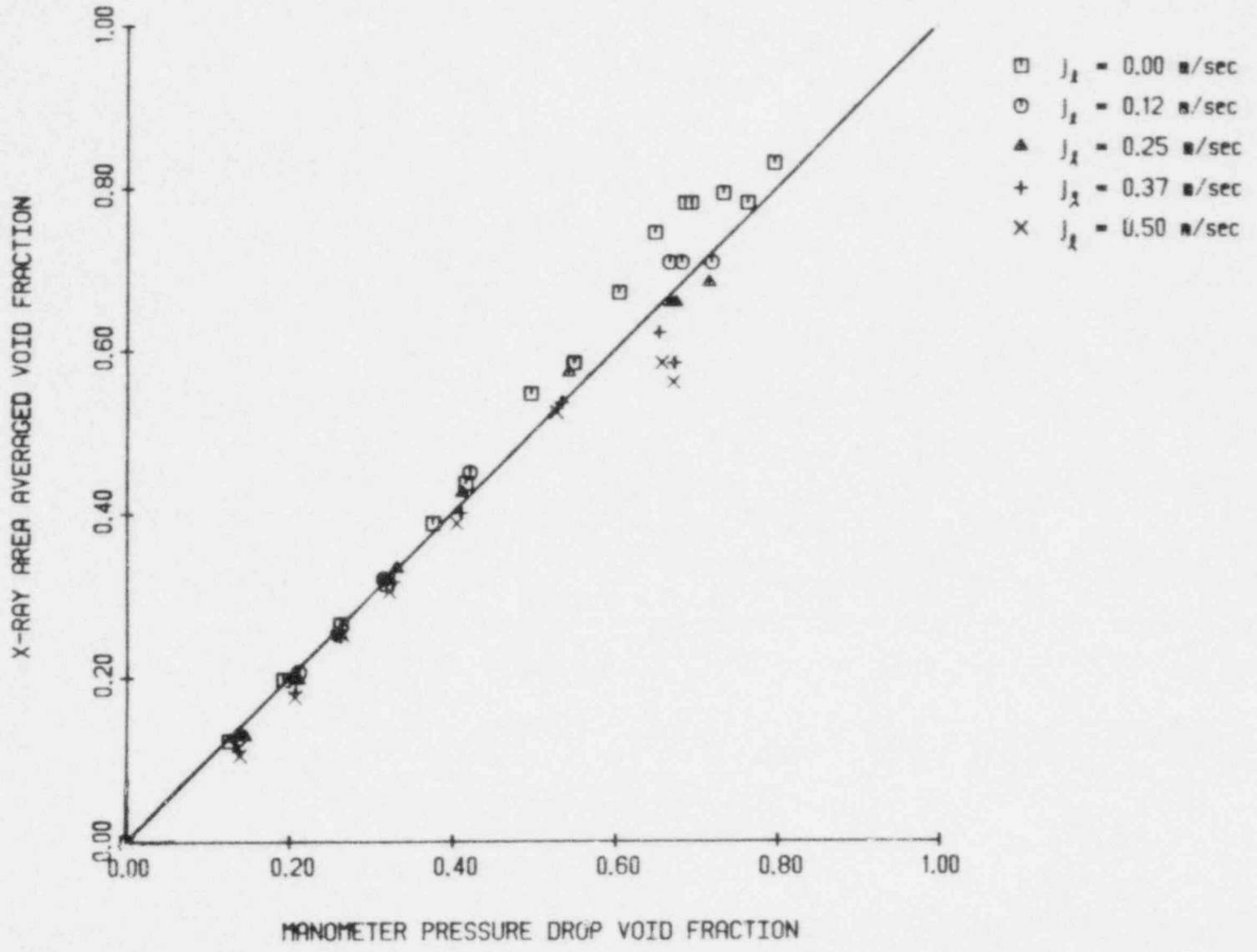

Figure 4.116 X-ray area-averaged vs. manometer pressure drop void fraction

4.4 Comparisons With Other Data

Many other researchers have studied two-phase flow. In particular, Nicklin, et.al. [42] proposed the following correlation for slug flow,

$$\frac{\langle j_g \rangle}{\langle \alpha \rangle} = 1.2\ (\langle j_\ell \rangle + \langle j_g \rangle) + 0.35(gD)^{1/2} \qquad (4.1)$$

where,

$\langle \alpha \rangle$ = cross-sectional average void fraction

$\langle j_\ell \rangle$ = liquid superficial velocity, ft/sec

$\langle j_g \rangle$ = vapor superficial velocity, ft/sec

The data taken by the x-ray system at zero superficial liquid velocity is compared with this correlation in Figure 4.117. Acceptable agreement is observed. Figures 4.118 and 4.119 compare the x-ray data and Nicklin's correlation at liquid superficial velocities of 0.12 and 0.25 m/sec. Data for 0.37 and 0.50 m/sec. liquid superficial velocity is compared to Nicklin's correlation in Figures 4.120 and 4.121. In all cases good agreement is observed, except at the larger voidage, where annular flow existed. A review of Nicklin's work showed that his own data showed a similar disagreement.

Zuber and Findlay [43] have presented a correlation for the vapor velocity and the mixture superficial velocity ($\langle j \rangle$). A plot in the $\langle j_g \rangle / \langle \alpha \rangle$ vs. $\langle j \rangle$ plane produces a straight line with a slope of 'C_o', the void concentration parameter, and a y-intercept of 'V_{gj}', the drift velocity. It has been previously shown [43] that

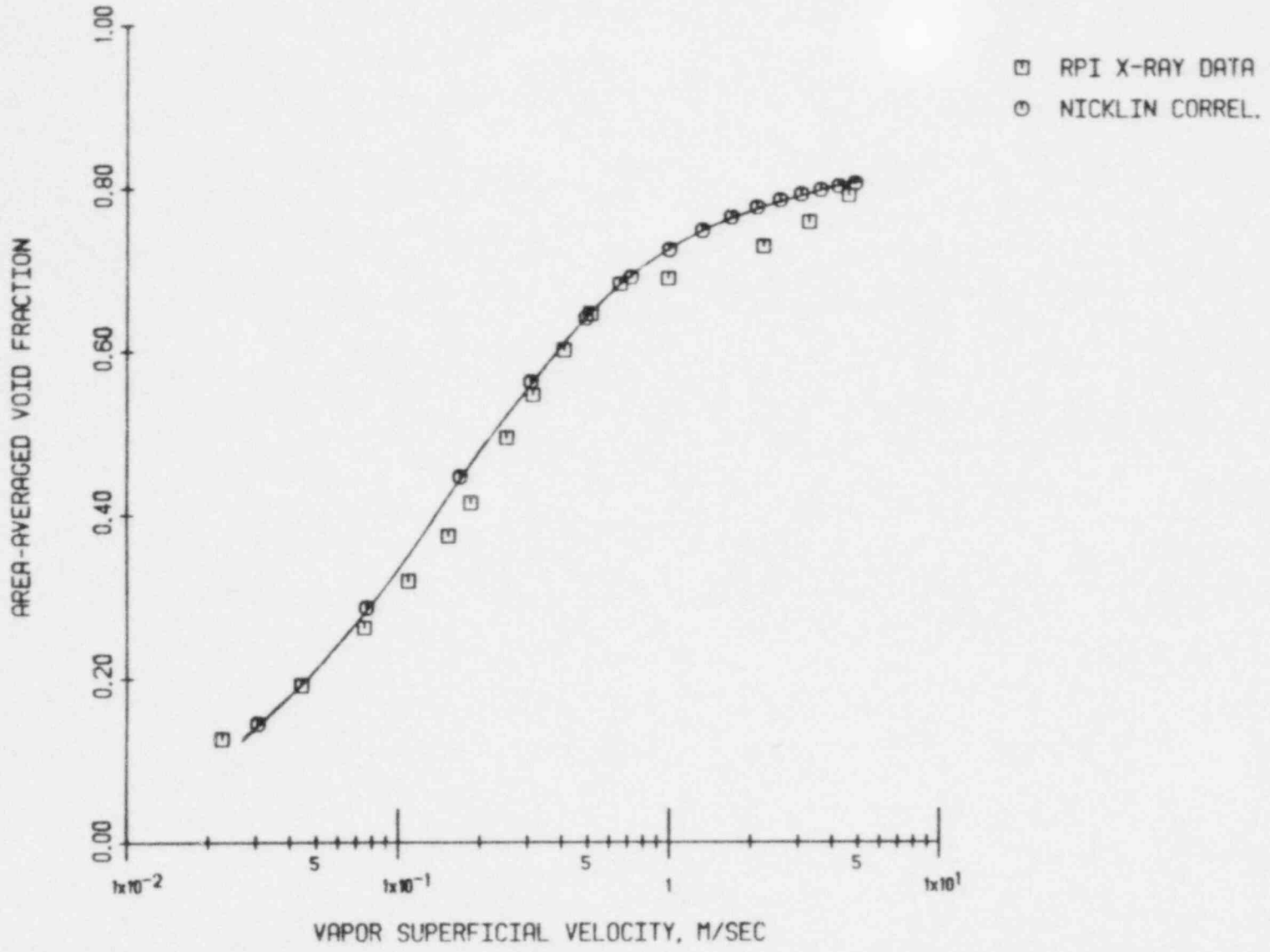

Figure 4.117 A comparison of RPI x-ray data and Nicklin's correlation (1962) for J_ℓ=0.00 m/sec

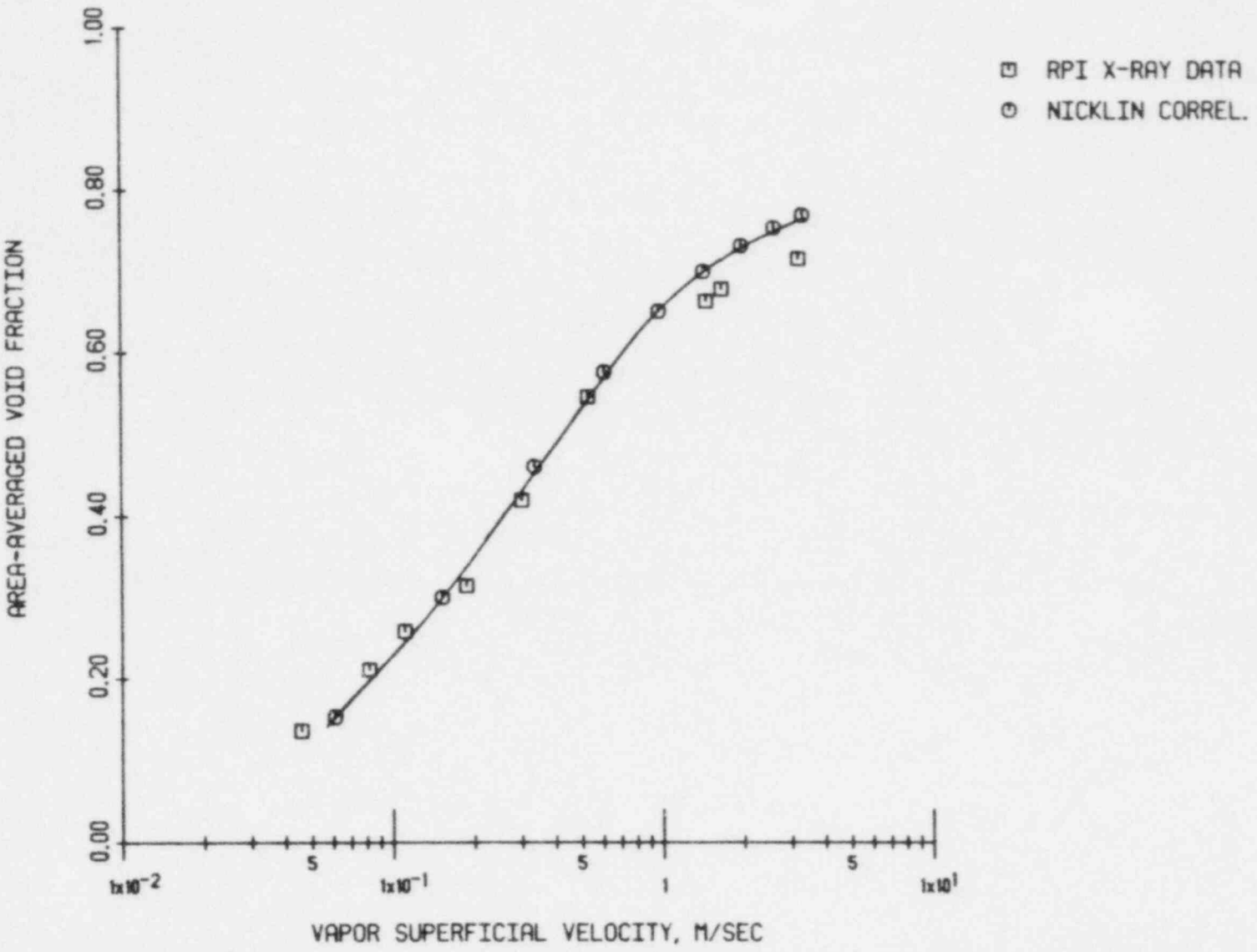

Figure 4.118 A comparison of RPI x-ray data and Nicklin's correlation (1962) for J_ℓ=0.12 m/sec

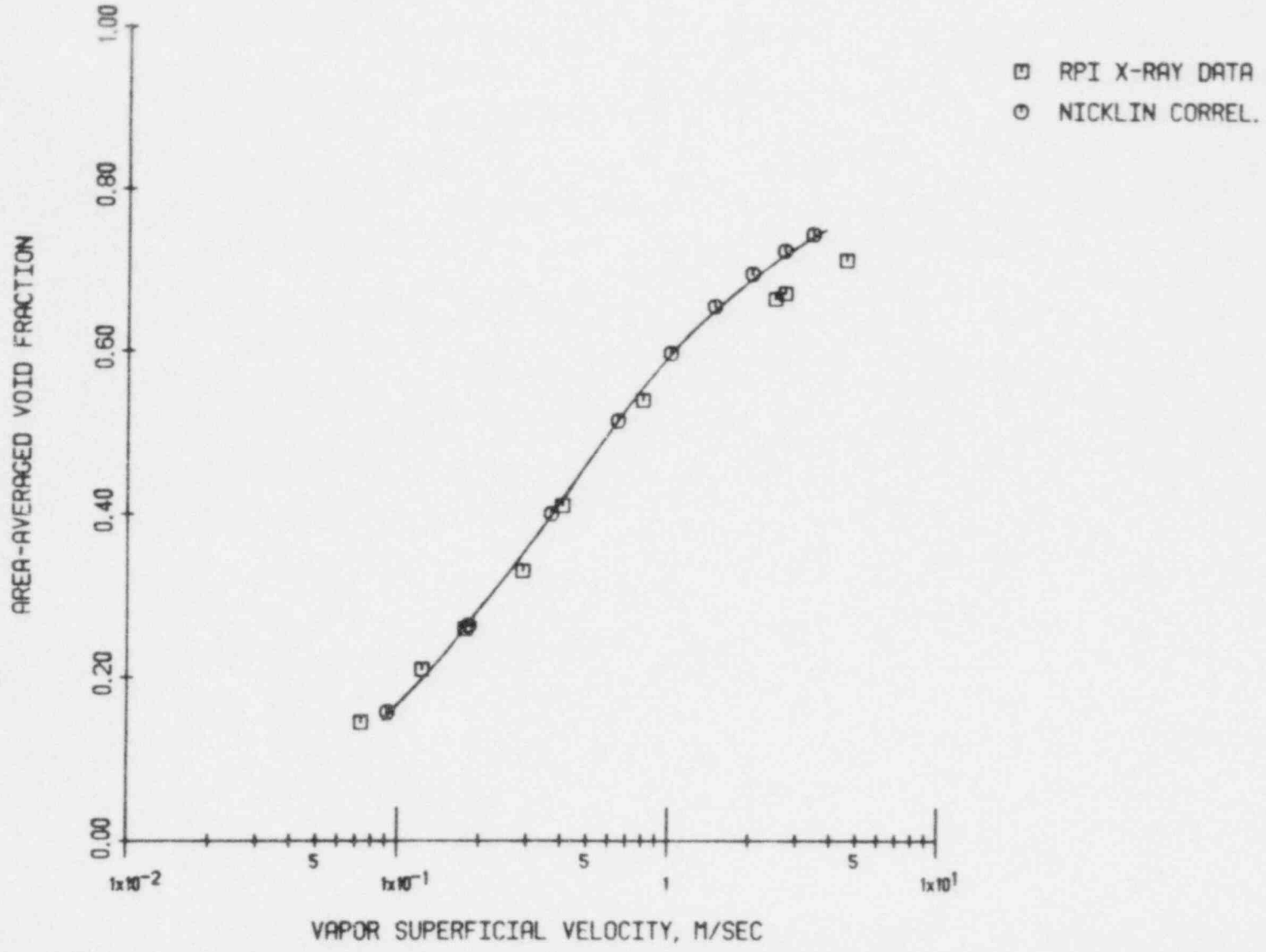

Figure 4.119 A comparison of RPI x-ray data and Nicklin's correlation (1962) for J_g=0.25 m/sec

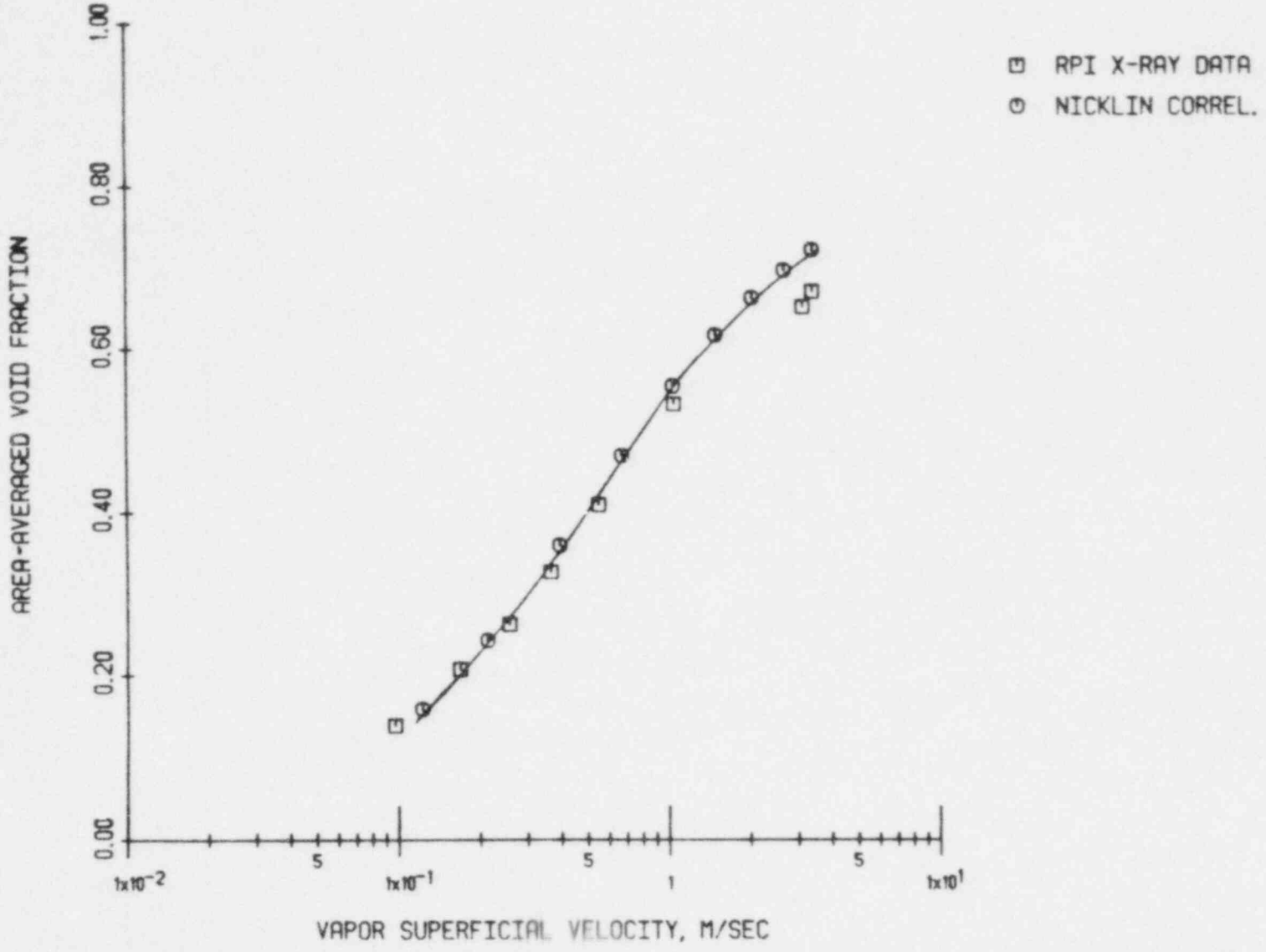

Figure 4.120 A comparison of RPI x-ray data and Nicklin's correlation (1962) for J_g =0.37 m/sec

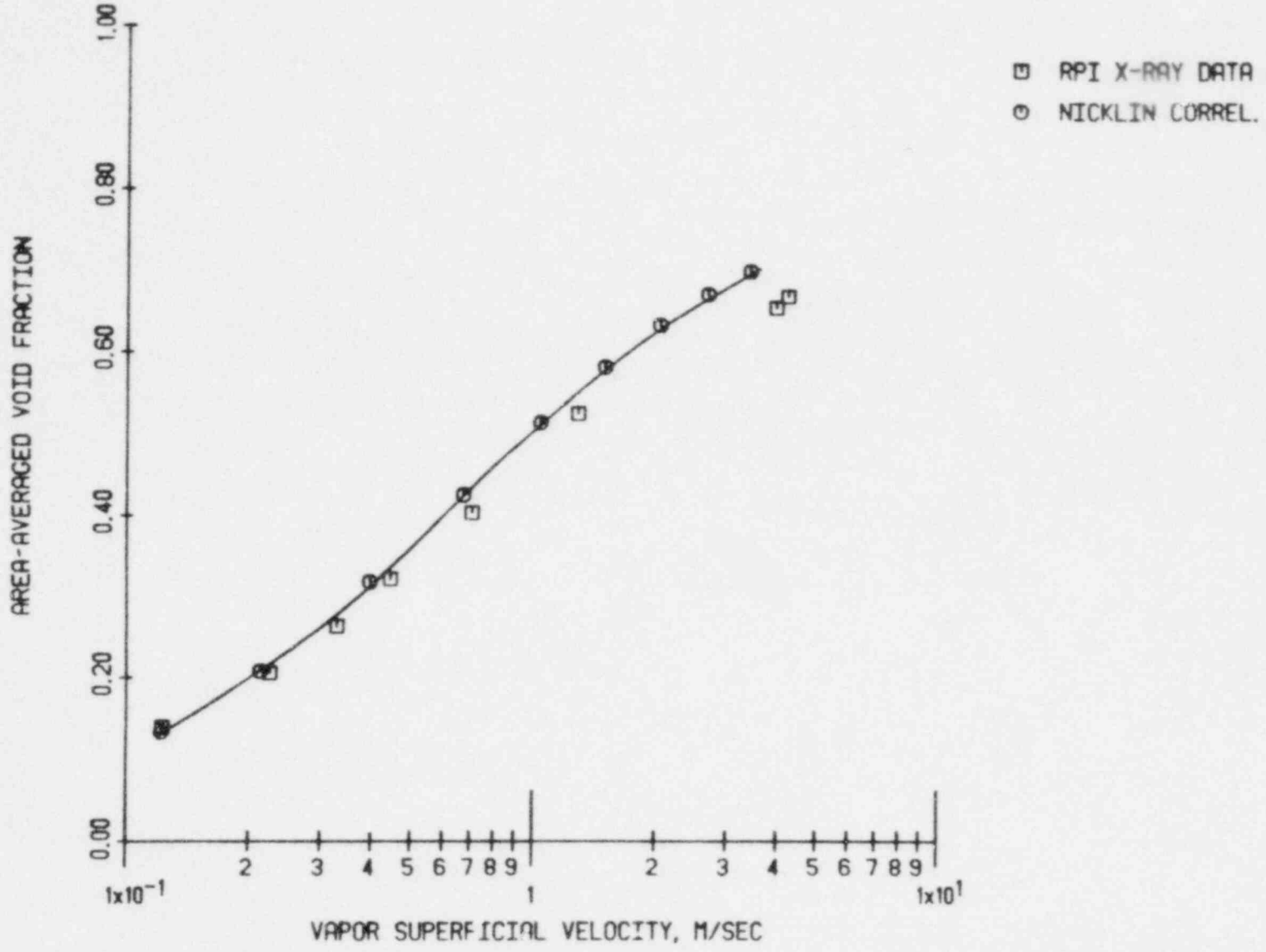

Figure 4.121 A comparison of RPI x-ray data and Nicklin's correlation (1962) for J_ℓ =0.50 m/sec

the 'C_o' parameter can range from 1.0 to 1.6 depending on the fluid system pressure and geometry while "V_{gj}" can vary from 0.3 to 1.2 ft./sec. The flow data and the void fraction data were combined to produce a plot in the "Zuber-Findlay" plane. This graph, shown in Figure 4.122, indicates that our data is correlated by a 'C_o' of 1.29 and a 'V_{gj}' of of 0.49 ft./sec. A least squares fit of the data produces a correlation coefficient of 0.999, (i.e.; near perfect correlation). Obviously, these values are well within the ranges indicated by Zuber and Findlay [43]. Since reasonable agreement with similar previous works was achieved, the x-ray data is believed to be accurate.

4.5 Recommended Flow Regime Indicator

The moments of the PDF and PSD associated with a variety of two-phase conditions were calculated. Even though flow regime information is evident in many of the moments calculated. The variance, or second moment about the mean, of the PDF appears to be the best flow regime indicator. For the pipe flow data analyzed, a variance greater than 0.04 indicated slug flow. Smaller variances indicate a bubbly or annular flow regime, depending on the mean void fraction. This flow regime indicator is not strongly dependent on the superficial liquid velocity, and is fairly independent of chordal measurement position, thus it appears to be a good choice.

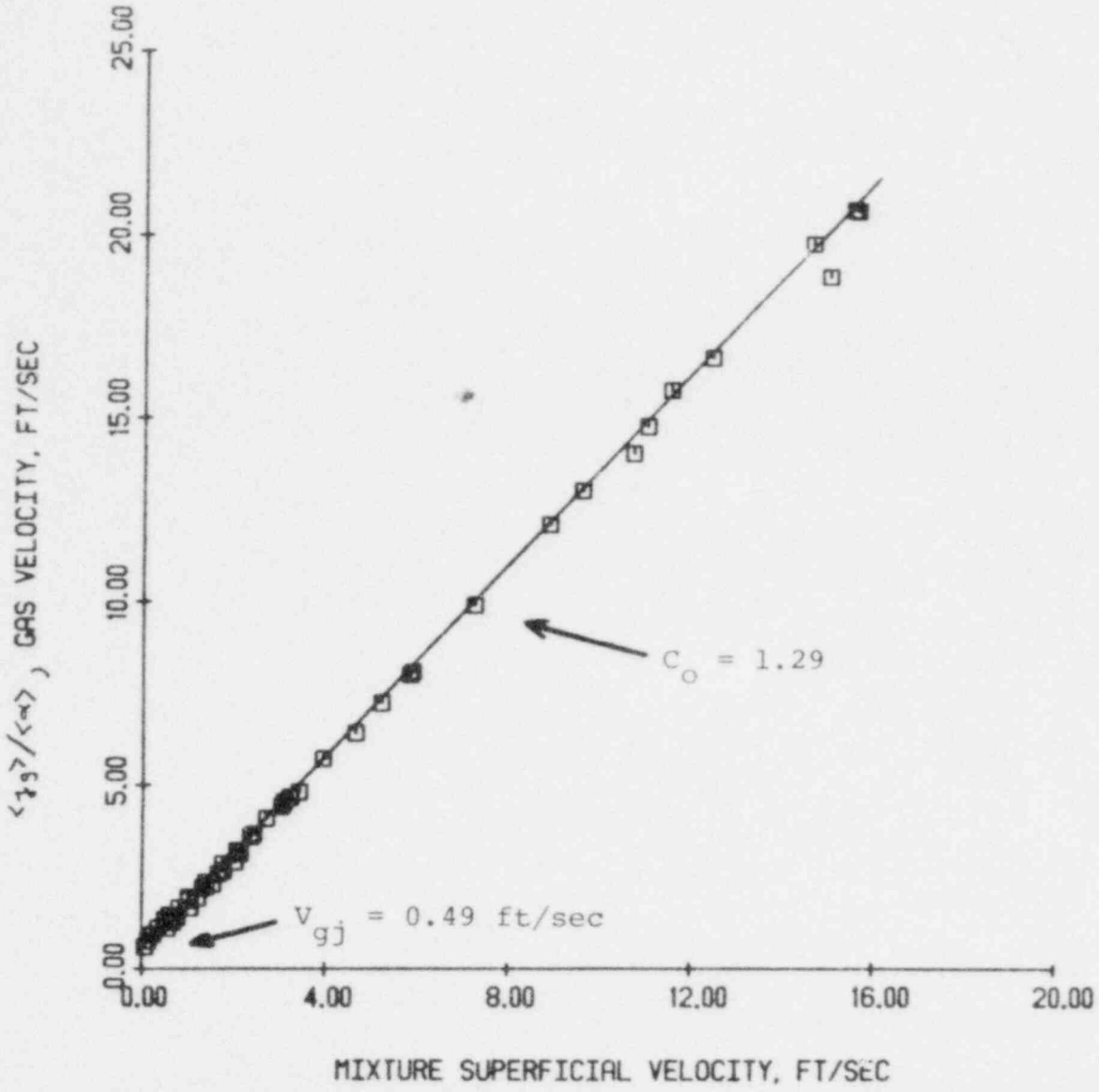

Figure 4.122 The RPI X-ray data in the Zuber-Findlay (1965) plane

The flow regime map determined using this criterion is shown in Figure 4.123. Comparing this figure with the flow regime boundaries indicated in Figure 4.2 (developed from direct visual observations), we see that the 0.04 variance criterion proposed does a good job.

This flow regime map disagrees somewhat with other maps. Figure 4.124 compares the results shown in Figure 4.123 with the map suggested by Taitel and Dukler [22]. It can be seen that the bubbly-slug (i.e. churn) transition boundary is in good agreement however the slug-annular transition is off significantly. This may be fortuitous since their flow regime criteria for the bubbly-slug flow regime transition is based on a constant area-averaged void fraction, a trend which was not observed in this study. Moreover, their slug-annular transition criterion of 15 m/sec is not supported by our data.

As shown in Figure 4.125, our 0.04 variance flow regime indicator produces reasonable agreement with Griffith and Wallis [21] map for the slug-annular transition. It also agrees with the Griffith and Wallis flow regime map for data acquired at zero liquid flow for the bubbly-slug transition. However a significant discrepency exists at the bubbly-slug transition for non-zero liquid flow.

Duns and Ros [44] also proposed a flow regime map. The variance criterion proposed herein disagrees with this map as shown in Figure 4.126. Duns and Ros predict the existence of bubbly flow when slug flow was visually observed and indicated by the variance criterion. Likewise,

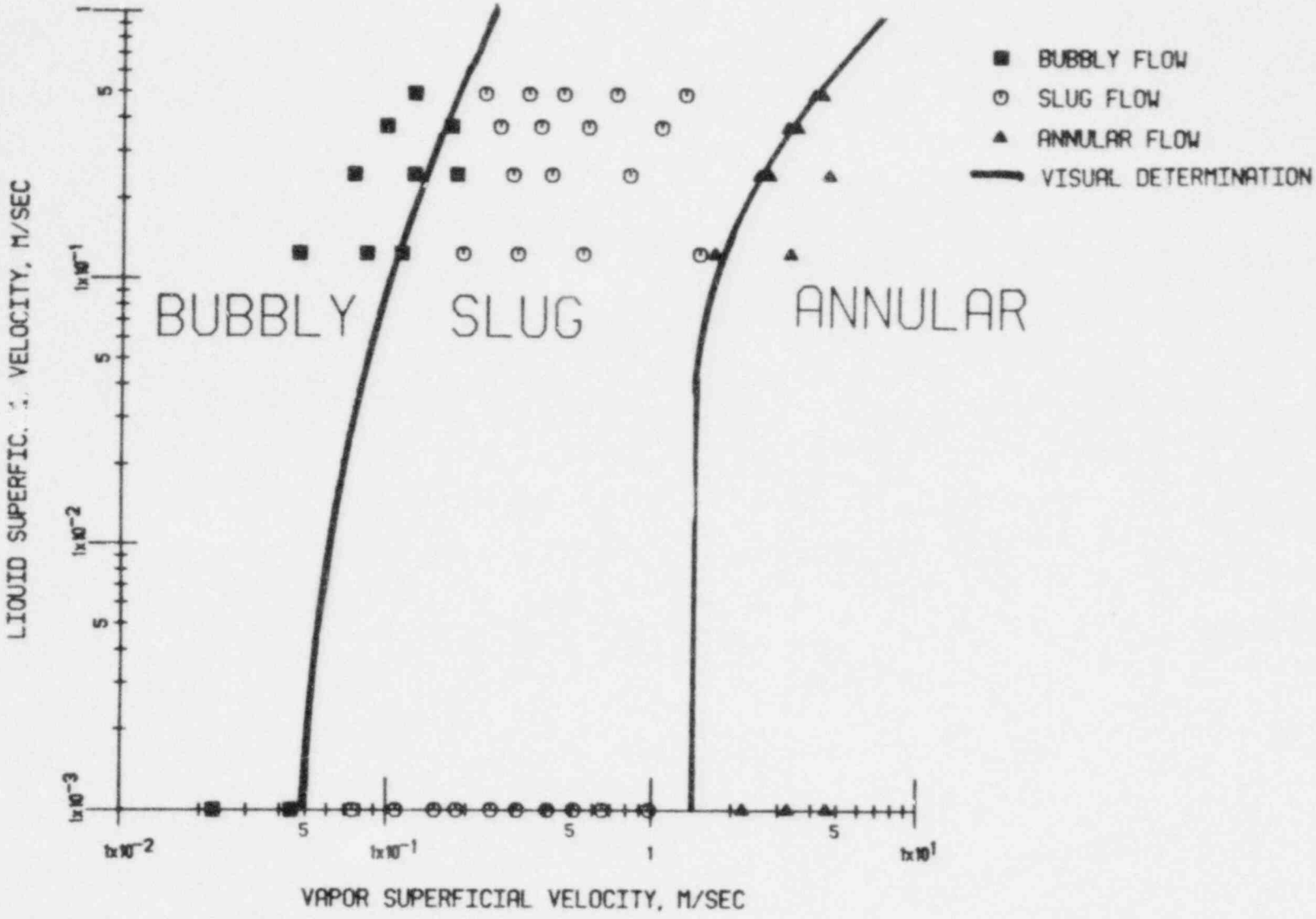

Figure 4.123 A flow regime map based on a PDF variance of 0.04

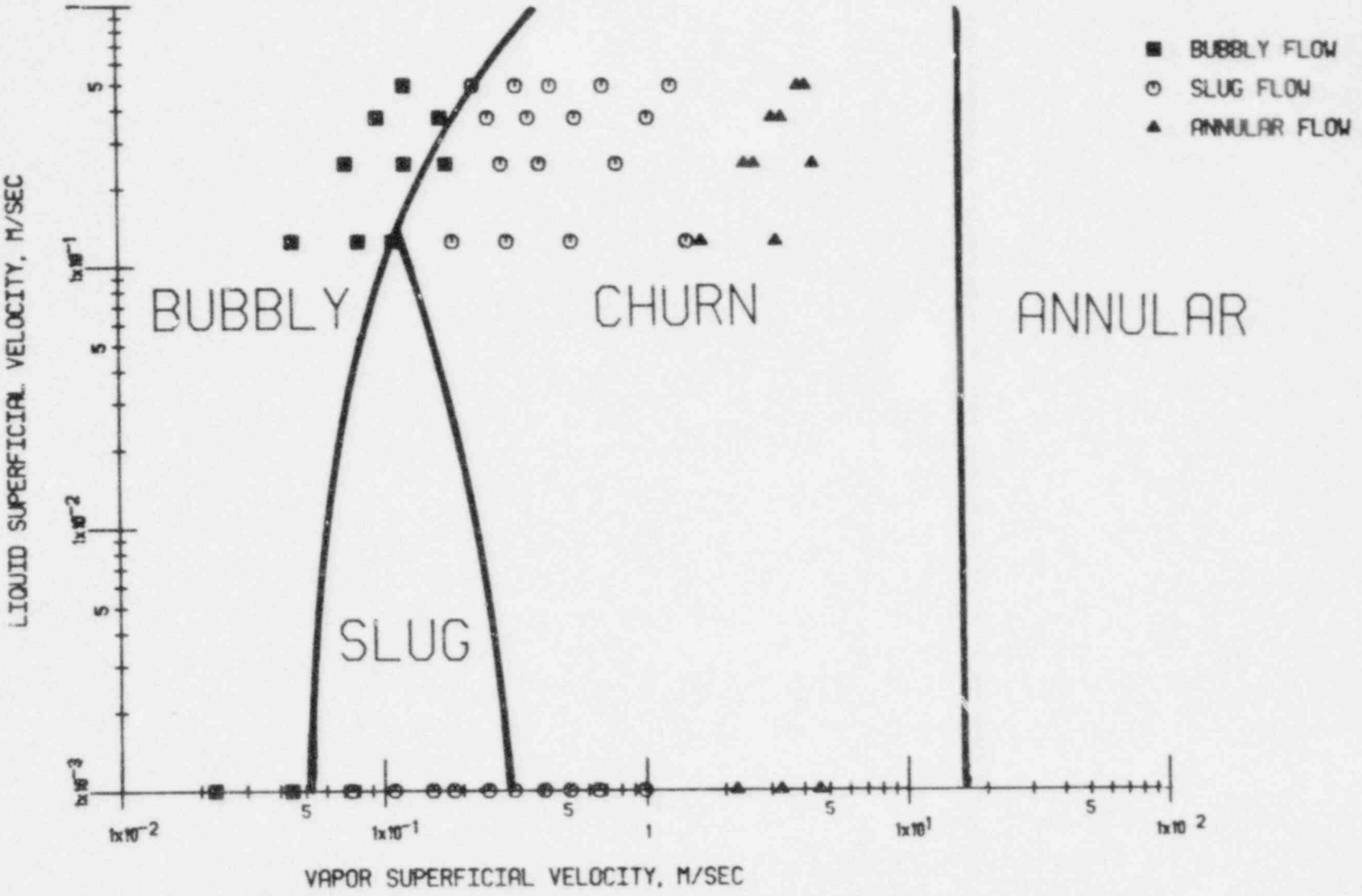

Figure 4.124 A comparison of the RPI X-Ray data and Taitel and Dukler (1976) correlations

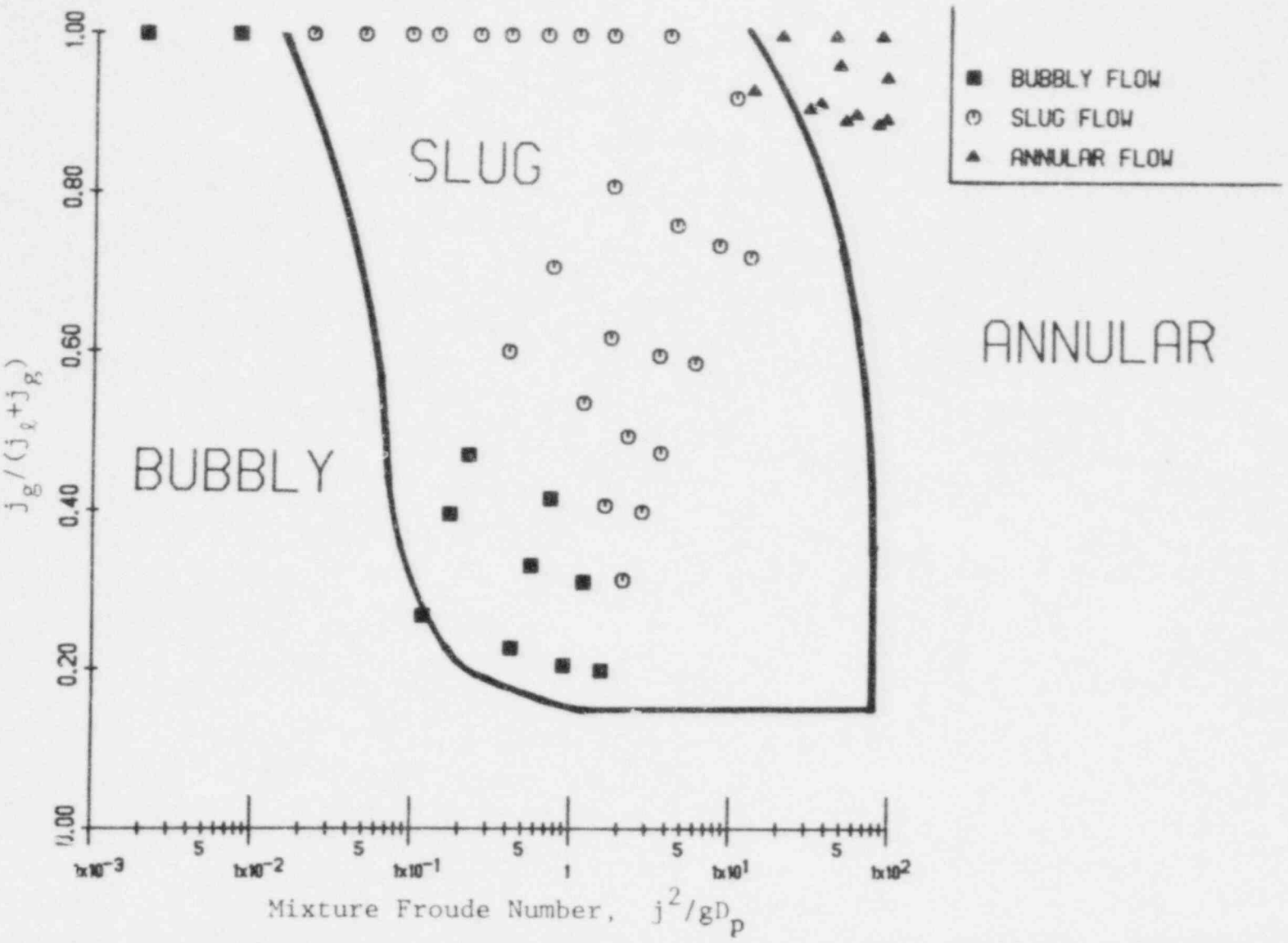

Figure 4.125 A plot of the RPI X-Ray data on the coordinates suggested by Griffith and Wallis (1961)

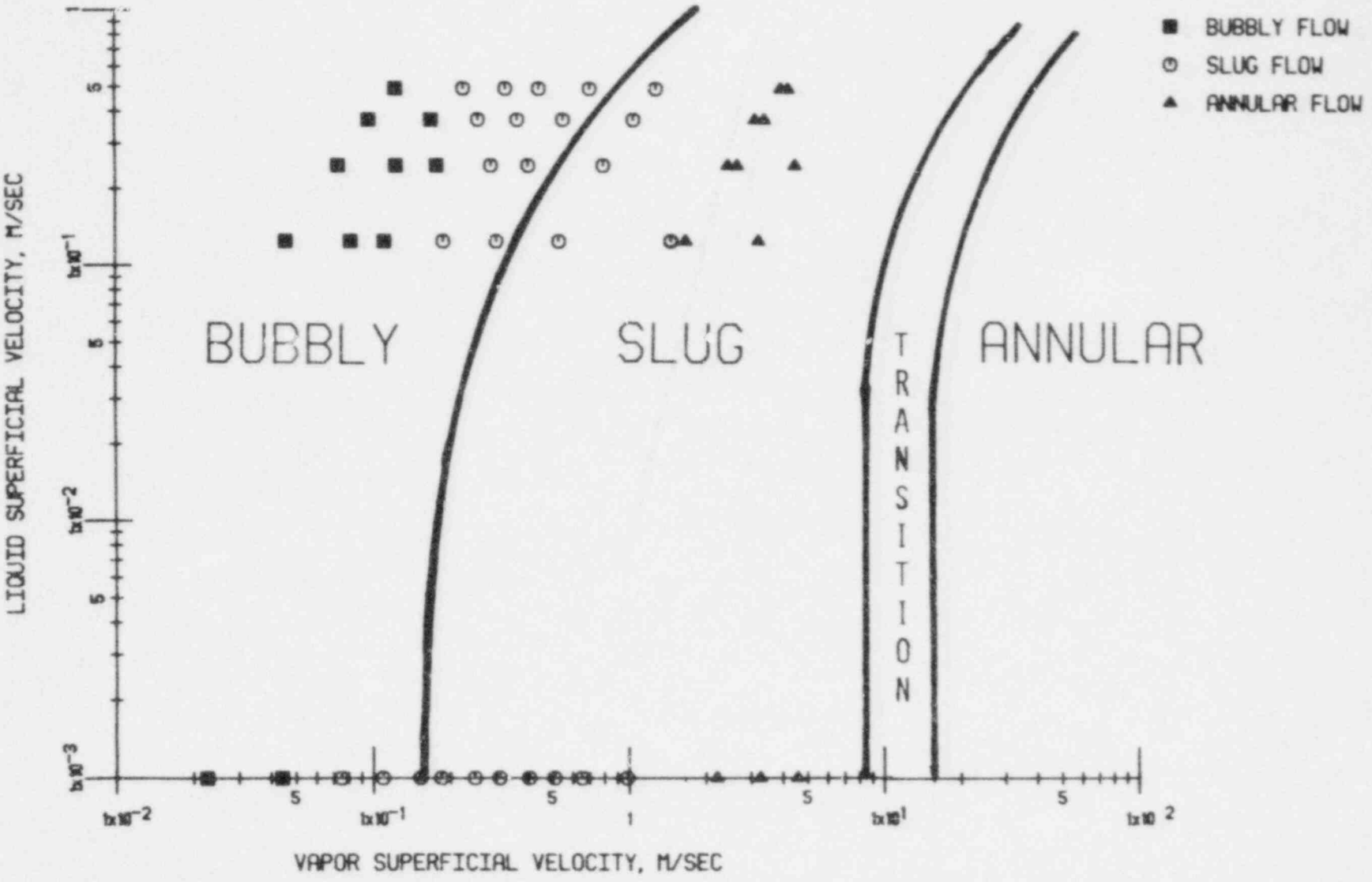

Figure 4.126 A comparison of the RPI X-Ray data and the flow regime map proposed by Duns and Ros (1963)

Duns and Ros predict slug flow when annular flow was observed and predicted by the variance criterion.

The map proposed by Govier and Aziz [45] is better but still differs somewhat from the variance criterion prediction at the bubbly-slug transition. As shown in Figure 4.127, the slug-annular transition predicted by the variance criterion is in reasonable agreement with the slug-froth transition shown by the Govier and Aziz flow regime map. It should be noted that the maps suggested by earlier researchers [21,22,44,45] do not completely agree amongst themselves, thus it is no surprise that our data does not agree with all of them. Indeed, this disagreement is a reflection of the subjective nature of previous investigators' flow regime maps, and clearly indicates the need for an objective criterion.

The physical characteristics of the flow regime are readily associated with variance. Bubbly flow has a relatively uniform void distribution in time, thus a small variance. In contrast, slug flow contains alternating regions of large and small void fraction, thus producing a relatively large variance. Annular flow, like bubbly flow, has a relatively uniform void distribution except near the wall, consequently a small variance is produced.

Some of the other moments of the PDF provide flow regime information, while others do not. However, for all other moments there were some problems associated with interpretating flow regime transition. The second raw

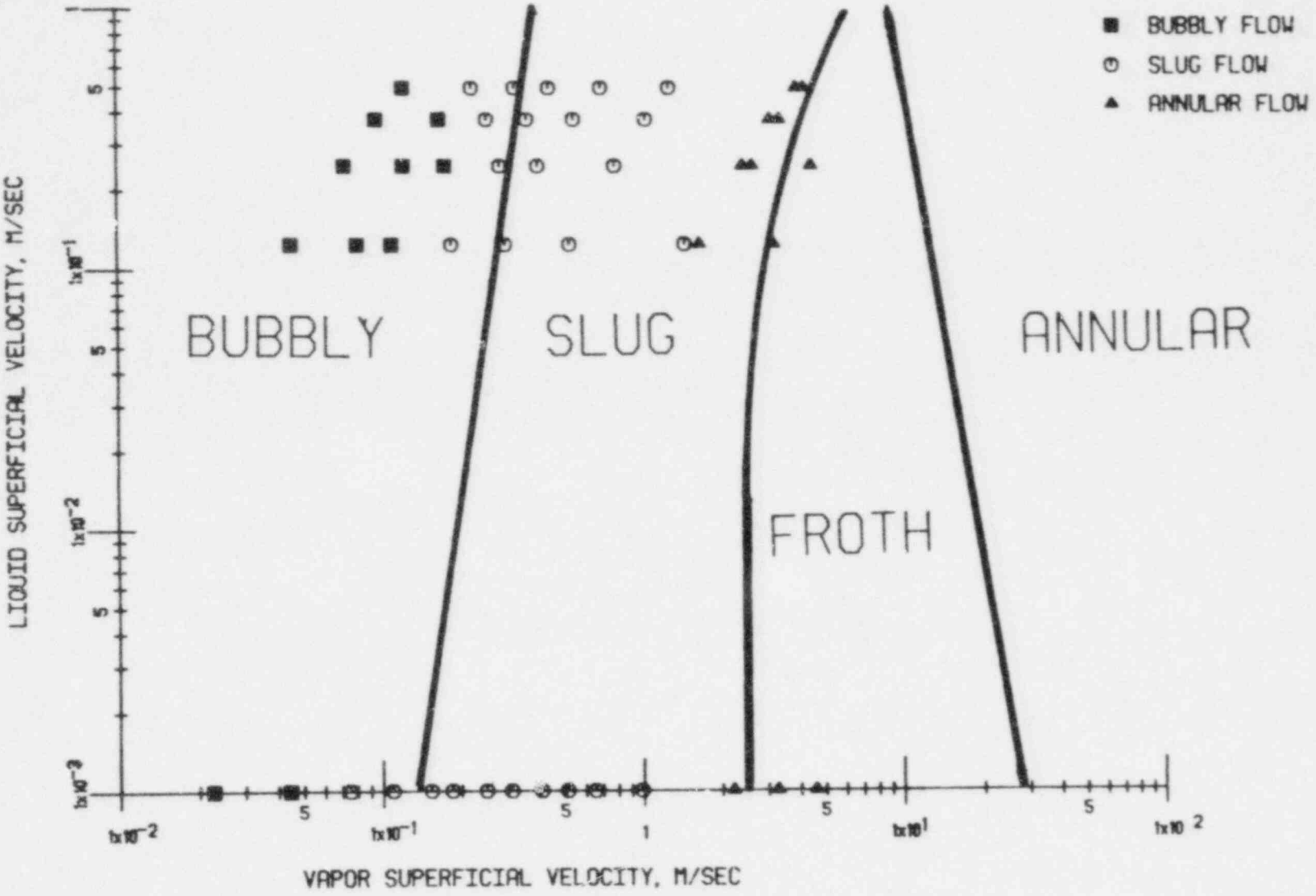

Figure 4.127 A comparison of the RPI X-Ray data and the flow regime map proposed by Govier and Aziz (1972)

moment, or second moment about the origin, does not exhibit any radical change with changing flow regime. Skewness, the third moment, has a trend similar to the variance, however, two phenomena are competing in the skewness resulting in an unclear indication of flow regime transition. The fourth moment, kurtosis, is relatively flat in the bubbly-slug transition region. In the slug-annular transition zone, however, the kurtosis does have possibilities. Unfortunately, at the larger void fractions this moment is very dependent on the chordal position of measurement and thus does not provide a good flow regime indicator.

All moments associated with the PSD exhibit a strong dependence on superficial liquid velocity. This characteristic is very undersirable because any correlation would require knowledge of the liquid superficial velocity. Void fraction measurements are sufficiently difficult, the requirement of a simultaneous liquid velocity measurement renders the use of PSD moments impractical. Moreover, only the variance of the PSD has possibilities for a flow regime indicator. The skewness and kurtosis are essentially independent of the flow regime. As a result, the moments of the PSD are not considered to be as valuable as the variance of the PDF for flow regime identification.

It should be stressed that our data base is limited to low pressure air/water flow in circular conduits, and thus the generality of using a constant PDF variance (i.e. 0.04) as a flow regime transition criterion needs

further verification. Nevertheless, based on what we have seen to date it appears to be a very promising criterion.

4.6 Error Analysis

Two types of errors are normally associated with void fraction measurements; static and dynamic. Static error is due to the geometry and count statistics associated with the measurement. Dynamic error may be caused by improper averaging of the phenomena under study.

4.6.1 Static Error

The static error may be calculated from geometric and counting statistics associated with the x-ray system. Equation 3.51 can be rearranged to yield the relative error.

$$\left(\frac{\Delta\alpha}{\alpha}\right)^2 = \frac{4\left(\frac{R_{SD}}{R_{ST}}\right)^2 (1-\alpha+\alpha^2) e^{[2\mu_w T+\mu_\ell C+\alpha(\mu_g-\mu_\ell)C]}}{A_d \theta\varepsilon I_o \mu_\ell C^2 \alpha^2} \quad (4.2)$$

where,

A_d = detector area struck by beam, cm^2

I_o = photon intensity on test section, photons/cm^2sec

R_{ST} = source to test section distance, cm

R_{SD} = source to detector distance, cm

μ_w = attenuation coefficient of walls of test section, cm^{-1}

μ_g = vapor phase attenuation coefficient, cm^{-1}

μ_ℓ = liquid phase attenuation coefficient, cm^{-1}

T = wall thickness of conduit, cm

C = chord length through two-phase mixture, cm

This expression can be evaluated at each chordal position to yield the relative chordal-average void fraction error at that location.

The flux needed for evaluation of Equation (4.2) must be measured and calculated. To this end, an ionization chamber was placed at the exit of the lead collimator associated with the x-ray beam. A lead sheet was used to cover the collimator entrance until x-ray operating conditions (40 ma, 32 kvp) were reached. The lead sheet was then removed remotely and the time of exposure carefully measured. After a sufficient period of time the x-ray machine was shut off. Division of the total dose (in rads) by the exposure time yielded a dose rate of twenty-two rads per minute. Several runs were made and this value was consistently measured.

The flux can be obtained by combining the dose rate, the x-ray spectrum and the true mass absorbtion coefficient. Relative intensities can be calculated by the expression, Equation 3.55, suggested by Krammer [37]. The operating conditions of 32 kv and 40 ma were substituted into Krammer's expression to produce Figure 4.128.

The photon flux can be calculated from the National Bureau on Standards Formulation,

$$D(E) = 1.6\times10^{11}\phi(E)\mu_T(E)\,E \qquad (4.3)$$

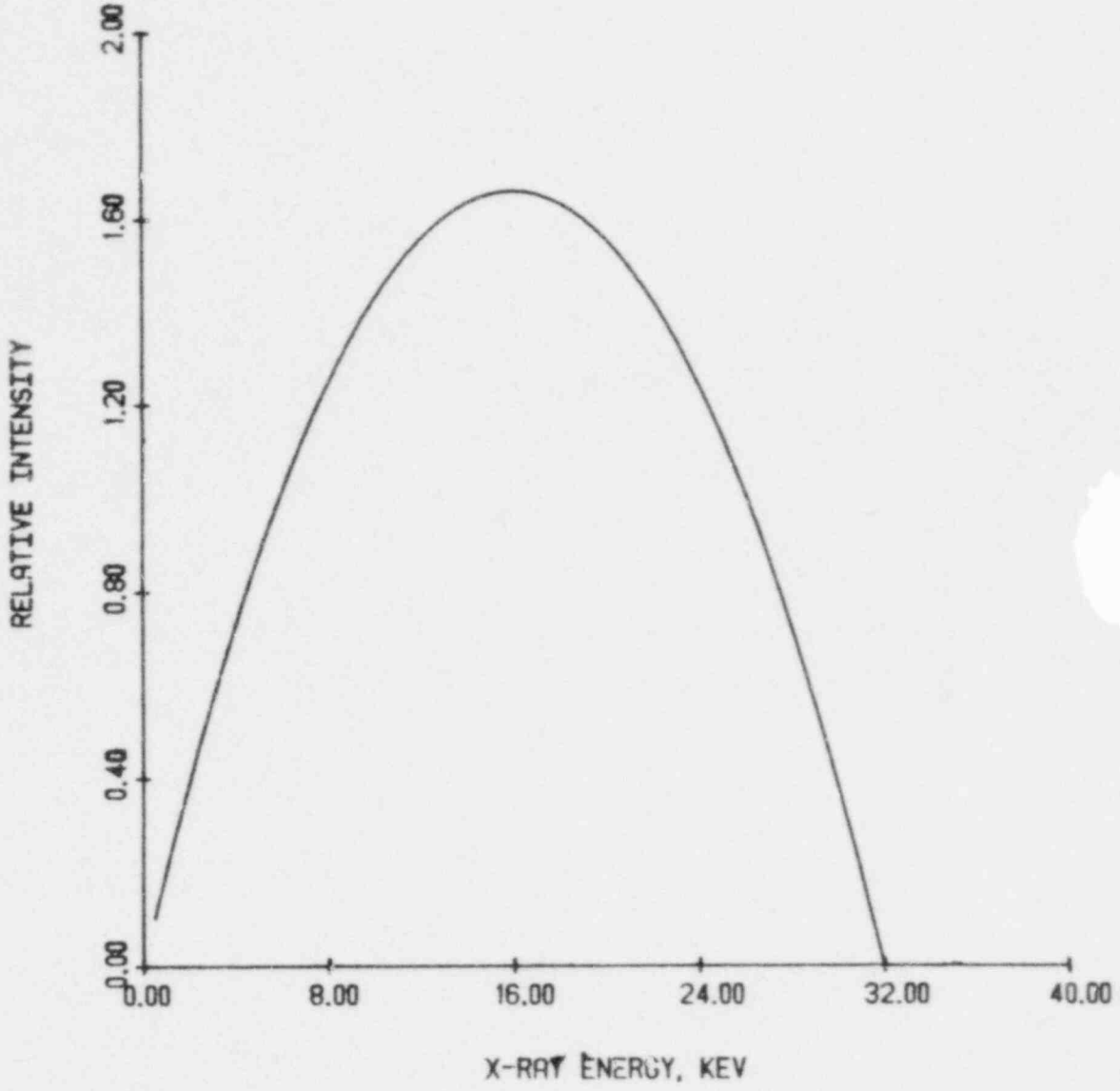

Figure 4.123 Relative x-ray spectrum based on Krammer (1923) for 32 kev, 40 ma.

where,

$D(E)$= dose rate, rads/sec

$\phi(E)$= photon flux, photons/cm^2-sec

$\mu_T(E)$= photoelectric or true mass absorption coefficient of detector medium, cm^2/gm

E = photon energy, kv

This expression is divided in several energy subintervals for integration because dose rate is a function of energy,

$$\int_{5kev}^{32kev} D(E)dE = 1.6\times10^{-11} \int_{5kev}^{32kev} \phi(E)\mu_T(E)E\,dE = \frac{22 \text{ rads}}{\text{min}} \quad (4.4)$$

Equation 4.4 illustrates the expression which must be evaluated. A lower limit of 5 kv was selected as a lower energy cutoff due to x-ray filtering. Equation (4.4) can be further reduced to,

$$\int_{5kev}^{32kev} \phi(E)\mu_T(E)EdE = \int_{5kev}^{12.5kev} \phi(E)\mu_T(E)EdE +$$

$$\int_{12.5kev}^{17.5kev} \phi(E)\mu_T(E)EdE + \int_{17.5kev}^{22.5kev} \phi(E)\mu_T(E)EdE +$$

$$\int_{22.5kev}^{27.5kev} \phi(E)\mu_T(E)EdE + \int_{27.5kev}^{32kev} \phi(E)\mu_T(E)EdE$$

$$= 2.3 \times 10^{10} \frac{\text{photons kv}^2}{\text{gm sec}} \quad (4.5)$$

Substitution of the mass absorption coefficient and the relative intensities into Equation (4.5) allows calculation of the energy dependent photon flux $\phi(E)$.

This calculated flux is a vector quantity, but x-ray intensity is a scalar. Since the photons are primarily uniaxial, the flux and intensity have the same magnitude. Thus the total integrated flux incident on the detector is,

$$\bar{\phi} = \int_{5kev}^{32kev} \phi(E)\, d\, E \qquad (4.6)$$

This expression can be integrated by the same scheme used earlier. Evaluation of this expression produced a flux of 4.5×10^{9} photon/cm^{2}-sec. This value was then used in Equation (4.2) to get the relative error.

Figure 4.129 shows the relative error associated with each chordal position as a function of void fraction. The curves shown account for all the variation in wall thickness and pathlength at the various chordal positions. The centerline chord produces the most accurate results since the largest portion of the x-ray is attenuated in the two-phase mixture. Correspondingly the wall chord contains the largest relative error.

The absolute error can be calculated by multiplying the relative error by the associated void fraction. These results are illustrated in Figure 4.130, for an integration time of 1 ms. It can be seen that the

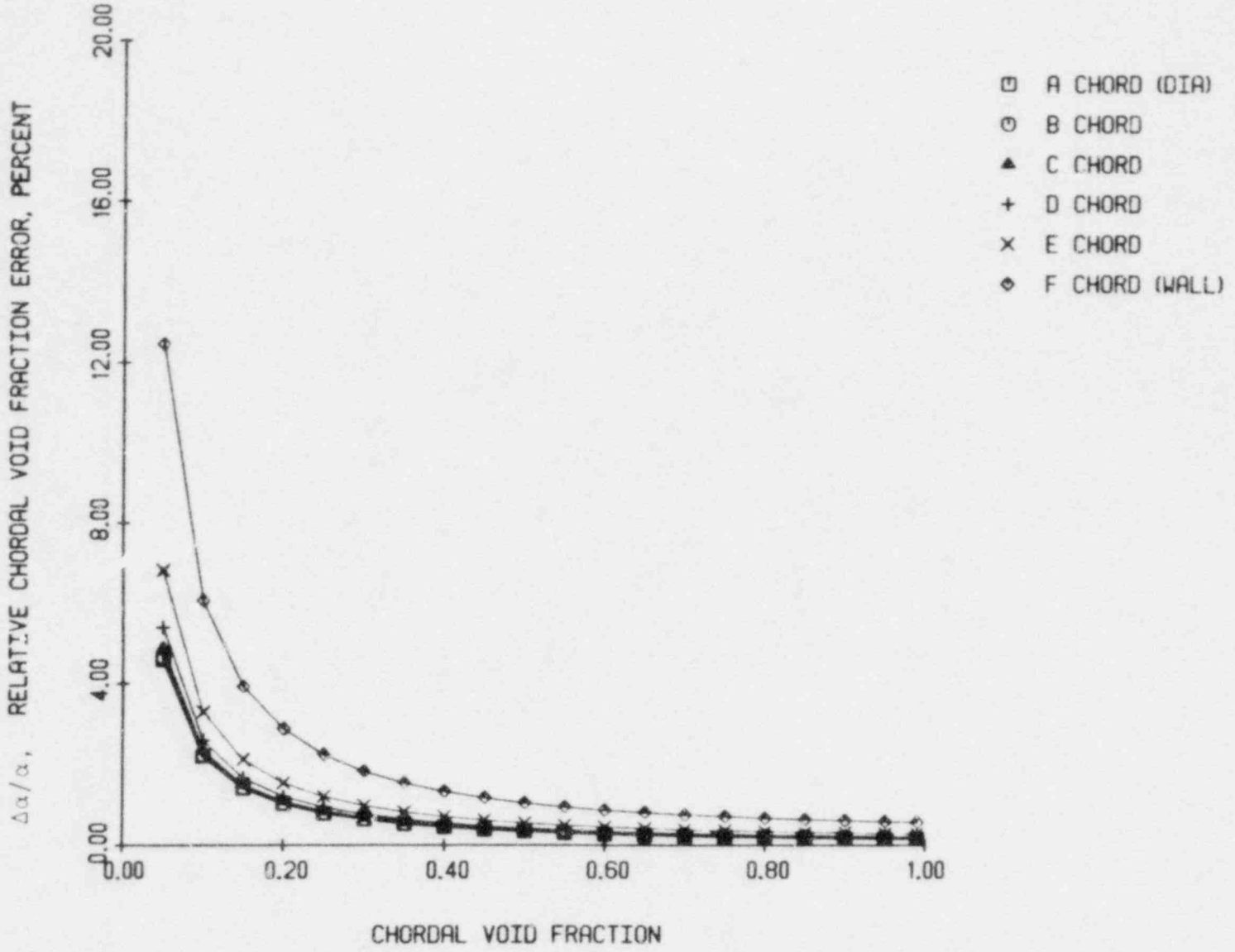

Figure 4.129 The relative chordal void fraction error ($\Delta\alpha/\alpha$) vs. chordal void fraction

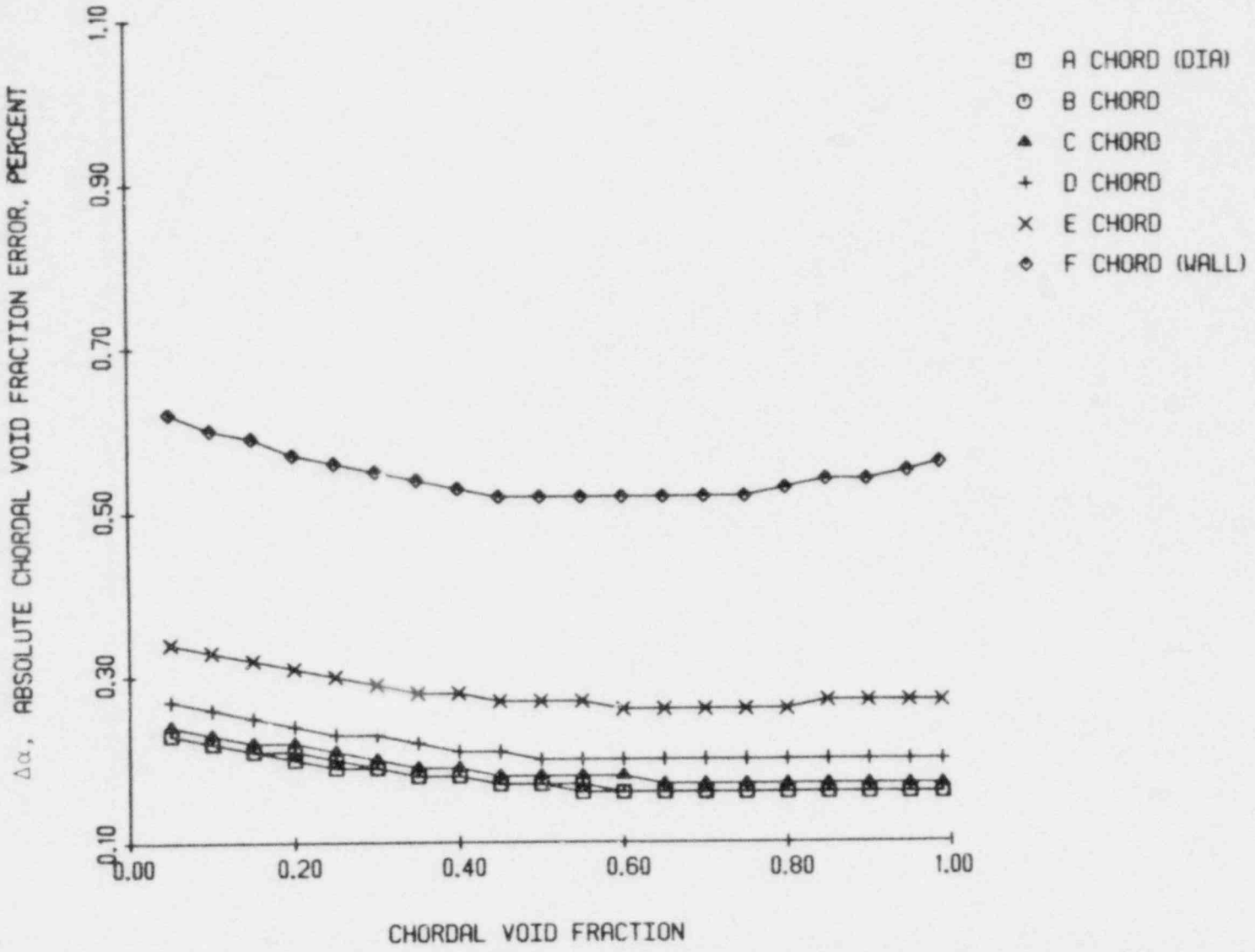

Figure 4.130 The absolute chordal void fraction error, $\Delta\alpha$ vs. chordal void fraction

design and operating conditions of this x-ray system produce measurements with acceptably small static error.

4.6.2 Dynamic Error

Dynamic error results because the logarithm of the time-average value of the measurement is not equal to the time-average of the logarithm of the measurement. That is,

$$\bar{\alpha} = \ell n \left[\frac{1}{T} \int_0^T \alpha \, dt \right] \neq \frac{1}{T} \int_0^T \ell n \, \alpha \, dt \qquad (4.7)$$

where,

$\bar{\alpha}$ = short-time and chordal average void fraction

T = averaging period, seconds

Most photon densitometers operate in the pulse mode; that is, they count single events. The relatively small source strength associated with gamma ray devices make this type of counting system necessary. Void fraction is normally calculated (see Appendix A.10) by,

$$\bar{\alpha} = \frac{\ell n \left(\frac{I_{2\phi}}{I_\ell} \right)}{\ell n \left(\frac{I_g}{I_\ell} \right)} \qquad (4.8)$$

where,

$\bar{\alpha}$ = chordal average void fraction

$I_{2\phi}$ = number of counts during time interval-T, when the test section is filled with a two-phase mixture

I_g = number of counts during time interval-T. when only the gas phase is present

I_ℓ = number of counts during time interval-T, when only the liquid phase is present

X-ray systems yield very high equivalent source strength. So high in fact that one can work in the current mode, and thus logarithms of the analog signal can be done electronically before data processing. Thus the measurement signal is linearized prior to time-averaging. The void fraction is then calculated with the linear relationship as shown in Equation (4.9),

$$\bar{\alpha}(t) = \frac{R_{2\phi} - R_L}{R_G - R_L} \tag{4.9}$$

where,

$\bar{\alpha}(t)$ = instantaneous chordal-average void fraction

$R_{2\phi}$ = instantaneous voltage associated with the two-phase mixture

R_G = voltage associated with the test section filled with vapor

R_L = voltage associated with test section filled with all liquid phase

Due to linearization, dynamic error was not present in our x-ray measurements.

5. Radio Frequency Excited Local Void Probe Results

5.1 Calibration Procedure

The response of the radio frequency excited void probe (RF Probe) was measured for a variety of two-phase conditions. Both level and derivative thresholding were tested. The previously described x-ray system was employed as the standard against which to calibrate this local impedance probe.

Initial operation of the local probe indicated that radial symmetry existed in the test section. Hence, subsequent data was only taken over one radius of the pipe. The radius was divided into ten equally spaced intervals. A local probe reading was taken at each interval's endpoint along the diameter. The point void fractions were numerically integrated by Simpson's Rule to determine the chordal average void fraction. Simultaneously, the chordal average void fraction was measured with the x-ray system. The stepping motor system, described in Chapter 3, was used to move the probe remotely.

A coarse calibration was necessary to determine the appropriate level and derivative threshold setting. This calibration consisted of operating the probe in a steady two-phase flow while varying the threshold value. Two graphs, for level and derivative thresholding, are illustrated in Figures 5.1 and 5.2. These curves show three general regions:

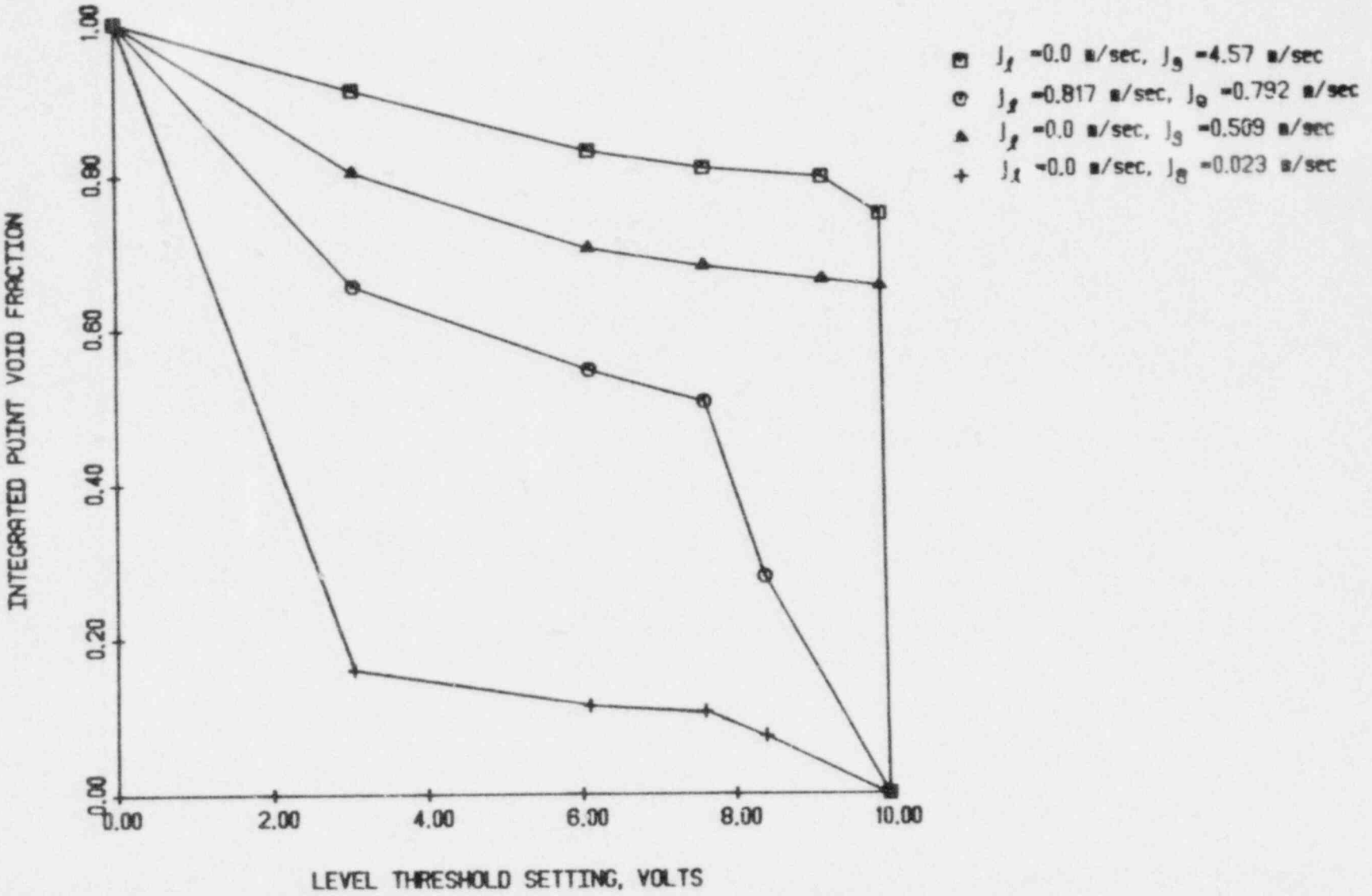

Figure 5.1 The integrated point void fraction response vs. level threshold setting

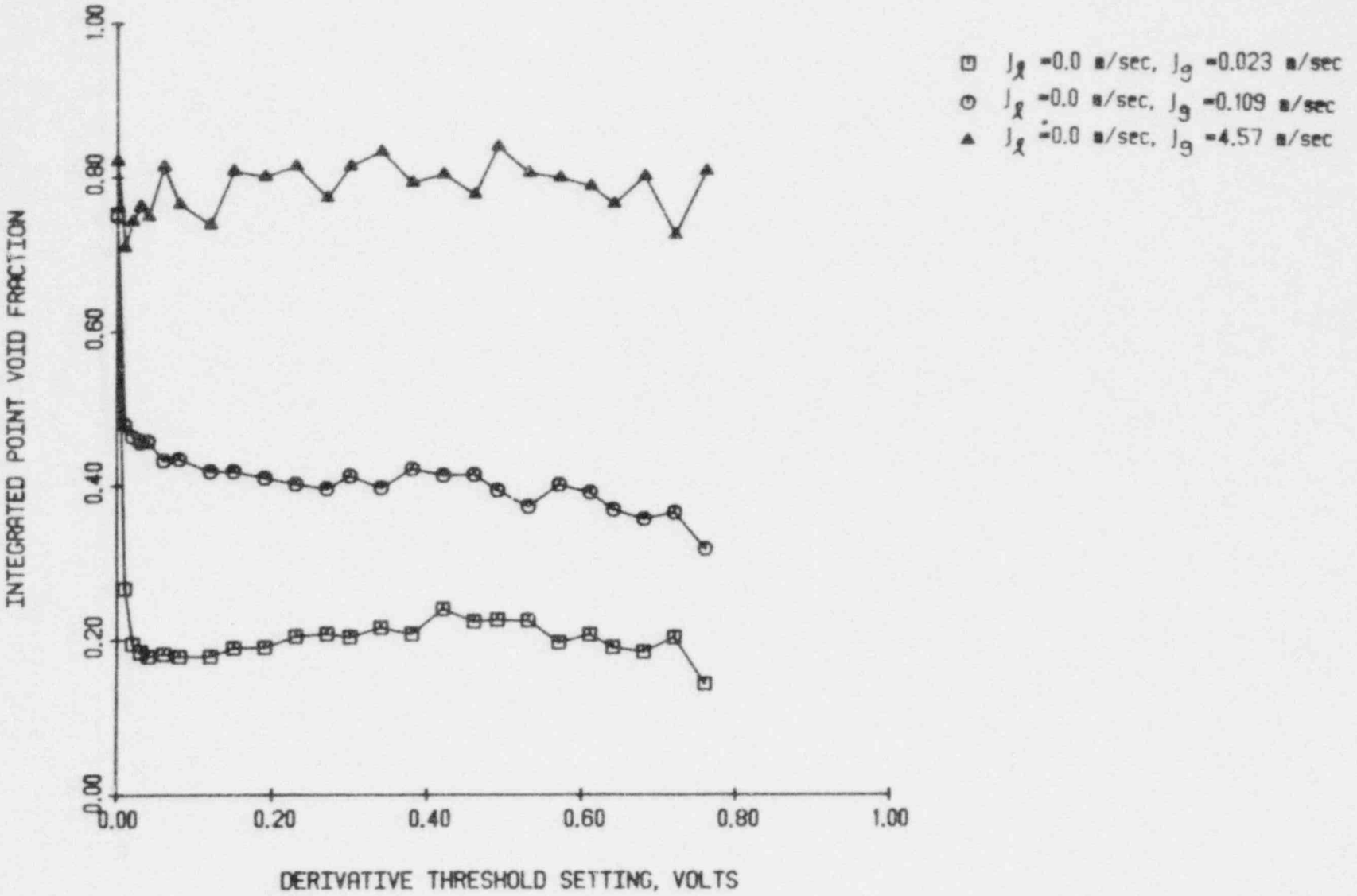

Figure 5.2 The integrated point void fraction response vs. derivative threshold setting

1) A region of high void fraction response caused by too low a threshold setting.
2) A region of fairly flat void response (i.e. a plateau), where the measured void fraction is relatively independent of threshold setting.
3) A region of decreasing void fraction response where the threshold is large, ultimately going to zero when the threshold level exceeds the signal.

It can be seen that the plateau is more pronounced for the derivative thresholding system, indicating that it is a more forgiving technique.

These graphs are very similar to the curve of photons counted as a function of the discriminator level employed in nuclear radiation detectors. Thus, the same criteria in selecting an operating point can be employed. The threshold should be large enough to eliminate noise, but not be too large, or actual void pulses will not be counted. Obviously, the level should be set in the middle of plateau region. Based on these conditions, a level threshold of 4.0 volts and a derivative level of 0.24 volts were selected.

This procedure is considerably different from the usual scheme used with level thresholding on other probes. Normally, the threshold is set to give the correct response for the two-phase conditions encountered. Some type of densitometer is required to be operated in parallel. Calibrating the probe at a constant threshold setting will

produce results of comparable accuracy, moreover the user does not need to know the flow conditions prior to operation. The probe's response can be corrected before data processing, thus giving the probe practicality in transient flows.

Twenty-two test conditions in air/water flow were selected for calibration. These ranged from bubbly to annular flow. Ten data sets were taken in stagnant liquid. Twelve data sets were taken at various non-zero liquid flow rates up to a superficial liquid velocity of one half meter per second.

5.2 Level Thresholding

Data was acquired using the RF probe and level thresholding. The integrated response of this local probe is compared with the x-ray measured chordal void fractions in Figure 5.3. These data sets were taken in stagnant liquid. The probe significantly underestimates the void fraction. The response of the probe to changing liquid velocity at constant void fraction is illustrated in Figure 5.4. Increasing the velocity causes the probe's measurement to approach the true value. Nassos and Bankoff [46] have indicated that the minimum liquid velocity for small flow effects is about one half meter per second. This velocity, unfortunately, was the maximum attainable in our air/water loop.

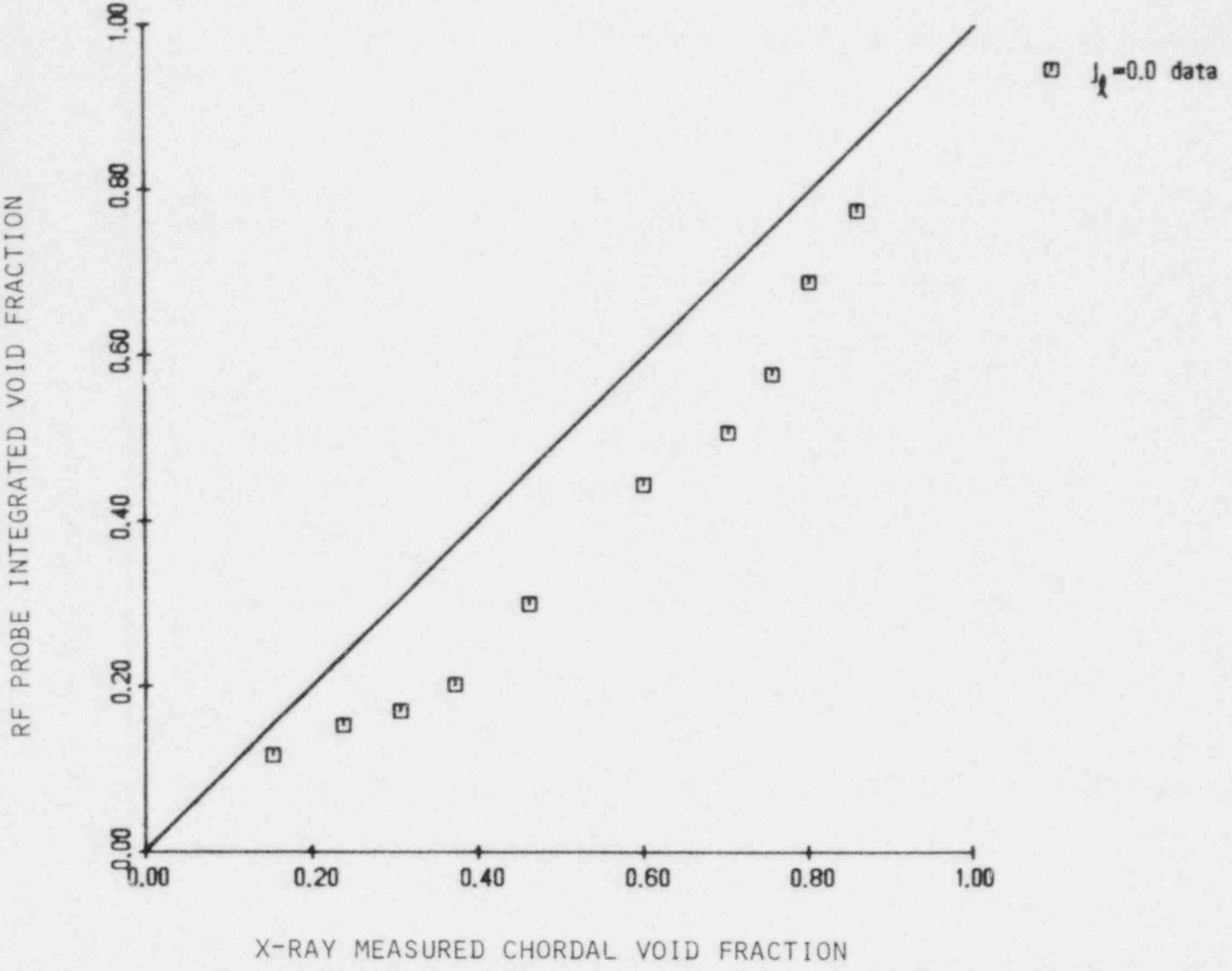

Figure 5.3 RPI RF void probe calibration curve with level thresholding for zero liquid velocity

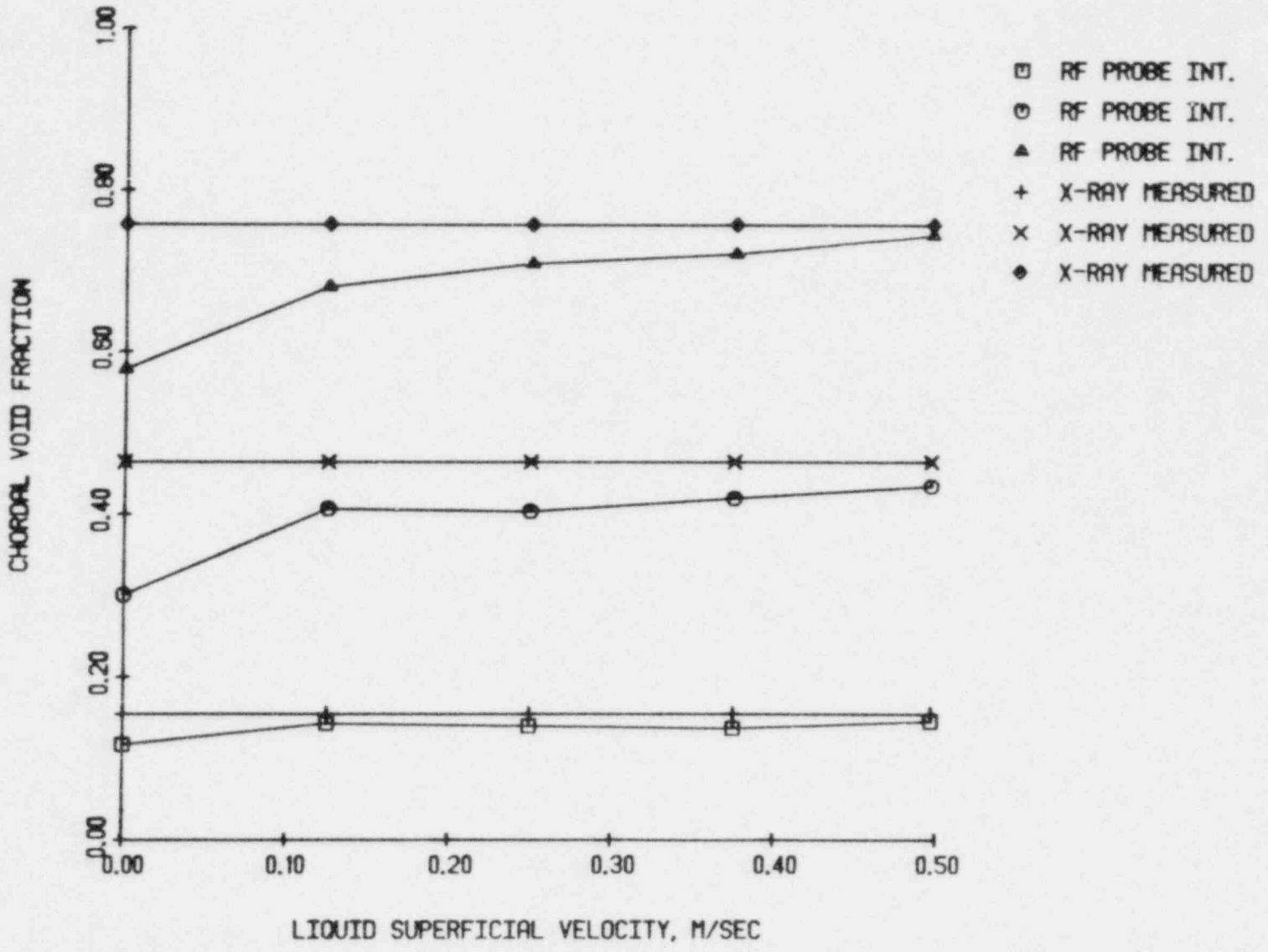

FIGURE 5.4 RPI RF void probe calibration curve with level thresholding for non-zero liquid velocity

Two phenomena are responsible for these data trends; void penetration by the probe and residual water film wetting the probe. Void penetration problems dominate at the lower void fraction and flow rates. Surface tension effects are inversly proportional to the radius, hence small voids are the most difficult for the probe to penetrate. Increasing the liquid velocity allows the probe to more easily penetrate the liquid/vapor interface and decreases void deflection.

The residual water film effects may be significant in the slug and annular flow regimes. The larger voids have less surface tension and would allow easier penetration. The probe also spends considerable time in the vapor phase. Formation of a liquid film would cause the probe to falsely indicate the presence of liquid phase. However, the increasing vapor velocity associated with a larger liquid velocity minimizes the residual water on the tip. As a result the RF probe tends to indicate a higher with increasing liquid velocity.

Drift in the operating level of the RF probe was observed. This problem was caused by variations in water temperature. A small change in temperature will cause a change in the liquid phase dielectric constant [47], as shown in Figure 5.5. Since the dielectric constant is directly proportional to the capacitance of the fluid, the baseline capacitance shifts with temperature. This result can be significant since the change in capacitance between

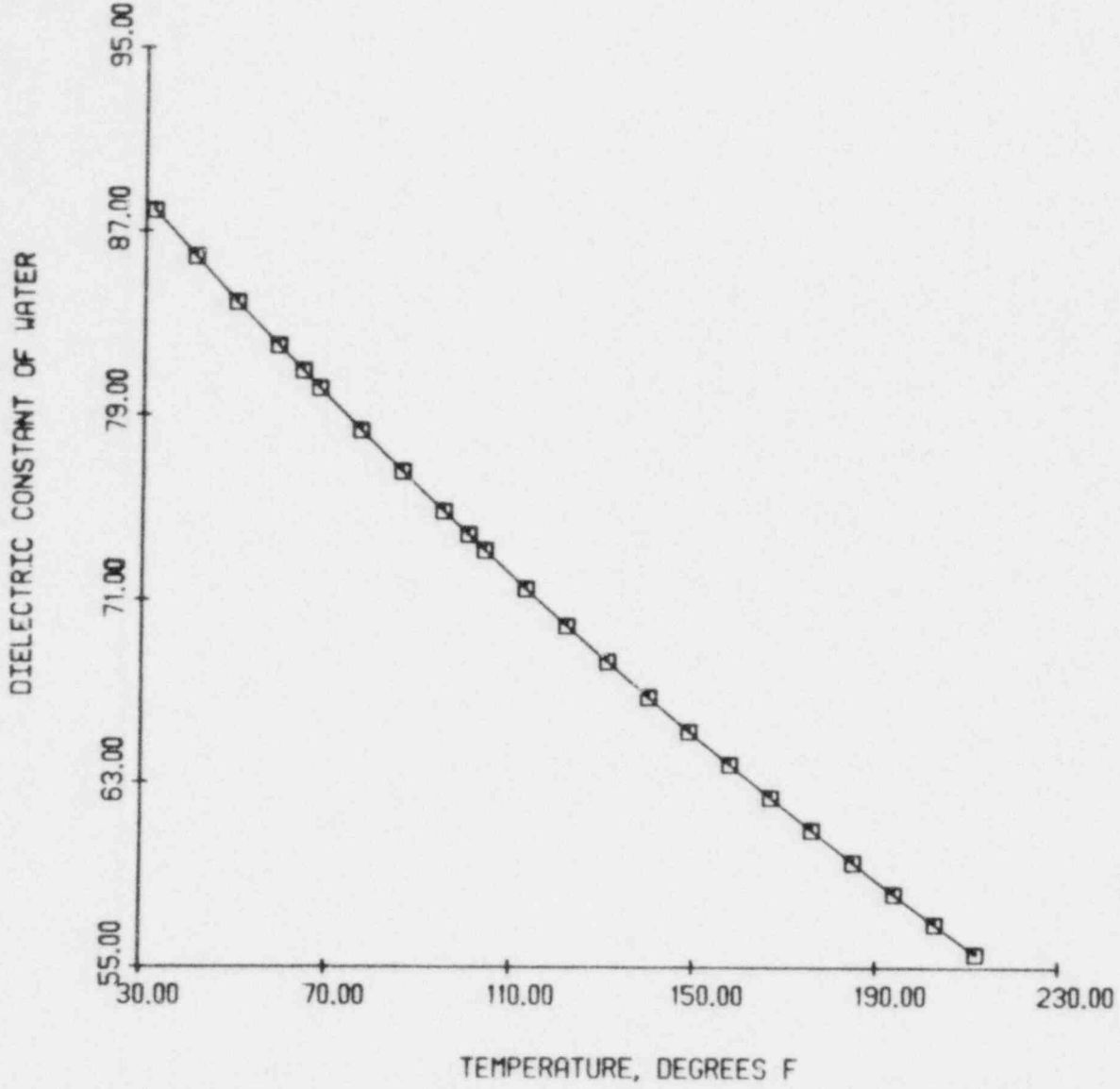

Figure 5.5 The dielectric constant of water as a function of temperature

phases is only 0.15 pf.

The observed drift in the baseline capacitance makes level thresholding difficult. A shift in the operating levels changes the effective discriminator level, thus during any sort of transient operation level thresholding could not perform satisfactorily.

5.3 Derivative Thresholding

Derivative thresholding was employed with the RF probe to remeasure the twenty-two selected two-phase flow conditions. The integrated response of this local probe is compared to the x-ray measured chordal void fractions in Figure 5.6. This data was taken with zero liquid flow. The probe overestimates the void fraction below 23 percent and underestimates the void fraction elsewhere. Flow effects still dominate the response.

Derivative thresholding, however, produces more accurate results then level thresholding. Figure 5.7 illustrates the effects of velocity. The response in bubbly flow is essentially independent of liquid velocity. Obviously this thresholding scheme tends to compensate for some of the liquid/vapor penetration problems just discussed. Slug and annular flow conditions still show some flow effects, however, like the data taken with a level threshold, the flow effects decrease with increasing liquid velocity.

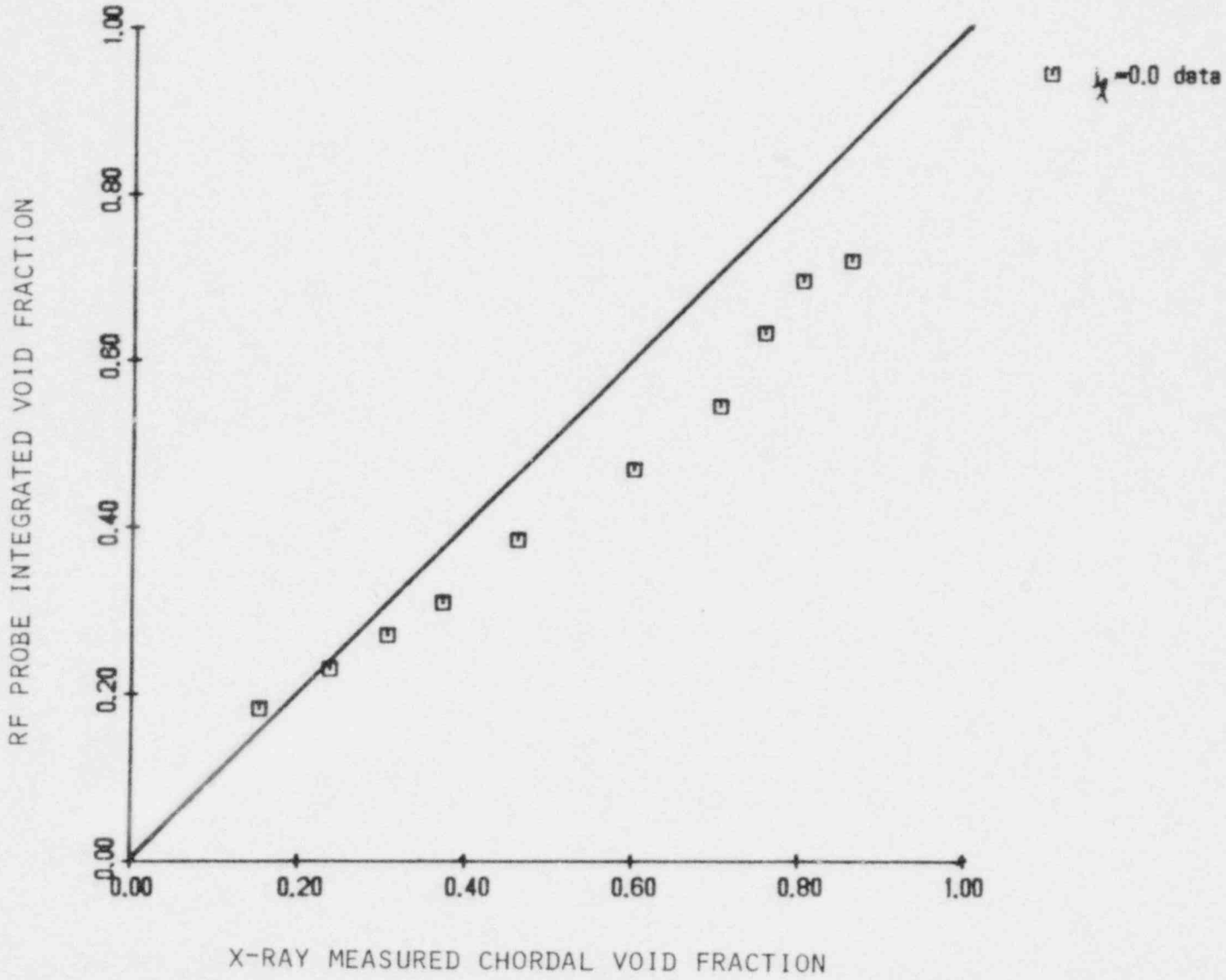

Figure 5.6 RPI RF void probe calibration curve with derivative thresholding for zero liquid velocity

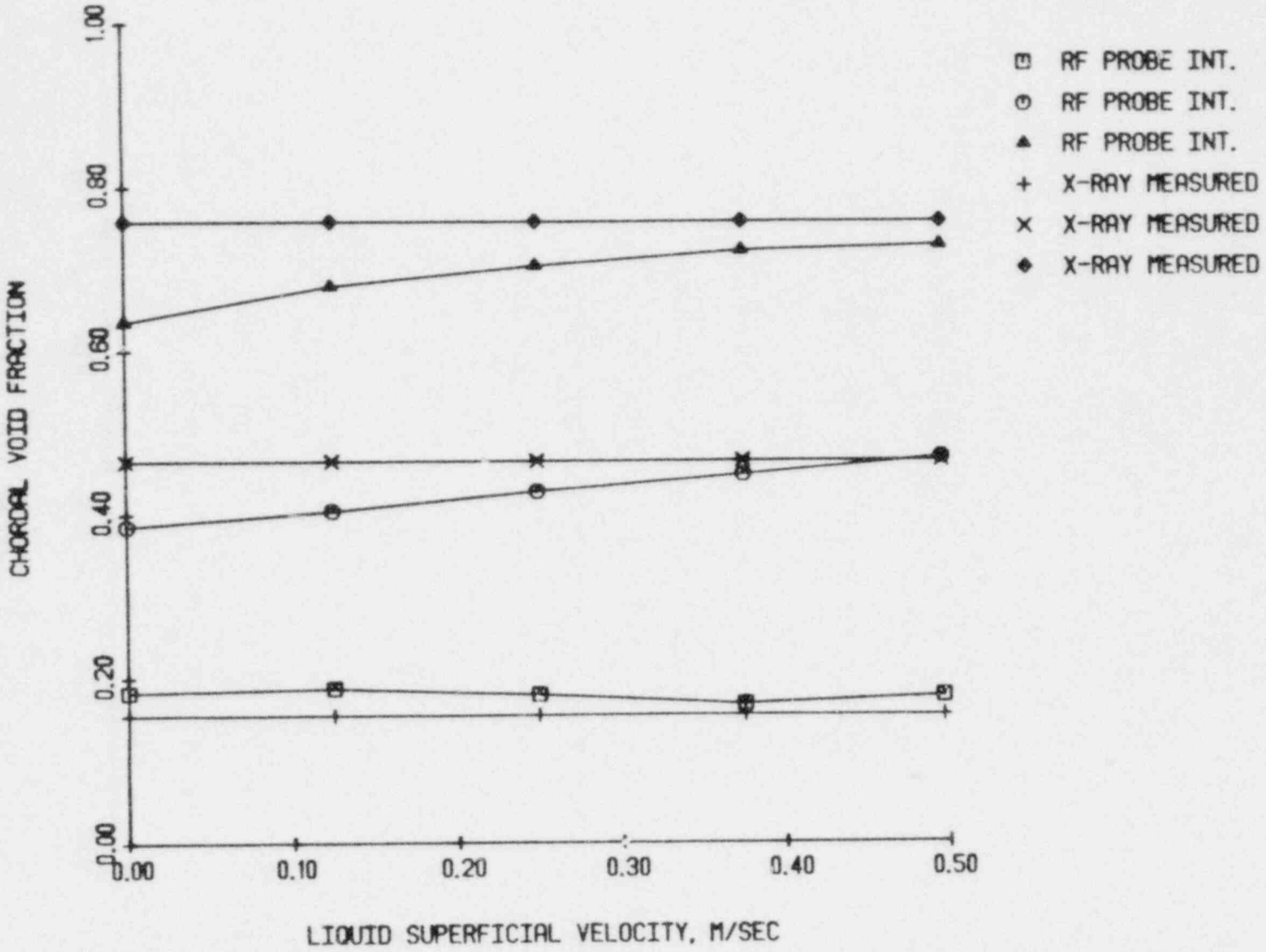

FIGURE 5.7 RPI RF void probe calibration curve with derivative thresholding for non-zero liquid velocity

Radial void profiles, taken for optimum settings with level and derivative thresholding, are presented in Figures 5.8 through 5.29. The integrated levels associated with each profile as well as the void fraction measured by the x-ray standard is shown. It can be seen that level thresholding fails to pickup some of the previously observed [48](Serizawa et al) details seen by derivative thresholding.

From this data correction curves for level and derivative thresholding can be constructed. The correction curves for zero liquid flow are shown in Figures 5.30 and 5.31,

The corresponding correction curves for non-zero liquid flow data are shown in Figures 5.32 and 5.33 for level and derivative thresholding. Like the zero liquid flow correction curves, these graphs are constructed by dividing the x-ray measured chordal-average void fraction by the integrated local probe measurements to obtain the correction factor.

The corrected radial void profiles for derivative thresholding are shown in Figures 5.34 to 5.55. These curves were constructed by multiplying each point void fraction reading by the chordal correction factor. This insures that the integral of the radial void profile will agree with the x-ray measured chordal-average void fraction. Only derivative thresholding results are shown due to the inherent problems with level thresholding previously

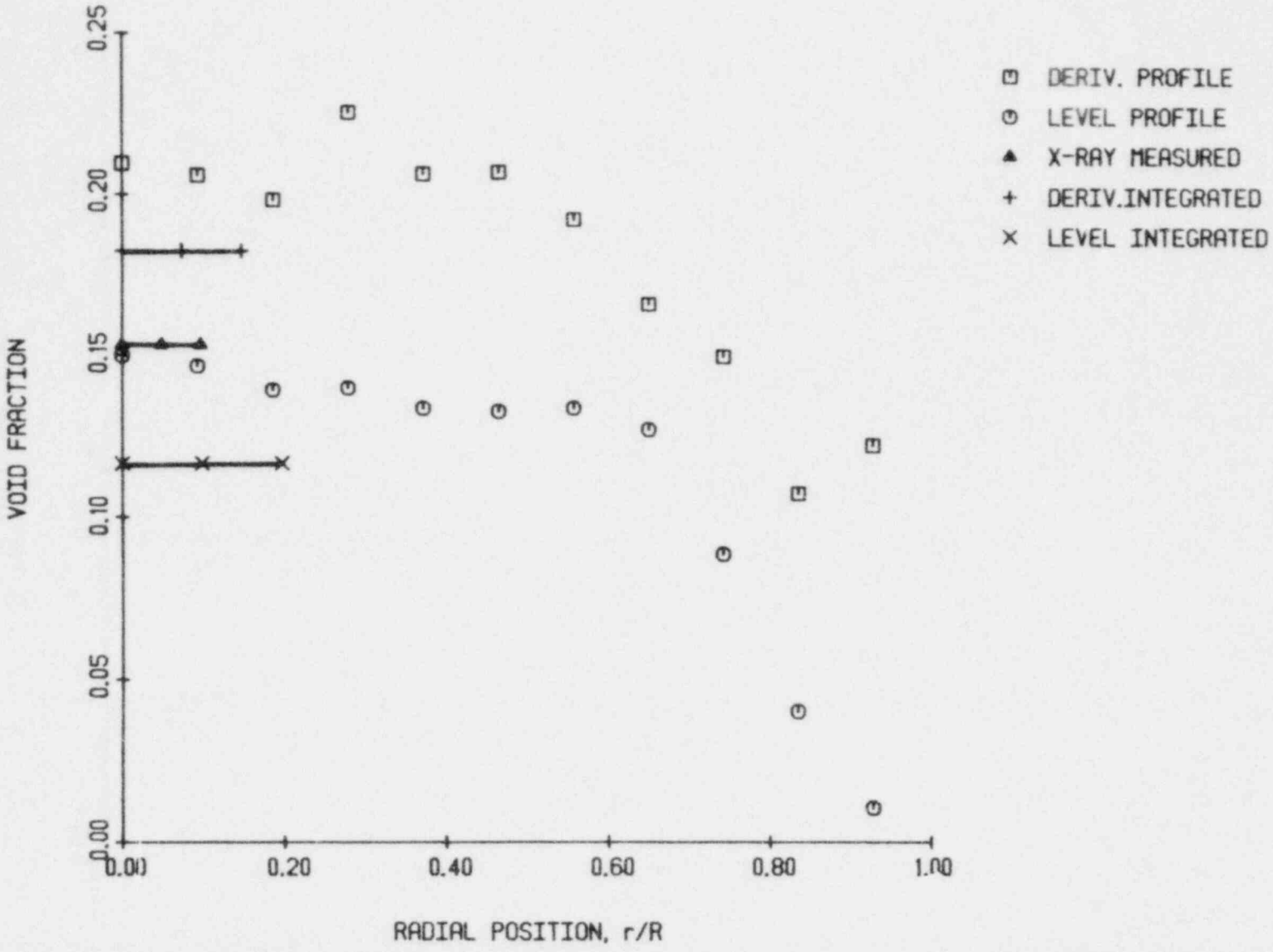

Figure 5.8 A comparison of the x-ray measured chordal void fraction and the integrated radial void profiles measured with the RF probe using level and derivative thresholding for j_ℓ=0.0 m/sec, j_g=0.023 m/sec

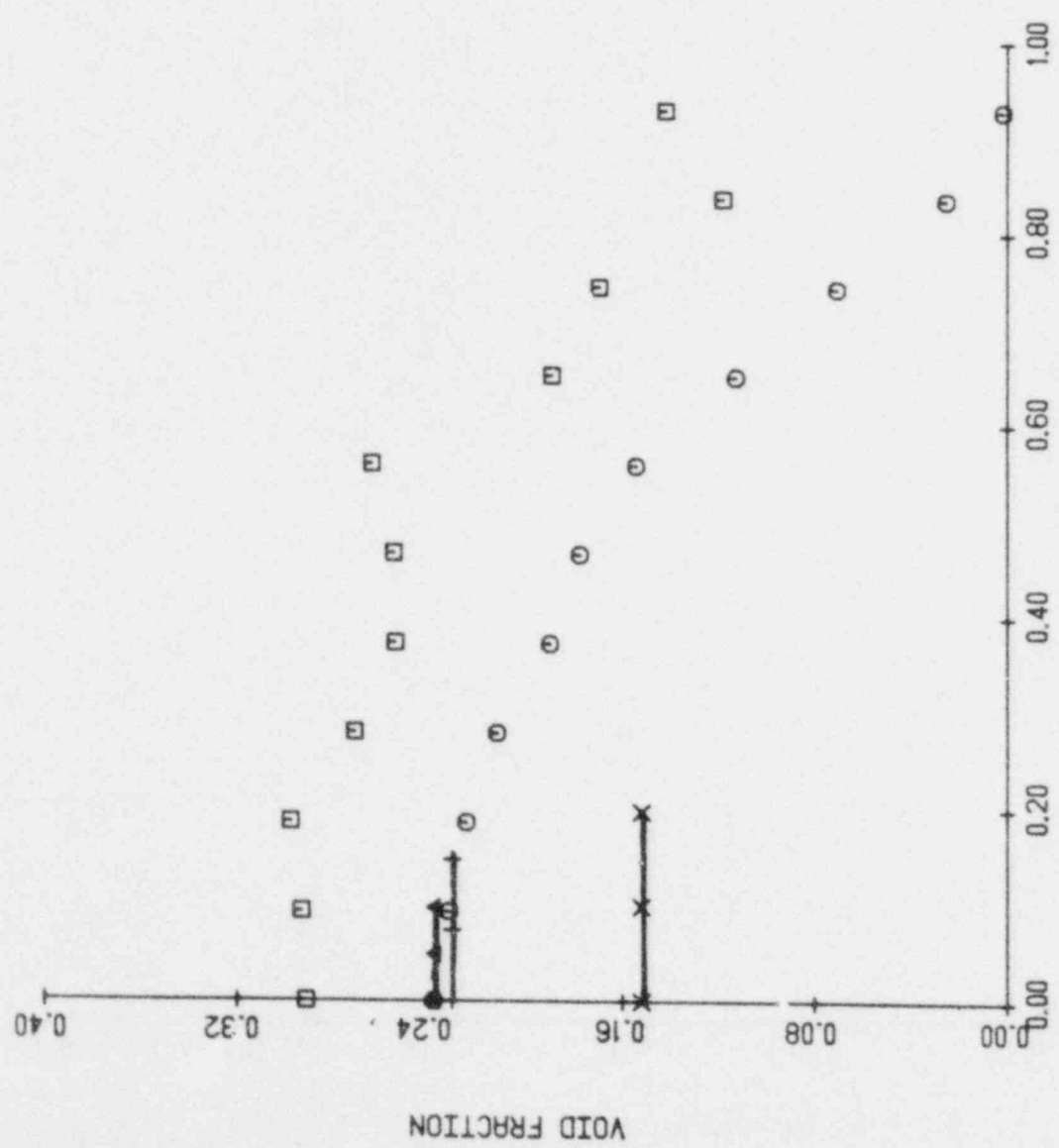

Figure 5.9 A comparison of the x-ray measured chordal void fraction and the integrated radial void profiles measured with the RF probe using level and derivative thresholding for j_ℓ=0.0 m/sec, j_g=0.044 m/sec

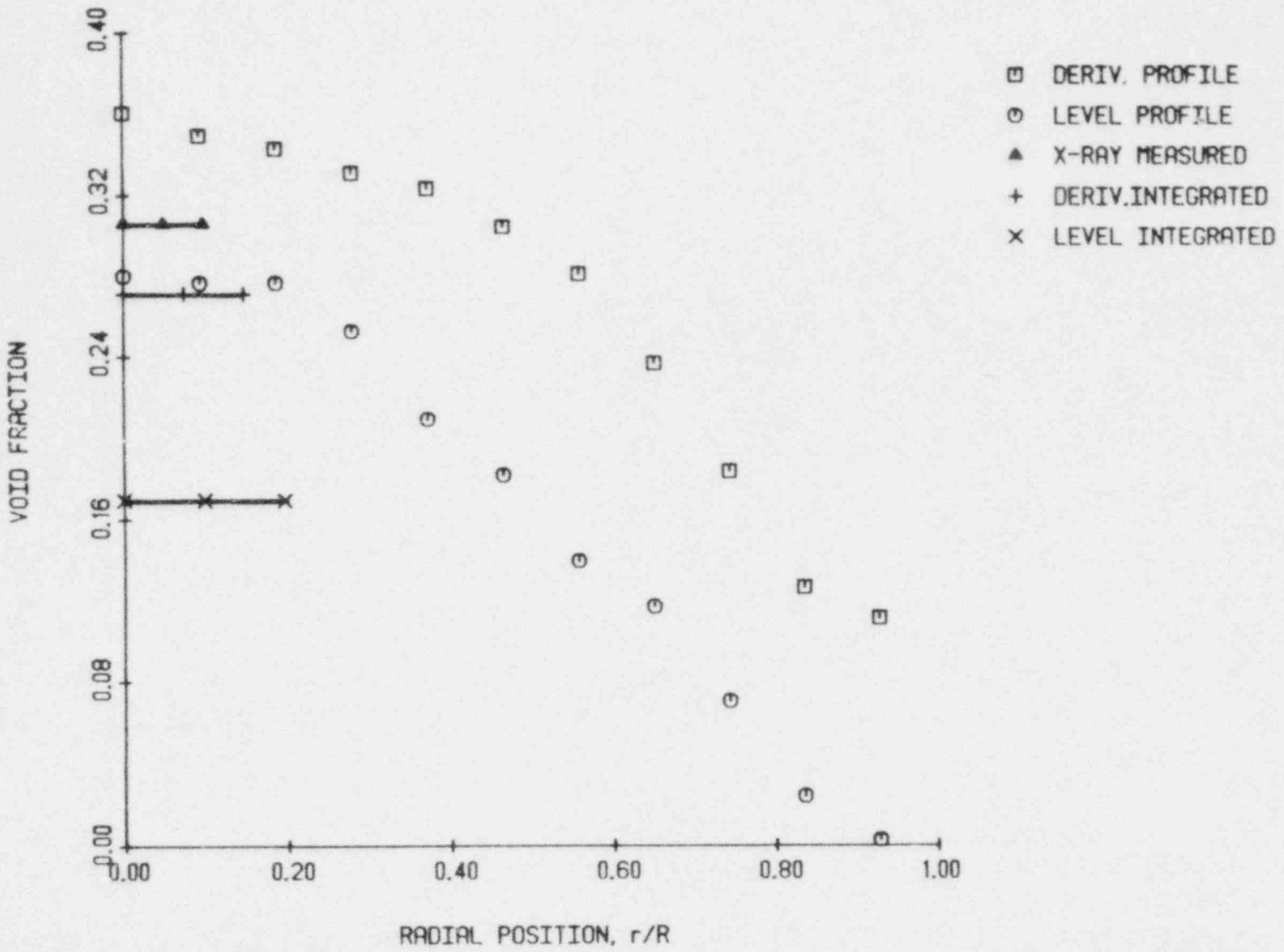

Figure 5.10 A comparison of the x-ray measured chordal void fraction and the integrated radial void profiles measured with the RF probe using level and derivative thresholding for j_ℓ=0.0 m/sec, j_g=0.075 m/sec

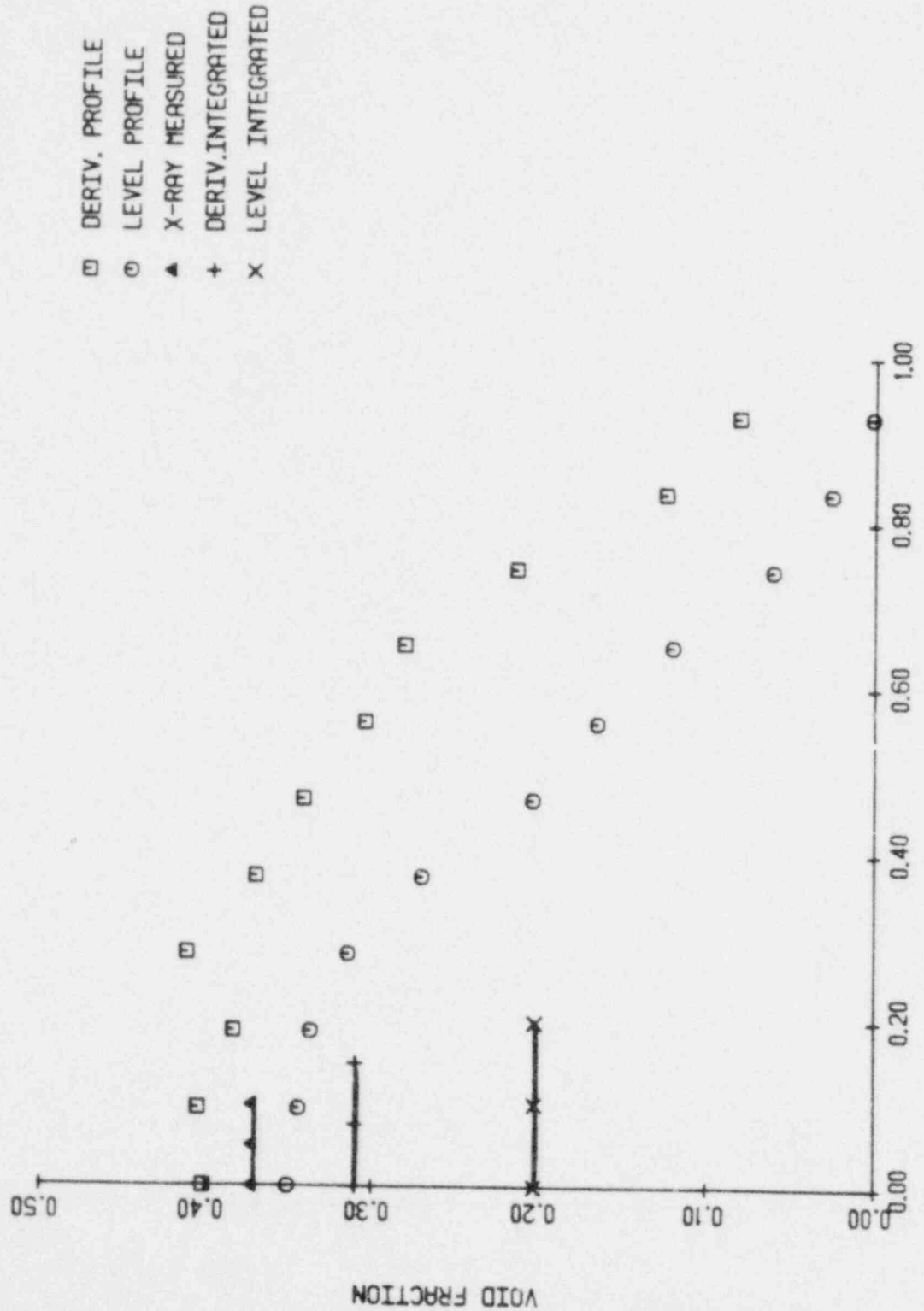

Figure 5.11 A comparison of the x-ray measured chordal void fraction and the integrated radial void profiles measured with the RF probe using level and derivative thresholding for j_ℓ=0.0 m/sec, j_g=0.109 m/sec

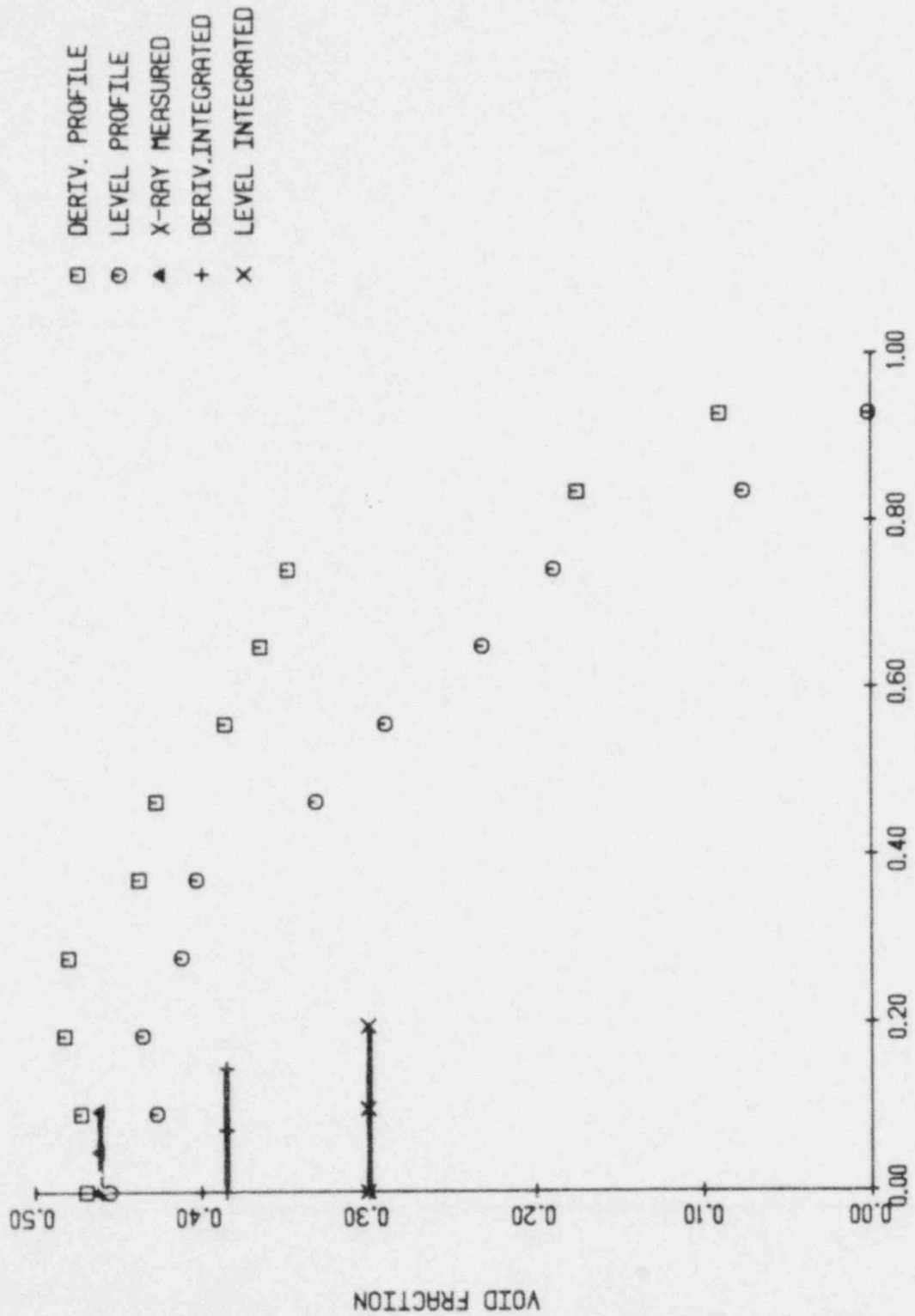

Figure 5.12 A comparison of the x-ray measured chordal void fraction and the integrated radial void profiles measured with the RF probe using level and derivative thresholding for j_ℓ=0.0 m/sec, j_g=0.184 m/sec

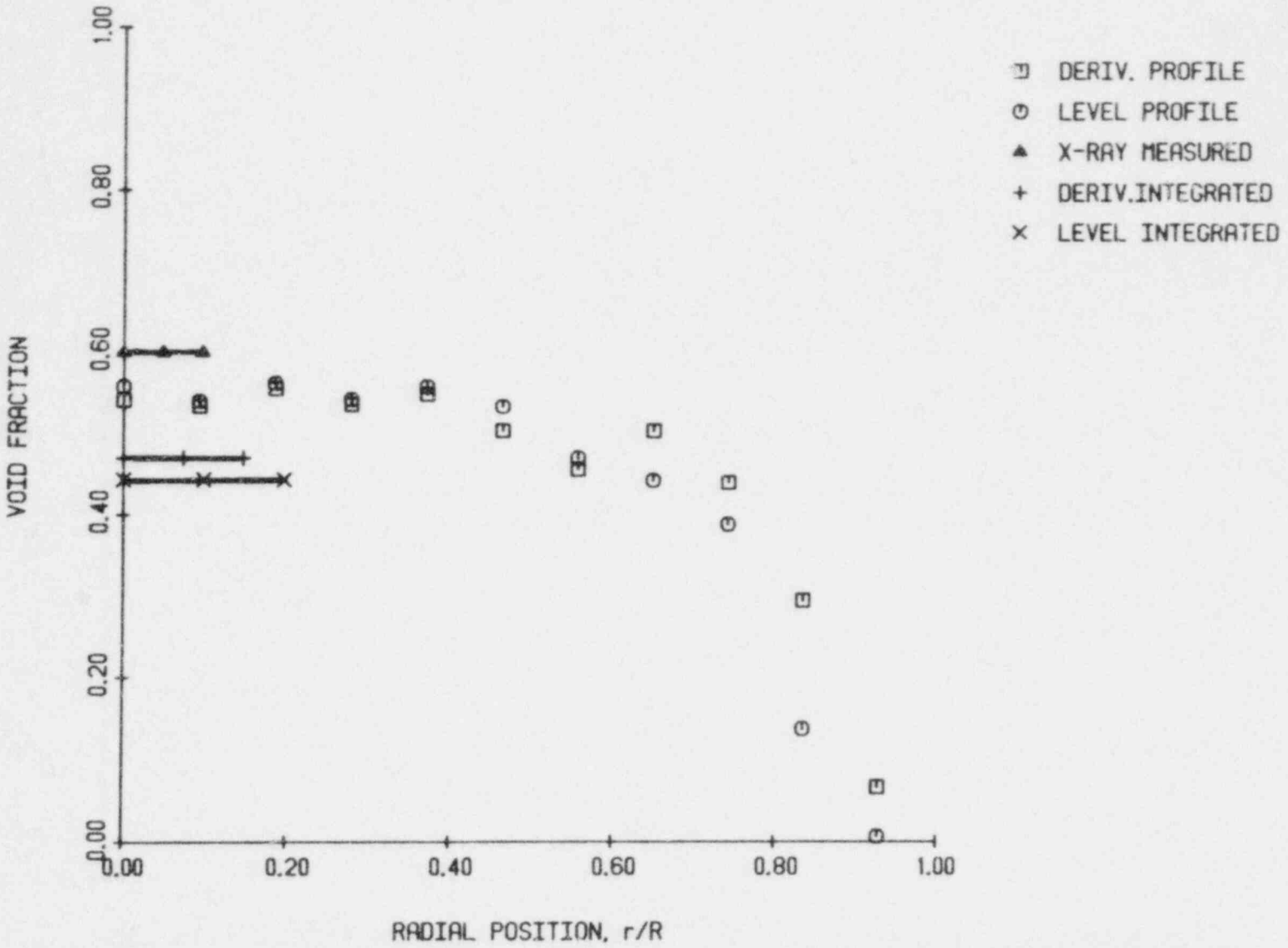

Figure 5.13 A comparison of the x-ray measured chordal void fraction and the integrated radial void profiles measured with the RF probe using level and derivative thresholding for j_ℓ=0.0 m/sec, j_g=0.311 m/sec

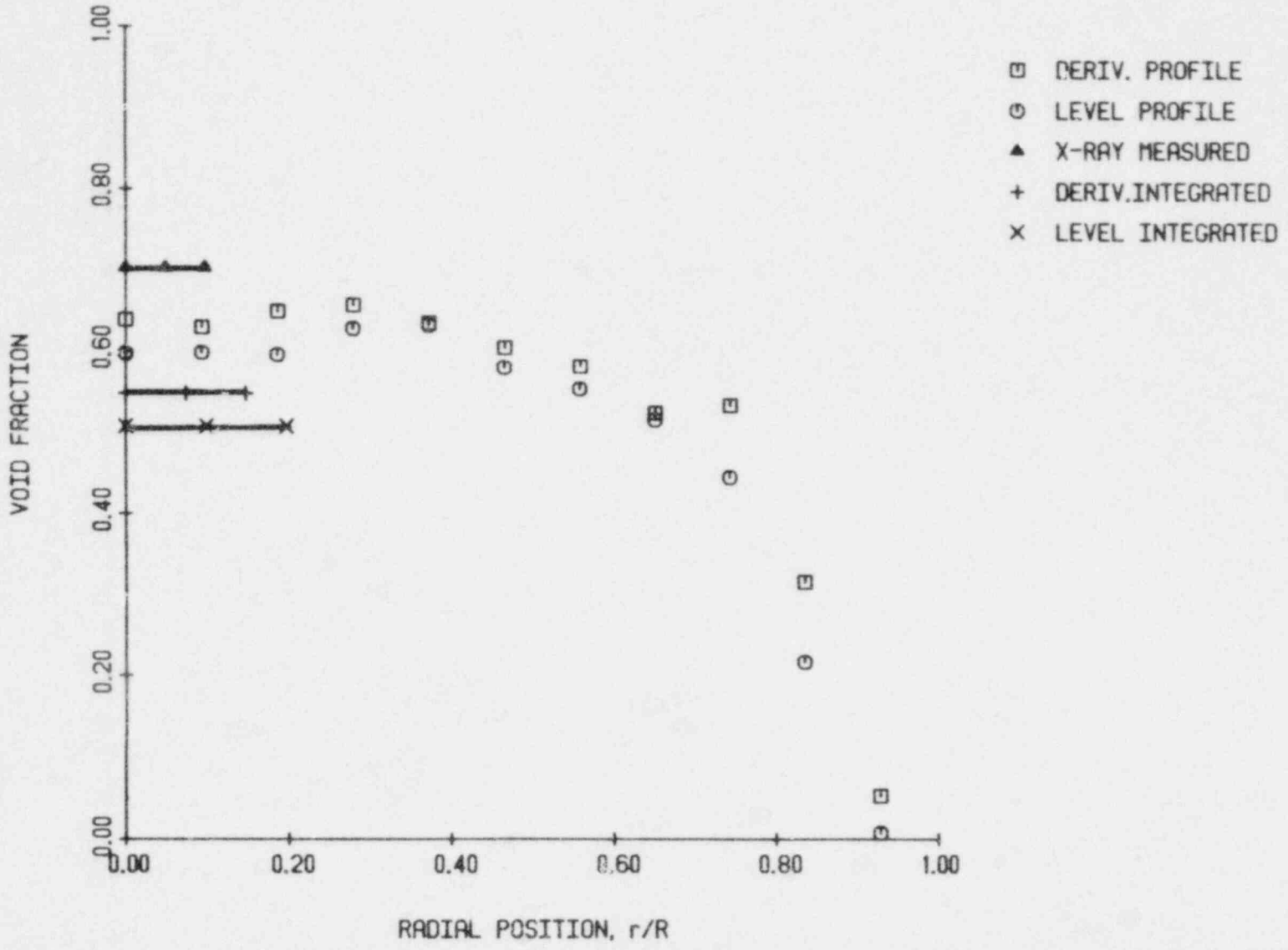

Figure 5.14 A comparison of the x-ray measured chordal void fraction and the integrated radial void profiles measured with the RF probe using level and derivative thresholding for j_ℓ=0.0 m/sec, j_g=0.509 m/sec

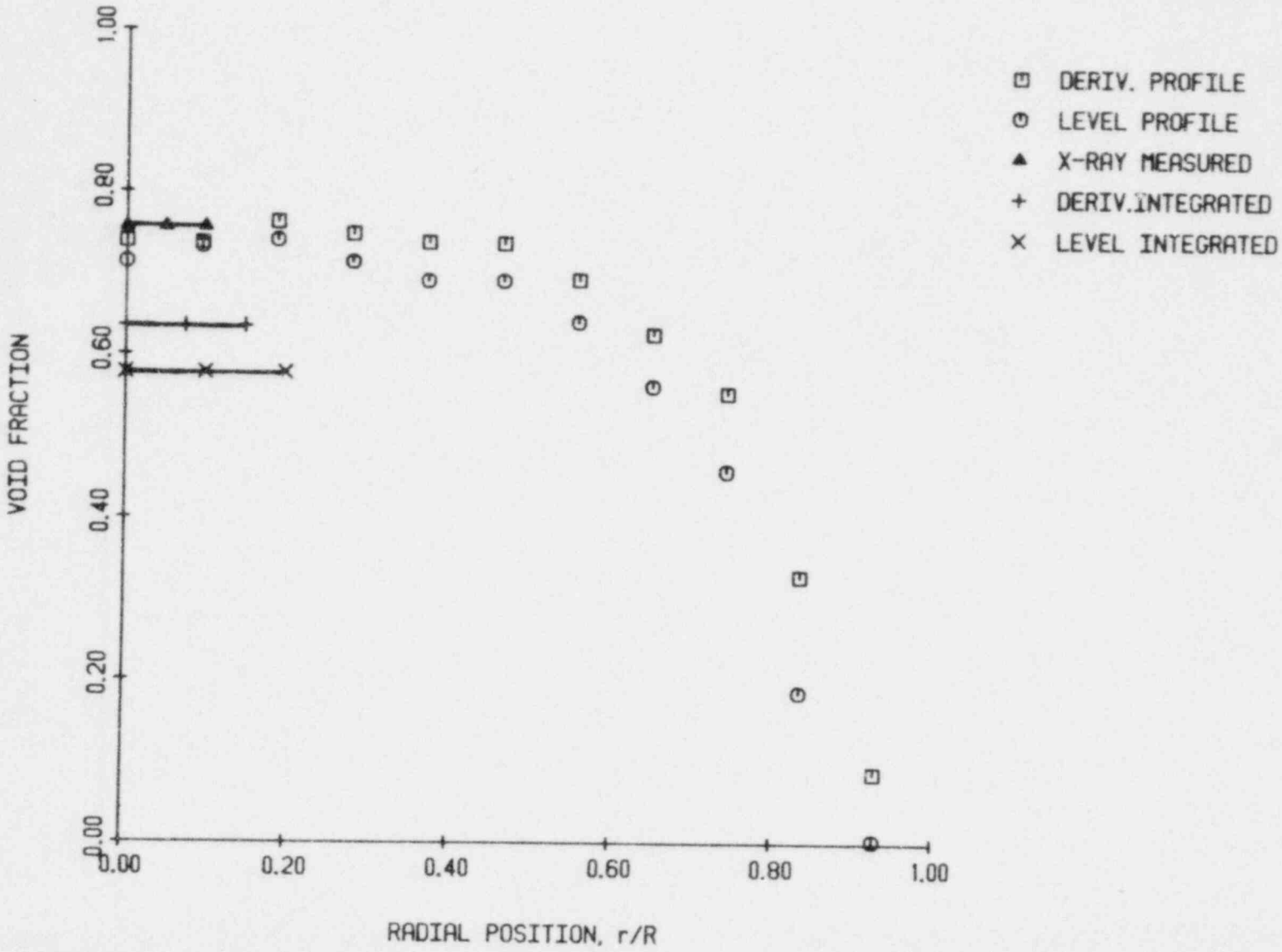

Figure 5.15 A comparison of the x-ray measured chordal void fraction and the integrated radial void profiles measured with the RF probe using level and derivative thresholding for j_ℓ=0.0 m/sec, j_g=0.981 m/sec

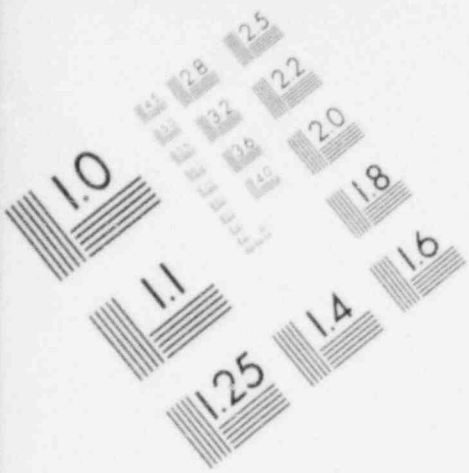

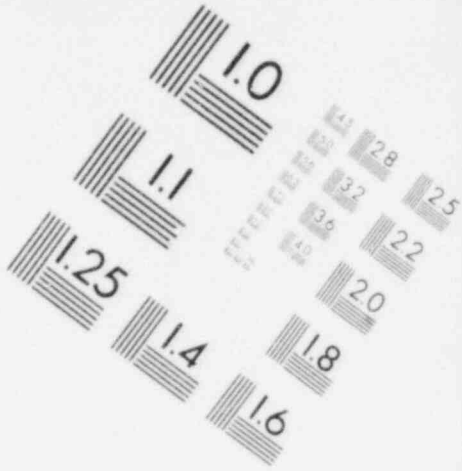

IMAGE EVALUATION
TEST TARGET (MT-3)

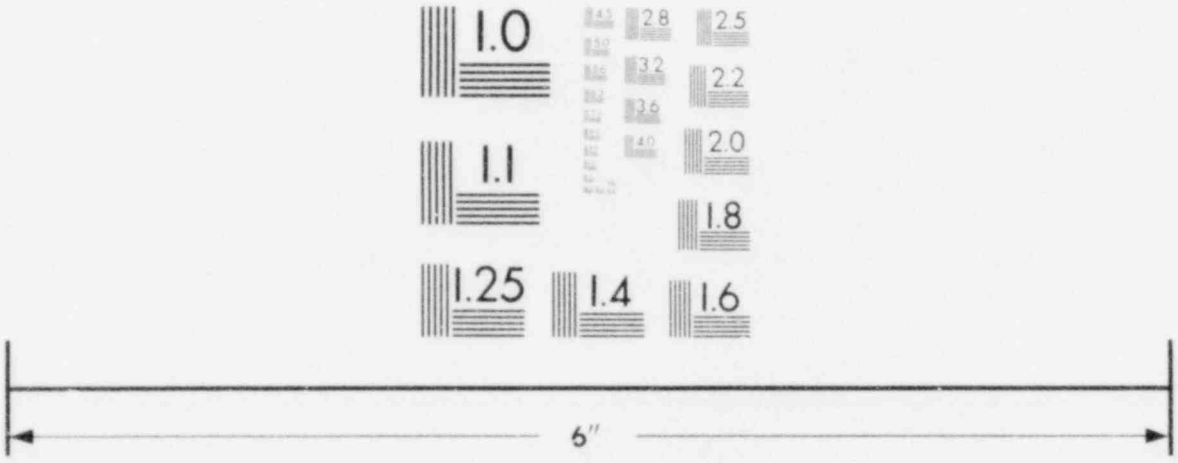

MICROCOPY RESOLUTION TEST CHART

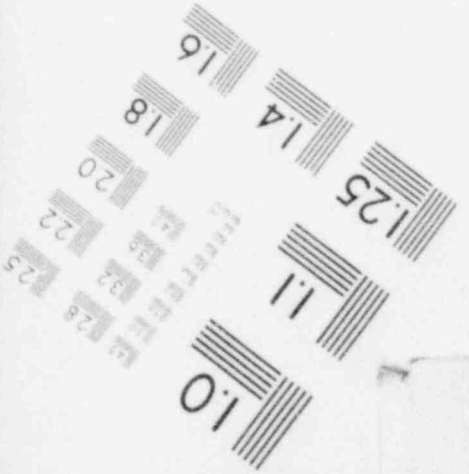

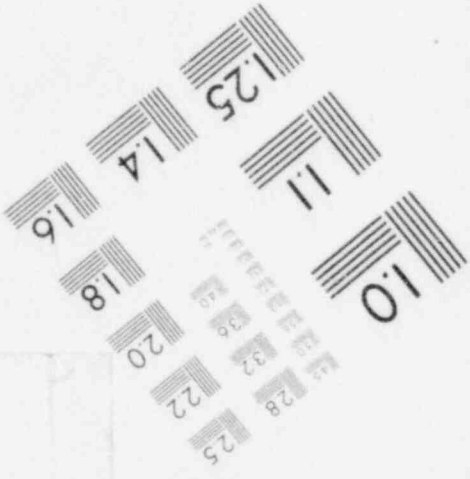

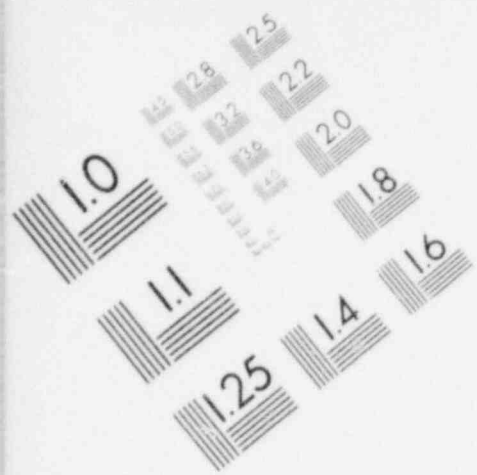

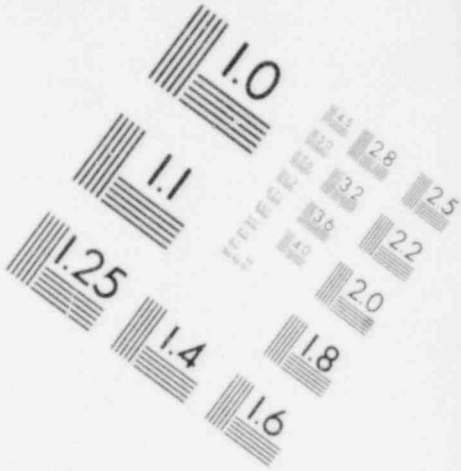

IMAGE EVALUATION
TEST TARGET (MT-3)

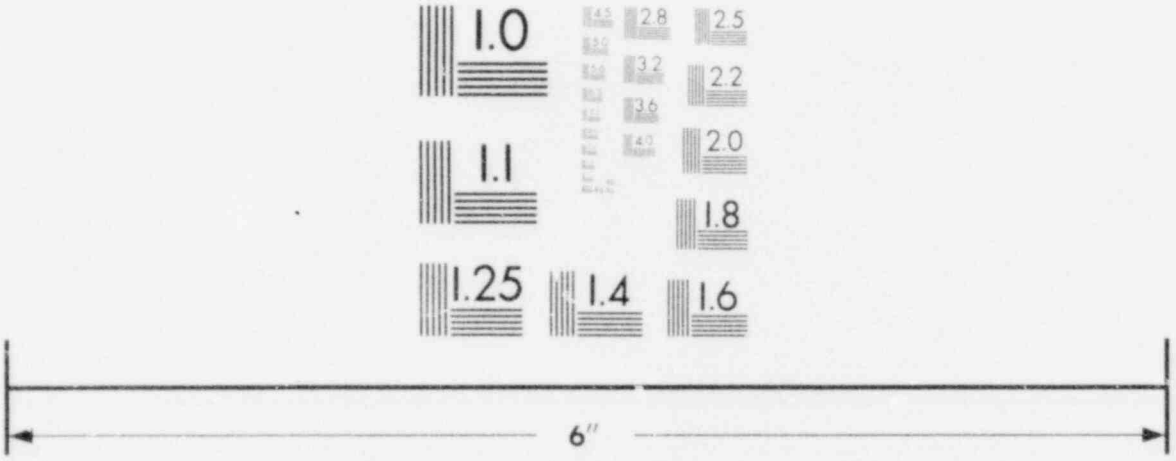

MICROCOPY RESOLUTION TEST CHART

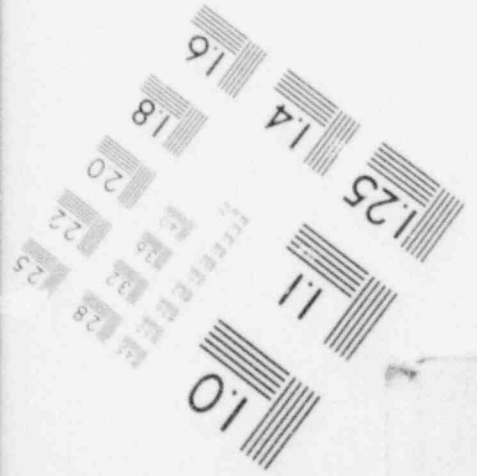

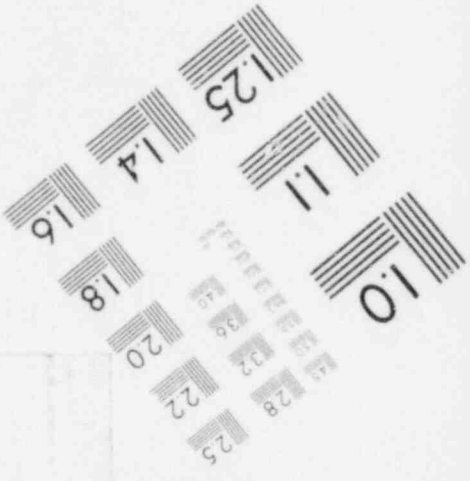

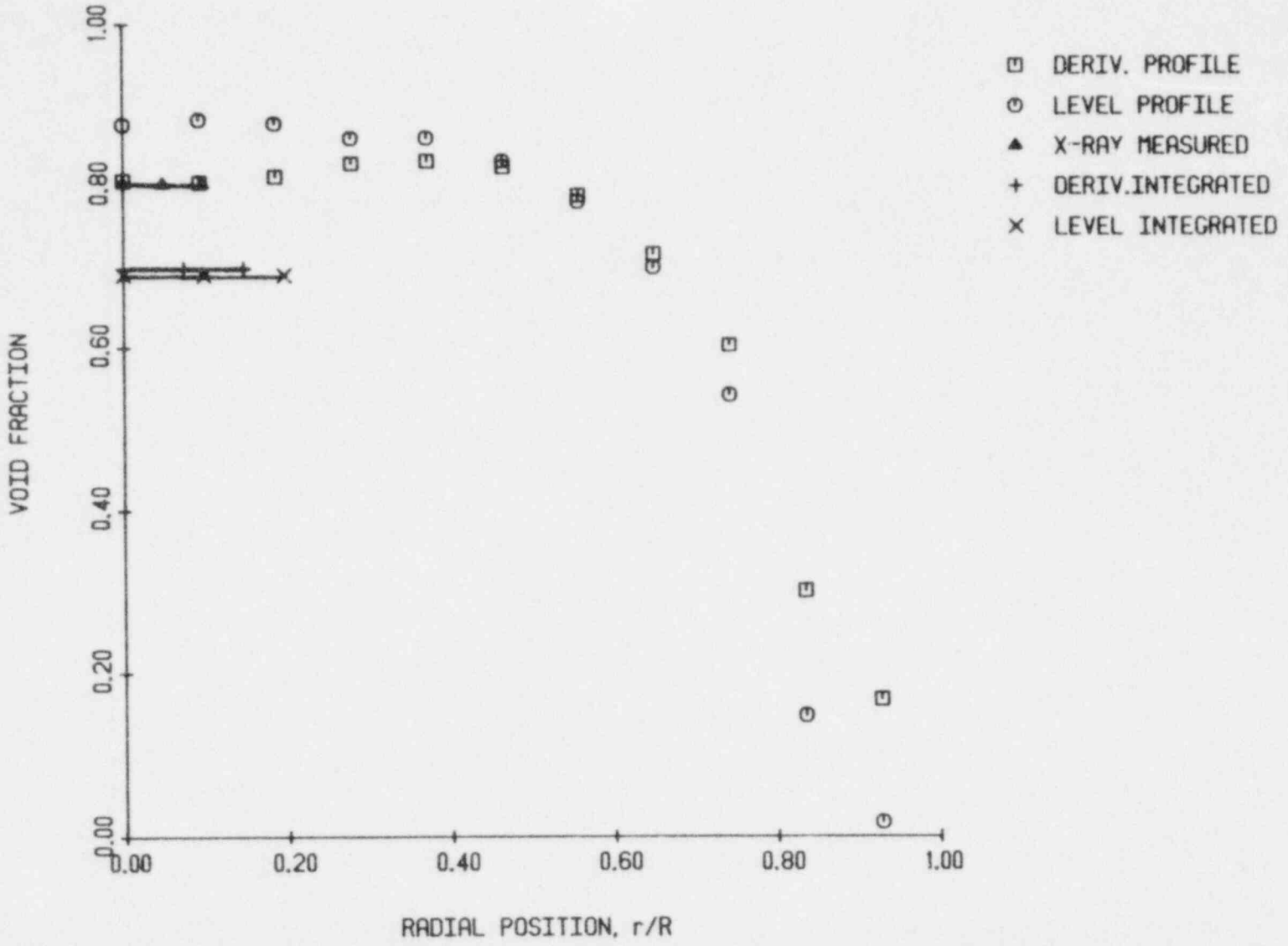

Figure 5.16 A comparison of the x-ray measured chordal void fraction and the integrated radial void profiles measured with the RF probe using level and derivative thresholding for j_ℓ=0.0 m/sec, j_g=2.21 m/sec

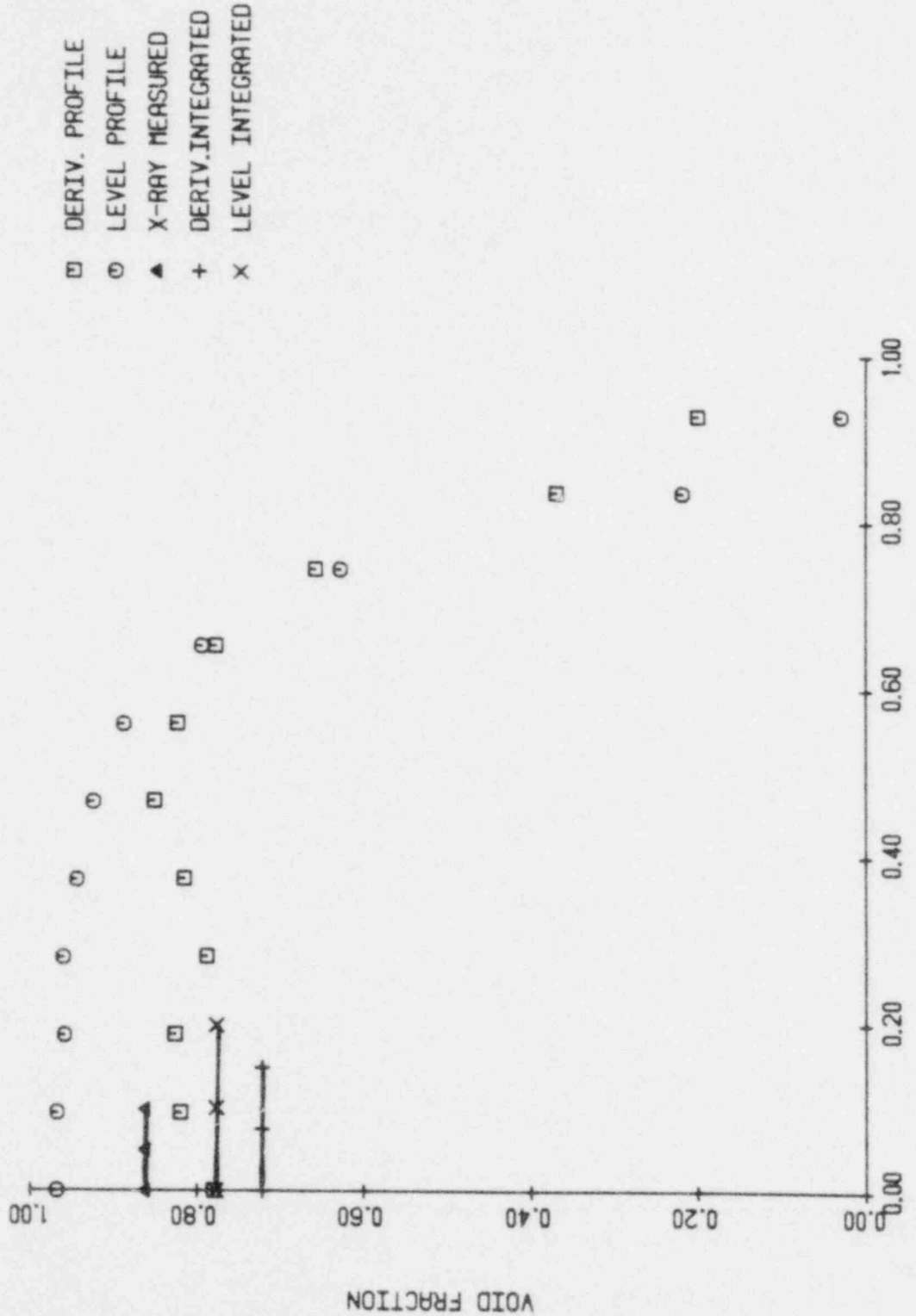

Figure 5.17 A comparison of the x-ray measured chordal void fraction and the integrated radial void profiles measured with the RF probe using level and derivative thresholding for j_ℓ=0.0 m/sec, j_g=4.57 m/sec

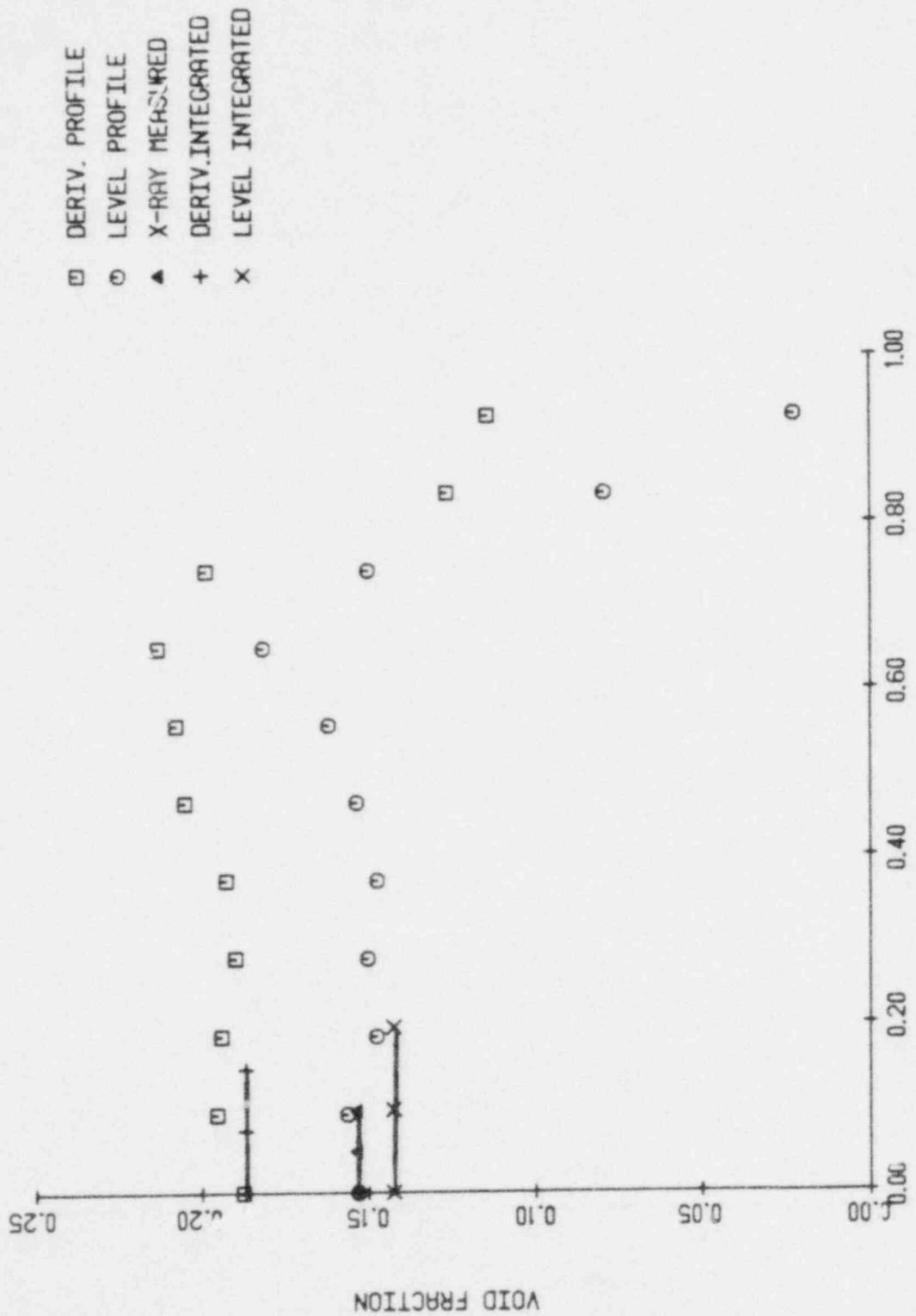

Figure 5.18 A comparison of the x-ray measured chordal void fraction and the integrated radial void profiles measured with the RF probe using level and derivative thresholding for j_ℓ=0.12 m/sec, j_g=0.046 m/sec

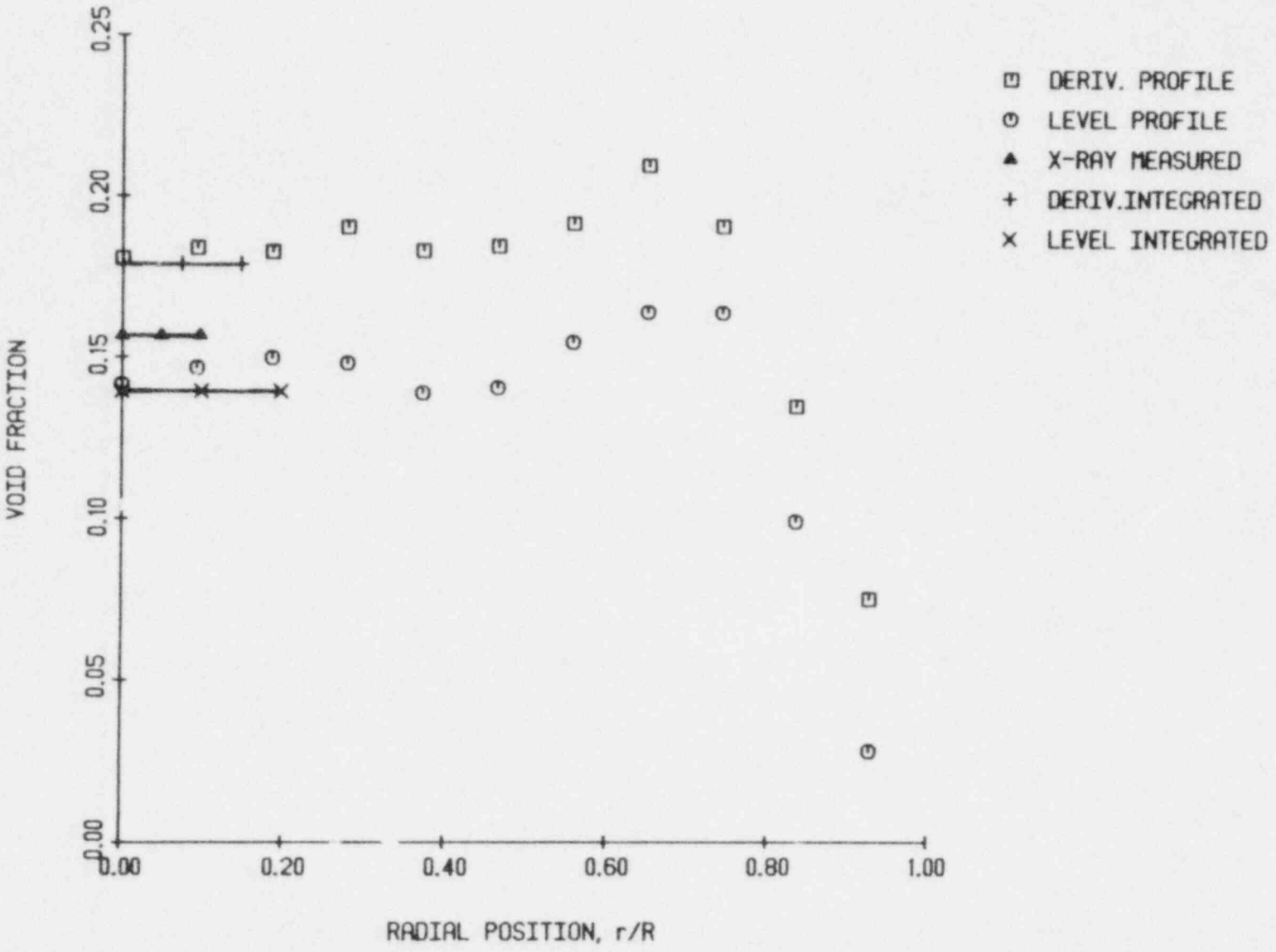

Figure 5.19 A comparison of the x-ray measured chordal void fraction and the integrated radial void profiles measured with the RF probe using level and derivative thresholding for j_ℓ=0.25 m/sec, j_g=0.073 m/sec

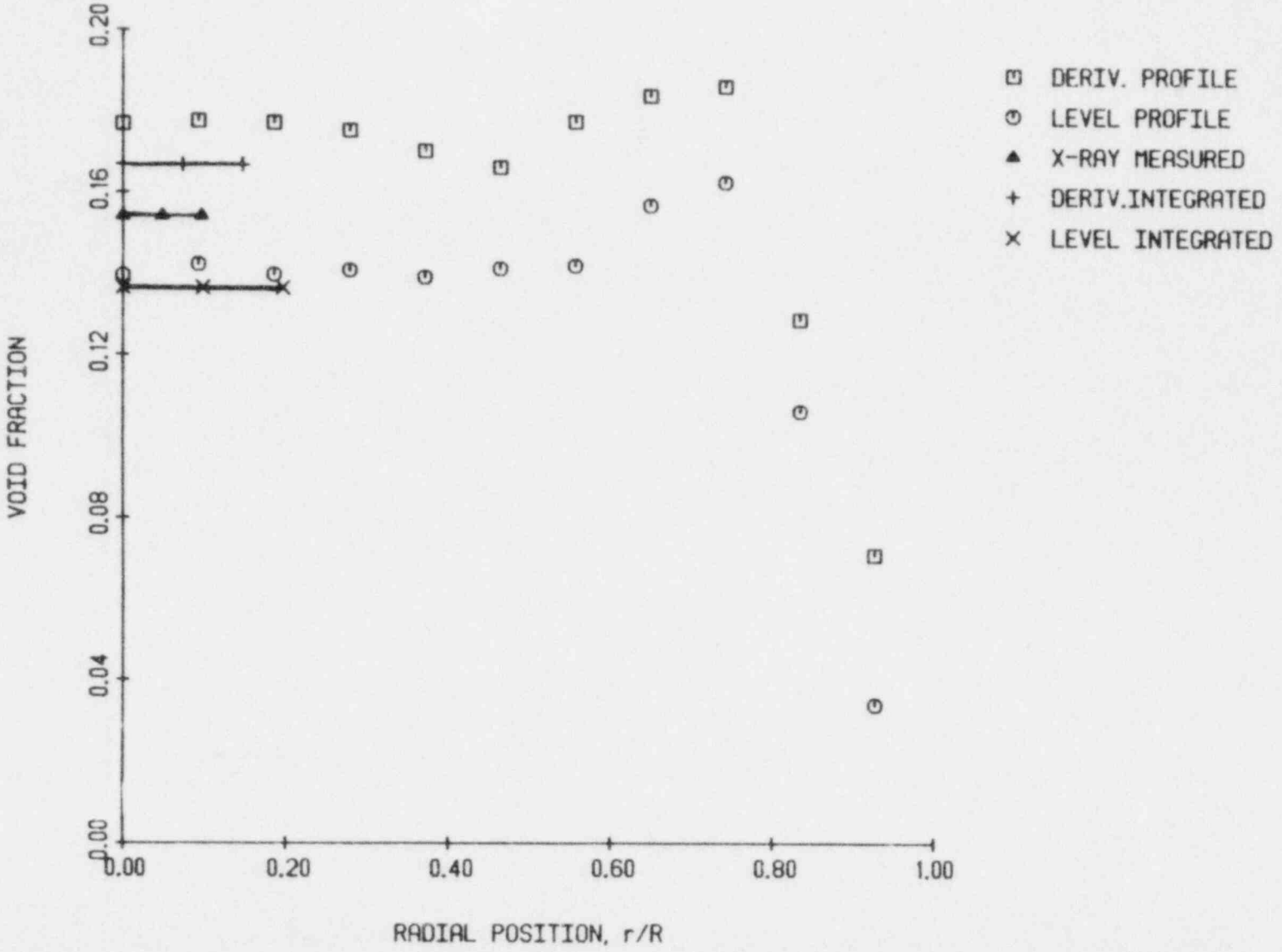

Figure 5.20 A comparison of the x-ray measured chordal void fraction and the integrated radial void profiles measured with the RF probe using level and derivative thresholding for j_ℓ=0.37 m/sec, j_g=0.097 m/sec

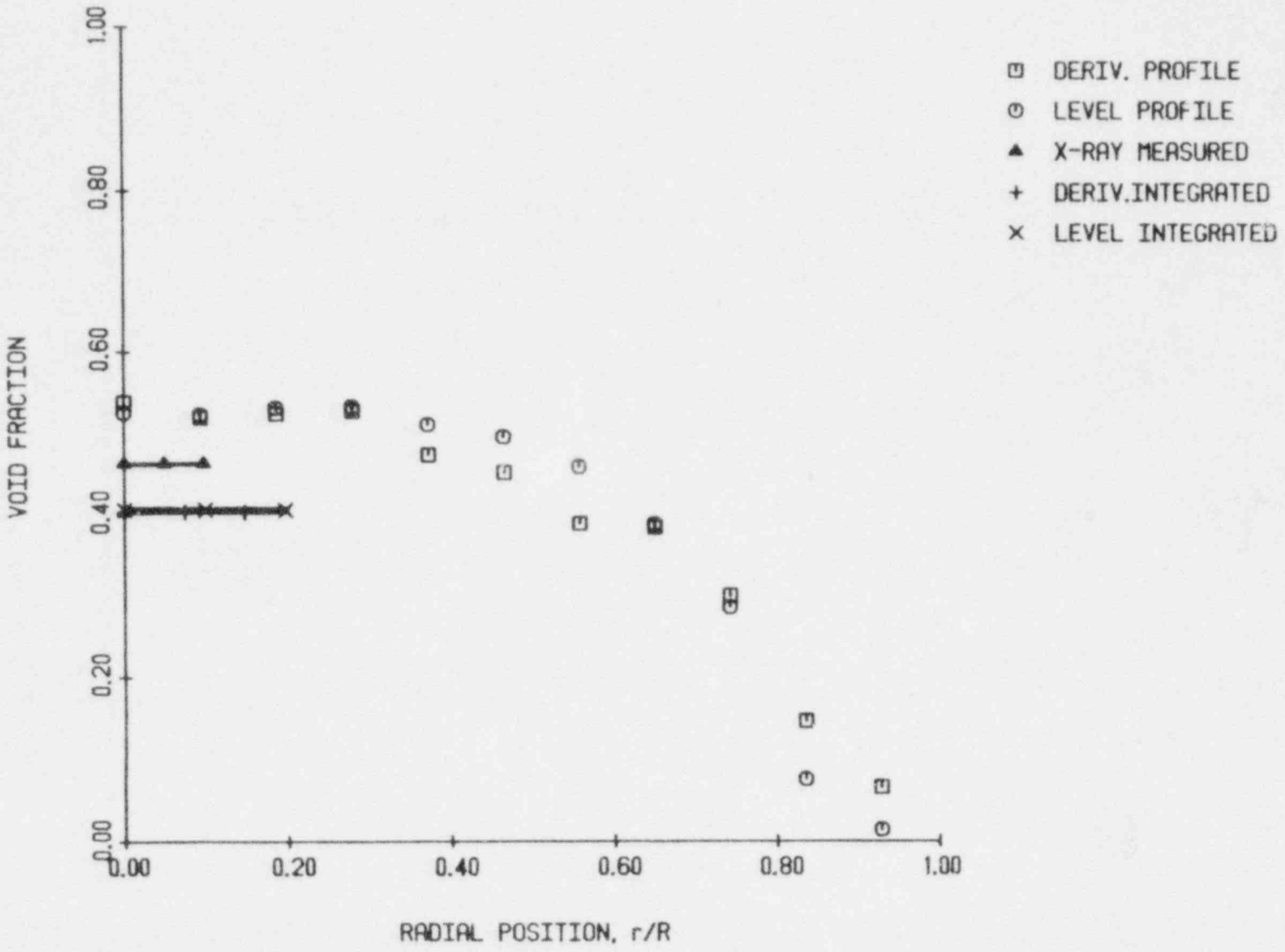

Figure 5.22 A comparison of the x-ray measured chordal void fraction and the integrated radial void profiles measured with the RF probe using level and derivative thresholding for j_ℓ=0.'_ m/sec, j_g=0.301 m/sec

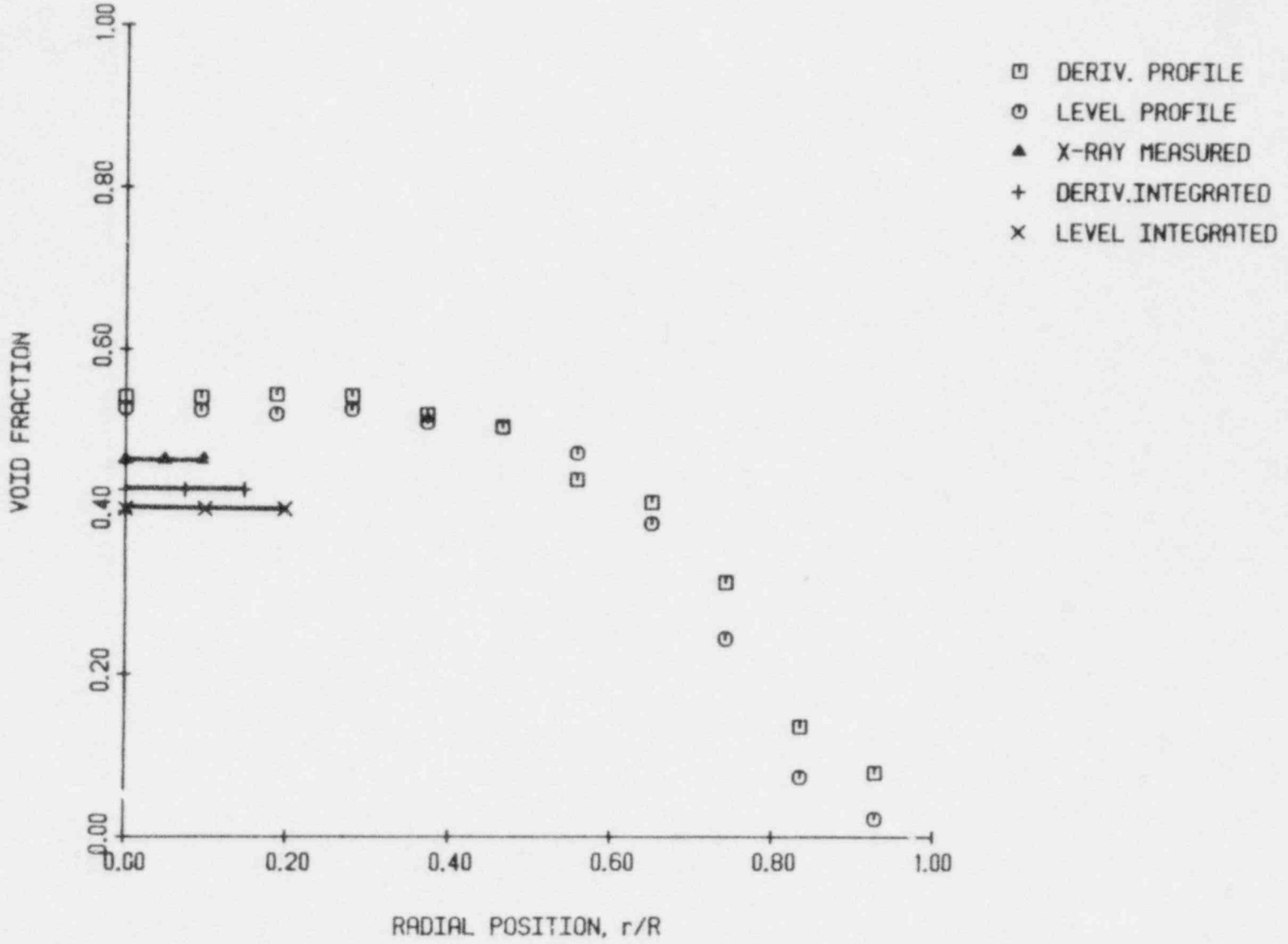

Figure 5.23 A comparison of the x-ray measured chordal void fraction and the integrated radial void profiles measured with the RF probe using level and derivative thresholding for j_ℓ=0.25 m/sec, j_g=0.402 m/sec

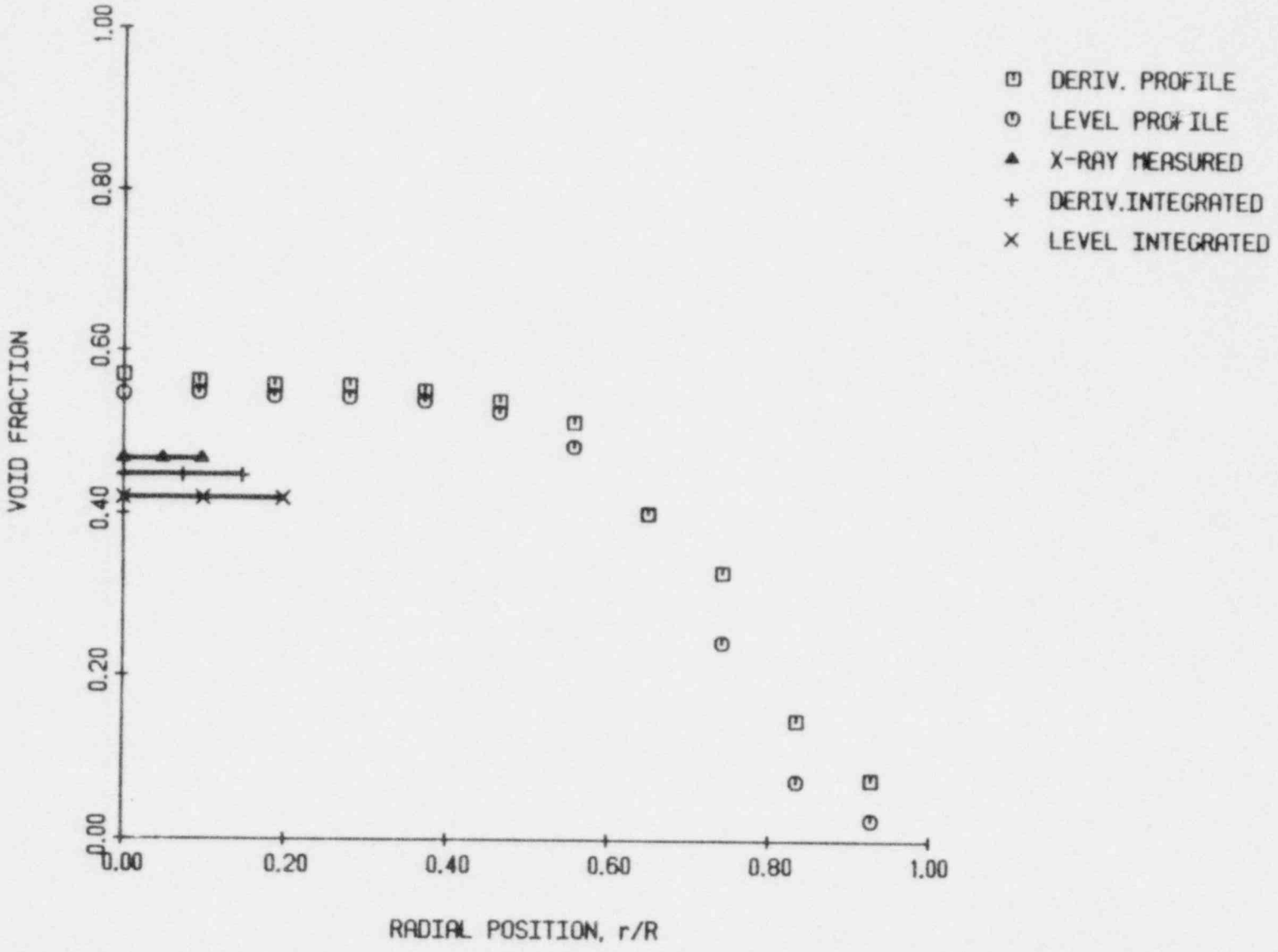

Figure 5.24 A comparison of the x-ray measured chordal void fraction and the integrated radial void profiles measured with the RF probe using level and derivative thresholding for j_ℓ=0.37 m/sec, j_g=0.552 m/sec

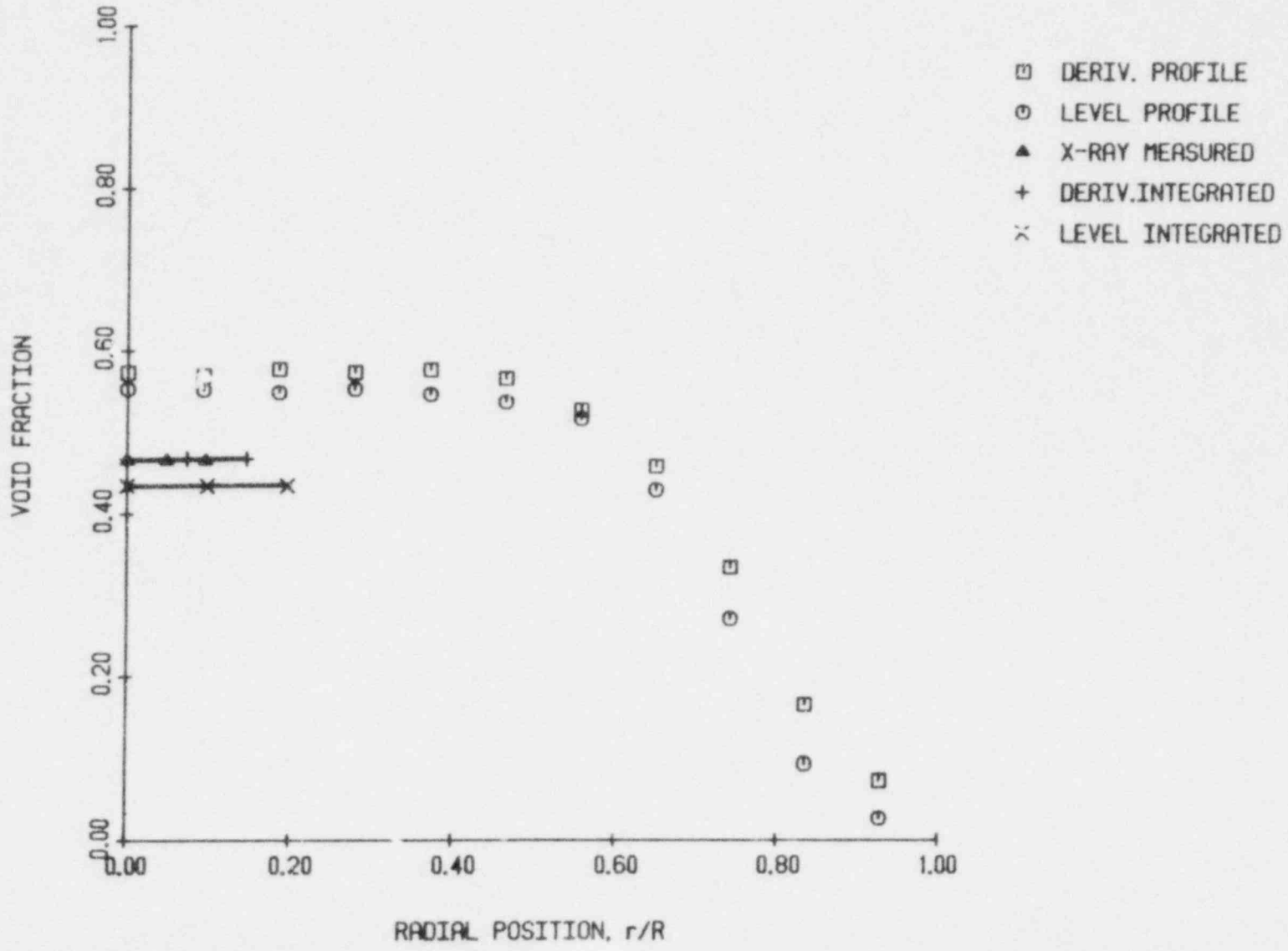

Figure 5.25 A comparison of the x-ray measured chordal void fraction and the integrated radial void profiles measured with the RF probe using level and derivative thresholding for j_ℓ=0.50 m/sec, j_g=0.704 m/sec

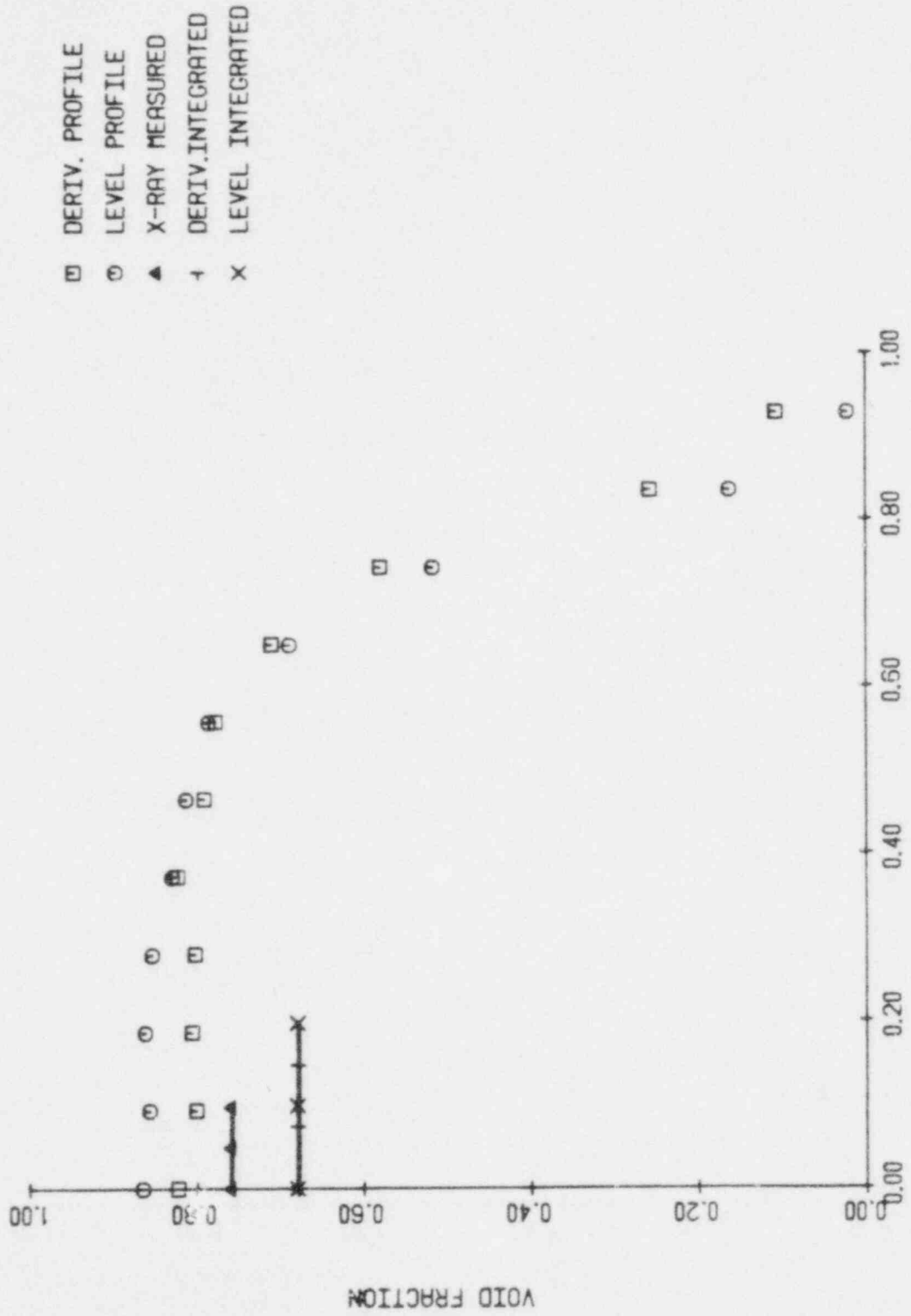

Figure 5.26 A comparison of the x-ray measured chordal void fraction and the integrated radial void profiles measured with the RF probe using level and derivative thresholding for j_ℓ=0.12 m/sec, j_g=1.67 m/sec

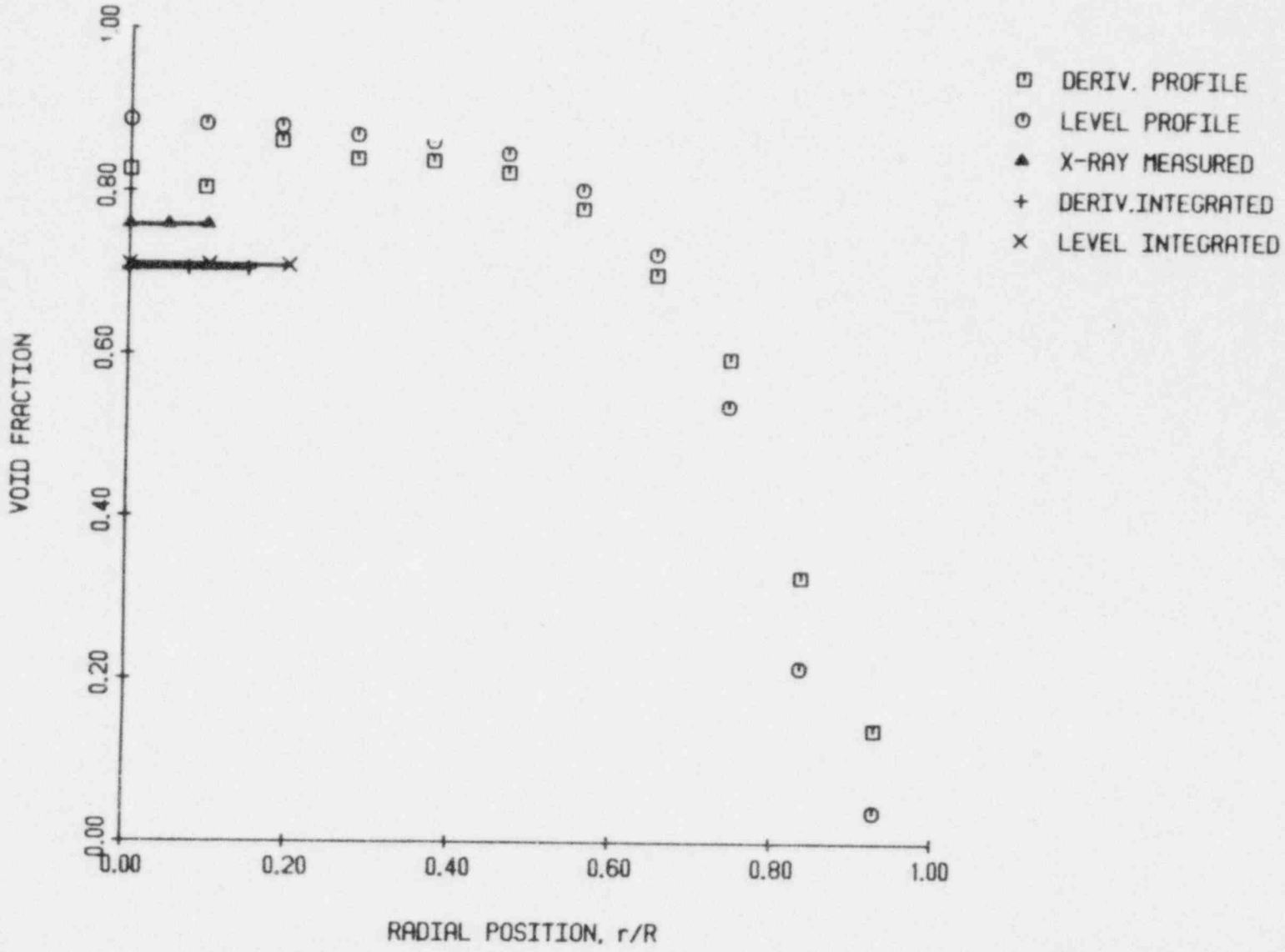

Figure 5.27 A comparison of the x-ray measured chordal void fraction and the integrated radial void profiles measured with the RF probe using level and derivative thresholding for j_ℓ=0.25 m/sec, j_g=2.67 m/sec

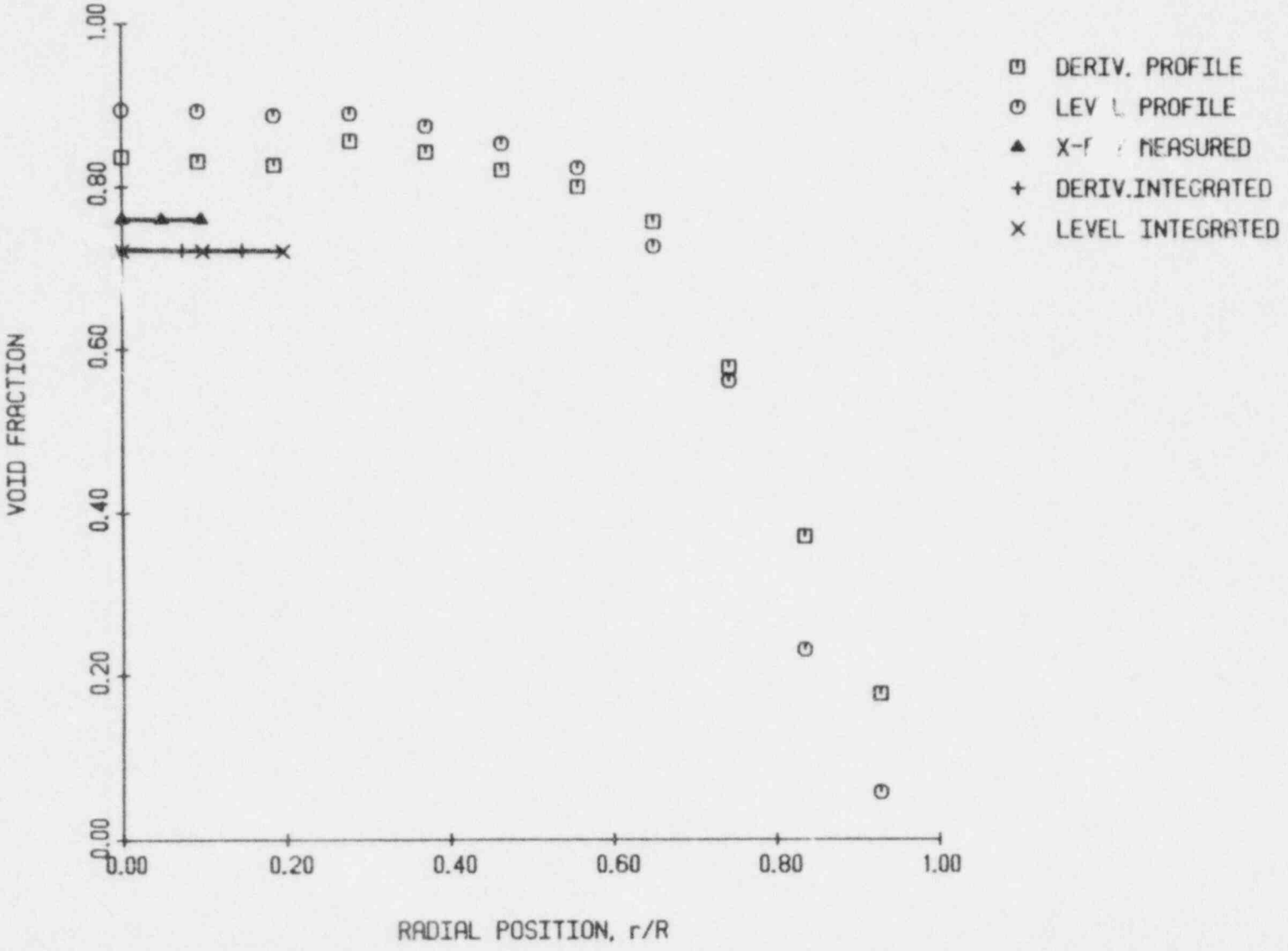

Figure 5.28 A comparison of the x-ray measured chordal void fraction and the integrated radial void rpfiles measured with the RF probe using level and derivative thresholding for j_ℓ=0.37 m/sec, j_g=3.41 m/sec

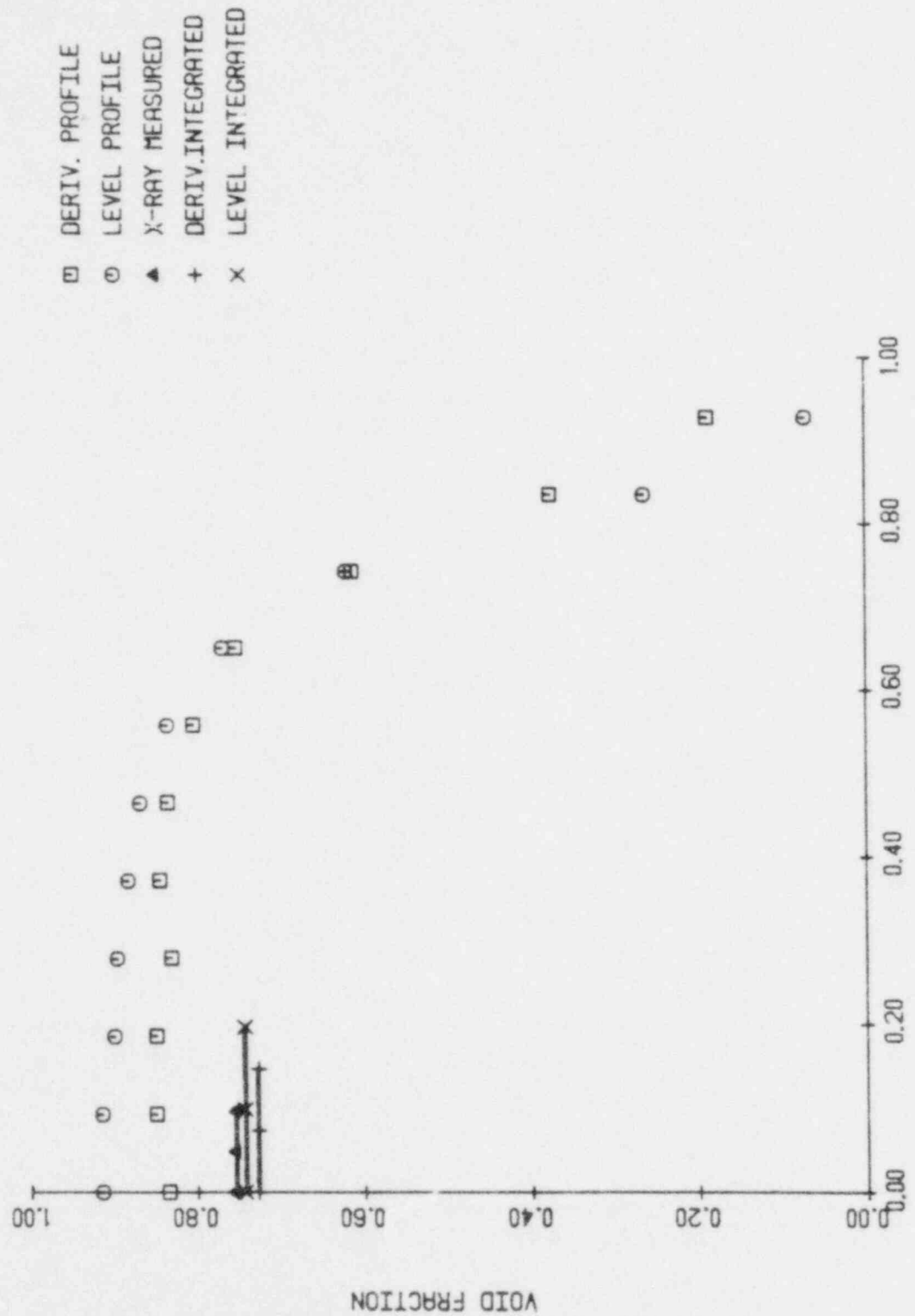

Figure 5.29 A comparison of the x-ray measured chordal void fraction and the integrated radial void profiles measured with the KF probe using level and derivative thresholding for j_ℓ=0.50 m/sec, j_g=4.24 m/sec

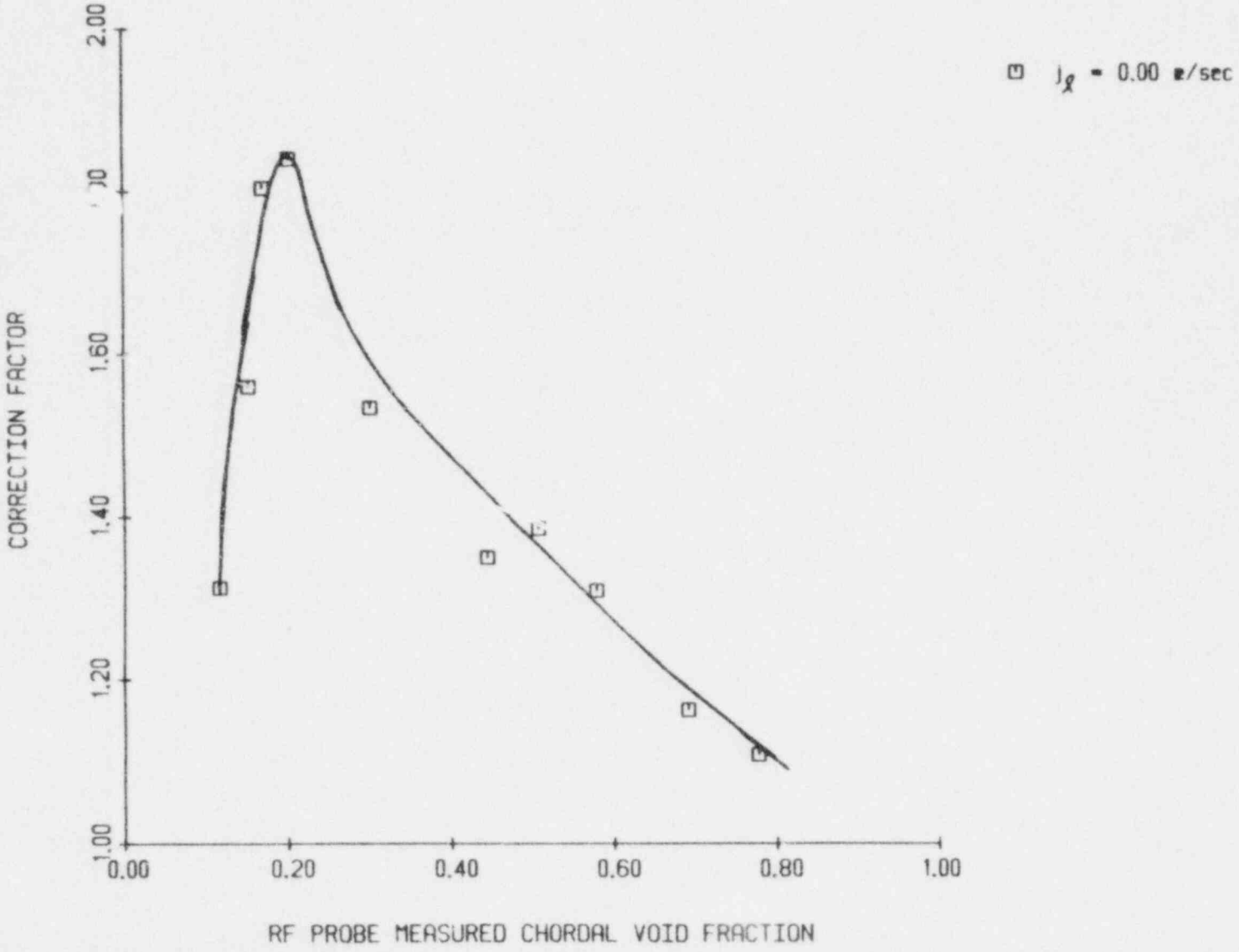

Figure 5.30 Level thresholding calibration curve for RF probe at j_g = 0.0 m/sec

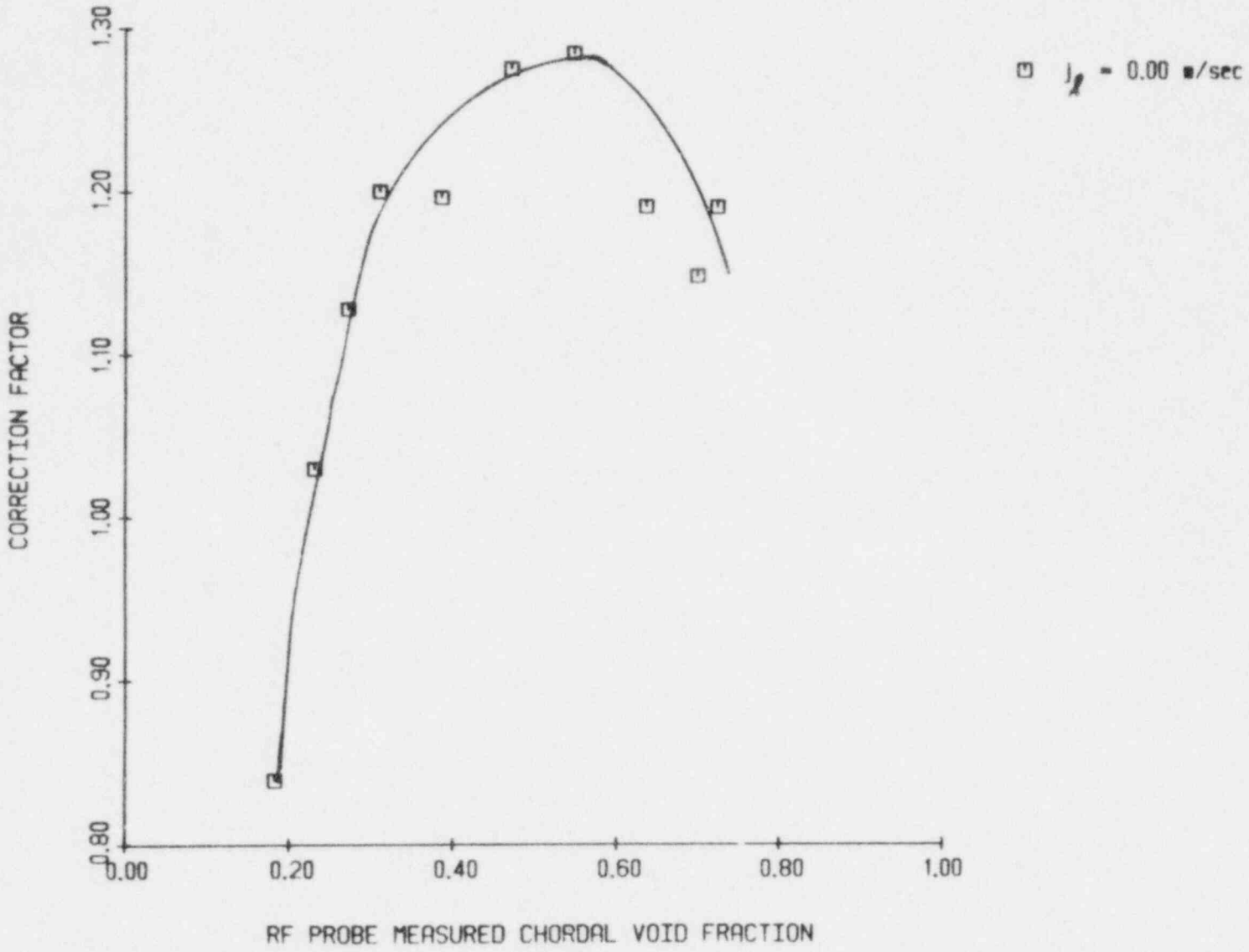

Figure 5.31 Derivative thresholding calibration curve for RF probe at J_ℓ = 0.0 m/sec

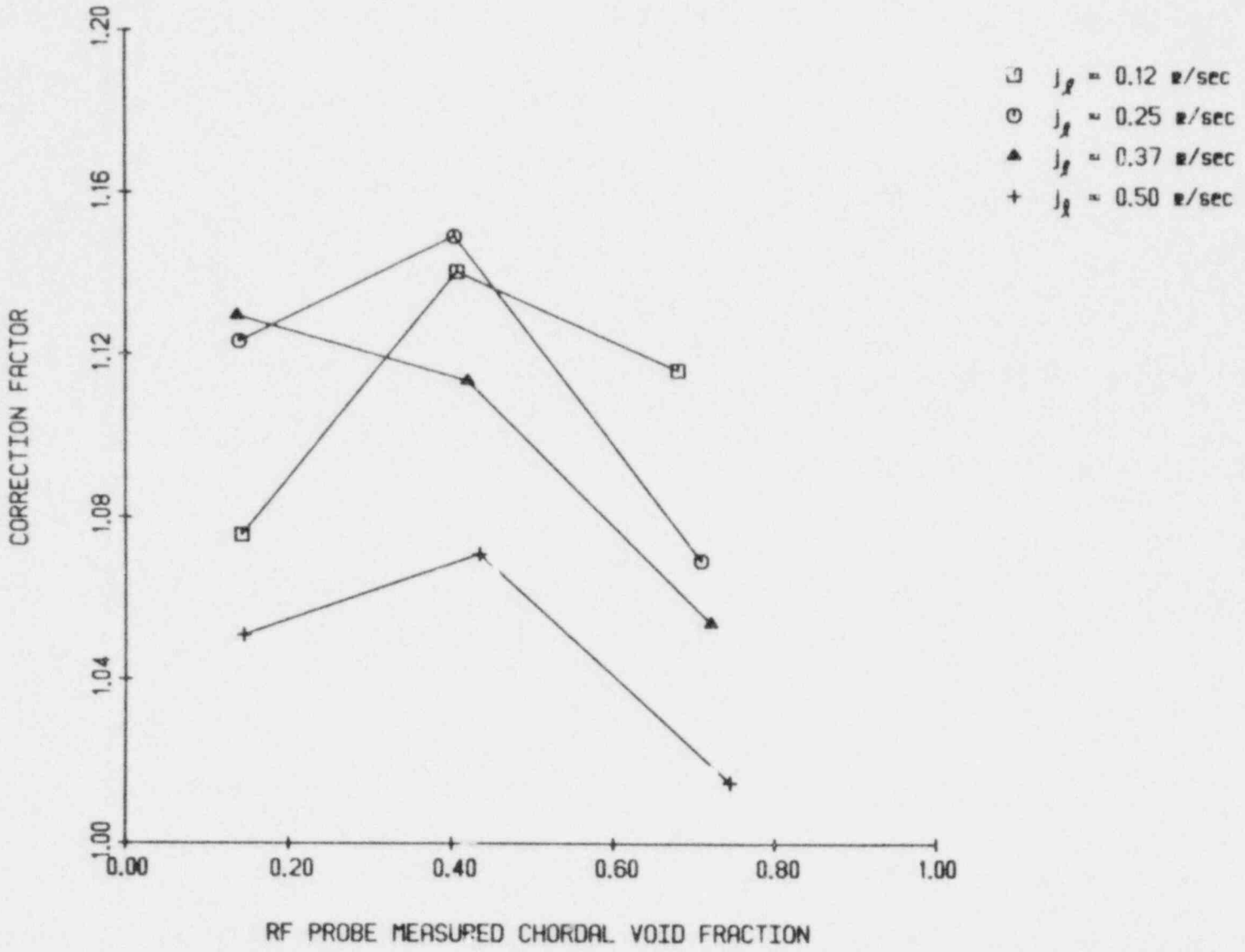

Figure 5.32 Level thresholding calibration curve for RF probe at non zero j_ℓ

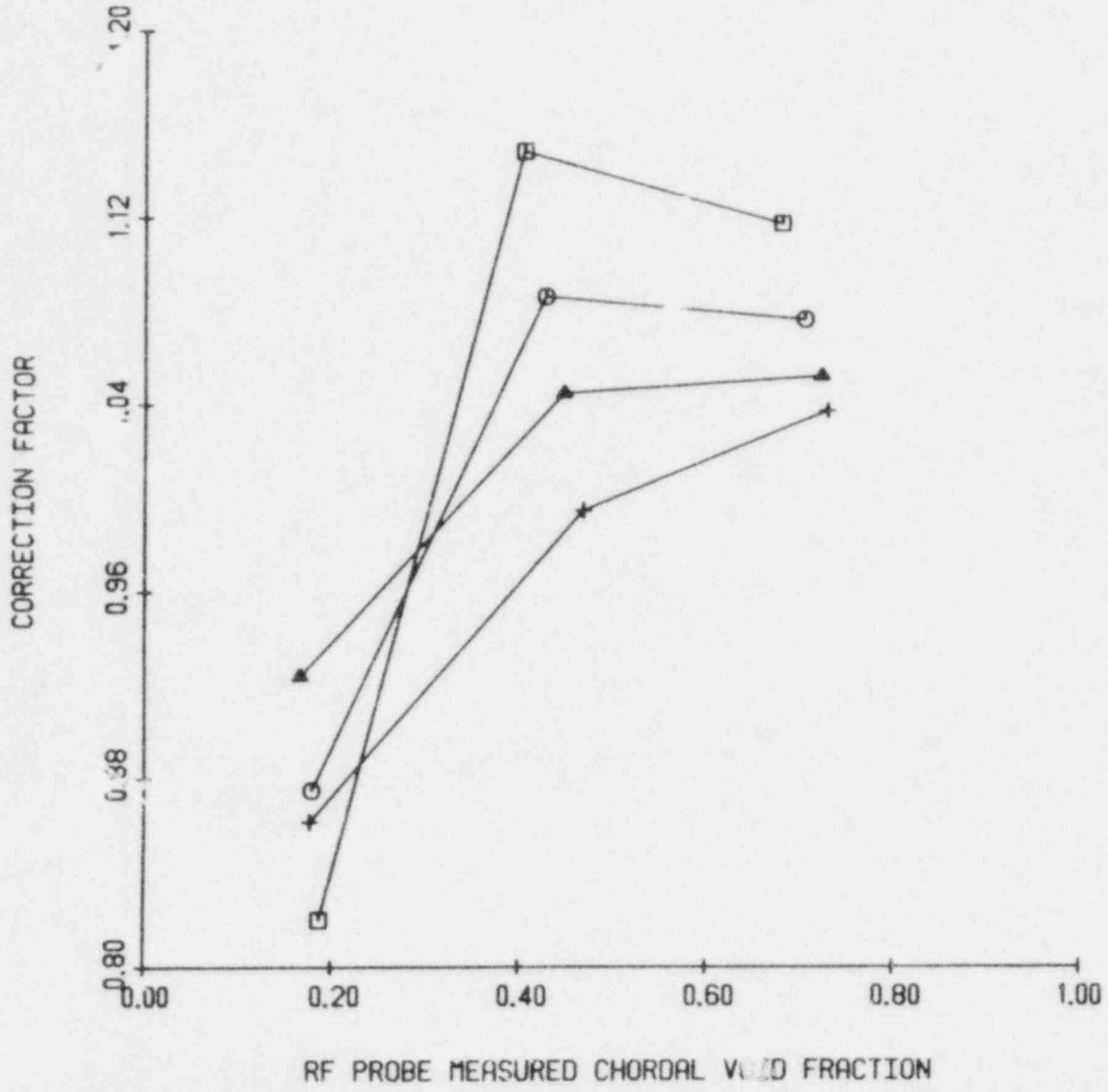

Figure 5.33 Derivative thresholding calibration curve for RF probe at non zero j_ℓ

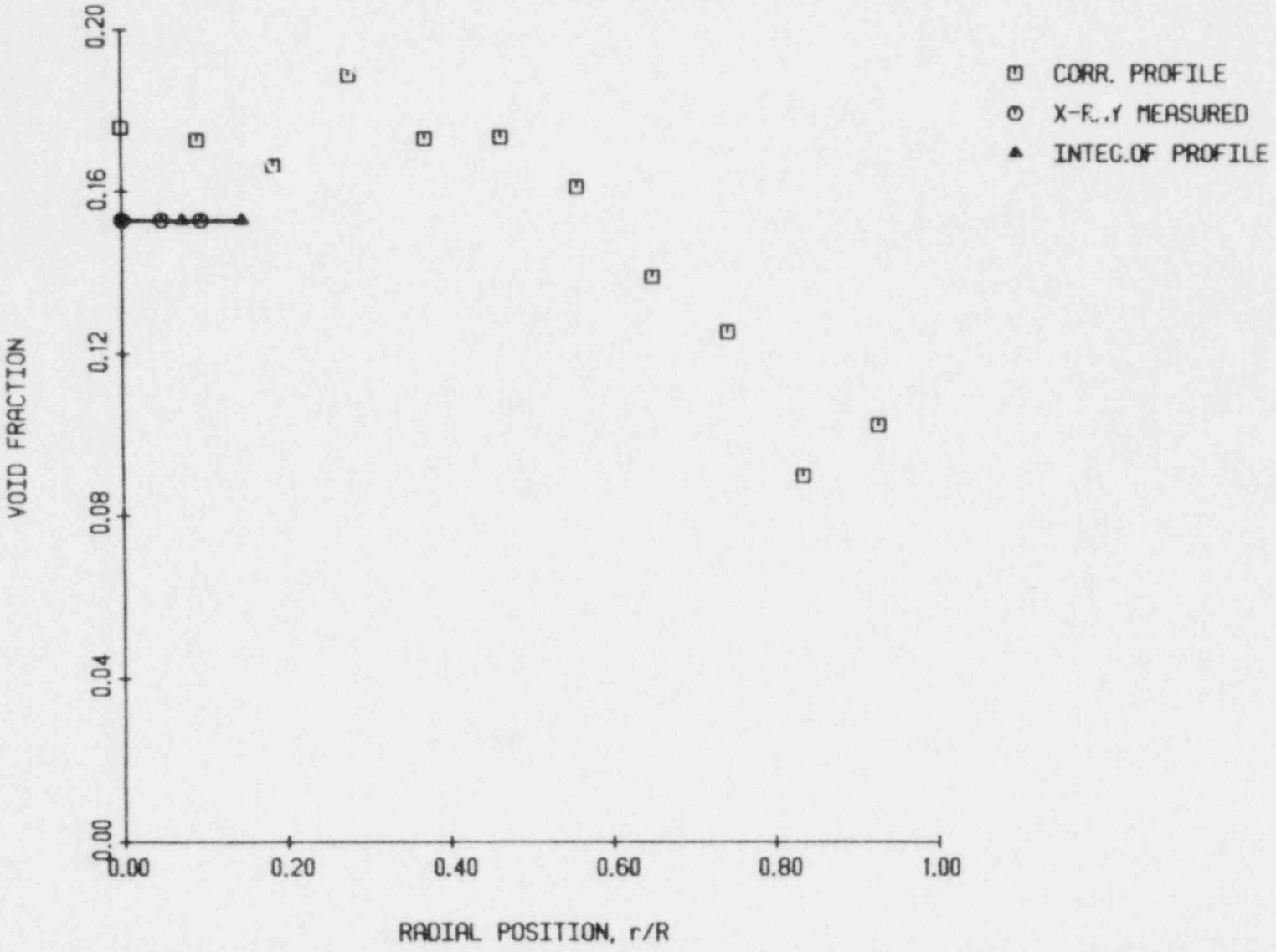

Figure 5.34 Corrected RF probe profiles taken with derivative thresholding for j_ℓ=0.00 ■/sec, j_g=0.023 ■/sec

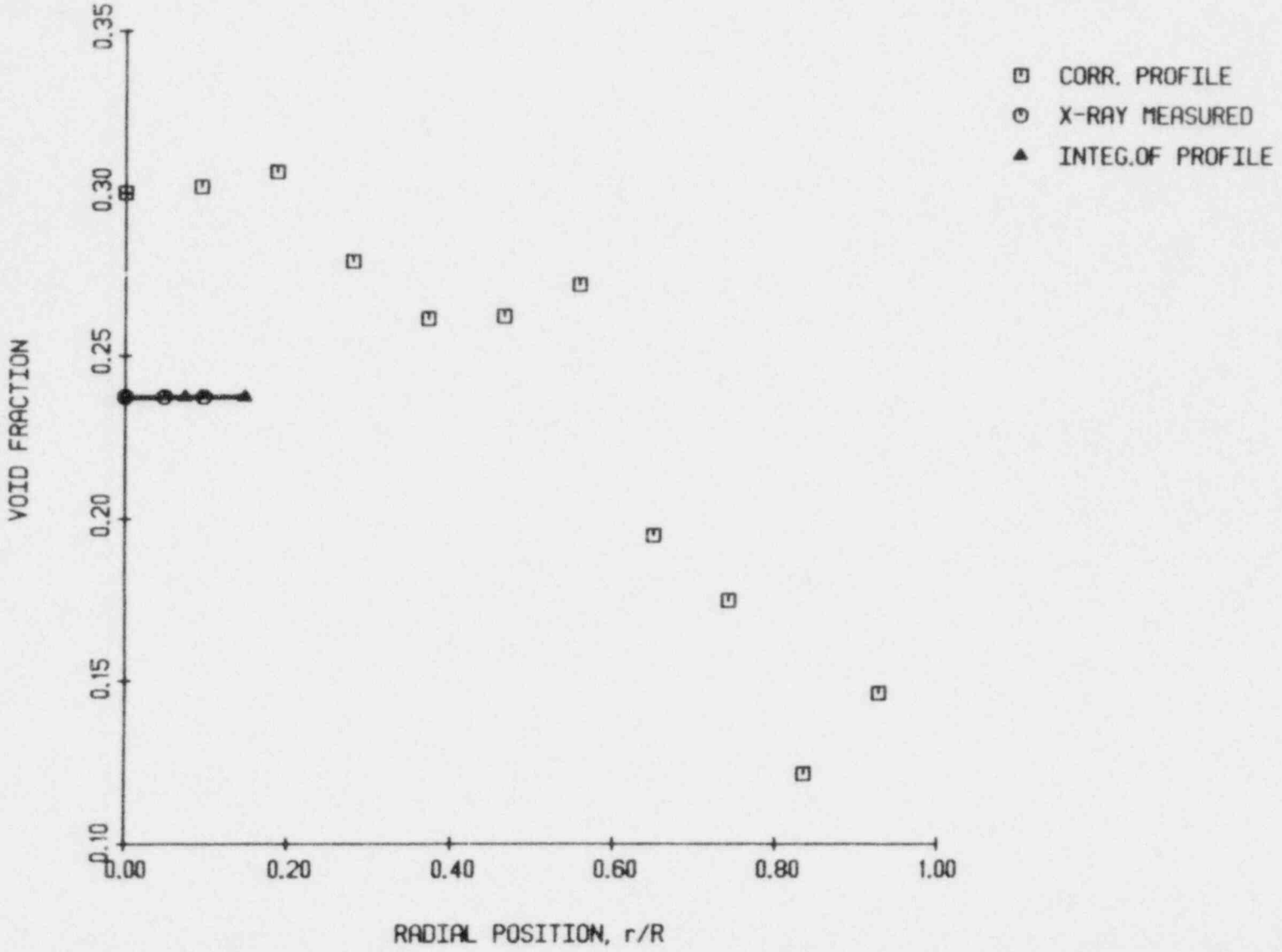

Figure 5.35 Corrected RF probe profiles taken with derivative thresholding for J_ℓ=0.00 ■/sec, J_g=0.044 ■/sec

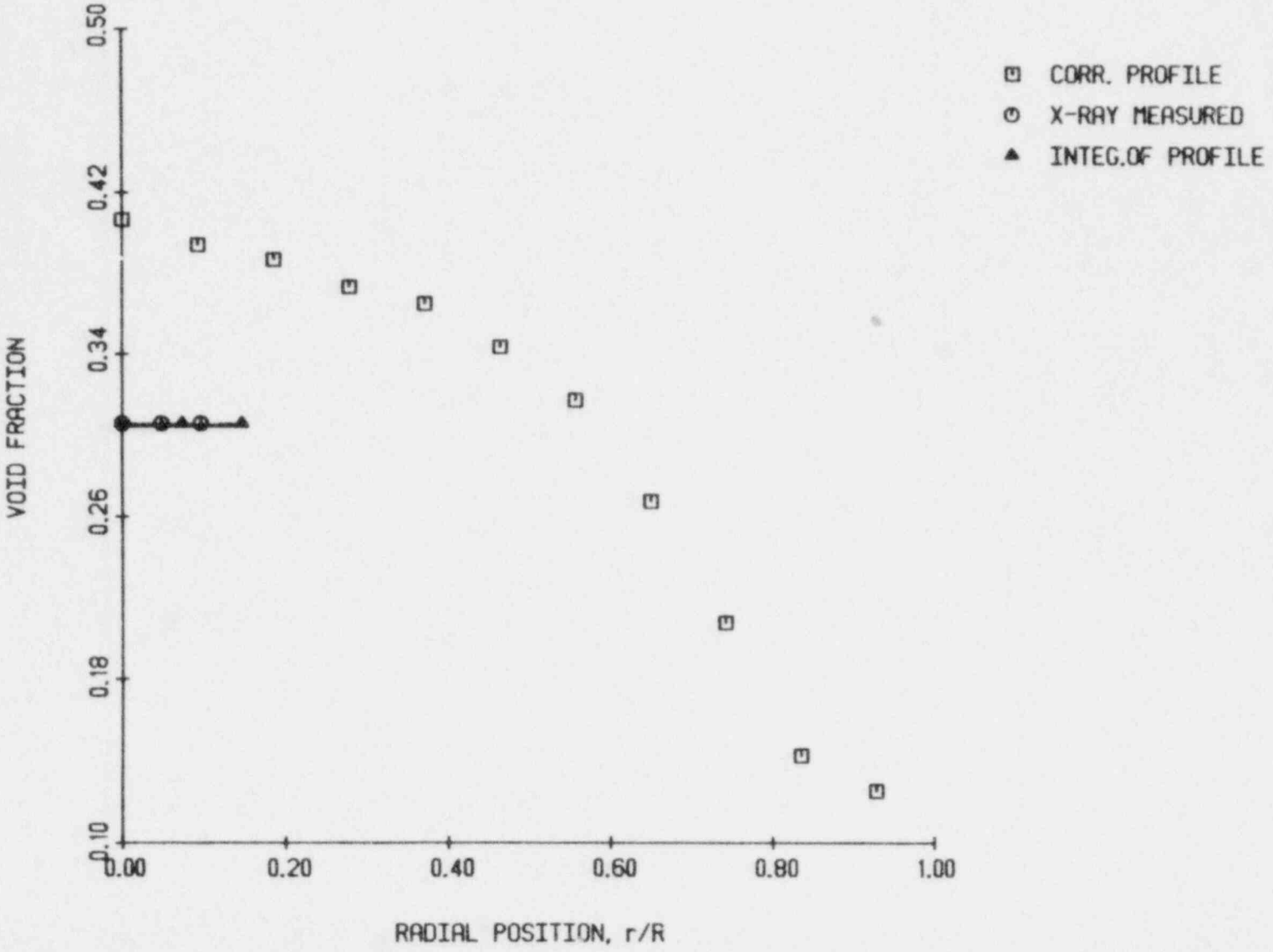

Figure 5.36 Corrected RF probe profiles taken with derivative thresholding for j_g =0.00 ■/sec, j_g =0.075 ■/sec

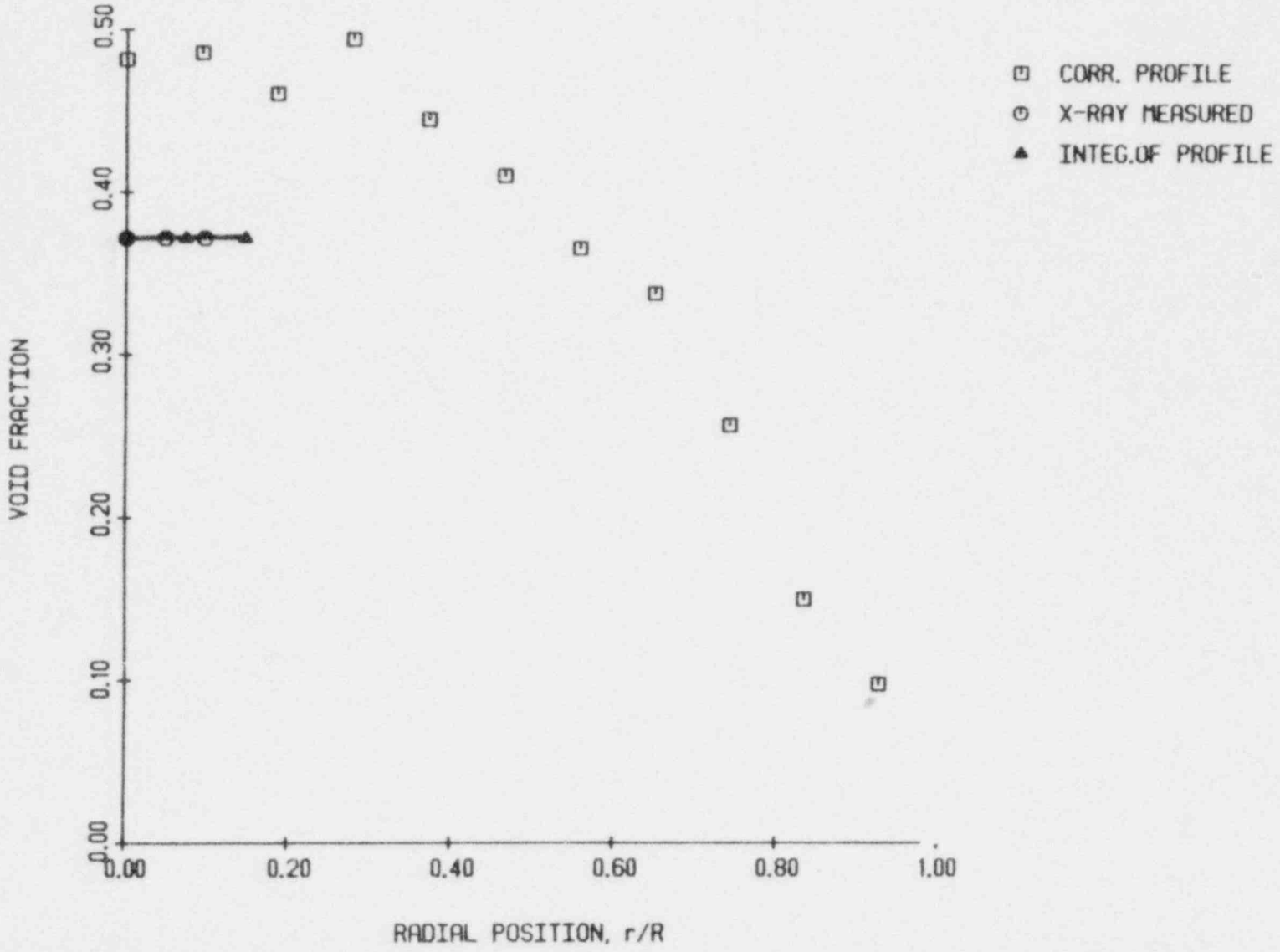

Figure 5.37 Corrected RF probe profiles taken with derivative thresholding for j_ℓ=0.00 m/sec, j_g=0.109 m/sec

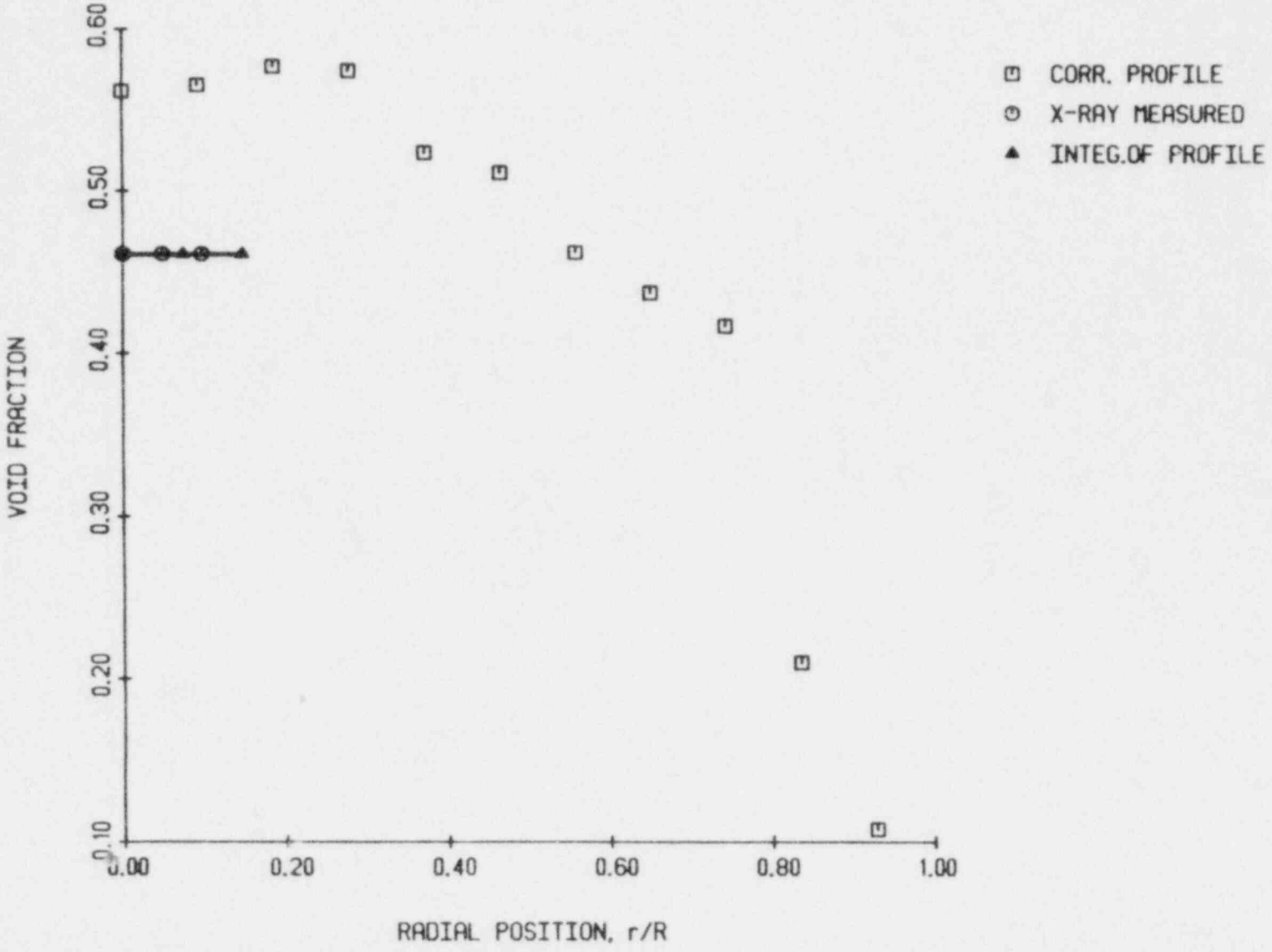

Figure 5.38 Corrected RF probe profiles taken with derivative thresholding for J_ℓ =0.00 m/sec, J_g =0.184 m/sec

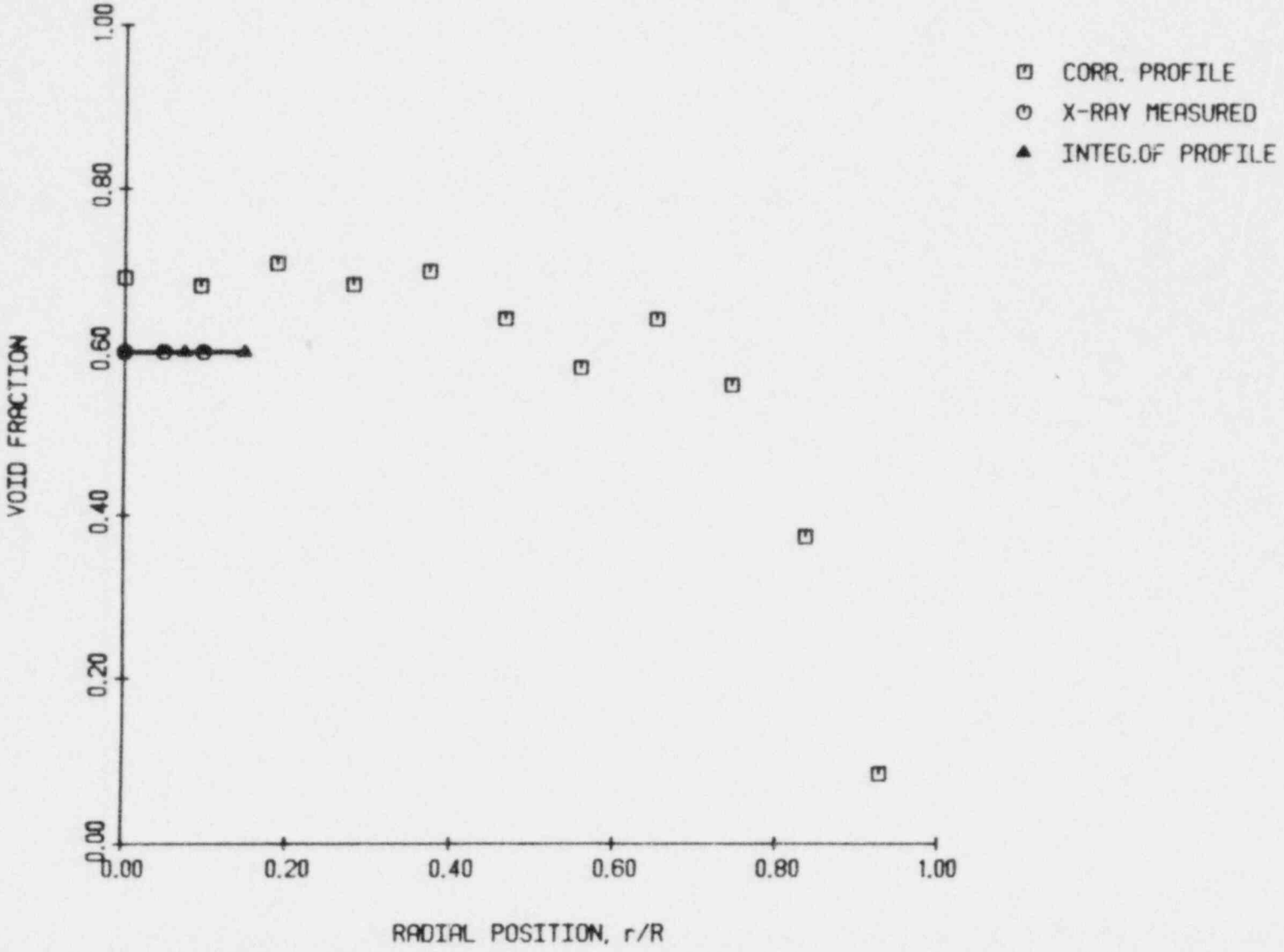

Figure 5.39 Corrected RF probe profiles taken with derivative thresholding for j_ℓ =0.00 m/sec, j_g =0.311 m/sec

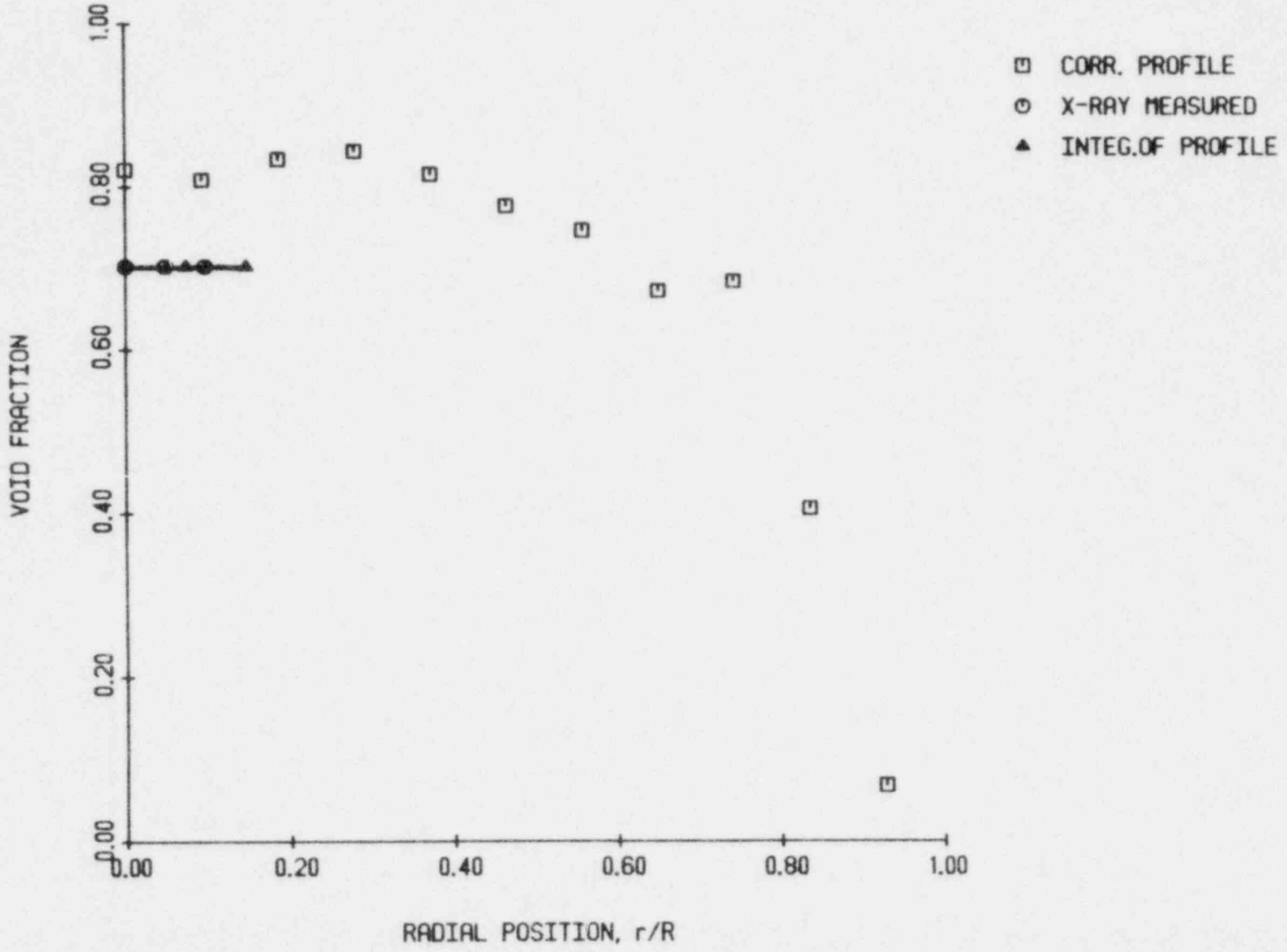

Figure 5.40 Corrected RF probe profiles taken with derivative thresholding for j_ℓ =0.00 ■/sec, j_g=0.509 ■/sec

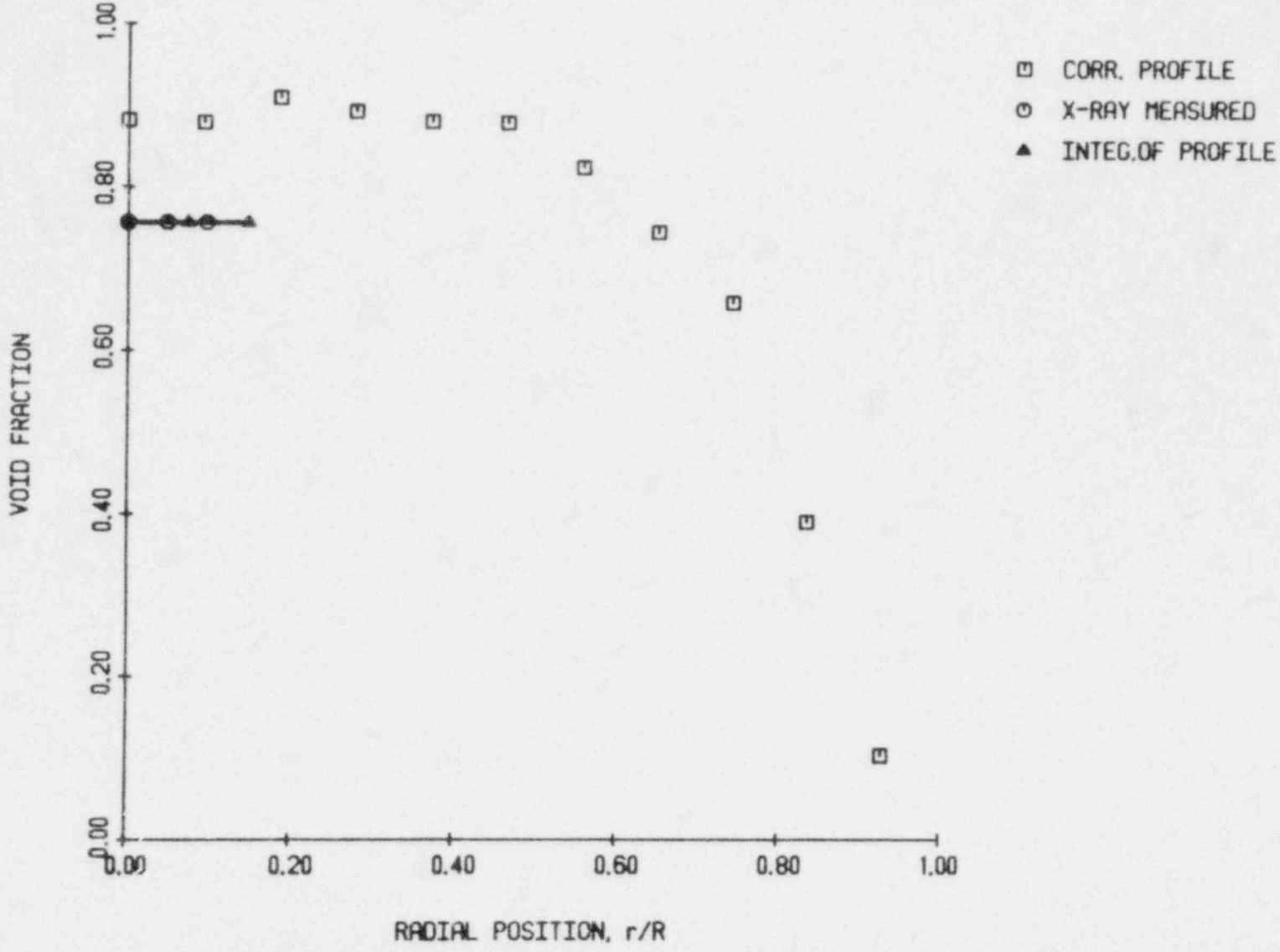

Figure 5.41 Corrected RF probe profiles taken with derivative thresholding for j_ℓ=0.00 m/sec, j_g=0.981 m/sec

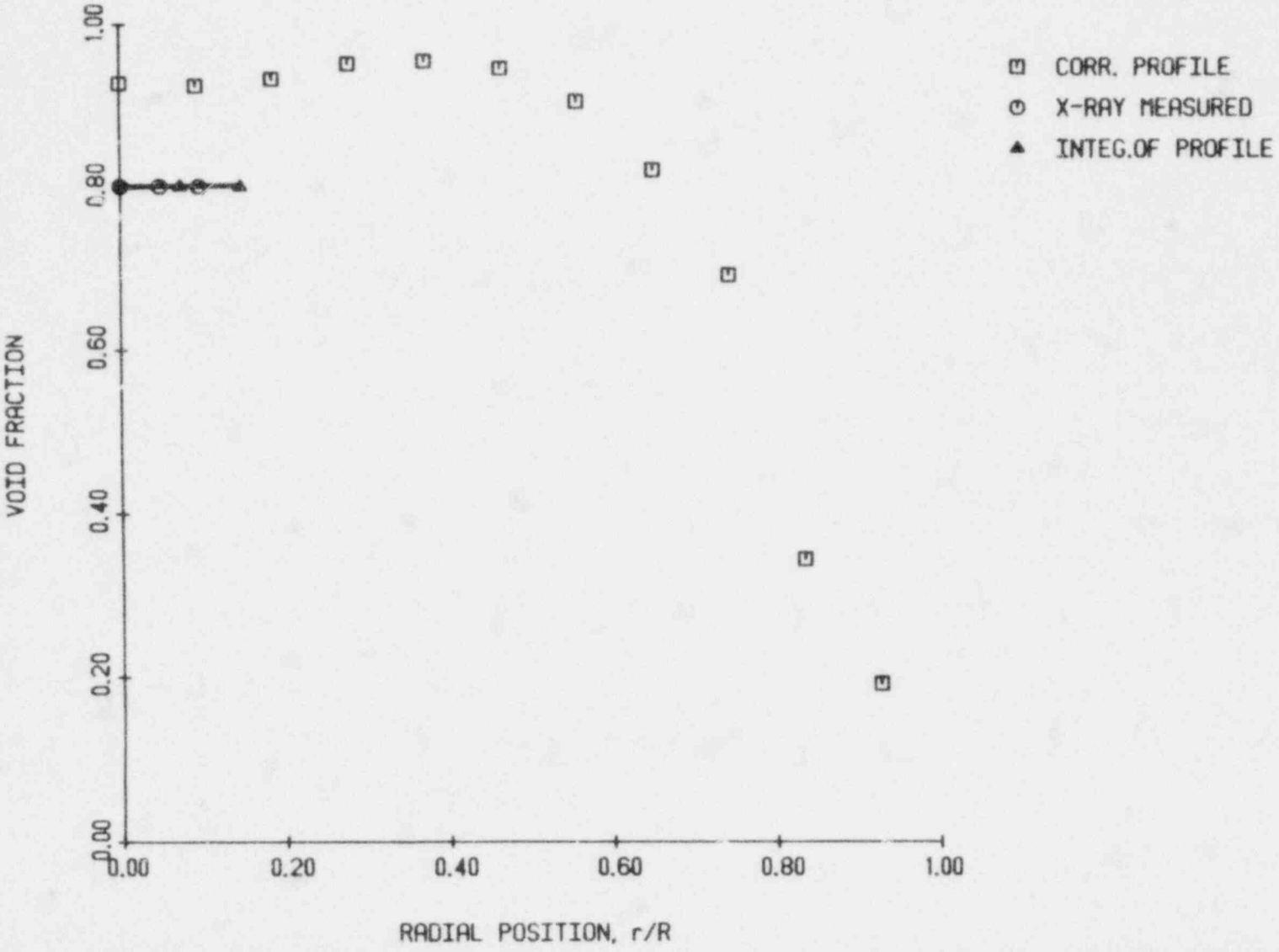

Figure 5.42 Corrected RF probe profiles taken with derivative thresholding for J_g =0.00 ■/sec, J_g =2.21 ■/sec

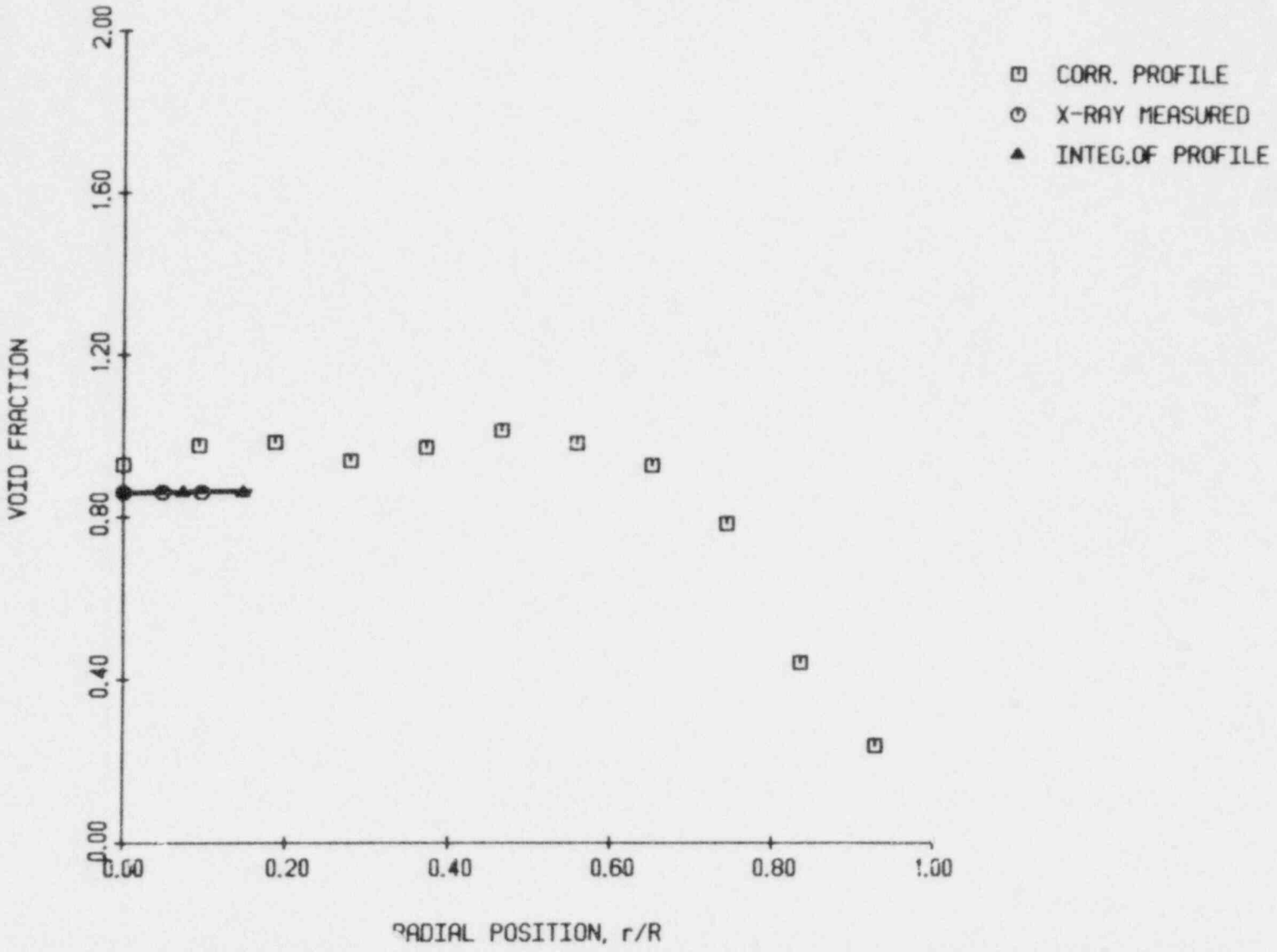

Figure 5.43 Corrected RF probe profiles taken with derivative thresholding for j_ℓ =0.00 m/sec, j_g =4.57 m/sec

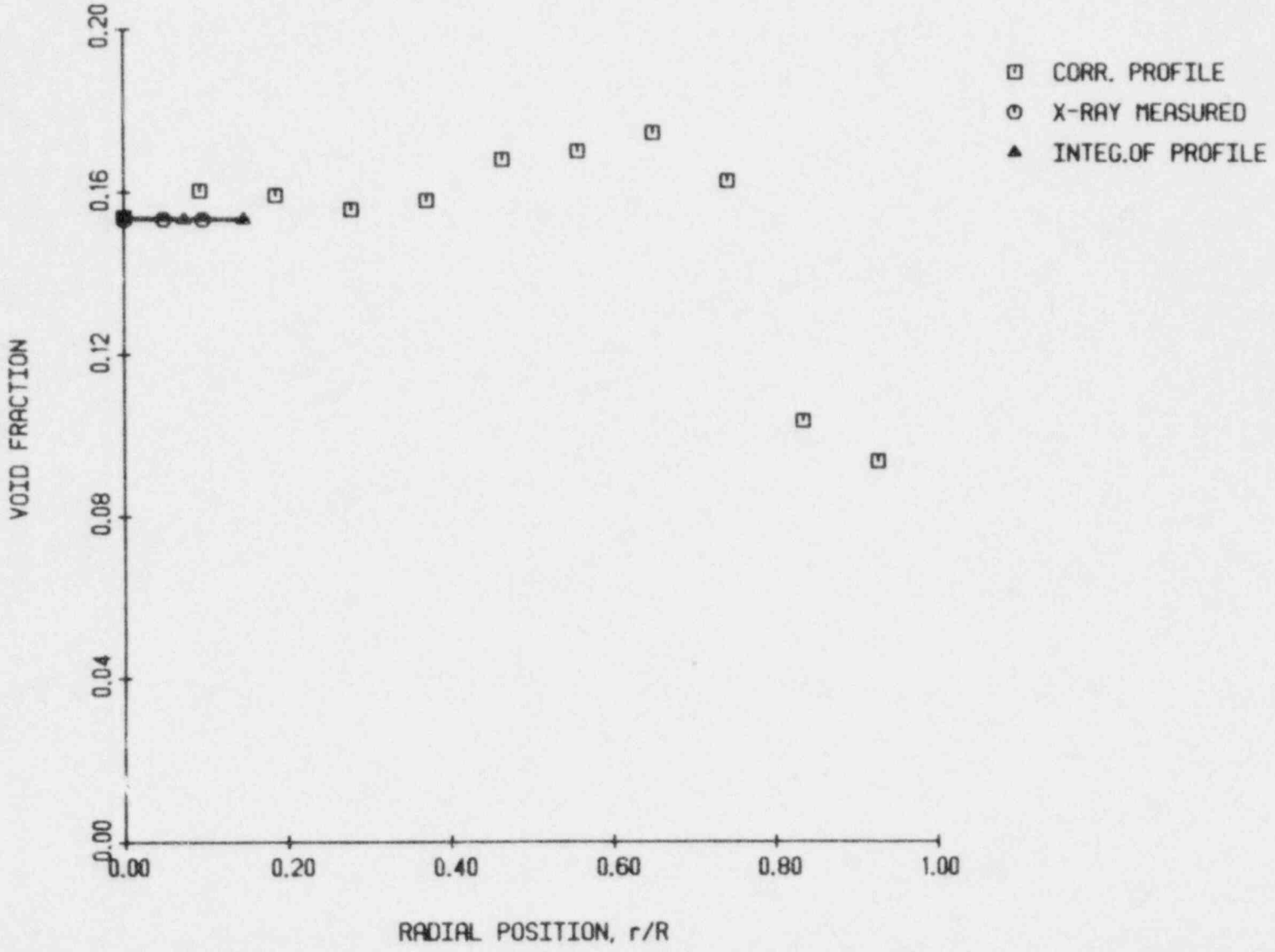

Figure 5.44 Corrected RF probe profiles taken with derivative thresholding for j_ℓ=0.12 m/sec, j_g=0.046 m/sec

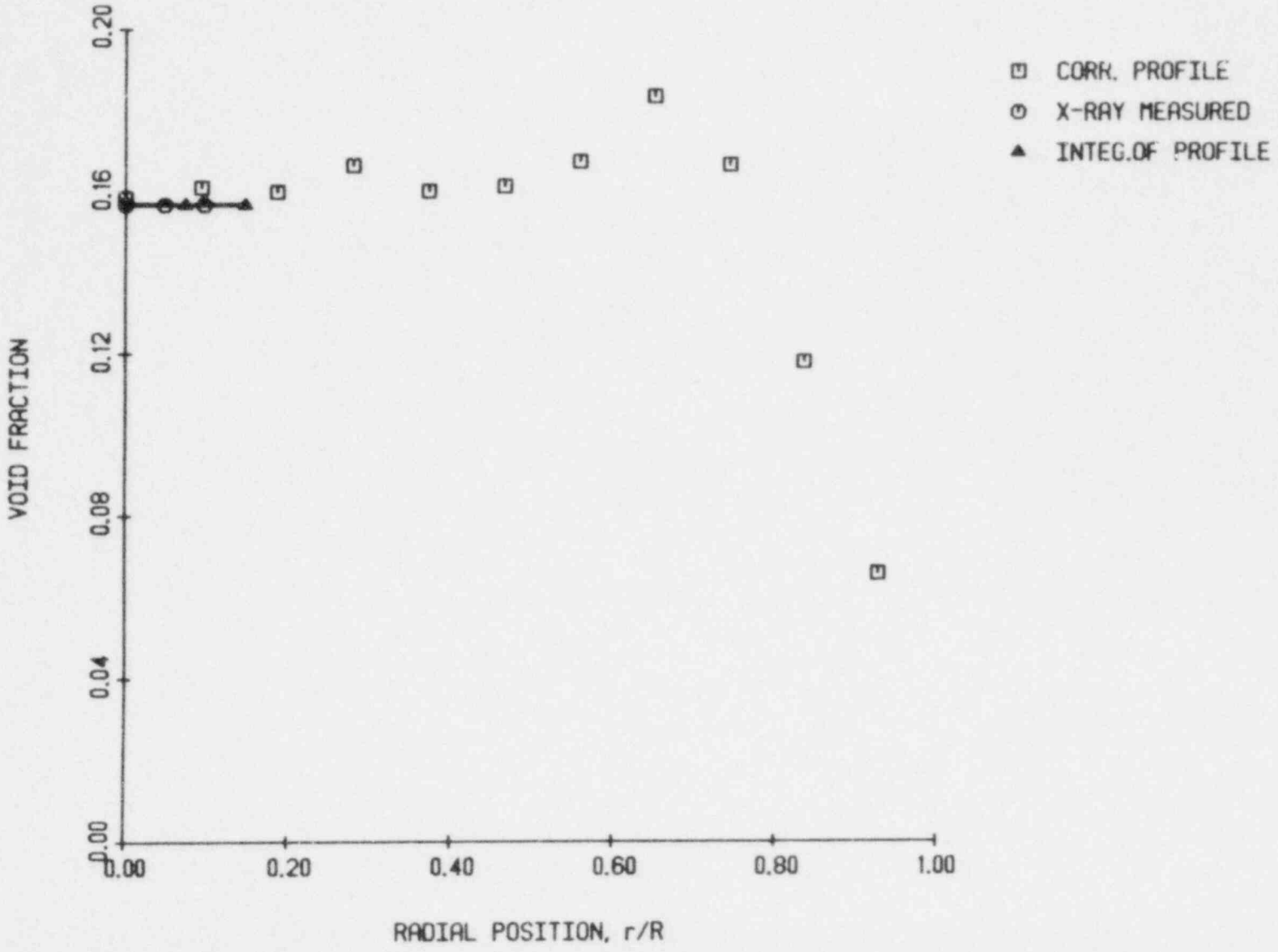

Figure 5.45 Corrected RF probe profiles taken with derivative thresholding for J_ℓ=0.25 ■/sec, J_g=0.073 ■/sec

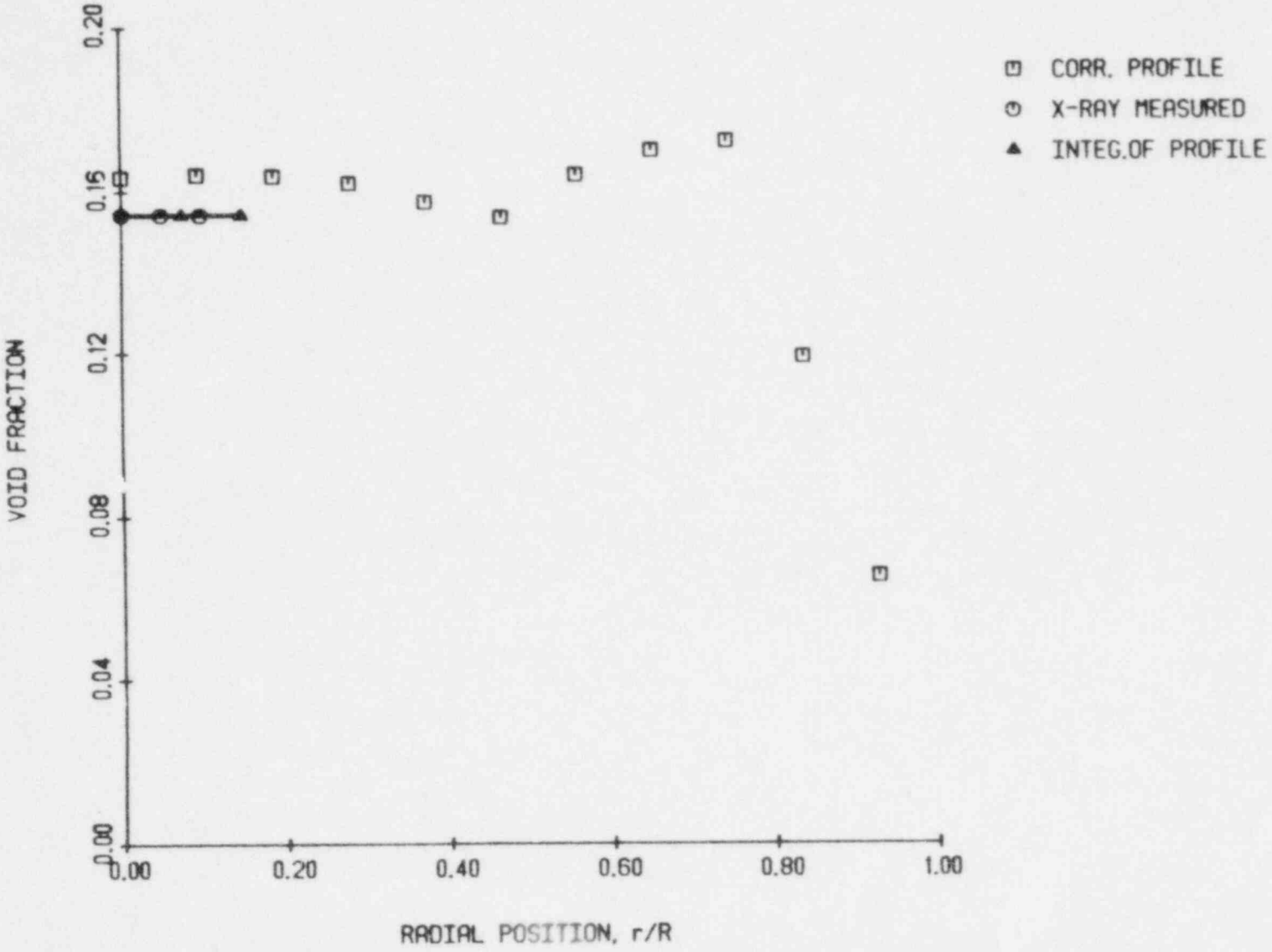

Figure 5.46 Corrected RF probe profiles taken with derivative thresholding for j_f =0.37 m/sec, j_g =0.097 m/sec

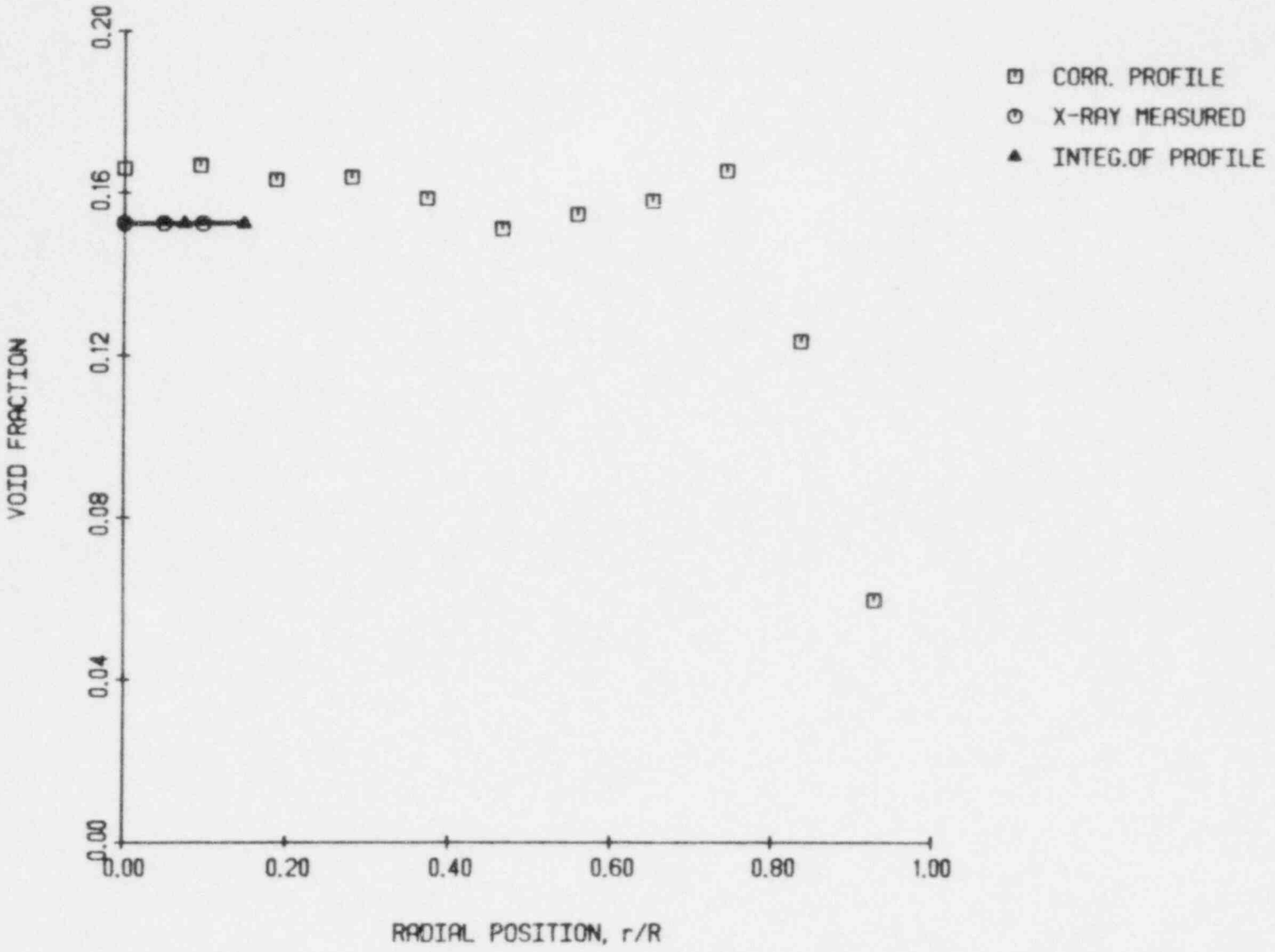

Figure 5.47 Corrected RF probe profiles taken with derivative thresholding for J_ℓ=0.50 m/sec, J_g=0.123 m/sec

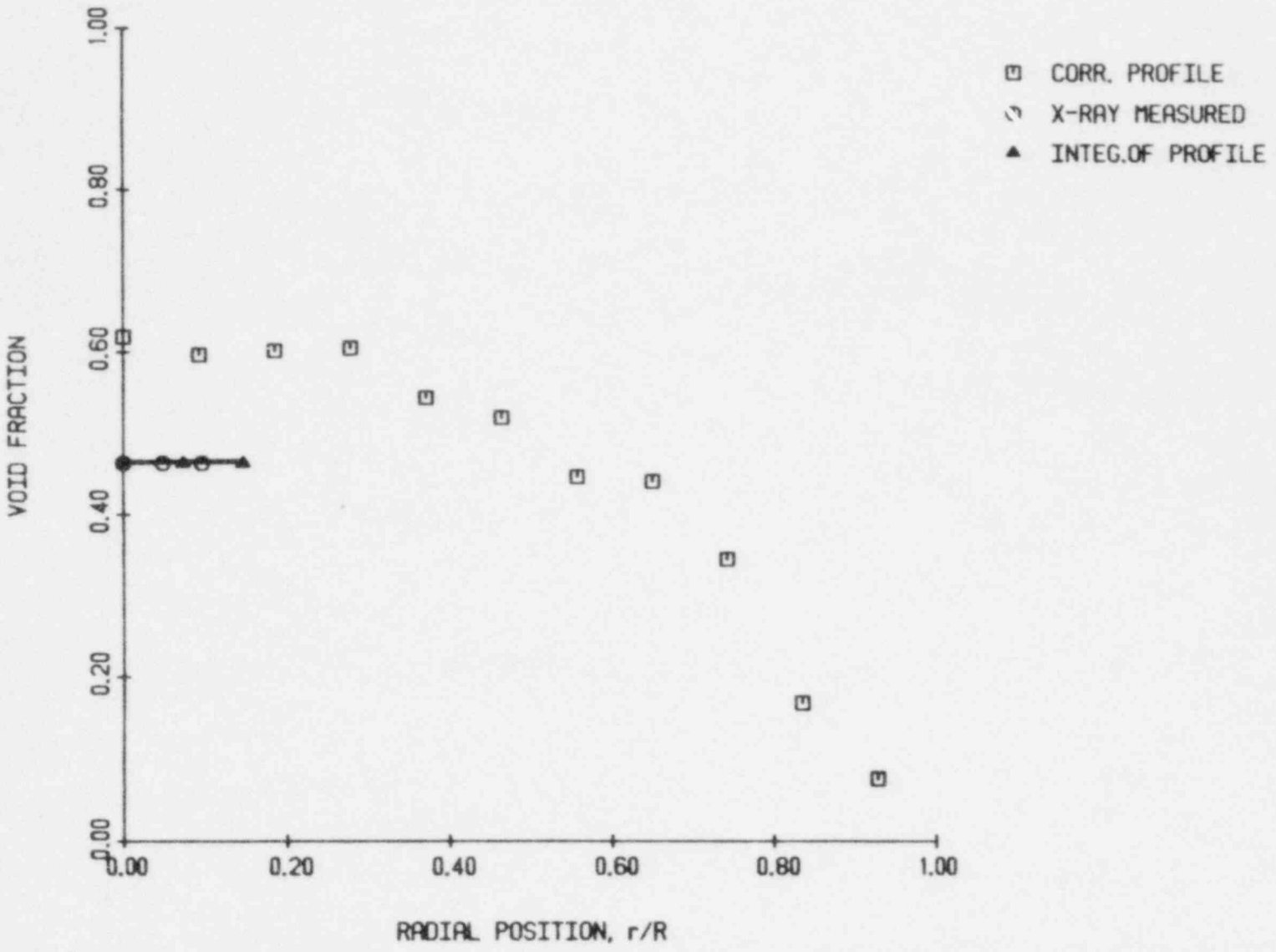

Figure 5.48 Corrected RF probe profiles taken with derivative thresholding for J_ℓ =0.12 ■/sec, J_g =0.301 ■/sec

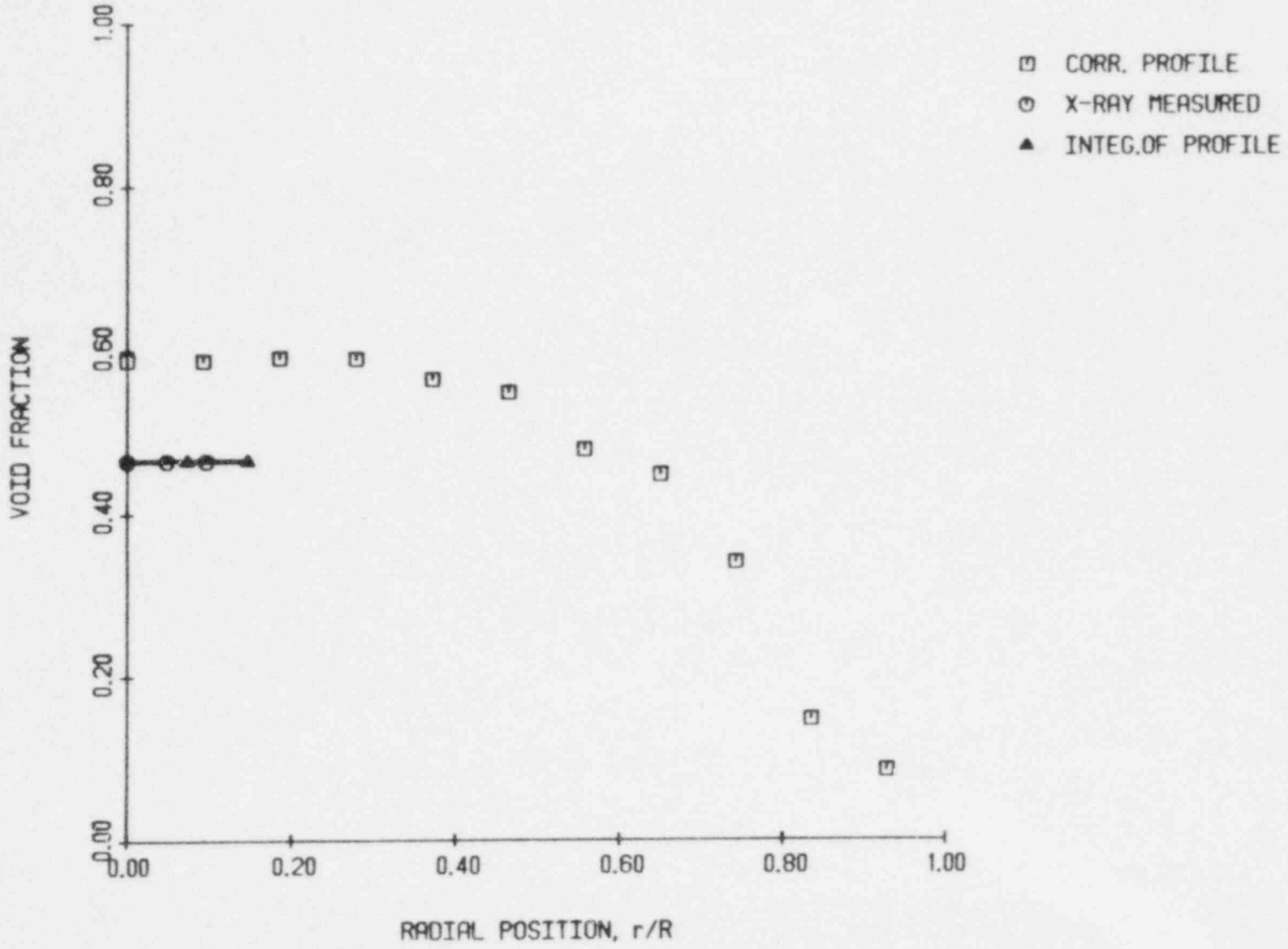

Figure 5.49 Corrected RF probe profiles taken with derivative thresholding for j_ℓ=0.25 m/sec, j_g=0.402 m/sec

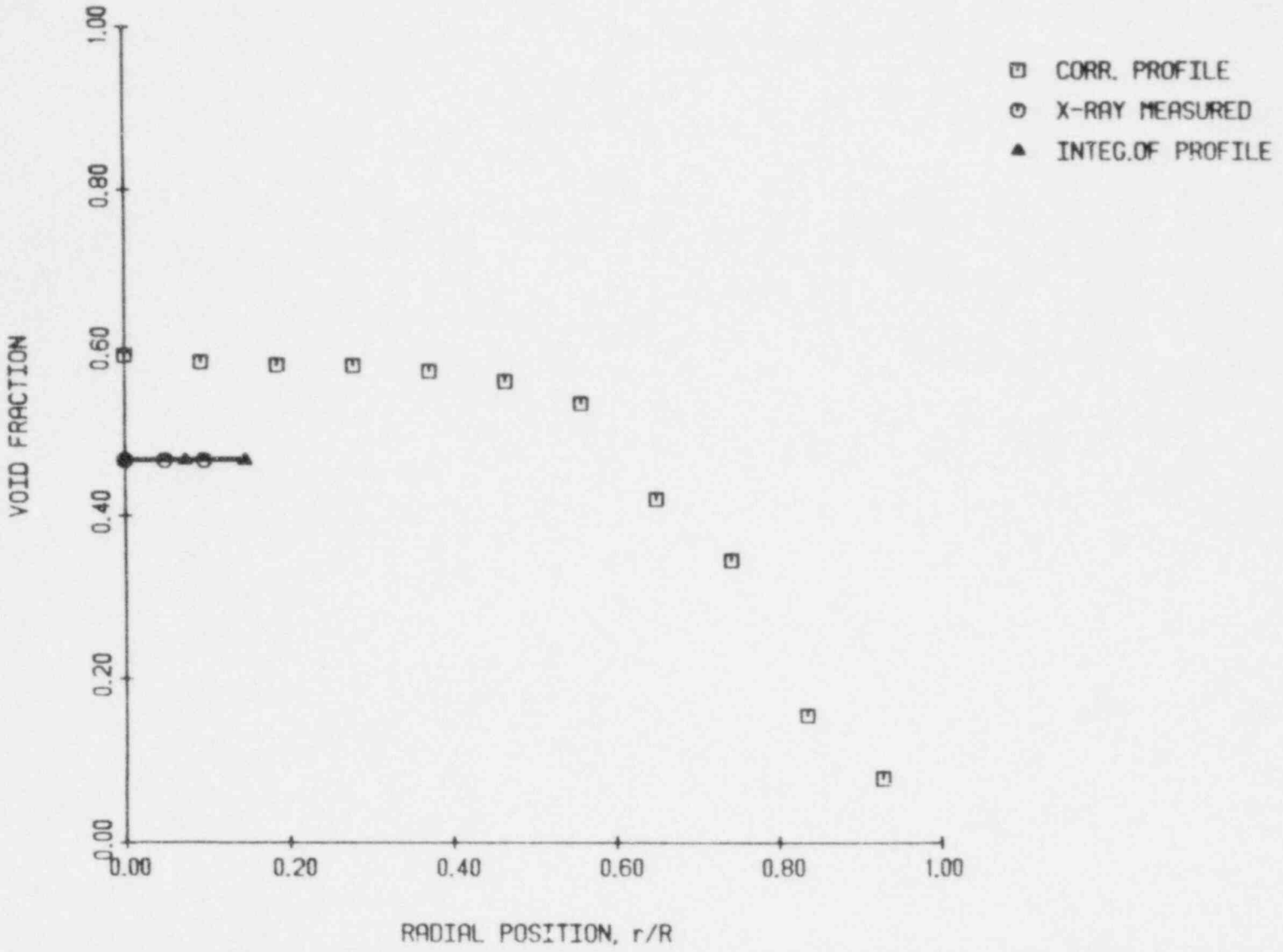

Figure 5.50 Corrected RF probe profiles taken with derivative thresholding for j_ℓ=0.37 m/sec, j_g=0.552 m/sec

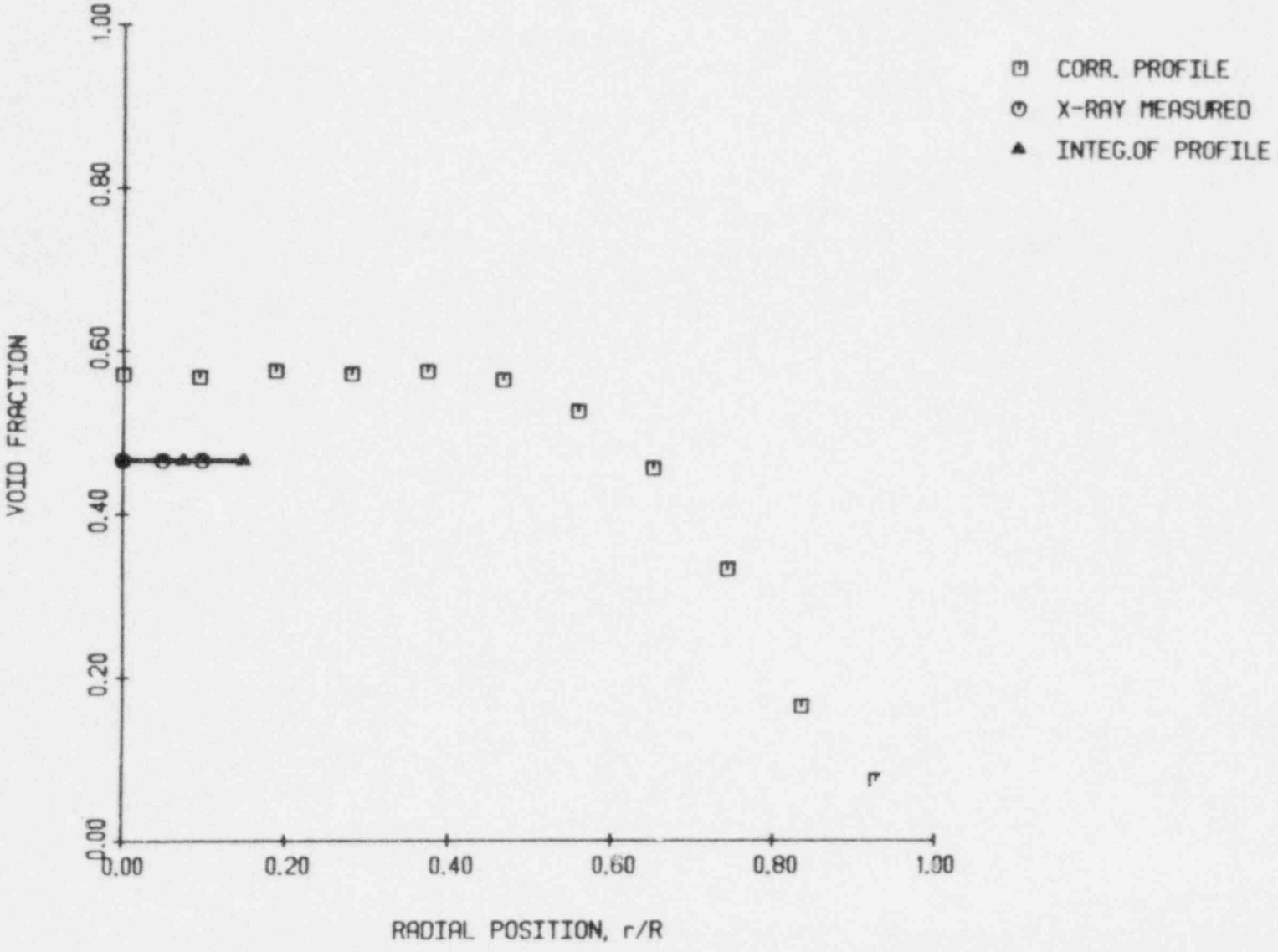

Figure 5.51 Corrected RF probe profiles taken with derivative thresholding for j_ℓ=0.50 m/sec, j_g=0.704 m/sec

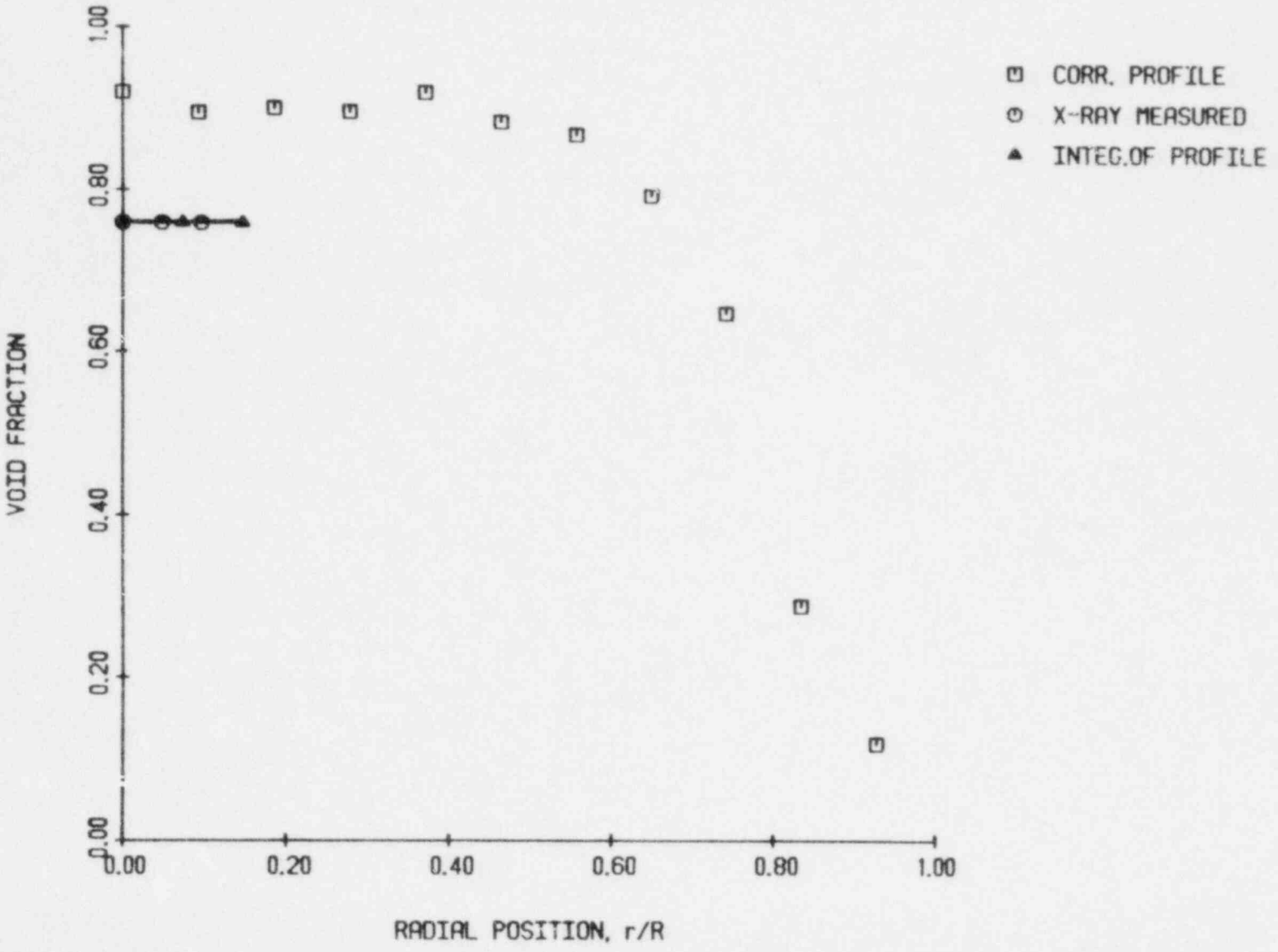

Figure 5.52 Corrected RF probe profiles taken with derivative thresholding for J_ℓ=0.12 m/sec, J_g=1.67 m/sec

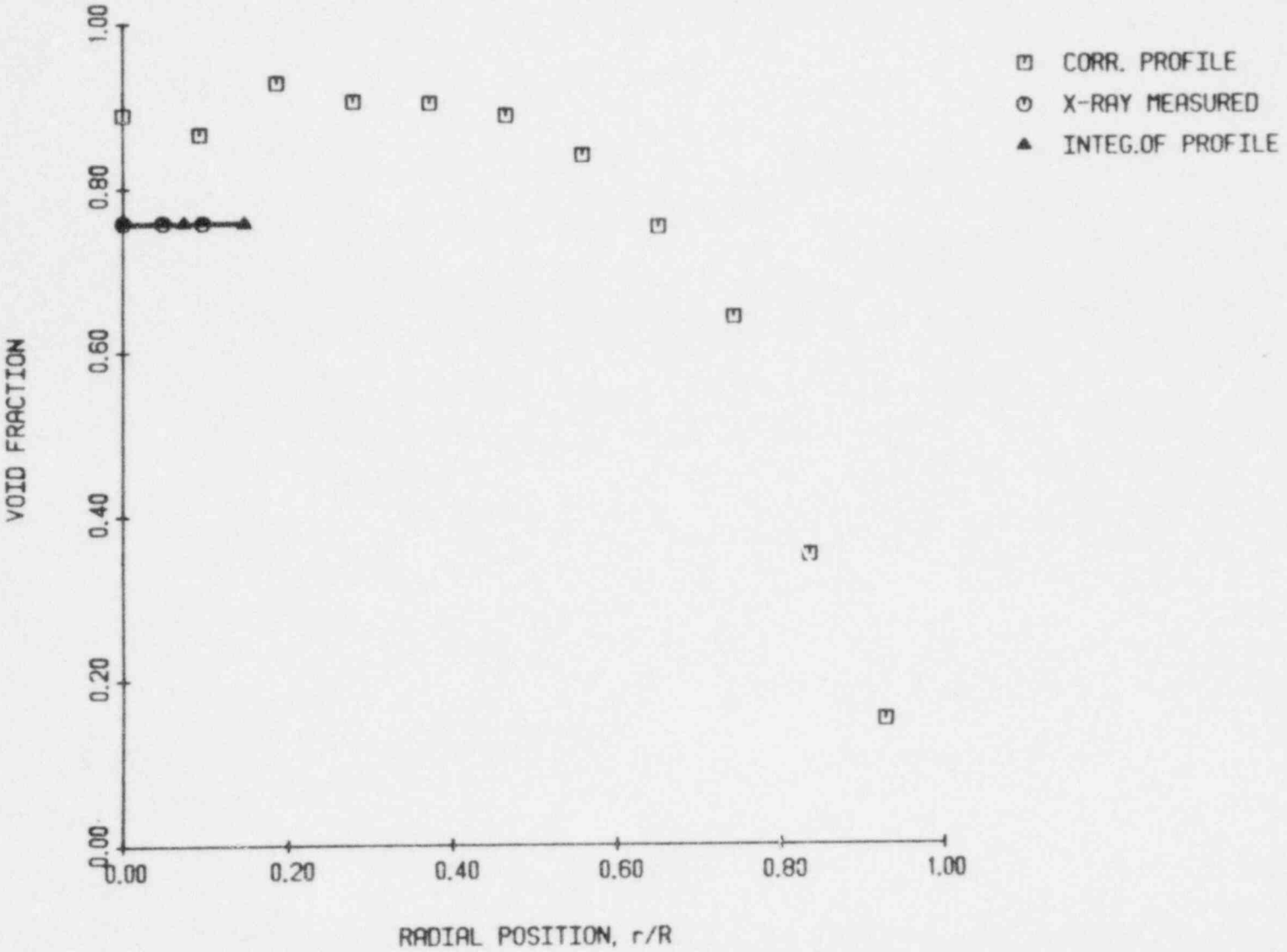

Figure 5.53 Corrected RF probe profiles taken with derivative thresholding for J_ℓ=0.25 m/sec, J_g=2.67 m/sec

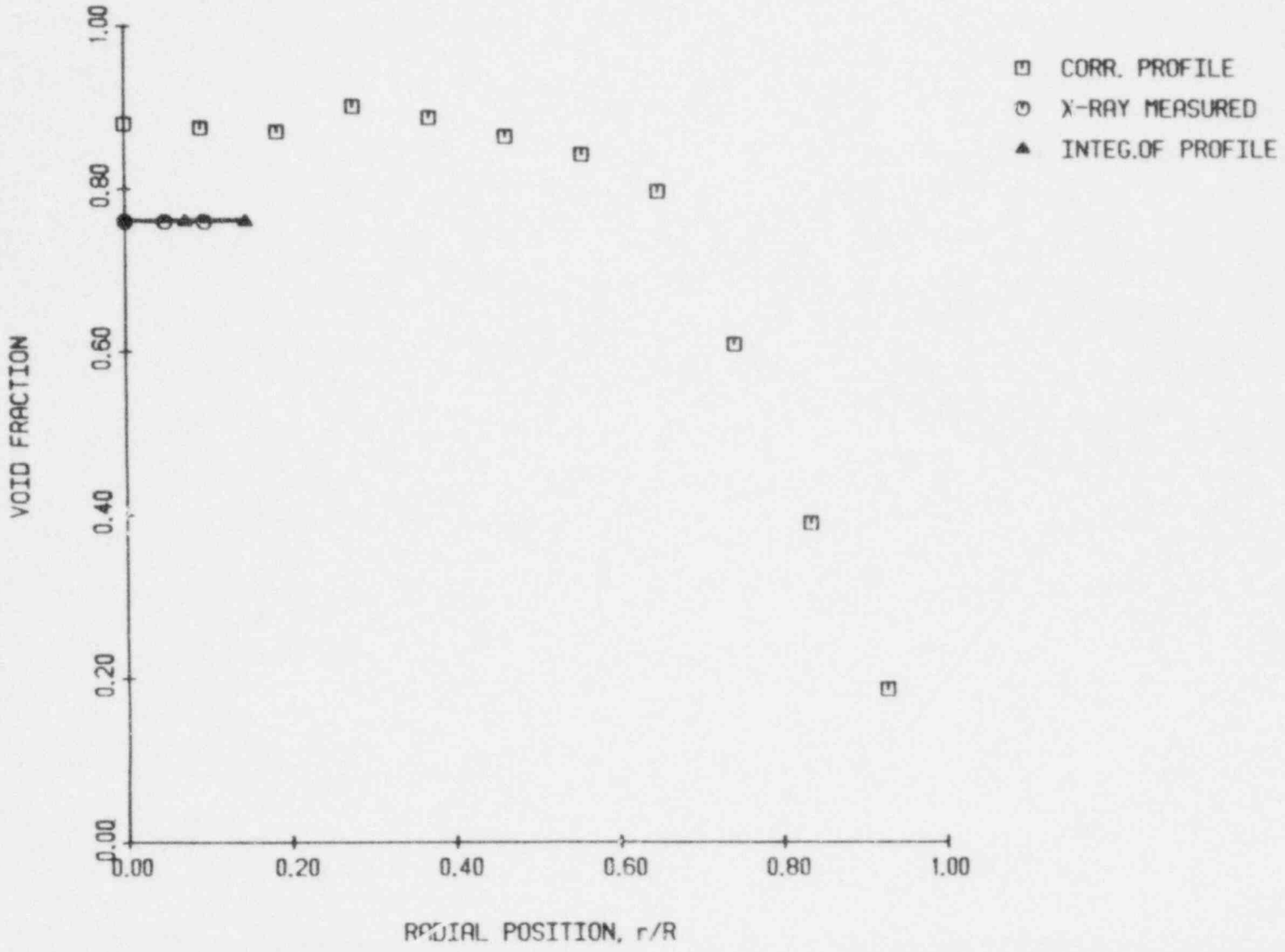

Figure 5.54 Corrected RF probe profiles taken with derivative thresho.ding for J_ℓ=0.37 m/sec, J_g=3.41 m/sec

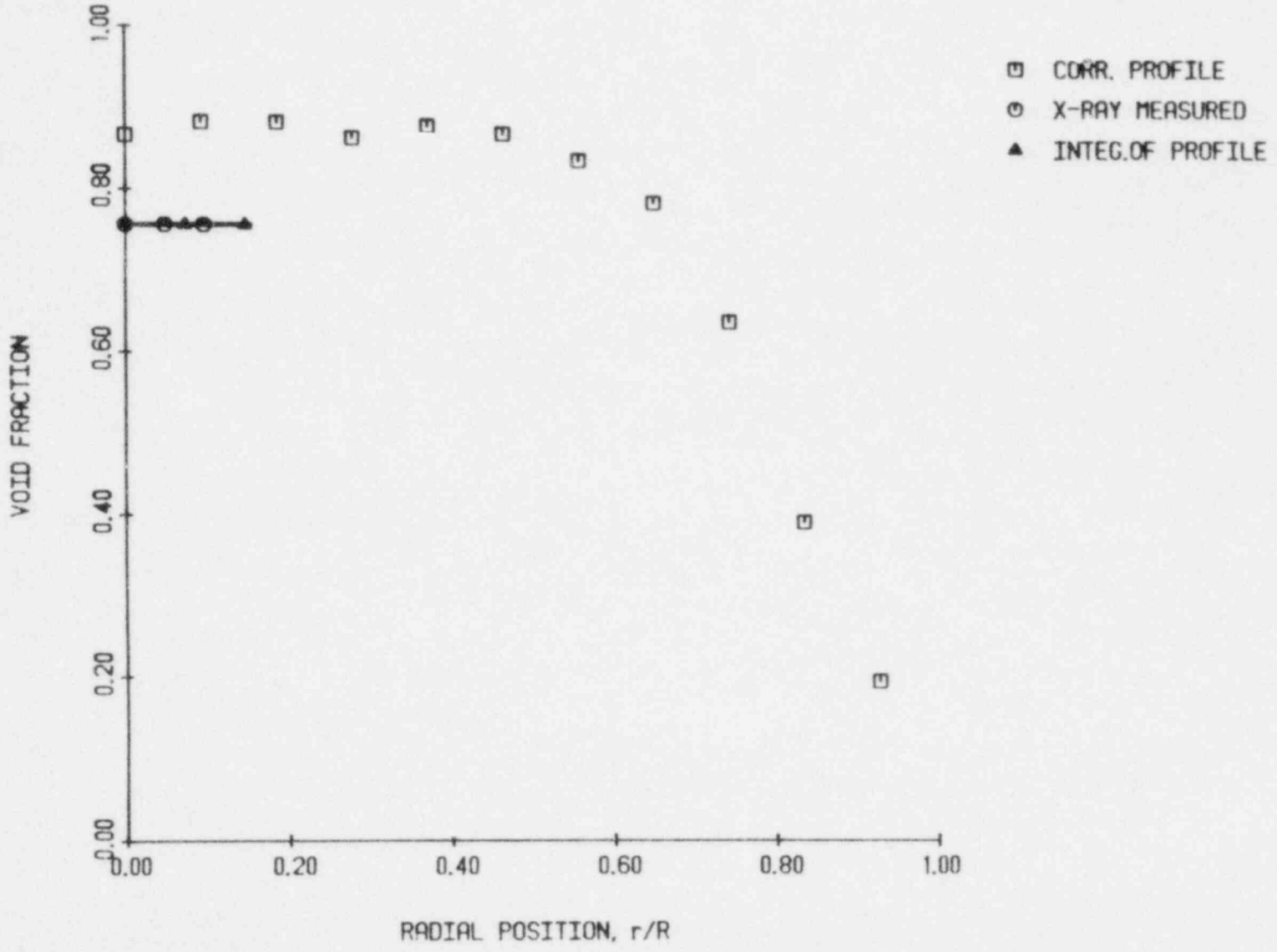

Figure 5.55 Corrected RF probe profiles taken with derivative thresholding for J_ℓ=0.50 m/sec, J_g=4.24 m/sec

discussed.

5.4 The Effect of Liquid Phase Resistivity

Three zero liquid flow cases were studied with three tablespoons of iodized table salt added to the water. The addition of salt changed the conductivity associated with the liquid phase; from 135.9 micromhos to 6.7 millimhos. The addition of salt also increased surface tension and consequently increased flow effects. Figures 5.56 through 5.58 compare the uncorrected pure and salt water void taken with derivative thresholding. The bubbly flow profile shown in Figure 5.56 is considerably altered due to flow effects. Neither the slug flow void profile, shown in Figure 5.57, nor the annular flow void profile, shown in Figure 5.58, is strongly effected by the addition of salt.

Level thresholding was not even operable with the salt water condition, since the addition of salt changed the dielectric constant of the water. As a result the baseline capacitance changed considerably. This changing baseline requires a new discriminator setting; a very undesirable situation, in that complete recalibration would be necessary. It was clear that derivative thresholding is the preferred technique for the signal processing of RF excited local impedance probes.

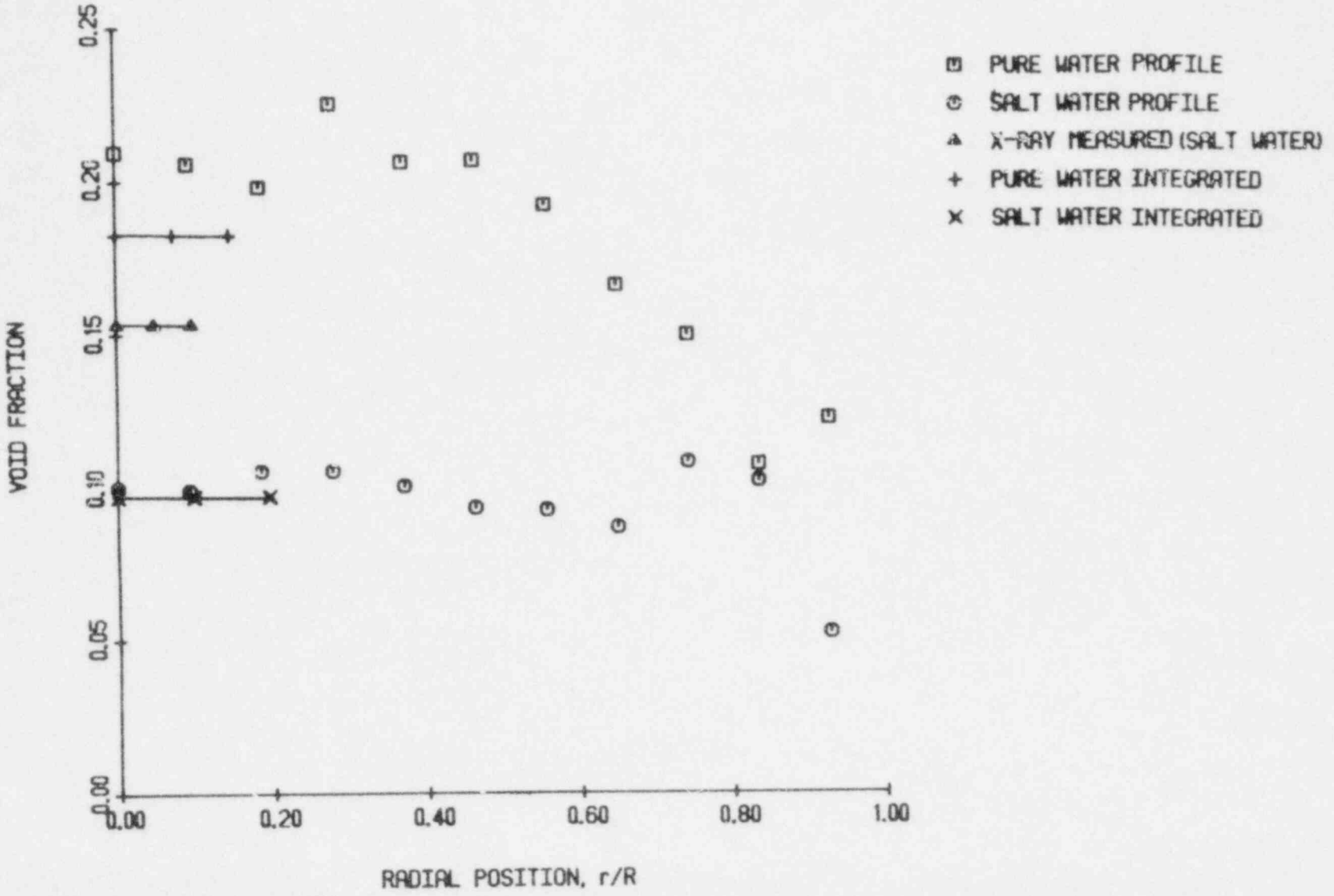

Figure 5.56 A comparison of the x-ray measured chordal void fraction and the RF probe integrated void profile for pure and salt water at j_ℓ = 0.00 m/sec. and j_g = 0.020 m/sec.

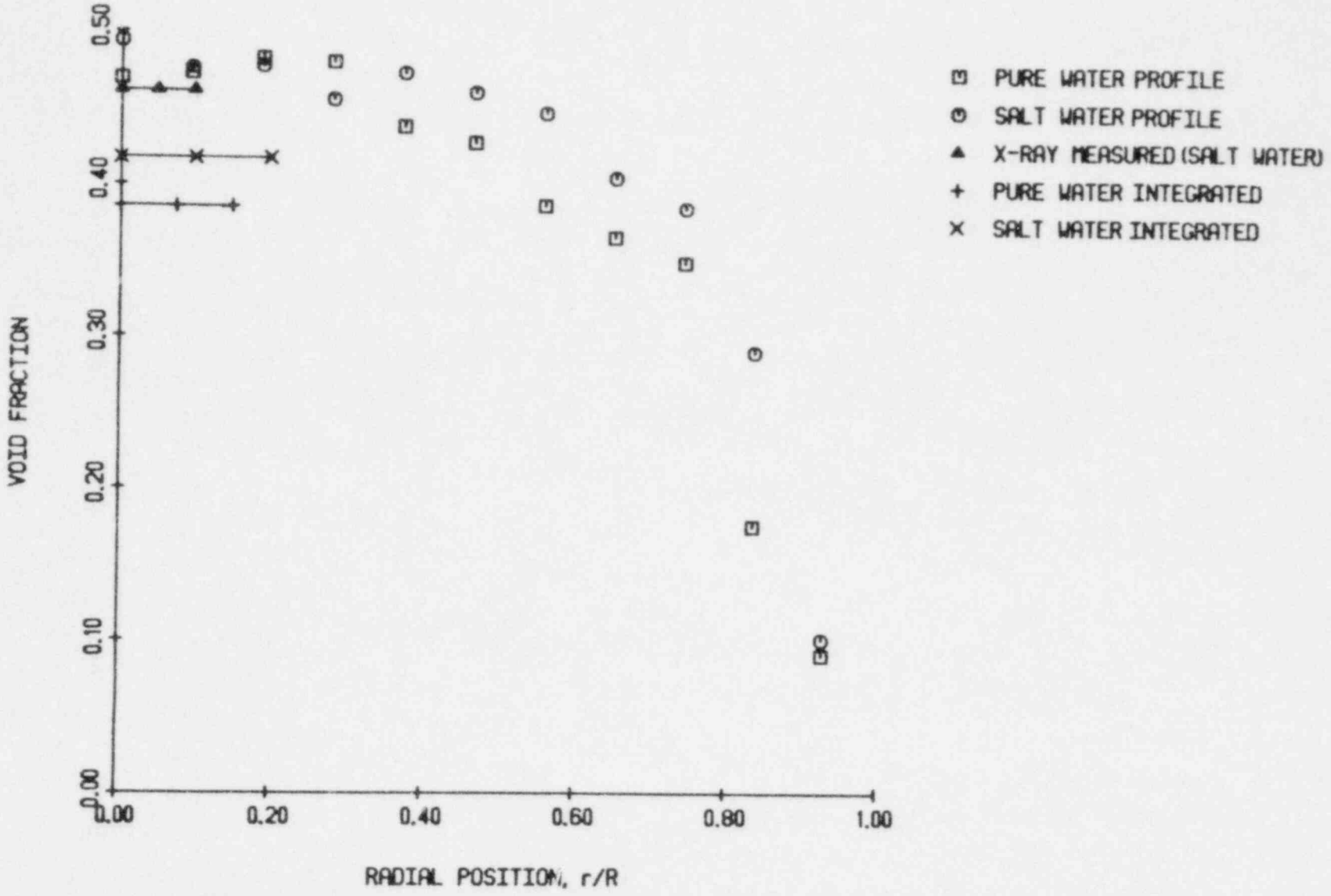

Figure 5.57 A comparison of the x-ray measured chordal void fraction and the RF probe integrated void profile for pure and salt water at j_ℓ = 0.00 m/sec. and j_g = 0.180 m/sec.

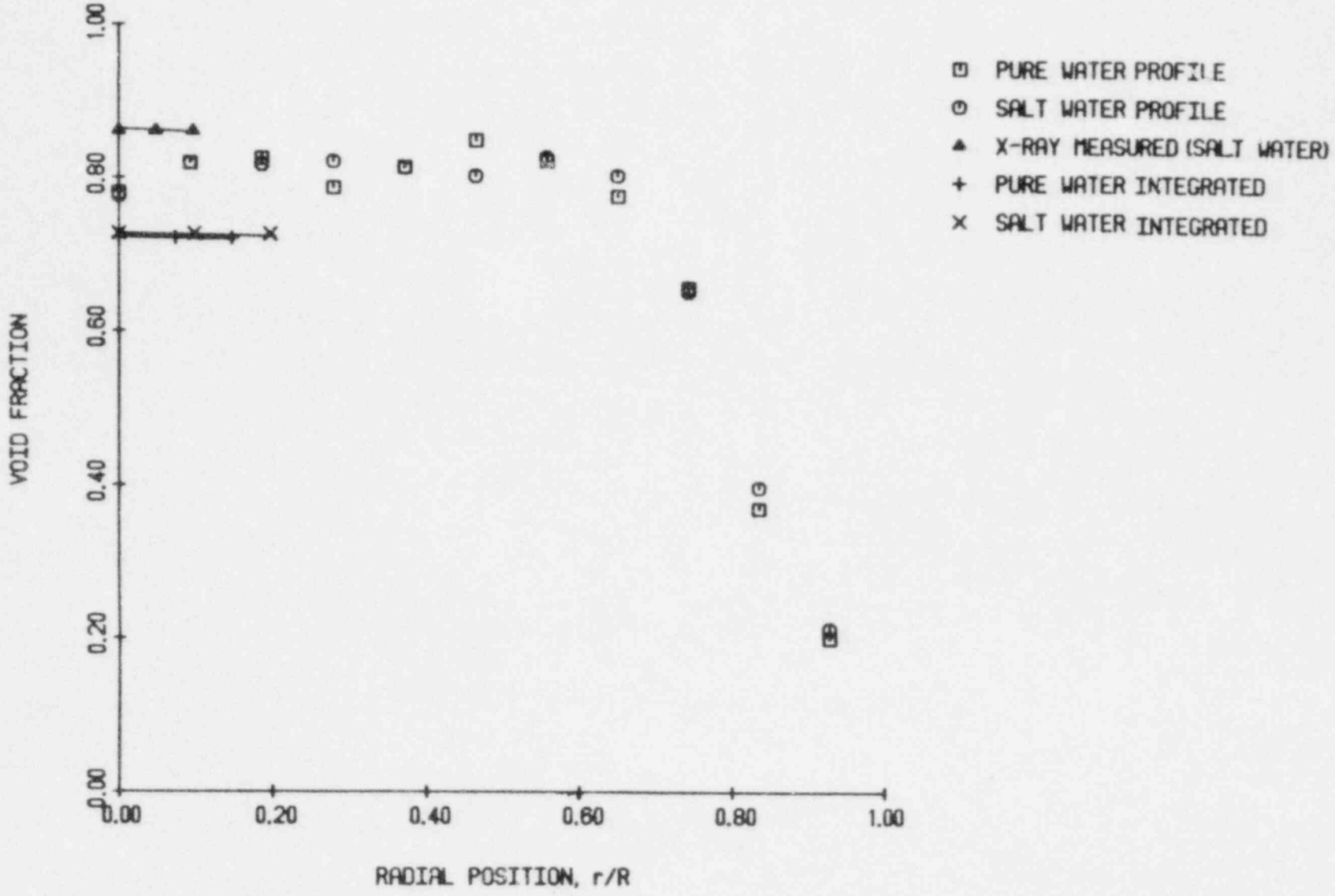

Figure 5.58 A comparison of the x-ray measured chordal void fraction and the RF probe integrated void profile for pure and salt water at j_ℓ = 0.00 m/sec. and j_g = 4.57 m/sec.

5.5 Conclusion

Derivative thresholding of an RF excited local probe gives much better local void fraction results than those obtained with level thresholding. Moreover, the scheme is less sensitive to liquid velocity changes and water purity than level thresholding. Indeed, it has been found that level thresholding is not really practical.

6. Summary and Recommendations

6.1 Flow Regime Identification

Forty-nine two-phase flows were studied with a dual beam x-ray system. The chordal-averaged void fraction was measured at six chordal locations across the pipe for each air/water flow. The probability density function (PDF) and power spectral density (PSD) function, and their first four moments, were calculated for each chordal position.

An objective flow regime indicator was developed from the first four moments associated with the PDF and PSD. The variance of the PDF is recommended. This moment responded to the changes in flow regime and was found to be independent of liquid superficial velocity.

Substantial physical significance can be associated with the variance of the PDF. Bubbly flow consists of small, distributed voids and thus any void fraction measurement should have a small variance. Annular flow is mostly vapor and correspondingly will also have a small variance. Slug flow, however, contains discrete regions of large and small void fraction. The variance about the mean will thus be large. For the conditions tested in this study the level of variance which indicated the bubbly-slug and slug-annular flow regime transition was found to be 0.04, independent of flow rate.

The moments of the PSD need to be correlated with liquid superficial velocity in order to be useful. This

would require the simultaneous measurement of the liquid superficial velocity. Thus the PSD, and its moments, are not recommended as a flow regime indicator.

Finally, it was observed that the commonly used [22] flow regime transition criterion of constant void fraction was inadequate, since it does not capture the observed flow effect.

6.2 Radio Frequency Probe Operation and Thresholding

A local impedance void probe excitation scheme was developed and tested. This device operated at radio frequency (RF) and drove a Karlsruhe type local impedance probe. Two signal thresholding techniques were used: single level and derivative. Single level thresholding triggers on the magnitude of the void signal while derivative thresholding responds to the slope of the analog void signal.

The RF probe was satisfactorily tested in tap and salt water. The probe, when operated with derivative thresholding, did not exhibit a substantial resistivity dependence, confirming that the RF excited probe was independent of liquid phase resistivity.

Level thresholding did not operate adequately particularly when fluid resistivity changed. This thresholding technique is very sensitive to baseline capacitance which will vary with temperature and water purity. As a result, derivative thresholding is

recommended. It was noticed that flow effects dominated the probe's operation especially at low void fraction and flow rates. This was true regardless of the method of thresholding and is due to inherent surface tension and fluid dynamic effects.

6.3 Optical Techniques

A high temperature diamond tipped optical probe was shown to be feasible for local void fraction measurements. Nevertheless, high cost and various manufacturing considerations (eg: seals, differential thermal expansion, etc.) remain problems to be overcome before these probes are practical.

An optical global void probe, called digital interferometer, was built and tested. This device operated reasonably well for high and low void fractions in small diameter ducts. The device is also capable of detecting droplets in annular flow. Application of this technique to large diameter pipes does not appear to be practical since it is very difficult to collimate the light beams across large gaps.

6.4 Future Work

Several areas require future work. The proposed flow regime indicator (i.e. the variance) should be evaluated in a high pressure steam environment. In

addition, different geometries, such as larger diameter pipes, triangular and eccentric annular test sections, and rod bundles, should be studied in air/water flows.

The RF excited local probe with derivative thresholding should be tested at larger liquid superficial velocities, and high pressure steam/water proof tests should be conducted.

A high temperature optical local probe should be developed along the lines presented herein. While such probes will likely be quite expensive they should be inherently insensitive to fluid conditions, and thus easily interpretable.

APPENDIX A.1

ACQUISTION AND CONVERSION OF X-RAY DATA

This appendix contains two computer codes. The first code, FLOW6, samples the analog-to-digital (A/D) converter and stores the binary results on the outer 16 tracks of the PDP-9 disk. This code also computes the running time average. The code will prompt the user for the appropriate inputs.

The second code, TFORM, reads the binary data placed on the disk by FLOW6 and converts it to the 4I4 format of FORTRAN. This code then writes the converted data to a DECtape for permanent storage. Like FLOW6, TFORM will prompt the user for the necessary input.

```
/       FILE NAME:  FLOW6 SRC
/
/       THIS PROGRAM KEEPS A RUNNING SUM OF THE
/       SAMPLE INPUTS AND THE NUMBER OF SAMPLES
/       THEN PRINTS OUT THE AVERAGE WHEN THE
/       RUN IS COMPLETED.
/
/       PROGRAM TO SAMPLE ADC 30K TIMES AND STORE
/       DATA ON THE 16 OUTER TRACKS OF THE DISK
/       WRITTEN BY JOHN W. PETTIT  2/25/77
/
DSRS=707262
DSSF=707001
DSCN=707044
DSCF=707041
DSFX=707042
DLAH=707064
DLAL=707024
DSCD=707242
CMSK=704201
        .TITLE  FLOW6
        .IODEV  4
        .GLOBL  AVEOUT,SAMP
        .INIT   4,1,PLP1
/
/       SET UP INTERUPT FOR CAMAC
/
        CAL     0
        16
/
/       SKIP CHAIN NAME
/
        CMSK
/
/       INTERUPT HANDLER
/
        CMINT
/
/       SET UP DISK
/
        CAL     0
        16
/
/       DISK SKIP CHAIN
/
        DSSF
/
/       INTERUPT HANDLER
/
        DKOK
        LAC     (3)
        IOT     704
/
/       CALL ROUTINE TO GET NUMBER OF DATA SAMPLES
/
```

```
        JMS*    SAMP
        JMP     .+1+1
        .DSA    NSAMP
        LAC     NSAMP
        CMA
        DAC     DONE
        ISZ     DONE
        LAC     (BAD1)
        DAC     POINT
        LAC     (0)
        DLAH
        LAC     (5)
        DSCF
        DSFX
        LAC     TRKAD
        DLAL
/
/       ENABLE THE INTERUPT I.E. ALLOW COMPUTER TO BE INTERUPTED
/       CRATE 1, FUNCTION 26 ENABLE, STATION 1, SUBADDRESS 1
/
        LAC     ENINS
        704204
        LAC     TWO
        704244
        704254
/
/       ENABLE THE DATA PULSER TO THE LINEAR GATE
/       CRATE 1, FUNCTION 26 ENABLE, STATION 19, SUBADDRESS 2
/
        LAC     ENGT
        704204
        LAC     TWO
        704244
        704254
/
/       DATA DISPLAY SECTION
/
PLP1    LAC     BUFSW
        SZA
        JMP     DBUF2
        LAC     (BAD1)
PLP2    DAC     ADCT1
        LAC     FHUN
        DAC     ADCT2
        DZM     ADCT3
PLP3    LAC     ADCT3
        IOT     506
        TAD     FOUR
        DAC     ADCT3
        LAC*    ADCT1
        IOT     646
        ISZ     ADCT1
        ISZ     ADCT2
        JMP     PLP3
        LAC     DTEST
```

```
        AND     (1)
        SNA
        JMP     PLP1
/
/       WRITE TO TELETYPE TO INDICATE CORRECT DATA ACQUISITION
/
        .WRITE  4,2,WRD1,4
        .WAIT   4
/
/       CALL SUBROUTINE TO WRITE OUT VOID FRACTION
/
        JMS*    AVEOUT
        JMP     .+3+1
        .DSA    PCT
        .DSA    RUNVL
        .DSA    RUNCT
        .EXIT
DBUF2   LAC     (BAD2)
        JMP     PLP2
/
/       INTERUPT HANDLING SECTION
/
CMINT   DAC     ACSAV
        LAC*    (0)
        DAC     INTSAV
/
/       READ A TO D CONVERTER INTO PDP-9 ACCUMMULATOR
/       CRATE 1, FUNCTION 1, STATION 1, SUBADDRESS 1
/
        LAC     ADC
        704204
        LAC     TWO
        704244
        704254
        704212
        DAC*    POINT
        AND     (1777)
        TAD     RUNVL
        SMA
        JMP     POP
        ISZ     PCT
        AND     (377777)
POP     DAC     RUNVL
        ISZ     RUNCT
        ISZ     BUFCT
        JMP     OUT
        LAC     BUFSW
        SZA
        JMP     BUF2
        LAC     (TAG2)
        DAC     POINT
        ISZ     BUFSW
        LAC     (TAG1)
        DAC*    (37)
        JMP     DATCH
```

```
BUF2    LAC     (TAG1)
        DAC     POINT
        .ZM     BUFSW
        LAC     (TAG2)
        DAC*    (37)
DATCH   LAC     FHUN
        DAC*    (36)
        DA      BUFCT
        DSCN
        ISZ     DONE
        JMP     OUT
/
/       DISABLE THE DATA PULSER TO THE LINEAR GATE
/       CRATE 1, FUNCTION 24, STATION 19, SUBADDRESS 2
/
        LAC     DAGT
        704204
        LAC     TWO
        704244
        704254
/
/       DISABLE THE INTERUPT FOR DATA
/       CRATE 1, FUNCTION 24,STATION 1,SUBADDRESS 1
/
        LAC     DAINS
        704204
        LAC     TWO
        704244
        704254
        ISZ     DTEST
OUT     ISZ     POINT
        LAC     ACSAV
        ION
        JMP*    INTSAV
DKOK    DAC     ACSAV
        LAC*    (0)
        DAC     INTSAV
        CLA
        DSRS
        AND     (200)
        DSCD
        NOP
        JMP     BAC
/
/       WRITE TO TELETYPE TO INDICATE DISK ERROR
/
        .WRITE  4,2,WRD2,4
        .WAIT   4
        .EXIT
BAC     LAC     ACSAV
        ION
        JMP*    INTSAV
/
/       STORAGE LOCATIONS
/
```

```
ENGT    072462
DAGT    070462
TRKAD   700000
NSAMP   0
PCT     0
RUNVL   0
RUNCT   0
FOUR    4
DTEST   0
TWO     2
DAINS   070021
ENINS   072021
ADC     041021
POINT   0
FHUN    -400
BUFSW   0
TAG1    0
        .REPT   400
BAD1    0
TAG2    0
        .REPT   400
BAD2    0
BUFCT   -400
TRADV   400
DONE    -200
ACSAV   0
INTSAV  0
ADCT1   0
ADCT2   0
ADCT3   0
WRD1    002092
        0
        .ASCII  ' DATA TAKING COMPLETED'<015><012>
WRD2    005002
        0
        .ASCII  ' DISK TRANSFER ERROR'<015><012>



        SUBROUTINE SAMP(I)
10      WRITE(4,1)
1       FORMAT(1X,23HINPUT NUMBER OF SAMPLES)
        READ(4,3) IB
3       FORMAT(I6)
        IF(IB .GT. 128) GO TO 20
        I=IB
        RETURN
20      WRITE(4,2)
2       FORMAT(1X,25HCANNOT BE LARGER THAN 128)
        GO TO 10
        END
```

```
      SUBROUTINE AVEOUT(IA,IB,IC)
C
      DIMENSION SCALE(2,6)
C
      DATA SCALE/19.94,955.66,33.0,953.03,81.03,941.68,
     1167.71,918.13,295.59,859.93,443.46,740.90/
C
C     READ IN CHORDAL SELECT
C     ENTER ZERO TO ENTER EXTERNAL VALUES
C
      WRITE(4,100)
100   FORMAT(1X,31HENTER CHORDAL SELECT, I4 FORMAT)
C
      READ(4,200) ISELCT
200   FORMAT(I4)
      A=FLOAT(IA)
      B=FLOAT(IB)
      C=FLOAT(IC)
      D=((131072.0*A)+B)/C
C
C     CHECK FOR OPTIONAL DATA INPUT
C
      IF (ISELCT.NE.0) GO TO 7
C
C     READ IN ALL VAPOR SCALE FACTOR
C
      WRITE(4,300)
300   FORMAT(/,1X,41HENTER ALL VAPOR BIAS FACTOR, F10.3 FORMAT)
      READ(4,400) SCALEF
400   FORMAT(F10.3)
C
C     READ IN ALL LIQUID SCALE FACTOR
C
      WRITE(4,500)
500   FORMAT(1X,34HENTER ALL WATER BIAS, F10.3 FORMAT)
      READ(4,400) DCBIAS
C
C     READ IN DATA SAMPLING RATE
C
      WRITE(4,600)
600   FORMAT(1X,33HENTER SAMPLING RATE, F10.3 FORMAT)
      READ(4,400) SAMRA
C
      GO TO 750
C
C     SET PRESET VALUES
C
700   SCALEF=SCALE(2,ISELCT)
      DCBIAS=SCALE(1,ISELCT)
      SAMRAT=200.
C
C     WRITE OUT SCALING FACTORS
C
750   WRITE(4,800) DCBIAS
```

```
800     FORMAT(1X,24HALL WATER BIAS VALUE IS:,F10.3)
        WRITE(4,900) SCALEF
900     FORMAT(/,1X,24HALL VAPOR BIAS VALUE IS:,F10.3)
C
C       SCALE VOID FRACTION
C
        D=(D-DCBIAS)/(SCALEF-DCBIAS)
        WRITE(4,1000) D
1000    FORMAT(/,1X,26HAVERAGE VOID FRACTION IS: ,F10.4)
        WRITE(4,1100) C
1100    FORMAT(/,1X,21HNUMBER OF SAMPLES IS:,2X,F10.4)
C
C       CALCULATE INTEGRATION TIME
C
        C=C/SAMRAT
C
        WRITE(4,1200) C
1200    FORMAT(/,1X,18HINTEGRATION TIME: ,F10.4,8H SECONDS)
        RETURN
        END
```

```
C       PROGRAM TO PUT 30K DATA ON DECTAPE
        DIMENSION IB(257),FIL(2)
        DATA FIL(1),FIL(2)/5H LODA,4HTSRC/
C
C       OUTPUT DECTAPE UNIT
C
        IUNIT3=7
C
C       TELETYPE UNIT NO.
C
        IUNIT4=4
C
        WRITE(IUNIT4,2)
2       FORMAT(1X,23HINPUT NUMBER OF RECORDS)
        READ(IUNIT4,3) N
3       FORMAT(I6)
C
C       OPEN OUTPUT FILE ON DECTAPE
C
        CALL ENTER(IUNIT3,FIL)
C
C       LOOP TO WRITE N BLOCKS OF 256
C
        DO 10 I=1,N
        CALL RDIN(IB(1))
        DO 20 IC=2,257,4
C
C       LOOP TO WRITE TO OUTPUT FILE
C
        ID=IC+1
        IE=ID+1
        IG=IE+1
        WRITE(IUNIT3,30) IB(IC),IB(ID),IB(IE),IB(IG)
30      FORMAT(1X,4I4)
20      CONTINUE
10      CONTINUE
C
C       CLOSE OUTPUT FILE
C
        CALL CLOSE(IUNIT3)
        STOP
        END
```

```
DLAH=707064
DSGO=707047
DLAL=707024
DSSF=707001
DSCD=707242
        .TITLE  RDIN
        .GLOBL  RDIN,.DA
RDIN    0
        JMS*    .DA
        JMP     .+1+1
MIN     .DSA    0
        LAC     FST
        SZA
        JMP     GO
        ISZ     FST
        CAL     0
        16
        DSSF
        DKOK
GO      LAC     (0)
        DLAH
        LAC     MIN
        DAC*    (37)
        LAC     (-400)
        DAC*    (36)
        LAC     TRKAD
        DLAL
        TAD     (400)
        DAC     TRKAD
        LAC     (3)
        DSGO
BAC     JMP     BAC
DKOK    DSCD
        ION
        JMP*    RDIN
TRKAD   700000
FST     0
        .END
```

APPENDIX A.2

POOF, A COMPUTER CODE TO CALCULATE THE DISCRETE PDF AND PSD

This appendix contains a FORTRAN computer code to calculate the discrete probability density function (PDF) and the discrete power spectral density (PSD) function. The moments of these distributions are also calculated. This code will operate on a PDP-9 or PDP-15 with 32k memory. The code is described in detail in the code's abstract.

The computer will prompt the operator for the necessary inputs. This code is highly modular. Each major task is performed by separate subroutines. All input and output unit numbers are assigned to variables.

```
C
C
C       ************************************************************
C       ************************************************************
C       ****                                                    ****
C       ****                                                    ****
C       ****   PPPPPP     000000     000000     FFFFFF         ****
C       ****   PPPPPPP    000000     000000     FFFFFF         ****
C       ****   PP  PP     00  00     00  00     FF             ****
C       ****   PP  PP     00  00     00  00     FF             ****
C       ****   PPPPPP     00  00     00  00     FFFFFF         ****
C       ****   PPPPPP     00  00     00  00     FFFFFF         ****
C       ****   PP         000000     000000     FF             ****
C       ****   PP         000000     000000     FF             ****
C       ****                                                    ****
C       ****                                                    ****
C       ************************************************************
C       ************************************************************
C
C
C
C
C       FORTRAN SOFTWARE PACKAGE TO CALCULATE THE DISCRETE
C       PROBABILITY DENSITY FUNCTION AND THE DISCRETE
C       POWER SPECTRAL DENSITY FUNCTION
C
C       WRITTEN FOR A PDP-9 OR PDP-15 WITH 32K MEMORY
C
C
C       WRITTEN AS PART OF A DOCTORAL THESIS BY:
C
C               MARK VINCE
C               NUCLEAR ENGINEERING DEPARTMENT
C               LINAC
C               RENSSELAER POLYTECHNIC INSTITUTE
C               TROY, NEW YORK 12181
C
C
C
C               ****        ABSTRACT        ****
C
C
C          THIS FORTRAN SOFTWARE PACKAGE CALCULATES THE
C       DISCRETE PROBABILITY DENSITY FUNCTION (PDF) AND
C       THE DISCRETE POWER SPECTRAL DENSITY FUNCTION (PSD)
C       FROM DIGITIZED DATA. THE PDF IS FORMED BY READING
C       THE INPUT DATA AND SIMULTANEOUSLY INCREMENTING THE
C       APPROPRIATE PDF BIN. THIS PROCEDURE STORES ONLY
C       PROCESSED DATA, THUS REDUCING CONSIDERABLY THE
C       CENTRAL MEMORY STORAGE REQUIRED. THE PROCESSED
C       PDF IS WRITTEN TO PERMANENT STORAGE FOR LATER
C       USE AND A PLOT OF THE NORMALIZED PDF IS
C       PRODUCED.
C          THE PDF IS INTEGRATED TO CALCULATE THE
C       CUMMULATIVE DISTIBUTION VALUE. FIVE MOMENTS
```

```
C       ARE GENERATED INCLUDING THE MEAN (FIRST MOMENT
C       ABOUT THE ORIGIN), THE VARIANCE (SECOND
C       MOMENT ABOUT THE MEAN) AND THE SECOND MOMENT
C       ABOUT THE ORIGIN. THE COEFFICIENTS OF
C       SKEWNESS AND KURTOSIS ARE FORMED FROM THE
C       THIRD AND FOURTH MOMENTS, RESPECTIVELY.
C          THE PSD CALCULATION IS BASED ON A DISCRETE FAST-
C       FORIER TRANSFORM (DFT). A SERIES OF DATA POINTS ARE
C       REREAD FROM THE INPUT DATA UNIT, STORED IN CENTRAL
C       MEMORY AND WRITTEN TO A PERMANENT STORAGE DEVICE.
C       THE MEAN VALUE OF THESE POINTS IS CALCULATED
C       FROM THE SIMPLE AVERAGE. THIS MEAN IS REMOVED FROM
C       THE DATA BEFORE APPLICATION OF ANY DATA SMOOTHING
C       WINDOW. AVAILABLE WINDOWS FOR TIME DOMAIN DATA
C       SMOOTHING INCLUDE A BOXCAR (NO WINDOW), HAMMING
C       AND HANNING. THE DATA'S LOCATION IS BIT-SHUFFLED
C       SO THAT THE DFT OUTPUT IS UNSCRAMBLED. A FORTRAN
C       DFT ROUTINE IS APPLIED TO CALCULATE THE FOURIER
C       TRANSFORM. THE PSD IS FORMED BY DIVIDING THE SUM OF
C       THE SQUARES OF THE REAL AND IMAGINARY COMPONENTS
C       CALCULATED FROM THE DFT BY HALF THE INTEGRATION TIME.
C       PLOT OF THE NORMALIZED PSD IS GENERATED AFTER
C       LISTING IT BY FREQUENCY. THE MOMENTS OF THE PSD
C       ARE ALSO CALCULATED.
C          THIS CODE IS ASSEMBLED VERY FLEXIBLY. EACH MAJOR
C       TASK IS PERFORMED BY A SEPARATE SUBROUTINE. INPUT AND
C       OUTPUT UNIT NUMBERS ARE ASSIGNED TO VARIABLES. ALL
C       INPUT SETUP DATA IS LISTED FOR REFERENCE. THE CODE
C       PLACES NO LIMIT ON THE NUMBER OF TIME DATA POINTS
C       USED IN THE PDF CALCULATION. THE DFT CAN HANDLE
C       A MAXIMUM OF 1024 POINTS.
C
C
C              ****       VARIABLES       ****
C
C
C
C       BINDAT(IVAL)     PROBABILITY OF THE I'TH PDF
C                        BIN, I.E. THE Y-COORDINATE OF
C                        PDF HISTOGRAM
C
C       DCbIAS           MINIMUM POSSIBLE DATA VALUE
C
C       DLVOID           DIFFERENCE BETWEEN SUCESSIVE
C                        PDF BINS
C
C       FILEN(2)         INPUT DATA FILE, NAMED
C                        FLODAT SRC
C
C       FILEO(2)         OUTPUT DATA FILE, VARIABLE NAME
C
C       I                TOTAL NUMBER OF RAW DATA POINTS
C                        DIVIDED BY N
C
```

```
C       IBNPNT(IVAL)    ARRAY CONTAINING NUMBER OF
C                       POINTS IN EACH PDF BIN
C
C       IDATA(N)        ARRAY FOR STORAGE OF INITIAL
C                       DATA FOR PDF OR FFT
C
C       IFPNTS          NUMBER OF DATA POINTS TO BE
C                       USED IN FFT ROUTINE
C
C       IPROCS          INPUT DATA SOURCE
C                         0 - ORIGINAL DATA
C                         1 - PREVIOUSLY PROCESSED
C                             DATA
C
C       IRPFFT          TRIP FOR FFT CALCULATION
C                           0 - FFT HAS NOT BEEN
C                               COMPUTED
C                           1 - FFT WILL BE
C                               RECOMPUTED
C
C       IXAL            NUMBER OF BINS (IVAL) + 1
C
C       IXBIN           NUMBER OF EXTRA PDF BINS TO
C                       BE PLACED ON LEFT AND RIGHT
C                       OF PDF TO COLLECT POSSIBLE
C                       SPURIOUS DATA OR NOISE
C
C       IVAL            NUMBER OF PDF BINS
C
C       JCT             COUNTER FOR INPUT DATA POINTS
C
C       N               NUMBER OF INPUT DATA POINTS
C                       PER RECORD
C
C       PI              ARITHMETIC CONSTANT, 3.14159
C
C       PLSZE           MAXIMUM X-AXIS VALUE FOR FFT
C                       PLOT
C
C       SAMRAT          DATA ACQUISTION SAMPLING RATE
C
C       SCALE(2,6)      PRESET TABLE CONTAINING
C                       MINIMUM AND MAXIMUM VALUES
C                       OF DATA
C
C       SCALEF          MAXIMUM POSSIBLE DATA VALUE
C
C       STARS(IXAL)     TEMPORARY STORAGE ARRAY FOR
C                       PLOTTING ROUTINE
C
C       VDRNG(IXAL)     X-COORDINATE OF PDF
C
C       X1(1024)        REAL DATA ARRAY FOR INPUT
C                       TO FFT
C
```

```
C       X2(2)   IMAGINARY DATA ARRAY FOR INPUT
                TO FFT
C
C
C
C
C
      DIMENSION IDATA(4),IBNPNT(120),BINDAT(120),FILEN(2),
     1FILEO(2),VDRNG(121),STARS(1024),X1(1024),X2(1024)
C
      EQUIVALENCE(STARS,X2)
C
      DATA FILEN(1),FILEN(2)/5HFLODA,4HTSRC/
      DATA FILEO(2)/4HTSRC/
C
C     SET CONSTANTS
C
      PI=3.14159
      N=4
      JCT=0
      IRPFFT=0
C
C     SET VARIOUS INPUT/OUTPUT UNIT NUMBERS
C
C     DATA INPUT UNIT
C
      IUNIT1=9
C
C     INPUT/OUTPUT DECPACK UNIT
C
      IUNIT2=6
C
C     OUTPUT PRINTER UNIT
C
      IUNIT3=7
C
C     TELETYPE OUTPUT
C
      IUNIT4=4
C
C     SET PLOT TRIP FOR TYPE OF ANALYSIS BEING PERFORMED
C
      IPLOT=1
C
C     READ IN OUTPUT FILE NAME
C
      WRITE(IUNIT4,100)
100   FORMAT(1X,33HENTER OUTPUT FILE NAME, A5 FORMAT)
      READ(IUNIT4,200) FILEO(1)
200   FORMAT(A5)
C
C     WRITE OUT INPUT DATA FILE FOR TAGGING PURPOSES
C
      WRITE(IUNIT3,250) FILEO(1)
      WRITE(IUNIT4,250) FILEO(1)
```

```
250     FORMAT(1X,16HDATA TAKEN FROM ,A5,5H FILE)
C
C       READ INPUT PARAMETERS AND INITIALIZE BINS
C
        CALL TILZER(IBNPNT,BINDAT,DLVOID,IVAL,SCALEF,I,IXBIN,
        1IUNIT3,IUNIT4,DCBIAS,SAMRAT,IFPNTS,PLSZE,IPROCS)
C
C       OPTION FOR ALREADY PROCESSED DATA
C
        IF (IPROCS.GT.0) GO TO 400
C
C       OPEN DATA FILE FROM X RAY UNIT
C
        CALL SEEK(IUNIT1,FILEN)
C
C       OPEN OUTPUT FILE
C
        CALL ENTER(IUNIT2,FILEO)
C
C       LOOP TO READ IN DATA AND PLACE IN BINS
C
        DO 300 II=1,I
C
        CALL REDATA(N,IDATA,IUNIT1)
C
        CALL BINS(N,IDATA,IBNPNT,SCALEF,IVAL,IXBIN,DCBIAS)
C
C       INCREMENT COUNTER TO KEEP TRACK OF DATA POINTS READ
C
        JCT=JCT+N
C
300     CONTINUE
C
C       NORMALIZE DATA
C
        CALL ORMALZ(JCT,DLVOID,BINDAT,IBNPNT,IVAL,IXBIN,VDRNG,
        1IUNIT2,IUNIT3,IUNIT4,IPROCS)
C
C       CLOSE INPUT DATA FILE
C
        CALL CLOSE(IUNIT1)
C
C       AVOID PREVIOUSLY PROCESSED DATA ROUTINES
C
        GO TO 500
C
C       FILL APPROPRIATE ARRAYS WITH PREVIOUSLY
C       PROCESSED DATA
C
400     CALL PRESET(N,BINDAT,VDRNG,IBNPNT,IUNIT1,IUNIT2,
        1FILEO,IUNIT3,IPROCS)
C
        IF (IRPFFT.EQ.1) GO TO 600
C
C       COMPUTE MOMENTS ASSOCIATED WITH DISTRIBUTION
```

```
C
500     CALL MOMENT(DLVOID,BINDAT,ALPHAB,IUNIT3,IUNIT4,
        1SRAWMM,SECMOM,SKEW,TOSIS,GRAPNM,IVAL,VDRNG,IPLOT)
C
C       PLOT NORMALIZED PROBABILITY DIST. FUNCTION
C
        CALL PLOT(STARS,IBNPNT,IVAL,BINDAT,IXBIN,VDRNG,
        1IUNIT3,IUNIT4,IPLOT,GRAPNM)
C
C       RESET VOID SCALING FACTOR
C
        SCALEF=SCALEF/DLVOID
C
C       SET UP PARAMETERS FOR FAST FOURIER ANALYSIS
C
        IDIR=1
        IPLOT=2
        IVAL=IVAL-(2*IXBIN)
        IXBIN=0
C
C       REOPEN INPUT DATA FILE, IF PROCESSING
C       ORIGINAL DATA
C
        IF (IPROCS.EQ.0) CALL SEEK(IUNIT1,FILEN)
C
C       BEGIN FAST FOURIER ANALYSIS
C
C       READ IN REAL ARRAY, SET IMAGINARY PART EQUAL TO ZERO
C       APPLY APPROPRIATE SCALING TO DATA
C
600     CALL REDATB(X1,X2,N,IFPNTS,SCALEF,DCBIAS,IUNIT1,
        1IPROCS,IUNIT2)
C
C       CLOSE INPUT DATA UNIT FOR ORIGINAL DATA
C
        IF (IPROCS.EQ.0) CALL CLOSE(IUNIT1)
C
C       CONVERT DATA TO A ZERO MEAN
C
        CALL DCMOVE(IFPNTS,X1,IUNIT3,IUNIT4)
C
C       SET NPTS FOR FFT ANALYSIS
C
        NPTS=IFPNTS
C
C       PROVIDE APPROPRIATE DATA WINDOW
C
        CALL WINDOW(X1,NPTS,PI,IUNIT3,IUNIT4,IWNDOW)
C
C       PERFORM FAST FOURIER TRANSFORM
C
        CALL FFT(X1,X2,NPTS,IDIR,SAMRAT)
C
C       COMPUTE POWER SPECTRAL DENSITY
C
```

```
      CALL PSD(X1,X2,NPTS,SAMRAT,IWNDOW)
C
C     POWER SPECTRAL DENSITY IS SYMMETRIC IN THIS CASE,
C     ONLY NEED TO PLOT ONE HALF OF IT
C
      NPTS=NPTS/2
C
C     CALCULATE FREQUENCY SPACING
C
      DLFREQ=SAMRAT/(FLOAT(NPTS*2))
C
C     CALCULATE MOMENTS OF THE POWER SPECTRAL DENSITY
C
      CALL MOMENT(DLFREQ,X1,ALPHAB,IUNIT3,IUNIT4,
     1SRAWMM,SECMOM,SKEW,TOSIS,GRAPNM,NPTS,X2,IPLOT)
C
C     WRITE ACTUAL PSD DATA VALUES TO PRINTER
C
      CALL WRITEA(X1,NPTS,IUNIT3,SAMRAT)
C
C     SET UP FREQUENCY AXIS
C
      CALL FREQST(IVAL,VDRNG,PLSZE,VDSZE)
C
C     COMPRESS DATA FOR GRAPHING PURPOSES
C
      CALL COMPRS(X1,NPTS,BINDAT,IVAL,PLSZE,SAMRAT,IUNIT4,
     1VDSZE)
C
C     PLOT PSD DATA
C
      CALL PLOT(STARS,IBNPNT,IVAL,BINDAT,IXBIN,VDRNG,
     1IUNIT3,IUNIT4,IPLOT,GRAPNM)
C
C     CLOSE DECPACK UNIT
C
      CALL CLOSE(IUNIT2)
C
C     CHECK IF ADDITIONAL DATA PROCESSING WITH
C     ADDITIONAL WINDOWS IS DESIRED
C
      WRITE(IUNIT4,700)
700   FORMAT(1H0,33HIF ADDITIONAL WINDOWS ARE DESIRED,//,
     11X,21HTYPE 1, IF NOT TYPE 0)
C
      READ(IUNIT4,800) IRPFFT
800   FORMAT(I4)
C
C     CHECK FOR REPEAT OF FFT CALCULATION
C
      IF (IRPFFT.GT.0) GO TO 400
C
      STOP
      END
```

```
      SUBROUTINE TILZER(IBNPNT,BINDAT,DLVOID,IVAL,SCALEF,I,IXBIN,
     1IUNIT3,IUNIT4,DCBIAS,SAMRAT,IFPNTS,PLSZE,IPROCS)
C
      DIMENSION SCALE(2,6),IBNPNT(120),BINDAT(120)
C
      DATA SCALE/19.94,955.66,33.0,953.03,81.03,941.68,
     1167.71,918.13,295.59,859.93,443.46,740.90/
C
C     READ IN VOID INCREMENT SIZE
C
      WRITE(IUNIT4,100)
100   FORMAT(1H0,39HENTER VOID INCREMENT VALUE, F8.7 FORMAT)
      READ(IUNIT4,200) DLVOID
200   FORMAT(F8.7)
C
C     READ IN PARAMETER TO SELECT APPROPRIATE
C     VOID DATA SCALING
C
      WRITE(IUNIT4,300)
300   FORMAT(1X,39HENTER CHORDAL SELECT VALUE IN I4 FORMAT)
      READ(IUNIT4,400) ISELCT
400   FORMAT(I4)
C
C     CHECK FOR OPTION DATA INPUT
C
      IF (ISELCT.NE.0) GO TO 800
C
C     READ IN ALL VAPOR SCALE FACTOR
C
      WRITE(IUNIT4,500)
500   FORMAT(1X,41HENTER ALL VAPOR BIAS FACTOR, F10.3 FORMAT)
      READ(IUNIT4,600) SCALEF
600   FORMAT(F10.3)
C
C     READ IN ALL LIQUID SCALE FACTOR
C
      WRITE(IUNIT4,700)
700   FORMAT(1X,34HENTER ALL WATER BIAS, F10.3 FORMAT)
      READ(IUNIT4,600) DCBIAS
C
      GO TO 900
C
C     SELECT ALL WATER BIAS VALUE FROM TABLE
C
800   DCBIAS=SCALE(1,ISELCT)
C
C     SELECT ALL VAPOR SCALING FACTOR FROM TABLE
C
      SCALEF=SCALE(2,ISELCT)
C
C     READ NUMBER OF SETS OF DATA POINTS, IN UNITS OF 256
C
900   WRITE(IUNIT4,1000)
1000  FORMAT(1X,34HENTER NUMBER OF DATA POINT RECORDS)
```

```
      F AD(IUNIT4,400) I
C
C     READ IN NUMBER OF DATA POINTS IN FOURIER TRANSFORM ROUTINE
C
      WRITE(IUNIT4,1100)
1100  FORMAT(1X,35HENTER NUMBER OF DATA POINTS FOR FFT)
      READ(IUNIT4,400) IFPNTS
C
C     READ IN DATA SAMPLING RATE
C
      WRITE(IUNIT4,1200)
1200  FORMAT(1X,36HENTER DATA SAMPLING RATE, PER SECOND)
      READ(IUNIT4,600) SAMRAT
C
C     READ IN TYPE OF FREQUENCY RANGE DESIRED IN PSD PLOT
C
      WRITE(IUNIT4,1300)
1300  FORMAT(1X,35HENTER MAXIMUM FREQUENCY OF INTEREST,
     117H, IN F10.3 FORMAT)
      READ(IUNIT4,600) PLSZE
C
C     READ IN PARAMETER TO INDICATE TYPE
C     OF DATA TO BE PROCESSED
C
      WRITE(IUNIT4,1400)
1400  FORMAT(1HO,26HENTER DATA TYPE PARAMETER ,//,
     11X,22HORIGINAL DATA, ENTER 0,//,
     21X,23HPROCESSED DATA, ENTER 1)
C
      READ(IUNIT4,400) IPROCS
C
C     DATA TAKEN FOUR AT A TIME,
C     MODIFY I FOR NUMBER OF SETS
C
      I=I*64
C
C     READ/WRITE EXTRA SIDE BINS
C
      WRITE(IUNIT4,1500)
1500  FORMAT(1X,34HENTER EXTRA SIDE BINS IN I4 FORMAT)
      READ(IUNIT4,400) IXBIN
      WRITE(IUNIT3,1600) DCBIAS
      WRITE(IUNIT4,1600) DCBIAS
1600  FORMAT(/,1X,25HTHE WATER BIAS VALUE IS: ,F8.3)
      WRITE(IUNIT3,1700) IXBIN
      WRITE(IUNIT4,1700) IXBIN
1700  FORMAT(/,1X,20HEXTRA SIDE BINS ARE:,I4,2X,8HPER SIDE)
C
C     DETERMINE NUMBER OF BINS
C
      IVAL=IFIX(1.0/DLVOID)
C
C     ADD IXBIN BINS TO EACH SIDE TO ALLOW FOR UNDER/OVERFLOW
C
      IVAL=IVAL+(2*IXBIN)
```

```
C
      WRITE(IUNIT3,1800) IVAL
      WRITE(IUNIT4,1800) IVAL
1800  FORMAT(/,1X,15HNUMBER OF BINS=,I4)
C
C     SET BINS AND BIN DATA POINT COUNTERS EQUAL TO ZERO
C
      DO 1900 IV=1,IVAL
C
      IBNPNT(IV)=0
      BINDAT(IV)=0.0
1900  CONTINUE
C
C     SET SCALEF FOR LATER USE
C
      SCALEF=(SCALEF-DCBIAS)*DLVOID
C
      WRITE(IUNIT3,2000) SCALEF
      WRITE(IUNIT4,2000) SCALEF
2000  FORMAT(/,1X,24HVOID BIN SCALING FACTOR=,F10.4)
C
C     WRITE OUT NUMBER OF FFT POINTS AND SAMPLING RATE
C
      WRITE(IUNIT3,2100)IFPNTS
      WRITE(IUNIT4,2100)IFPNTS
2100  FORMAT(/,1X,24HTIME DATA POINTS IN FFT= ,I6)
C
      WRITE(IUNIT3,2200) SAMRAT
      WRITE(IUNIT4,2200) SAMRAT
2200  FORMAT(/,1X,16HDATA ACQUIRED AT,F7.2,19H SAMPLES PER SECOND)
C
C     WRITE OUT MAXIMUM FREQUENCY DESIRED IN PSD PLOT
C
      WRITE(IUNIT3,2300) PLSZE
      WRITE(IUNIT4,2300) PLSZE
2300  FORMAT(/,1X,20HTHE PLOT WILL COVER ,F8.3,6H HERTZ)
C
C     SIGNIFY TYPE OF DATA BEING USED
C
      IF (IPROCS) 2400,2400,2600
C
2400  WRITE(IUNIT3,2500)
      WRITE(IUNIT4,2500)
2500  FORMAT(1HO,24HORIGINAL DATA BEING USED)
      RETURN
C
2600  WRITE(IUNIT3,2700)
      WRITE(IUNIT4,2700)
2700  FORMAT(1HO,36HPREVIOUSLY PROCESSED DATA BEING USED)
C
      RETURN
      END
```

```
      SUBROUTINE REDATA(N,IDATA,IUNIT1)
C
C     SUBROUTINE TO READ IN N [illegible] POINTS FROM DEC TAPE
C
      DIMENSION IDATA(4)
      READ(IUNIT1,100) (IDATA(NN),NN=1,N)
100   FORMAT(1X,4I4)
      RETURN
      END
```

```
      SUBROUTINE BINS(N,IDATA,IBNPNT,SCALEF,IVAL,IXBIN,DCBIAS)
C
      DIMENSION IDATA(4),IBNPNT(120)
C
      DO 200 NN=1,N
C
C     SELECT BIN USING INTEGER DIVISION
C
      F=FLOAT(IDATA(NN))
C
C     APPLY DC BIAS FOR ALL WATER VALUE
C
      F=F-DCBIAS
C
      IV=IFIX(F/SCALEF)
C
C     INCREMENT BINS
C
      IVI=IV+IXBIN+1
C
      IBNPNT(IVI)=IBNPNT(IVI)+1
C
200   CONTINUE
      RETURN
      END
```

```
      SUBROUTINE ORMALZ(JCT,DLVOID,BINDAT,IBNPNT,IVAL,
     1IXBIN,VDRNG,IUNIT2,IUNIT3,IUNIT4,IPROCS)
C
      DIMENSION BINDAT(120),IBNPNT(120),VDRNG(121)
C
C     WRITE OUT HEADINGS
C
      WRITE(IUNIT3,75)
75    FORMAT(1HO,1X,10HVOID RANGE,5X,10H PDF VALUE ,
```

```
     15X,16HNUMBER OF POINTS)
C
C    CALCULATE NORMALIZING VALUE FOR NUMBER OF POINTS IN
C    EACH BIN
C
     RMALZR=FLOAT(JCT)
C
C    SET VOID CALCULATION ONE HIGH TO FILL RANGE
C
     IXAL=IVAL+1
C
C    TAG DECPACK DATA
C
     WRITE(IUNIT2,50) IXAL
50   FORMAT(1X,I4)
C
C    APPLY NORMALIZING VALUE
C
     DO 200 IV=1,IXAL
     BINDAT(IV)=FLOAT(IBNPNT(IV))/RMALZR
C
C    CALCULATE VOID BIN
C
     VDRNG(IV)=FLOAT(IV-1-IXBIN)*DLVOID
C
     WRITE(IUNIT2,100) VDRNG(IV),BINDAT(IV),IBNPNT(IV)
     WRITE(IUNIT3,100) VDRNG(IV),BINDAT(IV),IBNPNT(IV)
100  FORMAT(1X,F10.5,5X,F10.4,9X,I8)
C
200  CONTINUE
C
C    SUM UP ALL POINTS IN PDF FOR COMPARISON
C
     ITOTAL=0
C
     DO 400 IV=1,IVAL
     ITOTAL=ITOTAL+IBNPNT(IV)
400  CONTINUE
C
C    WRITE OUT VALUES FOR  COMPARISON
C
     WRITE(IUNIT3,500) ITOTAL,JCT
     WRITE(IUNIT4,500) ITOTAL,JCT
500  FORMAT(/,1X,28HTHE TOTAL NUMBER IN THE PDF=,I8,3X,
     127HTHE TOTAL NUMBER OF POINTS=,I8)
C
     RETURN
     END
```

```
      SUBROUTINE PRESET(N,BINDAT,VDRNG,IBNPNT,IUNIT1,
     1IUNIT2,FILEO,IUNIT3,IPROCS)
      DIMENSION BINDAT(120),IBNPNT(120),VDRNG(121),
     1FILEO(2)
      JCT=0
C
C     SET TRIP FOR USE OF PREVIOUSLY
C     PROCESSED DATA
C
      IPROCS=1
C
C     ACCESS PREVIOUS DATA
C
      CALL SEEK(IUNIT2,FILEO)
C
C     READ AND WRITE NUMBER OF DATA POINT SETS
C
      READ(IUNIT2,100) IXAL
100   FORMAT(1X,I4)
C
      IVAL=IXAL-1
C
      WRITE(IUNIT3,200) IVAL
200   FORMAT(1H ,I6,12H BINS IN PDF)
C
C     READ IN PDF DATA
C
      DO 400 IV=1,IXAL
      READ(IUNIT2,300) VDRNG(IV),BINDAT(IV),IBNPNT(IV)
300   FORMAT(1X,F10.5,5X,F10.4,9X,I8)
C
400   CONTINUE
C
C     REFORM PDF TO INSURE NUMERICAL REPRODUCIBILITY
C
C     SUM UP POINTS FOR NORMALIZATION
C
      DO 500 IX=1,IXAL
      JCT=JCT+IBNPNT(IX)
500   CONTINUE
C
      RMALZR=FLOAT(JCT)
C
C     FORM PDF
C
      DO 600 IX=1,IXAL
      BINDAT(IX)=(FLOAT(IBNPNT(IX)))/RMALZR
600   CONTINUE
C
C     RESET INPUT DATA UNIT
C
      IUNIT1=IUNIT2
C
      RETURN
      END
```

```
      SUBROUTINE MOMENT(DLVOID,BINDAT,ALPHAB,IUNIT3,
     1IUNIT4,SRAWMM,SECMOM,SKEW,TOSIS,GRAPNM,IVAL,VDRNG,
     2IPLOT)
C
      REAL LIMITS(11)
C
      DIMENSION BINDAT(120),VDRNG(121),HEADNG(11),TYPE(2)
      DATA TYPE(1),TYPE(2)/3HPDF,3HPSD/
C
C     INITIALIZE MOMENT REGISTERS AND PDF INTEGRATION
C
      ALPHAB=0.0
      SRAWMM=0.0
      GRAPNM=0.0
      GRALIM=0.1
      ILIM=1
      SECMOM=0.0
      THDMOM=0.0
      FTHMOM=0.0
C
C     INTEGRATE THE PDF TO DETERMINE NORMALIZING CONSTANT
C
      DO 100 IV=1,IVAL
C
      ADVOID=VDRNG(IV)
C
      GRAPNM=GRAPNM+BINDAT(IV)
C
      IF (IPLOT.EQ.2) GO TO 100
C
C     CHECK FOR LIMIT
C
      IF (ADVOID.GE.GRALIM.AND.GRAPNM.LT.0.9999) CALL LIMIT(
     1ADVOID,GRALIM,LIMITS,ILIM,HEADNG,GRAPNM)
C
100   CONTINUE
C
      IF (IPLOT.EQ.2) GO TO 235
C
C     RESET LIMIT FOR PRINTING PURPOSES
C
      ILIM=ILIM-1
C
C     WRITE OUT INTEGATED PDF AND VOID FRACTION LIMIT
C
      WRITE(IUNIT3,200) (HEADNG(IL),IL=1,ILIM)
      WRITE(IUNIT4,200) (HEADNG(IL),IL=1,ILIM)
200   FORMAT(1H0,22HCRITICAL VOID FRACTION,6X,11(F6.3,3X))
C
      WRITE(IUNIT3,225) (LIMITS(IL),IL=1,ILIM)
```

```
      WRITE(IUNIT4,225) (LIMITS(IL),IL=1,ILIM)
225   FORMAT(1HO,'25HINTEGRATED AREA/REMAINDER,2X,11(F7.2,2X))
C
C     WRITE TOTAL INTEGRAL OF PDF
C
235   WRITE(IUNIT3,250) TYPE(IPLOT),GRAPNM
      WRITE(IUNIT4,250) TYPE(IPLOT),GRAPNM
250   FORMAT(1HO,15HINTEGRATION OF ,A3,1H=,F12.7)
C
C
C     COMPUTE FIRST AND SECOND MOMENTS, I.E. MEAN
C     AND VARIANCE ABOUT THE ORIGIN
C
      DO 150 IV=1,IVAL
C
C     CALCULATE X AXIS VALUE
C
      ADVOID=VDRNG(IV)+(DLVOID/2.0)
C
      CONPRT=ADVOID*BINDAT(IV)
C
C     CALCULATE MEAN VALUE
C
      ALPHAB=ALPHAB+CONPRT
C
C     CALCULATE VARIANCE
C
      SRAWMM=SRAWMM+(ADVOID*CONPRT)
C
150   CONTINUE
C
C     COMPUTE SECOND, THIRD AND FOURTH MOMENTS
C     ABOUT THE MEAN
C
      DO 300 IV=1,IVAL
C
C     CALCULATE X AXIS DIFFERENCE FROM MEAN
C
      ADVOID=((VDRNG(IV)+(DLVOID/2.0))-ALPHAB)
C
C     CALCULATE MOMENTS WITH RESPECT TO MEAN
C
      CONPRT=(ADVOID**2)*BINDAT(IV)
C
      SECMOM=SECMOM+CONPRT
C
      THDMOM=THDMOM+(ADVOID*CONPRT)
C
      FTHMOM=FTHMOM+((ADVOID**2)*CONPRT)
C
300   CONTINUE
C
C     FORM COEFFICIENTS OF SKEWNESS AND KURTOSIS
C
C     SKEWNESS
```

```
C
      SKEW=THDMOM/(SECMOM**1.5)
C
C     KURTOSIS
C
      TOSIS=FTHMOM/(SECMOM**2.0)
C
C     WRITE OUT FIRST MOMENT, I.E. MEAN
C
      WRITE(IUNIT3,350) ALPHAB
      WRITE(IUNIT4,350) ALPHAB
350   FORMAT(1HO,27HTHE AVERAGE VOID FRACTION= ,F10.5)
C
C     WRITE OUT VARIANCES, I.E. SECOND MOMENT
C
C     ABOUT THE ORIGIN
C
      WRITE(IUNIT3,375) SRAWMM
      WRITE(IUNIT4,375) SRAWMM
375   FORMAT(1HO,31HTHE VARIANCE ABOUT THE ORIGIN= ,F10.5)
C
C     ABOUT THE MEAN
C
      WRITE(IUNIT3,400) SECMOM
      WRITE(IUNIT4,400) SECMOM
400   FORMAT(1HO,29HTHE VARIANCE ABOUT THE MEAN= ,F10.5)
C
C     WRITE OUT COEFFICIENT OF SKEWNESS
C
      WRITE(IUNIT3,500) SKEW
      WRITE(IUNIT4,500) SKEW
500   FORMAT(1HO,29HTHE COEFFICIENT OF SKEWNESS= ,F10.5)
C
C     WRITE OUT THE COEFFICIENT OF KURTOSIS
C
      WRITE(IUNIT3,600) TOSIS
      WRITE(IUNIT4,600) TOSIS
600   FORMAT(1HO,29HTHE COEFFICIENT OF KURTOSIS= ,F10.5)
C
C     RESET GRAPNM WHEN PSD MOMENTS HAVE BEEN CALCULATED
C
      IF (IPLOT.EQ.2) GRAPNM=1.0
C
      RETURN
      END
```

```
      SUBROUTINE LIMIT(ADVOID,GRALIM,LIMITS,ILIM,HEADNG,GRAPNM)
C
      REAL LIMITS(11),HEADNG(11)
C
C     STORE LIMITING VALUE
C
      LIMITS(ILIM)=GRAPNM/(1.0-GRAPNM)
      HEADNG(ILIM)=GRALIM
C
C     INCREMENT LIMIT COUNTER
C
      ILIM=ILIM+1
C
C     INCREMENT INTEGRATION LIMITS
C
      GRALIM=GRALIM+0.10
C
      RETURN
      END



      SUBROUTINE PLOT(STARS,IBNPNT,IVAL,BINDAT,IXBIN,VDRNG,
     1IUNIT3,IUNIT4,IPLOT,GRAPNM)
C
      DIMENSION STARS(1024),IBNPNT(120),VDRNG(121),BINDAT(120),
     1TYPE(2),BINSTO(121)
C
      DATA ASTAR/1H*/
      DATA BSTAR/1H /
      DATA CSTAR/1H+/
      DATA TYPE(1),TYPE(2)/3HPDF,3HPSD/
C
C     SET PLOT SIZE
C
      SIZE=40.0
      ISIZE=IFIX(SIZE)
C
C     SCALE DATA FOR PLOTTING
C
      SCALEN=0.0
C
C     FIND MAX PDF VALUE
C
      DO 100 IV=1,IVAL
      SCLCHK=BINDAT(IV)
      IF (SCLCHK.GT.SCALEN) SCALEN=SCLCHK
100   CONTINUE
C
C     WRITE OUT MAXIMUM VALUE
C
```

```
      WRITE(IUNIT3,200) TYPE(IPLOT),SCALEN
      WRITE(IUNIT4,200) TYPE(IPLOT),SCALEN
200   FORMAT(/,1X,8HMAXIMUM ,A3,8H VALUE= ,F10.4)
C
C     SELECT PLOT SCALING
C
      CALL SCALAT(SCALEN,IPLCNT,IUNIT4)
C
C     SET SCALING CONSTANT
C
      SCALR=SIZE/SCALEN
C
C     SKIP SOME SPACES
C
      WRITE(IUNIT3,300)
300   FORMAT(1H1,1X,//////)
C
C     SET Y-AXIS INCREMENT FOR PDF GRAPH
C
      SCALEN=SCALEN/(10.0**IPLCNT)
C
      PLCMNT=SCALEN/SIZE
C
C     APPLY SCALING
C
      DO 400 IV=1,IVAL
      BINSTO(IV)=BINDAT(IV)/((10.0**IPLCNT)*GRAPNM)
400   CONTINUE
C
C     PLOT GRAPH
C
      DO 900 IN=1,ISIZE
C
C     SET MAGNITUDE NEEDED FOR PLOT LINE
C
      TEST=SCALEN-(0.5*PLCMNT)
C
C     FILL ARRAY FOR THIS LINE
C
      DO 700 IV=1,IVAL
C
      IF (BINSTO(IV)-TEST) 500,600,600
C
C     PUT IN A BLANK IF INSUFFICIENT MAGNITUDE
C
500   STARS(IV)=BSTAR
      GO TO 700
C
C     PUT IN STAR TO INDICATE PLOT VALUE
C
600   STARS(IV)=ASTAR
C
700   CONTINUE
C
C     MAKE ACTUAL PLOT
```

```
C
C       ROUTE FOR APPROPRIATE FORMAT
C
        ICA=IN/2
        ICA=ICA*2
        IF (ICA.EQ.IN) GO TO 825
        WRITE(IUNIT3,800) SCALEN,(STARS(IV),IV=1,IVAL)
800     FORMAT(1X,F5.3,2H +,120A1)
        GO TO 875
C
825     WRITE(IUNIT3,850) (STARS(IV),IV=1,IVAL)
850     FORMAT(6X,2H I,120A1)
C
C       RESET PLOT VALUE FOR NEXT PASS
C
875     SCALEN=SCALEN-PLCMNT
        IF (SCALEN.LT.0.0005) SCALEN=0.0
900     CONTINUE
C
C       WRITE IN BOTTOM SCALE OF GRAPH
C
C       SET BOTTOM SCALE
C
        ISCALE=10
C
C       SET IXAL TO PICKUP LAST POINT
C
        IXAL=IVAL+1
C
C       WRITE OUT BOTTOM SCALE
C
        WRITE(IUNIT3,1000) SCALEN,(CSTAR,IC=1,IXAL,ISCALE)
1000    FORMAT(1X,F5.3,1X,1H*,A1,12(9H----+----,A1))
C
        WRITE(IUNIT3,1100) (VDRNG(IV),IV=1,IXAL,ISCALE)
1100    FORMAT(5X,F6.2,15(4X,F6.2))
C
        IF (IPLOT.GT.1) GO TO 1300
C
        WRITE(IUNIT3,1200)
1200    FORMAT(/,62X,13HVOID FRACTION)
        GO TO 1500
C
1300    WRITE(IUNIT3,1400)
1400    FORMAT(/,50X,16HFREQUENCY, HERTZ)
C
C       WRITE OUT Y-AXIS SCALING FACTOR
C
1500    WRITE(IUNIT3,1600) IPLCNT
        WRITE(IUNIT4,1600) IPLCNT
1600    FORMAT(1H ,19HPLOT SCALED BY 1.0E,I2)
        RETURN
        END
```

```
      SUBROUTINE SCALAT(SCALEN,IPLCNT,IUNIT4)
C
C     INITIALIZE COUNTER
C
      IPLCNT=0
C
C     PLACE SCALING VALUE
C
100   IF (SCALEN.LE.1.0) GO TO 200
C
C     SCALING VALUE IS TOO LARGE
C
      SCALEN=SCALEN/10.0
      IPLCNT=IPLCNT+1
      GO TO 100
C
C     SUFFICIENTLY SMALL SCALING VALUE
C
200   IF (SCALEN.GT.0.1) GO TO 300
C
C     SCALING VALUE TOO SMALL
C
      SCALEN=SCALEN*10.0
      IPLCNT=IPLCNT-1
      GO TO 200
C
C     SCALING FACTOR IN APPROPRIATE RANGE,
C     SELECT EXACT SCALER
C
300   DO 400 NN=1,5
C
      XETA=(FLOAT(NN))*0.2
C
      IF (XETA.GT.SCALEN) GO TO 600
C
C     INCORRECT VALUE IS FOUND
C
400   CONTINUE
C
C     ERROR FLAG
C
      WRITE(IUNIT4,500)
500   FORMAT(1H0,27HINCORRECT SCALING OPERATION)
C
C     SET CORRECT VALUE
C
600   SCALEN=XETA*(10.0**IPLCNT)
C
      RETURN
      END
```

```
      SUBROUTINE REDATB(X1,X2,N,IFPNTS,SCALEF,DCBIAS,IUNIT1,
     1IPROCS,IUNIT2)
      DIMENSION X1(1024),X2(1024),IDATA(4)
C
C     READ IN INPUT DATA
C
      DO 200 II=1,IFPNTS,N
C
C     READ 4 INTEGER VALUES
C
      CALL REDATA(N,IDATA,IUNIT1)
C
      IF (IPROCS.EQ.0) WRITE(IUNIT2,300) (IDATA(NN),NN=1,N)
300   FORMAT(1X,4I4)
C
      DO 100 IJ=1,N
C
C     DO INITIAL SCALING
C
      IPOS=II+IJ-1
C
C     SET UP REAL COMPONENT
C
      X1(IPOS)=(FLOAT(IDATA(IJ))-DCBIAS)/SCALEF
C
C     SET UP IMAGINARY ARRAY
C
      X2(IPOS)=0.0
C
100   CONTINUE
C
200   CONTINUE
C
      RETURN
      END




      SUBROUTINE DCMOVE(N,X1,IUNIT3,IUNIT4)
      DIMENSION X1(1)
C
C     SUM ALL DATA POINT USED IN FFT CALCULATION
C
      XTOTAL=0.0
C
      DO 100 NI=1,N
      XTOTAL=XTOTAL+X1(NI)
100   CONTINUE
```

```
C
C       CALCULATE THE AVERAGE VALUE
C
        AVAL=XTOTAL/FLOAT(N)
C
        WRITE(IUNIT3,200) AVAL
        WRITE(IUNIT4,200) AVAL
200     FORMAT(1H1,1X,33HTHE AVERAGE VOID FRACTION IN PSD=,F7.4)
C
C       REMOVE DC VALUE FROM DATA
C
        DO 300 NI=1,N
        X1(NI)=X1(NI)-AVAL
300     CONTINUE
C
        RETURN
        END



        SUBROUTINE WINDOW(X1,N,PI,IUNIT3,IUNIT4,IWNDOW)
C
        DIMENSION X1(1),COEF(2,2)
C
C       HANNING WINDOW COEFFICIENTS
C
        DATA COEF(1,1),COEF(1,2)/0.50,0.50/
C
C       HAMMING WINDOW COEFFICIENTS
C
        DATA COEF(2,1),COEF(2,2)/0.54,0.46/
C
        DATA1=FLOAT(N-1)
C
C       SELECT WINDOW OPTION
C
C       NO WINDOW, TYPE 0
C
C       HANNING WINDOW, TYPE 1
C
C       HAMMING WINDOW, TYPE 2
C
        WRITE(IUNIT4,100)
100     FORMAT(/,1X,20HSELECT WINDOW OPTION)
        WRITE(IUNIT4,200)
200     FORMAT(/,1X,23HNO WINDOW OPTION-TYPE 0)
        WRITE(IUNIT4,300)
300     FORMAT(/,1X,2_HHANNING WINDOW-TYPE 1)
        WRITE(IUNIT4,400)
400     FORMAT(/,1X,21HHAMMING WINDOW-TYPE 2)
        READ(IUNIT4,500) IWNDOW
500     FORMAT(I4)
```

```
C
      IF (IWNDOW-1) 510,520,530
C
510   WRITE(IUNIT4,250)
      WRITE(IUNIT3,250)
250   FORMAT(/,1X,18HNO WINDOW EMPLOYED,/)
      RETURN
520   WRITE(IUNIT4,350)
      WRITE(IUNIT3,350)
350   FORMAT(/,1X,23HHANNING WINDOW EMPLOYED,/)
      GO TO 700
530   WRITE(IUNIT4,450)
      WRITE(IUNIT3,450)
450   FORMAT(/,1X,23HHAMMING WINDOW EMPLOYED,/)
C
C
C     HANNING/HAMMING WINDOW OPTIONS
C
700   DO 750 NI=1,N
C
      GAMMA=FLOAT(NI-1)
C
      ALPHA=COS(PI*((DATA1-(2.0*GAMMA))/DATA1))
C
      X1(NI)=X1(NI)*(COEF(IWNDOW,1)+(COEF(IWNDOW,2)*ALPHA))
C
750   CONTINUE
      RETURN
      END



      SUBROUTINE FFT(X1,X2,N,IDIR,SAMRAT)
C
C
C     ******** FAST FOURIER TRANSFORM FOR 2**P=9 *******
C
C                  ***FORTRAN-IV VERSION***
C
C
C     VARIABLES IN 'REAL' FORMAT.
C
C
C     AUTHORS: E. DE BOER AND H.R. DE JONGH.
C
C
      DIMENSION X1(1),X2(1)
C
      PI=3.14159
      TWPI=2.0*PI
      XN=N
      NQUART=N/4
C
```

```
C       CALCULATE POWER OF 2 FOR NUMBER OF DATA POINTS
C
        NSTAGE=ALOG(XN)/ALOG(2.)+0.01
C
C       CALCULATE UNIFORM NORMALIZATION FACTOR
C       I.E. MINIMUM PERIOD IN DATA
C
        SQRTST=1.0/SAMRAT
C
C       REGULAR ENTRY: SHUFFLE INPUT DATA:
C       SCRAMBLE INPUT ARRAYS SO THAT FFT OUTPUT IS UNSCRAMBLED
C       THIS ROUTINE PERFORMS BIT REVERSAL ON THE ARRAY
C       ARGUMENTS, I.E. MOVES NUMBER IN ARRAY LOCATION
C       01011 TO 11010 POSITION
C
        CALL RSHUF2(X1(1),X2(1),N)
C
C       THE MAIN BODY OF THE TRANSFORM
C       CONTAINS THREE NESTED LOOPS:
C
        IA=1
        INDEX1=N
C
C       OUTER LOOP:
C
        DO 100 ISTAGE=1,NSTAGE
C
        IB=IA
        IA=IA*2
        INDEX1=INDEX1/2
C
C       INNER LOOP:
C
        DO 100 I=1,N,IA
C
        IND=1
        L=I
        M=L+IB
C
C       INNERMOST LOOP:
C
        DO 100 J=1,IB
C
C       CALCULATE SINE FUNCTION VALUE
C
        SINS=SIN(TWPI*FLOAT(IND-1)/XN)
C
C       CHECK FOR INVERSE TRANSFORM
C
        IF (IDIR .LT. 0) SINS=-SINS
C
C       INCREMENT COUNTER BY 90.0 DEGREES TO CALCULATE COSINE VALUE
C
        IND2=IND+NQUART
C
```

```
C       CALCULATE COSINE FUNCTION VALUE
C
        COSS=SIN(TWPI*FLOAT(IND2-1)/XN)
C
C       PULL VALUES FROM DATA ARRAY
C
        X2M=X2(M)
        X1M=X1(M)
        X2L=X2(L)
        X1L=X1(L)
C
        A=X2M*SINS+X1M*COSS
        B=X1M*SINS-X2M*COSS
C
        X1(L)=X1L+A
        X2(L)=X2L-B
        X1(M)=X1L-A
        X2(M)=X2L+B
C
        L=L+1
        M=M+1
100     IND=IND+INDEX1
C
C       END OF TRANSFORM ROUTINE.
C
C       NORMALIZE OUTPUT DATA:
C
        DO 1000 I=1,N
        X1(I)=X1(I)*SQRTST
        X2(I)=X2(I)*SQRTST
1000    CONTINUE
C
        RETURN
        END
```

```
        .TITLE RSHUF2
/
/* * * * SHUFFLING ROUTINE * * * * * *
/
/
/       RSHUF2 PERFORMS SIMULTANEOUS SHUFFLING OF TWO REAL ARRAYS
/       AS PREPARATION FOR FAST FOURIER TRANSFORM, F4 VERSION.
/
/       AUTHOR: H.R. DE JONGH.
/
/       MODIFIED FOR USE AT RPI BY:
/
/                       BILL RUTZ
/                       MARK VINCE
/
/                       JANUARY 1979
```

```
/
/
/       CALLING SEQUENCE IN FORTRAN:
/
/       CALL RSHUF2(ARRAY NAME 1(1) , ARRAY NAME 2(1) , N )
/
/       ARRAY NAMES MUST REFER TO REAL ARRAYS.
/
/       FORTRAN CALL MUST BE MADE TO FIRST ELEMENT OF EACH ARRAY
/
/       N MUST BE A REAL POWER OF 2,
/       AND N=2**I, WHERE I IS AN INTEGER
/
/
        .GLOBL RSHUF2,.DA
RSHUF2  XX
        JMS*    .DA
        JMP     .+4
ARR1    0               /REFER TO ADDRESS OF FIRST WORD OF ARRAY #1.
ARR2    0               /THE SAME FOR ARRAY #2.
WC      0
        LAW     -21     /MAXIMUM SIZE IS 2^17.
        DAC     SH1#
        LAC     (1
        DAC     SHINDX#
        DAC     SHPOW#
        RCL
        SAD*    WC      /FIND THE PERTINENT POWER OF TWO.
        JMP     .+5
        ISZ     SHPOW
        ISZ     SH1
        JMP     .-5
        JMP     SHERR
        LAW     -3
        TAD*    WC
        CMA
        DAC     SHCNT#  /WC-2  DATA TO BE SHUFFLED.
        LAC     SHPOW   /CONTAINS THE POWER OF TWO.
        CMA
        TAD     (1
        DAC     SHPOW
/
/       INITIALIZE SHUFFLE LOOP;
/       FIRST PERFORM BIT REVERSION:
/
INIT    LAC     SHPOW
        DAC     SH1
        DZM     ADR2#
        LAC     SHINDX
        DAC     ADR1#   /SHINDX & ADR2 ARE GOING TO CONTAIN THE
SHLOOP  LAC     ADR1    /INDEXES OF THE 2 ELEMENTS THAT MUST BE
        RCR             /INTERCHANGED.
        DAC     ADR1
        LAC     ADR2
        RAL
```

```
        DAC     ADR2
        ISZ     SH1     /BIT REVERSION DONE?
        JMP     SHLOOP
        CMA             /AFTER THIS LOOP HAS BEEN COMPLETED, ADR2
/                       /CONTAINS THE NUMBER ORIG. STORED IN ADR1 ,N
/                       /BIT-REVERSED ORDER.
        TAD     (1
        TAD     SHINDX  /THIS NUMBER MUST BE > THAN THE
        SMA             /ORIGINAL CONTENTS OF ADR1.
        JMP     NOSHUF  /IF NOT, NO SHUFFLING IS NEEDED.
        LAC     ADR2    /SHINDX AND ADR2 STILL CONTAIN THE
        RCL
        DAC     ADR4*   /TWO NUMBERS CORRESPONDING WITH
        TAD     ARR1    /THE DATA WORDS THAT MUST BE INTERCHANGED.
        DAC     ADR2    /NOW THE REAL ADDRESSES OF THESE
        LAC     ADR4    /WORDS MUST BE FETCHED.
        TAD     ARR2
        DAC     ADR4
        LAC     SHINDX
        RCL
        DAC     ADR3*
        TAD     ARR1
        DAC     ADR1
        LAC     ADR3
        TAD     ARR2
        DAC     ADR3
        LAW     -2
        DAC     SH2*
/
/       INTERCHANGE THE TWO ELEMENTS:
/
        LAC*    ADR1    /GET FIRST DATA WORD FROM FIRST ARRAY.
        DAC     SH1     /STORE TEMPORARILY.
        LAC*    ADR2    /GET SECOND WORD.
        DAC*    ADR1    /INTERCHANGE.
        LAC     SH1
        DAC*    ADR2
        LAC*    ADR3    /DO THE SAME FOR THE SECOND ARRAY.
        DAC     SH1
        LAC*    ADR4
        DAC*    ADR3
        LAC     SH1
        DAC*    ADR4
        ISZ     ADR1
        ISZ     ADR2
        ISZ     ADR3
        ISZ     ADR4
        ISZ     SH2
        JMP     .-21
NOSHUF  ISZ     SHCNT   /ALL DONE?
        SKP             /NO.
        JMP*    RSHUF2  /YES, EXIT FROM SUBROUTINE.
        ISZ     SHINDX  /TRY NEXT INDEX.
        JMP     INIT    /GO BACK TO INITIALIZATION FOR
/                       /SHLOOP.
```

```
/
/
/
SHERR   LAW     67      /ERROR: SIZE LARGER THAN 2^17 OR
        JMP*    (4      /SIZE IS NOT AN INTEGER POWER OF 2.
/
```

```
        SUBROUTINE PSD(X1,X2,N,SAMRAT,IWNDOW)
C
        DIMENSION AMPSFT(3),X1(1),X2(1)
C
        DATA AMPSFT/1.0,2.0,1.8519/
C
C       CALCULATE POWER SPECTRAL DENSITY USING RESULTS FROM FFT15
C
C       NOTE THAT FFT15 NORMALIZES DATA TO THE TIME BETWEEN
C       ADJACENT DATA POINTS
C
C       CONSIDER N DATA POINTS, TAKEN AT A SAMPLING RATE
C       OF SAMRAT, TAKEN OVER N/SAMRAT SECONDS, I.E. T
C
C       PSD COMPUTED = (2/T)*((X1**2)+(X2**2))
C
        IAMPDW=IWNDOW+1
C
C       PSD IS MULTIPLIED BY 2.0 BECAUSE DATA IS STRICTLY REAL
C
C       CALCULATE SCALING COEFFICIENT, I.E. 2.0/T
C
        TEE=2.0*AMPSFT(IAMPDW)*SAMRAT/FLOAT(N)
C
        DO 100 I=1,N
C
C       CALCULATE MAGNITUDE OF PSD
C       MULTIPLICATION BY THE SCALING FACTOR MAKES THE PSD'S
C       MAGNITUDE CORRECT
C
        X1(I)=(X1(I)**2+X2(I)**2)*TEE
        X2(I)=(FLOAT(I-1)/FLOAT(N))*SAMRAT
C
100     CONTINUE
C
        RETURN
        END
```

```
      SUBROUTINE WRITEA(X1,N,IUNIT3,SAMRAT)
      DIMENSION X1(1024),FREK(4),XOUT(4)
C
      DATA BLANK/1H /
C
C     CALCULATE FREQUENCY SPACING
C
      DELFRQ=FLOAT(2*N)/SAMRAT
      IRTFRQ=N/4
C
C     WRITE OUT HEADING
C
      WRITE(IUNIT3,100) (BLANK,NQ=1,4)
100   FORMAT(1HO,4(9HFREQUENCY,2X,9HPSD VALUE,3X,A1))
C
C     WRITE OUT PSD VALUES AS A FUNCTION OF FREQUENCY
C
      DO 400 NJ=1,IRTFRQ
C
      DO 200 NQ=1,4
C
      ISPOT=NJ+((NQ-1)*IRTFRQ)
C
C     CALCULATE FREQUENCY
C
      FREK(NQ)=FLOAT(ISPOT-1)/DELFRQ
C
C     SELECT PSD VALUE
C
      XOUT(NQ)=X1(ISPOT)
C
200   CONTINUE
C
      WRITE(IUNIT3,300) (FREK(NQ),XOUT(NQ),NQ=1,4)
300   FORMAT(1H ,4(F7.3,1X,F10.4,6X))
C
400   CONTINUE
C
      RETURN
      END
```

```
      SUBROUTINE FREQST(IVAL,VDRNG,PLSZE,VDSZE)
      DIMENSION VDRNG(121)
C
C     SET COUNTER 1 HIGH TO ALLOW FOR DC VALUE
C
      IXAL=IVAL+1
C
C     SET PLOTTING SCALER
```

```
C
      VDSZE=FLOAT(IVAL)/PLSZE
C
C     CALCULATE FREQUENCY VALUES FOR PLOT
C
      DO 100 NI=1,IXAL
C
      VDRNG(NI)=FLOAT(NI-1)/VDSZE
C
100   CONTINUE
C
      RETURN
      END



      SUBROUTINE COMPRS(X1,N,BINDAT,IVAL,PLSZE,SAMRAT,IUNIT4,
     1VDSZE)
      DIMENSION X1(1024),BINDAT(121)
C
C     RESET BINDAT ARRAY
C
      DO 250 IN=1,IVAL
      BINDAT(IN)=0.0
250   CONTINUE
C
C     SET UP INITIAL CONSTANTS
C
      ICOUNT=0
C
      ASIZE=FLOAT(2*N)/SAMRAT
C
      IB=1
C
      PTOT=FLOAT(N)
C
      NCOUNT=IFIX(PLSZE*2.0*PTOT/SAMRAT)
C
C     PERFORM ERROR CHECK
C
      IF (NCOUNT.LE.N) GO TO 100
C
      WRITE(IUNIT4,200)
200   FORMAT(1X,29H**** PLOT SIZE INCORRECT ****)
      STOP
C
C     LOOP THROUGH APPROPRIATE DATA AND BIN ACCORDINGLY
C
100   DO 500 IP=1,NCOUNT
C
      FREQ=FLOAT(IP-1)/ASIZE
C
      COMPAR=((FLOAT(IB))-0.5)/VDSZE
```

```
C
C       BIN CHECK
C
        BINCHK=FREQ/COMPAR
C
        IF (BINCHK.LT.1.0) GO TO 300
C
C       AVERAGE PREVIOUS DATA
C
        BINDAT(IB)=BINDAT(IB)/FLOAT(ICOUNT)
C
C       RESET/INCREMENT COUNTERS
C
        ICOUNT=1
        IB=IB+1
C
C       STORE FIRST POINT OF NEXT BIN
C
        BINDAT(IB)=BINDAT(IB)+X1(IP)
C
        GO TO 500
C
C       INCREMENT COUNTER AND TALLY POINT
C
300     ICOUNT=ICOUNT+1
        BINDAT(IB)=BINDAT(IB)+X1(IP)
500     CONTINUE
C
        RETURN
        END
```

APPENDIX A.3

START UP AND DATA ACQUISITION PROCEDURE

A consistent technique was applied in starting the x-ray machine and acquiring the void fraction data. This scheme assured accuracy and repeatability of results. The technique is provided in instruction form.

Prior to Operation

1. Make sure grounded rod is applied to capacitors.
2. Bring battery water level to correct mark.
3. Clean battery terminals.
4. Fully charge batteries.(Over night is best)
5. Remove battery charger from high voltage field.
6. Start water flow through test section at 2 gpm.
7. Start cooling air flow to reference attenuator (2 valve turns).

X-ray Start-Up Procedure

1. Visually inspect air/water loop and x-ray tube for leaks or cracks.
2. Make sure local probe (if used) is fully inserted,i.e.

set micrometer drive at 0.100 in.

3. Plug in log-amp box.
4. Plug in 220 volt cable for x-ray unit.
5. Close lead covered door and plug in door interlock.
6. Turn on radiation detectors' power supply and slowly increase to 1200 volts.
7. Remove grounding rod from capacitors and place in interlocked bracket.
8. Set timer to 23 hours.
9. Turn high voltage control counter clock wise.
10. Unlock wall breaker switch and place in "ON" position.
11. Press "START" on main x-ray control panel to activate FA-60 cooling water pump. (Green light should come on.)
12. Visually observe x-ray cooling water flow from 3/4 in. copper pipe into drainage sink.
13. Turn on filament voltage supply and reduce to lowest possible current.
14. Press "ON" on main x-ray control panel.(After 20 seconds, a timer will turn on the red light, switch off the green light and activate the yellow x-ray warning light)
15. Slowly increase high voltage control, stopping for 5 minutes at increments of 5 kv. (This will prolong x-ray tube life)
16. Increase filament voltage supply to desired operating level. (Check the operational curve associated with the specific x-ray tube to determine the possible operating

conditions)

X-ray Set Up for Data Acquisition

1. Allow x-ray machine to operate for 5 hours making sure high voltage and current stay constant. Readjust if necessary.
2. Stop test section water flow and empty test section with large air flow.
3. Move x-ray unit to right side of test section with crank (Watch the voltage of the output line to the PDP-9 computer. This voltage will reach a minimum at the pipe edge)
4. Set dial micrometer to read 0.625 inches.
5. Move x-ray unit to left side of test section with crank. Micrometer should read 0.375 inches (If not, repeat steps 3 through 5 to get equal travel on each side.)
6. Return x-ray unit to the center of the pipe. Micrometer should read 0.000 inches.
7. Adjust reference attenuator (Knob near crank labelled 'c') to obtain zero output voltage from logarithmic amplifiers.
8. Refill test section with water and verify all water voltage.
9. Empty test section and reverify the zero voltage at the

logarithmic amplifier output.

10. Go to the computer room and measure cable voltage at input to the linear gate(It should be 4.00 volts).
11. Refill test section.
12. Return to computer room and set external pulser for correct frequency and pulse width.
13. Perform two-phase experiment.

X-ray Shutdown Procedure

1. Slowly reduce high voltage control to full counter-clockwise position. (Kilovolt meter should read zero)
2. Reduce filament voltage control to full counter-clockwise position.
3. Turn off filament supply.
4. Press "OFF" switch on main x-ray control panel.
5. Press "STOP" on main x-ray control panel.
6. Turn wall breaker switch to "OFF" position and lock in place.
7. Ground high voltage side of capacitors with grounding rod.
8. Shut off air flow to reference attenuator and set test section water flow rate to 1 gpm.
9. Reduce slowly and turn off radiation detectors' power

supply.

10. Enter x-ray test area and inspect for leaks or any abnormalities.
11. Disconnect logarithmic amplifier power supply.
12. Leave room and close lead covered door.

APPENDIX A.4

HIGH TEMPERATURE OPTICAL LOCAL PROBE

Two-phase flows are encountered in a wide variety of industrial applications. Accurate measurement of various liquid and vapor phase parameters on a local or global basis, is required for equipment design and computer model verification. To this end a high temperature local probe was developed at RPI. The next section will present the underlying analysis. The final section will present the design considerations.

Analysis

Phase detection, using light, is theoretically possible since the refractive index of vapor and liquid vary considerably. Employing high temperature fiber optics, light can be introduced into the two-phase environment. Moreover, the high frequency of visible and infrared light results in a small response time. A negligible dependence on other water properties, such as purity, would be expected since the probe only uses the phase refractive index for discrimination.

Local optical probes to measure the local void fraction of a flowing two-phase mixture have previously been designed and built [26,27]. These probes operate on the principles of Snell's Law,

$$n_1 \sin\phi_1 = n_2 \sin\phi_2 \qquad (1)$$

where,

n_1, n_2 = the refractive indices

ϕ_1 = the angle of incidence, measured with respect to a normal to the surface

ϕ_2 = the angle of refraction, measured with respect to a normal to the surface

Unfortunately since these early probes were made of glass, they were not suited for the high velocity, temperature, and pressure environment encountered in many important processes(eg: nuclear reactor safety experiments).

Nevertheless, employing the operational idea of Snell's Law, but using an optically clear, high temperature tip, a rugged probe can be developed. An optically clear diamond was used in this study since they are available at reasonable cost. The refractive index of diamond (2.41) is much greater than water (1.33), or air (1.00). This makes critical angle reflection possible. The manufacture of a small diamond for the a probe tip is straightforward since miniature synthetic diamonds are commonly cut as stereo turntable needles.

A conical-tipped cylindrical diamond was selected as the probe tip. A conical tip will provide easier penetration of the vapor/liquid interface, and minimize bubble distortion. The cylindrical shaft section of the tip

provides a region for mechanical attachment of the diamond to the protective outer tube. Figure A.4.1 illustrates the general tip shape.

The optical response of the diamond tip depends on numerous physical parameters. Length, radius, and tip angle are some of the important parameters. Other parameters include the optical properties of the incoming and outgoing light fibers as well as the relative ratio of input to output fiber area.

The fabrication and testing of a series of diamond tips to determine an optimum probe design would be costly. Thus, a computer simulation was developed to provide an easier and less expensive alternative. The code, known as DOPE-1, was written (Appendix-A.5) and used to model the optical response of the diamond tip. This two-dimensional simulation assumes that light rays move in straight lines of the form,

$$y_{ray} = m_{ray} x_{ray} + b_{ray} \qquad (2)$$

where,

y_{ray} = y-coordinate of the ray

m_{ray} = slope of the ray

x_{ray} = x-coordinate of the ray

b_{ray} = y-intercept of the ray

Several optical laws including Snell's Law for refraction, Beer's Law for attenuation [14], and Fresnel's Laws for reflection and refraction losses [14] were employed.

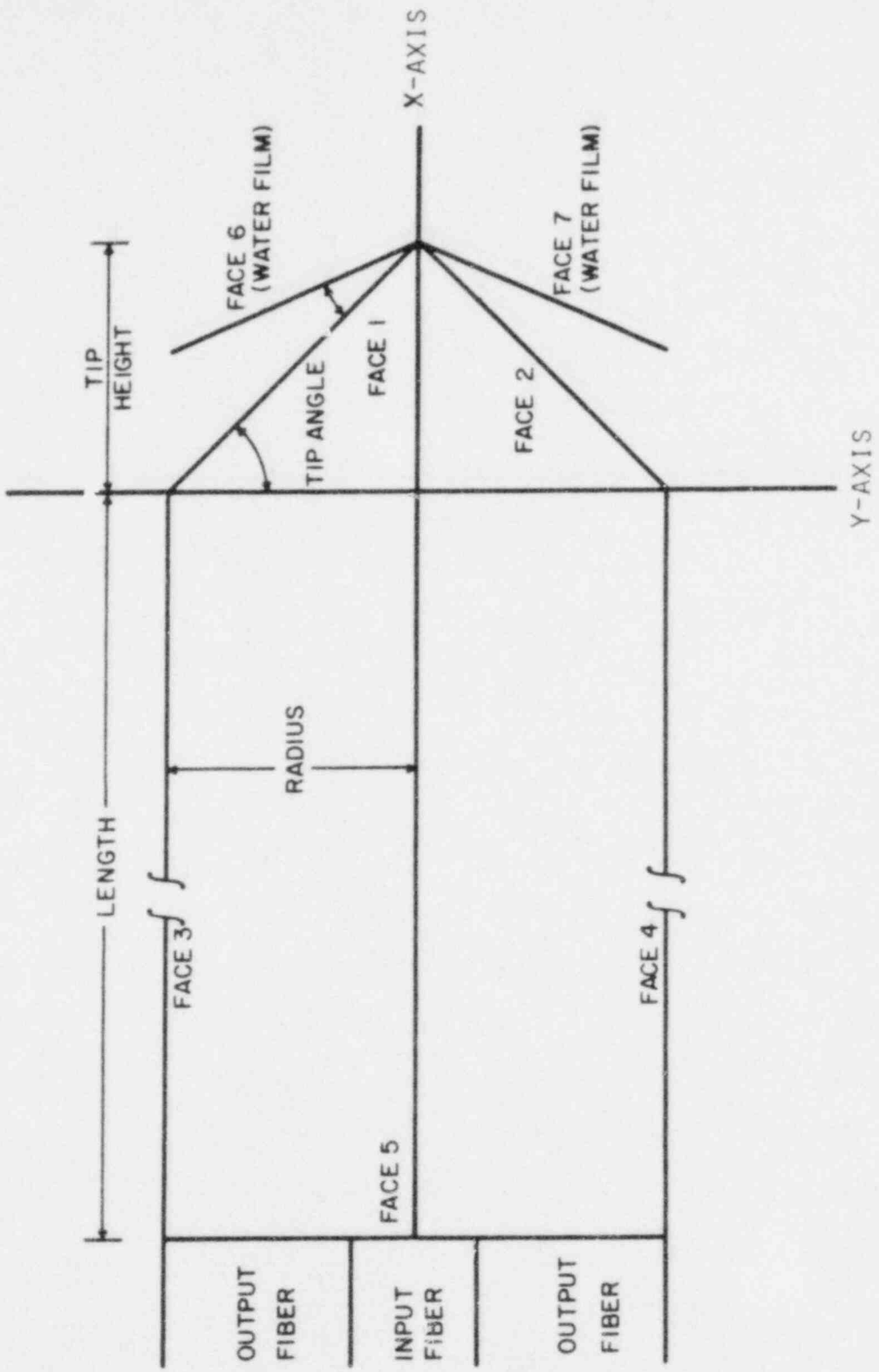

Figure A.4.1
The general diamond tip shape

Modeling options include the simulation of a residual water film on the tip and the angular distribution of the input light. A relative intensity is also calculated for each light ray. Variation of the important diamond parameters for optimum design is easily accomplished through code input.

Information obtained from DOPE-1 includes a coded summary of the ultimate fate of each light ray. This information is listed below in tabular form:

1	light transmitted through face 1
2	light transmitted through face 2
3	light transmitted through face 3
4	light transmitted through face 4
51	light at incorrect angle at face 5
52	light at incorrect position at face 5
6	light transmitted through face 6 (water film option only)
7	light transmitted through face 7 (water film option only)
88	light reflected back to acceptance region in fiber optic within acceptance cone
91	light transmitted out face 1 film edge
92	light transmitted out face 2 film edge

Table 1: Ray Trace Indicators

An option is available for listing the actual ray paths.

Modeling

The simulation is divided into five sections:

1) Establishment of a coordinate system.
2) Introduction of the light rays.
3) General ray tracing scheme.
4) Water film ray tracing.
5) Light intensity loss calculation.

The first three sections may be considered the nucleus of the simulation, while parts four and five can be viewed as refinements to the code. Visualizing the model in this fashion made an efficient development possible.

Geometric calculations form the basis of light ray tracing. The simulated light rays move in one coordinate system while the angle of incidence is calculated with respect to a system based on the normal of the intersected surface. Proper selection of a coordinate system will minimize the computational effort required to calculate the reflected light equation using the angle of incidence.

Figure A.4.1 illustrated the coordinate system employed in the DOPE-1 code. The x-axis is parallel to the sides of the diamond shaft and passes through the tip's apex. A y-axis was selected to pass through the conical tip's base. This choice makes face discrimination possible

by coordinates as summarized in Table 2.

	SIGN OF X-COORDINATE	SIGN OF Y-COORDINATE
FACE 1	+	+
FACE 2	+	-
FACE 3	-	+
FACE 4	-	-

TABLE 2: Polarity of Optical Coordinate System

The entering light rays must be initialized along the input optical fibers. Thus the light rays are assumed to originate along the back face (face 5). The selected coordinate system fixes the x-coordinate of these starting points at minus the diamond shaft length. A total distance available for light input, corresponding to the sum of the width of all input fibers, is calculated. From this total distance, a uniform spacing (i.e., the space between adjacent light rays) is computed. The first light ray is started below the uppermost boundary of the first input fiber. A second light ray is originated at an interval below the first. This process is repeated until the specified number of rays have been assigned initial 'x' and 'y' coordinate positions. It should be noted that the uniform spacing distance consists of one input fiber width.

If a ray is estimated to originate in a non-input region, the total width of this region is added to the light ray's estimated origin. This will shift the origin to a point inside an input fiber region.

Since the slope of the input light ray and the ray origin coordinates are known. only 'b', the y-intercept has to be calculated. Equation (2), can be rearranged to yield the ray's intercept,

$$b_{ray} = y_i - m_{ray} x_i \qquad (3)$$

where,

y_i = initial y-coordinate

x_i = initial x-coordinate

Now the initial light ray equation is complete.

General Ray Tracing Procedure

Simultaneous solution of the diamond face equation,

$$y_{face} = m_{face} x_{face} + b_{face} \qquad (4)$$

and the light ray equation,

$$y_{ray} = m_{ray} x_{ray} + b_{ray} \qquad (5)$$

will yield the 'x' and 'y' coordinates of an intersection point. The x-coordinate of this point is easily calculated by,

$$XXX = \frac{b_{face} - b_{ray}}{m_{ray} - m_{face}} \qquad (6)$$

where,

xxx = x-coordinate of intersection of ray and face

Should xxx be less than the diamond tip height or greater than minus the diamond shaft length, the y-coordinate is calculated by,

$$yyy = m_{ray}xxx + b_{ray} \tag{7}$$

where,

yyy = y-coordinate of intersection of ray and face

The parameter yyy must be less than the radius or greater than minus the radius. If these conditions have been met, the face under consideration has been intersected. When the conditions on xxx or yyy are not met, the next face in numerical order, is studied. This process is repeated until an intersection is found.

Depending on the angle of incidence, reflection or refraction may occur at an intersected face; as shown in Figure A.4.2. This angle is calculated from the face and ray slopes. Plane geometry dictates that angles ϕ_1, β, and θ should sum to 90 degrees,

$$\frac{\pi}{2} = \phi_1 + (-\beta) + \theta \tag{8}$$

where,

ϕ_1 = angle of incidence, with respect to the face normal

β = angle between the face and the axis (i.e., the arctangent of the face slope)

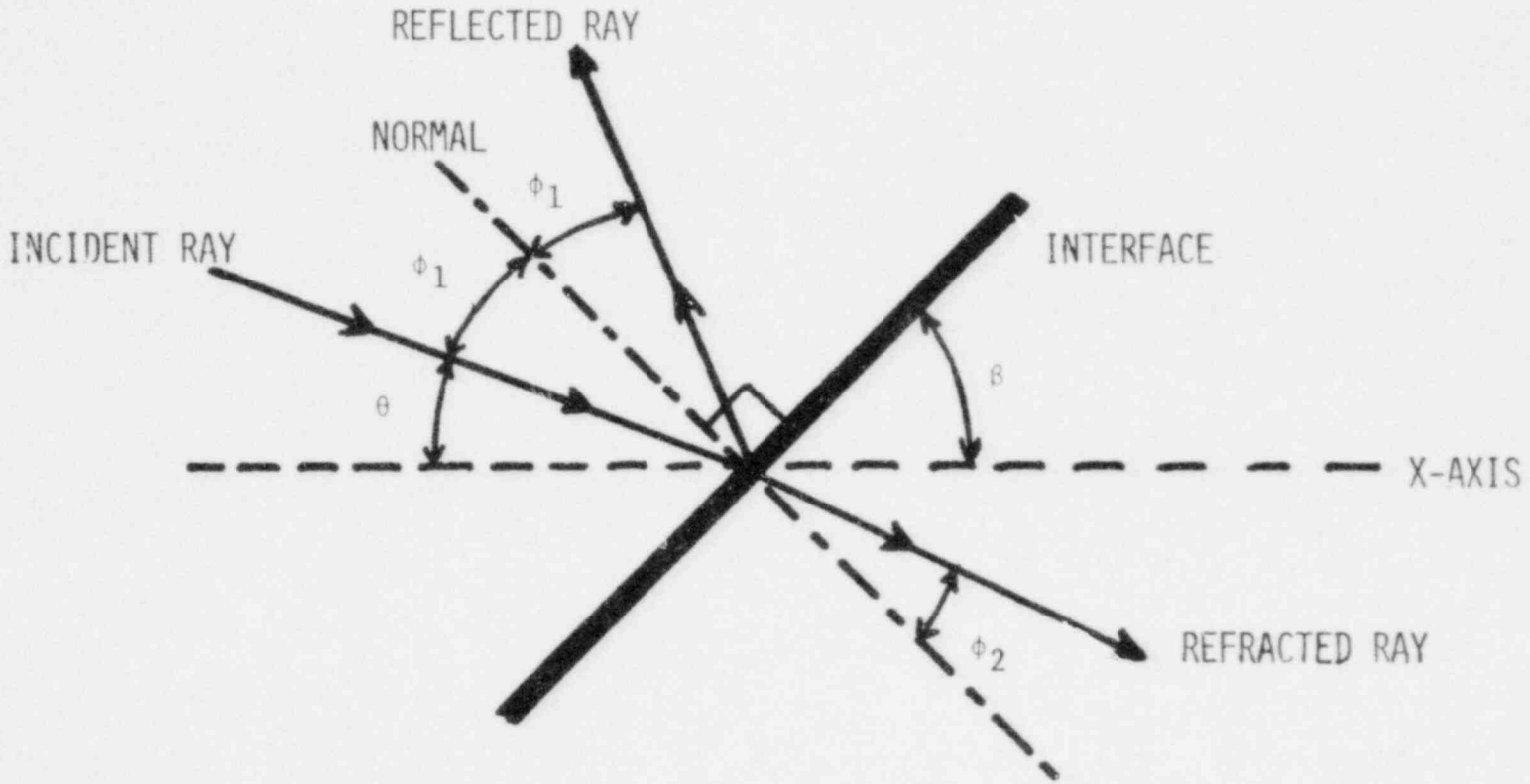

Figure A.4.2 Light ray reflection and refraction at an interface

θ = angle between the incident light ray and the x-axis (i.e., the arctangent of the ray's slope)

The angle of incidence can be obtained by rearranging Equation (8),

$$\phi_1 = \frac{\pi}{2} - (-\beta + \theta) \tag{9}$$

This angle is compared with the critical angle for that interface to determine if reflection or refraction has occurred.

For angles of incidence greater than the critical angle, internal reflection occurs, and a new ray tracing equation must be calculated. Refraction of the ray would usually terminate the tracing procedure and result in the ray being appropriately coded. When the water film option is used, and the rays are refracted through the appropriate faces, a refracted ray equation is generated. The ray tracing procedure is then continued within the liquid film.

A new equation for the reflected light ray can be obtained by assuming that the angle of incidence is equal to the angle of reflection. The 'x' and 'y' coordinates of a point on the ray are known as well as the slope of the face intersected. Combining these three quantities a new ray equation can be generated.

Two possible face-slope reflection situations could exist:

1) Slope of the reflected ray equal to zero.

2) Slope of the reflected ray not equal to zero. Figure A.4.3 illustrates three possible face/ray intersections, however the positive or negative slope cases yield the same analytical expression. The zero slope case is the simplest. A reflected ray's slope will just change sign. Then using the intersection coordinates and the new slope, the new ray intercept is calculated by Equation (3). A refelcted ray equation is now complete.

Generation of the reflected ray equation when the face slope is not zero is more complicated. Consider a normal to the diamond's face, the slope of the normal is the negative reciprocal of the face's slope,

$$\text{Normal Slope} = -\frac{1}{\text{Face Slope}} \tag{10}$$

Using plane geometry, the slope of the reflected ray can be related to the angle of incidence and surface normal,

$$\text{rayslp} = \tan(\phi_1 + \alpha) \tag{11}$$

where,

rayslp = slope of reflected ray

ϕ_1 = the angle of incidence, measured with respect to the normal

α = the angle between the normal and the positive x-coordinate axis, (i.e., the arctangent of the normal's slope)

RPI's IBM 3033 computer's tangent functions are valid only in the first and fourth quadrants. This

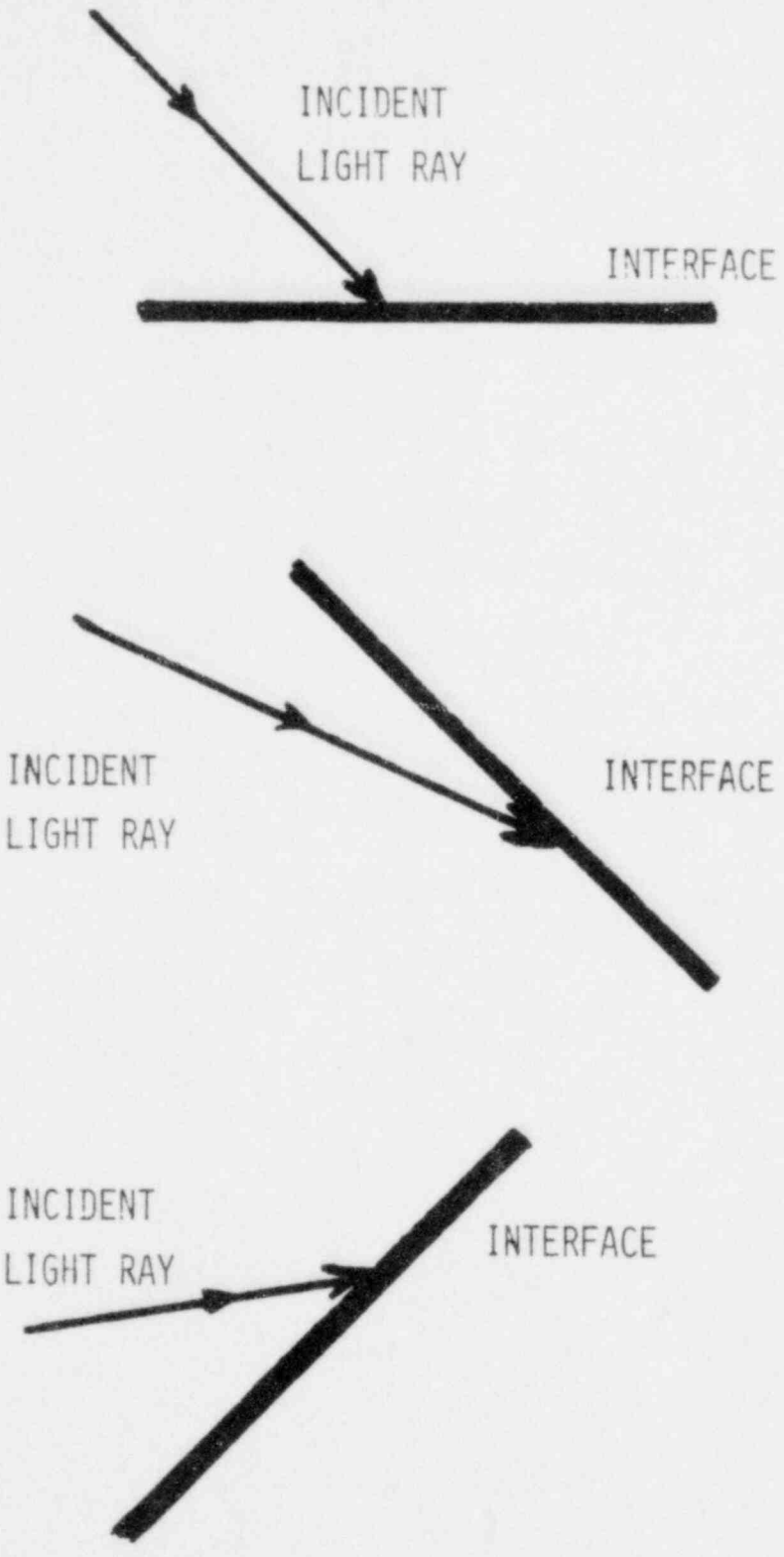

Figure A.4.3 Three possible surface/light ray intersections

condition imposes a limitation on the use of Equation (11), since the code may calculate an equation identical to the incident light ray equation. For this case, the new light ray equation must be corrected by an additional angle.

This adjustment angle is obtained from plane geometry. Using Figure A.4.2, the adjustment angle is calculated by,

$$\theta_{adj} = 2\left(\frac{\pi}{2} - \phi_1\right) \tag{12}$$

where,

ϕ_{adj} = adjustment angle, required to compensate for the computer's tangent function algorithm

ϕ_1 = angle of incidence, measured with respect to the normal

A new ray slope is then computed by adding the adjustment to the previously calculated angle,

$$rayslp_{new} = \tan\left(\tan^{-1}\left(rayslp_{old}\right) + \theta_{adj}\right) \tag{13}$$

where,

$rayslp_{new}$ = new light ray slope

$rayslp_{old}$ = previously calculated light ray slope

Θ_{adj} = adjustment angle, calculated by Equation (12)

The y-intercept is now calculated by using the new slope in Equation (3).

Light rays which have been retroreflected must meet two criteria before being considered fully accepted

into the fiber optic bundle connected to Face-5. First, these rays must strike the back face (Face-5) at an angle less than the acceptance cone angle. Light at a greater angle will be refracted out of the fiber optic bundle. Secondly, in our design only light rays which return to the zones designated as output fibers will be considered accepted. Any other retroreflected rays will not be detected by the signal-processing electronics.

The angle of incidence on the back face is easily computed since this face is vertical. This angle is obtained by taking the arctangent of the incident ray slope,

$$\bar{\phi}_1 = \tan^{-1}(\text{rayslp}) \tag{14}$$

where,

$\bar{\phi}_1$ = angle of incidence on back face (face-5)

rayslp = slope of incident light ray

The angle of incidence is positive by definition, therefore only the magnitude is considered. This angle of incidence, is compared to the acceptance angle of the optical fibers to determine if acceptance is possible.

Reflected light rays which satify the angle criterion are then checked for position. The y-coordinate of face-5 intersection is calculated and compared to fiber optic boundaries. When the fiber which has been struck is located, it is checked to see if it is and output fiber. Light rays striking an output fiber are considered accepted while all others are rejected and assumed lost.

Residual liquid phase may wet the probe tip during the vapor's presence. A simulation of this film was developed after a review of basic boundary layer models for wedge flows [49,50] indicated the possibility of such films. The residual liquid model employed is assumed to have zero thickness at the probe's apex and increase linearly along the conical tip.

Ray tracing in the water film begins by calculating the angle of refraction at the diamond/film interface. This angle is obtained from application of Snell's Law, Equation (1). A new ray equation is formulated by using the refraction angle as the angle of incidence in the previously described ray generation techniques.

Light rays in the liquid film that are moving away from the diamond tip can intersect with the (assumed) smooth liquid/vapor interface. The angle of incidence is compared with the critical angle to determine if refraction or reflection occurs. Reflection would result in generation of a new ray equation at an angle equal to the angle of incidence. Refraction at this point would stop the ray tracing routine and result in the appropriate ray coding.

Rays which strike the region of the water film colinear with face 3 or 4 are considered lost. These rays could originate due to a reflection on the liquid/vapor interface or come directly from the diamond. In either case, the rays are coded appropriately and the ray tracing is terminated.

Reflection at the liquid/vapor interface returns rays to the diamond tip. Snell's Law, Equation (1), is used to calculate the angle of refraction at the film/diamond interface. This angle is used as an angle of incidence to generate a new ray equation. The technique is identical to the one described for light rays leaving the diamond and entering the liquid film. Ray tracing techniques used for the general case are now employed to continue the ray trace.

As the light travels through the diamond the rays will be attenuated in two ways:

1) Attenuation along the path.

2) Attenuation at an interface.

Beer's Law, is used to calculate the attenuation along the ray path,

$$I = I_o \, e^{-\bar{\mu}x} \tag{15}$$

where,

I = intensity at a distance, 'x', into the media, photons/cm^2-sec

I_o = source intensity, photons/cm^2-sec

$\bar{\mu}$ = attenuation coefficient, dependent on media and light wavelength, cm^{-1}

x = pathlength through media, cm

The computer model stores the previous ray intersection coordinates and computes the pathlength as follows,

$$x = \sqrt{(x_n - x_o)^2 + (y_n - y_o)^2} \tag{16}$$

where,

x_n = x-coordinate of present ray position, cm

x_o = x-coordinate of previous ray position, cm

y_n = y-coordinate of present ray position, cm

y_o = y-coordinate of previous ray position, cm

Beer's Law is applied after intersection so that the light ray intensity is always current. This allows the ray to move into different media and keep the calculation procedure simple.

Fresnel's Laws are used to calculate the intensity of the transmitted and reflected rays. These laws account for the fact that an intensity loss occurs at an interface if the total reflection does not occur. In fact, the reflected light ray component may have a larger intensity than the transmitted. Fresnel's Laws are,

$$\frac{R_{st}}{E_s} = - \frac{\sin(\phi_1-\phi_2)}{\sin(\phi_1+\phi_2)} \tag{17}$$

and,

$$\frac{E_{st}}{E_s} = \frac{2\sin\phi_2\cos\phi_1}{\sin(\phi_1+\phi_2)} \tag{18}$$

and,

$$\frac{R_{pr}}{E_p} = \frac{\tan(\phi_1-\phi_2)}{\tan(\phi_1+\phi_2)} \tag{19}$$

and,

$$\frac{E_{pt}}{E_{pr}} = \frac{2\sin\phi_2\cos\phi_1}{\sin(\phi_1+\phi_2)\cos(\phi_1-\phi_2)} \tag{20}$$

where,

R_{sr} = perpendicular component of reflected light

E_s = perpendicular component of incident light

E_{st} = perpendicular component of transmitted light

R_{pr} = parallel component of reflected light

E_p = parallel component of incident light

E_{pr} = parallel component of reflected light

ϕ_1 = angle of incidence

ϕ_2 = angle of refraction

The reflectance is calculated by squaring Equation (17) for the perpendicular component, and squaring Equation (19) for parallel light.

Calculation of the transmitted intensity is not as simple. The total energy must be conserved. The total energy is obtained by multiplying the respective light ray intensity by its area,

$$\left(\frac{R}{E}\right)^2 + \frac{n_2}{n_1}\left(\frac{E_T}{E}\right)\frac{\cos\phi_2}{\cos\phi_1} = 1 \qquad (21)$$

This expression will apply to parallel or perpendicular light. Note that the refractive indices enter the analysis to conserve energy.

APPENDIX A.5

DIAMOND OPTICAL PROBE EVALUATION, VERSION 1, DOPE-1

This appendix contains a FORTRAN listing of the DOPE-1 code. This computer code traces the paths of light rays moving through a diamond tipped optical probe. Snell's Law is employed to calculate the angle of refraction. Beer's Law is used to calculate light ray attenuation along its path, while Fresnel's Laws are employed to calculate intensity losses at an interface.

The code is variably dimensioned for maximum flexibility. Using an IBM 3033 computer, one to two seconds of C.P.U. time is required per run.

```
C
C     DDDDDDD      OOOOOOOOO    PPPPPPP      EEEEEEEEE              111
C     DDDDDDDD     OOOOOOOOO    PPPPPPPP     EEEEEEEEE             1111
C     DDD   DDD    OOO   OOO    PPP  PPPP    EE                   11111
C     DDD   DDD    OOO   OOO    PPP  PPP     EEEEEEEEE    ----      111
C     DDD   DDD    OOO   OOO    PPPPPPPP     EEEEEEEEE    ----      111
C     DDD   DDD    OOO   OOO    PPPPPPP      EEE                    111
C     DDDDDDDD     OOOOOOOOO    PPP          EEEEEEEEE            111111111
C     DDDDDDD      OOOOOOOOO    PPP          EEEEEEEEE            111111111
C
C
C
C     DIAMOND OPTICAL PROBE EVALUATION, VERSION 1
C     $       $       $     $                    $
C
C
C
C                          SEPTEMBER 1978
C
C
C
C     DEVELOPED AT RENSSELAER POLYTECHNIC INSTITUTE FOR:
C
C                     UNITED STATES NUCLEAR REGULATORY COMMISSION
C                     WASHINGTON, D.C.
C                     CONTRACT AT(49-24)-0301
C                     DR T. T. HSU, DIRECTOR
C
C
C
C
C
C     AUTHOR:
C
C                     MARK VINCE
C                     NUCLEAR ENGINEERING AND SCIENCE BUILDING
C                     RENSSELAER POLYTECHNIC INSTITUTE
C                     TROY, NEW YORK 12181
C
C
C
C
C     WRITTEN IN PARTIAL FULFILLMENT OF THE REQUIREMENTS
C     FOR THE DEGREE OF DOCTOR OF PHILOSOPHY
C     IN NUCLEAR ENGINEERING
C
C
C
C
C
C     DOCTORAL COMMITTEE:
C
C                     DR. RICHARD T. LAHEY, JR. CHAIRMAN
C                     DR. HENRY E. BREED
C                     MR. GEORGE KRYCUK
C                     DR. RODNEY GAY
C                     DR. JOHN C. CORELLI
C
C
C
```

```
C
C                DOPE-1 PLANE GEOMETRY
C
C
C                          FACE 3
C
C      XXXXXXXX**********************************  CC
C               **********************************  OO       FACE 6
C               **                                ** CC
C       OUTPUT  **                                 ** OO (WATER FILM)
C               **                                  ** CO
C               **                          FACE 1   ** OO
C      XXXXXXXX**                                    ** OO
C               **                                     ** OO
C       INPUT   ** FACE 5                               **CC
C               **                                     ** OO
C      XXXXXXXX**                                     **  OO
C               **                          FACE 2    **  OO
C               **                                   **  CO
C       OUTPUT  **                                  **  CO     FACE 7
C               **                                 **  CC
C               **********************************  OO    (WATER FILM)
C      XXXXXXXX**********************************  CO
C
C                          FACE 4
C
C
C       FIBER              DIAMOND
C       OPTICS               TIP
C
C
C                        *** ABSTRACT ***
C
C
C          ACCURATE MEASUREMENT OF VOID FRACTION IN TWO PHASE FLOWS IS
C      NECESSARY FOR EQUIPMENT DESIGN AND COMPUTER MODEL VERIFICATION.
C      OPTICAL VOID MEASURING TECHNIQUES HAVE BEEN DEVELOPED(1,2), BUT
C      THESE DEVICES ARE NOT SUITED FOR HARSH INDUSTRIAL ENVIRONMENTS.
C          A DIAMOND TIPPED PROBE HAS BEEN PROPOSED(3) FOR USE IN A
C      HIGH TEMPERATURE AND PRESSURE ENVIRONMENT. THIS COMPUTER MODEL
C      SIMULATES THE PROBE'S OPTICAL RESPONSE IN TWO PHASE FLOW. THE
C      CALCULATIONS ARE PERFORMED IN 2-D GEOMETRY DUE TO THE SYMMETRY OF
C      THE CONICAL-TIPPED, CYLINDRICAL DIAMOND. SNELL'S LAW(4),
C
C                    N1 * SIN(THETA 1) = N2 * SIN(THETA 2)              (1)
C
C      EQUATION 1, IS USED TO CALCULATE THE ANGLE OF REFRACTION.
C          THE SIMULATION BEGINS BY INTRODUCING LIGHT RAYS ON THE
C      VERTICAL, BACK FACE (FACE 5). RAYS CAN ONLY ORIGINATE IN THE LIGHT
C      INPUT ZONES. AT THESE POINTS, AN EQUATION FOR THE LIGHT RAY LINE
C      IS GENERATED. SIMULTANEOUS SOLUTION OF THE LIGHT RAY EQUATION
C      AND THE TIP FACE EQUATIONS WILL YIELD THE COORDINATES OF
C      INTERSECTION. THE ANGLE OF INCIDENCE IS CALCULATED AND COMPARED
C      TO THE CRITICAL ANGLE FOR THAT INTERFACE. REFRACTION OF THE RAY
C      WILL TERMINATE THE RAY TRACING PROCEDURE AND RESULT IN APPROPRIATE
C      RAY CODING. REFLECTED RAYS ARE ASSUMED TO REFLECT AT AN ANGLE
C      EQUAL TO THE ANGLE OF INCIDENCE. A NEW LIGHT RAY EQUATION IS THEN
C      GENERATED REPRESENTING THE REFLECTED RAY. THE PROCESS OF
C      RAY TRACING IS REPEATED UNTIL THE RAY IS TRANSMITTED FROM THE
C      TIP OR RETURNED TO THE BACK FACE (FACE 5).
```

```
C       A RAY RETURNING TO THE BACK FACE (FACE 5) IS CHECKED FOR ITS
C     ANGLE OF INCIDENCE. THIS ANGLE MUST BE LESS THAN OR EQUAL TO THE
C     FIBER OPTICS ACCEPTANCE ANGLE. IF THIS CRITERION IS MET, THE RAY
C     IS THEN CHECKED TO ASSURE INTERSECTION WITH AN ACCEPTANCE FIBER.
C     IF THESE TWO CRITERIA HAVE BEEN SATISIFIED, THE RAY IS CODED 88,
C     I.E. TOTALLY REFLECTED BACK TO THE ACCEPTANCE REGIONS OF THE
C     PICKUP FIBER.
C       TWO LIGHT INTENSITY REDUCTION LAWS ARE INCORPORATED INTO
C     THE SIMULATION. BEER'S LAW(5), EQUATION 2, IS USED TO CALCULATE
C
C                                   I = IO*EXP(-UX)                (2)
C
C     ATTENUATION ALONG THE RAY PATH. INTENSITY LOSSES DUE TO
C     REFLECTION OR REFRACTION AT AN INTERFACE ARE CALCULATED BY
C     FRESNEL'S LAWS(6).
C       RESIDUAL LIQUID IS EXPECTED TO WET THE PROBE TIP DURING
C     THE PRESENCE OF THE VAPOR PHASE. THE COMPUTER MODEL FOR THIS
C     PHENOMENA ASSUMES A LINEAR VARIATION IN WATER FILM THICKNESS,
C     WHERE THE FILM WIDTH IS ZERO AT THE PROBE'S APEX. LIGHT
C     REFRACTION AND REFLECTION IN THE WATER FILM ARE CONSIDERED BY
C     APPROPRIATE CACULATIONS.
C       THIS SIMULATION CAN MODEL A MAXIMUM ACCEPTANCE ANGLE OF 16
C     DEGREES. A TIP WITH 5 FACES IS RECOMMENDED. THE PROGRAM IS
C     VARIABLY DIMENSIONED FOR MAXIMUM FLEXIBILITY. TEN(10) RAYS AT
C     EACH ANGLE CAN BE INDEPENDENTLY TRACED PER RUN.
C       OUTPUT CONSISTS OF A TRANSMISSION MATRIX. THIS ARRAY CONTAINS
C     A SUMMARY OF EACH RAY TRACE IN TABULAR FORM. THE NORMALIZED
C     INTENSITY ASSOCIATED WITH EACH RAY IS ALSO PRINTED. ALL INPUT
C     DATA IS LISTED FOR REFERENCE AND ERROR CORRECTION. USING THE
C     PROPER INPUT CODE, THE ACTUAL RAY PATHS AND RAY DATA CAN BE
C     PRINTED OUT.
C
C     *** REFERENCES ***
C
C     1. MILLER,N. AND MITCHIE,R.E., "MEASUREMENT OF LOCAL VOIDAGE
C        IN LIQUID/GAS TWO-PHASE FLOW SYSTEMS', JOUR. OF BRITISH
C        NUCLEAR ENERGY SOCIETY, VOL. 9,#2, 1970
C
C     2. DANIEL,F. AND DELHAYE,J.M., "SONDE OPTIQUE POUR MESURE DU
C        TAUX DE PRESENCE LOCAL ECOULEMENT DIPHASIQUE', MESURES,
C        REGULATION, AUTOMATISE, AUGUST-SEPTEMBER, 1971
C
C     3. LAHEY,R.T., TWO-PHASE FLOW PHENOMENA IN NUCLEAR REACTOR
C        TECHNOLOGY, QUARTERLY PROGRESS REPORT, NO. 1., RENSSELAER
C        POLYTECHNIC INSTITUTE, TROY, NEW YORK, OCT. 1, 1976.
C
C     4. JENKINS,F.A., AND WHITE,H.E., "FUNDAMENTALS OF OPTICS',
C        FOURTH EDITION, MCGRAW HILL, INC., 1976, PAGE 11
C
C     5. REFERENCE 4, PAGE 231.
C
C     6. REFERENCE 4, PAGE 524.
C
C
C
C
C
C
C
```

```
C
C                          *** SUBROUTINES ***
C
C     ANSB          SUBROUTINE TO WRITE OUT TRANSMISSION MATRIX AND
C                   APPROPRIATE HEADINGS
C
C     BEERS         SUBROUTINE TO PERFORM BEER'S LAW INTENSITY
C                   ATTENUATION FOR LIGHT RAYS
C
C     CALCCF        SUBROUTINE TO CALCULATE PARAMETERS FOR USE IN
C                   FRESNEL'S EQUATIONS
C
C     CIDNGL        FUNCTION SUBROUTINE TO CALCULATE THE ANGLE OF
C                   INCIDENCE GIVEN RAY AND FACE SLOPE
C
C     DIST          FUNCTION SUBROUTINE TO CALCULATE THE DISTANCE
C                   BETWEEN TWO POINTS,I.E. THE DISTANCE FORMULA
C
C     EQUAT         SUBROUTINE TO DETERMINE EQUATIONS OF DIAMOND FACET
C                   AND WATER FILM FACES
C
C     FACHER        FUNCTION SUBROUTINE TO CHECK IF LIGHT RAY
C                   INTERSECTS WATER FILM WITHIN TIP CONSTRAINTS
C
C     FIPRAY        SUBROUTINE TO FLIP RAY IN WATER FILM IF INCORRECT
C                   LIGHT EQUATION IS GENERATED
C
C     FRENEL        FUNCTION SUBROUTINE TO CACULATE THE INTENSITY OF
C                   A REFLECTED OR REFRACTED LIGHT RAY USING
C                   FRESNEL'S LAWS
C
C     GCNCGC        SUBROUTINE TO CALCULATE TRANSMISSION OR REFLECTION
C                   OF LIGHT RAYS
C
C     ICCEPT        FUNCTION SUBROUTINE USED TO CHECK IF RETURNING LIGHT
C                   RAY IS WITHIN FIBER ACCEPTANCE CONE
C
C     MATFER        FUNCTION SUBROUTINE TO DETERMINE APPROPRIATE
C                   CRITICAL ANGLE FOR INTERFACE
C
C     MAYFLP        FUNCTION SUBROUTINE TO DETERMINE IF RAY
C                   FLIPPING IS NECESSARY
C
C     NCVRGE        FUNCTION SUBROUTINE USED TO DETERMINE FACE
C                   INTERSECTED BY LIGHT RAY
C
C     OPTFRP        SUBROUTINE USED TO READ IN REFRACTIVE INDICES AND
C                   COMPUTE CRITICAL ANGLES
C
C     RAYEQT        SUBROUTINE TO GENERATE INPUT LIGHT RAY EQUATIONS
C
C     RAYNEW        SUBROUTINE TO CALCULATE A REFLECTED RAYS EQUATION
C
C     RAYSRG        SUBROUTINE TO POSITION LIGHT RAYS EQUALLY SPACED
C                   ALONG INPUT SURFACES
C
C     READTA        SUBROUTINE TO READ VARIOUS INPUT PARAMETER
C
C     SETENZ        SUBROUTINE TO INITIALIZE INTENSITY ARRAY
C
```

```
241     C       SNELL           FUNCTION SUBROUTINE TO CALCULATE ANGLE OF
242     C                       REFRACTION USING SNELL'S LAW
243     C
244     C       SUMMER          SUBROUTINE TO SUM UP REFLECTED RAYS FOR EACH INPUT
245     C                       ANGLE
246     C
247     C       WATRAC          SUBROUTINE TO DO RAY TRACE IN WATER FILM
248     C
249     C       WTEQCT          SUBROUTINE TO CALCULATE EQUATIONS OF WATER FILM
250     C
251     C       XSET            SUBROUTINE TO CALCULATE INTERSECTION COORDINATES
252     C                       FOR USE IN BEER'S LAW ATTENUATION CALCULATION
253     C
254     C       ZONCHK          FUNCTION SUBROUTINE TO DETERMINE IF REFLECTED RAY
255     C                       INCIDENT ON FIFTH FACE STRIKES AN ACCEPTANCE REGION
256     C
257     C
258     C
259     C
260     C                               *** VARIABLES ***
261     C
262     C
263     C
264     C       A                       FLOATING POINT NUMBER EQUAL TO NOPNTS
265     C                               USED AS DUMMY VARIABLE IN SUBROUTINE SUMMER
266     C
267     C       ADDGLE                  TWICE THE DIFFERENCE BETWEEN THE ANGLE OF
268     C                               INCIDENCE AND 90.0 DEGREES
269     C
270     C       ANGLE                   ANGLE OF INCIDENCE FOR A LIGHT RAY ON A
271     C                               FACE, IN RADIANS
272     C
273     C       CDTNGL                  TANGENT OF ANGLE OF INCIDENCE
274     C
275     C       CHECK                   ABSOLUTE VALUE OF RAY ANGLE (DEGREES),
276     C                               WHEN INCIDENT ON FACE 5
277     C
278     C       CRTANG(IL)              ARRAY CONTAINING CRITICAL ANGLES BETWEEN
279     C                               VARIOUS INTERFACES
280     C
281     C       DAB                     RADIUS WITH EXTRA TOLERANCE (0.00001) USED
282     C                               FOR COMPARISONS IN FUNCTION NCVRGE
283     C
284     C       DEGNGL                  ANGLE OF INCIDENCE CONVERTED TO DEGREES
285     C
286     C       FACCOF                  COEFFICIENT USED IN FRESNEL REFLECTION/
287     C                               REFRACTION CALCULATION
288     C
289     C       EB                      1.0 PER CENT OF A LIGHT RAY'S SLOPE
290     C
291     C       ERRCB1                  ABSOLUTE VALUE OF THE DIFFERENCE BETWEEN
292     C                               THE ORIGINAL RAY SLOPE AND THE REFLECTED
293     C                               RAY SLOPE
294     C
295     C       ERRCB2                  ABSOLUTE VALUE OF THE DIFFERENCE BETWEEN
296     C                               THE ORIGINAL RAY Y-INTERCEPT AND THE
297     C                               REFLECTED RAY Y-INTERCEPT
298     C
299     C       EP                      1.0 PER CENT OF A LIGHT RAY'S Y-INTERCEPT
300     C
```

```
C     FACLGT                  TIE FACE LENGTH
C
C     FACSLP                  SLOPE OF FACE STRUCK BY LIGHT RAY
C
C     GAMMA                   DUMMY VARIABLE USED IN RAYEQT FOR THE ANGLE
C                             OF INCOMING LIGHT, IN DEGREES
C
C     GAMMA                   DUMMY VARIABLE USED TO STORE WIDTH OF
C                             FIBERS LESS THAN SIZE OF SPACE
C
C     HFANGL                  MAXIMUM ANGLE OF INCOMING LIGHT, INTEGER
C
C     HGT                     HEIGHT OF DIAMOND CONE, BASED ON RADIUS AND
C                             TIE ANGLE
C
C     ICHECK                  CHECK FOR LIGHT RAY INTERSECTION IN
C                             WATER FILM
C                                0 SUITABLE INTERSECTION
C                                1 INTERSECTION OUTSIDE WATER FILM
C                                  RANGE
C
C     IFLIP                   RAY FLIPPING PARAMETER
C                                0 NO RAY FLIPPING REQUIRED
C                                1 INCORRECT RAY EQUATION, MUST FLIP
C
C     IFRESL                  PARAMETER TO DETERMINE IF THE REFLECTED
C                             OR REFRACTED INTENSITY IS TO BE CALCULATED
C                                0 REFRACTED TRANSMITTANCE
C                                1 REFLECTED TRANSMITTANCE
C
C     IHEAD(NOPNTS)           VECTOR CONTAINING ONE TO NOPNT VALUES
C                             USED SOLELY FOR PRINTING HEADING ON OUTPUT
C
C     INTCPT                  FACE INTERSECTED BY LIGHT RAY
C
C     INTFAC                  INTERFACE PARAMETER:
C                                1 AIR
C                                2 WATER
C                                3 WATER FILM ONLY
C
C     IPRINT                  RAY PATH PRINTING OPTION CODE
C                             0-PRINT RAY PATH  1-NO PRINTING
C
C     ITRANS(HFANGL,NOPNTS)   TRANSMISSION MATRIX SHOWING ULTIMATE FATE
C                             OF EACH LIGHT RAY, BY ANGLE AND POSITION
C                                1 TRANSMITTED THROUGH FACE 1
C                                2 TRANSMITTED THROUGH FACE 2
C                                3 TRANSMITTED THROUGH FACE 3
C                                4 TRANSMITTED THROUGH FACE 4
C                               51 LIGHT AT INCORRECT ANGLE AT FACE 5
C                               52 LIGHT AT INCORRECT POSITION AT FACE 5
C                                6 TRANSMITTED THROUGH FACE 6 (WATER FILM
C                                  OPTION ONLY)
C                                7 TRANSMITTED THROUGH FACE 7 (WATER FILM
C                                  OPTION ONLY)
C                               88 REFLECTED BACK TO ACCEPTANCE REGION IN
C                                  FIBER OPTIC WITHIN ACCEPTANCE CONE
C                               91 LIGHT TRANSMITTED OUT FACE 1 FILM EDGE
C                               92 LIGHT TRANSMITTED OUT FACE 2 FILM EDGE
C
```

```
C       IWTCAL          WATER FILM OPTION CALL PARAMETER
C                          0 WATER FILM OPTION NOT CALLED
C                          1 WATER FILM OPTION WAS CALLED
C
C       L               NUMBER OF MATERIALS IN SYSTEM, USUALLY 3
C
C       LGT             LENGTH OF DIAMOND SHAFT,IN MILS
C
C       LL              DO-LOOP PARAMETER USED FOR REFRACTIVE
C                       INDICES
C
C       LT              MATERIAL IN WHICH ATTENUATION OCCURS
C                          1 AIR
C                          2 WATER
C                          3 DIAMOND
C
C       MU(L)           ATENUATION COEFFICENTS' ARRAY
C
C       NF              DO-LOOP PARAMETER USED FOR TIP FACES
C
C       NFACE           NUMBER OF TIP FACES, USUALLY 5
C
C       NH              DO-LOOP PARAMETER USED FOR INPUT
C                       ACCEPTANCE ANGLES
C
C       NN              COUNTER FOR STARTED RAYS
C
C       NCENTS          NUMBER OF FACE WHERE LIGHT RAY STARTS,
C                       INITIALLY SET EQUAL TO 0, MAXIMUM VALUE IS
C                       NFACE, WITH WATER FILM OPTION MAXIMUM
C                       VALUE IS
C
C       NP              DO-LOOP PARAMETER USED FOR NUMBER
C                       OF LIGHT RAYS
C
C       NXX             INDEX FOR CENTERLINE ZONE, USED TO SET
C                       CENTERLINE ZONE EQUAL TO 0.0
C
C       NZ              DO-LOOP PARAMETER USED FOR NUMBER
C                       OF FIBER OPTIC INPUT/OUTPUT ZONES
C
C       NZCODE(NZDIM2)  INTEGER ARRAY CONTAINING THE CODE NUMBER
C                       FOR EACH LIGHT AREA
C                          0 REGION OF NO LIGHT TRANSMISSION
C                          1 REGION OF LIGHT INPUT
C                          2 REGION OF LIGHT PICKUP
C
C       NZDIM1          DIMENSIONING PARAMETER FOR ZONE ARRAYS
C
C       NZDIM2          DIMENSIONING PARAMETER FOR ZONE ARRAYS
C
C       NZPOS           NZONES+1
C
C       NZONES          ONE HALF NUMBER OF ZONES ON FIBER OPTICS
C
C       NZONE2          TWICE NZONES + 1
C
C       OANGLE          STORED ANGLE OF INCIDENCE, IN RADIANS,
C                       USED AS THE ANGLE OF INCIDENCE IN
C                       FRESNEL'S LAWS CALCULATION
```

```
C
C     P1                  VARIABLE CONTAINING FRACTION OF LIGHT
C                         RAYS REFLECTED BACK AND ACCEPTED AT
C                         FACE 5
C
C     PARACP              PARALLEL COMPONENT OF LIGHT INTENSITY
C
C     PERPCP              PERPENDICULAR COMPONENT OF LIGHT INTENSITY
C
C     PERTAB              ARRAY CONTAINING TALLY OF TOTALLY REFLECTED
C                         LIGHT RAYS BY ANGLE
C
C     PHETA               SINE OF ANGLE SNELL IN FUNCTION SNELI
C
C     PHI1                TIP BASE ANGLE, IN DEGREES
C
C     PI                  ARITHMETIC CONSTANT, 3.14159
C
C     RAD                 TIP RADIUS, IN MILS
C
C     RAYCPT              Y-INTERCEPT IN LIGHT RAY EQUATION
C
C     RAYSLP              SLOPE IN LIGHT RAY EQUATION
C
C     RFINDX(LL)          ARRAY CONTAINING REFRACTIVE INDICES
C
C     RFTNGI              TANGENT OF ANGLE OF REFRACTION
C
C     RYCRON(NOPNTS)      ARRAY CONTAINING Y-COORDINATE OF STARTING
C                         LIGHT RAYS ALONG FIFTH FACE
C
C     SLKEEP              VARIABLE CONTAINING DIFFERENCE BETWEEN
C                         LIGHT RAY STARTING POSITION AND ZONE
C                         BOUNDARY, USED TO KEEP RAYS EQUALLY SPACED
C
C     SLOPE(NFACE)        ARRAY CONTAINING SLOPE OF DIAMOND FACE
C                         LINES
C
C     SLOPE1              DUMMY VARIABLE FOR INITIAL RAY SLOPE
C
C     SNELLD              ANGLE SNELL (IN DEGREES)
C
C     SPACE               DISTANCE BETWEEN LIGHT RAY STARTING
C                         POSITIONS
C
C     SPCIRP              TRIP PARAMETER FOR FIBERS SMALLER THAN
C                         SPACE
C
C     TENSTY(NH,NP)       ARRAY CONTAINING THE VARIOUS LIGHT RAY
C                         INTENSITIES BY ANGLE AND POSITION
C
C     THETA               ANGLE PHI1, IN RADIANS
C
C     TITLE               ARRAY CONTAINING TITLE OF PARTICULAR RUN
C
C     TRIP                PARAMETER USED TO CONTINUE OR DICONTINUE
C                         A PARTICULAR RAY TRACING
C                            1.0 RAY LOST, STOP TRACING
C                           -1.0 RAY STILL WITHIN SYSTEM
C
```

```
C      DX                      ATTENUATION COEFFICIENT TIMES THE
C                              STRAIGHT LINE DISTANCE THROUGH MEDIUM
C
C      WATHIK                  MAXIMUM WATER FILM THICKNESS
C
C      WATFLM                  PARAMETER TO INDICATE WATER FILM OPTION
C                                 0 NO WATER FILM ON TIP
C                                 1 WEDGE-SHAPED FILM PRESENT ON TIP
C
C      WFANG1                  WATER FILM ANGLE
C
C      WFANG2                  WFANG1+(90.0-PHI1)
C
C      WFHGT                   HEIGHT OF WATER FILM ALONG Y-AXIS
C
C      XETA                    X-COORDINATE OF STARTING LIGHT RAYS
C
C      XNEW                    NEW X-COORDINATE OF INTERSECTION
C
C      XOLD                    OLD X-COORDINATE OF INTERSECTION
C
C      XXX                     DUMMY VARIABLE TO KEEP POSSIBLE INITIAL RAY
C                              POSITIONS
C
C      XXX                     DUMMY VARIABLE USED TO INDICATE THE
C                              INTERSECTION OF A LIGHT RAY AND A TIP FACE
C
C      YCEPT(NFACE)            Y-INTERCEPT ARRAY FOR LIGHT INPUT REGION
C
C      YCEPT1                  DUMMY VARIABLE FOR INITIAL RAY INTERCEPT
C
C      YNEW                    NEW Y-COORDINATE OF INTERSECTION
C
C      YOLD                    OLD Y-COORDINATE OF INTERSECTION
C
C      YTTL                    TOTAL LENGTH OF LIGHT INPUT REGION
C
C      YXX                     DUMMY VARIABLE REPRESENTING LENGTH OF
C                              INPUT REGION AVAILABLE FOR STARTING RAY
C
C      YYY                     Y VALUE OF POSSIBLE LIGHT RAY/FACE
C                              INTERSECTION POINT
C
C      ZNUMB                   DUMMY VARIABLE USED TO CONTAIN THE SIZE OF
C                              THE INPUT ZONE UNDER STUDY
C
C      ZONES(NZDIM1)           ARRAY CONTAINING THE DIMENSIONS OF THE
C                              FIBER OPTIC INPUT/OUTPUT ARRAY
C
C      ZZDEC)                  RATIO OF FACE SLOPE TO RAY SLOPE,
C                              USED FOR CHECKING REFLECTED RAY
C                              EQUATIONS
C
C
C
      DIMENSION RFINDX(3),SLOPE(7),YCEPT(7),OBTANG(3),ITRANS(16,20),
     1PEITAN(16),IBEAD(20),ZONES(11),NZCODE(10),BYCRGN(20),
     2TITLE(20),INTSTY(16,20)
C
      REAL LGT,MU(3)
```

```
      INTEGER HFANGL,ZONCHK,WATERM
C
C     SET CONSTANTS
C
      L=3
      PI=3.14159
C
C     READ INPUT DATA
C
      CALL READATA(HFANGL,PHI1,NCPNTS,RAD,HGT,PI,LGT,NFACE,NZONES,
     1INTFAC,WATERM,TITLE,IPRINT,WATHIK)
C
C     SET ARRAY DIMENSIONS
C
      CALL SETDIM(NZONES,WATERM,NFACE,NZDIM1,NZDIM2)
C
C     CALCULATE DIAMOND FACE EQUATIONS
C
      CALL EQUAT(PHI1,SLOPE,YCEPT,PI,RAD,LGT,NFACE,WATHIK,
     1WATERM)
C
C     READ REFRACTIVE INDICES
C     COMPUTE CRITICAL ANGLES
C
      CALL CRTPRP(L,REINDX,CRTANG,PI,IPRINT,MU)
C
C     DETERMINE ZONES AND ZONE CODES
C
      CALL ZONER(NZONES,ZONES,NZCODE,NZDIM1,RAD,NIX,NZDIM2)
C
C     DETERMINE STARTING RAY POSITIONS
C
      CALL RAYORG(NOPNTS,RYORGN,NZCODE,NZDIM1,ZONES,NZDIM2,NZONES,
     1IPRINT)
C
C     INITIALIZE INTENSITY ARRAY
C
   50 CALL SETENZ(NCPNTS,HFANGL,TENSTY)
C
C     DO RAY TRACE
C
      DO 500 NH=1,HFANGL
C
C     LOOP THRU EACH ANGLE REPETIVELY
C
      SGN=-1.0
C
C     LOOP THRU EACH POSITION REPETIVELY
C
      DO 300 NP=1,NCPNTS
C
C     PRINT AND RESET EACH RAY AS CREATED ON
C
      CALL RESTRT(NH,NP,NSTART,IPRINT)
C
C     DETERMINE INPUT RAY EQUATIONS
C
      CALL RAYEQT(NH,NP,LGT,RAD,RAYSLP,RAYCPT,PI,NOPNTS,SGN,RYORGN,
     1IPRINT)
C
```

```
      C     SET INITIAL X AND Y STARTING COORDINATES FOR ATTENUATION
      C     CALCULATION
      C
            CALL XSET(XOLD,YOLD,RAYSLP,RAYCPT,LGT,NSTART,SLOPE,YCEPT,
           1NFACE)
      C
            GO TO 200
      C
      C     FLIPPING OPTION AFTER WATER TRACKING
      C
  100 IFLIP=0
      C
            IF (IWTCAL.LT.1) GO TO 150
      C
      C     CALCULATE IF FLIPPING IS NECESSARY
      C
            IFLIP=RAYFLP(NSTART,NFACE,RAYSLP,SLOPE)
      C
      C     CACCULATE REFLECTED RAY EQUATION
      C
  150 CALL RAYNEW(REFCR1,RAYSLP,RAYCPT,REFCR2,PI,INTCPT,YCEPT,SLOPE
           1,NFACE,ANGLE,IPRINT)
      C
      C     IF NECESSARY, FLIP RAY
      C
            IF (IFLIP.GT.0) CALL FLIPRAY(RAYSLP,RAYCPT,SLOPE,YCEPT,PI,ANGLE,
           1NFACE,NSTART,RAD,HGT,IPRINT)
      C
      C     RESET IFLIP AND WATER TRACKING OPTION
      C
            IFLIP=0
            IWTCAL=0
      C
      C
      C     DETERMINE REFLECTION OR TRANSMISSION OF RAY
      C
  200 CALL GONOGO(NH,NP,NFACE,SLOPE,RAYSLP,RAYCPT,CRYANG,
           1INTFAC,PI,TRIP,REFANGL,FACSLP,INTCPT,YCEPT,ITRANS,LGT,HGT,
           2NCPNTS,NSTART,RAD,ANGLE,NZONES,NZDIM1,NZDIM2,ZONES,NZCODE,
           3XXX,NXX,L,IPRINT,WATRFM,WATHIK,RFINDX,IWTCAL,TENSTY,MU,
           4XOLD,YOLD)
      C
      C     CHECK FOR REFLECTION
      C
            IF (TRIP.LT.0.0) GO TO 100
      C
  300 CONTINUE
  500 CONTINUE
      C
            CALL SUMMER(ITRANS,REFANGL,NCPNTS,PERTAN,PI)
      C
            CALL ANSR(ITRANS,REFANGL,NCPNTS,PERTAN,IHEAD,TITLE,DENSTY,
           1INTFAC)
      C
      C     CHECK TO SEE IF WATER EVALUATION HAS BEEN COMPLETED
      C
            IF (INTFAC.EQ.(WATRFM+2)) GO TO 999
            INTFAC=INTFAC+1
            GO TO 50
  999 STOP
```

```
      END
C
C     ********************
C     ********************
C     **                **
C     **                **
C     **  SUBROUTINES   **
C     **                **
C     **                **
C     ********************
C     ********************
C
      SUBROUTINE READATA(HFANGL,PHI1,NOPNTS,RAD,HGT,PI,LGT,NFACE,
     1NZONES,INTFAC,WATERM,TITLE,IPRINT,WATHIK)
      INTEGER HFANGL,WATERM
      REAL LGT
      DIMENSION TITLE(20)
C
C     READ/WRITE PROBLEM TITLE
C
      READ(5,100) TITLE
  100 FORMAT(20A4)
      WRITE(6,200) TITLE
  200 FORMAT(1H1,20A4)
C
C     READ IN PRINTING OPTION
C     1-NO RAY PATH PRINTING, 0-RAY PATH PRINTING
C
      READ(5,250) IPRINT
  250 FORMAT(I4)
C
C     READ IN VARIABLES DESCRIBING THE PROBLEM
C
      READ(5,300) HFANGL,NOPNTS,PHI1,RAD,LGT,NFACE,NZONES
  300 FORMAT(2I4,3F5.1,2I4)
C
C     CONVERT ANGLE TO RADIANS FOR PRINTING
C
      THETA=PHI1*PI/180.0
C
C     COMPUTE DIAMOND CONE HEIGHT
C
      HGT=RAD*TAN(THETA)
C
      WRITE(6,400) HFANGL,NOPNTS,PHI1,NFACE,RAD,LGT,HGT,NZONES
  400 FORMAT(1H0,T10,'HALF ANGLE OF INCOMING LIGHT',T40,I4,/
     1       ' ',T10,'NUMBER OF RAYS',T40,I4,/
     2       ' ',T10,'DIAMOND BASE ANGLE',T41,F5.2,/
     3       ' ',T10,'NUMBER OF DIAMOND FACES',T40,I4,/
     4       ' ',T10,'DIAMOND RADIUS',T41,F5.2,/
     5       ' ',T10,'DIAMOND SHAFT LENGTH',T41,F5.2,/
     6       ' ',T10,'DIAMOND CONE HEIGHT',T41,F5.2,/,
     7       ' ',T10,'ONE HALF NUMBER OF ZONES',T41,I4,/)
C
C     READ IN INTERFACE AND WATER FILM OPTION CODES
C
      READ(5,500) INTFAC,WATERM
  500 FORMAT(2I4)
C
C     CHECK FOR INTERFACE OPTIONS
```

```
      C
            IF (INTFAC-2) 550,700,900
        550 WRITE(6,600)
        600 FORMAT('-','AIR AND WATER WILL SURROUND THE PROBE',//)
            GO TO 900
        700 WRITE(6,800)
        800 FORMAT('-','ONLY WATER WILL COVER PROBE',//)
      C
      C     CHECK FOR WATER FILM OPTION
      C
        900 IF (WATRFM.EQ.1) GO TO 1100
            WRITE(6,1000)
       1000 FORMAT('-','NO WATER FILM OPTION',//)
      C
      C     SET WATER THICKNESS EQUAL TO ZERO
      C
            WATHIK=0.0
            RETURN
      C
       1100 WRITE(6,1200)
       1200 FORMAT('-','WATER FILM OPTION IN EFFECT',//)
      C
      C     READ/WRITE WATER FILM THICKNESS
      C
            READ(5,1300) WATHIK
       1300 FORMAT(F10.3)
      C
            WRITE(6,1400) WATHIK
       1400 FORMAT(' ','THE MAXIMUM WATER FILM THICKNESS IS:',F10.7,//)
            RETURN
            END
      C
            SUBROUTINE SETDIM(NZONES,WATRFM,NFACE,NZDIM1,NZDIM2)
            INTEGER WATRFM
      C
      C     INCREMENT IF WATER FILM OPTION DESIRED
      C
            IF (WATRFM.GT.0) NFACE=NFACE+2
      C
      C     SET ARRAY DIMENSIONS
      C
            NZDIM2=2*NZONES
            NZDIM1=NZDIM2+1
      C
            RETURN
            END
      C
            SUBROUTINE EQUAT(PHI1,SLOPE,YCEPT,PT,RAD,IGT,NFACE,WATHIK,
           1WATRFM)
            REAL IGT
            INTEGER WATRFM
            EXTERNAL WTEQUT
      C
      C     EVALUATE DIAMOND TIP EQUATIONS
      C
            DIMENSION SLOPE(NFACE),YCEPT(NFACE)
      C
      C     FOR SCINTED FACES
      C
            THETA=90.0-PHI1
```

```
C
C     CONVERT THETA TO RADIANS
C
      THETA=THETA*PI/180.0
C
C     COMPUTE SLOPES
C
      SLOPE(1)=-TAN(THETA)
      SLOPE(2)=-SLOPE(1)
C
C     COMPUTE Y-INTERCEPTS
C
      YCEPT(1)=RAD
      YCEPT(2)=-RAD
C
C     EVALUATE DIAMOND SHAFT EQUATIONS
C
C     SIDES
C
C     COMPUTE SLOPES
C
      SLOPE(3)=0.0
      SLOPE(4)=0.0
C
C     COMPUTE Y-INTERCEPTS
C
      YCEPT(3)=YCEPT(1)
      YCEPT(4)=YCEPT(2)
C
C     BACK EQUATIONS
C
      SLOPE(5)=1.0
      YCEPT(5)=-LGT
C
C     CONVERT PHI1 TO RADIANS
C
      PHI1=PHI1*PI/180.0
C
C     COMPUTE WATER FILM EQUATIONS, IF NECESSARY
C
      IF (WATRFM.GT.0) CALL WTEQUT(THETA,PHI1,SLOPE,YCEPT,PI,
     1RAD,NFACE,WATFIM)
C
C     WRITE OUT VALUES
C
      WRITE(6,200)
  200 FORMAT('-',1X,'FACE',8X,'SLOPE',9X,'Y-INTERCEPT  ',//)
C
      DO 300 NF=1,NFACE
      WRITE(6,400) NF,SLOPE(NF),YCEPT(NF)
  400 FORMAT(' ',I4,2(5X,1PE12.4))
  300 CONTINUE
      RETURN
      END
C
      SUBROUTINE WTEQUT(THETA,PHI1,SLOPE,YCEPT,PI,RAD,NFACE,WATHIK)
      DIMENSION SLOPE(NFACE),YCEPT(NFACE)
C
C     CALCULATE FACE LENGTH
C
```

```
      FACLG1=RAD/(COS(PHI1))
C
C     CALCULATE WATER FILM ANGLE
C
      WFANG1=ARSIN(WATHIK/FACLG1)
      WFANG2=WFANG1+IPETA
C
C     CALCULATE WATER FILM HEIGHT ALONG Y-AXIS
C
      WFHGT=WATHIK/(SIN(PHI1-WFANG1))
C
C     CALCULATE WATER FILM SLOPES AND Y-INTERCEPTS
C
      SLOPE(6)=-TAN(WFANG2)
      SLOPE(7)=-SLOPE(6)
C
      YCEPT(6)=WFHGT+RAD
      YCEPT(7)=-YCEPT(6)
C
      RETURN
      END
C
      SUBROUTINE CRITREF(L,RFINDX,CRTANG,PI,IPRINT,MU)
      REAL MU(L)
      DIMENSION RFINDX(L),CRTANG(L)
      EXTERNAL SNELL
C
C     READ/WRITE REFRACTIVE INDICES
C
      READ(5,100) (RFINDX(LL),LL=1,L)
  100 FORMAT(3F10.7)
      WRITE(6,200)
  200 FORMAT('0','REFRACTIVE INDICES',/,
     1'0',1X,'MATERIAL',3X,'INDEX')
      DO 400 LL=1,L
      WRITE(6,300) LL,RFINDX(LL)
  300 FORMAT(' ',I5,5X,F8.5)
  400 CONTINUE
C
C     COMPUTE CRITICAL ANGLES
C
        WRITE(6,500)
  500 FORMAT('0','MATERIALS',3X,'CRITICAL ANGLE')
      REFANG=PI/2.0
      DO 900 LL=1,L
      IF (LL.EQ.1) GO TO 600
      L1=L
      L2=LL
      GO TO 700
  600 L1=L-1
      L2=L-2
  700 CRTANG(LL)=SNELL(L1,L2,REFANG,RFINDX,L,PI,IPRINT)
C
C     CONVERT TO DEGREES  FOR PRINTING PURPOSES
C
      CRTANG(LL)=CRTANG(LL)*180.0/PI
C
C     WRITE OUT CRITICAL ANGLES
C
      WRITE(6,800) L1,L2,CRTANG(LL)
```

```
  800 FORMAT(' ',2X,I2,' TO',I2,6X,F7.4)
C
C     CONVERT BACK TO RADIANS
C
      OBTANG(LL)=OBTANG(LL)*PI/180.0
  900 CONTINUE
C
C     READ/WRITE LINEAR ATTENUATION COEFFICIENTS
C
      READ(5,1000) (MU(LL),LL=1,L)
 1000 FORMAT(3F10.7)
      WRITE(6,1100)
 1100 FORMAT('0','MATERIALS',5X,'LINEAR ATTENUATION COEFFICIENT')
      DO 1300 LL=1,L
      WRITE(6,1200) LL,MU(LL)
 1200 FORMAT(' ',3X,I3,17X,F10.7)
 1300 CONTINUE
      RETURN
      END
C
      FUNCTION SNELL(L1,L2,ANGLE,RFINDX,L,PI,IPRINT)
C
      DIMENSION RFINDX(L)
C
C     SNELL'S LAW TO YIELD REFRACTED RAY
C
      PHETA=((RFINDX(I2)/RFINDX(L1))*SIN(ANGLE))
C
C     CHECK TO MAKE SURE PHETA LESS THAN OR EQUAL TO 1
C
      IF (PHETA.GT.1.0) GO TO 200
C
      SNELL=ARSIN(PHETA)
C
      SNELLD=SNELL*180.0/PI
C
      IF (IPRINT.GT.0) GO TO 400
C
      WRITE(6,100) SNELLD
  100 FORMAT(' ',' THETA ANGLE= ',F10.4)
  400 RETURN
C
  200 WRITE(6,300)
  300 FORMAT(' ','*** ERROR IN RAY REFRACTION ***',//////)
C
      RETURN
      END
C
      SUBROUTINE ZONES(NZONES,ZONES,NZCODE,NZDIM1,RAD,NXX,NZDIM2)
      DIMENSION ZONES(NZDIM1),NZCODE(NZDIM2)
C
      NZPOS=NZONES+1
C
C     READ IN ZONE VALUES, NORMALIZED FROM ZERO TO ONE
C
      READ(5,100) (ZONES(NZPOS-NZ),NZ=1,NZONES)
  100 FORMAT(8F10.5)
C
C     READ IN ZONE CODE
C
```

```
      READ(5,200) (NZCODE(NZPOS-NZ),NZ=1,NZONES)
  200 FORMAT(8I4)
C
C     SPACE AND SCALE ZONES
C     SET CENTERLINE EQUAL TO ZERO
C
      NXX=(NZDIM1/2)+1
      ZONES(NXX)=0.0
C
      DO 300 NZ=1,NZONES
C
C     SCALE UP SIDE
C
      ZONES(NZ)=ZONES(NZ)*RAD
C
C     SCALE DOWN SIDE
C
      ZONES(NZDIM1+1-NZ)=-ZONES(NZ)
C
C      SET ZONE CODE
C
      NZCODE(NZDIM2+1-NZ)=NZCODE(NZ)
C
  300 CONTINUE
C
C      WRITE OUT RANGES AND MATERIAL
C
      NZONES=NZONES*2
      WRITE(6,400)
  400 FORMAT('1',4X,'UPPER',5X,'LOWER',/,
     1       ' ',4X,'BOUND',5X,'BOUND',8X,'CODE',//)
C
      DO 600 NZ=1,NZONES
      WRITE(6,500) ZONES(NZ),ZONES(NZ+1),NZCODE(NZ)
  500 FORMAT(' ',2F10.5,5X,I5)
  600 CONTINUE
C
      RETURN
      END
C
      SUBROUTINE RAYCFG(NCPNTS,RYCRGN,NZCODE,NZDIM1,ZONES,NZDIM2,NZONES,
     1IPRINT)
      DIMENSION RYCRGN(NCPNTS),NZCODE(NZDIM2),ZONES(NZDIM1)
C
      TTTL=0.0
C
      DO 100 NZ=1,NZONES
      IF (NZCODE(NZ).NE.1) GO TO 100
C
C
C     DETERMINE TOTAL LENGTH OF INPUT REGION
C
      TTTL=TTTL+(ZONES(NZ)-ZONES(NZ+1))
C
  100 CONTINUE
C
      SPACE=TTTL/(NCPNTS+1)
C
      WRITE(6,150) SPACE
  150 FORMAT(' ','SPACE= ',F10.5)
```

```
1021      C
1022            NN=0
1023            SLKEEP=0.0
1024      C
1025      C
1026      C     LOOP THROUGH ZONES, SPACING BAYS AT APPROPRIATE
1027      C     POSITIONS
1028      C
1029      C     REMEMBER CALCULATIONS DONE IN REAL SPACE, NOT
1030      C     PER CENT SCALED SPACE
1031      C
1032            DO 800 NZ=1,NZONES
1033            IF  (NZCODE(NZ).NE.1) GO TO 800
1034      C
1035      C     SET TRIP
1036      C     SET ZONE LIMIT
1037      C
1038            SPCTRP=1.0
1039      C
1040            ZNCHK=ZONES(NZ+1)
1041      C
1042      C     SUBTRACT SPACING, BUT ADD REMAINDER FROM ANY PREVIOUS ZONE
1043      C
1044            YYY=ZONES(NZ)-SPACE+SLKEEP
1045            GO TO 300
1046      C
1047        200 YYY=YYY-SPACE
1048      C
1049      C     SET ZONE CHECK A LITTLE LOW TO ALLOW FOR COMPUTER
1050      C     ROUND-OFF
1051      C
1052            ZNCHK=ZONES(NZ+1)-(ZONES(NZ+1)*0.00001)
1053        300 IF (YYY.LT.ZNCHK) GO TO 500
1054      C
1055      C     INCREMENT COUNTER, UNDO TRIP, AND SET BAY ORIGIN
1056      C
1057        400 NN=NN+1
1058            SPCTRP=0.0
1059            BYORGN(NN)=YYY
1060            WRITE(6,450) NN,BYORGN(NN),SLKEEP
1061        450 FORMAT(' ','BYORGN=',I4,2(5X,F10.5))
1062            GO TO 200
1063      C
1064        500 IF (SPCTRP.GT.0.0) GO TO 600
1065      C
1066      C     STORE REMAINDER OF ZONE FOR LATER USE
1067      C
1068            SLKEEP=ZONES(NZ+1)-YYY
1069            GO TO 800
1070      C
1071        600 GAMMA=ZONES(NZ)-ZONES(NZ+1)
1072            IF (SLKEEP.EQ.0.0) GO TO 700
1073      C
1074      C     SUBTRACT OFF SMALL FIBER WIDTH
1075      C
1076            SLKEEP=SLKEEP-GAMMA
1077            GO TO 800
1078      C
1079      C     SET SLKEEP, IF ZERO
1080      C
```

```
      700 SINBEB=GAMMA
      800 CONTINUE
C
          RETURN
          END
C
          SUBROUTINE SETENZ(NOPNTS,NBANGL,IENSTY)
          INTEGER NBANGL
          DIMENSION IENSTY(NBANGL,NOPNTS)
C
C     LOOP TO SET ARRAY TO UNIT INTENSITY
C
          DO 100 NB=1,NBANGL
          DO 100 NP=1,NOPNTS
C
          IENSTY(NB,NP)=1.0
      100 CONTINUE
          RETURN
          END
C
          SUBROUTINE RESTRT(NB,NP,NSTART,IPRINT)
C
C     WRITE OUT LIGHT RAY
C
          IF (IPRINT.GT.0) GO TO 500
C
          WRITE(6,400) NB,NP
      400 FORMAT(' ','*** LIGHT ANGLE=',I4,'  DEGREES, RAY NO.=',
         1I4,'  ***')
C
C     RESTART FOR NEXT RAY
C
      500 NSTART=0
C
          RETURN
          END
C
          SUBROUTINE RAYEQT(NB,NP,LGT,PAI,RAYSLP,RAYCPT,PI,NOPNTS,SGN,
         1RYCBGN,IPRINT)
          REAL LGT
          DIMENSION RYCBGN(NOPNTS)
C
C     CONVERT INPUT ANGLE(DEGREES) TO RADIANS
C
          GAMMA=NB*PI/180.0
C
C
C     COMPUTE INPUT RAY EQUATIONS
C
          XETA=SGN*LGT
          RAYSLP=TAN(GAMMA)
          RAYCPT=RYCBGN(NP)-(XETA*RAYSLP)
C
C     WRITE OUT CHECK AND RAY SLOPE AND INTERCEPT
C
          IF (IPRINT.GT.0) GO TO 200
C
          WRITE(6,100) RYCBGN(NP),RAYSLP,RAYCPT
      100 FORMAT(' ',3(5X,1PE12.4))
      200 RETURN
```

```
      END
C
      SUBROUTINE XSET(XOLD,YOLD,BAYSLP,BAYCPT,XXX,NSTART,SLOPE,YCEPT,
     1NFACE)
      DIMENSION SLOPE(NFACE),YCEPT(NFACE)
C
C     REMEMBER X AND Y COORDINATES
C
      XOLD=-XXX
C
      IF (NSTART.NE.0) XOLD=(YCEPT(NSTART)-BAYCPT)/(BAYSLP-SLOPE(NSTART)
     1)
C
C     OPTION FOR FACE 5
C
      IF (NSTART.EQ.5) XOLD=-XXX
C
      YOLD=(BAYSLP*XOLD)+BAYCPT
C
C     WRITE(6,100) XOLD,YOLD,NSTART
C 100 FORMAT(' ','XOLD=',F10.4,2X,'YOLD=',F10.4,2X,'NSTART=',I2)
C
      RETURN
      END
C
      SUBROUTINE BAYNEW(ERROR1,BAYSLP,BAYCPT,ERROR2,PI,INTCPT,YCEPT
     1,SLOPE,NFACE,ANGLE,IPRINT)
      DIMENSION SLOPE(NFACE),YCEPT(NFACE)
C
C     SET ERROR MARGINS
C
      EB=ABS(BAYSLP)*0.01
C
      EP=ABS(BAYCPT)*0.01
C
C     SET DUMMY VARIABLES
C
      SLOPE1=BAYSLP
      YCEPT1=BAYCPT
C
C
C     COMPUTE REFLECTED BAY EQUATION
C
C
C     SOLVE FACE AND BAY EQUATION SIMULTANEOUSLY
C
      XXX=(YCEPT(INTCPT)-BAYCPT)/(BAYSLP-SLOPE(INTCPT))
      YYY=(BAYSLP*XXX)+BAYCPT
C
C     CHECK FOR HORIZONTAL FACES
C
      ZZCHCK=SLOPE(INTCPT)/BAYSLP
      IF (ZZCHCK) 200,300,200
C
C     NOT HORIZONTAL FACE
C
  200 BAYANG=ANGLE+ATAN(-1.0/SLOPE(INTCPT))
      GO TO 500
C
C     HORIZONTAL FACE
```

```
1201      C
1202        300 BAYSLP=-BAYSLP
1203            GO TO 600
1204      C
1205      C     COMPUTE POSSIBLE RAY SLOPE AND INTERCEPT
1206      C
1207        500 BAYSLP=TAN(BAYANG)
1208        600 BAYCPT=YYY-(BAYSLP*XXX)
1209      C
1210      C     CHECK RAY TO AVOID REGENERATING  INCIDENT RAY EQUATION
1211      C
1212            ERRCR1=ABS(RAYSLP-SLOPE1)
1213            ERRCR2=ABS(YCEPT1-BAYCPT)
1214            IF (ERRCR1.LT.EP.AND.ERRCR2.LT.EP) GO TO 700
1215            GO TO 800
1216      C
1217      C     OPTION TO FLIP RAY IF SAME EQUATION IS GENERATED
1218      C
1219        700 ADDGLE=2.0*((PI/2.0)-ANGLE)
1220            RAYSLP=TAN(ATAN(RAYSLP)+ADDGLE)
1221            BAYCPT=YYY-(RAYSLP*XXX)
1222      C
1223      C     WRITE OUT  SLOPE AND INTERCEPT
1224      C
1225        800 IF (IPRINT.GT.0) GO TO 900
1226      C
1227            WRITE(6,100) RAYSLP,BAYCPT,XXX
1228        100 FORMAT(' ','NEW RAY SLOPE=',1PE12.4,'  NEW RAY INTERCEPT=',
1229           1 1PE12.4,'  XXX=',1PE12.4)
1230        900 RETURN
1231            END
1232      C
1233            SUBROUTINE GCNOGO(NR,NP,NFACE,SLOPE,RAYSLP,BAYCPT,CRIANG,INTFAC,
1234           1PI,TRIP,HFANGL,FACSLP,INTCPT,YCEPT,ITRANS,LGT,HGT,NCPNTS,NSTART,
1235           2RAD,ANGLE,NZONES,NZDIM1,NZDIM2,ZONES,NZCODE,XXX,NXX,I,IPRINT,
1236           3WATRFP,WATRIR,RFINDX,INTCAL,TENSTY,MU,XCLD,YCLD)
1237      C
1238            INTEGER HFANGI,ZCNCHK,WATFFP
1239            REAL LGT,MU(L)
1240      C
1241      C     CHECK FOR TRANSMISSION OR REFLECTION
1242      C
1243            DIMENSION SLOPE(NFACE),YCEPT(NFACE),CRIANG(L),ITRANS(HFANGL,
1244           1NCPNTS),ZONES(NZDIM1),NZCODE(NZDIM2),RFINDX(L),
1245           2TENSTY(HFANGL,NCPNTS)
1246            EXTERNAL CIRNGL,NCVRGE,ICCEPT,ZCNCHK,WATYPE,SNELL,WATRAC,
1247           1RAYNEW,FIPRAY,FACHEK,RAYFLP,BEERS,DIST,FRENEL,CALCOF,XSET
1248      C
1249      C     DETERMINE INTERSECTED FACE
1250      C
1251            INTCPT=NCVRGE(NFACE,LGT,HGT,SLOPE,YCEPT,RAYSLP,BAYCPT,NSTART,
1252           1RAD,NR,NP,IPRINT,WATRFP)
1253            NSTART=INTCPT
1254      C
1255      C     SET SELECT FOR MATERIAL ATTENUATION COEFFICIENT
1256      C
1257            LI=3
1258      C
1259      C     DO BEERS LAW ATTENUATION
1260      C
```

```
      CALL LEERS(EFANGL,NOPNTS,L,MU,TENSTY,XOLD,YOLD,NP,NH,LT,LGT,RAYCPT
     1,RAYSLP,NSTART,SLOPE,YCEPT,NFACE)
C
      IF (INTCPT.EQ.5) GO TO 200
C
      FACSLP=SLOPE(INTCPT)
C
C     DETERMINE ANGLE OF INCIDENCE
C
      ANGLE=CIDNGL(FACSLP,RAYSLP,PI,IPRINT)
C
C     SET TRIP, RESET LATER IF NECESSARY
C
      TRIP=1.0
C
C     SET ICHECK AND WATER FILM TRACKING
C
      ICHECK=0
      IWICAL=0
C
C     COMPARE ANGLES FOR REFLECTION
C
      LL=MATYPE(NSTART,INTFAC)
      IF (ANGLE.GT.CRTANG(LL)) GO TO 100
C
C     CHECK FOR WATER FILM OPTION
C
      IF (NSTART.LT.3.AND.INTFAC.EQ.3) CALL WATRAC(NSTART,NFACE,NH,NP,
     1SLOPE,YCEPT,ANGLE,FACSLP,RAYSLP,PI,WATHIK,L,RFINDX,IPRINT,
     2CRTANG,RAYCPT,INTCPT,TRIP,RAD,RGT,ICHECK,IWICAL,TENSTY,
     3EFANGL,NOPNTS,XOLD,YOLD,MU,LGT)
C
      IF (ICHECK.GT.0) GO TO 500
C
      IF (TRIP.LT.0.00) RETURN
C
C     SET ANGLE FOR FRESNEL REFLECTION CALCULATION
C
      OANGLE=ANGLE
C
C     CALCULATE ANGLE OF REFRACTION
C
      IF (NSTART.GT.5) GO TO 50
C
      L2=I
      I1=II
      GO TO 75
C
   50 L1=1
      L2=2
C
   75 ANGLE=SNELL(L1,L2,ANGLE,RFINDX,L,PI,IPRINT)
C
C     SET TRIP TO CALCULATE REFLECTED COMPONENT
C
      IFRENI=1
C
C     DO FRESNEL REFLECTION INTENSITY CALCULATION
C
      TENSTY(NH,NP)=TENSTY(NH,NP)*FRENEL(ANGLE,OANGLE,IFRENI,IPRINT,
```

```
1321           1L,BPINDX,L2,L1)
1322      C
1323                ITBANS(NH,NP)=NSTABT
1324                RETURN
1325      C
1326           100 TBIP=-1.0
1327                RETURN
1328      C
1329      C
1330      C         CHECK TO SEE IF WITHIN ACCEPTANCE CONE
1331      C
1332           200 ITBANS(NH,NP)=ICCEPT(HFANGL,RAYSLP,PI)
1333      C
1334      C         CALCULATE POINT OF FACE 5 INTERSECTION
1335      C
1336                XXX=(-RAYSLP*1GI)+RAYCPT
1337      C
1338                IF (IPPINT.GT.0) GO TO 400
1339      C
1340                WRITE(6,300) XXX
1341           300 FORMAT(' ','XXX= ',1PE12.4)
1342      C
1343           400 IF (ITBANS(NH,NP).EQ.88) ITBANS(NH,NP)=ZONCHK(NZONES,NZDIM1,
1344              1NZDIM2,ZONES,NZCODE,XXX,NXX)
1345                TBIP=1.0
1346                RETURN
1347      C
1348           500 IF (NSTABT-1) 600,600,700
1349      C
1350      C         OPTION FOR FACE 1
1351      C
1352           600 ITBANS(NH,NP)=91
1353                RETURN
1354      C
1355      C         OPTION FOR FACE 2
1356      C
1357           700 ITBANS(NH,NP)=92
1358                RETURN
1359                END
1360      C
1361      C
1362                FUNCTION CIDNGL(FACSLP,RAYSLP,PI,IPPINT)
1363      C
1364      C         COMPUTE ANGLE OF INCIDENCE GIVEN RAY AND FACE SLOPE
1365      C
1366                BETA=ATAN(RAYSLP)
1367                THETA=ATAN(FACSLP)
1368      C
1369      C         EQUATION DEVELOPED FROM 2-D OPTICS
1370      C
1371           200 CIDNGL=ABS((PI/2.0)-ABS(-BETA+THETA))
1372      C
1373      C         CONVERT ANGLE TO DEGREES FOR PRINTING PURPOSES
1374      C
1375                DEGNCI=CIDNGL*180.0/PI
1376      C
1377      C
1378      C         WRITE OUT ANGLE OF INCIDENCE
1379      C
1380                IF (IPPINT.GT.0) GO TO 500
```

```
1381      C
1382        300 WRITE(6,400) DEGNGL
1383        400 FORMAT('+',T90,'THE ANGLE OF INCIDENCE IS: ',F5.2,' DEGREES')
1384        500 RETURN
1385            END
1386      C
1387            FUNCTION NCVRGE(NFACE,LGT,HGT,SLOPE,YCEPT,RAYSLP,RAYCPT,NSTART,R
1388           1AD,NB,NP,IPBINT,WATERM)
1389            DIMENSION SLOPE(NFACE),YCEPT(NFACE)
1390            REAL LGT
1391            INTEGER WATERM
1392      C
1393      C     DETERMINE FACE INTERSECTED BY LIGHT RAY
1394      C
1395            DAB=RAD*1.00001
1396      C
1397      C     LOOP THRU FACES
1398      C
1399            DO 100 NF=1,NFACE
1400      C
1401      C     WRITE OUT FACE SCAN
1402      C
1403      C     WRITE(6,50) NF,NSTART
1404      C  50 FORMAT(' ',2I4)
1405            IF (NF.EQ.NFACE) GO TO 300
1406            IF (NSTART.EQ.NF) GO TO 100
1407            IF (NF.EQ.(NFACE-(2*WATERM))) GO TO 450
1408            XXX=(YCEPT(NF)-RAYCPT)/(RAYSLP-SLOPE(NF))
1409      C     WRITE(6,200) NF,XXX
1410            IF (XXX.GT.HGT.OR.XXX.LT.-LGT) GO TO 100
1411            YYY=(RAYSLP*XXX)+RAYCPT
1412      C     WRITE(6,200) NF,YYY
1413            IF (YYY.GT.DAB.OR.YYY.LT.-DAB) GO TO 100
1414            IF (NSTART.EQ.2.AND.NF.EQ.4.AND.XXX.GE.0.0) GO TO 100
1415            IF (NSTART.EQ.1.AND.NF.EQ.3.AND.XXX.GE.0.0) GO TO 100
1416            NCVRGE=NF
1417      C
1418      C     WRITE OUT INTERSECTED FACE AND POINT OF INTERSECTION
1419      C
1420            IF (IPBINT.GT.0) GO TO 500
1421      C
1422            WRITE(6,200) NF,XXX,NSTART
1423        200 FORMAT(' ',I2,'INTERSECTED FACE=',I2,'  POINT OF INTERSECTION=
1424           1',F9.5,'   STARTING FACE=',I2)
1425            RETURN
1426        100 CONTINUE
1427      C
1428      C     ERROR FLAG FOR BAD RAYS
1429      C
1430        300 WRITE(6,400) NF,NB
1431        400 FORMAT(' ','FIRST FACE INTERCEPTED IS 5 , RAY=',I4,2X,'ANGLE=
1432           1',I4)
1433            RETURN
1434      C
1435      C     NOTE XXX ALONG Y-AXIS
1436      C
1437        450 XXX=(-RAYSLP*LGT)+RAYCPT
1438      C
1439            NCVRGE=5
1440      C
```

```
      IF (IPRINT.GT.0) GO TO 500
C
      WRITE(6,200) NCYRGE,XXX,NSTART
  500 RETURN
      END
C
      FUNCTION ICCEPT(HFANGL,RAYSIP,II)
      INTEGER HFANGL
C
C     CHECK TO SEE IF INSIDE ACCEPTANCE CONE
C
      ICCEPT=51
      CHECK=ABS(ATAN(RAYSIP))
      THETA=FFANGL*PI/180.0
      IF (CHECK.LT.THETA) ICCEPT=88
      RETURN
      END
C
      FUNCTION ZCNCHK(NZCNES,NZDIM1,NZDIM2,ZCNES,NZCODE,XXX,NXX)
      INTEGER ZCNCHK
      DIMENSION ZCNES(NZDIM1),NZCODE(NZDIM2)
C
      NZCNEZ=NZCNES+1
C
      DO 100 NZ=2,NZCNEZ
      IF (ZCNES(NZ).GT.XXX) GO TO 100
C
C     ACCEPTANCE REGION ?????
C
      IF (NZCODE(NZ-1).EQ.2) GO TO 200
C
C     NOT AN ACCEPTANCE REGION
C
      GO TO 300
  100 CONTINUE
C
  200 ZCNCHK=88
      RETURN
  300 ZCNCHK=52
      RETURN
      END
C
C
C
      FUNCTION MATTER(NSTART,INTFAC)
C
C     CHECK FOR INCIDENT FACE
C
C     TIP FACES
C
      IF (NSTART.LT.3) GO TO 100
C
C     SIDE, BACK, OR WATER FILM FACES
C
      IF (NSTART-5) 300,400,600
C
C     CHECK FOR WATER OR AIR ON TIP
C
  100 IF (INTFAC.GT.1) GO TO 200
C
```

```
      C     AIR ON TOP
      C
            MATYPE=1
            RETURN
      C
      C     WATER ON TOP
      C
        200 MATYPE=2
            RETURN
      C
      C     SIDES
      C
        300 MATYPE=1
            RETURN
      C
      C     ERROR FLAG FOR BACK FACE
      C
        400 WRITE(6,500)
        500 FORMAT(1H1,'ZZZ *** ERROR IN TRACING *** ZZZ',////)
            RETURN
      C
      C     WATER FILM
      C
        600 MATYPE=3
            RETURN
            END
      C
            SUBROUTINE WATBAC(NSTART,NFACE,NH,NP,SLOPE,YCEPT,ANGLE,FACSLP,
           1RAYSLP,PI,WATHIK,L,REFINDX,IREFNT,CRTANG,RAYCPT,INTCPT,TRIP,
           2BAD,EGT,ICHECK,IWTCAL,INTENSTY,HFANGL,NOPNTS,XOLD,YOLD,MU,IGT)
      C
            INTEGER HFANGL
            REAL MU(L),LGT
            DIMENSION SLOPE(NFACE),YCEPT(NFACE),REFINDX(L),CRTANG(L),
           1INTENSTY(HFANGL,NCRNTS)
      C
            EXTERNAL SNELL,RAYNEW,CIRNGL,FIRRAY,FACHEK,MAYFLP,FRENEL,
           1DIST,ERRRS,CALCCP,XSET
      C
      C     SET WATER TRACK CALL
      C
            IWTCAL=1
      C
      C     SET ANGLE FOR FRESNEL REFRACTION CALCULATION
      C
            CANGLE=ANGLE
      C
      C     DETERMINE ANGLE OF REFRACTION
      C
      C     SET L1, L2 FOR ENTRANCE INTO WATER FILM
      C
            L1=2
            L2=3
      C
            ANGLE=SNELL(L1,L2,ANGLE,REFINDX,L,PI,IREINT)
      C
      C     SET TRIP TO CALCULATE REFRACTED COMPONENT
      C
            IFRENL=0
      C
```

```
C      DO FRESNEL REFRACTION INTENSITY CALCULATION
C
       TENSTY(NH,NP)=TENSTY(NH,NP)*FRENEL(ANGLE,OANGLE,IFRENL,IPRINT,
      1L,RFINDX,L2,L1)
C
C      SET FLIP OPTION
C
       IFLIP=0
C
C      CHECK IF RAY FLIPPING IS NECESSARY
C
       IFLIP=RAYFLP(NSTART,NFACE,RAYSLP,SLOPE)
C
C      SET INTERCEPTED DIAMOND FACE
C
  300  INTCPT=NSTART
C
C      GENERATE NEW RAY EQUATION
C
       CALL RAYNEW(ERROR1,RAYSLP,RAYCPT,ERROR2,PI,INTCPT,YCEPT,SLOPE
      1,NFACE,ANGLE,IPRINT)
C
C      FLIPPING OPTION
C
       IF (IFLIP.GT.0) CALL FLPRAY(RAYSLP,RAYCPT,SLOPE,YCEPT,PI,ANGLE,
      1NFACE,INTCPT,RAD,HGT,IPRINT)
C
C      RESET FLIP OPTION
C
       IFLIP=0
C
C      SET FOR INTERCEPTED WATER FILM FACE
C
       INTCPT=INTCPT+5
C
C      CHECK FOR AIR/WATER INTERFACE INTERSECTION OUTSIDE OF TIP
C
       ICHECK=FACHEK(RAYSLP,RAYCPT,NFACE,INTCPT,SLOPE,YCEPT,RAD,HGT)
       IF (ICHECK.GT.0) RETURN
C
C      SET SELECT FOR MATERIAL ATTENUATION COEFFICIENT
C
       LT=2
C
C      DO BEERS LAW ATTENUATION TO WATER/AIR INTERFACE
C
       CALL BEERS(BEANGL,NOPNTS,L,MU,TENSTY,XOLD,YOLD,NP,NH,LT,LGT,RAYCPT
      1,RAYSLP,INTCPT,SLOPE,YCEPT,NFACE)
C
C      SET FACE SLOPE
C
       FACSLP=SLOPE(INTCPT)
C
C      DETERMINE ANGLE OF INCIDENCE
C
       ANGLE=CIDNGL(FACSLP,RAYSLP,PI,IPRINT)
C
C      COMPARE ANGLE OF INCIDENCE TO CRITICAL ANGLE
C
       L1=MATTYP(INTCPT,INTFAC)
```

```
1621            IF (ANGLE.GE.CRITANG(LL)) GO TO 400
1622      C
1623      C     SET TRIP FOR TRANSMITTED RAY
1624      C
1625            NSTART=INTCPT
1626            TRIP=1.0
1627            RETURN
1628      C
1629      C     REFLECTED RAY CALCULATION
1630      C
1631          400 CALL RAYNEW(ERROR1,RAYSLP,RAYCPT,ERROR2,PI,INTCPT,YCEPT,SLOPE
1632           1,NFACE,ANGLE,IPRINT)
1633      C
1634      C     CHECK FOR WATER/DIAMOND INTERFACE INTERSECTION OUTSIDE OF TIP
1635      C
1636            ICHECK=FACHEK(RAYSLP,RAYCPT,NFACE,NSTART,SLOPE,YCEPT,RAD,HGT)
1637            IF (ICHECK.GT.0) RETURN
1638      C
1639      C     DO BEERS LAW ATTENUATION BACK TO DIAMOND/WATER INTERFACE
1640      C
1641            CALL BEERS(HPANGL,NCPNTS,L,PO,TENSTY,XOLD,YOLD,NP,NH,LT,LGT,RAYCPT
1642           1,RAYSLP,NSTART,SLOPE,YCEPT,NFACE)
1643      C
1644      C     SET L1, L2 FOR RE-ENTRANCE OF DIAMOND
1645      C
1646            L1=3
1647            L2=2
1648      C
1649      C     RESET FACE SLOPE, SINCE RETURNED TO DIAMOND
1650      C
1651            FACSLP=SLOPE(NSTART)
1652      C
1653      C     CALCULATE ANGLE OF INCIDENCE AND RESULTING ANGLE OF REFRACTION
1654      C
1655            ANGLE=CIDNGL(FACSLP,RAYSLP,PI,IPRINT)
1656      C
1657      C     SET ANGLE FOR FRESNEL REFRACTION CALCULATION
1658      C
1659            CANGLE=ANGLE
1660      C
1661            ANGLE=SNELL(L1,L2,ANGLE,RFINDX,L,PI,IPRINT)
1662      C
1663      C     SET TRIP TO CALCULATE REFRACTED COMPONENT
1664      C
1665            IFRENL=0
1666      C
1667      C     DO FRESNEL REFRACTION INTENSITY CALCULATION
1668      C
1669            TENSTY(NH,NP)=TENSTY(NH,NP)*FRENEL(CANGLE,ANGLE,IFRENL,IPRINT,
1670           1L,RFINDX,L1,L2)
1671      C
1672      C     RESET TRIP AND INTERSECTED FACE
1673      C
1674            TRIP=-1.0
1675      C
1676            INTCPT=NSTART
1677            RETURN
1678            END
1679      C
1680            FUNCTION RAYFLP(NSTART,NFACE,RAYSLP,SLOPE)
```

```
      C
            DIMENSION SLOPE(NFACE)
            IF (SLOPE(NSTART)) 100,800,200
        100 IF (ABS(RAYSLP).LT.ABS(SLOPE(NSTART))) GO TO 400
            GO TO 300
        200 IF (ABS(RAYSLP).GT.ABS(SLOPE(NSTART))) GO TO 400
      C
        300 MAYFLP=0
            RETURN
      C
        400 MAYFLP=1
            RETURN
      C
      C     ERROR MESSAGE FOR HORIZIONTAL FACE
      C
        800 WRITE(6,900)
        900 FORMAT(1H1,'WATER FILM HORIZIONTAL FACE',///)
            RETURN
            END
      C
            SUBROUTINE FIPRAY(RAYSLP,RAYCPT,SLOPE,YCEPT,PI,ANGLE,NFACE,INTCPT,
           1RAD,FG1,IPRINT)
      C
            DIMENSION SLOPE(NFACE),YCEPT(NFACE)
      C
      C     CALCULATE INTERSECTION POINT
      C
            XXX=(YCEPT(INTCPT)-RAYCPT)/(RAYSLP-SLOPE(INTCPT))
            YYY=(RAYSLP*XXX)+RAYCPT
      C
      C     ADD ON NECESSARY ANGLE SWING
      C
            ADDGLE=2.0*((PI/2.0)-ANGLE)
      C
      C     RECALCULATE RAY EQUATION
      C
            RAYSLP=TAN(ATAN(RAYSLP)+ADDGLE)
            RAYCPT=YYY-(RAYSLP*XXX)
      C
      C
            IF (IPRINT.GT.0) GO TO 300
      C
            WRITE(6,200) RAYSLP,RAYCPT,XXX
        200 FORMAT(' ','FLIP RAY SLOPE=',1PE12.4,'   FLIP RAY INTERCEPT=',
           1 1PE12.4,'  XXX=',1PE12.4)
        300 RETURN
            END
      C
            FUNCTION FACHEK(RAYSLP,RAYCPT,NFACE,INTCPT,SLOPE,YCEPT,RAD,HGT)
      C
            DIMENSION SLOPE(NFACE),YCEPT(NFACE)
      C
      C     CALCULATE INTERSECTION POINT
      C
            XXX=(YCEPT(INTCPT)-RAYCPT)/(RAYSLP-SLOPE(INTCPT))
            YYY=(RAYSLP*XXX)+RAYCPT
      C
      C     CHECK TO MAKE SURE INTERSECTION IS WITHIN DIAMOND/WATER FILM AREA
      C
            IF (XXX.LT.0.0.OR.XXX.GT.HGT) GO TO 100
```

```
1741      C
1742            IF (YYY.GT.BAD.OR.YYY.LT.-BAD) GO TO 100
1743      C
1744      C     INTERSECTION WITHIN BOUNDS
1745      C
1746            FACTOR=0
1747            RETURN
1748      C
1749      C     INTERSECTION IS OUT OF BOUNDS
1750      C
1751        100 FACTOR=1
1752            RETURN
1753            END
1754      C
1755            SUBROUTINE BEERS(HFANGL,NCENTS,L,MU,TENSTY,XOLD,YOLD,NP,NH,LT,LGT,
1756           1RAYCPT,RAYSLP,NSTART,SLOPE,YCEPT,NFACE)
1757            REAL MU(L),LGT
1758            INTEGER HFANGL
1759            DIMENSION TENSTY(HFANGL,NCENTS),SLOPE(NFACE),YCEPT(NFACE)
1760            EXTERNAL XSET,DIST
1761      C
1762      C     DETERMINE NEW X AND Y COORDINATES
1763      C
1764            CALL XSET(XNEW,YNEW,RAYSLP,RAYCPT,LGT,NSTART,SLOPE,YCEPT,NFACE)
1765      C
1766      C     CALCULATE PATH LENGTH USING DISTANCE EQUATION TIMES ATTENUATION
1767      C     COEFFICIENT
1768      C
1769            OX=(DIST(XOLD,YOLD,XNEW,YNEW)*MU(LT))
1770      C
1771      C     APPLY BEER'S LAW  I=IO*EXP(-OX)
1772      C
1773            TENSTY(NH,NP)=TENSTY(NH,NP)*EXP(-OX)
1774      C
1775      C     RESET XOLD AND YOLD FOR LATER USE
1776      C
1777            XOLD=XNEW
1778            YOLD=YNEW
1779      C
1780      C     WRITE OUT TENSTY
1781      C
1782      C     WRITE(6,100) TENSTY(NH,NP),OX,XOLD,YOLD
1783      C 100 FORMAT(' ',4(2X,F10.5))
1784      C
1785            RETURN
1786            END
1787      C
1788      C
1789            FUNCTION DIST(XOLD,YOLD,XNEW,YNEW)
1790      C
1791      C     ROUTINE TO APPLY DISTANCE EQUATION
1792      C
1793            DIST=SQRT(((XNEW-XOLD)**2)+((YNEW-YOLD)**2))
1794      C
1795            RETURN
1796            END
1797      C
1798            SUBROUTINE CALCOP(OANGLE,ANGLE,RADCOF,CDTNGL,RFTNGL,IFRENI)
1799      C
1800      C     CALCULATE TANGENT OF INCIDENT ANGLE
```

```
      C
            CDTNGL=TAN(CANGLE)
      C
      C     CALCULATE ANGLE OF REFRACTED ANGLE
      C
            RFTNGL=TAN(ANGLE)
      C
      C     CALCULATE LEADING COEFFICIENT
      C
            RADCOF=0.5*(RFTNGL/CDTNGL)
      C
            IF (IFRENL.GT.0) RADCOF=0.5*(CDTNGL/RFTNGL)
      C
            RETURN
            END
      C
            FUNCTION FRENEL(CANGLE,ANGLE,IFRENL,IPRINT,L,RFINDX,L1,L2)
            DIMENSION RFINDX(L)
            EXTERNAL CALCOF
      C
            IF (CANGLE.LT.0.01) GO TO 100
      C
            CALL CALCOF(CANGLE,ANGLE,RADCOF,CDTNGL,RFTNGL,IFRENL)
      C
            IF (IFRENL.GT.0) GO TO 75
      C
      C     CALCULATE TRANSMITTED INTENSITY
      C
      C     CACCLATE PARALLEL COMPONENT
      C
            PARACF=((CDTNGL-RFTNGL)*(1.0-(CDTNGL*RFTNGL)))/
     1        ((CDTNGL+RFTNGL)*(1.0+(CDTNGL*RFTNGL)))
      C
      C     CALCULATE PERPENDICULAR COMPONENT
      C
            PERPCF=((COS(ANGLE)*SIN(CANGLE))-(SIN(ANGLE)*COS(CANGLE)))/
     1        ((SIN(CANGLE)*COS(ANGLE))+(COS(CANGLE)*SIN(ANGLE)))
      C
      C     COMBINE INTO TOTAL TRANSMITTED INTENSITY
      C
            FRENEL=RADCOF*(2.0-(PARACF**2)-(PERPCF**2))
            GO TO 200
      C
      C     CALCULATES REFLECTED INTENSITY
      C
      C     CALCULATE PERPENDICULAR COMPONENT
      C
         75 PERPCF=(2.0*SIN(ANGLE)*COS(CANGLE))/((SIN(CANGLE)*COS(ANGLE))
     1+(COS(CANGLE)*SIN(ANGLE)))
      C
      C     CALCULATE PARALLEL COMPONENT
      C
            PARACF=PERPCF*(1.0/((COS(CANGLE)*COS(ANGLE))+(SIN(CANGLE)*
     1SIN(ANGLE))))
      C
      C     COMBINE INTO TOTAL TRANSMITTED COMPONENT
      C
            FRENEL=1.0-(RADCOF*((PARACF**2)+(PERPCF**2)))
            GO TO 200
      C
```

```
C      ZERO ANGLE OF INCIDENCE CASE
C
C      REFLECTED COMPONENT
C
  100 RRENEL=((RFINDX(L2)-RFINDX(L1))/(RFINDX(L2)+RFINDX(L1)))**2
C      TRANSMITTED COMPONENT
C
       IF (IFRENL.EQ.0) RRENEL=(1.0-RRENEL)*(RFINDX(L2)/RFINDX(L1))
C
C
  200 IF (IRRINT.GT.0) RETURN
C
C      WRITE OUT NEW INTENSITY
C
       WRITE(6,300) RRENEL,PARACP,PERPCP
  300 FORMAT('0','NEW RELATIVE INTENSITY= ',1PE12.5,'WITH A PARALLEL CO
     1MP= ',1PE12.5,' AND A PERPENDICULAR COMP= ',1PE12.5)
C
       RETURN
       END
C
       SUBROUTINE SUMREF(ITRANS,MFANGL,NCPNTS,PERTAN,PI)
       INTEGER MFANGL
       DIMENSION ITRANS(MFANGL,NCPNTS),PERTAN(MFANGL)
C
C      SUM UP REFLECTED RAYS FOR EACH ANGLE
C
       A=NCPNTS
       DO 200 NH=1,MFANGL
       PERTAN(NH)=0.0
       DO 100 NP=1,NCPNTS
       IF (ITRANS(NH,NP).NE.88) GO TO 100
       PERTAN(NH)=PERTAN(NH)+1
  100 CONTINUE
       PERTAN(NH)=PERTAN(NH)/A
  200 CONTINUE
       RETURN
       END
C
C
       SUBROUTINE ANSR(ITRANS,MFANGL,NCPNTS,PERTAN,IHEAD,TITLE,
     1TENSITY,INTFAC)
       INTEGER MFANGL
       DIMENSION IHEAD(NCPNTS),TITLE(20),TENSITY(MFANGL,NCPNTS)
       DIMENSION ITRANS(MFANGL,NCPNTS),PERTAN(MFANGL)
C
       PI=0.0
C
C      WRITE OUT TITLE
C
       WRITE(6,75) TITLE
   75 FORMAT(1H1,20A4)
       WRITE(6,100) INTFAC
  100 FORMAT('0','*** TRANSMISSION AND INTENSITY MATRIX FOR CASE',
     1' NO. ',I2,' ***',///)
C
C      SET TABLE HEADING
C
       DO 50 NP=1,NCPNTS
       IHEAD(NP)=NP
```

```
 1921          50 CONTINUE
 1922             WRITE(6,200) (IHEAD(NP),NP=1,NOPNTS)
 1923         200 FORMAT(' ',T2,'ANGLE OF',53X,'*** RAY POSITION***',/,
 1924            1       ' ','INPUT LIGHT',10(8X,I2))
 1925             WRITE(6,250)
 1926         250 FORMAT('+',T125,'TOTAL',//)
 1927             DO 400 NH=1,NFANGL
 1928             WRITE(6,300) NH,(IIRANS(NH,NP),NP=1,NOPNTS)
 1929         300 FORMAT('0',1X,I4,6X,10(8X,I2))
 1930             WRITE(6,350) FERTAN(NH)
 1931         350 FORMAT('+',T125,F5.2)
 1932             R1=R1+FERTAN(NH)
 1933       C
 1934             WRITE(6,375) (INTENSITY(NH,NP),NP=1,NOPNTS)
 1935         375 FORMAT(' ',17X,10(F6.4,4X))
 1936       C
 1937         400 CONTINUE
 1938       C
 1939             R1=R1/NFANGL
 1940             WRITE(6,450) R1
 1941         450 FORMAT('0','FRACTION REFLECTED BACK IS:',F10.5)
 1942             WRITE(6,500)
 1943         500 FORMAT(1H1)
 1944             RETURN
 1945             END
 1946       C
END OF FILE
```

APPENDIX A.6

AN OPTICAL TECHNIQUE FOR GLOBAL VOID FRACTION

Several important two-phase flow parameters have been measured using light transmission techniques. Langlois, et. al. [51] employed this technique to measure interfacial area. Lockett and Safekourdi [31] measured gas holdup in gas/liquid systems using light transmission Lahey, et. al. [52] have developed a device to measure the instantaneous global void fraction and phase distribution.

Light transmission techniques are very attractive for two-phase flow measurements. Light can be introduced and detected non-intrusively. High efficiency fiber optics can be employed to transmit light with minimal losses. The propagational speed of light is very fast, thus the response time of an optical device would depend only on the signal processing electronics.

The next section presents the basis of the optics associated with the light transmission technique. A two-dimensional computer model, BUBRAY, was developed and used to quantify the light ray reflection and refraction patterns in two-phase mixtures. This code is presented in Appendix-A.7. This section consists of two major parts. The modeling part discusses the assumptions and mathematics employed in the analysis. The second section discusses specific details associated with the computer code. An example is described and programmed in Appendix A.7.

Modeling

Light ray intersection with voids in a two-phase media is a function of three dimensions and time. A total description of the phenomena would require the simultaneous solution of four variables. The problem can be reduced by making a series of assumptions. These assumptions simplify the analytical effort and result in a solution which indicates the basic physics involved. The specific assumptions are:

1) Light rays move in straight lines.
2) Light rays move independently of each other.
3) Constant optical properties exist within each phase.
4) Light rays move only in the x-y plane,(i.e., in two dimensions only).
5) The time dependence of the ray tracing can be discretized.

As in DOPE-1, light is assumed to move in a straight line,

$$y = mx + b \tag{1}$$

where,

y = y-coordinate of the ray
m = slope of the ray
x = x-coordinate of the ray
b = y-intercept of the ray

It is well known that light rays do move in this fashion. Assumptions (2) and (3) also represent reasonable physical

assumptions.

The fourth assumption is the most significant. Light is emitted from a source with a conical pattern. The rays are moving through three dimensions. Light ray reflection and refraction occur in a plane but this plane is positioned in three dimensions. The fourth assumption implies that the 'z' component of this plane is constant. Ray tracing done in two-dimensions is strictly valid only for those light rays moving in a plane parallel to the x-y axis, and for voids made up of cylindrical axial sections, each of which have no axial 'z' curvature.

The time dependence of the light ray paths is simulated by performing the tracing on successive planes through an ellipsoidal bubble. These planes are equally spaced through the void and are parallel to the x-y plane.

Several equations form the basis of the ray tracing scheme. A brief description of these equations are presented here to provide a basic understanding of the technique employed.

The coordinates of a light ray and interface intersection point must be calculated accurately. These coordinates are necessary since they will determine the normal to the interface and the angle of incidence. Simultaneous solution of Equation (1) and Equation (2),

$$\frac{(x-a)^2}{A} + \frac{(y-d)^2}{B} + \frac{(z-c)^2}{C} = R^2 \qquad (2)$$

where,

x,y,z = the coordinates of a point on the interface

a,d,c = the coordinates of the center of the ellipsoid

A,B,C = the x, y, and z coefficients of the ellipsoid

R = the effective radius

the expression for a three dimensional ellipsoid, will yield the coordinates of the point of intersection,

$$\frac{(x-a)^2}{A} + \frac{(mx+b-d)^2}{B} + \frac{(z-c)^2}{C} = R^2 \qquad (3)$$

Equation (3) is obtained from the direct substitution of 'y' in Equation (1), into Equation (2). The value of 'z' is fixed in a given plane parallel to the x-y axis, thus the third term of Equation (3) can be considered a constant. Simplification of this expression is done by defining the following constants,

$$Q \triangleq b-d \quad Z \triangleq R^2 - \frac{(z-c)^2}{C} \qquad (4)$$

Equations (3) and Equation (4) yield,

$$\frac{(x^2 - 2ax + a^2)}{A} + \frac{((mx)^2 + 2mx\,Q + Q^2)}{B} = Z \qquad (5)$$

After substitution of Equation (4) and expansion of terms, Equation (5) can be multiplied through 'AB' and regrouped

to yield,

$$(B+Am^2)x^2+(2AmQ - 2Ba)x+(a^2B+AQ^2- ZAB = 0 \qquad (6)$$

This equation has the form of a quadratic equation. Solution is possible by using the well known quadratic formula,

$$X = \frac{-BBB\pm\sqrt{(BBB)^2- 4(AAA\ CCC)}}{2AAA} \qquad (7)$$

where,

$AAA = B+Am^2$

$BBB = 2(AmQ-Ba)$

$CCC = a^2B+AQ^2-ZAB$

Two values for a possible x-coordinate are produced. Substitution of each x-coordinate value into Equation (1) will yield a corresponding y-coordinate value. These values are then substituted back into Equation (2). Only the coordinates of the intersection will satisify the equation. The coordinates of intersection are now established.

The normal to the interface must now be calculated so that the angle of incidence can be determined. The derivative of Equation (2), at constant 'z' is,

$$\frac{2(x-a)}{A}\,dx + \frac{2(y-d)}{B}\,dy = 0 \qquad (8)$$

Equation (8) gives the tangent to the interface as,

$$\frac{dy}{dx} = - \frac{A(y-d)}{B(x-a)} \qquad (9)$$

The normal is easily calculated since it is just the negative reciprocal of the tangent,

$$\text{Normal} = -\frac{1}{\text{interface slope}} = \frac{B(x-a)}{A(y-d)} \tag{10}$$

Reflection or refraction may now occur at an interface depending on the angle of incidence. This angle is calculated from the interface and ray slope, as shown in Figure A.c.1. Plane geometry dictates that angles ϕ_1, β, and θ should sum to 90 degrees,

$$\frac{\pi}{2} = \phi_1 + (-\beta) + \theta \tag{11}$$

where,

ϕ_1 = angle of incidence, with respect to the interface normal

β = angle between the interface and the x-axis, (i.e., the arctangent of the interface slope)

θ = angle between the incident light ray and the x-axis, (i.e., the arctangent of the ray slope)

The angle of incidence can be obtained by rearranging Equation (11),

$$\phi_1 = \frac{\pi}{2} - (-\beta+\theta) \tag{12}$$

This angle is compared with the critical angle for that interface to determine if reflection or refraction has

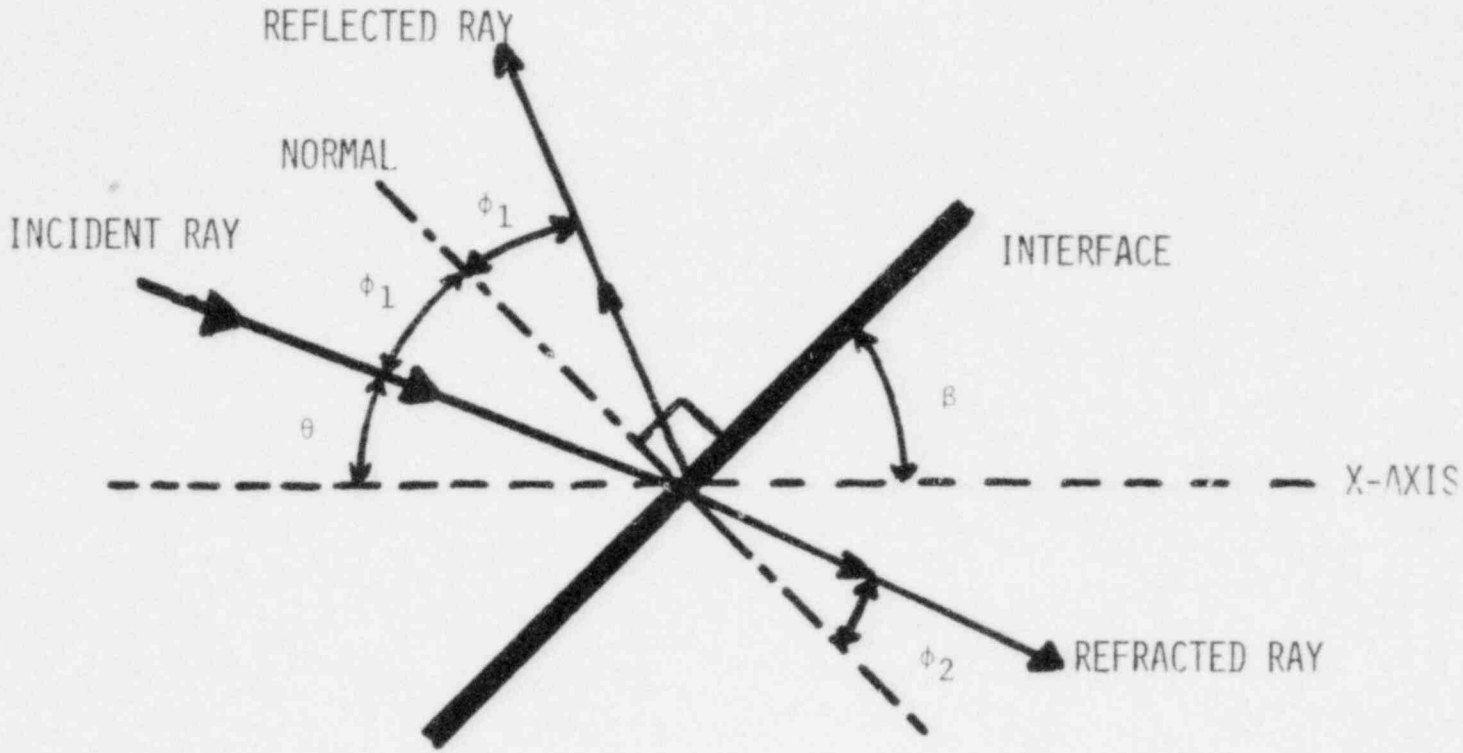

Figure A.6.1 Light ray reflection and refraction at an interface

occurred.

A new equation for the reflected light ray can be obtained by assuming that the angle of incidence is equal to the angle of reflection. The 'x' and 'y' coordinates of a point on the ray are known as well as the interface slope. Combining these three quantities a new ray equation can be generated.

Two possible reflection situations could exist:

1) The slope of the reflected ray is equal to zero.
2) The slope of the reflected ray is not equal to zero.

Figure A.6.2 illustrates three possible face/light ray intersections, note that the positive or negative slope cases yield the same analytical expression. The zero slope case is the simplest. A reflected light ray's slope will just change sign. Thus using the intersection coordinates and the new slope the new ray intercept is calculated by rearranging Equation (1).

Generation of the reflected ray when the surface slope is not zero is somewhat more complicated. Consider a normal to the bubble's interface. The slope of the normal is the negative reciprocal of the surface slope, as previously shown in Equation (10). Using plane geometry, the slope of the reflected ray can be related to the angle of incidence and the surface normal,

$$\text{rayslp} = \tan(\phi_1 + \alpha) \qquad (13)$$

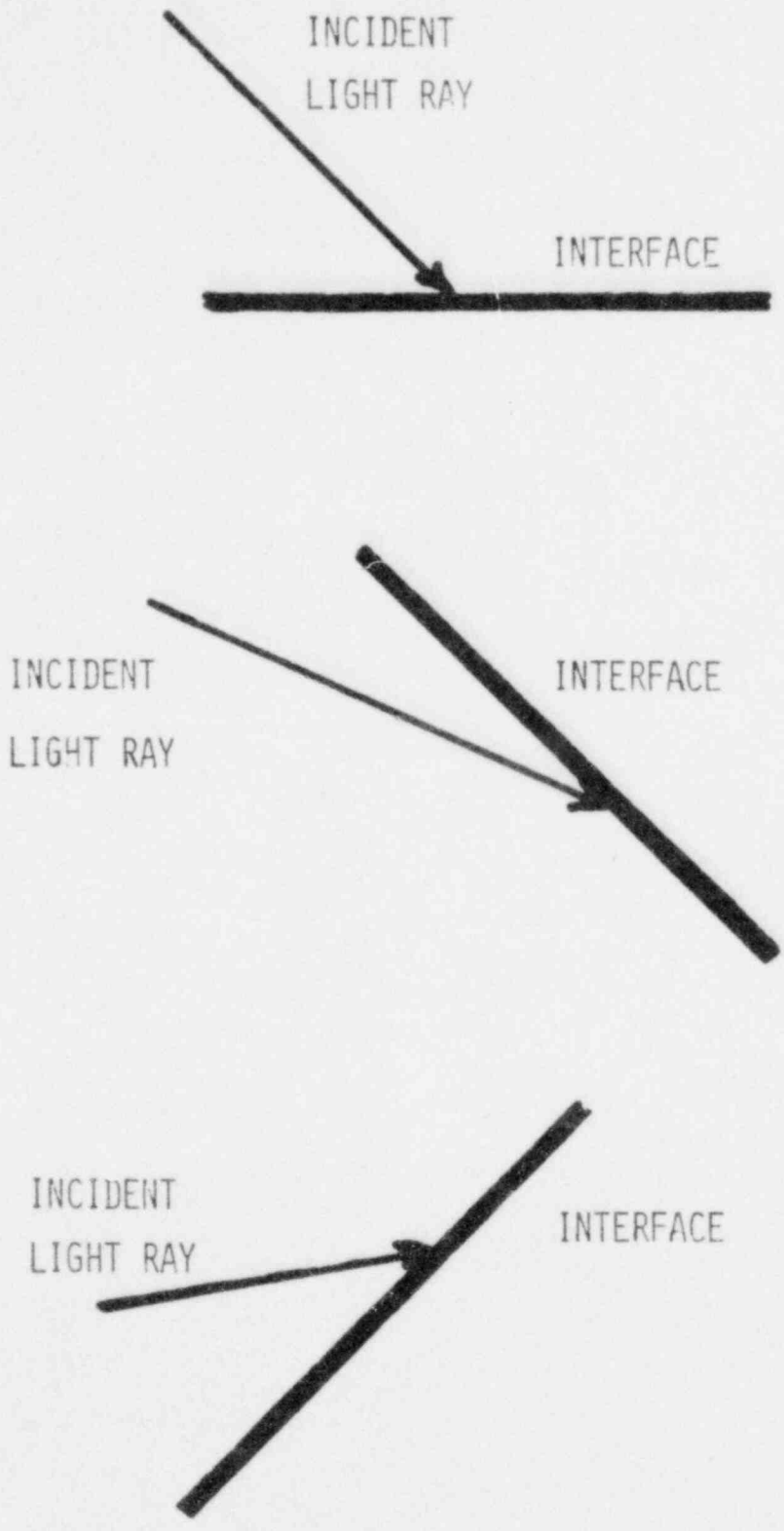

Figure A.6.2 Three possible surface/light ray intersections

where,

rayslp = slope of reflected ray

ϕ_1 = the angle of incidence, measured with respect to the normal

α = the angle between the normal and the positive x-coordinate axis, (i.e.,the arctangent of the normal's slope)

The IBM 3033 computer's tangent function operates only in the first and fourth quadrants. As with DOPE-1, this condition imposes a limitation on the use of Equation (13), since regeneration of the incident light ray is possible. If regeneration occurs, the ray equation must be corrected by an additional angle.

This adjustment is obtained from plane geometry. Using the schematics of Figure A.6.1, the adjustment angle is calculated by,

$$\theta_{adj} = 2\left(\frac{\pi}{2} - \phi_1\right) \tag{14}$$

where,

θ_{adj} = adjustment angle, required to compensate for the computer's tangent function

ϕ_1 = angle of incidence, measured with respect to the normal

A new ray is then computed by adding the adjustment angle to the previously calculated angle,

$$rayslp_{new} = \tan(\tan^{-1}(rayslp_{old}) + \theta_{adj}) \tag{15}$$

where,

$rayslp_{new}$ = new light ray slope

$rayslp_{old}$ = previously calculated ray slope

θ_{adj} = adjustment angle, calculated by Equation (14)

The y-intercept is now calculated by using the new slope in Equation (1).

Light rays which are not reflected when striking the liquid/vapor interface are refracted. Snell's Law,

$$n_1 \sin\phi_1 = n_2 \sin\phi_2 \tag{16}$$

where,

n_1, n_2 = refractive indices of medium 1 and 2, respectively

ϕ_1 = the angle of incidence, measured with respect to a normal to the surface

ϕ_2 = the angle of refraction measured with respect to a normal to the surface

can now be used to calculate the angle of refraction. This angle is used with the reflected ray generation technique to calculate the equation of the refracted ray.

This computer model can also model a liquid film along the wall of a conduit. The film is assumed to be of constant thickness, except at the place where the light rays enter. Here a variable angle for this part of the film can be selected. Snell's Law, Equation (16), is used to calculate the light ray refraction at the liquid film/vapor

interface. The actual ray tracing procedures employed in the liquid film are identical to those used outside the the film.

Computer Model

The previously described mathematics have been used in the BUBRAY computer code. This code's flowchart is illustrated in Figures A.6.3a and A.6.3b. Output from the BUBRAY code includes a chart indicating the number of rays which strike a given region on the square duct's inner surface. This table is printed as a function of input light angle. An appropriate chart is generated for each 'z' increment. All input data is printed for reference, and to allow verification. Appendix A.7 provides a FORTRAN listing of the code, and a typical I/O data preparation instructions.

The time step viewing of the two-phase mixture is illustrated in Figure A.6.4. The 'z' component of the bubble is assumed constant at each step. The plane of refraction is based on the projection of the true normal on the x-y plane since the 'z' component of the liquid/vapor interface normal is assumed to be sero.

Normally BUBRAY is used for the analysis of two-phase flow in a pipe. However, the code was modified and a geometry commonly used in two-phase flow experiments conducted at Rensselaer Polytechnic Institute (RPI) was studied with the BUBRAY code. This geometry consists of a

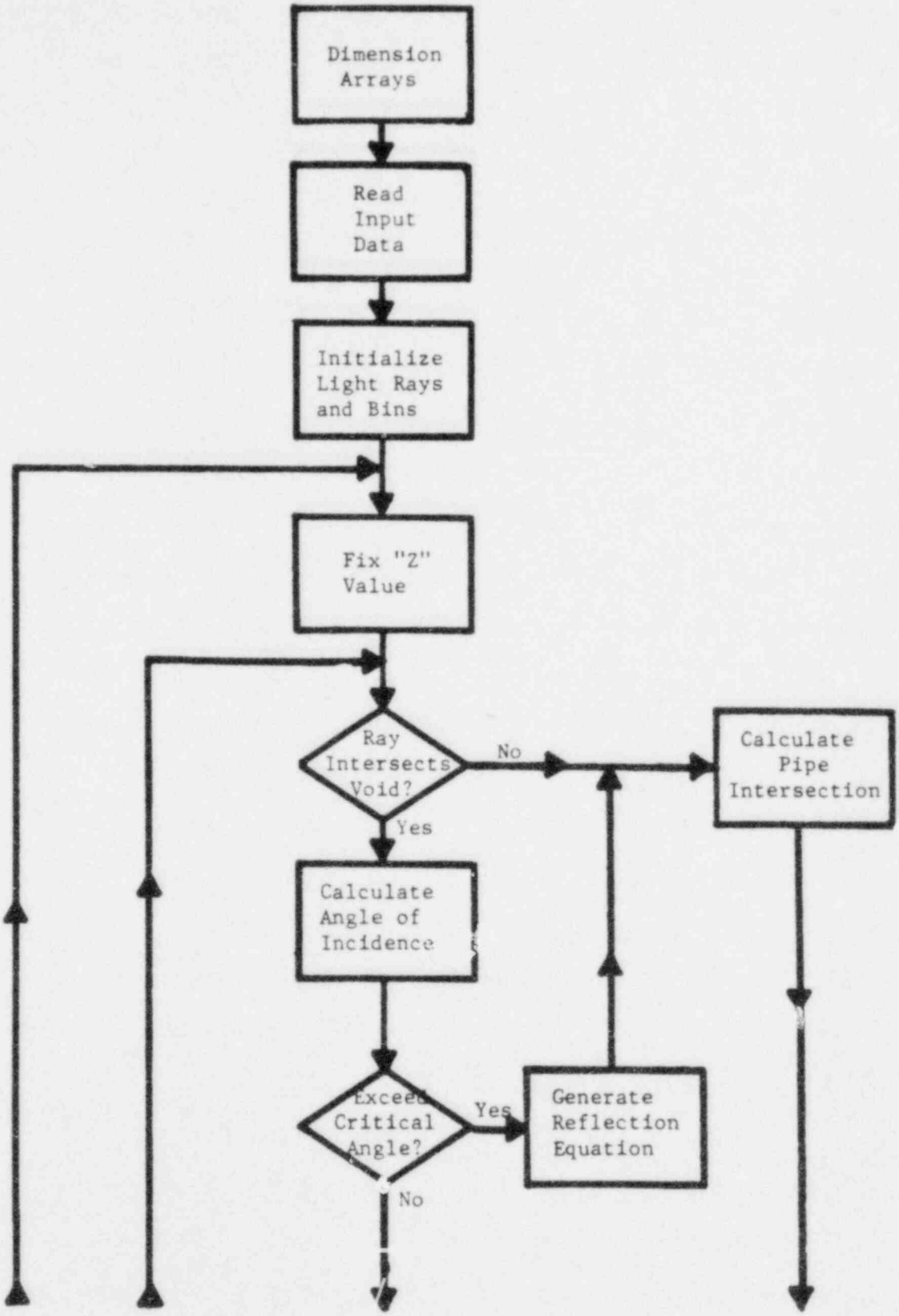

Figure A.6.3 a
BUBRAY flowchart

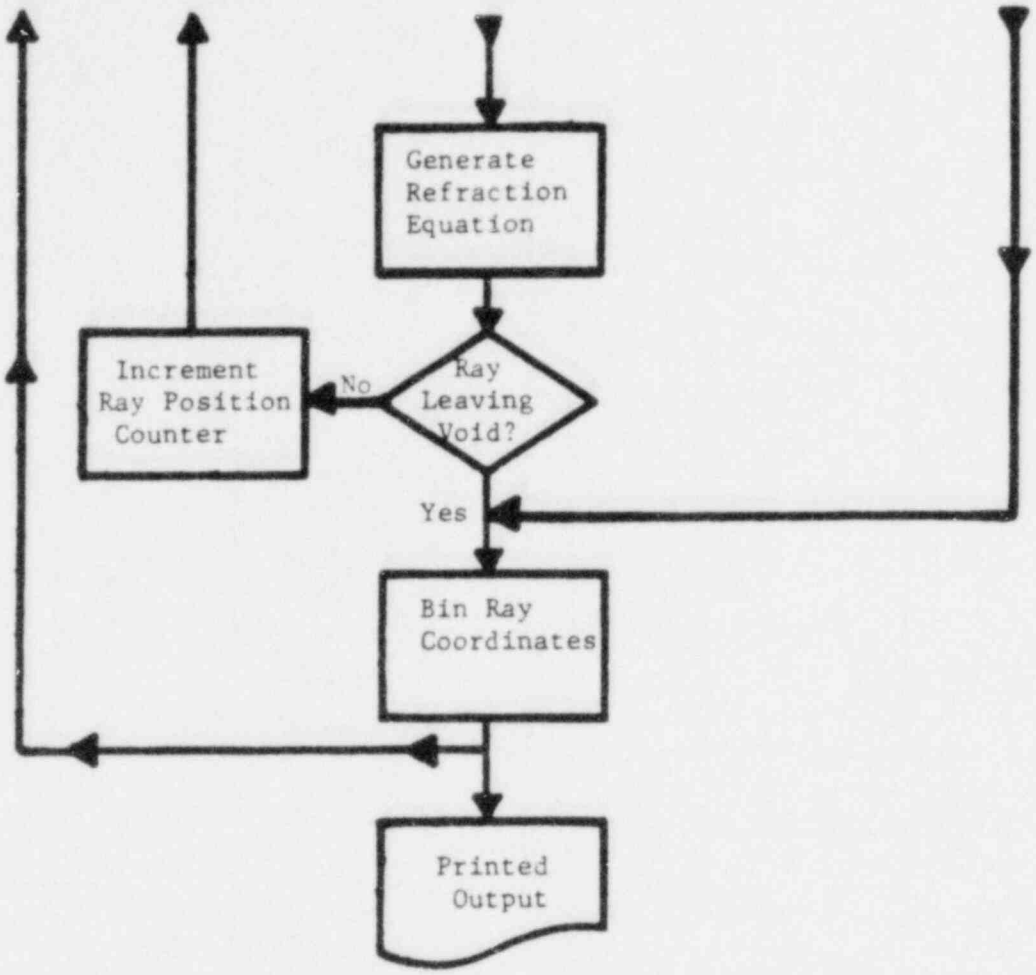

Figure A.6.3b Continued

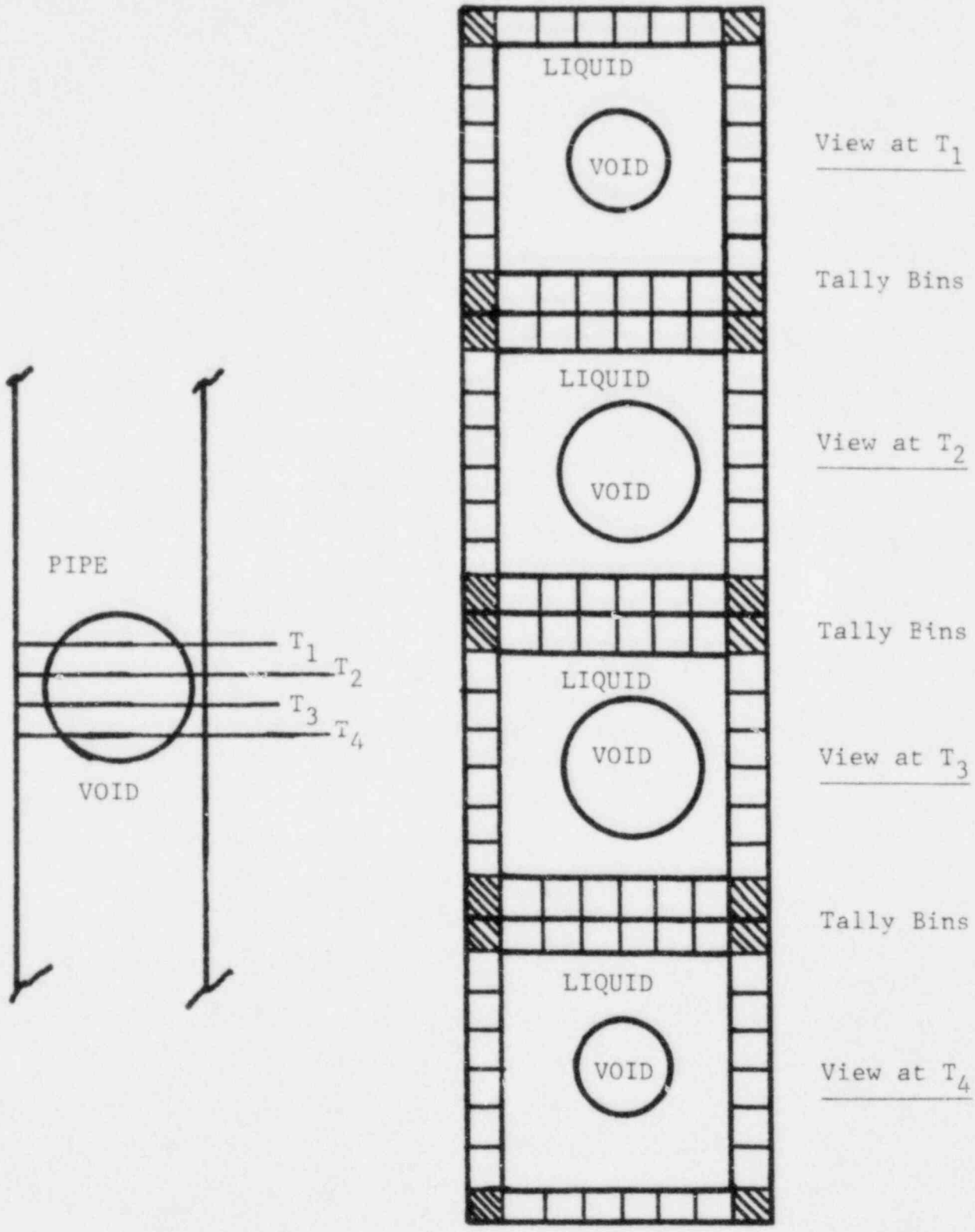

Figure A.6.4 Time step viewing used in BUBRAY

1.2 inch square duct containing a single air bubble in water. Visible red light, with a wave length of 690 nanometers, was introduced through 0.125 inch diameter sapphire pipes. This ray tracing simulation has verified the operating principle of the digital optical interferometer.

APPENDIX A.7

PROGRAMMING INSTRUCTIONS FOR THE BUBRAY CODE

BUBRAY is a two computer simulation of light ray interaction with a two-phase mixture. Light rays are initiated uniformly over the specified input region. The rays are then assumed to move in straight lines. Snell's Law for refraction is employed if a liquid/vapor interface is intersected. Tally bins are equally positioned around the pipe circumference to sum up the rays and their position, when they return to the pipe surface.

All input data is listed for reference and verification. Output consists of a listing of the number of rays striking each bin as a function of input light angle. A separate listing is provided for each time step.

BUBRAY is written in Fortran-IV. The code is variably dimensioned and requires a small amount of input data. Execution time is about 3 c.p.u. seconds on an IBM-370/3033. A brief description of all subroutines and the important variables is provided at the beginning of the program listing.

The input data required to perform a BUBRAY run is listed in Table 1. Any dimenstional units can be used as long as all are consistent. A brief description of each card follows to further explain the input data.

First Card

The title of the run being performed is written here. This card is used only for references. It can be left blank if desired.

Second Card

Two types of geometry, circular pipe or square duct, were considered when this code was developed. The user should enter 0 for the circular pipe option and enter 1 for the square duct option.

Third Card

This card contains various specifications for the voids, pipe and light rays. The first entry sets the number of surface equations required, usually 2. One surface equation is required to describe the pipe and one for each void or droplet studied. The second entry specifies the thickness of any water film, while the third entry sets the width of a square duct test section. These two parameters can be set equal to zero or set to appropriate values for the now complete square test section option. The radius of the input light beam is the fourth entry on this card. Specification of the maximum light ray angle composing the light beam is the fifth entry. This beam is assumed to be composed of a finite number of rays. The sixth entry of the card is the total number of these rays. The number of planes in the 'Z' direction, i.e., the number of time steps to be considered, is the seventh data entry on this card. The last entry is the number of tally bins to be placed around the pipe. Forty (40) is the suggested value as well

as the maximum value. Use of less bins reduces discrimination while inclusion of more bins results in an output too wide for computer paper.

Fourth Card

This card specifies if intermediate values calculated are to be printed. Inputting 0 suppresses printing but use of 1 will generate detailed information concerning the ray tracing. It is recommended that this parameter be 0 because substantial output is generated.

Fifth Card(s)

The parameters specifying the equation of the various surfaces are input here. The center 'x', 'y', 'z' coordinates of the surface are first to be input. Three more data entries on the same card specify the 'x', 'y', 'z' coefficients of this equation. The seventh entry on this card is the radius squared. (For a more detailed explanation of these parameters, see Equation (2) in Appendix A.6). A final entry on this card specifies the material contained within the surface. The liquid phase is designated by 1, while entry of 2 will specify vapor.

Two precautions must be taken when inputting this information. The card which contains data describing the pipe surface should be first. Void data follows the pipe information. Secondly, the 'Z' coefficient causes Equation (2) in Appendix A.6 to reduce to the equation of an elliptic cylinder in three dimensional space. 10^{30} is sufficiently large enough to avoid computer underflow.

Sixth Card

Refractive indices are specified on this card. The liquid refractive index is specified first. The second entry will set the refractive index on vapor. Care should be taken to enter appropriate indices bearing in mind that the refractive index is a function of light wavelength.

Seventh Card

The final data card contains the linear attenuation coefficients. No attenuation calculations are performed, so this data can be set equal to zero.

A Code Listing and Sample Problem

A BUBRAY listing and sample problem are provided. The simulation consists of a 0.055 inch radius air bubble in a 0.5 inch radius pipe. The pipe is full of water with a void positioned concentrically. Visible red light is input through 0.0626 inch radius light pipes. The code output is attached.

TABLE 1. - BUBRAY Input Data

Card Sequence	Columns	Format	Description
1 Card	1-80	20A4	Title of simulation being run
1 Card	2-5	I4	Type of geometry being modeled 0 - circular pipe 1 - square duct
1 Card	2-5	I4	Number of surface equations needed in the simulation
	6-15	F10.5	Thickness of residual water film
	16-25	F10.5	Width of square duct test section
	26-35	F10.5	Radius of input light beam
	37-40	I4	Maximum angle of input light rays
	42-45	I4	Number of light rays composing light beam
	47-50	I4	Number of 'Z' or time steps to be considered
	52-55	I4	Number of tally bins around pipe circumference
1 Card	2-5	I4	Intermediate printing code 0 - no printing 1 - print intermediate values
NBUB cards	1-10	E10.3	x-coordinate of void or pipe center
	11-20	E10.3	y-coordinate of void or pipe center
	21-30	E10.3	z-coordinate of void or pipe center
	31-40	E10.3	x-coefficient of void or pipe equation
	41-50	E10.3	y-coefficient of void or pipe equation
	51-60	E10.3	z-coefficient of void or pipe equation

	61-70	E10.3	Equivalent radius squared of void or pipe
	72-75	I4	Material inside surface equation 1 - liquid 2 - vapor
1 Card	1-10	F10.7	Refractive index of liquid
	11-20	F10.7	Refractive index of vapor
1 Card	1-10	F10.7	Linear attenuation coefficient of liquid
	11-20	F10.7	Linear attenuation coefficient of vapor

```
1     /COMPILE
2     C
3     C
4     C     BBBBBB    UU   UU    BBBBBB    BBBBBB      AAA      YY  YY    2222222
5     C     BB   BB   UU   UU    BB   BB   BB   BB    AAAAA     YY  YY   22222222
6     C     BB   BB   UU   UU    BB   BB   BB   BB    A   A     YYYYYY         222
7     C     BBBBBB    UU   UU    BBBBBB    BBBBBB    AAAAAAA     YYYY      222222
8     C     BB   BB   UU   UU    BB   BB   BB   BB   AAAAAAA      YY      222
9     C     BB   BB   UUUUUU    BBBBBB    BB   BB   AA   AA      YY     22222222
10    C     BBBBBB    UUUUUU    BBBBBB    BB   BB   AA   AA      YY     22222222
11    C
12    C
13    C
14    C
15    C      BUBBLE RAY TRACING, VERSION 2
16    C      $$$    $$$                  3
17    C
18    C
19    C
20    C
21    C
22    C                        DECEMBER 1979
23    C
24    C
25    C
26    C      DEVELOPED AT RENSSELAER POLYTECHNIC INSTITUTE FOR:
27    C
28    C                      UNITED STATES NUCLEAR REGULATORY COMISSION
29    C                      WASHINGTON, D.C.
30    C                      CONTRACT AT(49-24)-0301
31    C                      DR Y. Y. HSU, DIRECTOR
32    C
33    C
34    C
35    C
36    C
37    C      AUTHOR OF BUBRAY:
38    C
39    C                      MARK VINCE
40    C                      NUCLEAR ENGINEERING AND SCIENCE BUILDING
41    C                      RENSSELAER POLYTECHNIC INSTITUTE
42    C                      TROY, NEW YORK 12181
43    C
44    C
45    C
46    C      WRITTEN IN PARTIAL FULFILLMENT OF THE REQUIREMENTS
47    C      FOR THE DEGREE OF DOCTOR OF PHILOSOPHY
48    C      IN NUCLEAR ENGINEERING
49    C
50    C
51    C
52    C
53    C      MODIFIED FROM BUBRAY TO BUBRAY2  BY:
54    C
55    C                      GLENN SYLVESTER
56    C                      RENSSELAER SOCIETY OF ENGINEERS
57    C                      RENSSELAER POLYTECHNIC INSTITUTE
58    C                      TROY, NEW YORK  12180
59    C
60    C
```

```
C      DOCTORAL COMMITTEE:
C
C                    DR. RICHARD T. LAREY, JR. CHAIRMAN
C                    DR. HENRY E. BREED
C                    MR. GEORGE KRYCUK
C                    DR. RODNEY GAY
C                    DR. JOHN C. COBELLI
C
C
C
C                                   BUREAU SECRETARY
C
C                                      ********
C                                    ******  ******
C                                  *****      *****
C                                ***              ***
C                              **      *****       **
C                            ***     ***   ***     ***
C      ** INPUT **          **       ***     ***      **
C      ** LIGHT **        **         **       **       **
C                       **          **         **       **
C                      **           **  VOID   **        **
C      REFRACTED   11111**111111111**1         **         **
C                     **            **  1      **         **
C                     **            **   1     **         **
C                     **            **    1    **         **
C      REFLECTED   22222**222222222**     1    **   LIQUID **
C                     **            2 ***  ***             **
C                      **             2  ****1              **
C      TRANSMITTED 3333333**33333333333333333333333333333333**
C                        **                2       1          **
C                         **   LIQUID     2       1         **
C                          **              2       1        **
C                            **            2       1      **
C                              ***         2       ***
C                                *****     2   *****
C                                   ******  ******
C                                      ********
C
C
C
C
C
C                          *** SUBROUTINES ***
C
C
C     BINEE                SUBROUTINE TO TALLY LIGHT RAYS IN
C                          APPROPRIATE BINS
C
C     BINZZ                FUNCTION SUBROUTINE TO CALCULATE THE SIZE
C                          OF A BIN, IN RADIANS
C
C     CEPT                 SUBROUTINE TO CALCULATE THE Y-INTERCEPT OF
C                          THE INITIAL LIGHT RAYS
C
C     CIDNGL               FUNCTION SUBROUTINE TO CALCULATE THE
C                          ANGLE OF INCIDENCE GIVEN RAY AND
```

```
C                       INTERFACE SLOPE
C
C       EQUAT           SUBROUTINE TO CALCULATE THE WATER FILM
C                       EQUATIONS WHEN SQUARE GEOMETRY IS USED
C
C       FIPRAY          SUBROUTINE TO FLIP RAY IF INCORRECT RAY
C                       EQUATION IS GENERATED
C
C       FSRSET          SUBROUTINE TO SELECT THE APPROPIATE
C                       REFRACTIVE INDICES AT AN INTERFACE
C
C       GEOM            SUBROUTINE TO READ AND WRITE PIPE AND
C                       BUBBLE GEOMETRY
C
C       INFCHK          FUNCTION SUBPROGRAM TO CHECK FOR INFINTE
C                       LOOPING DUE TO NO SOLUTION TO QUADRATIC
C                       EQUATION
C
C       MAYFLP          FUNCTION SUBROUTINE TO DETERMINE IF RAY
C                       FLIPPING IS NECESSARY
C
C       OPTPRP          SUBROUTINE USED TO READ IN REFRACTIVE
C                       INDICES AND COMPUTE CRITICAL ANGLES
C
C       RAYNEW          SUBROUTINE TO CALCULATE A REFLECTED RAY'S
C                       EQUATION
C
C       RAYSET          SUBROUTINE TO POSITION LIGHT RAYS
C                       EQUALLY SPACED ALONG INPUT SURFACE
C
C       READTA          SUBROUTINE TO READ VARIOUS INPUT PARAMETERS
C
C       RESET           FUNCTION SUBPROGRAM TO RESET RAY SLOPE TO
C                       START RAY TRACING
C
C       SECT            SUBROUTINE TO CALCULATE TWO POSSIBLE
C                       X-COORDINATES FOR BUBBLE/RAY INTERSECTION
C
C       SETZRO          SUBROUTINE TO SET TALLY BINS EQUAL TO ZERO
C                       BEFORE RAY TRACING
C
C       SNELL           FUNCTION SUBPROGRAM TO CALCULATE ANGLE OF
C                       REFRACTION USING SNELL'S LAW
C
C       TANGNT          FUNCTION SUBROUTINE TO CALCULATE INTERFACE
C                       SLOPE AT POINT OF LIGHT RAY INTERSECTION
C
C       WRITE           SUBROUTINE TO WRITE OUT RESULTS
C
C       XLECT           SUBROUTINE TO SELECT CORRECT X-COORDINATE
C                       OF RAY/INTERFACE INTERSECTION
C
C       XSTART          SUBROUTINE TO CALCULATE STARTING
C                       X-COORDINATE OF INPUT LIGHT RAYS
C
C       ZEE             FUNCTION SUBPROGRAM TO CALCULATE VALUE OF
C                       Z-COORDINATE
C
C       FILMSUB         SUBROUTINE TO CALCULATE AND WRITE FILM
C                       EQUATIONS
```

```
181     C
182     C       PLSEC1,PLSEC2           SUBROUTINES TO CALCULATE RAY-FILM
183     C                               INTERSECTIONS
184     C
185     C       PLRNW1,PLRNW2           SUBROUTINES TO CALCULATE RAY EQUATIONS
186     C                               AFTER FILM INTERSECTIONS
187     C
188     C
189     C                               *** VARIABLES ***
190     C
191     C
192     C
193     C       ADDCLE                  TWICE THE DIFFERENCE BETWEEN THE ANGLE OF
194     C                               INCIDENCE AND 90.0 DEGREES
195     C
196     C       ANGLE                   ANGLE OF INCIDENCE FOR A LIGHT RAY ON A
197     C                               INTERFACE, IN RADIANS
198     C
199     C       BINS(NBIN,HFANGL)       ARRAY CONTAINING NUMBER OF RAYS STRIKING
200     C                               EACH BIN AS A FUNCTION OF INPUT LIGHT ANGLE
201     C
202     C       BINSZ                   SIZE OF A BIN, IN RADIANS
203     C
204     C       CCEF(4,NBOB)            X,Y,Z ELLIPSOID COEFFICIENTS AND RADIUS
205     C                               SQUARED
206     C
207     C       CCBI(3,NBOB)            X,Y,AND Z COORDINATES OF ELLIPSOID "CENTER"
208     C
209     C       CHBIS(NBIN)             HEADING FOR RAY BINS, +180 TO -180 DEGREES
210     C
211     C       CRITANG(LL)             ARRAY CONTAINING CRITICAL ANGLES BETWEEN
212     C                               VARIOUS INTERFACES
213     C
214     C       DEGNGL                  ANGLE OF INCIDENCE CONVERTED TO DEGREES
215     C
216     C       EP                      1.0 PER CENT OF A LIGHT RAY'S Y-INTERCEPT
217     C
218     C       DZES                    NUMBER OF Z PLANES AT WHICH RAY TRACES ARE
219     C                               PERFORMED
220     C
221     C       ES                      1.0 PER CENT OF A LIGHT RAY'S SLOPE
222     C
223     C       ESSCS1                  ABSOLUTE VALUE OF THE DIFFERENCE BETWEEN
224     C                               THE ORIGINAL RAY SLOPE AND THE REFLECTED
225     C                               RAY SLOPE
226     C
227     C       ESSCS2                  ABSOLUTE VALUE OF THE DIFFERENCE BETWEEN
228     C                               THE ORIGINAL RAY Y-INTERCEPT AND THE
229     C                               REFLECTED RAY Y-INTERCEPT
230     C
231     C       FACSLP                  INTERFACE SLOPE
232     C
233     C       HFANGL                  ANGLE OF INPUT LIGHT
234     C
235     C       IFLIP                   RAY FLIPPING PARAMETER
236     C                                  0 NO RAY FLIPPING REQUIRED
237     C                                  1 RAY FLIPPING NECESSARY
238     C
239     C       JGEOM                   GEOMETRY SELECTOR
240     C                                  0 CIRCULAR GEOMETRY
```

```
241     C                               1 SQUARE GEOMETRY
242     C
243     C       ILOPCT                  INFINITY CHECKING PARAMETER
244     C                                  0 NO INFINTE LOOP INDICATED
245     C                                  1 INFINITE LOOP INDICATED
246     C
247     C       ISECT                   INTERFACE INTERSECTED
248     C                                  0 BUBLE INTERSECTED
249     C                                  1 NO BUBBLE INTERSECTION
250     C                                  2 VALUE AT START OF SIMULATION
251     C
252     C       IPRINT                  PRINTING OPTION TRIP
253     C                                  0 PRINT ONLY RAY TRACING SUMMARY
254     C                                  1 DUMP OUT ALL INFORMATION PERTAINING
255     C                                    TO RAY PATHS
256     C
257     C       L                       NUMBER OF MATERIALS IN SYSTEM, USUALLY 2
258     C
259     C       NBIN                    NUMBER OF BINS AVAILABLE TO COLLECT LIGHT
260     C
261     C       NBLE                    BUBBLE COUNTER
262     C                                  1 PIPE
263     C                                  2 VOID INSIDE PIPE
264     C
265     C       NBOE                    NUMBER OF BUBBLES + 1
266     C
267     C       NH                      DO-LOOP PARAMETER USED FOR INPUT LIGHT
268     C                               ANGLES
269     C
270     C       NP                      DO-LOOP PARAMETER USED FOR COUNTER OF RAYS
271     C
272     C       NSTART                  LIGHT RAY POSITION INDICATOR
273     C                                  1 LIGHT RAY MOVING INTO TWO PHASE REGION
274     C                                  2 LIGHT RAY ENTERING VOID
275     C                                  3 LIGHT RAY LEAVING VOID
276     C
277     C
278     C       NZ                      DO-LOOP PARAMETER USED FOR STEPPING IN THE
279     C                               Z-DIRECTION
280     C
281     C       PHETA                   SINE OF ANGLE SNELL IN FUNCTION SNELL
282     C
283     C       PI                      ARITHMETIC CONSTANT, 3.14159
284     C
285     C       RAD                     RADIUS OF INPUT LIGHT REGION
286     C
287     C       RAYCPT                  Y-INTERCEPT IN LIGHT RAY EQUATION
288     C
289     C       RAYSLP                  SLOPE IN LIGHT RAY EQUATION
290     C
291     C       RFINDX(LL)              ARRAY CONTAINING REFRACTIVE INDICES
292     C
293     C       RYCBGN(NOPNTS)          ARRAY CONTAINING Y-COORDINATE OF STARTING
294     C                               LIGHT RAYS
295     C
296     C       SNELLD                  ANGLE SNELL (IN DEGREES)
297     C
298     C       SPACE                   DISTANCE BETWEEN LIGHT RAY STARTING
299     C                               POSITIONS
300     C
```

```
C      TESTHK                  TEST SECTION THICKNESS (SQUARE GEOMETRY
C                              ONLY)
C
C      TITLE                   ARRAY CONTAINING TITLE OF PARTICULAR RUN
C
C      WATFIK                  WATER FILM THICKNESS (SQUARE GEOMETRY ONLY)
C
C      X1                      FIRST POSSIBLE INTERSECTION X-COORDINATE
C
C      X2                      SECOND POSSIBLE INTERSECTION X-COORDINATE
C
C      XCOOR(NOPNTS)           X-COORDINATE OF LIGHT RAY STARTING POSITION
C
C      XXX                     Y VALUE OF LIGHT/RAY INTERFACE INTERSECTION
C
C
C      YCEPT(NOPNTS)           Y-INTERCEPT OF STARTING LIGHT RAYS
C      YYY                     Y VALUE OF LIGHT RAY/INTERFACE INTERSECTION
C
C      ZZZ                     VALUE OF Z-COORDINATE FOR A GIVEN POSITION
C
C      WATAIR                  PIPE CONTENTS OPTION
C                              0  AIR AND DROPLET
C                              1  WATER AND BUBBLE
C
C      WATANG                  ANGLE OF WATER FILM IN REGION OF INPUT
C                              LIGHT
C
C      FLMSHP                  SLOPE OF WATER FILM IN REGION OF INPUT
C                              LIGHT
C
C      MATRAP                  PARAMETER USED TO DETERMINE IF RAY IS
C                              TRAPPED INSIDE DROPLET
C
C      SHEILA                  RAY INTERSECTION OPTION
C                              0   DROPLET INTERSECTION
C                              5   PIPE INTERSECTION
C
C
C        ***** MAIN PROGRAM *****
C
C
C
C
      DIMENSION TITLE(20),COORD(3,10),COEF(4,10),SURFAC(4),FYCRGN(50),
     1REFINDX(3),MATYPE(10),MU(3),CRTANG(3),XCOOR(50),YCEPT(50)
C
      INTEGER DZES,RFANGL,BINS(41,10),CHRIS(41),SHEILA,WATAIR
C
      PI=3.14159
      L=2
C
C     SET UP PROBLEM
C
      CALL READATA(NBOE,WATHIK,TITLE,TESTHK,RAD,RFANGL,NOPNTS,IGEOM,
     1DZES,IPRINT,NBIN,WATAIR,WATANG,PI)
C
      CALL GEOM(NBOE,COORD,COEF,MATYPE)
C
      CALL CRTPRP(L,REFINDX,CRTANG,PI,IPRINT,MU)
```

```
      C
      C     OPTION FOR SQUARE TEST SECTION
      C
            IF (IGEOM.EQ.0) CALL EQUAT(WATBIR,TESTHR,SURFAC)
      C
      C     CALCULATE WATER FILM SLOPE
      C
            IF(WATAIR.EQ.0) CALL FLMSHP(WATANG,SURFAC,FLMSLP,B,RAD,PI,
     1IPRINT)
      C
      C     CALCULATE RAY STARTING POINTS, I.E. Y-COORDINATE
      C
            CALL RAYSRT(NCPNTS,RAD,RYCRGN,IPRINT)
      C
      C     CALCULATE APPROPRIATE X STARTING COORDINATES
      C
            CALL XSTART(XCCCR,NCPNTS,RYCRGN,COEF,CORD,NRUR,IPRINT,ZZZ,
     1TESTHR,WATRIR,IGEOM)
      C
      C     SET BINING PARAMETERS
      C
            BINSZ=BINZZ(COEF,NRUR,NRIN,PI,TESTHR,IGEOM)
      C
      C     DO LOOP FOR Z FRAMES
      C
            DO 900 NZ=1,DZES
      C
      C     FIX Z VALUE
      C
            ZZZ=ZEE(NZ,DZES,COEF,NRUR,IPRINT)
      C
      C     SET BINS EQUAL TO ZERO
      C
            CALL SETZRO(RINS,NRIN,RFANGL)
      C
      C     LOOP FOR ANGLES
      C
            DO 700 NR=1,RFANGL
      C
      C     CALCULATE Y INTERCEPT FOR THIS ANGLE'S STARTING RAYS
      C
            CALL CEPT(XCCCR,NOPNTS,RYCRGN,YCEPT,NR,IPRINT,PI)
      C
      C     LOOP FOR INDIVIDUAL LIGHT RAYS
      C
            DO 500 NP=1,NCENTS
      C
      C     RESET RAY SLOPE FOR NEXT RAY
      C
            RAYSLP=REESET(NP,PI)
      C
      C     SET Y INTERCEPT
      C
            RAYCPT=YCEPT(NP)
      C
      C     CALCULATE INTERSECTION WITH FILM
      C
            IF(WATAIR.EQ.0) CALL FLSEC1(FLMSLP,B,RAYSLP,RAYCPT,XXX,YYY,
     1WATANG,SURFAC,IPRINT)
      C
```

```
421      C      CALCULATE NEW BAY EQUATION
422      C
423            IF(WATAIR.EQ.0) CALL FLRNW1(L1,L2,MATYPE,WATANG,PIMSLP,BAYSLP,
424           1BAYCPT,IPRINT,ANGLE,RPINDX,PI,XXX,YYY,NBUB,L)
425      C
426      C      SET UP TRIP TO PROTECT AGAINST INFINITE LOOPS DUE TO POSSIBLE
427      C      NON CONVERGENCE OF SOLUTION TO QUADRATIC EQUATION
428      C
429            ILOPCT=0
430      C
431      C      SET INTERSECTION TRIP ONE HIGH TO START
432      C
433            ISECT=2
434      C
435      C      SET PARAMETER FOR BAY BEING TRAPPED IN DROPLET
436      C      SET BUBBLE BEING LOCKED FOR
437      C      SET PIPE-DROPLET OPTION FOR SQUARE GEOMETRY
438      C
439            MATRAP=0
440            NSTART=1
441            SHEILA=0
442         50 NBLE=2
443      C
444      C      CHECK FOR BAY TRAPPED IN DROPLET
445      C
446            MATRAP=MATRAP+1
447            IF(MATRAP.GT.4) GO TO 490
448            GO TO 200
449      C
450        100 NBLE=1
451      C
452      C      CHECK FOR INFINITE LOOP
453      C
454            ILOPCT=INFCHK(ILOPCT,NH,NF,NZ)
455      C
456      C      PROVIDE MEANS TO BREAK OUT OF INFINITE LOOP
457      C
458            IF (ILOPCT.GT.1) GO TO 500
459      C
460      C      SOLVE FOR SECOND FILM INTERSECTION AND NEW BAY
461      C
462            IF(WATAIR.EQ.0) CALL FLSEC2(SUBPAC,BAYSLP,BAYCPT,XXX,YYY,
463           1IPRINT)
464            IF(WATAIR.EQ.0) CALL FLRNW2(SUBPAC,ANGLE,BAYSLP,PI,IPRINT,
465           1MATYPE,RPINDX,XXX,YYY,BAYCPT,L,NBUB)
466      C
467      C      CHECK FOR SQUARE PIPE INTERSECTION
468      C
469            IF(IGEOM.EQ.0) SHEILA=5
470      C
471      C
472      C      SOLVE FOR LIGHT BAY/BUBBLE INTERSECTION
473      C
474        200 CALL SECT(NBUB,COEF,CORD,X1,X2,ZZZ,BAYCPT,BAYSLP,NBLE,IPRINT,
475           1TESTER,XXX,YYY,IGEOM,SHEILA)
476      C
477      C      SELECT CORRECT SOLUTION OF QUADRATIC EQUATION
478      C
479      C      NO QUADRATIC EQUATION IF AT SQUARE PIPE INTERSECTION
480      C
```

```
      IF(SHEILA.EQ.5) GO TO 210
C
      CALL XLECT(X1,X2,NP,NH,NBOB,CCEP,CCRD,RAYCPT,RAYSLP,YYY,
     1ISECT,XYX,NBLE,ZZZ,NSTART,IPRINT,IGEOM)
C
C     CHECK FOR INTERSECTION WITH PIPE
C
  210 CONTINUE
      IF (NBLE.EQ.1) GO TO 400
C
C     TRIP FOR NO INTERSECTION WITH BUBBLE
C
      IF (ISECT.EQ.1) GO TO 100
C
C     CALCULATE SLOPE OF FACE AT POINT: XXX, YYY
C
      FACSLP=TANGNT(CCRD,COEF,YYY,ZXX,NBOB,NBLE,IPRINT)
C
C     CALCULATE ANGLE OF INCIDENCE
C
      ANGLE=CIDNGL(FACSLP,RAYSLP,PI,IPRINT)
C
C     CHECK AGAINST CRITICAL ANGLE
C
      LL=1
      IF (NSTART.GT.1) LL=2
C
      IF (ANGLE.GT.CRIANG(LL)) GO TO 300
C
C     ********** ***************************************************
C     *****                                                    *****
C     *****              RAY REFRACTION OPTION                 *****
C     *****                                                    *****
C     ************************************************************
C
C     SELECT REFRACTIVE INDICES
C
      CALL REKSET(L1,L2,NSTART,MATYPE,NBOB)
C
C     CALCULATE ANGLE OF REFRACTION
C
      ANGLE=SNELL(L1,L2,ANGLE,RFINDX,L,PI,IPRINT)
C
C     RESET CHECK FOR PIPE INTERSECTION OPTION
C
      NSTART=NSTART+1
C
C     ************************************************************
C     *****                                                    *****
C     *****              RAY GENERATION SCHEME                 *****
C     *****                                                    *****
C     ************************************************************
C
C     SET FLIP OPTION
C
  300 IFLIP=0
C
C     CHECK IF RAY FLIPPING IS NECESSARY
C
      IFLIP=RAYFLP(RAYSLP,FACSLP,NSTART,NH,WATAIR,YYY)
```

```
C
C     GENERATE NEW RAY EQUATION
C
      CALL RAYNEW(ERROR1,RAYSLP,RAYCPT,ERROR2,PI,XXX,YYY,FACSLP,
     1ANGLE,IPRINT,NATAIR)
C
C     FLIPPING OPTION
C
      IF (IFLIP.GT.0) CALL FIPRAY(RAYSLP,RAYCPT,FACSLP,PI,ANGLE,IPRINT,
     1XXX,YYY)
C
C     RESET FLIP OPTION
C
      IFLIP=0
C
      IF (NSTART-2) 100,50,100
C
C     PUT COORDINATES IN APPROPRIATE BINS
C
C     MIGHT USE SQUARE BINNING
C
  400 IF(IGEOM.EQ.0) SHEILA=5
C
      CALL BINER(BINS,BINSZ,XXX,YYY,NBIN,HFANGL,NH,IPRINT,TESTHK,
     1SHEILA,PI)
      GO TO 500
C
C
  490 CONTINUE
      WRITE(6,495)
  495 FORMAT('0','RAY TRAPPED IN DROPLET')
  500 CONTINUE
  700 CONTINUE
C
C     WRITE OUT RESULTS FOR THIS DZ
C
      CALL WRIB(ZZZ,BINS,NBIN,HFANGI,PI,CHRIS,BINSZ,IGEOM)
C
  900 CONTINUE
C
      STOP
      END
C
C     **********************************************************************
C     **********************************************************************
C     *****                                                            *****
C     *****                                                            *****
C     *****                      SUBROUTINES                           *****
C     *****                                                            *****
C     *****                                                            *****
C     **********************************************************************
C     **********************************************************************
C
      SUBROUTINE READATA(NROB,WATHIK,TITLE,TESTHK,RAD,HFANGI,NOPNTS,
     1IGEOM,DZES,IPRINT,NBIN,NATAIR,NATANG,PI)
      DIMENSION TITLE(20)
      INTEGER DZES,HFANGL,NATAIR
C
C     READ/WRITE TITLE OF SIMULATION
C
```

```
      READ(5,100) TITLE
  100 FORMAT(20A4)
      WRITE(6,200) TITLE
  200 FORMAT('1',20A4)
C
C     READ IN GEOMETRY CODE
C     0 SQUARE
C     2 CIRCULAR
C
      READ(5,125) IGEOM,WATAIR,WATANG
  125 FORMAT(1X,I4,1X,I4,1X,F7.4)
C
      IF (IGEOM.EQ.0) GO TO 175
  150 WRITE(6,160)
  160 FORMAT('-','CIRCULAR GEOMETRY SELECTED',//)
      GO TO 290
C
  175 WRITE(6,180)
  180 FORMAT('-','SQUARE GEOMETRY SELECTED',//)
C
C     WRITE PIPE CONTENTS AIR-WATER OR WATER-AIR
C
      IF(WATAIR.EQ.0) GO TO 191
      WRITE(6,190)
  190 FORMAT(' ','PIPE FILLED WITH WATER AND BUBBLE',//)
      GO TO 195
C
  191 WRITE(6,192)
  192 FORMAT(' ','PIPE FILLED WITH AIR AND DROPLET',//)
      DWTANG=WATANG*180.0/PI
      WRITE(6,193) DWTANG
  193 FORMAT('0','WATER FILM ANGLE=',F8.4)
  195 CONTINUE
C
C     READ IN NUMBER OF BUBBLE/DROPLET SURFACES AND WATER FILM THICKNESS
C     ALSO READ IN TEST SECTION THICKNESS AND RADIUS OF INPUT/OUTPUT
C
  290 READ(5,300) NBUB,WATHIK,TESTHK,RAD,HFANGL,NCPNTS,DZES,NBIN
  300 FORMAT(1X,I4,3F10.5,4(1X,I4))
C
      READ(5,350) IPRINT
  350 FORMAT(1X,I4)
C
C     WRITE OUT DATA
C
      WRITE(6,400) NBUB,WATHIK,TESTHK,RAD,HFANGL,NCPNTS,DZES,NBIN
  400 FORMAT('0','NUMBER OF BUBBLES OR DROPLETS TO BE STUDIED',I4,/,
     1       ' ','WATER FILM THICKNESS',22X,F10.5,/,
     2       ' ','TEST SECTION THICKNESS',20X,F10.5,/,
     3       ' ','RADIUS OF INPUT/OUT REGIONS',15X,F10.5,/,
     4       ' ','HALF ANGLE OF IN COMING LIGHT',14X,I4,/,
     5       ' ','NUMBER OF LIGHT RAYS TO BE TRACED',10X,I4,/,
     6       ' ','NUMBER OF Z SLICES USED',20X,I4,/,
     7       ' ','SCATTERED LIGHT PINS',23X,I4,/)
C
      RETURN
      END
C
      SUBROUTINE GEOM(NBUB,COBD,COEF,MATYPE)
      DIMENSION COBD(3,NBUB),COEF(4,NBUB),MATYPE(NBUB)
```

```
      C
      C     READ IN CENTER COORDINATE AND RADIUS SQUARED,THEN WRITE OUT
      C
            WRITE(6,100)
        100 FORMAT('-','BUBBLE',5X,'X-COORDINATE',2X,'Y-COORDINATE',2X,'Z-COOR
           1DINATE',2X,'X-COEFFICIENT',2X,'Y-COEFFICIENT',
           22X,'Z-COEFFICIENT',2X,'RADIUS SQUARED',5X,'MATERIAL TYPE')
            DO 400 NN=1,NBUB
            READ(5,200) (CCRD(NP,NN),NP=1,3),(CCEF(NP,NN),NP=1,4),MATYPE(NN)
        200 FORMAT(7E10.3,1X,I4)
      C
            WRITE(6,300) NN,(CCRD(NP,NN),NP=1,3),(CCEF(NP,NN),NP=1,4),MATYPE(N
           1N)
        300 FORMAT('0',I4,3X,4(3X,1PE11.4),1X,3(4X,1PE11.4),11X,I4)
        400 CONTINUE
      C
            RETURN
            END
      C
            SUBROUTINE OPTPRP(L,RFINDX,CRTANG,PI,IPRINT,MU)
            REAL MU(L)
            DIMENSION RFINDX(L),CRTANG(L)
            EXTERNAL SNELL
      C
      C     READ/WRITE REFRACTIVE INDICES
      C
            READ(5,100) (RFINDX(LL),LL=1,L)
        100 FORMAT(3F10.7)
            WRITE(6,200)
        200 FORMAT('0','REFRACTIVE INDICES',//,
           1'0',1X,'MATERIAL',3X,'INDEX')
            DO 400 LL=1,L
            WRITE(6,300) LL,RFINDX(LL)
        300 FORMAT(' ',I5,5X,F8.5)
        400 CONTINUE
      C
      C     COMPUTE CRITICAL ANGLES
      C
              WRITE(6,500)
        500 FORMAT('0','MATERIALS',3X,'CRITICAL ANGLE')
            REFANG=PI/2.0
            DO 900 LL=1,L
      C
            IF(RFINDX(1).LT.RFINDX(2)) GO TO 750
      C
            L2=LL
            L1=1
      C
        700 CRTANG(LL)=SNELL(L2,L1,REFANG,RFINDX,L,PI,IPRINT)
      C
      C     CONVERT TO DEGREES  FOR PRINTING PURPOSES
      C
            CRTANG(LL)=CRTANG(LL)*180.0/PI
      C
      C     WRITE OUT CRITICAL ANGLES
      C
            WRITE(6,800) L2,L1,CRTANG(LL)
            GO TO 850
      C
        750 CONTINUE
```

```
      I1=II
      I2=1
C
      CRTANG(LL)=SNELL(I1,I2,REFANG,RFINDX,L,PI,IPBINT)
      CRTANG(LL)=CRTANG(LL)*180.0/PI
C
      WRITE(6,800) I1,I2,CRTANG(LL)
  800 FORMAT(' ',2X,I2,' TO',I2,6X,F7.4)
  850 CONTINUE
C
C     CONVERT BACK TO RADIANS
C
      CRTANG(LL)=CRTANG(LL)*PI/180.0
  900 CONTINUE
C
C     READ/WRITE LINEAR ATTENUATION COEFFICIENTS
C
      READ(5,1000) (MU(LL),LL=1,L)
 1000 FORMAT(3F10.7)
      WRITE(6,1100)
 1100 FORMAT('0','MATERIALS',5X,'LINEAR ATTENUATION COEFFICIENT')
      DO 1300 LL=1,L
      WRITE(6,1200) LL,MU(LL)
 1200 FORMAT(' ',3X,I3,17X,F10.7)
 1300 CONTINUE
      RETURN
      END
C
      FUNCTION SNELL(I1,I2,ANGLE,RFINDX,L,PI,IPBINT)
C
      DIMENSION RFINDX(L)
C
C     SNELL'S LAW TO YIELD REFRACTED RAY
C
      PHETA=((RFINDX(I2)/RFINDX(I1))*SIN(ANGLE))
C
C     CHECK TO MAKE SURE PHETA LESS THAN OR EQUAL TO 1
C
      IF (PHETA.GT.1.0) GO TO 200
C
      SNELL=ARSIN(PHETA)
C
      SNELLD=SNELL*180.0/PI
C
      IF (IPBINT.EQ.0) GO TO 400
C
      WRITE(6,100) SNELLD
  100 FORMAT(' ',' THETA ANGLE=  ',F10.4)
  400 RETURN
C
  200 WRITE(6,300)
  300 FORMAT(' ','*** ERROR IN RAY REFRACTION ***',///////)
C
      RETURN
      END
C
      SUBROUTINE EQUAT(MATHIK,TESTHK,SURFAC)
      DIMENSION SURFAC(4)
C
      SURFAC(1)=(TESTHK/2.0)
```

```
781           SURFAC(2)=-SURFAC(1)
782     C
783     C     CALCULATE LINE FOR WATER BOUNDRIES
784     C
785     C
786     C
787     C     WRITE TEST SECTION BOUNDRIES
788     C
789           WRITE(6,100) SURFAC(1),SURFAC(2)
790       100 FORMAT('0','TEST SECTION BOUNDRIES AT X= ',F6.3,' AND AT X= ',
791          1F6.3)
792     C
793           IF (WATHIK.EQ.0.0) RETURN
794     C
795           SURFAC(3)=SURFAC(1)-WATHIK
796           SURFAC(4)=-SURFAC(3)
797     C
798     C     WRITE OUT WATER FILM BOUNDRIES
799     C
800           WRITE(6,200) SURFAC(3),SURFAC(4)
801       200 FORMAT('0','FILM BOUNDRIES AT X= ',F6.3,' AND AT X= ',F6.3)
802           RETURN
803           END
804     C
805           SUBROUTINE RAYSRT(NORNTS,RAD,RYORGN,IPRINT)
806           DIMENSION RYORGN(NORNTS)
807     C
808     C     SPACE STARTING RAYS EQUAL OVER THE INPUT LIGHT PIPE
809     C
810           SPACE=(2.0*RAD)/(NORNTS+1)
811     C
812     C     SET FIRST POINT
813     C
814           RYORGN(1)=RAD-SPACE
815     C
816     C     LOOP TO FILL IN REST OF POINTS
817     C
818           DO 100 NP=2,NORNTS
819           RYORGN(NP)=RYORGN(NP-1)-SPACE
820       100 CONTINUE
821     C
822           IF (IPRINT.EQ.0) RETURN
823     C
824     C     WRITE OUT STARTING POSITIONS
825     C
826           WRITE(6,200)
827       200 FORMAT('0','RAY NO.',7X,'RAY ORIGIN')
828     C
829           DO 400 NP=1,NORNTS
830           WRITE(6,300) NP,RYORGN(NP)
831       300 FORMAT(' ',I4,8X,F10.4)
832       400 CONTINUE
833     C
834           RETURN
835           END
836     C
837           SUBROUTINE XSTART(XCOOR,NOPNTS,RYORGN,COEF,CORD,NRUR,IPRINT,ZZZ,
838          1IESTER,WATHIK,IGEOM)
839           DIMENSION XCOOR(NOPNTS),RYORGN(NOPNTS),COEF(4,NRUR),CORD(3,NRUR)
840     C
```

```
      INTEGER HFPNTS
C
      HFPNTS=NOPNTS/2
C
C     CHECK FOR SQUARE GEOMETRY
C
      IF(IGEOM.EQ.0) GO TO '25
C
      DO 100 NP='',HFPNTS
C
      XCOOR(NOPNTS-NP)=XCOOR(NP)
      ZETA=(COEF(4,1)-(((BYORGN(NP)-COORD(2,1))**2)/COEF(2,1))
C
      XCOOR(NP)=COORD(1,1)-SQRT(COEF(1,1)*ZETA)
      NP=NP-1
C
C
  100 CONTINUE
C
  125 DO 150 NP=1,HFPNTS
      GO TO 175
C
      XCOOR(NP)=-TESTHK/2
      NP=NP-1
      XCOOR(NOPNTS-NP)=XCOOR(NP)
  150 CONTINUE
  175 IF (IPRINT.EQ.0) RETURN
C
      DO 300 NP=1,NOPNTS
      WRITE(6,200) NP,XCOOR(NP)
  200 FORMAT(' ','NP=',I4,5X,'XCOOR=',F10.5)
  300 CONTINUE
      RETURN
      END
C
      FUNCTION ZEE(NZ,DZES,COEF,NBUB,IPRINT)
      DIMENSION COEF(4,NBUB)
      INTEGER DZES
C
C     CALCULATE Z VALUE AT THIS INTERVAL
C
      FDZES=FLOAT(DZES)
      FNZ=FLOAT(NZ)
C
      ACCRE=FDZES+1.0
      ABCCI=SQRT(COEF(4,2))
C
      ZET=(FNZ/ACCRE)*(2.0*ABCCI)
      ZEE=ABCCI-ZET
C
      IF (IPRINT.EQ.0) RETURN
      WRITE(6,100) NZ,ZEE
  100 FORMAT(' ','NZ=',I4,5X,'ZEE=',F10.5)
      RETURN
      END
C
      FUNCTION EINZZ(COEF,NBUB,NBIN,PI,TESTHK,IGEOM)
      DIMENSION COEF(4,NBUB)
C
C     CHECK FOR SQUARE GEOMETRY
```

```
      C
            IF(IGEOM.EQ.0) GO TO 50
      C
      C     CALCULATE BINING PARAMETERS, IN RADIANS FOR CIRCULAR GEOMETRY
      C
            BINZZ=2.0*PI/(FLOAT(NBIN))
      C
            WRITE(*,100) BINZZ
            RETURN
      C
      C     CALCULATE BINING PARAMETERS FOR SQUARE GEOMTRY
      C
         50 CONTINUE
            BINZZ=(TESTHK/2.0)/(FLOAT(NBIN/8))
      C
            WRITE(6,200) BINZZ
        100 FORMAT(' ','BIN SIZ =',F6.4,' RADIANS')
        200 FORMAT(' ','BIN SIZE=',F6.4)
      C
            RETURN
            END
      C
            FUNCTION REESET(NE,PI)
      C
            SLP=FLOAT(NH-1)*PI/180.0
            REESET=TAN(SLP)
      C
            RETURN
            END
      C
            FUNCTION INPCHK(ILOPCT,NH,NP,NZ)
      C
      C     INCREMENT COUNTER
      C
            INPCHK=ILOPCT+1
      C
            IF (INPCHK.GT.1) WRITE(6,100) NP,NH,NZ
        100 FORMAT('1','*** INFINITE LOOP AT NP=',I2,' NH=',I2,' NZ=',I2)
      C
            RETURN
            END
      C
            SUBROUTINE SETZRO(BINS,NBIN,HPANGL)
            INTEGER HPANGL
            INTEGER BINS(NBIN,HPANGL)
      C
      C     LOOP TO FILL WITH ZEROES
      C
            DO 100 NE=1,NBIN
            DO 100 NH=1,HPANGL
            BINS(NE,NH)=0
        100 CONTINUE
      C
            RETURN
            END
      C
            SUBROUTINE CEPT(XCOOR,NOPNTS,BYORGN,YCEPT,NH,IPRINT,PI)
      C
            DIMENSION XCOOR(NOPNTS),BYORGN(NOPNTS),YCEPT(NOPNTS)
            EXTERNAL REESET
```

```
      C
      C     SET BAY SLOPE
      C
            BAYSLP=RESET(NB,PI)
      C
            DO 200 NP=1,NCPNTS
            YCEPT(NP)=BYCRGN(NP)-(BAYSLP*XCOOR(NP))
      C
            IF (IPRINT.EQ.0) GO TO 200
      C
            WRITE(6,100) NP,YCEPT(NP)
        100 FORMAT(' ','NP=',I4,5X,'YCEPT=',F10.5)
        200 CONTINUE
      C
            RETURN
            END
      C
            SUBROUTINE SECT(NBUB,CCEF,CCBD,X1,X2,ZZZ,BAYCPT,BAYSLP,NBLE,
           1IPRINT,ISTHK,XXX,YYY,IGECM,SPEILA)
            DIMENSION CCEF(4,NBUB),CCBD(3,NBUB)
            INTEGER SPEILA
      C
      C     CHECK FOR SQUARE PIPE INTERSECTION
      C
            IF(SPEILA.EQ.5) GO TO 300
      C
      C     CALCULATE INITIAL SIMPLIFING VARIABLES
      C
            C=BAYCPT-CCBD(2,NBLE)
            Z=CCEF(4,NBLE)-(((ZZZ-CCBD(3,NBLE))**2)/CCEF(3,NBLE))
      C
      C     FORM EQUATION OF THE FORM AX**2+BX+C=0
      C
            AAA=CCEF(2,NBLE)+((CCEF(1,NBLE))*(BAYSLP**2))
      C
            BBB=2.0*((CCEF(1,NBLE)*BAYSLP*C)-(CCEF(2,NBLE)*CCBD(1,NBLE)))
      C
            ZAB=2*CCEF(1,NBLE)*CCEF(2,NBLE)
      C
            CCC=((CCBD(1,NBLE)**2)*CCEF(2,NBLE))+(CCEF(1,NBLE)*(C**2))-ZAB
      C
      C     FORM PARTS OF QUADRATIC FORMULA
      C
            BB2=BBB**2
            CA4=4.0*AAA*CCC
            AA2=2.0*AAA
      C
            B24AC=BB2-CA4
      C
      C     CHECK FOR ZERO OR NEGATIVE NUMBER UNDER SQUARE ROOT
      C
            IF (B24AC.LE.0.0) GO TO 200
      C
      C     TWO POSSIBLE X SOLUTIONS ARE
      C
            X1=(-BBB-SQRT(B24AC))/AA2
      C
            X2=(-BBB+SQRT(B24AC))/AA2
      C
            IF (IPRINT.EQ.0) RETURN
```

```
1021            WRITE(6,100) Q,Z,AAA,BBB,CCC,ZAB,X1,X2
1022          100 FORMAT(' ',T43,8(1PE10.3))
1023        C
1024            RETURN
1025        C
1026        C       CEICK FOR ZERO OR LESS UNDER SQUARE ROOT
1027        C       BY SETTING THESE VALUES VERY HIGH, NO INTERSECTION IS INDICATED
1028        C
1029          200 X1=1.0E04
1030            X2=X1
1031            RETURN
1032        C
1033          300 CONTINUE
1034            X1=TESTHK/2
1035            Y1=RAYSLP*X1+RAYCPT
1036            IF(ABS(Y1).LT.X1) GO TO 320
1037            GO TO 340
1038          320 CONTINUE
1039            XXX=X1
1040            YYY=Y1
1041            GO TO 390
1042          340 IF(Y1.LT.0.0) GO TO 360
1043            GO TO 380
1044          360 CONTINUE
1045            YYY=-X1
1046            XXX=(YYY-RAYCPT)/RAYSLP
1047            GO TO 390
1048          380 CONTINUE
1049            YYY=X1
1050            XXX=(YYY-RAYCPT)/RAYSLP
1051          390 CONTINUE
1052            IF(IPRINT.EQ.0) RETURN
1053        C
1054            WRITE(6,400) XXX,YYY
1055          400 FORMAT(' ','PIPE INTERSECTION AT  XXX=',F6.3,' AND YYY=',F6.3)
1056            RETURN
1057        C
1058            END
1059            SUBROUTINE XLECT(X1,X2,NP,NB,NBUB,CCEF,CCED,RAYCPT,RAYSLP,YYY,
1060           1ISECT,XXX,NBLE,ZZZ,NSTART,IPRINT,IGECM)
1061        C
1062            DIMENSION CORD(3,NBUB),COEF(4,NBUB)
1063        C
1064            IF (IPRINT.EQ.0) GO TO 200
1065            WRITE(6,100) NSTART
1066          100 FORMAT(' ','NSTART=',I2)
1067        C
1068        C       SELECTOR ONCE INSIDE BUBBLE
1069        C
1070          200 IF (NSTART-2) 400,700,400
1071        C
1072        C       SELECTOR FOR RAYS THAT MISS BUBBLE
1073        C
1074          400 IF (NBLE.EQ.1) GO TO 700
1075        C
1076        C       CHECK FIRST POINT
1077        C
1078            XXX=X1
1079          600 YYY=(RAYSLP*XXX)+RAYCPT
1080        C
```

```
      C     COMBINE INTO GENERAL ELLIPSOID EQUATION
      C
            X22=((XXX-CORD(1,NELE))**2)/COEF(1,NELE)
            Y22=((YYY-CORD(2,NELE))**2)/COEF(2,NELE)
            Z22=((ZZZ-CORD(3,NELE))**2)/COEF(3,NELE)
            XX1=X22+Y22+Z22-COEF(4,NELE)
      C
            XCHECK=ABS(XX1)
            IF (XCHECK.LT.0.001) GO TO 9100
            IF (XXX.EQ.X2) GO TO 800
      C
      C     CHECK SECOND X COORDINATE
      C
        700 XXX=X2
            GO TO 600
      C
        800 IF(IPRINT.EQ.0) GO TO 1000
            WRITE(6,900) NP
        900 FORMAT('+',T15,1X,'*** NO INTERSECTION FOR RAY',I4,' ***')
      C
       1000 ISECT=1
            RETURN
      C
      C     SET FLAG TO INDICATE INTERSECTION
      C
       1100 ISECT=0
            IF (IPRINT.EQ.0) RETURN
            WRITE(6,1200) XXX,YYY
       1200 FORMAT('+',T30,'XXX=',F10.5,2X,'YYY=',F10.5)
      C
            RETURN
            END
      C
            FUNCTION TANGNT(CORD,COEF,YYY,XXX,NRUB,NELE,IPRINT)
            DIMENSION COEF(4,NRUB),CORD(3,NRUB)
      C
      C     CALCULATE TANGENT TO ELIPSOID AT POINT (XXX,YYY)
      C
            ALPHA=COEF(2,NELE)*(XXX-CORD(1,NELE))
      C
            BETA=COEF(1,NELE)*(YYY-CORD(2,NELE))
      C
            TANGNT=(-ALPHA)/BETA
      C
            IF (IPRINT.EQ.0) RETURN
      C
            WRITE(6,100) TANGNT
        100 FORMAT(' ','FACE SLOPE=',1PE12.5)
            RETURN
            END
      C
            FUNCTION CIDNCI(FACSLP,RAYSLP,PI,IPRINT)
      C
      C     COMPUTE ANGLE OF INCIDENCE GIVEN RAY AND FACE SLOPE
      C
            BETA=ATAN(RAYSLP)
            THETA=ATAN(FACSLP)
      C
      C     EQUATION DEVELOPED FROM 2-D OPTICS
      C
```

```
      200 CIDNGI=ABS((PI/2.0)-ABS(-BETA+THETA))
C
C     CONVERT ANGLE TO DEGREES FOR PRINTING PURPOSES
C
      DEGNGI=CIDNGI*180.0/PI
C
C
C     WRITE OUT ANGLE OF INCIDENCE
C
      IF (IPRINT.EQ.0) GO TO 500
C
      300 WRITE(6,400) DEGNGI
      400 FORMAT('+',T40,'THE ANGLE OF INCIDENCE IS: ',F5.2,' DEGREES')
      500 RETURN
          END
C
          SUBROUTINE PARSET(L1,L2,NSTART,MATYPE,NPOB)
          DIMENSION MATYPE(NPOB)
C
          IF (NSTART.NE.1) GO TO 100
C
C     WATER TO BUBBLE CASE
C
          L1=MATYPE(2)
          L2=MATYPE(1)
          RETURN
C
C     BUBBLE TO WATER CASE
C
      100 L1=MATYPE(1)
          L2=MATYPE(2)
          RETURN
          END
C
          SUBROUTINE BAYNEW(ERROR1,BAYSLP,BAYCPT,ERROR2,PI,XXX,YYY
         1,SLOPE,ANGLE,IPRINT,WATAIR)
          INTEGER WATAIR
C
C     SET ERROR MARGINS
C
          EB=ABS(BAYSLP)*0.01
C
          EP=ABS(BAYCPT)*0.01
C
C     SET DUMMY VARIABLES
C
          SLOPE1=P YSLP
          YCEPT1=BAYCPT
C
C     CHECK FOR HORIZONTAL LIGHT RAYS
C
          IF (ABS(BAYSLP).LT.0.00001) GO TO 225
C
C     COMPUTE REFLECTED RAY EQUATION
C
C     CHECK FOR HORIZONTAL FACES
C
          ZZCHCK=SLOPE/BAYSLP
          IF (ZZCHCK) 225,300,225
C
```

```
      C     NOT HORIZIONTAL FACE
      C
  200 RAYANG=ANGLE+ATAN(-1.0/SLOPE)
      GO TO 500
      C
  225 CONTINUE
      C
      C     CHECK FOR AIR-DROPLET, WATER-BUBBLE IN PIPE
      C
      IF(WATAIR.EQ.0) GO TO 250
      GO TO 200
  250 FACANG=ATAN(-1.0/SLOPE)
      IF(FACANG) 200,275,275
  275 RAYANG=FACANG-ANGLE
      GO TO 500
      C
      C     HORIZIONTAL FACE
      C
  300 RAYSLP=-RAYSLP
      GO TO 600
      C
      C     COMPUTE POSSIBLE RAY SLOPE AND INTERCEPT
      C
  500 RAYSLP=TAN(RAYANG)
  600 RAYCPT=YYY-(RAYSLP*XXX)
      C
      C     CHECK RAY TO AVOID REGENERATING  INCIDENT RAY EQUATION
      C
      ERROR1=ABS(RAYSLP-SLOPE1)
      ERROR2=ABS(YCEPT1-RAYCPT)
      IF (ERROR1.LT.EP.AND.ERROR2.LT.EP) GO TO 700
      GO TO 800
      C
      C     OPTION TO FLIP RAY IF SAME EQUATION IS GENERATED
      C
  700 ADDGLE=2.0*((PI/2.0)-ANGLE)
      RAYSLP=TAN(ATAN(RAYSLP)+ADDGLE)
      RAYCPT=YYY-(RAYSLP*XXX)
      C
      C     WRITE OUT  SLOPE AND INTERCEPT
      C
  800 IF (IPRINT.EQ.0) GO TO 900
      C
      WRITE(6,100) RAYSLP,RAYCPT,XXX
  100 FORMAT(' ','NEW RAY SLOPE=',1PE12.4,'  NEW RAY INTERCEPT=',
     1E12.4,'  XXX=',1PE12.4)
  900 RETURN
      END
      C
      FUNCTION MAYFLP(RAYSLP,FACSLP,NSTART,NH,WATAIR,YYY)
      INTEGER WATAIR
      C
      C     CALCULATE NORMAL
      C
      ORMAL=-1.0/FACSLP
      C
      C     SET INITIAL TRIP
      C
      MAYFIP=0
      C
```

```
      C     CHECK PIPE CONTENTS OPTION
      C
            IF(DATAIR.EQ.0) GO TO 400
      C
      C     ROUTE ACCORDING TO INTERSECTED FACE
      C
            IF (NSTART-2) 100,200,300
      C
      C     SET TRIP FOR SCATTERED LIGHT RAYS
      C
  100 IF (NR.NE.1) RETURN
      C
            IF (FACSLP.GT.0.0) MAYFLP=1
            RETURN
      C
      C     FIRST REFRACTION COMPONENT
      C
  200 IF (FACSLP.GT.0.0) RETURN
      C
            IF (ABS(OBMAL).GT.ABS(RAYSLP)) MAYFLP=1
      C
            RETURN
      C
      C     SECOND REFRACTION COMPONENT
      C
  300 IF (RAYSLP.GT.0.0) MAYFLP=1
      C
            IF (ABS(OBMAL).LT.ABS(RAYSLP)) MAYFLP=1
      C
  400 CONTINUE
            IF(NSTART-2) 700,500,600
  500 CONTINUE
      C
      C     FIRST RAY REFRACTION
      C
            IF(RAYSLP.LT.0.0) GO TO 550
            IF(FACSLP.GT.0.0) RETURN
            IF(RAYSLP.GT.OBMAL) MAYFLP=1
            RETURN
  550 CONTINUE
            IF(FACSLP.LT.0.0) RETURN
            IF(RAYSLP.LT.OBMAL) MAYFLP=1
            RETURN
      C
  600 CONTINUE
      C
      C     SECOND RAY REFRACTION
      C
            IF(RAYSLP.LT.0.0) GO TO 650
            IF(FACSLP.GT.0.0) RETURN
            IF(RAYSLP.GT.OBMAL) MAYFLP=1
            RETURN
  650 CONTINUE
            IF(FACSLP.LT.0.0) RETURN
            IF(RAYSLP.LT.OBMAL) MAYFLP=1
      C
  700 CONTINUE
      C
            RETURN
            END
```

```
      C
            SUBROUTINE PIPBNY(RAYSLP,RAYCPT,FACSLP,PI,ANGLE,IPBINT,XXX,YYY)
      C
      C     ADD ON NECESSARY ANGLE SWING
      C
            ADDGLE=2.0*((PI/2.0)-ANGLE)
      C
      C     RECALCULATE RAY EQUATION
      C
            RAYSLP=TAN(ATAN(RAYSLP)+ADDGLE)
            RAYCPT=YYY-(RAYSLP*XXX)
      C
      C
            IF (IPBINT.EQ.0) GO TO 300
      C
            WRITE(6,200) RAYSLP,RAYCPT,XXX
        200 FORMAT(' ','PLIP RAY SLOPE=',1PE12.4,'    PLIP RAY In...',
           1'1PE12.4,'  XXX=',1PE12.4)
        300 RETURN
            END
      C
            SUBROUTINE BINNER(BINS,BINSZ,XXX,YYY,NBIN,HFANGL,NH,IPBINT,
           1TESTBK,SHEILA,PI)
      C
      C
            REAL PI
            INTEGER HFANGL,SHEILA
            INTEGER BINS(NBIN,HFANGL)
      C
      C     CHECK FOR SQUARE PIPE BINNING
      C
            IF(SHEILA.EQ.5) GO TO 250
      C
            BBIE=ATAN((ABS(YYY))/(ABS(XXX)))
            NBIB=(IPIX(BBIB/BINSZ))+1
      C
      C     KEEP ORIGINAL BIN
      C
            NKEEP=NBIB
      C
      C     CHECK FOR POSITIVE XXX
      C
            IF (XXX.GE.0.0) GO TO 100
      C
      C     CHECK FOR POSITIVE YYY
      C
            IF (YYY.LT.0.0) NBIB=NBIN-NBIB+1
      C
            GO TO 700
      C
        100 NBIB=(NBIN/2)-NBIB+1
      C
            IF (YYY.LT.0.0) NBIB=NBIB+((2*NKEEP)-1)
            GO TO 700
      C
        250 CONTINUE
            BBIB=ATAN((ABS(YYY))/(ABS(XXX)))
            TCBIT=45.0*PI/180.0
      C
      C     CHECK WHICH SURFACE OF SQUARE PIPE IS INTERSECTED
```

```
1381      C
1382            IF(FFIF-TCRIT) 300,300,350
1383          300 N=IFIX(ABS(YYY)/BINSZ)+1
1384            GO TO 400
1385          350 N=NBIN/4-IFIX(ABS(XXX)/BINSZ)
1386          400 IF(YYY.LT.0.0) GO TO 550
1387            IF(XXX.LT.0.0) GO TO 450
1388            GO TO 500
1389          450 NBIB=N
1390            GO TO 700
1391          500 NBIB=(NBIN/2+1)-N
1392            GO TO 700
1393          550 IF(XXX.LT.0.0) GO TO 600
1394            GO TO 650
1395          600 NBIB=NBIN-N+1
1396            GO TO 700
1397          650 NBIB=NBIN/2+N
1398      C
1399          700 IF(IFBINT.EQ.0) GO TO 900
1400      C
1401            WRITE(6,800) NBIB,NN
1402          800 FORMAT('+',T90,'NBIB=',I3,1X,'NN=',I3)
1403      C
1404          900 BINS(NBIB,NN)=BINS(NBIB,NN)+1
1405      C
1406            RETURN
1407            END
1408      C
1409            SUBROUTINE WBIB(ZZZ,BINS,NBIN,HFANGI,PI,CHBIS,BINSZ,IGEOM)
1410            INTEGER HFANGI
1411            INTEGER BINS(NBIN,HFANGI)
1412            INTEGER CHBIS(41),IPTTAL(10),IANGTI(41)
1413      C
1414            DATA BAR/4H----/
1415      C
1416            NTERM=NBIN+1
1417      C
1418      C     TEST FOR SQUARE GEOMETRY
1419      C
1420            IF(IGEOM.EQ.0) GO TO 60
1421      C
1422            CHBIS(1)=180
1423      C
1424            NBEILE=(360/NBIN)
1425      C
1426            DO 50 NB=2,NTERM
1427            CHBIS(NB)=CHBIS(NB-1)-NBEILE
1428         50 CONTINUE
1429            GO TO 90
1430         60 CONTINUE
1431            CHBIS(1)=1
1432            DO 75 NB=2,NTERM
1433            CHBIS(NB)=CHBIS(NB-1)+1
1434         75 CONTINUE
1435         90 CONTINUE
1436      C
1437      C     CHECK     SQUARE GEOMETRY
1438      C
1439            IF(IGEOM.EQ.0)    TO 110
1440            WRITE(6,100) ZZZ
```

```
      100 FORMAT('1','LIGHT BINING SUMMARY SHEET FOR  Z=',F7.4,/,
     1       '0',55X,'ANGLE AROUND TUBE, DEGREES')
          GO TO 140
      110 CONTINUE
          WRITE(6,130) ZZZ
      130 FORMAT('1','LIGHT BINING SUMMARY SHEET FOR  Z=',F7.4,/,
     1       '0',55X,'BIN NUMBER AROUND PIPE')
C
      140 CONTINUE
          WRITE(6,150) (CHRIS(NB),NB=1,NTEMP,2)
      150 FORMAT('0','LIGHT',1X,I4,20(2X,I4),/,' ','ANGLE')
C
          DO 300 NH=1,NFANGL
          NHP=NH-1
C
          WRITE(6,200) NHP,(BINS(NB,NH),NB=1,NBIN)
      200 FORMAT('-',I3,5X,41(1X,I2))
C
      300 CONTINUE
C
C     SUM UP TOTAL NUMBER OF POINTS FOR EACH ANGLE
C
          DO 350 NH=1,NFANGL
          IPTTAL(NH)=0
      350 CONTINUE
C
          DO 400 NB=1,NBIN
          IANGTL(NB)=0
          DO 400 NI=1,NFANGL
          IPTTAL(NI)=IPTTAL(NI)+BINS(NB,NI)
      400 CONTINUE
C
          DO 500 NH=1,NFANGL
          DO 500 NB=1,NBIN
          IANGTL(NB)=IANGTL(NB)+BINS(NB,NH)
      500 CONTINUE
C
C     DRAW IN LINE
C
          WRITE(6,550) (BAR,NB=1,32)
      550 FORMAT(' ',1X,32A4)
C
          WRITE(6,600) (IANGTL(NB),NB=1,NBIN)
      600 FORMAT('0','TOTALS',2X,40(1X,I2))
C
          DO 800 NH=1,NFANGL
          NQ=NH-1
          WRITE(6,700) NQ,IPTTAL(NH)
      700 FORMAT('0','TOTAL POINTS FOR ',I2,' DEGREES LIGHT ANGLE= ',I2)
      800 CONTINUE
          RETURN
          END
C
          SUBROUTINE FLMSRP(WATANG,SUBFAC,FLMSLP,E,BAD,PI,IPRINT)
          DIMENSION SUBFAC(4)
C
   97     IF(ABS(WATANG).LT.0.00001) GO TO 200
C
          GAMMA=PI/2.0-ABS(WATANG)
          IF(WATANG.GT.0.0) GO TO 100
```

```
      FLMSLP=TAN(GAMMA)
      GO TO 300
  100 CONTINUE
      FLMSLP=-TAN(GAMMA)
      GO TO 300
  200 CONTINUE
      IF(IPRINT.EQ.0) RETURN
      WRITE(6,250)
  250 FORMAT(' ','WATER FILM SLOPE IS INFINITE,NORMAL TO FILM IS 0')
      RETURN
  300 CONTINUE
      IF(WATANG.GT.0.0) GO TO 400
      B=-BAC-FLMSLP*SUBFAC(4)
      GO TO 500
  400 CONTINUE
      B=BAC-FLMSLP*SUBFAC(4)
  500 CONTINUE
      IF(IPRINT.EQ.0) RETURN
      WRITE(6,600) FLMSLP,B
  600 FORMAT(' ','FILM SLOPE=',1PE12.4,'   Y-INTERCEPT OF FILM=',
     1 1PE12.4)
      RETURN
      END
C
      SUBROUTINE FLSEC1(FLMSLP,B,BAYSLP,BAYCPT,XXX,YYY,WATANG,
     1SUBFAC,IPRINT)
      DIMENSION SUBFAC(4)
C
      IF(WATANG.LT.0.00001) GO TO 100
      XXX=(B-BAYCPT)/(BAYSLP-FLMSLP)
      YYY=BAYSLP*XXX+BAYCPT
      GO TO 200
  100 CONTINUE
      XXX=SUBFAC(4)
      YYY=BAYSLP*XXX+BAYCPT
  200 CONTINUE
      IF(IPRINT.EQ.0) RETURN
      WRITE(6,300) XXX,YYY
  300 FORMAT('0','FILM INTERSECTION AT XXX=',F8.4,'   AND YYY=',
     1F8.4)
      RETURN
      END
C
      SUBROUTINE FLSNS1(L1,L2,MATYPE,WATANG,FLMSLP,BAYSLP,BAYCPT,
     1IPRINT,ANGLE,BFINDX,PI,XXX,YYY,NBUB,L)
      DIMENSION MATYPE(NBUB),BFINDX(L)
C
      L1=MATYPE(1)
      L2=MATYPE(2)
      IF(ABS(WATANG).LT.0.00001) GO TO 100
      ANGLE=ABS(ATAN(-1./FLMSLP)-ATAN(BAYSLP))
      FLMANG=ATAN(-1.0/FLMSLP)
      GO TO 200
  100 CONTINUE
      ANGLE=ATAN(BAYSLP)
      FLMANG=0.0
  200 CONTINUE
      IF(IPRINT.EQ.0) GO TO 300
      DANGLE=ANGLE*180.0/PI
      WRITE(6,250) DANGLE
```

```
      250 FORMAT(' ','ANGLE OF INCIDENCE=',F8.4)
      300 CONTINUE
          ANGLE=SNELL(L1,L2,ANGLE,RFINDX,L,PI,IPRINT)
C
          RAYANG=ATAN(RAYSLP)
C
          IF(RAYANG.GT.PIPANG) GO TO 350
          RAYANG=PLMANG-ANGLE
          GO TO 400
      350 CONTINUE
          RAYANG=PLMANG+ANGLE
      400 CONTINUE
C
          RAYSLP=TAN(RAYANG)
          RAYCPT=YYY-RAYSLP*XXX
C
          IF(IPRINT.EQ.0) RETURN
          WRITE(6,450) RAYSLP,RAYCPT,XXX
      450 FORMAT(' ','NEW RAY SLOPE=',1PE12.4,'   NEW RAY INTERCEPT=',
     1E12.4,'   XXX=',1PE12.4)
C
          RETURN
          END
C
          SUBROUTINE PLSEC2(SURFAC,RAYSLP,RAYCPT,XXX,YYY,IPRINT)
          DIMENSION SURFAC(4)
C
          XX1=SURFAC(3)
          YY1=RAYSLP*XX1+RAYCPT
C
          IF(ABS(YY1).GT.XX1) GO TO 100
          XXX=XX1
          YYY=YY1
          GO TO 300
C
      100 CONTINUE
          IF(YY1.GT.0.0) GO TO 200
          YYY=-XX1
          XXX=(YYY-RAYCPT)/RAYSLP
          GO TO 300
C
      200 CONTINUE
          YYY=XX1
          XXX=(YYY-RAYCPT)/RAYSLP
C
      300 CONTINUE
          IF(IPRINT.EQ.0) RETURN
          WRITE(6,400) XXX,YYY
      400 FORMAT('0','SECOND FILM INTERSECTION AT XXX=',F8.4,'  AND YYY=
     1',F8.4)
C
          RETURN
          END
C
          SUBROUTINE PLANE2(SURFAC,ANGLE,RAYSLP,PI,IPRINT,MATYPE,RFINDX,
     1XXX,YYY,RAYCPT,L,NBOB)
          DIMENSION SURFAC(4),RFINDX(L),MATYPE(NBOB)
C
          IF(ABS(YYY).EQ.SURFAC(3)) GO TO 100
          ANGLE=ABS(ATAN(RAYSLP))
```

```
1621            GO TO 200
1622      C
1623        100 CONTINUE
1624            ANGLE=ABS(PI/2.0-ABS(ATAN(RAYSLP)))
1625        200 CONTINUE
1626            IF(IPRINT.EQ.0) GO TO 400
1627            DANGLE=ANGLE*180.0/PI
1628            WRITE(6,300) DANGLE
1629        300 FORMAT(' ','ANGLE OF INCIDENCE=',F8.4)
1630      C
1631        400 CONTINUE
1632            L1=RAYPE(2)
1633            L2=RAYPE(1)
1634            ANGLE=SNELL(L1,L2,ANGLE,REINDX,L,PI,IPRINT)
1635      C
1636            IF(ABS(YYY).LT.SURFAC(3)) GO TO 600
1637            IF(YYY.LT.0.0) GO TO 500
1638            RAYANG=PI/2.0-ANGLE
1639            GO TO 800
1640        500 CONTINUE
1641            RAYANG=ANGLE-PI/2.0
1642            GO TO 800
1643        600 CONTINUE
1644            IF(RAYSLP.LT.0.0) GO TO 700
1645            RAYANG=ANGLE
1646            GO TO 800
1647        700 CONTINUE
1648            RAYANG=-ANGLE
1649      C
1650        800 CONTINUE
1651            RAYSLP=TAN(RAYANG)
1652            RAYCPT=YYY-RAYSLP*XXX
1653      C
1654            IF(IPRINT.EQ.0) RETURN
1655            WRITE(6,900) RAYSLP,RAYCPT,XXX
1656        900 FORMAT(' ','NEW RAY SLOPE=',1PE12.4,'    NEW RAY INTERCEPT=',
1657           1 1PE12.4,'    XXX=',1PE12.4)
1658            RETURN
1659            END
1660      C
1661      /DATA
END OF FILE
```

ADVANCED TWO PHASE FLOW DEMONSTRATION CASE

CIRCULAR GEOMETRY SELECTED

NUMBER OF BUBBLES OR DROPLETS TO BE STUDIED	2
WATER FILM THICKNESS	0.0
TEST SECTION WIDTH	0.0
RADIUS OF INPUT/OUT REGIONS	0.06250
HALF ANGLE OF IN COMING LIGHT	10
NUMBER OF LIGHT RAYS TO BE TRACED	50
NUMBER OF Z SLICES USED	5
SCATTERED LIGHT BINS	40

BUBBLE	X-COORDINATE	Y-COORDINATE	Z-COORDINATE	X-COEFFICIENT	Y-COEFFICIENT	Z-COEFFICIENT	RADIUS SQUARED	MATERIAL TYPE
1	0.0	0.0	0.0	1.0000E+00	1.0000E+00	1.0000E+30	2.5000E-01	1
2	0.0	0.0	0.0	1.0000E+00	1.0000E+00	1.0000E+00	3.0000E-03	2

REFRACTIVE INDICES

MATERIAL	INDEX
1	1.33330
2	1.00000

MATERIALS	CRITICAL ANGLE
2 TO 1	48.5921
2 TO 2	90.0000

MATERIALS	LINEAR ATTENUATION COEFFICIENT
1	0.0
2	0.0

BIN SIZE=0.1571 RADIANS

LIGHT BINING SUMMARY SHEET FOR Z= 0.0

LIGHT ANGLE	ANGLE AROUND TUBE, DEGREES																																		
	180	162	144	126	108	90	72	54	36	18	0	-18	-36	-54	-72	-90	-108	-126	-144	-162	-180														
0	0	0	0	0	0	0	0	0	1	1	2	0	2	3	2	3	4	7	7	4	3	2	3	2	0	2	1	1	0	0	0	0	0	0	0	0	0
1	0	0	0	0	0	0	0	0	1	1	1	2	2	1	3	4	4	10	4	4	3	2	1	2	2	1	1	1	0	0	0	0	0	0	0	0	0
2	0	0	0	0	0	0	0	0	0	1	2	1	1	2	2	2	4	11	6	5	4	3	2	1	1	0	1	1	0	0	0	0	0	0	0	0	0
3	0	0	0	0	0	0	0	0	0	1	1	2	1	2	2	2	5	17	3	4	5	3	2	0	0	0	0	0	0	0	0	0	0	0	0	0	0
4	0	0	0	0	0	0	0	0	0	2	1	1	1	2	3	2	4	21	3	2	8	2	0	0	0	0	0	0	0	0	0	0	0	0	0	0	0
5	0	0	0	0	0	0	0	0	0	1	1	2	2	2	2	2	5	24	3	2	2	2	0	0	0	0	0	0	0	0	0	0	0	0	0	0	0
6	0	0	0	0	0	0	0	0	0	1	1	1	1	2	1	3	3	8	24	2	2	1	0	0	0	0	0	0	0	0	0	0	0	0	0	0	0
7	0	0	0	0	0	0	0	0	0	0	2	2	0	2	2	2	3	15	21	1	0	0	0	0	0	0	0	0	0	0	0	0	0	0	0	0	0
8	0	0	0	0	0	0	0	0	0	1	1	1	2	2	1	3	3	22	14	0	0	0	0	0	0	0	0	0	0	0	0	0	0	0	0	0	0
9	0	0	0	0	0	0	0	0	0	1	1	2	0	2	3	2	1	26	10	0	0	0	0	0	0	0	0	0	0	0	0	0	0	0	0	0	0
TOTALS	0	0	0	0	0	0	0	0	0	3	12	13	12	15	19	23	25	96	**	35	26	26	16	8	5	5	2	4	1	2	0	0	0	0	0	0	0	0

TOTAL POINTS FOR 0 DEGREES LIGHT ANGLE= 50

TOTAL POINTS FOR 1 DEGREES LIGHT ANGLE= 50

TOTAL POINTS FOR 2 DEGREES LIGHT ANGLE= 50

TOTAL POINTS FOR 3 DEGREES LIGHT ANGLE= 50

TOTAL POINTS FOR 4 DEGREES LIGHT ANGLE= 50

TOTAL POINTS FOR 5 DEGREES LIGHT ANGLE= 50

TOTAL POINTS FOR 6 DEGREES LIGHT ANGLE= 50

TOTAL POINTS FOR 7 DEGREES LIGHT ANGLE= 50

TOTAL POINTS FOR 8 DEGREES LIGHT ANGLE= 50

TOTAL POINTS FOR 9 DEGREES LIGHT ANGLE= 50

APPENDIX A.8

LOCAL FRACTION PROBE CALIBRATION TECHNIQUE

Calibration of local impedance probes is performed by measuring the chordal void fraction with an x-ray machine while simultaneously measuring the point void fraction along the same chord. The point measurements can be integrated using Simpson's Rule and compared to x-ray measured chordal void fraction. The threshold setting can then be adjusted as necessary to obtain agreement.

The following procedures outline the techniques used to calibrate the RF probe. All calibration was performed along the diameter of the circular test section.

Prior to X-ray Operation

1) Manually move local probe to 0.150 in.
2) Plug in local probe driver box and immediately press the "reset" button.
3) Move probe to 0.100 in., using stepping motor and driver box.
4) Employ regular x-ray start-up procedures, Appendix A.3, and direct x-ray beam along test section's diameter.

Actual Calibration

1) Set "zero" on RF circuitry box to 2.00 volts for test section containing all water.
2) Set "span" on RF circuitry box to 10.0 volts for test section containing all air.
3) Repeat steps 1 and 2 until the correct values are achieved. It may be necessary to move the probe from the wall to remove residual water on probe tip.
4) Select appropriate signal thresholding and employ in circuit. Set level thresholding at 4.0 volts or derivative thresholding at 0.24 volts.
5) Set up two-phase flow conditions
6) Take x-ray measurement of chordal void fraction.
7) Take one minute readings of local void fraction at each point along the chord. Use the stepping motor system to move the probe accurately.
8) Retake x-ray measurement of chordal void fraction to assure accuracy
9) Repeat steps 5 through 8 for all two-phase cases studied.

APPENDIX A.9

DERIVATION OF THE WEIGHTING FACTORS USED TO CALCULATE AREA AVERAGED VOID FRACTION FROM CHORDAL VOID FRACTION MEASUREMENTS

Pike et. al. [41] has derived an expression which relates chordal void fraction measurements and the area-averaged void fraction. His result was used in this study, thus for completeness his weighting factors will be rederived herein.

Figure A.9.1 shows the circular geometry Pike used to develop his expression. The area averaged void fraction is,

$$\langle\alpha\rangle = \frac{A_g}{A_{x-s}} = \frac{\int_{-R}^{R} \ell\, dr}{\pi R^2} \qquad (1)$$

where,

$\langle\alpha\rangle$ = cross sectional area averaged void fraction

A_g = cross sectional area of vapor phase , cm^2

A_{x-s} = cross sectional area of pipe, cm^2

R = pipe radius, cm

ℓ = pathlength in vapor phase, cm

r = perpendicular distance from centerline to chord, cm

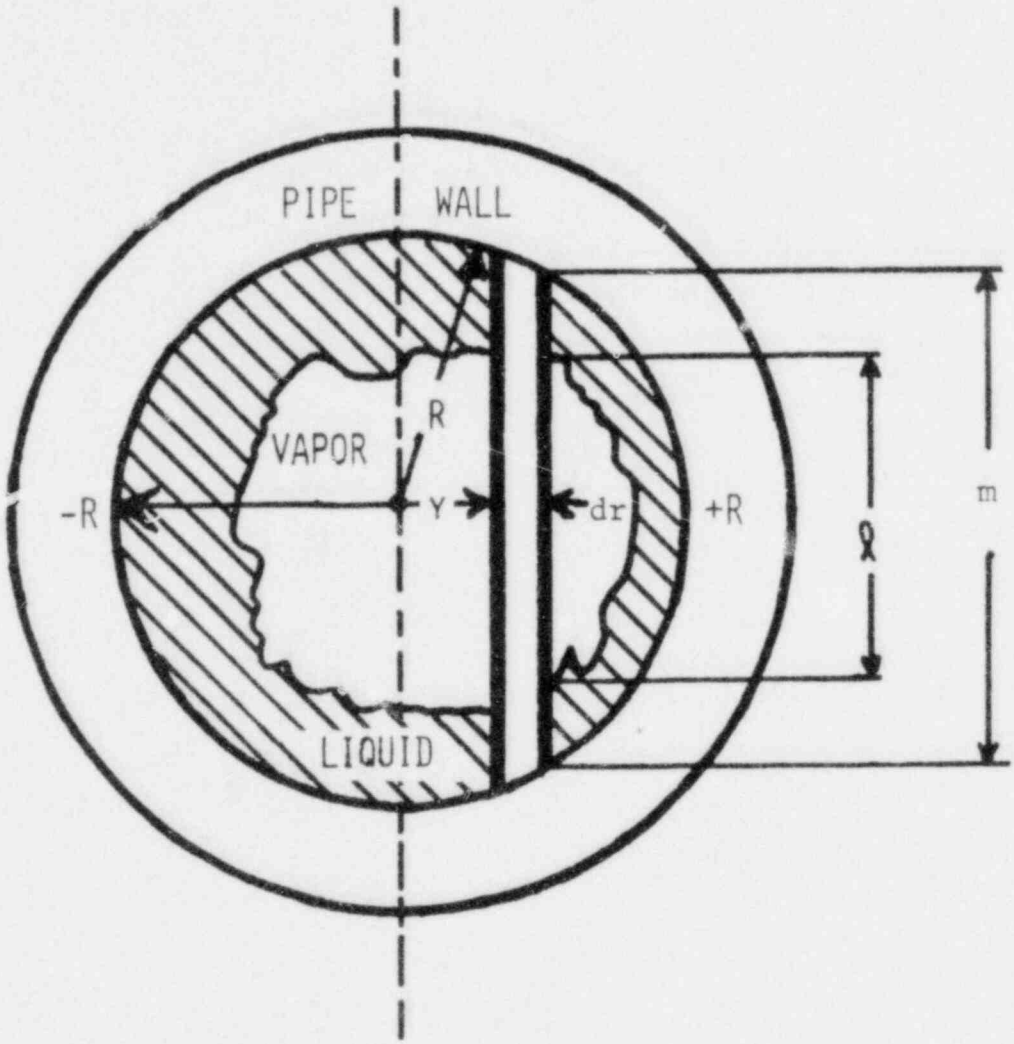

Figure A.9.1 The idealized void geometry used by Pike [41]

The chordal void fraction taken over an incremental width, dr, is,

$$\alpha(r) = \frac{\ell}{m} = \frac{\ell}{2\sqrt{R^2-r^2}} \tag{2}$$

where,

$\alpha(r)$ = chordal measured void fraction

m = total chord length, cm

Equations (1) and (2) are combined to yield,

$$\langle\alpha\rangle = \frac{\int_{-R}^{R} 2\alpha(r)\sqrt{R^2-r^2}\ dr}{\pi R^2} \tag{3}$$

A parameter, 'y', can be defined as,

$$y = \frac{r+R}{2R} \tag{4}$$

Taking the derivative of 'y' with respect to 'r' and rearranging,

$$dr = 2Rdy \tag{5}$$

Rearranging Equation (4) to get 'r' in terms of 'y' yields,

$$r = R(2y-1) \tag{6}$$

Equations (5) and (6) can be combined with Equation (3) to yield,

$$\langle\alpha\rangle = \frac{8}{\pi}\int_{0}^{1}\alpha(y)\sqrt{y(1-y)}\ dy \tag{7}$$

The void weighting factor is $\sqrt{y(1-y)}$. This integral can be integrated with Simpson's Rule if the weights are known at the appropriate locations. The pipe studied earlier in this report had a 0.5 in radius. For this case the weight factors are tabulated in Table A.9.1,

r(in)	y	$\sqrt{y(1-y)}$
0.0	0.5	0.500
0.1	0.6	0.490
0.2	0.7	0.458
0.3	0.8	0.400
0.4	0.9	0.300
0.475	0.975	0.156

Table A.9.1: Chordal Weighting Factors for a one Inch I.D. Pipe

APPENDIX A.10

DERIVATION OF VOID FRACTION USING RADIATION ATTENUATION

Equation (4.8) is commonly used to calculate void fraction, from radiation attenuation measurement. For completeness, this result will now be derived. Radiation attenuation in a media follows Beer's Law,

$$I = I_o e^{-\bar{\mu}x} \tag{1}$$

where,

I = unattenuated intensity at distance 'x' into the media, photons/cm^2-sec

I_o = source intensity, photons/cm^2-sec

$\bar{\mu}$ = energy dependent attenuation coefficient of media, cm^{-1}

x = thickness of attenuating media, cm

If the two-phase media may be considered to be well mixed the two-phase attenuation coefficient can be written,

$$\mu_{2\phi} = \alpha \mu_g + (1-\alpha)\mu_\ell \tag{2}$$

where,

$\mu_{2\phi}$ = two-phase attenuation coefficient, cm^{-1}

α = chordal void fraction

μ_g = attenuation coefficient of gas phase, cm^{-1}

μ_ℓ = attenuation coefficient of liquid phase, cm^{-1}

It is now necessary to consider two specific cases:

1) Only liquid phase present, i.e., $\langle\alpha\rangle$=0.0

2) Only vapor phase present, i.e., $\langle\alpha\rangle = 1.0$.

Equation (1) can now be evaluated for these two cases,

$$\frac{I_\ell}{I_o} = e^{-\mu_\ell x}, \quad \text{for } \langle\alpha\rangle = 0.0 \tag{3}$$

$$\frac{I_g}{I_o} = e^{-\mu_g x}, \quad \text{for } \langle\alpha\rangle = 1.0 \tag{4}$$

where,

I_ℓ = transmitted intensity during the presence of only the liquid phase, photons/cm^2-sec

I_g = transmitted intensity during the presence of only the vapor phase, photons/cm^2-sec

Equations (3) and (4) can be divided to remove the 'I_o' term resulting in,

$$\frac{I_\ell}{I_g} = e^{(\mu_g - \mu_\ell)x} \tag{5}$$

The expression for the two-phase transmitted intensity is developed by substituting Equation (2) into Equation (1),

$$I_{2\phi} = I_o\, e^{-(\alpha\mu_g + (1-\alpha)\mu_\ell)x} \tag{6}$$

where,

$I_{2\phi}$ = two-phase transmitted intensity, photons/cm^{2}sec

This expression can be related to the all liquid case, $\langle\alpha\rangle = 0.0$, by dividing by Equation (3),

$$\frac{I_{2\phi}}{I_\ell} = e^{(\mu_\ell - \mu_g)x} \tag{7}$$

Equations (5) and (7) relate the void fraction to the all liquid, all vapor and two-phase intensity ratios,

$$\alpha = \frac{\ln\left(\frac{I_{2\phi}}{I_{\ell}}\right)}{\ln\left(\frac{I_{g}}{I_{\ell}}\right)} \tag{8}$$

This expression is commonly used to calculate the chordal void fraction measured with gamma densitometers.

REFERENCES

[1] Wallis, G.B., One-Dimensional Two-Phase Flow, McGraw-Hill, Inc., 1969

[2] Hsu, Y.Y. and Graham, R.W., Transport Processes In Boiling and Two-Phase Systems, McGraw-Hill Book Company, 1976

[3] Hsu, Y.Y., Simoneau, R.J., Simon, F.F. and Graham, R.W., "Photographic and other Optical Techniques for Studying Two- Phase Flow.", ASME Symposium Volume:Two-Phase Flow Instrumentation, 1969

[4] Govier, G.W., Radford, B.A. and Dunn, J.S.C., "The Upwards Vertical Flow of Air-Water Mixtures", The Canadian Journal of Chemical Engineering, August, 1957

[5] Hubbard, M.G. and Dukler, A.E, "The Characterization of Flow Regimes for Horizontal Two-Phase Flow", Proceedings of the 1966 Heat Transfer and Fluid Mechanics Institute, Stanford University Press, 1966

[6] Jones, O.C. and Zuber, N., "The Interrelation of Void Fraction Fluctuations and Flow Patterns in Two-Phase Flow", International Journal of Multiphase Flow, Vol. 2, 1975

[7] Green, A.E., and Bourne, A.J., Reliability Technology, Wiley-Interscience, 1972

[8] Hahn and Shapiro, Statistical Models in Engineering, John Wiley and Sons, 1967

[9] Thie, J.A., Reactor Noise , ANS Monograph, 1963

[10] Bendat, J.S. and Piersol, A.G., Random Data: Analysis and Measurement Procedures, Wiley-Interscience, 1971

[11] Lahey, R.T., "A Review of Selected Void Fraction and Phase Velocity Measurement Techniques", Two-Phase Flow Measurements, Fluid Dynamics Institute Short Course 78-1, Dartmouth College, Hanover, New Hampshire, August 1978

[12] Hsu, Y.Y. et al, Two-Phase Instrumentation Review Group Meeting Report, United States Nuclear Regulatory Commission, NUREG-0375, January, 1977*

[13] Reimann, J., Arnold, G., Demski, A., John, H. and Muller, S., Bestimmung der Stromungsform in Horizontaler Luft-Wasser-Sowie Dampf-Wasser-Stromung mit einer lok alen Impendanz-Sonde, Kernforschungszentrum Karlsruhe, 1977

[14] Jenkins, F.A. and White, H.E., Fundamentals of Optics, 4th Edition, McGraw Hill Book Company, 1976

[15] Chrenko, R.M. and Strong, H.M., Physical Properties of Diamond, G.E. Report No. 75CRD089, General Electric Company Corporate Research and Development, October, 1975

[16] Seal, M. and Drukker, D., "The Increasing Applications of Diamond as an Optical Material and in the Electronics Industry", Industrial Diamond Review, January, 1978

[17] Austin, I.G. and Wolfe, R., "Electrical and Optical Properties of a Semiconducting Diamond", Proceedings of The Physical Society, London, 1956

[18] Calderbank, R.H., "The Interfacial Area in Gas-Liquid Contacting with Mechanical Agitation", Transactions of The Institute of Chemical Engineers, Vol. 36, 1958,

[19] Baker, O., "Simultaneous Flow of Oil and Gas", The Oil and Gas Journal, July 26, 1954

[20] Govier, G.W. and Short, W.L., "The Upward Vertical FLow of Air Water Mixtures", The Canadian Journal of Chemical Engineering, October, 1958

[21] Griffith, P. and Wallis, G.B., "Two-Phase Slug Flow", Transactions of the ASME, Vol. C, Journal of Heat Transfer, August, 1961

[22] Taitel, Y., Bornea, D. and Dukler, A.E., "Modeling Flow Pattern Transitions for Steady Upward Gas-Liquid in Vertical Tubes", American Institute of Chemical Engineers Journal, Vol. 26, No. 4, 1980

[23] Bergles, A.E., "Electrical Probes for Study of Two-Phase Flows", ASME Symposium Volume: Two-Phase Flow Instrumentation, 1969

[24] Delhaye, J.M., "Hot Film Anemometry In Two-Phase Flow" ASME Symposium Volume: Two-Phase Flow Instrumentation, 1969

[25] Kobori, T. and Terada, M., "Application of Needle Contact Probe to Blow-Down Test", Proceding of CSNI Specialist Meeting on Transient Two-Phase Flow, Paris, France, June 1978

[26] Miller, N. and Mitchie, R.E., "The Development of a Universal Probe for The Measurement of Local Voidage in Liquid/Gas Two-Phase Flow Systems", ASME Symposium Volume: Two-Phase Flow Instrumentation, 1969

[27] Lanel, F. and Delhaye, J.M., "Sonde Optique pour Mesure du Taux de Presnece Local and Ecoulement Diphasique", Mesures, Regulation, Automatisme, Aout-Septembre, 1971

[28] Delhaye, J.M., Gallup, J.P., Reocreux, M., and Ricque, R., Metrology of Two-Phase Flow - Different Methods, CEA-R-4457, September 1973.

[29] Disamatic Inc., Type 555 Two-Phase Flow Equipment, DISA Electronics Technical Bulletin, New Jersey, USA 1978

[30] Davis, G.E., "Scattering of Light By an Air Bubble in Water", Journal of the Optical Society of America, Vol. 45, No. 7, July 1955

[31] Lockett, M.J. and Safekourdi, A.A., "Light Transmission Through Bubble Swarms", AICHE Journal, Vol. 23, No. 3, May 1977

[32] Schrock, V.E., "Radiation Attenuation Techniques in Two-Phase Flow Measurements", ASME Symposium Volume: Two-Phase Flow Instrumentation, 1969

[33] Lassahn, G.D., Stephens, A.G, Taylor, D.J., and Wood, D.B., "X-Ray and Gamma Ray Transmission Densitometry", International Colloquim on Two-Phase Flow Instrumentation, June, 1979

[34] Smith, A.V., "Transient Density Measurements in Two-Phase Flows Using X-Rays", Journal of British Nuclear Engineering Society, Vol. 10, No. 2, 1971

[35] Kline, S.J. and McClintock, F., "Describing Uncertainties in Single Sample Experiments", Journal of Mechanical Engineering, January, 1953

[36] Petrick, M. and Swanson, B.S., "Radiation Attenuation Method of Measuring Density of a Two-Phase Fluid", Rev. Sci. Instr., Vol. 29, No. 12, 1958

[37] Krammers, H.A., "On The Theory of X-Ray Absorption and of the Continuous X-Ray Spectrum", Philisophical Magazine, Vol. 46, 1923

[38] Skanamatics Corporation, Pico-Skan Fiber Optic Skanner S58 Series, Elbridge N.Y., 1974

[39] Lahey, R.T., Two-Phase Flow Phenomena in Nuclear Reactor Technology, Quarterly Report No. 5, December 1977, NUREG/CR-0023*

[40] Blackman, R.B., and Tukey, J.W., The Measurement of Power Spectra, Dover Publications, New York, 1958

[41] Pike, R.W., Wilkins, B. and Ward, H.C., "Measurement of the Void Fraction in Two-Phase Flow By X-Ray Attenuation", A.I.Ch.E. Journal, September, 1965

[42] Nicklin, D.J., Wilkes, J.O. and Davidson, J.F., "Two-Phase Flow in Vertical Tubes", Trans. Instn. Chem. Engnrs., Vol. 40, 1962

[43] Zuber, N. and Findlay, J.A., "Average Volumetric Concentration in Two-Phase Flow Systems", Journal of Heat Transfer, Nov., 1965

[44] Duns, H. and Ros, N.C.J., "Vertical Flow of Gas and Liquid Mixtures from Boreholes", Sixth World Petroleum Congress, Sect. 2, Paper 22, Frankfurt, West Germany, June, 1963

[45] Govier, G. W. and Aziz, K., The Flow of Complex Mixtures in Pipes, Van Nostrand Reinhold Co., New York, 1972

[46] Nassos, G.P. and Bankoff, S.G., "Local Resistivity for Study of Point Properties of Gas-Liquid Flows", The Canadian Journal of Chemical Engineering, Vol. 45, October 1967

[47] Hamer, W.J., Theoretical Mean Activity Coefficents in Strong Electrolytes in Aqueous Solutions From 0 to 100 Degrees C., NSRDS-NBS-24, No. c13.48:24, 1968

[48] Serizawa, A., Fluid-Dynamic Characteristics of Two-Phase Flow, Ph.D Thesis, Kyoto University,Japan, 1974

[49] Eckert, E.R.G., and Drake, R.M., Analysis of Heat and Mass Transfer, McGraw-Hill Book Company, 1972

[50] Schlichting, H., Boundary Layer Theory, Sixth Edition, McGraw-Hill Book Company, 1968

[51] Langolis, G.E., Gullberg, J.F., and Vermuelen, T., "Determination of Interfacial Area in Unstable Emulsions by Light Transmission", The Review of Scientific Instruments, Vol. 25, No. 4, April, 1954

[52] Lahey, R.T., Vince, M., and Krycuk, G., "The Development of an Optical Digital Interferometer", Proceedings of 2nd Multiphase Flow and Heat Transfer Symposium-Workshop, April, 1979

*Available for purchase from the NRC/GPO Sales Program, U.S. Nuclear Regulatory Commission, Washington, DC 20555, and the National Technical Information Service, Springfield, VA 22161.

NRC FORM 335 (7.77)

U.S. NUCLEAR REGULATORY COMMISSION

BIBLIOGRAPHIC DATA SHEET

1. REPORT NUMBER (Assigned by DDC)
NUREG/CR-1692

4. TITLE AND SUBTITLE (Add Volume No., if appropriate)
Flow Regime Identification and Void Fraction Measurement Techniques in Two-Phase Flow

2. (Leave blank)

3. RECIPIENT'S ACCESSION NO.

7. AUTHOR(S)
M. A. Vince and R. T. Lahey, Jr.

5. DATE REPORT COMPLETED
MONTH: May | YEAR: 1980

9. PERFORMING ORGANIZATION NAME AND MAILING ADDRESS (Include Zip Code)
Department of Nuclear Engineering
Rensselaer Polytechnic Institute
Troy, New York 12181

DATE REPORT ISSUED
MONTH: October | YEAR: 1980

6. (Leave blank)

8. (Leave blank)

12. SPONSORING ORGANIZATION NAME AND MAILING ADDRESS (Include Zip Code)
U. S. Nuclear Regulatory Commission
Office of Nuclear Regulatory Research
Washington, DC 20555

10. PROJECT/TASK/WORK UNIT NO.

11. CONTRACT NO.
NRC-04-76-301
FIN No. B7272

13. TYPE OF REPORT
TOPICAL

PERIOD COVERED (Inclusive dates)
6/1/76 - 5/31/80

15. SUPPLEMENTARY NOTES

14. (Leave blank)

16. ABSTRACT (200 words or less)

This report presents a study concerning the development of various instruments for the measurement of void fraction. In addition, an objective technique for flow regime identification is presented.

17. KEY WORDS AND DOCUMENT ANALYSIS

17a. DESCRIPTORS

Two-phase instrumentation
Flow regime determination
Two-phase flow

17b. IDENTIFIERS/OPEN-ENDED TERMS

18. AVAILABILITY STATEMENT
Unlimited

19. SECURITY CLASS (This report)
Unclassified

21. NO. OF PAGES
534

20. SECURITY CLASS (This page)
Unclassified

22. PRICE
$